The Geochemistry of Feldspar-Free Volcanic Rocks.

Thesis

UNRESTRICTED

The Geochemistry of Feldspar-Free Volcanic Rocks

A thesis presented for the degree of

Doctor of Philosophy

by

Doreen Elizabeth James

B.A. (Honours)

Department of Earth Sciences

The Open University

1995

Date of submission: 2 October 1995
Date of award: 29 February 1996

ProQuest LLC.
789 East Eisenhower Parkway
P.O. Box 1346
Ann Arbor, MI 48106 – 1346

ABSTRACT

Highly silica-undersaturated magmas which form feldspar-free volcanic rocks have been erupted at some time on most continents and in all major ocean basins. In this study 488 oceanic and continental feldspar-free volcanic rocks have been analyzed for major and trace elements. The results are presented in a new compilation covering five continents and three oceans. This type of volcanism is associated with intraplate volcanic activity and occurs within extensional tectonic regimes in continental areas or as late-stage, post-erosional volcanism on oceanic islands. It is restricted almost entirely to the continental circum-cratonic Proterozoic lithosphere and to the margins of ocean basins where the Phanerozoic oceanic lithosphere is older.

The magmas responsible for oceanic (OIN) and continental (CON) nephelinites are dominated by asthenosphere-derived melts. Nephelinitic rocks are enriched in elements which partition strongly into carbonate melts. Small silicate melt fractions may have been enriched by a carbonate precursor liquid derived by 0.1% melting of the same source, the carbonate addition being ca.10% for OIN and up to 20% for CON. K and Rb variation in OIN and CON indicate derivation from amphibole (ca. 2%)-garnet lherzolite sources by carbonate-silicate liquid mixing. Amphibole is residual at small degrees of partial melting but consumed before larger degrees of melting appropriate to most OIB are reached. In a few somewhat K-enriched sources phlogopite is indicated. OIN are characterised by HIMU and EMI trace-element ratios but amphibole implies shallow sources rather than the deep mantle location proposed for the HIMU component. OIN and CON are enriched in carbonate-phobic incompatible elements. This may be the result of remobilization of asthenosphere-derived melts from the base of the lithosphere. Continental lithosphere involvement is also indicated by the greater variability of CON in incompatible element compositions.

Potassic rocks from the Western Rift (WR) and New South Wales (NSW) are extremely enriched in incompatible elements. This may be evidence of metasomatised lithospheric mantle involvement in magma genesis. Carbonate liquids are involved in most WR magmas but not in NSW magmas where H_2O-rich fluids are indicated. Phlogopite (probably with amphibole) dominates both sources. Olivine-poor nephelinites (COP) are also enriched in incompatible elements but have similar normalised profiles to OIN and CON. COP may be derived by liquid immiscibility from highly carbonated asthenospheric magmas and are related to CON by two-stage silicate-carbonate liquid partitioning effects, crystal fractionation, and contamination by lithospheric mantle.

ACKNOWLEDGEMENTS

I am especially grateful to Dr Godfrey Fitton for originating this project and for his support and advice throughout its duration, to Dr Martin Menzies and Professor Brian Upton for finding a way for me to undertake the work in the first place, to Professor Ian Gass for his wisdom in the early stages, and to Dr Nick Rogers for his encouragement and support while I have been completing the work.

In particular, I am indebted to Godfrey Fitton for helping me to finance four field trips and, in the early stages, for his assistance with locating suitable collections of rocks and selecting samples for study. It has been difficult to do justice to the large amount of data collected in the course of this work. Godfrey has provided guidance and inspiration in the face of confusion and indecision and helped me to remain focussed on the original objectives in spite of the many interesting details which threatened to bog down or redirect the main thrust of the project. I have greatly appreciated the careful and constructive criticisms of the first draft made by Godfrey and Nick and also their tolerance of my mistakes and misunderstandings. I am also grateful to Nick Rogers for providing INAA analyses at the Open University; to Dave Gerlach for ID analyses at Leeds University; and to Godfrey Fitton, Brian Upton, Barry Dawson, Cassi Paslick, and Hilary Downes for company, advice, and humour in the field.

A large proportion of the samples analyzed in the course of this study have been donated. The following are thanked for responding so willingly to my requests for material: Professors K.G.Cox, J.B. Dawson, D.H. Green, S. Maaløe, and B.G.J. Upton; Drs D.S. Barker, H. Downes, J.G. Fitton, R.V. Fodor, R.W. Johnson, M.J. Le Bas, D.P. Mattey, J.H. Natland, T.F.D. Neilsen, H-U. Schmincke, J.C. Stormer, F.L. Sutherland, R. Varne, L.A.J. Williams, A.R. Woolley. The Smithsonian Institute is thanked for samples from Oahu and Kauai. Valerie Jones provided essential help in locating samples from the collections of the British Museum (Natural History) and cutting suitable pieces for analysis. Peder Aspen also located material within the collections of the Grant Institute. The Curator, Department of Earth Sciences, Cambridge University, is thanked for providing samples collected by A.D. Coombs from the Western Rift.

Over the years, I have received immeasurable support and encouragement from staff and students at the Grant Institute. I cannot mention all by name but, in particular, I must acknowledge the friendship and help of Brian Upton, Barry Dawson, Hilary Downes, Tracy Watson, Pauline Smedley, and latterly, Mike Norry, Chris Brake, and Ian Snape.

Finally, to Nick, Samantha, and Jonathan, thanks! Without the understanding and loyalty of my family this work would neither have been started nor completed. They have tolerated my frequent mood changes, tiredness, and even being ignored for weeks on end, without complaint, criticism, or doubt in my ability to reach this point. I am also indebted to Simba, Kali Paka, and Figaro for providing company in the middle of the night. They have personally inspected every page in this work, leaving muddy marks of approval or dismay, and have never failed to be fascinated by the whole process. But for them the whole thing might have been finished sooner.

CONTENTS

LIST OF FIGURES

Chapter 2

Chapter 3

Chapter 4

Chapter 5

LIST OF TABLES

Chapter 1
Introduction

1.1 Introduction and Basic Rationale

Mafic lavas are derived by variable degrees of partial melting in the Earth's mantle and thus have the potential to provide information about the chemistry and mineralogy of their mantle sources.

Large-ion lithophile elements (LILE) are highly incompatible in major mantle phases and, therefore, become concentrated in liquids during partial melting. Small degrees of partial melting are thus more enriched in LILE than large degrees of partial melting from the same source, and LILE and other incompatible element concentrations in large melt fractions tend to reflect the source composition of these elements. Incompatible trace-element concentrations in mafic lavas range from <10 x chondrite in mid-ocean ridge basalts (MORB) to approximately 100 x chondrite in ocean island basalts (OIB) and up to 1000 x chondrite in some continental basic alkaline volcanic rocks.

Intraplate basic alkaline volcanic rocks are thus strikingly enriched in incompatible elements and none more so than the highly undersaturated feldspar-free varieties such as nephelinite and melilitite. Feldspar-free basic volcanic rocks may, therefore, represent the smallest degrees of partial melting observed and as such the magmas should contain information about source characteristics and also mantle mineralogy before the onset of melting since only very minor phases will be consumed during their formation. Many nephelinites and melilitites have high MgO/(MgO+FeO) and often contain peridotite xenoliths. These volcanic rocks could, therefore, represent primary melts or be very close to primary melt compositions.

Nephelinite, melilitite, and related highly undersaturated feldspar-free volcanic rocks occur in both oceanic and continental environments. A geochemical study of these rock types on a global scale could thus provide valuable information about the nature of the upper mantle and the sources of intraplate basic magmas.

1.2 Background and General Objectives

MORB have low concentrations of LILE, and isotope ratios which indicate that the MORB source has had low Rb/Sr and Nd/Sm (and, by implication, low concentrations of LILE in general) for a considerable period of time. MORB are, therefore, generally regarded as large-degree melts (10-20%) from LILE-depleted shallow mantle sources which lie beneath mid-ocean ridges. These degrees of melting are unable to fractionate the highly incompatible elements and therefore the incompatible trace-element chemistry of MORB represents the relative abundance of these elements in the MORB source.

Intraplate basic alkaline volcanic rocks are, on the other hand, highly enriched in incompatible elements. As in the case of MORB, isotope ratios frequently imply source regions for these magmas which have a long-term depletion in LILE although not quite so depleted as the MORB source. If highly LILE-enriched nephelinite and melilitite are generated by partial melting of a depleted source (for example, the MORB source) then the degree of melting required to concentrate LILE to the observed levels in these magmas must be very small indeed (much less than 1%). It has, traditionally, been considered impossible to extract melt fractions of this magnitude from the mantle source and therefore complex melting and enrichment processes such as zone refining (Harris, 1957) and wall-rock reaction (Green & Ringwood, 1967) have been proposed. More recently models in which the mantle source is metasomatically enriched shortly before the onset of melting, by H_2O- and CO_2-rich fluids originating from deeper within the mantle, have been invoked to account for the high concentrations of incompatible elements observed in both oceanic

(e.g. Wright, 1984) and continental (e.g. Frey *et al.*, 1978; Menzies & Murthy, 1980a; Bailey, 1982) intraplate environments.

Support for metasomatic enrichment processes has been derived from studies of metasomatised mantle xenoliths found in alkali basalts and kimberlites in continental provinces (e.g. Boettcher & O'Neil, 1980; Menzies & Murthy, 1980b; Wass & Rogers, 1980; Bailey, 1982; Wilkinson & Le Maitre, 1987). The mineralogical composition of these xenoliths indicates that they are almost certainly derived from the continental lithosphere. However, it is not clear whether the formation of the metasomatic mineral assemblages is a cause or consequence of magmatism. Nevertheless, considerable experimental and analytical effort has been expended on establishing criteria for the presence of hydrous phases in the sub-continental lithosphere (e.g. Kushiro, 1972; Boettcher *et al.*, 1975; Mysen & Boettcher, 1975; Wendlandt & Eggler, 1980a; Wendlandt & Eggler, 1980b; Schneider & Eggler, 1986) and the consequences of melting these regions (Brey *et al.*, 1983; Olafsson & Eggler, 1983; Wyllie, 1987).

The mantle sources of intraplate basic alkaline volcanic rocks may reside in the oceanic lithosphere or the continental lithosphere, and/or the convecting asthenosphere. The continental lithosphere is older and thicker than the oceanic lithosphere and has the capability to store, for long periods of time, the products of lithospheric mantle interaction with upwardly percolating metasomatising fluids and, continuously- or episodically-derived small melt fractions from the asthenosphere which may be incorporated and retained in its base. Either of these processes could be responsible for local enrichment in incompatible elements which could be superimposed on earlier enrichment events related to subduction processes at active continental margins. The oceanic lithosphere should be equally subjected to fluid-migration effects and yet metasomatised mantle fragments are extremely rare in ocean island rocks. If fluid percolation and accumulation is episodic or the rate of production is slow, the oceanic lithosphere may be too young for significant volumes of metasomatised mantle material to have been preserved. The oceanic lithosphere may, therefore, be at least as depleted in LILE as the MORB source. The asthenosphere, in

contrast with the continental lithosphere, is generally assumed to be homogeneous in composition as a result of convective mixing or, more accurately, to be similarly heterogeneous, on the scale of individual convection cells, beneath both continents and ocean basins.

Fitton & Dunlop (1985) showed that Cameroon line mafic magmas from continental and oceanic sectors are essentially indistinguishable in normalised incompatible-element patterns and concentrations. They concluded, therefore, that the magmas must have a common source within the asthenosphere. McKenzie (1984) developed equations to describe the process of partial melting and these predict that very small melt fractions will be removed from the mantle source region if their viscosity is low. Highly undersaturated alkaline magmas, wherever they occur, may thus be dominated by small melt fractions derived from sources which lie within the asthenosphere. Experimental evidence indicates that these cannot be produced from volatile-free mantle peridotite and that small amounts of both H_2O and CO_2 are essential ingredients in the source regions of nephelinitic and melilititic magmas.

Le Bas (e.g. 1987, 1989a) has classified nephelinitic rocks as belonging to the carbonatite-nephelinite (olivine-poor) association or the basalt-nephelinite (olivine-rich) association. Olivine-poor melanephelinite is almost totally absent from ocean islands but occurs commonly in continental rift provinces. Although the parental or derivative status of some carbonatitic magmas is debated (Twyman & Gittins, 1987; Le Bas, 1987; Gittins, 1989) it is generally agreed that conjugate silicate and carbonate magmas can arise from liquid immiscibility processes in the sub-continental mantle. The parental magma in this process is thought to be CO_2-rich olivine nephelinite in composition and separation of the two liquids may be accompanied by extensive fractionation of olivine. If this is so, olivine-poor nephelinites may be no more than evolved variants of olivine-rich varieties from similar sources and there would be no need to appeal to fundamentally different processes, or sources within the continental lithosphere, to account for the difference in mineralogy.

The case for metasomatic enrichment of mantle sources as an essential precursor to all intraplate alkaline magmatism has been significantly weakened. Furthermore, a growing body of analytical data suggests that highly undersaturated magmas in both oceanic and continental environments are commonly derived from sources in the asthenosphere and that volatiles (H_2O and/or CO_2) play a vital part in their genesis. However, the extremely high concentrations of LILE found in a number of feldspar-free intraplate continental volcanic rocks, particularly those where $K_2O>Na_2O$, suggest that small degrees of melting alone may not be able to account for the levels of enrichment observed (Fitton & James, 1986). In these cases the magmas may be generated from metasomatically enriched continental lithosphere and retain information about the mineralogy of continental lithospheric sources.

Ocean-basin magmatism is uncomplicated by the potential for direct involvement of continental lithosphere. Comprehensive studies of ocean basin magmatism have sought to characterise the nature of the asthenosphere which is the source for MORB and OIB. It is now well established that the MORB and OIB sources undergo considerable cross-contamination (e.g. Saunders *et al.*, 1988; Halliday *et al.*, 1995a), and that chemical and isotopic heterogeneities exist within OIB, on a large scale (Hart, 1984) and on a local scale (e.g. Hoernle & Schmincke, 1993b; Davies *et al.*, 1989; Gerlach *et al.*, 1987). Highly undersaturated magmas in ocean basins may be derived by small degrees of partial melting of the MORB source but isotopic evidence suggests that OIB have been generated from mixtures of sources involving mantle components that have remained isolated from the convecting mantle for time periods in excess of 1 Ga. In recent years a number of mantle reservoirs, domains, and components with distinct isotopic and chemical characteristics, have been put forward as possible end-member sources for ocean island magmatism (Zindler & Hart, 1986 and references therein) and a number of mechanisms and locations for the isolation of these sources have been proposed (e.g. Zindler *et al.*, 1982; Hofmann & White, 1982; Cohen & O'Nions, 1982; Ringwood, 1982; McKenzie & O'Nions, 1983; White, 1985; Hart *et al.*, 1986; Hawkesworth *et al.*, 1986) and discussed (e.g. Sun & McDonough, 1989; Weaver, 1991; Baker, 1992). While it is convenient to visualise the

isotopic variation of OIB in terms of hypothetical end-member compositions, there is little evidence in reality for the existence or involvement of these. However, it is possible that the smallest degrees of partial melting represented by feldspar-free volcanic rocks on ocean islands may be preferentially derived from chemically and isotopically anomalous mantle material or, at least, have a tendency to be different, both chemically and isotopically, from the larger melt fractions.

The purpose of this study has been to use major- and trace-element data from highly undersaturated feldspar-free volcanic rocks to investigate the mineralogy and source characteristics of the mantle from which small melt fractions are derived. The information obtained has then been used to address the problems introduced in this section in an attempt to constrain the minor phases which may be present in both asthenospheric and lithospheric mantle sources, to identify global variations in mantle source characteristics, and to model the partial-melting processes responsible for the generation of small melt fractions.

1.3 Specific Objectives

(i) To review the nomenclature and establish a classification for feldspar-free volcanic rocks.

(ii) To review the temporal and spatial distribution of highly undersaturated volcanism, the range of geological settings, and their relationship with tectonic environments.

(iii) To present major- and trace-element data for oceanic and continental feldspar-free volcanic rocks in order to establish the geochemical characteristics of these rock types and to demonstrate similarities and differences from asthenosphere-derived OIB.

(iv) To compare the compositional range of oceanic nephelinites and melilitites (OIN) with OIB in general. The geochemical characteristics of small melt fractions might reveal

a) the presence of residual phases in the mantle source which are consumed in larger degrees of melting, and

b) unusual source characteristics which might reflect the isotopic variations found in OIB, or

c) that OIN are simply the smallest melt fractions from the same sources as other OIB.

(v) To compare the compositional range of oceanic and continental highly undersaturated magmas in order to establish whether continental types are derived by small degrees of melting from asthenospheric sources or from enriched lithospheric sources. The composition of continental feldspar-free volcanic rocks may vary with

a) tectonic setting, and

b) previous history of the lithosphere.

(vi) To compare the compositional range of olivine-rich nephelinites of the basalt-nephelinite association with olivine-poor nephelinites of the carbonatite-nephelinite association. Trace-element concentrations might indicate that

a) there is nothing more fundamental in the classification than degree of differentiation, and

b) that olivine-poor nephelinites contain evidence for the operation of liquid immiscibility in highly carbonated magmas.

1.4 Previous Work

A comparative study of nephelinites from East africa with similar rocks from the rest of the world was undertaken some time ago by Wood (1968) in an attempt to place nephelinite genesis in the broader field of basalt magmatism. The conclusions were based

on new analyses of rocks from East Africa and a small number of other provinces, and a considerable amount of published data of varying age and reliability. Trace-element analysis was restricted to a few elements considered to be diagnostic in terms of the partial melting, crystal fractionation, and other magma enrichment models which were popular at that time. Wood's interpretation, however, was strongly prejudiced by the notion that trace-element enriched basaltic magmas are derived by crystal fractionation processes from trace-element depleted parents (e.g. picritic tholeiite) originating from greater depths (e.g. O'Hara, 1965; 1965; Tilley & Yoder, 1964; Green & Ringwood, 1964; 1966). Partial melting models (Yoder & Tilley, 1962; Kushiro & Kuno, 1963), incongruent melting of pargasite (Varne, 1965) and alternative enrichment mechanisms (Harris, 1957; Green & Ringwood, 1967) were considered but found wanting in the context of highly enriched nephelinitic magmas. Wood concluded that a composite model involving upwardly percolating picritic magmas, high-pressure pyroxene fractionation, and additional low-pressure enrichment processes (either by zone refining, wall-rock reaction, or both) was appropriate to his data. A predisposition to crystal fractionation processes for enriched magmas did, however, lead him to the conclusion that olivine-poor and olivine-rich melanephelinites are related by such a mechanism.

Since Wood's (1968) work was completed a wealth of analytical and experimental data has been accumulated which suggests that partial melting and source enrichment processes are significantly more important in the genesis of alkaline magmas than he thought and that highly LILE-enriched primary liquids can be derived directly from mantle sources.

Progress in understanding the petrogenesis of alkaline igneous rocks has been assessed by several authors in recent years. Reviews have been published in a number of well-known texts (e.g. Sørensen, 1974; Basaltic Volcanism Study Project, 1981; Fitton & Upton, 1987) and in specialised volumes dealing with particular rock types and associations (e.g. Le Bas, 1977; Gupta & Yagi, 1980; Kornprobst, 1984; Mitchell, 1986;

Ross, 1989; Bell, 1989). These contributions contain copious references to the primary literature and the reader is referred to

(i) Edgar (1974, 1987) and Eggler (1989) for experimental studies

(ii) Bailey (1974) for the early petrogenetic models for alkaline rocks in general and nephelinite in particular, and Ringwood (1989) for more recent models

(iii) Le Bas (1977, 1987, 1989a) for nephelinite associations and petrogenetic models for olivine-rich and olivine-poor varieties

(iv) Kjarsgaard & Hamilton (1989), Wyllie (1989), and Gittins (1989) for experimental evidence for the origins of olivine-poor nephelinite and carbonatite

(v) Mitchell (1986) and Wyllie (1989) for the petrogenesis of melilititic rocks associated with kimberlite

(vi) Sahama (1974), Gupta & Yagi (1980), Bergman (1987) and Mitchell & Bergman (1991) for the petrogenesis of lamproite, leucitite, kamafugite and other potassic rocks.

The volume and extent of the work carried out in the last 25 years makes it difficult to summarize but a number of important observations and results have emerged which have redirected petrological thinking and served to constrain petrogenetic models.

(i) Olivine-rich nephelinite and melilitite are unlikely to be related to tholeiitic or alkaline picritic parental magmas by fractional crystallization processes (Bultitude & Green, 1971) and are by implication, therefore, primary magmas.

(ii) Polybaric partial melting behaviour of mantle lherzolite (O'Hara, 1968) predicts that magmas become more SiO_2-poor and MgO-rich with increasing depth and that highly undersaturated mafic magmas are derived from garnet and/or spinel lherzolite assemblages.

(iii) With increasing alkalinity the derivation of mafic and ultramafic magmas from a volatile-free lherzolite mantle source, or one with H_2O as the only volatile

component, becomes increasingly difficult (Bultitude & Green, 1967; 1971; Allen *et al.*, 1975; Merrill & Wyllie, 1975).

(iv) Olivine-rich nephelinite represents small melt fractions derived from amphibole-bearing peridotite in the presence of small amounts of H_2O and CO_2 (<0.37 wt%) at shallow depths (ca. 50 km) while melilitite and melilite nephelinite are derived from greater depths (50 - 90 km) where CO_2 is an essential and predominant volatile component (Eggler, 1978).

(v) Melilitite is produced at shallower depths than kimberlite (Brey *et al.*, 1983) and is no longer considered to be genetically related to kimberlite except in the sense that both are thought to be products of metasomatised mantle sources (Mitchell, 1986).

(vi) Three groups of potassic and ultrapotassic rocks from differing tectonic settings have been recognised (lamproite, kamafugite and Roman Province leucitite) with distinct mineralogies and chemistries which precludes any simple genetic relationship between them (Mitchell & Bergman, 1991).

(vii) Kamafugites and lamproites both occur in intraplate environments but the only common aspect in their petrogenesis is the requirement for a metasomatized mantle source (Edgar, 1987; Mitchell & Bergman, 1991).

(viii) The kamafugitic group cannot be generated from lherzolitic mantle sources where H_2O is the only volatile phase (Edgar *et al.*, 1976) and these rocks are believed to represent melts derived either from clinopyroxenite (Edgar & Arima, 1983) or from phlogopite peridotite (Wendlandt & Eggler, 1980b).

(ix) In the presence of small amounts of H_2O and CO_2 liquids become increasingly K_2O-rich and SiO_2-poor as depth increases from 100 to 150 km (Wendlandt & Eggler, 1980a).

(x) Olivine-poor nephelinite and associated carbonatite are produced by liquid immiscibility processes from a highly carbonated nephelinitic parental magma. The depth at which this occurs may be deep (Twyman & Gittins, 1987) or at lower crustal levels (Le Bas, 1987) and may be accompanied by extensive fractionation of olivine.

A consensus seems now to have been reached that highly LILE-enriched magmas can be derived by small degrees of partial melting from mantle sources. Exactly which sources, and where they originate or may have been transported, is still debated as is the role of source enrichment in magma generation. Experimental results favour strongly the involvement of both H_2O and CO_2 in the generation of highly alkaline magmas, and dissolved volatiles may be an essential ingredient which reduces the viscosity of the smallest melt fractions and permits their escape from the source region.

Many recent papers have dealt with the occurrence of highly undersaturated rocks in specific provinces or volcanic complexes as part of more detailed studies of the isotopic and trace-element characteristics of possible sources. Sometimes the work has been sufficiently detailed to warrant a separate contribution for the highly undersaturated rocks (e.g. Clague & Frey, 1982) but more commonly these are not considered in isolation because the rock types are relatively rare (e.g. Ewart *et al.*, 1988). The relevant papers are too numerous to list individually here but they are cited in the following chapters where appropriate. Individual pieces of work have also been used by others to formulate all-encompassing chemical geodynamic mantle models which account for both oceanic and continental intraplate basic magmas with compositions ranging from kimberlite to tholeiite (e.g. Allègre, 1982; Allègre & Turcotte, 1985; Zindler & Hart, 1986; Zindler & Jagoutz, 1988).

Wood's work was completed in 1968. Despite a better understanding of phase relationships, partial melting processes, mineral/melt partition coefficients, and the role of volatiles in melting regimes, no similar global study of highly undersaturated feldspar-free rocks has been undertaken and the potential of these rock types to reveal coherent information about the nature of the upper mantle and the sources of intraplate basic magmas has been somewhat neglected.

1.5 Nomenclature and Definitions

Alkaline rocks have, traditionally, been classified on the basis of their mineralogy and frequently have been named by a "type locality". This has led to a plethora of rock names (see Glossary in Sørensen, 1974) which convey no direct information about the mineralogy of the rock and, despite seemingly precise definitions of the mineralogy for the type localities, they are often difficult to apply unambiguously elsewhere. Fortunately many of these names have fallen out of use but a number persist in the literature and continue to be used. Some are feldspar-free volcanic varieties and the following have been encountered in identifying possible rock samples for inclusion in this study

(i) Ankaratrite - biotite olivine melanephelinite

(ii) Etindite - leucite nephelinite

(iii) Katungite - olivine melilitite containing kalsilite (no pyroxene)

(iv) Limburgite - olivine and augite phenocrysts in alkali-rich glass

(v) Mafurite - olivine kalsilitite

(vi) Tannbuschite - augite ankaratrite or olivine melanephelinite

(vii) Ugandite - olivine melaleucitite

(viii) Kamafugite - collective name for the ***ka***tungite-***maf***urite-***ug***andite association

These names have been used as appropriate when referring to older literature and describing the temporal and spatial distribution of feldspar-free volcanic rocks in Chapter 2. Elsewhere in this work mineralogical names (e.g. nephelinite, melilitite, leucitite) have been adopted except in the case of the kamafugites from the Western Rift of eastern Africa where the locality names (katungite, mafurite, and ugandite) are well known and are still in common use.

In general the recommendations of Le Bas (1989b) have been followed in naming the feldspar-free volcanic rocks used in this work. Nephelinites *(sensu lato)* are referred to as nephelinitic rocks to avoid confusion with the use of nephelinite *(sensu*

stricto). Mafic nephelinitic rocks are referred to as melanephelinites, either olivine melanephelinite or pyroxene melanephelinite depending on the phenocryst assemblage, while nephelinite *(sensu stricto)* is restricted to the olivine-free or olivine-poor variety consisting of nepheline and augite. Melilitite (melilite and augite) and leucitite (leucite and augite) are reserved for olivine-free or olivine-poor rocks containing abundant melilite and leucite, respectively. The former practice of using nepheline basalt, leucite basalt and melilite basalt to describe olivine-bearing varieties of nephelinite, leucitite, and melilitite is considered misleading where rocks so named do not contain feldspar. Throughout this work these are referred to as olivine nephelinite, olivine leucitite, and olivine melilitite, respectively.

The rock samples used in this study are feldspar-free volcanic rocks and as such are defined as having no modal feldspar. They comprise nephelinite, melanephelinite, melilitite, melilite nephelinite, leucitite, and kamafugite (ugandite, mafurite, and katungite) as defined above. In view of the effort that has been devoted to the study of kimberlites and lamproites in recent years, it was decided to exclude these rock types, and also leucitites associated with subduction zones, from this work. All the rocks included in this study are from intraplate settings in either oceanic or continental environments. The abbreviations OIN (for ***O***cean ***I***sland ***N***ephelinitic rocks) and CON (***CO***ntinental ***N***ephelinitic rocks) are used frequently to distinguish the two groups. COK and COP are used to distinguish ***CO***ntinental potassic (***K***-rich) rocks and ***CO***ntinental olivine-***P***oor rocks respectively. OIB (***O***cean ***I***sland ***B***asalt) and MORB (***M***id-***O***cean ***R***idge ***B***asalt) are used where appropriate in this work but otherwise acronyms have been avoided.

1.6 Sample Selection and Classification

The majority of samples used in this study were donated from research collections. Many occurrences of feldspar-free volcanic rocks are well documented and reviewed (e.g. East African Rift) and, thanks to the generosity and help of the geological

fraternity around the world, samples were obtained fairly easily. In most cases rock samples or chips were obtained but in some instances only powders were available.

Other occurrences of feldspar-free volcanic rocks are known only from obscure references in the literature (e.g. Manchurian Province) and it proved impossible to locate material for many of these. Older literature and catalogues frequently refer to potentially suitable rock types by "exotic" names (see section 1.5) and, in some cases, there was a strong possibility that rocks had not been named rigorously or may have been misidentified altogether. Thus, for example, many nephelinites *(sensu lato)* might prove to be phonolite or basanite containing small amounts of plagioclase feldspar and not, therefore, suitable for inclusion. Similarly limburgite could be nephelinitic or basanitic in chemical composition despite an apparent absence of feldspar in thin section. For this reason, rather more samples were gathered initially from collections than would ultimately be included in the data base. Where samples were not easily obtainable from individuals and institutions, opportunities were taken to collect material whenever possible. By virtue of four short field excursions rocks were collected from the Eifel and Rhine Graben (Germany), from Raton-Clayton (New Mexico), from the Hopi Buttes (Arizona), and from Northern Tanzania.

The simple definition of feldspar-free volcanic rocks given in Section 1.5 is quite unambiguous, namely those volcanic rocks with no modal feldspar. However, as with most simple definitions, this became inadequate when applied to the practicalities of sample selection. Many nephelinitic rocks have a very fine grained or glassy groundmass and it is not always possible to determine whether feldspar is present in thin section or not. As a result of this common difficulty in applying mineralogical definitions satisfactorily, chemical distinctions have been sought (e.g. Irvine & Baragar, 1971; Le Maitre, 1976, 1984; De la Roche *et al.,* 1980; Le Bas *et al.,* 1986; Le Bas, 1989b). The samples obtained as rocks or chips were, in the first instance, examined petrographically for the presence or absence of modal feldspar. All the samples were then analyzed by X-ray fluorescence at Edinburgh University for major elements. On the basis of the analyses obtained it was

possible to determine which samples should be included in the data base and to screen those for which no thin section was available.

In selecting samples for this study the chemical criteria determined by Le Bas (1989b) have been used. However, for the purposes of this work it has been less important to name the rock samples accurately than to select those in which feldspar is absent, or virtually absent. For this reason the boundary criteria set by Le Bas (1989b) for nephelinitic rocks have been applied less rigorously than would be the case if nomenclature were of paramount importance. The criteria used for selection and classification of samples included in the data base are as follows

(i) ***Absence, or apparent absence, of modal feldspar***

(ii) ***MgO > 4 wt.%***

unless samples were from carbonatite-nephelinite associations when data were retained to study the relationship between olivine-rich and olivine-poor types

(iii) ***Melilitite*** (> 10% modal melilite; Streckeisen, 1980)

SiO_2 < 40 wt.%

CaO > 15 wt.%

Normative calcium orthosilicate > 10 wt.%

(iv) ***Melilite Nephelinite***

SiO_2 < 40 wt.%

CaO > 12 wt.%

Normative calcium orthosilicate present but < 10 wt.%

(v) ***Olivine Melanephelinite*** (olivine phenocrysts, augite in groundmass)

SiO_2 < 42 - 44 wt.%

MgO > 10 wt.%

Total alkalies < 7 wt.% (Le Bas, 1989b recommends < 8 wt.%)

Normative albite < 7 wt.% (Le Bas, 1989b recommends < 5 wt.% but the higher value used here allows for some zeolitisation of the sample)

Normative nepheline = 4 - 22 wt.% (Le Bas, 1989b recommends < 20 wt.%)

(vi) ***Pyroxene Melanephelinite*** (augite phenocrysts, sparse olivine)

As above but with MgO = 4 - 10 wt.%

(vii) ***Nephelinite*** (nepheline and augite phenocrysts, no olivine phenocrysts)

SiO_2 < 47 - 49 wt.%

MgO = 4 - 7 wt.%

Total alkalies = 7 - 15 wt.% (Le Bas, 1989b recommends > 8 wt.%)

Normative nepheline = 22 - 40 wt.% (Le Bas, 1989b recommends > 20 wt.%)

Normative albite < 12 wt.% (Le Bas, 1989b suggests < 20 wt.%).

(viii) ***Leucitite*** (modal leucite)

$K_2O > Na_2O$

(ix) ***Kamafugite*** (katungite, mafurite, and ugandite as defined in section 1.5)

$K_2O > Na_2O$

The samples selected for study numbered 488 in all. Of these 174 were from oceanic islands (OIN) and 314 were from continental provinces. The continental data set was further subdivided into mafic melanephelinites and nephelinites (CON; 215 samples), potassic leucitites and kamafugites from the Western Rift in Uganda and New South Wales in SE Australia (COK; 59 samples), and a further 40 samples of olivine-poor nephelinite (COP; MgO < 4 wt.%) from carbonatite-nephelinite associations. All these samples were analysed by X-ray fluorescence at Edinburgh University for major and trace elements. Details of the techniques used are given in Appendix B and the data obtained appear in Appendix C. The sources of the samples are listed in Appendix F.

At the same time as this data base was being compiled a large collection (904 samples) of ocean island volcanic rocks, ranging in composition from tholeiite to melilitite, was assembled and analysed. These data were obtained to provide a data base of analyses which would be internally consistent and directly comparable with the data obtained for the feldspar-free volcanic rocks. As has already been discussed, OIB are free from the direct involvement of continental lithosphere in their mantle source regions and can, therefore, be taken to represent the range of possible magma products from asthenospheric sources

across a wide spectrum of degrees of partial melting. The OIB data base has been used extensively throughout this study of feldspar-free volcanic rocks for comparative purposes. In view of the large number of samples involved the OIB analyses are not tabulated in this work. Average data for all the islands represented in the data base and of OIB in general are, however, given in Appendix E and in the summary tables in Chapters 3 and 4.

Chapter 2

The Global Distribution and Tectonic Setting of Feldspar-Free Volcanic Rocks

2.1 Introduction

Highly silica-undersaturated, feldspar-free volcanic rocks, although rare, have been erupted at some time on most continents and in all major ocean basins (Fig. 2-1). This type of volcanism is associated, almost exclusively, with intraplate volcanic activity. There are no known occurrences at constructive plate margins or at destructive continental margins, and no occurrences which can be directly related to island arc volcanism, although feldspar-free volcanic rocks have been found in Japan (Nakamura *et al.*, 1985) and on Ambitle (Feni Islands) in the south-west Pacific (Johnson *et al.*, 1976).

Other authors have reviewed the global distribution of these rock types (Wood, 1968; Le Bas, 1977; Gupta & Yagi, 1980) or their distribution in specific provinces, volcanic associations, or tectonic environments (e.g. chapters in Sørensen, 1974; Fitton & Upton, 1987; Johnson, 1989; Bell, 1989; and, Mitchell, 1986; Woolley, 1987; Mitchell & Bergman, 1991). The following overview and discussion refers, in general terms, to samples analysed in this study or to samples for which recently-published data are used for comparative purposes. Details of the locations of the samples, their tectonic environments, ages, and the associated volcanic products are given in Appendix A. The sources of the samples used in this study are given in Appendix F.

2.2 Oceanic Islands

Feldspar-free volcanic rocks most often occur on oceanic islands as a late-stage rejuvenation episode following a period of quiescence and erosion (e.g. Oahu and Kauai,

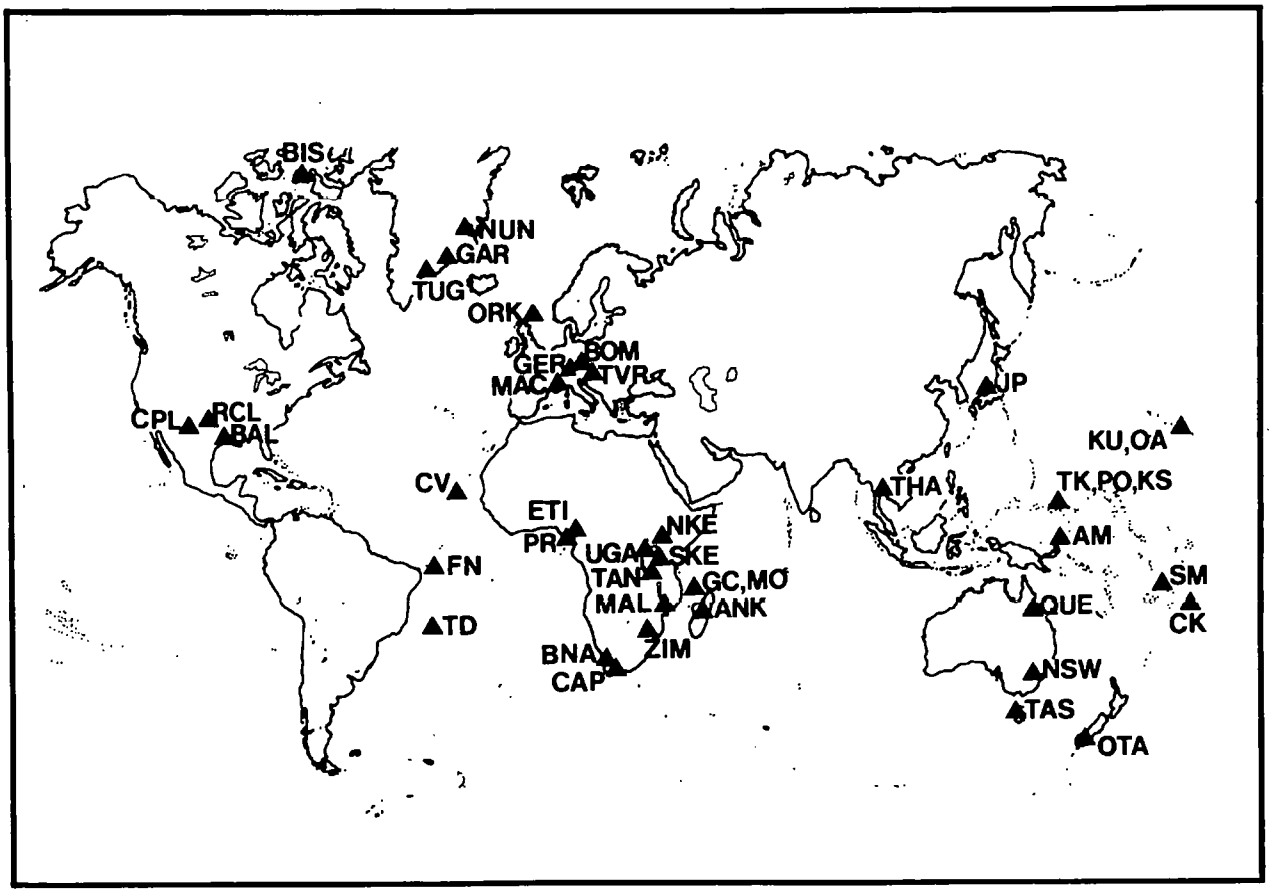

Figure 2-1. Locations of feldspar-free samples used in this study.

Ocean Islands (OIN)
AM Ambitle, Feni Islands, New Ireland
CK Aitutaki, Cook Islands
CV Cape Verdes
FN Fernando de Noronha
GC Grande Comore, Comores Islands
JP Nagahama, Japan
KS Kusaie, Caroline Islands
KU Kauai, Hawaiian Islands
MO Moheli, Comores Islands
OA Oahu, Hawaiian Islands
PO Ponape, Caroline Islands
PR Principe, Gulf of Guinea
SM Upolo, Samoa
TD Trinidade
TK Truk, Caroline Islands

Continental Provinces (CON & COP)
ANK Ankaratra Mtns, Malagasy
BAL Balcones, Texas
BIS Bathurst Island, Canadian Arctic
BNA Bushmanland-Namaqualand, S Africa
BOM Bohemian Massif, Czech (inc. COP)
CAP Cape Province, S Africa

Continental Provinces (CON & COP) cont.
CPL Colorado Plateau, Arizona
ETI Etinde, Cameroon (inc. COP)
GAR Gardiner, E Greenland
GER Germany (inc. COP)
MAC Massif Central, France
MAL Chilwa, Malawi (inc. COP)
NKE E African Rift, N Kenya & E Uganda (inc. COP)
NUN Nunatak Zone, E Greenland
ORK Orkney
OTA Otago, New Zealand (inc. COP)
QUE Central Queensland, E Australia (inc. COP)
RCL Raton-Clayton, New Mexico (inc. COP)
SKE East African Rift, S Kenya (inc. COP)
TAN N Tanzania (inc. COP)
TAS Tasmania (inc. COP)
THA Chantaburi, Thailand (inc. COP)
TUG Tugtilik, E Greenland (inc. COP)
TVR Graz Basin, Austria (inc. COP)
ZIM Nuanetsi, Zimbabwe (inc. COP)

Continental Provinces (COK)
NSW New South Wales, E Australia
UGA Western Rift, Uganda

Hawaiian Islands). More rarely, highly undersaturated volcanics may dominate an entire volcanic complex (e.g. Moheli, Comores Islands). The rock type occurs in island groups where there is a clearly definable hot-spot trace (e.g. Hawaiian Islands), where an age progression is less evident (e.g. Cape Verde Islands), and where no age progression is apparent (e.g. Gulf of Guinea Islands).

Apart from the Hawaiian Islands and Cook-Austral Islands in the southern Pacific, all the islands where these rock types occur are constructed on oceanic crust of Jurassic to Cretaceous age, around the margins of ocean basins, and well away from the regions of high geothermal gradient closer to mid-ocean ridges where, presumably, the degree of melting is too high to produce highly undersaturated volcanic rocks. However, not all islands in these locations have erupted highly undersaturated magmas (e.g. Madeira Group) and only two islands lying in the isotopically anomalous DUPAL region of the southern hemisphere have produced feldspar-free volcanic rocks (Upolo, Samoan archipelago and Aitutaki, Cook Islands).

Most ocean island volcanic rocks which are classified as feldspar-free are olivine-bearing melanephelinite. Only on Oahu (Hawaiian Islands), the Canary Islands, and Cape Verde Islands are melilite-bearing rocks found. In the Cape Verde and Canary Island groups these are mainly olivine-poor melanephelinite and associated with older intrusive carbonatite complexes which are exceedingly rare in the oceanic environment.

2.2.1 Atlantic Ocean Islands

Feldspar-free volcanic rocks occur on a number of islands in the southern and central Atlantic Ocean. Trinidade (Baker, 1973) and Fernando de Noronha (Gerlach *et al.*, 1987) represent the youngest volcanism along volcanic chains which extend eastwards from the continental margin of South America and follow the lines of major fracture zones in the oceanic crust. Principe (Dunlop & Fitton, 1979; Fitton & Hughes, 1977) is situated off the west coast of Africa and is part of the "Cameroon line" volcanic chain which

extends from the Cameroon Highlands south-westwards into the Gulf of Guinea. There is no apparent age progression along the Cameroon line as a whole or within the oceanic sector of the chain. Etinde (Fitton & Hughes, 1981; Fitton, 1987; Nkoumbou *et al.*, 1995) is also part of this chain and is located on the coast of the Republic of Cameroon. Although underlain by attenuated continental lithosphere, it is appropriate to consider Etinde with Principe in the general context of Cameroon line volcanism since highly undersaturated volcanic rocks are not found elsewhere in the Cameroon line. Volcanism on Trinidade, Fernando de Noronha, and Principe could be related to the separation of Africa and South America which was initiated in the upper Cretaceous.

The Cape Verde Islands (Davies *et al.*, 1989) and the Canary Islands (Hoernle & Schmincke, 1993a; 1993b) lie off the west coast of northern Africa on oceanic crust of Jurassic to Cretaceous age. Early volcanism at these locations is probably associated with the opening of the Central Atlantic in the Jurassic but the islands are now situated on positive topographic anomalies on the sea floor which are thought to result from oceanic crustal thrusting and dynamic uplift of the lithosphere due to ascending thermal plumes in the upper mantle (Courtney & White, 1986). Plume activity is almost certainly involved in the re-establishment of volcanism at these locations in the Miocene and Pliocene but it has also been noted that the Canary Islands lie close to the edge of the continental shelf and have carbonatite intrusions similar in age to those in the Atlas Mountains. It has therefore been suggested that the Canary Islands might represent an extension of the structures formed in the Alpine orogenic episode that affected Europe and North Africa at that time (Woolley, 1989 and references therein). The carbonatite intrusions in the Cape Verde Islands are younger and cannot be related directly to these events. The Cape Verde Islands lie close to the pole of rotation of the African plate and the oceanic lithosphere has moved, relative to the fixed frame of reference provided by mantle plumes, only some 200 km north-eastwards in the past 50 to 60 m.y. There is no clear age progression in either island group although the south-western islands appear to be younger in both cases. Volcanism in both island groups may, therefore, be the consequence of a plume impinging on the base of a thickened and relatively slow-moving plate.

2.2.2 Indian Ocean Islands

Most of the volcanic islands in the Indian Ocean are only mildly alkaline but nephelinite and olivine melanephelinite occur in the Comores archipelago on the islands of Gran Comoro, Moheli, and Mayotte (Upton, 1982; Nougier *et al.*, 1986). The four principal islands of the Comores group form a NW-SE trending chain across the northern end of the Mozambique Channel between the coast of East Africa and northern Madagascar. Highly undersaturated lavas belonging to the same petrographic province as the Comores Islands also occur on Madagascar itself. There is an apparent decrease in age of the volcanism from SE to NW along the chain which has been attributed to the movement of the lithosphere in a direction ESE over a mantle plume which currently lies beneath Gran Comoro. However, volcanism appears to be a consequence of the separation of Madagascar from eastern Africa in the Jurassic. Geophysical evidence strongly suggests that Madagascar moved southwards from a position adjacent to southern Somalia, Kenya, and Tanzania, by transform motion along the Davie fracture zone. Relative motion between Madagascar and Africa appears to have ceased about 120 million years ago (Rabinowitz *et al.*, 1983).

Xenoliths from the volcanic rocks have been interpreted by Strong & Flower (1969) as evidence that the northern part of the Mozambique Channel is underlain by continental basement rocks. This conclusion is not supported by the magnetic anomaly patterns which indicate that the islands rise from ocean floor of Jurassic age. However, the Comores Islands, like the Canary Islands, may not be oceanic islands underlain by oceanic lithosphere despite their apparently oceanic environment.

2.2.3 Pacific Ocean Islands

Olivine melanephelinite and, more rarely, melilite melanephelinite occur in several island chains in the Pacific Ocean. In the Hawaiian Islands (central Pacific) and the

Caroline Islands (western Pacific), the age of the volcanism decreases eastwards along the island chains. These islands are widely accepted to be a consequence of a mantle plume impinging on the base of the north-westward moving Pacific plate. Feldspar-free volcanic rocks represent a post-erosional rejuvenation episode on Kauai (Maaløe *et al.*, 1992) and Oahu (Clague & Frey, 1982), in the Hawaiian chain, and on Truk, Ponape, and Kusaie, in the Carolines (Mattey, 1982). Increasing alkalinity of the lavas and the decrease in total erupted volume with time along the Carolines chain suggests that the strength of the plume decreased while the islands were being formed (Keating *et al.*, 1984). On the basis of sea-floor topography west of Truk, Bracy & Andrews (1974) have suggested that the Caroline ridge west of Truk may be part of a relict island arc.

The Cook-Austral Islands, in the southern Pacific, form a series of sub-parallel archipelagoes trending north-westwards from the volcanically active McDonald Seamount, in the south-east, to the Samoan Islands near the Tonga-Kermadec trench (Palacz & Saunders, 1986). These islands show no simple age progression from west to east and cannot, therefore, be related to the activity of a single plume. The islands of the Samoan group actually appear to be propagating to the west but this may be due to the long period of quiescence which follows the shield building phase. Voluminous post-erosional activity gives the older shield volcanoes in the west the appearance of youthful volcanoes although the shield-building activity may be getting younger to the east (Natland, 1980).

On Aitutaki, Cook Islands (Fodor *et al.*, 1982) and Upolo, Samoa (Wright & White, 1987) the sub-aerial highly undersaturated volcanism represents a post-erosional phase of activity similar to that found on other islands in the Pacific Ocean. However, Natland (1980) considers the near-simultaneous eruption of post-erosional lavas along 1500 km of the Samoan Island chain in Pleistocene to historic times to be a result of lateral bending of the Pacific plate at the point where the axis of the Tonga-Kermadec trench swings from an orientation almost due north-south to a line trending 70° west of north. Upolo currently lies at the point where lateral bending becomes significant while the

islands further west are moving along the line of the flexure as subduction of the Pacific plate beneath the Australian plate continues.

The Samoan and Cook Islands lie within the DUPAL isotopically anomalous region of the southern hemisphere and the feldspar-free volcanic rocks from these islands are the only known occurrence of this rock type among the islands in the DUPAL region. The DUPAL component in the OIB reservoir is generally accepted to be derived from an enriched mantle source, in this case the EMII domain of Zindler & Hart (1986).

2.2.4 Island Arc-related Volcanism

Most Cenozoic volcanic rocks in Japan belong to the calc-alkaline basalt-andesite-dacite-rhyolite series and are associated with island arc magmatism. However, alkaline rocks of Quaternary age occur in a small province situated on the north-eastern coast of the Sea of Japan and extending from south-western Honshu and northern Kyushu into North Korea and Manchuria. The volume of alkaline rocks is small but it includes isolated occurrences of olivine melanephelinite and melilite melanephelinite at Nagahama, south-west Honshu. Alkaline volcanism in the circum-Japan Sea belt may be related to the formation of the Japan Sea behind the active trench-arc system which began at the end of the Palaeogene (Minato *et al.*, 1965). The volcanic rocks retain an island arc chemical signature (Nb depletion) which appears to decrease in intensity southwards along the Japanese coast and disappear completely as distance from the active arc increases westwards into North Korea and Manchuria (Nakamura *et al.*, 1985).

The Tabar, Lihir, Tanga, and Feni groups of islands in the south-west Pacific form a chain lying roughly parallel to the coast of the Tertiary island arc system of New Ireland and about 50 km to the north-east (Wallace *et al.*, 1983). The islands are not associated directly with the island arc system, or a mantle plume trace, and the tectonic setting of the islands is still uncertain. Strongly undersaturated rocks occur in the Tanga and Feni groups but the only feldspar-free rocks are from Ambitle in the Feni group

(Johnson *et al.*, 1976). The trace-element chemistry of these samples is completely different from all other samples encountered in this study, being highly enriched in Rb, K, Pb and Sr, and depleted in all other incompatible elements, particularly Nb. Depletion in Nb is the only feature common to both the Ambitle samples and those from Nagahama.

2.3 Intraplate Continental Environments

Feldspar-free volcanic rocks in continental environments are almost invariably associated with extensional tectonic regimes. They are found, most commonly, within rift systems (e.g Eastern African Rift) and on the margins of ocean basins which almost certainly developed from continental rift systems (e.g. East Greenland, N Atlantic borderlands). However, they also occur in extensional marginal basins associated with collision zones (e.g. Pannonian Basin, Hungary), in provinces co-linear with lines of structural weakness which result from earlier orogenic episodes (e.g. Balcones, Texas), in regions of major transcurrent faulting (e.g. Thailand), and areas of rapid uplift (e.g. Colorado Plateau). Many major provinces involve more than one of these tectonic features (e.g. uplift and rifting in East Africa).

Ocean island nephelinite and melilitite rocks tend to be younger than their continental counterparts which range in age from Jurassic/Cretaceous to recent. Post-erosional highly undersaturated suites generally occur as late-stage volcanic products on islands which have been constructed on ocean floor which is Jurassic, or younger, in age. Continental provinces are not subject to this constraint. Furthermore, linear plume traces of the type seen in ocean basins are generally absent or at least equivocal in continental environments.

Continental volcanic provinces can be potassic, that is $K_2O > Na_2O$, (e.g. Western Rift, Uganda) or sodic (e.g. Eastern Rift, Kenya) in character and the highly undersaturated rocks retain the sodic or potassic nature of the more silica-saturated

varieties in the same provinces. Potassic rocks are considerably more common on the continents than in the ocean basins where they are restricted to the DUPAL regions of the southern hemisphere. Potassic character is thus thought to be a consequence of highly enriched sub-continental lithospheric mantle in the source region of these magmas. Sodic continental provinces, and most ocean island basalts, may be dominated by sources within the asthenosphere.

Many continental provinces lie in close proximity to destructive margins or in areas where the continental lithosphere may have been affected by earlier subduction processes (e.g. Eastern Australia; New Zealand; Thailand). Mantle sources may contribute a chemical signature inherited from the subduction episode (e.g. Nb depletion) to magmas erupted in these provinces either preferentially in small degrees of melting, or throughout the entire range of volcanic products (e.g. Raton-Clayton, New Mexico).

Highly undersaturated magmas can be erupted from fissures or central-vent volcanoes (e.g. Miocene province, East African Rift). Fissure eruptions generally produce olivine melanephelinite whereas central-vent volcanoes can erupt olivine-rich and olivine-poor melanephelinite, and melilitite, often within the same complex. Melilitite and olivine-poor melanephelinite are generally associated with carbonatite intrusive complexes in areas of domal uplift and rifting (e.g. Tanzania, East Afican Rift). Such complexes are almost totally absent from the oceanic environment.

2.3.1 Australasia

A number of examples of nephelinite volcanism associated with basalt and allied extrusive rocks of Mesozoic to Holocene age occur along the east coast of Australia from the Torres Strait to Tasmania (Knutson, 1989). A highly potassic Miocene suite forms a narrow band centred on New South Wales and some 200 km inland (Cundari, 1973). This volcanism appears to get younger to the south.

The cause of the volcanism is complex. Eastern Australia was close to the active margin of the Indo-Australian plate throughout the Mesozoic and the folded belts parallel to the continental margin may represent a series of collisions resulting from subduction of the Pacific plate beneath the continental margin. Compressional tectonics were followed by extensional events in the Cretaceous. The volcanism is thought to relate to spreading in marginal basins close to the eastern edge of the Indo-Austalian plate and to the opening of the ocean between Antarctica and Australia, and Antarctica and southern New Zealand. Volcanism has continued to the present day but the main eruptive pulse occurred at 55 to 30 Ma. Central-vent volcanic activity began at about 34 Ma and has progressed southwards to the present day. This type of volcanism is thought to be due to the presence of a mantle plume (Duncan & McDougall, 1989).

Volcanic rocks of a similar age and composition are also found in New Zealand on both islands. New Zealand straddles the tectonically active boundary between the Pacific plate and the Indo-Australian plate. Widespread Cenozoic volcanism is found on the South Island, and is almost entirely on the Pacific plate. Highly undersaturated volcanism is rare and associated only with short-lived monogenetic centres peripheral to the Dunedin volcano in the Otago Province (Coombs *et al.*, 1986).

2.3.2 South-East Asia

Upper Cenozoic alkaline volcanic rocks form an extensive igneous province in Thailand, Kampuchea, Laos, Vietnam, and Malaysia (Barr & MacDonald, 1981). The volcanic rocks have been erupted in an area of uplift, complex transcurrent faulting, and extensional tectonics (Wood, 1985; Whitford-Stark, 1983). They are thought to be related to the active subduction zones lying to the south-west, south, and east, and to the associated marginal basin development in the Andaman Sea to the south-west, and in the China Sea to the east. Major transcurrent faulting and basin development in south-east Asia appears to be a consequence of the collision between India and Eurasia but no consistent spatial relationship of basins and faults with volcanism has been documented. Similarly, no

pattern of volcanism with space or time has been established (Barr & James, 1990). Volcanic rocks are more voluminous in Vietnam, eastern Kampuchea, and southern Laos than elsewhere in the region and feldspar-free rocks occur only in south-eastern Thailand.

2.3.3 North America

Feldspar-free volcanic rocks are rare in North America. Nephelinitic rocks are found in the Cretaceous Balcones igneous province in Texas roughly co-linear with the buried Ouachita structural belt and slightly north of the Balcones fault zone. Igneous activity occurred some 150 m.y. after the deformation in the Ouachita belt and approximately 60 m.y. before the movement on the Balcones faults. Volcanism is not, therefore, related directly to either of these events but the location of the volcanism and intrusions may have been controlled by structural weaknesses resulting from the Ouachita orogenic episode in the early Mesozoic. According to Spencer (1969), the igneous activity took place in a shallow continental-shelf sea.

The Raton-Clayton volcanic field in New Mexico is part of an extensive late Cenozoic igneous province in the south-western United States. Feldspathoidal rocks occur as flows, plugs, and dykes (Phelps *et al.*, 1983). Intra-plate alkaline magmatism in this region followed the cessation of subduction of the Farallon plate beneath the western USA in the Mesozoic and early Cenozoic. Volcanism is related to uplift of the Colorado Plateau and surrounding area and to lithospheric extension and subsidence of the Basin and Range Province, which began in the late Miocene. The Raton-Clayton field lies to the east of the northern end of the Rio Grande rift and forms part of the transition zone around the Colorado Plateau (Fitton *et al.*, 1988; 1991).

Isolated occurrences of feldpar-free volcanic rocks are also found on the Colorado Plateau in Arizona and are related to the tectonic events described above. The Navajo volcanic field is scattered over a large area around the Four Corners (the junction of Arizona, New Mexico, Colorado and Utah). Most of the volcanic activity was explosive

and generally potassic in nature. The Navajo diatremes and dykes were emplaced in the Cenozoic towards the end of the subduction episode (Laughlin *et al.*, 1986). The Hopi Buttes lie to the south-west of the Navajo diatremes. These are often considered to be part of the same igneous province but the rocks are sodic in composition and were mostly erupted in the Pliocene. Volcanism was explosive and pyroclastic deposits and lava flows appear to have been erupted into shallow fresh water (Shoemaker *et al.*, 1962).

2.3.4 The North Atlantic Borderlands

The early Tertiary to Recent volcanism of eastern Greenland is thought to be associated with the opening of the North Atlantic. Attenuation of the Laurasian lithosphere reached a climax in the early Tertiary and was accompanied by intrusion of dykes and widespread fissure eruptions. The bulk of the activity took place in eastern Greenland between 54 and 52 Ma and was followed by the intrusion of sills and the development of central-vent volcanoes on major fault lines. Volcanism in the most intense areas of activity may not have ceased until around 30 Ma, long after sea-floor spreading had been initiated (Upton, 1988). Highly undersaturated alkaline rocks have been reported in the Gardiner ultramafic complex, at the western end of the Kangerdlugssuaq fjord in central east Greenland, and in the Tugtilik coastal dyke swarm to the south. Nephelinite flows cap nunataks to the north in Arnold Eschers Land and Hobbs Land.

Early Tertiary olivine melanephelinite rocks from Freeman's Cove on Bathurst Island, in the North West Territories of Canada, probably relate to the same episode (Mitchell & Platt, 1983; 1984). The volcanism appears to be controlled by major north-east and north trending faults.

2.3.5 Europe

Alkaline volcanic rocks of the late Tertiary to Quaternary magmatic province in western and central Europe are associated with an extensive rift system, which

developed in the early Cenozoic and evolved during the later stages of the Alpine orogeny. Magmatism was probably a response to the change in direction of convergence of Africa and Europe in the Neogene (Ziegler, 1982) and could be due to lithospheric flexure or to the development of a series of plumes in the upper mantle. However, the bulk of the volcanism occurs on horst blocks adjacent to the graben structures, or near to important structural boundaries in the lithosphere formed during the Hercynian orogeny 360 m.y. ago (Wilson and Downes, 1991).

Both sodic (Forez horst) and potassic (Cantal, Massif Central) types of highly undersaturated volcanism have occurred in France. In Germany sodic (often olivine-poor) melanephelinite is found on the flanks of the Rhine Graben and within the carbonatitic Kaiserstuhl complex at the southern end of the rift. Potassic olivine melanephelinite occurs in the Eifel region where it is associated with uplift of the Rhenish Massif at the northern end of the graben. In the North Hessian depression, and to the east in the Bohemian Massif (Czechoslovakia), the rocks are again sodic. The Pannonian Basin extends from eastern Austria across the Hungarian Plains to western Romania. Alkaline volcanism occurred in the northern part of the basin during the Pliocene and closely followed subduction-related calc-alkaline volcanism, of Eocene to Pliocene age (Embey-Isztin *et al.*, 1993). Feldspar-free volcanic rocks occur only at Stradner Kogel, in the Graz Basin, which lies on the west side of the Pannonian Basin in south-eastern Austria.

A suite of monchiquitic dykes in the Orkney Islands are Permian in age and are contemporaneous with the basaltic magmatism in south and central Scotland (Upton *et al.*, 1992). These are not part of the North Atlantic Thulean magmatic province or the European province associated with the Alpine orogeny but are included in this geographical section.

2.3.6 Eastern Africa

The abundance of highly undersaturated volcanic rocks associated with the East African rift system is well documented. The rift system is generally considered to be the failed arm of a triple junction centred on the southern end of the Red Sea and the Gulf of Aden. It extends some 3500 km from Afar south-westwards into Malawi and Mozambique and can be divided into two sectors: the eastern rift (Ethiopia, Kenya, and northern Tanzania) and the western rift (Uganda and southern Tanzania). The two branches pass either side of the Tanganyika craton and appear to join, in a broad area of normal faulting, in southern Tanzania and continue southwards through Malawi into Mozambique (King, 1970).

The Tertiary rift system overprints a number of older rift structures which were active in the Permo-Triassic and Jurassic, and which are almost certainly associated with the formation and subsequent fragmentation of Pangaea. It can be divided into a number of distinct zones which are thought to be a consequence of major transform faulting in at least two places. The rift axis could be offset by some 700 km between the northern end of the western rift in Uganda, and the southern end of the eastern rift, in northern Tanzania. Similarly, the Rukwa rift in southern Tanzania appears to be a broad zone of strike-slip faulting which offsets the southern end of the western rift from the Malawi rift (Rosendahl, 1987).

Tertiary rifting in eastern Africa was accompanied by major episodes of epeirogenic uplift and the formation of large elongate domes (ca. 1000 km across) in Ethiopia and Kenya (Baker *et al.*, 1972). Uplift is thought to have begun in the early Miocene, with the main pulse in the Pliocene-Pleistocene, but the timing of uplift is disputed. Uplift has, however, been accompanied by extensive volcanism of fissure and central-vent types but volcanism does not appear to be directly related to rifting since some sections of the rift system are devoid of volcanic rocks. Central-vent volcanoes have dominated the Quaternary activity in Kenya and northern Tanzania and two main

magmatic types have been identified: the carbonatite-nephelinite (olivine-poor) association and the basalt-nephelinite (olivine-rich) association (Le Bas, 1977; 1978a; 1978b; 1987; 1989).

Feldspar-free olivine melanephelinite, nephelinite, and melilite melanephelinite occur on the margins of the rift in a province stretching from Turkana to northern Tanzania. Volcanism appears to have begun in the eastern rift at about 30 Ma with explosive activity from the central-vent volcanoes on the Kenya-Uganda border (Baker *et al.*, 1971; King & Chapman, 1972). Some of these overlie a group of earlier carbonatitic intrusive complexes (King *et al.*, 1972) and are dominated by olivine-poor melanephelinite, but further to the north and in the Kavirondo trough to the south, both olivine-poor and olivine-rich melanephelinite are found. Volcanism to the east of the northern end of the rift is less strongly alkaline and is often associated with widespread fissure eruptions and monogenetic cones, but a number of nephelinite occurrences, of both types, are found on the shoulders of the Narok-Nguruman escarpment on the western side of the southern end of the Kenya rift system (Crossley, 1979).

In northern Tanzania the rift system is less distinct and more splayed out. A major phase of Tertiary rifting gave rise to a broad depression and was followed by the eruption of considerable volumes of basaltic and trachytic magmas from large shield volcanoes. This volcanism was separated, by a second phase of faulting, from upper Pleistocene to Recent explosive activity which produced more limited quantities of melanephelinite, phonolite, and carbonatite (Dawson, 1989). Olivine-poor nephelinite associated with phonolite and intrusive carbonatite is characteristic of the Quaternary shield volcanoes in the western part of the province, while the volcanoes further to the east are generally of mixed association having both olivine-poor and olivine-rich varieties.

The volcanic rocks of the western rift are strongly potassic. Feldspar-free varieties including olivine melilitite, olivine melanephelinite, leucite nephelinite, and ankaratrite occur in the northern part of this branch of the rift but the volcanic rocks

become less undersaturated further to the south. Carbonatite is not exposed but occurs as volcanic bombs in the pyroclastics at Katwe and in the Fort Portal area further to the north (Higazy, 1954; Bell & Powell, 1969).

The oldest (Early Cretaceous) volcanic rocks associated with the East African rift system occur in Malawi and Mozambique where nephelinite dykes and plugs occur with intrusive carbonatite complexes in the Chilwa province. Volcanicity post-dates Karoo magmatism but it is closely associated with uplift and rifting that may have been initiated in Karoo times (Woolley & Jones, 1987).

2.3.7 Southern Africa

Highly undersaturated volcanic rocks occur in two widely separated areas of southern Africa and in distinctly different associations. The Nuanetsi nephelinite flows, which are found at the base of the Karoo flood basalt sequence in south-eastern Zimbabwe, are related to the fragmentation of eastern Gondwanaland in the Jurassic (Bristow, 1984).

Melilitite and nephelinite intrusions of Late Cretaceous to Early Tertiary age (post-Karoo) are found in close association with clusters of kimberlite diatremes in a zone, about 400 km wide, parallel to the coast of South Africa and Namibia (Boctor & Yoder, 1986). The magmatism is restricted to Upper Palaeozoic mobile belts adjacent to cratonic areas in southern Africa. The intrusion of highly undersaturated magmas at these locations is believed to be related to the landward extension of transform faults associated with the opening of the South Atlantic in the Cretaceous or, alternatively, to be part of linear trends connecting recent oceanic volcanism in the South Atlantic with Cretaceous kimberlite activity in South Africa (Duncan *et al.*, 1978). The youngest rocks (olivine melilitite sometimes associated with phonolite) are found near the coast whereas farther inland (e.g. Sutherland Commonage and Bushmanland-Namaqualand) older olivine melilitite plugs occur with carbonatite intrusions and kimberlite pipes (Dawson *et al.*, 1985; Moore & Erlank, 1979).

2.4 Conclusion

Highly undersaturated volcanic rocks in continental regions occur in greater profusion, more diverse associations, and apparently more varied tectonic settings than their oceanic counterparts. Since the asthenospheric mantle beneath continents and oceans is likely to be broadly homogeneous in composition or, at least, similarly heterogeneous, the distinct possibility exists that contributions from enriched continental lithospheric mantle sources are responsible for the diversity and frequency observed. The extent and manifestation of this contribution may be a consequence of the age of the lithosphere, the thickness of the lithosphere, and movement of the lithosphere relative to the underlying asthenosphere.

Continental lithospheric sources are not available to ocean island volcanism except by processes which involve recycling continental lithospheric mantle into the asthenosphere where its effect may be diluted by melting of adjacent material. The following chapters attempt to identify possible source components of highly undersaturated magmas by exploring the effects of decreasing degree of partial melting and the environment involved.

Chapter 3

Major-Element Characteristics of Feldspar-Free Volcanic Rocks

3.1 Introduction

Partial melting of the Earth's upper mantle produces primary magmas which are basic to ultrabasic in composition in most tectonic environments. The major-element composition of primary magmas is determined by the mineral assemblage of the mantle source from which they are derived. Studies of the mineralogy and chemical composition of mantle xenoliths together with the results of melting experiments indicate that the source of most basic magmas is a four-phase lherzolite consisting of olivine, orthopyroxene, clinopyroxene, and an aluminous phase (garnet and/or spinel). Thus, while magmas with particular major-element characteristics may be associated with some tectonic regimes, major elements are not, in general, sensitive indicators of tectonic setting. However, the composition of primary magmas also depends on minor variations in source mineralogy, chemical characteristics of the source region, and the depth and degree of partial melting. All of these may vary markedly across the range of possible tectonic settings and environments in which magmas may be generated.

There is now little doubt that volatile components, H_2O and CO_2 for example, play an essential part in the generation of highly alkaline magmas (Chapter 1). There is also a growing body of evidence for a significant carbon component in the mantle which may be in the form of primary carbonate minerals (magnesite and dolomite) or CO_2-rich vapour. Current estimates of the concentration of carbon vary from 0.1 wt.% (McKenzie, 1985) to < 0.2 wt.% (Turner *et al.*, 1990). The effect of carbonate in mantle sources is to create a cusp on the solidus which produces an almost isobaric decrease in solidus temperature at ca. 70 km. This has the effect of lowering the carbonate-peridotite solidus

by ca. 200°C, relative to the dry-peridotite solidus, at depths > 70 km (Wyllie & Huang, 1975; Eggler, 1978; Olafsson & Eggler, 1983; Falloon & Green, 1989; 1990). Thus, the carbonate-peridotite solidus may be very close to typical mantle temperatures at depths corresponding to the asthenosphere-lithosphere boundary (Wyllie, 1987).

A small increase in the ambient mantle temperature may result in the production of a small quantity of near-solidus melt which has low viscosity and low density (Treiman & Schedl, 1983) and which will, therefore, readily segregate from the source region and percolate upwards (Richter & McKenzie, 1984; McKenzie, 1984). Initial melts produced in this way from carbonated peridotite are carbonate liquids[1] (Koster van Groos, 1975; Wendlandt & Eggler, 1980a, 1980b; Wallace & Green, 1988; Thibault *et al.*, 1992). These liquids are small in volume and will, therefore, maintain the ambient mantle temperature as they rise, solidifying again where the geotherm intersects the solidus. This may occur within the thermal boundary layer or within the mechanical boundary layer in regions of thicker (> 100 km) lithosphere. If the temperature of the carbonate liquid during ascent is somewhat higher than that of the geotherm (as might be the case if ascent is rapid) then the carbonate liquid may rise to shallower mantle levels, solidifying and decarbonating where the temperature path intersects the solidus cusp at ca. 70 - 80 km. Carbonate minerals are not stable at depths less than ca. 70 km but carbon is present in the shallow mantle as CO_2 vapour. A carbonate liquid which rises very rapidly may reach the surface as primary carbonatite. However, given the physical properties of carbonate liquids (Treiman & Schedl, 1983) and the thermal regime in which they are likely to be generated, this is thought to be the least likely destination for mantle-derived carbonate melt. Most carbonatite is, in fact, believed to be produced by the immiscible separation of carbonatitic liquids from carbonated silicate liquids at low pressure.

Solidification of carbonate liquid, decarbonation reactions, and the upward passage of CO_2-rich fluids may cause extensive modal (Wyllie & Rutter, 1986; Wilshire, 1987; Meen, 1987; Meen *et al.*, 1989) and cryptic (Dawson, 1984) metasomatism of the

[1] Throughout this work , the term "liquid" is used to mean melt. The term "fluid" is used specifically to refer to fluids other than melts.

lithosphere. Metasomatic enrichment by fugitive H_2O-rich fluids and CO_2-rich fluids produced in decarbonation reactions may also be responsible for the formation of K-rich phases (amphibole and/or phlogopite) in mantle sources. The continental lithosphere and, possibly, old oceanic lithosphere are the most likely mantle regions where enriched material may be created and preserved. Feldspar-free volcanic rocks are associated almost exclusively with intraplate volcanic activity (Chapter 2) but occur in both oceanic (ocean island) and continental (mainly rift) intraplate environments. In oceanic environments highly undersaturated rocks are restricted to areas where the oceanic lithosphere is old (Chapter 2) but there may, nevertheless, be significant compositional differences between highly undersaturated magmas derived from sub-oceanic asthenosphere and lithosphere and those from sub-continental asthenospheric and lithospheric sources because the continental lithosphere is even older. These differences appear to be particularly significant in considering the origins of the highly potassic magmas erupted in some intraplate continental provinces (Chapter 1).

It would appear that carbonate liquids, formed as a result of small thermal perturbations in the mantle, either solidify in the thermal or mechanical boundary layers or rise and decarbonate causing metasomatism of the shallower mantle. However, if the mantle decompresses through the solidus for carbonated peridotite, silicate melting should occur. In this case, initial carbonate liquids may be incorporated into the silicate liquids and erupted. It is possible that highly undersaturated magmas, and possibly all alkaline magmas, represent silicate liquids which have had a carbonate liquid precursor. Most intraplate magmatism has been attributed to the presence of mantle plumes or "hotspots". In this scenario, only a relatively small volume of mantle around the core of the plume might be above the dry-peridotite solidus temperature, whereas a much larger volume, possibly an order of magnitude larger (Watson & McKenzie, 1991), of surrounding mantle will be above the temperature of the carbonated peridotite solidus. Thus, although the actual volume of initial carbonate liquid produced might be small compared with the volume of silicate melt, a much larger volume of mantle is involved in the melting process. Carbonate liquids, therefore, have the opportunity to become significantly enriched in

elements which partition strongly into them. This process is enhanced by high diffusion rates (Minarik & Watson, 1991) which enable carbonate liquids to scavenge incompatible elements from the grain boundaries of mantle minerals. Mixing of carbonate and silicate liquids will produce a magma in which the elements which partition strongly into carbonate liquids might dominate the composition of the mixture at small total melt fractions. The influence of the carbonate will, however, decline rapidly as melting proceeds.

Many feldspar-free volcanic rocks have high MgO/(MgO+FeO) and contain peridotite xenoliths. They are also strikingly enriched in elements which are incompatible in major mantle phases (Chapter 1). These rocks may, therefore, be representative of primary melts or be very close to primary melt compositions. They may also be the products of the smallest degrees of mantle melting of normal mantle sources or melting of sources which have experienced modal and cryptic metasomatism by carbonate liquids or H_2O- and CO_2-rich fluids. At very small degrees of partial melting only minor mantle phases will be consumed during the melting process and highly undersaturated volcanic rocks such as nephelinite and melilitite should, therefore, contain information about mantle mineralogy and source characteristics immediately before melting begins. In particular, if carbonate plays a significant part in the generation of highly undersaturated magmas in both continental and oceanic environments then evidence for the involvement of this component should be found in the major-element composition of those elements which are strongly partitioned into carbonate liquids.

3.2 Major-Element Data Tables

The feldspar-free volcanic rocks selected for this study numbered 488 in all. Major-element data for these samples appear in Appendix C. The tables of Appendix C contain analyses of oceanic island nephelinite (174 samples), continental nephelinite (215 samples), potassic continental kamafugite and leucitite (59 samples), and olivine-poor

nephelinite (40 samples) as described in Chapter 1. The OIB data base referred to in Chapter 1 comprises 904 analyses also obtained during the course of this work. The OIB analyses are not presented here individually but appear in summary tables (e.g. Table 3-1 and Appendix Table E-5) as an average OIB composition.

Table 3-1 Summary Table of Averages

	SiO_2	Al_2O_3	Fe_2O_3	MgO	CaO	Na_2O	K_2O	TiO_2	MnO	P_2O_5
Ocean Island Basalts										
OIB (average of 904 analyses)	44.87	13.48	13.06	9.01	10.56	2.97	1.18	2.94	0.18	0.61
(average of 39 islands)	44.84	13.42	13.07	8.94	10.35	2.97	1.24	3.09	0.18	0.67
Ocean Island Nephelinites										
OIN (average of 169 analyses)	39.81	10.56	14.25	13.25	12.50	2.89	1.06	3.08	0.20	0.78
(average of 13 islands)	39.39	10.86	13.98	12.72	12.30	3.19	1.35	3.33	0.20	0.95
Continental Nephelinites										
CON (average of 215 analyses)	39.93	11.13	13.18	10.01	13.13	3.41	1.83	3.10	0.23	1.02
(average of 37 groups)	39.87	10.91	13.07	10.92	12.79	3.39	1.84	3.03	0.22	1.04
Potassic Continental Rocks										
Western Rift (average of 53 analyses)	40.20	8.85	12.62	11.77	12.57	2.02	4.18	4.33	0.20	0.80
New South Wales (av. of 6 analyses)	44.93	9.17	11.28	10.77	8.17	1.90	6.01	4.64	0.15	0.96
Olivine-poor Nephelinites										
COP (average of 89 analyses)	42.64	14.85	10.95	4.60	10.38	6.39	3.01	2.28	0.27	0.98
(average of 25 groups)	42.11	14.49	11.52	5.12	10.25	6.27	2.88	2.33	0.27	1.00

Average compositions of ocean island nephelinite (OIN), continental nephelinite (CON), potassic continental rocks from the Western Rift (Uganda) and New South Wales (SE Australia), and olivine-poor continental nephelinite are given in Appendix Tables E-1 to E-4, respectively. Each of these tables gives averages by island, volcanic complex, or province, as appropriate, and an overall average for the subset of data. Table E-5 of Appendix E similarly presents averages for all the islands represented in the OIB data base. A summary of Appendix Tables E-1 to E-5 is given above in Table 3-1.

3.3 Preliminary Comparison of Major-Element Data

The statistics presented in Table 3-1 indicate that, compared with OIB, average OIN is significantly lower in SiO_2 and Al_2O_3, and higher in MgO, CaO, and the incompatible elements TiO_2 and P_2O_5. A surprising feature is that OIN and OIB have similar average K_2O. Potassium is incompatible in typical mantle phases and would be expected to behave in the same way as the other incompatible elements. LILE are low field-strength elements (LFSE) and are, therefore, mobile in secondary alteration processes. OIN may thus have lost potassium as a consequence of alteration but it is difficult to envisage how OIN could be more susceptable to potassium loss by this mechanism than OIB in general. The apparently low levels of K_2O in OIN may, therefore, indicate the existence of residual potassic phases in the mantle source at very small degrees of partial melting. The problem of LILE mobility will be addressed in more detail in Chapter 4.

The differences between OIB and OIN may be explained in general terms by consideration of polybaric partial melting of a four-phase mantle lherzolite assemblage in the CaO-MgO-Al_2O_3-SiO_2 (CMAS) quaternary system (O'Hara, 1968). Within this system it is possible to predict that initial partial melts become less siliceous and more magnesian with increasing pressure and as the coexisting mineral assemblage changes from spinel lherzolite to garnet lherzolite with increasing depth. OIN may simply originate from deeper levels in the mantle than OIB in general and the low concentrations of Al_2O_3 in OIN may be a consequence of residual aluminous phases (garnet and/or spinel) at smaller degrees of partial melting than OIB. Incompatible elements such as TiO_2 and P_2O_5 will become concentrated in melt fractions which are smaller than those of average OIB.

Continental nephelinites (CON) are, on average, similar to OIN but are somewhat lower in MgO and higher in Al_2O_3, CaO, K_2O, TiO_2, and P_2O_5 than OIN. These tendencies are rather more extreme in olivine-poor continental nephelinites. However, olivine-poor nephelinites have lower average CaO and higher SiO_2 than continental

nephelinites in general. It is possible, therefore, that olivine-poor continental nephelinites, in particular, and continental nephelinites, in general, have all lost olivine and augite by crystal fractionation during ascent and/or high-level magma storage and that this process is more common in continental than oceanic environments due to the possibility of basic magmas being trapped in low density continental crust.

Potassic continental rocks, in addition to having higher concentrations of K_2O than OIN and CON, are notably more SiO_2-, TiO_2-, and P_2O_5-rich, and Al_2O_3-poor. These differences are not easy to interpret within the simple model involving polybaric melting, small melt fractions, and crystal fractionation discussed so far. While OIN and many continental feldspar-free volcanic rock compositions may be related by such simple mechanisms to the magmas generally derived from the OIB source, it appears that continental potassic rocks originate by partial melting of a source not generally available in ocean basins or most continental environments and which has significantly different chemical characteristics and mineralogy.

3.4 Correction for Crystal Fractionation Processes

Since crystal fractionation appears to have been an important differentiation process modifying magma compositions in continental regions, it is more meaningful to compare major-element chemistry after this component of variation has been removed.

Samples with high concentrations of MgO may be assumed to be very close to primary magma compositions and thus to have lost only olivine by fractional crystallization processes. Samples with MgO > 10 wt.% in the OIB data base, and in both oceanic and continental data sets, were corrected for crystal fractionation by incremental addition of olivine until the magma composition was calculated to be in equilibrium with typical mantle olivine. The details of the method appear in Appendix D and are described by Fitton & James (1986). The composition of mantle olivine for these calculations was

taken to be Fo_{90} (Boyd, 1987) and the distribution (K_D) of Fe^{2+} and Mg between olivine and melt to be 0.3 (Roeder & Emslie, 1970). The primary magma compositions calculated in this way are presented in Appendix D. The tables of Appendix D contain data for oceanic nephelinite (148 samples), continental nephelinite (82 samples), and potassic continental rocks (26 samples). None of the olivine-poor continental nephelinites had MgO > 10 wt.%. These rocks could not be considered close representatives of primary magmas and may have been subjected to extensive crystallization of both olivine and augite before eruption. They were not, therefore, included in the primary magma calculations.

Using the criterion of MgO > 10 wt.% to select suitable compositions it was possible to correct 85% of the OIN analyses but only 40% of the continental nephelinite and potassic continental rock analyses. These percentages are consistent with the suggestion already made that lower average MgO concentrations in continental nephelinites may be due to crystal fractionation processes. A summary table of averages for calculated primary magmas appears as Table 3-2. Again an average primary OIB composition is given for comparison.

3.5 Preliminary Comparison of Calculated Primary Magma Compositions

The averages presented in Table 3-2 indicate that primary OIN is more SiO_2- and Al_2O_3-poor than primary OIB but requires the same amount of olivine (ca. 12.4%) addition to bring the average composition back to equilibrium with mantle olivine (Fo_{90}). Continental nephelinites and potassic continental rocks, however, require only ca. 8% added olivine. Continental magmas are likely to be subjected to at least as much crystal fractionation as oceanic magmas as, in general, they traverse greater thicknesses of lithosphere on their way to the surface. The average continental feldspar-free magma composition, therefore, would also be expected to require olivine addition of ca. 12%.

Table 3-2 Summary Table of Averages (Calculated Primary Magmas)

	%Ol added	%Fo	SiO_2	Al_2O_3	Fe_2O_3	FeO	MgO	CaO	Na_2O	K_2O	TiO_2	MnO	P_2O_5
Ocean Island Basalts													
OIB (average of 328 analyses)	12.44	90.02	42.68	10.29	1.43	10.73	16.28	10.12	2.32	0.87	2.49	0.17	0.56
St Dev	7.05		2.53	1.06	0.09	0.80	1.20	1.69	0.62	0.38	0.55	0.02	0.27
Ocean Island Nephelinites													
OIN (average of 148 analyses)	12.35	90.02	39.80	9.36	1.51	11.28	17.11	11.30	2.57	0.92	2.77	0.18	0.70
St Dev	7.13		1.46	0.69	0.08	0.82	1.23	1.65	0.61	0.38	0.51	0.01	0.24
Continental Nephelinites													
CON (average of 82 analyses)	8.28	90.06	39.32	8.79	1.48	10.67	16.27	12.15	2.59	1.40	3.00	0.19	0.87
St Dev	7.86		2.57	2.35	0.21	1.48	2.23	1.94	0.84	0.64	1.29	0.02	0.44
CON (average of 82 analyses)	12.30	90.71	39.38	8.49	1.43	10.61	17.44	11.73	2.50	1.35	2.89	0.18	0.84
St Dev	8.75		2.48	2.30	0.20	1.41	2.32	1.93	0.81	0.62	1.23	0.02	0.42
Potassic Continental Rocks													
New South Wales (average of 5 analyses)	7.92	90.01	44.60	8.21	1.26	9.20	13.96	7.53	1.90	5.32	4.35	0.14	0.92
St Dev	1.88		1.15	0.49	0.05	0.40	0.60	0.41	0.49	0.53	0.25	0.01	0.18
New South Wales (average of 5 analyses)	11.60	90.71	44.48	7.94	1.22	9.21	15.13	7.28	1.84	5.15	4.21	0.13	0.89
St Dev	2.07		1.12	0.48	0.05	0.39	0.64	0.38	0.47	0.52	0.24	0.01	0.17
Western Rift (average of 21 analyses)	8.87	90.03	39.57	7.49	1.38	10.08	15.32	12.80	1.49	3.43	3.91	0.18	0.74
St Dev	7.50		3.62	2.04	0.07	0.80	1.17	2.53	0.65	1.50	0.91	0.02	0.31
Western Rift (average of 21 analyses)	12.87	90.71	39.62	7.28	1.33	10.06	16.52	12.35	1.44	3.32	3.77	0.18	0.71
St Dev	8.21		3.49	1.98	0.06	0.77	1.26	2.43	0.62	1.47	0.89	0.02	0.30

A larger addition of olivine may be achieved in primary magma calculations if the equilibrium olivine composition for continental magmas has a higher forsterite content. Peridotite xenoliths have been shown by Boyd (1987) to fall into two groups: a low-temperature group where Fo > 91.5 and a high-temperature group with Fo < 91.5. The low-temperature group is associated with continental cratonic regions where the lithosphere may have become depleted in basaltic components by the removal of komatiitic liquids in the Archaean, whereas the high-temperature group is restricted to circum-cratonic and oceanic environments. The equilibrium olivine composition for continental feldspar-free volcanic rocks may thus be higher than Fo_{90} and it was found, by trial and error, that calculating primary compositions for the continental rocks using $Fo_{90.7}$ as the equilibrium olivine composition returned a similar amount of olivine to the average magma composition as was calculated for OIB and OIN using Fo_{90}.

Average major-element compositions for continental nephelinites and potassic continental kamafugites and leucitites calculated back to mantle olivine at $Fo_{90.7}$ are also given in Table 3-2 for comparison with the compositions which would be in equilibrium with Fo_{90}. The forsterite content used in the average primary magma calculation for continental rocks can be taken as the likely lower limit of the olivine composition. The actual average forsterite content may be significantly higher but performing the calculations with higher values is an *ad hoc* process which cannot be constrained by any independent criterion in this case. This approach has not, therefore, been pursued.

Figures 3-1 and 3-2 illustrate the levels of enrichment and depletion of primary OIN, CON, Western Rift kamafugites, and the New South Wales leucitites, over average primary OIB. The general profile of OIN (Fig. 3-1a), together with the unexpectedly small enrichment of K_2O by comparison with other incompatible elements, has already been noted (Section 3.3). Small amounts of H_2O in the mantle could result in the stabilization of amphibole, at the expense of clinopyroxene, without changing the concentration of potassium in the source (i.e $^{K}C_0$ = constant). A small amount of amphibole would, however, cause a significant increase in the bulk D value for K as potassium is normally

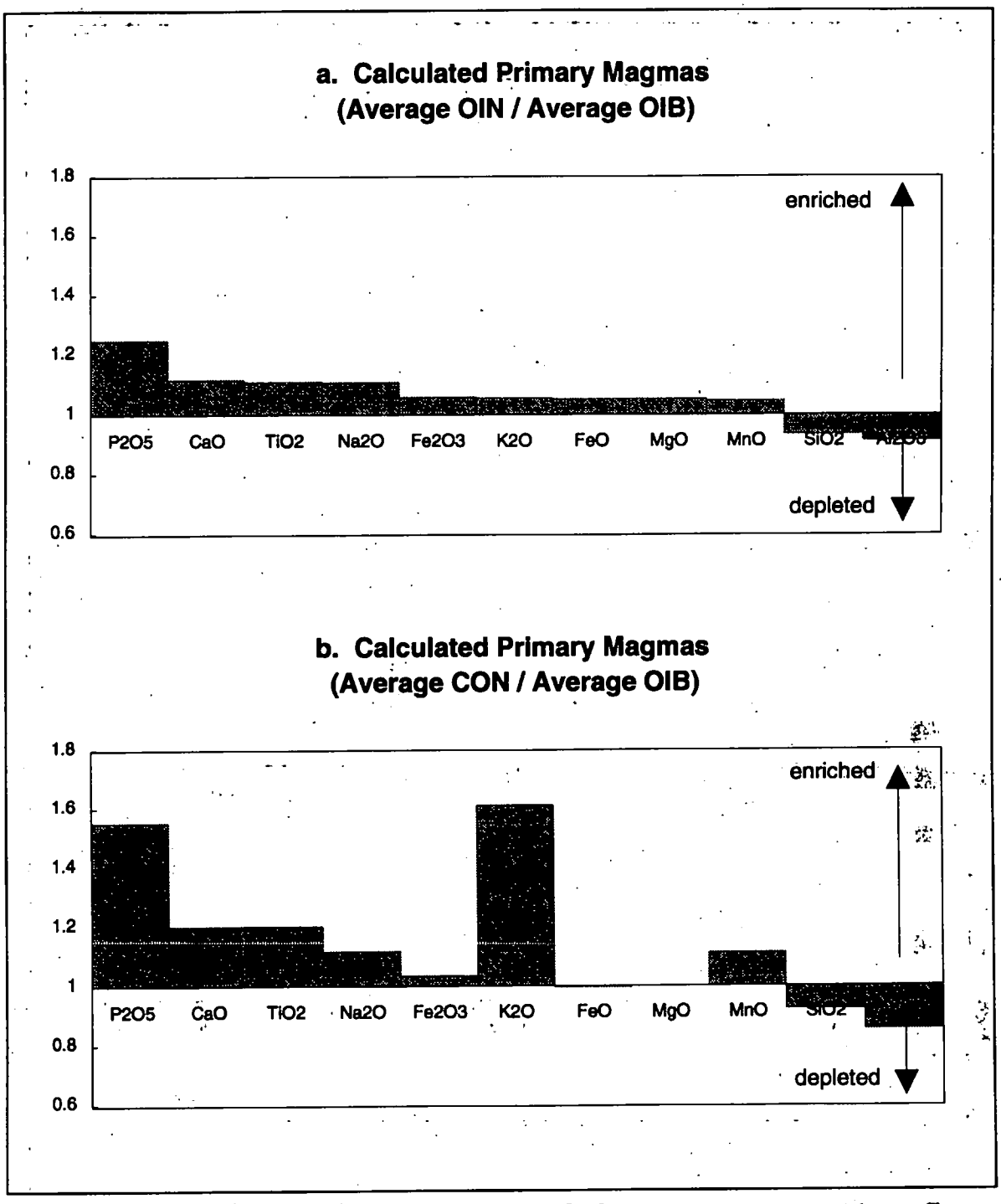

Figure 3-1. Enrichment/depletion in major elements compared with average primary OIB for
a. average primary ocean island nephelinites (OIN)
b. average primary continental nephelinites (CON)
Primary magma compositions calculated using $K_D = 0.30$ for the distribution of Fe^{2+} and Mg between olivine and coexisting silicate melt and an equilibrium forsterite content of Fo_{90}.

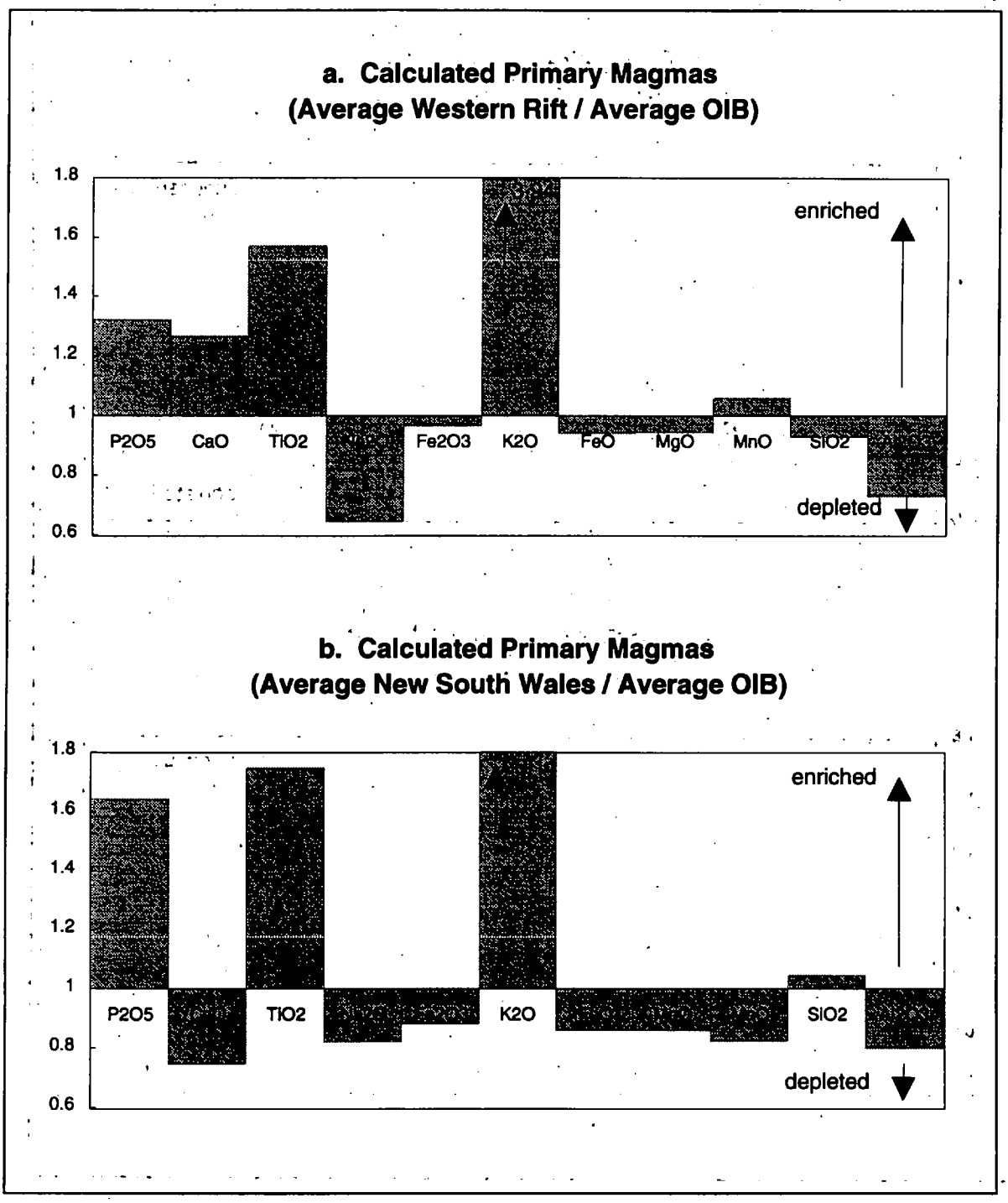

Figure 3-2. Enrichment/depletion in major elements compared with average primary OIB for
a. average primary potassic magmas from the Western Rift, Uganda
b. average primary potassic magmas from New South Wales, SE Australia
Primary magma compositions calculated using $K_D = 0.30$ for the distribution of Fe^{2+} and Mg between olivine and coexisting silicate melt and an equilibrium forsterite content of Fo_{91}.

highly incompatible in anhydrous mantle phases ($^{Bulk}D_K \cong 10^{-3}$ in normal mantle). For example, if the mantle contains 2% clinopyroxene and this is all converted to amphibole then $^{Bulk}D_K$ (where $^{amph}D_K = 1.2$) would increase by an order of magnitude. At small degrees of partial melting (e.g. $F \cong 0.001$) an order of magnitude increase in $^{Bulk}D_K$ would lead to a *decrease* of the same order in the concentration (C_L) in the liquid (where C_L is given by $C_L/C_0 = 1/(D + F - DF)$. The partition coefficient of titanium in amphibole is approximately the same as that of potassium ($^{amph}D_{Ti} = 1.5$). However, Ti is not as incompatible as K in other mantle phases and so $^{Bulk}D_{Ti}$ is less affected than $^{Bulk}D_K$ by the stabilization of amphibole. For example, C_L decreases by a factor of only ca. 1.5 by the stabilization of 2% amphibole in the OIN source.

OIN (Fig. 3-1a) and CON (Fig. 3-1b) have broadly similar patterns but CON are more strikingly enriched in CaO, MnO, and the incompatible elements (P_2O_5, K_2O and, to a lesser extent, TiO_2) than OIN. In Section 3.3 it was proposed that OIN may be the products of smaller degrees of partial melting from deeper sources than OIB in general, where garnet and, possibly, a K-rich mineral which is rapidly consumed over a small temperature interval close to the solidus, are residual mantle phases. Continental nephelinites may, therefore, represent even smaller degrees of partial melting than OIN. These may be derived from a similar source mineralogy but, to account for the higher average level of potassium, some continental sources must contain more potassium than the OIN source. This implies the involvement of metasomatically enriched mantle where high potassium may be a characteristic resulting from cryptic or modal metsomatism of the source. In this case, $^KC_0$ is higher than in the OIN source. Amphibole and phlogopite have been proposed as the most likely K-rich mantle phases as these minerals are frequently found in mantle-derived xenoliths in continental regions.

Potassic continental rocks have noticeably different patterns from OIN and CON, and from each other. The Western Rift (Fig. 3-2a) is highly enriched in TiO_2 and K_2O but depleted in Na_2O relative to OIB. New South Wales (Fig. 3-2b) has a similar pattern but is depleted in CaO and MnO, and enriched in SiO_2. This is the only data group

which exhibits this type of enrichment-depletion pattern. Following from the discussion above, the highly potassic rocks found in the Western Rift and New South Wales must also be derived from enriched sources containing amphibole and/or phlogopite.

Mantle sources in which a small amount of amphibole has been stabilized by hydration of clinopyroxene will produce liquids where K_2O/Na_2O is determined by the ratio of the D values of these elements in amphibole. ${}^{amph}D_K \cong {}^{amph}D_{Na}$ and Na tends to be buffered by other mantle phases. A low average K_2O/Na_2O, as observed in OIN and most CON, would suggest that the potassic phase is, therefore, predominantly amphibole. Mantle sources in which phlogopite is the predominant potassic phase have been enriched by metasomatising fluids with high K_2O/Na_2O. Melting phlogopite lherzolite generates magmas with high K_2O/Na_2O. In both the Western Rift and New South Wales K_2O/Na_2O is so high that the presence of phlogopite is indicated (Wilkinson & Le Maitre, 1987). The high concentrations of titanium in both the Western Rift and New South Wales samples suggests that the mantle sources of these magmas are also enriched in titanium. Studies of amphibole and mica in metasomatised spinel lherzolite xenoliths (e.g. Stolz & Davies, 1988) indicate that titanium concentrations in these minerals can be extremely variable. The source regions of potassic continental magmas may therefore contain Ti-rich amphibole (kaersutite) and mica introduced as a result of extensive metasomatism of the mantle by K- and Ti-rich fluids.

The presence of hydrous minerals, such as phlogopite and amphibole, and CO_2-rich fluid inclusions in olivine and pyroxene crystals in many mantle-derived xenoliths suggests that decarbonation reactions and CO_2- and H_2O-rich fluids may be important agents in metasomatic alteration of normal mantle minerals. The most soluble major elements in H_2O-rich fluids seem to be Si, Al, and K (Odling & Randle, 1992). Major elements, however, have a very low solubility in CO_2-rich fluids (Meen *et al.*, 1989; Fielding, 1992). Thus, while H_2O-rich fluids could be significant in the generation of some continental potassic magmas, CO_2-rich fluids (not to be confused with carbonate melts) will probably have little effect on major-element compositions.

Modally or cryptically metasomatised lithospheric sources have been considered, by many workers, to be essential to the production of highly undersaturated continental magmas in order to account for the high concentrations of incompatible elements, but it is not clear how this kind of enrichment process can influence the composition of oceanic magmas. If, however, carbonate liquids can become incorporated into more voluminous silicate melts, as described in Section 3.1, magmas may become preferentially enriched in elements which partition strongly into carbonate liquids. A detailed study of element partitioning between carbonate and silicate liquids has recently been completed by Fielding (1992). Fielding's experimental data (Table 3-3) are presented below for reference. On the basis of these data, if carbonate liquids are involved, strong enrichments in CaO and P_2O_5, coupled with depletion in SiO_2, TiO_2, and Al_2O_3, would be expected. Major elements which partition less strongly into carbonate liquids, Mg and Mn for example, might also be enriched in carbonate-silicate liquids but the effect will be less well marked.

Table 3-3 **Partitioning between carbonate (Lc) and silicate (Ls) liquids under mantle conditions (data from Fielding, 1992)**

Element (i)	Ls/Lc_{D_i}	Element (i)	Ls/Lc_{D_i}
Na	2	Si	10
K	1.5	Ti	5
Rb	1	Zr	10
Cs	0.8	Hf	18
Mg	0.5	P	0.2
Ca	0.15	V	1
Sr	0.1	Nb	1.2
Ba	<0.1	Ta	3
Mn	0.6		
Fe	1	Pb	0.5
		Th	8
Al	50	U	2
Y	0.8		
La	0.2	Mo	0.2
Ce	0.25		
Nd	0.3		
Sm	0.35		

This preliminary study of the characteristic enrichment-depletion patterns for primary magma compositions suggests that oceanic nephelinites and most continental feldspar-free volcanic rocks may be generated from similar sources but that element partitioning in carbonate liquids together with the effect of potassic phases in the mantle source, which may be residual in the melting process or rapidly consumed in the early stages of partial melting, may be responsible for much of the major-element variation observed.

The composition of OIN is uncomplicated by the possibility of direct involvement of continental lithosphere in the mantle source region. A more detailed study of OIN should, therefore, make it possible to identify the source mineralogy and characteristics, and the mantle processes which may be common to the generation of highly undersaturated nephelinitic magmas wherever they occur.

3.6 Major-Element Composition of Primary Ocean Island Nephelinites

From consideration of data averages, it was proposed in Section 3.3 that OIN are smaller degrees of partial melting which may be generated from deeper mantle sources than OIB in general and that garnet may be residual in the melting process. Figure 3-3a shows a general inverse correlation between SiO_2 and MgO for primary OIB and OIN which would support this simple model. The OIN data set is not a co-magmatic suite and it is clear from Figure 3-3a that there is considerable variation in OIN which makes it impossible to progress further by considering OIN as a whole. For this reason, the largest sub-group of primary OIN (78 samples of nephelinite and melilitite from Kauai) was examined in detail.

A similar negative correlation exists between SiO_2 and MgO in the Kauai data (Fig. 3-3b) but a small number of samples seem to have low SiO_2 and lie below the trend formed by the majority of the Kauai samples. The data have, therefore, been divided

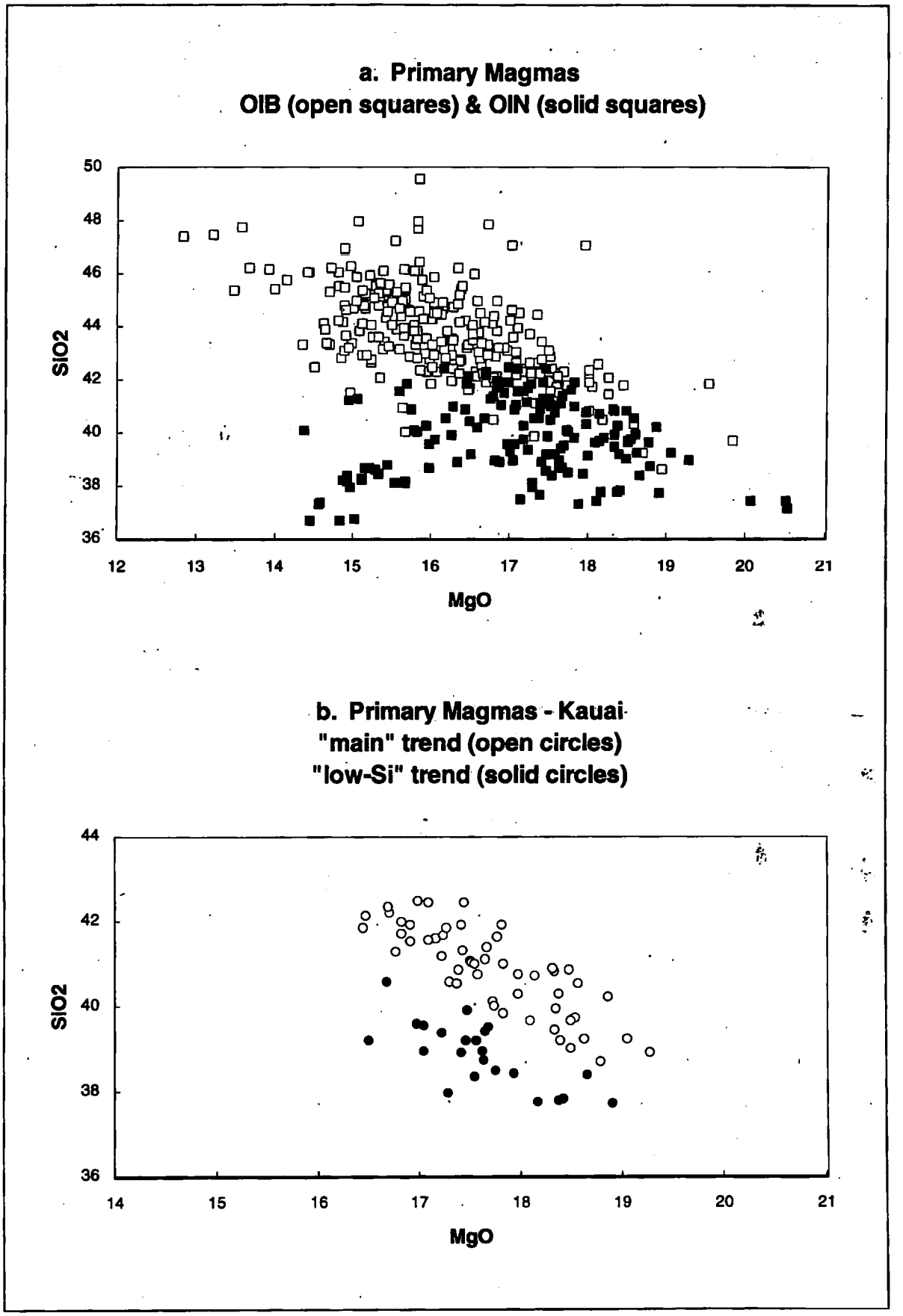

Figure 3-3. SiO_2 *versus* MgO for calculated primary magma compositions. Primary magma compositions calculated as in Figure 3-1. The terms "main" trend and "low-Si" trend have been chosen to describe SiO_2/MgO variation. The division between the trends is arbitrary.

arbitrarily into two groups for plotting purposes (a "main" group and a "low-Si" group) such that they form two parallel trends on Figure 3-3b. The division into these two groups is preserved in plots of MgO *versus* Al_2O_3 (Fig. 3-4a), CaO (Fig. 3-4b), TiO_2 (Fig. 3-4c), and P_2O_5 (Fig. 3-4d). It is not easy to account for the apparent existence of two trends in Figure 3-3b with any model involving small degrees of partial melting and residual aluminous phases by reference to the CMAS system. However, the "low-Si" trend of Figure 3-3b can be made colinear with the "main" trend if the primary compositions indicated by the solid symbols on Figure 3-3b are either recalculated to a higher equilibrium forsterite content, or a higher coefficient for the distribution of Fe^{2+} and Mg between olivine and coexisting melt is used in the calculations. Both possibilities have the effect of increasing the MgO concentration and reducing the SiO_2 concentration of the compositions represented by the solid symbols such that these points would then fall towards the bottom right-hand end of the "main" trend shown on Figure 3-3b. A higher forsterite content implies a more depleted source. Conventional wisdom places depleted sources (e.g. the MORB source) at shallower mantle depths than enriched sources (O'Nions, 1987). A more depleted source for the rocks of the "low-Si" trend is unlikely, therefore, to be consistent with a deeper origin for these samples.

The distribution (K_D) of Fe^{2+} and Mg between olivine ($_{ol}$) and silicate melt ($_{Ls}$) is defined by $K_D = [Fe^{2+}/Mg]_{ol}/[Fe^{2+}/Mg]_{Ls}$. In order to achieve a higher K_D the ratio $[Fe^{2+}/Mg]_{Ls}$ must be reduced at constant olivine composition. This may result from the addition of a liquid component to the melt which has a lower $[Fe^{2+}/Mg]$ than $[Fe^{2+}/Mg]_{Ls}$. A $K_D > 0.3$ would be appropriate for the addition of carbonate liquid ($_{Lc}$) to a silicate melt ($_{Ls}$) since $[Fe^{2+}/Mg]_{Lc} < [Fe^{2+}/Mg]_{Ls}$ because Mg partitions more strongly into carbonate liquid than silicate liquid whereas Fe^{2+} partitions equally (Fielding, 1992).

The results of using Fo_{90} and $K_D = 0.33$ for the compositions represented by the solid symbols are shown for MgO *versus* SiO_2 (Fig. 3-5a), Al_2O_3 (Fig. 3-5b), CaO (Fig. 3-5c), TiO_2 (Fig. 3-5d), and P_2O_5 (Fig. 3-5e). Fielding's (1992) partition coefficients indicate that carbonate liquids are strongly enriched in Ca ($^{Ls/Lc}D_{Ca} = 0.15$) and P ($^{Ls/Lc}D_P = 0.2$).

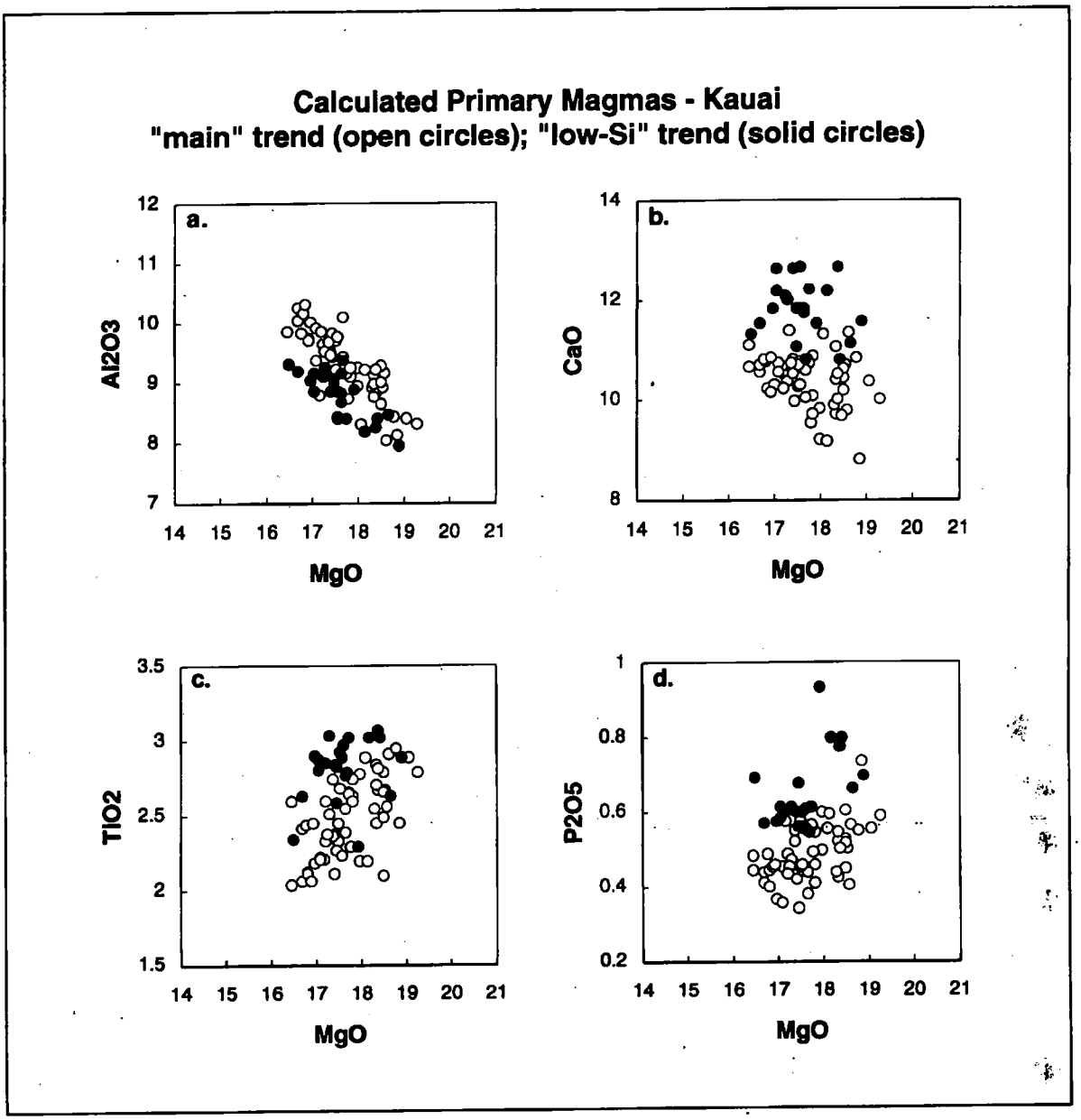

Figure 3-4. Kauai calculated primary magma compositions.
Primary magma compositions calculated as in Figure 3-1.
The terms "main" trend and "low-Si" trend are defined in Figure 3-3.

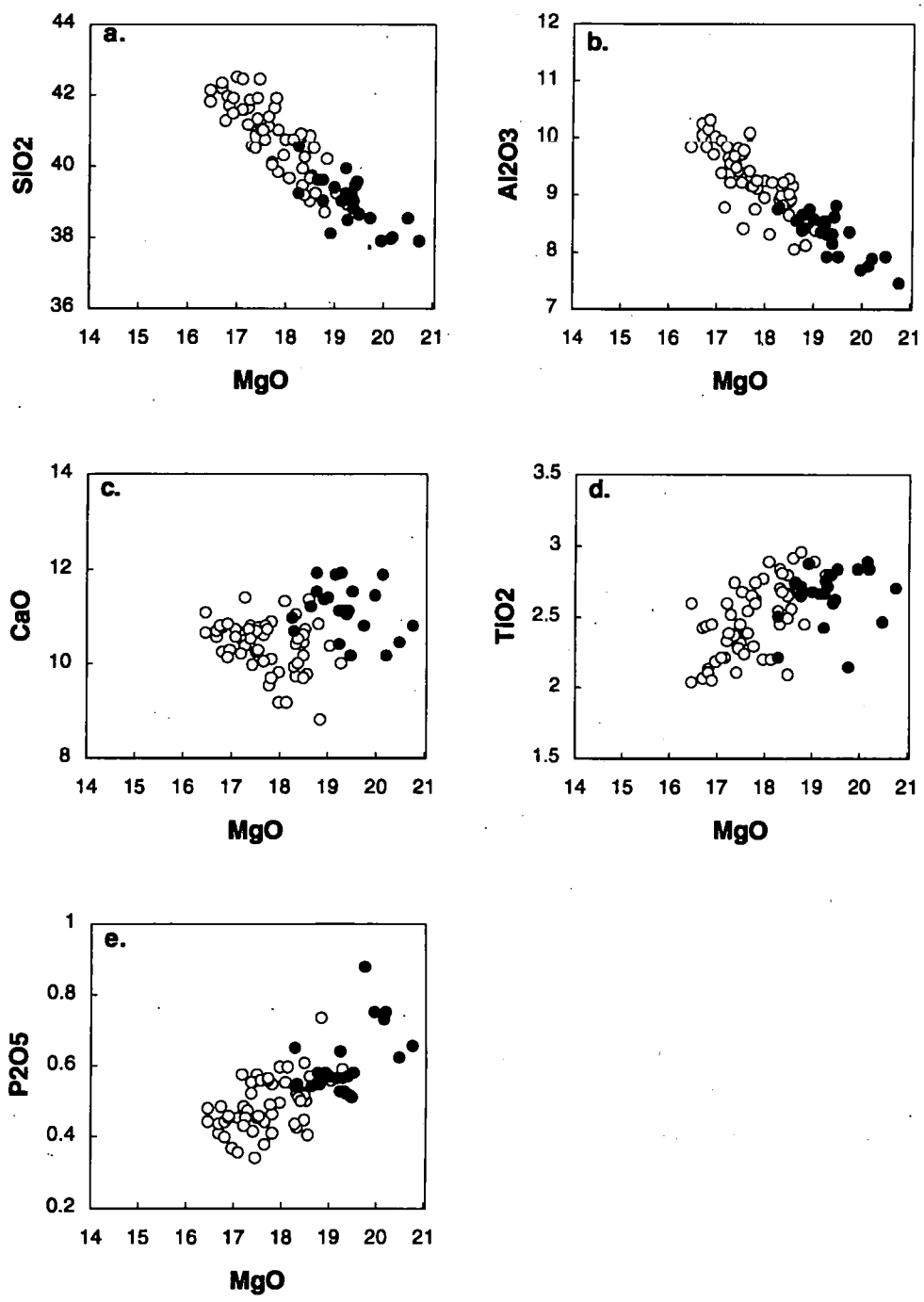

Figure 3-5. Kauai calculated primary magma compositions.
Primary magma compositions calculated as in Figure 3-1 but using K_D = 0.33 for the "low-Si" trend and K_D = 0.30 for the "main" trend.
The terms "main" trend and "low-Si" trend are defined in Figure 3-3.

However, Mg ($^{Ls/Lc}D_{Mg}$ = 0.5) and Mn ($^{Ls/Lc}D_{Mn}$ = 0.6) are less strongly partitioned into carbonate liquids while Si ($^{Ls/Lc}D_{Si}$ = 10), Ti ($^{Ls/Lc}D_{Ti}$ = 5), and particularly Al ($^{Ls/Lc}D_{Al}$ = 50) strongly favour silicate liquids. The correlations illustrated in Figure 3-5 for Kauai may be a consequence of varying amounts of carbonate liquid which are incorporated into silicate melt fractions and mixing of carbonate and silicate liquids could, therefore, be a feature of OIN in general.

Most OIN lie at lower SiO_2 and MgO values than the samples forming the Kauai "main" trend (Fig. 3-6). Many lie close to the Kauai "low-Si" trend but extreme compositions are found among the Cape Verde samples. Using the same procedure as for Kauai it is possible to show that a K_D between 0.36 and 0.40 might be appropriate for the Cape Verde magmas. The effect of recalculating the Cape Verde magmas using K_D = 0.40 is shown for SiO_2, Al_2O_3, CaO, TiO_2, and P_2O_5 *versus* MgO in Figure 3-7(a-e). The Kauai data (using K_D = 0.30 and 0.33) are shown on these diagrams for comparison.

Using the relationships

(1) $^{ol/Ls}K_D = {}^{ol/Ls}D_{Fe} / {}^{ol/Ls}D_{Mg} = 0.30$ (Roeder & Emslie, 1970)

(2) $^{ol/Lsc}K_D = {}^{ol/Lsc}D_{Fe} / {}^{ol/Lsc}D_{Mg} = 0.33$ (for Kauai "low-Si" trend)

where $_{Lsc}$ denotes mixed silicate-carbonate liquid

(3) $^{Ls/Lc}D_{Fe} = 1$ and **(4)** $^{Ls/Lc}D_{Mg} = 0.5$ (Fielding, 1992)

it is possible to derive an estimate of the amount of carbonate liquid in the Kauai magmas. From **(3)** it follows that $^{ol/Lsc}K_D$ is a linear function of the proportion (x) of carbonate liquid in the Kauai magmas. From **(3)** and **(4)** $^{Ls/Lc}K_D = {}^{Ls/Lc}D_{Fe} / {}^{Ls/Lc}D_{Mg} = 2$

But $^{ol/Lc}K_D = {}^{ol/Ls}K_D \cdot {}^{Ls/Lc}K_D$

Therefore $^{ol/Lc}K_D = 2\ (0.3) = 0.6$

For mass balance $^{ol/Lsc}K_D = (x)\ {}^{ol/Lc}K_D + (1-x)\ {}^{ol/Ls}K_D$

where x is the mass fraction of carbonate liquid.

The proportion of carbonate liquid is thus $x = (^{ol/Lsc}K_D - {}^{ol/Ls}K_D) / (^{ol/Lc}K_D - {}^{ol/Ls}K_D)$

$x = (0.33 - 0.3) / (0.6 - 0.3)$

$\underline{x = 0.1}$

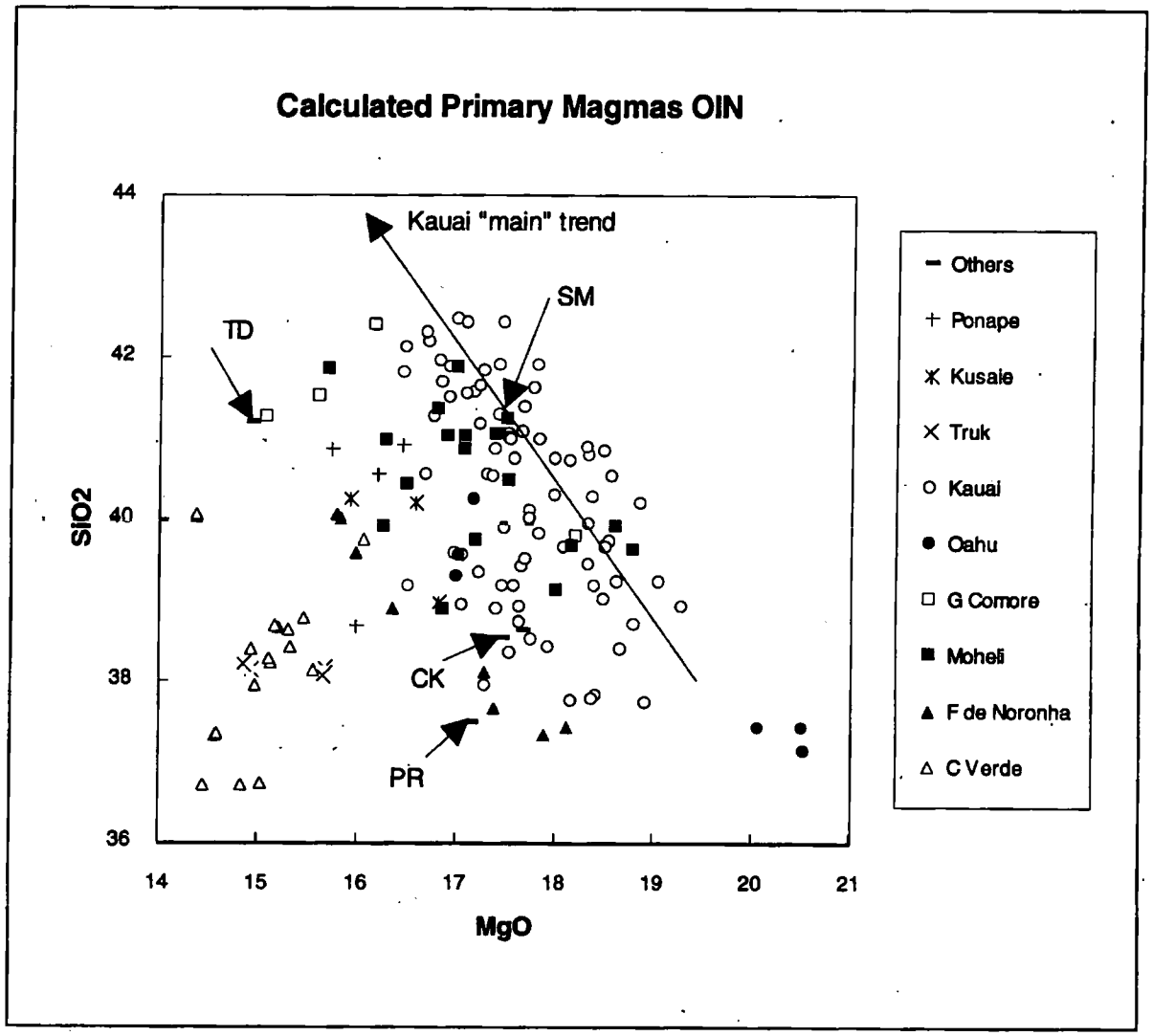

Figure 3-6. SiO_2 *versus* MgO for all ocean island nephelinites (OIN).
Primary magma compositions calculated as in Figure 3-1.
"Others" covers islands for which only one or two samples are included.
These are Principe (PR), Trinidade (TD), Samoa (SM), and Aitutaki (CK).

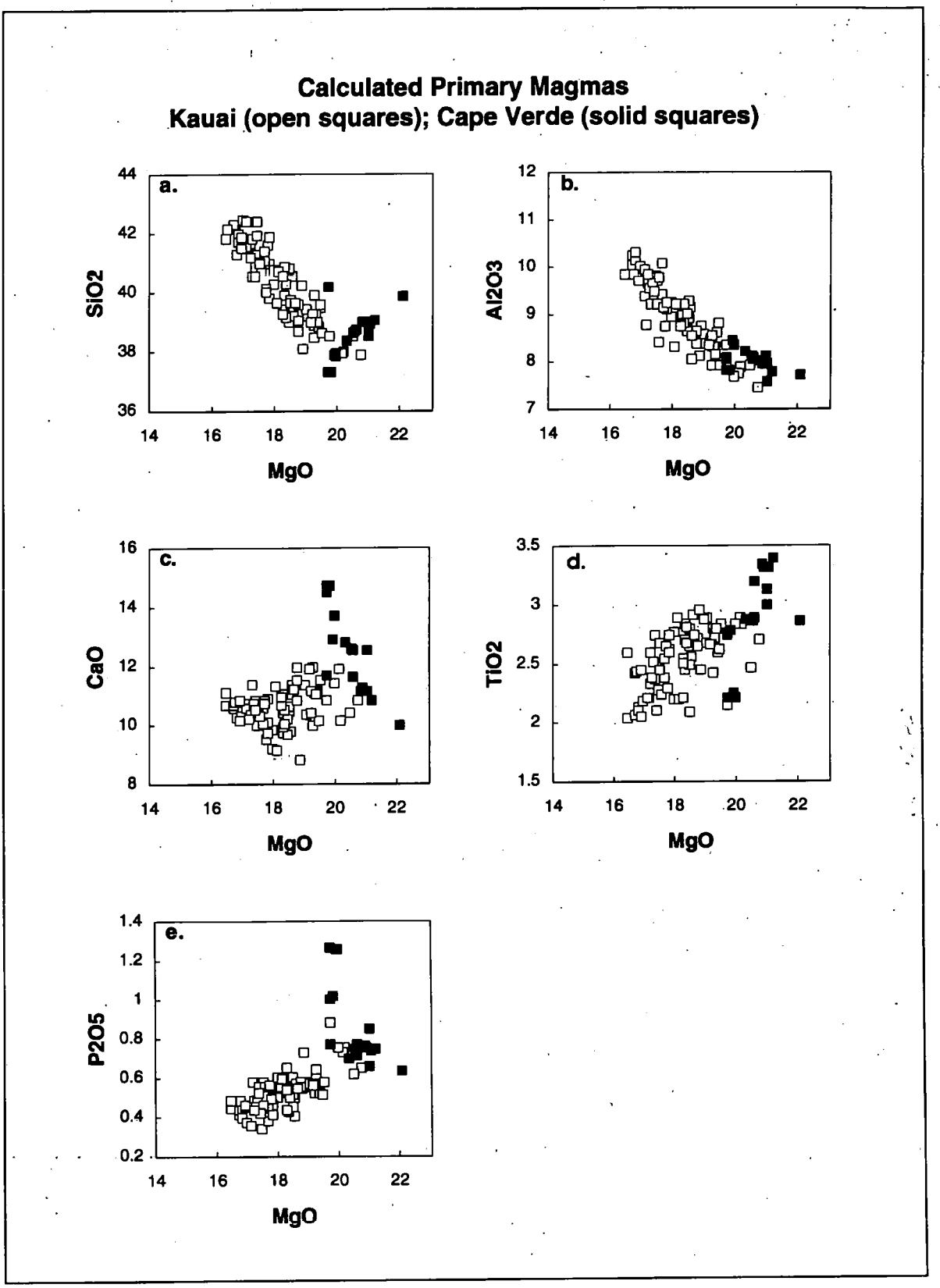

Figure 3-7. Kauai and Cape Verde primary magma compositions.
Primary magma compositions calculated as in Figure 3-1 but using K_D = 0.33 and 0.30 for the Kauai "low-Si" and "main" trends respectively and K_D = 0.40 for Cape Verde.

The amount of carbonate liquid in Kauai magmas represented by the "low-Si" trend is, therefore, ca. 10%. Similar calculations can be performed for the Cape Verde magmas using K_D values between 0.36 and 0.40. The results indicate that between 20% and 33% carbonate liquid addition is appropriate for Cape Verde. However, these calculations probably indicate a lower limit of carbonate involvement as it is possible that the samples defining the "main" Kauai trend are also carbonate-silicate mixtures.

Carbonate precursor liquids may impose low-SiO_2, low-Al_2O_3, high-CaO and high-P_2O_5 characteristics on OIN in general. If this is the case then major-element correlations should be consistent with Fielding's (1992) partitioning data. For example, SiO_2, Al_2O_3, and TiO_2 should correlate negatively with MgO but for CaO and P_2O_5 the correlations should be positive. This is shown to be so for Kauai in Figure 3-5 except that TiO_2 correlates positively with MgO, not negatively. In fact TiO_2 appears to correlate positively with elements which favour carbonate liquids (e.g. Fig. 3-8c & d) and negatively with those that do not (Fig. 3-8a & b). Thus, either titanium partitions more strongly into carbonate liquid than silicate liquid, which is contrary to the results of Fielding's (1992) experiments, or some other process is involved in the control of the Kauai "main" trend. As already suggested, this trend may simply reflect variations in the depth and degree of partial melting. Titanium would be expected to behave as an incompatible element during small degrees of silicate melting and would be enriched in silicate liquids. TiO_2 concentrations in carbonate-silicate liquid mixtures may, therefore, be governed by the concentration in the silicate fraction. The same argument could apply to P_2O_5. The positive correlations in CaO and P_2O_5 *versus* TiO_2 (Figure 3-8) might, therefore, be a consequence of both incompatible-element enrichment in small melt fractions and carbonate liquid partitioning. Clearly mantle processes may compete or act in concert to produce the magmas which eventually appear at the surface and it is often impossible to interpret the consequences unambiguously.

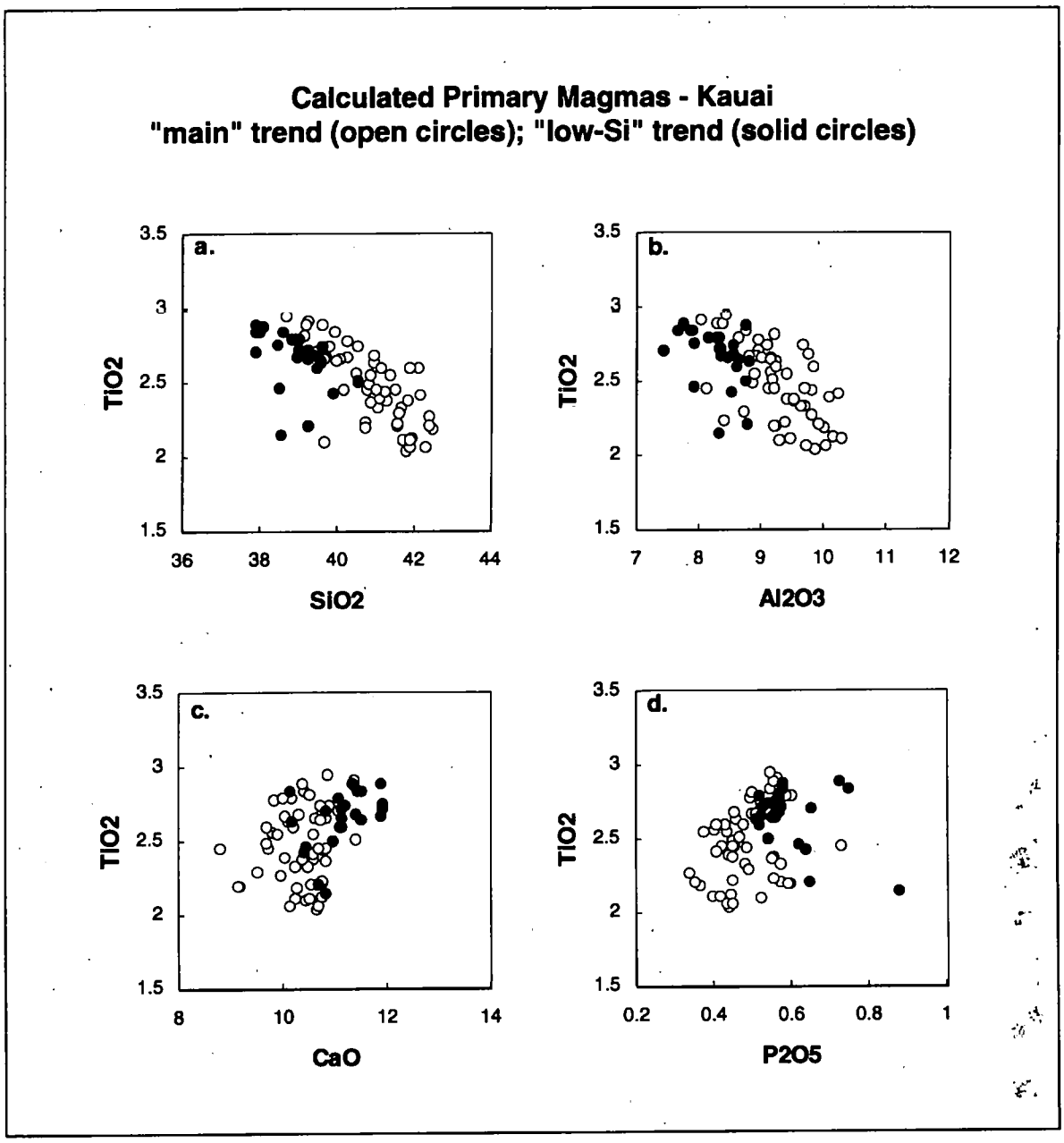

Figure 3-8. Kauai calculated primary magma compositions.
Primary magma compositions calculated as in Figure 3-1 but using K_D = 0.33 for the "low-Si" trend, K_D = 0.30 for the "main" trend.

Although major-element correlations in the Kauai data have been shown to be consistent with carbonate-silicate liquid partitioning and, in the case of titanium, with incompatible element behaviour in small melt fractions, it has also been proposed (Section 3.3) that low Al_2O_3 may result from the presence of residual aluminous phases in the mantle source. High-pressure melting studies indicate that melting of carbonated mantle peridotite occurs at depths corrresponding to the garnet and garnet-spinel stability fields (Olafsson & Eggler, 1983; Brey *et al.*, 1983) and that three or more phases will be on the liquidus at up to ca. 20% partial melting (Mysen & Kushiro, 1977; Jaques & Green, 1980). Primary magmas should, therefore, be saturated in mantle phases which are residual at temperatures and pressures corresponding to the depth of segregation. Yttrium has a high partition coefficient in garnet. Thus, if garnet is residual in the melting processes which generate OIN, and no other process is involved, a positive correlation between Al_2O_3 and Y might be expected. In the case of Kauai, Y appears to be negatively correlated with Al_2O_3 (Fig. 3-9b). REE partition strongly into carbonate liquids (Table 3-3). HREE and Y ($^{L_s/L_c}D_Y$=0.8) partition less strongly than LREE but nevertheless favour carbonate over silicate liquid. In the Kauai magmas Y correlates positively with elements which partition strongly into carbonate liquids (Fig. 3-9c & d) and negatively with those which do not (Fig. 3-9a & b). Yttrium also correlates positively with MnO (Fig. 3-9e), which partitions weakly into carbonate ($^{L_s/L_c}D_{Mn}$=0.6). It is thus likely that the Y and Al_2O_3 concentrations in Kauai magmas are influenced by carbonate liquid partitioning as well as the depth and degree of partial melting and the residual mineralogy of the source. In the case of yttrium the effects are competing, while for aluminium the effects reinforce each other.

For elements which partition fairly weakly into silicate liquids, TiO_2 ($^{L_s/L_c}D_{Ti}$=5), Na_2O ($^{L_s/L_c}D_{Na}$=2), and K_2O ($^{L_s/L_c}D_K$=1.5), negative correlations with Y might be expected. This is only observed in the case of Na_2O (Fig. 3-10b). There is no correlation between K_2O and Y (Fig. 3-10c) and TiO_2 (Fig. 3-10a) appears to correlate positively with Y. There is also an absence of correlation between K_2O and other incompatible elements (Fig. 3-10d & e). Both Na_2O and K_2O correlate negatively with MgO and CaO but positively with SiO_2 and Al_2O_3 (Figure 3-11). This behaviour is consistent with carbonate-silicate partitioning

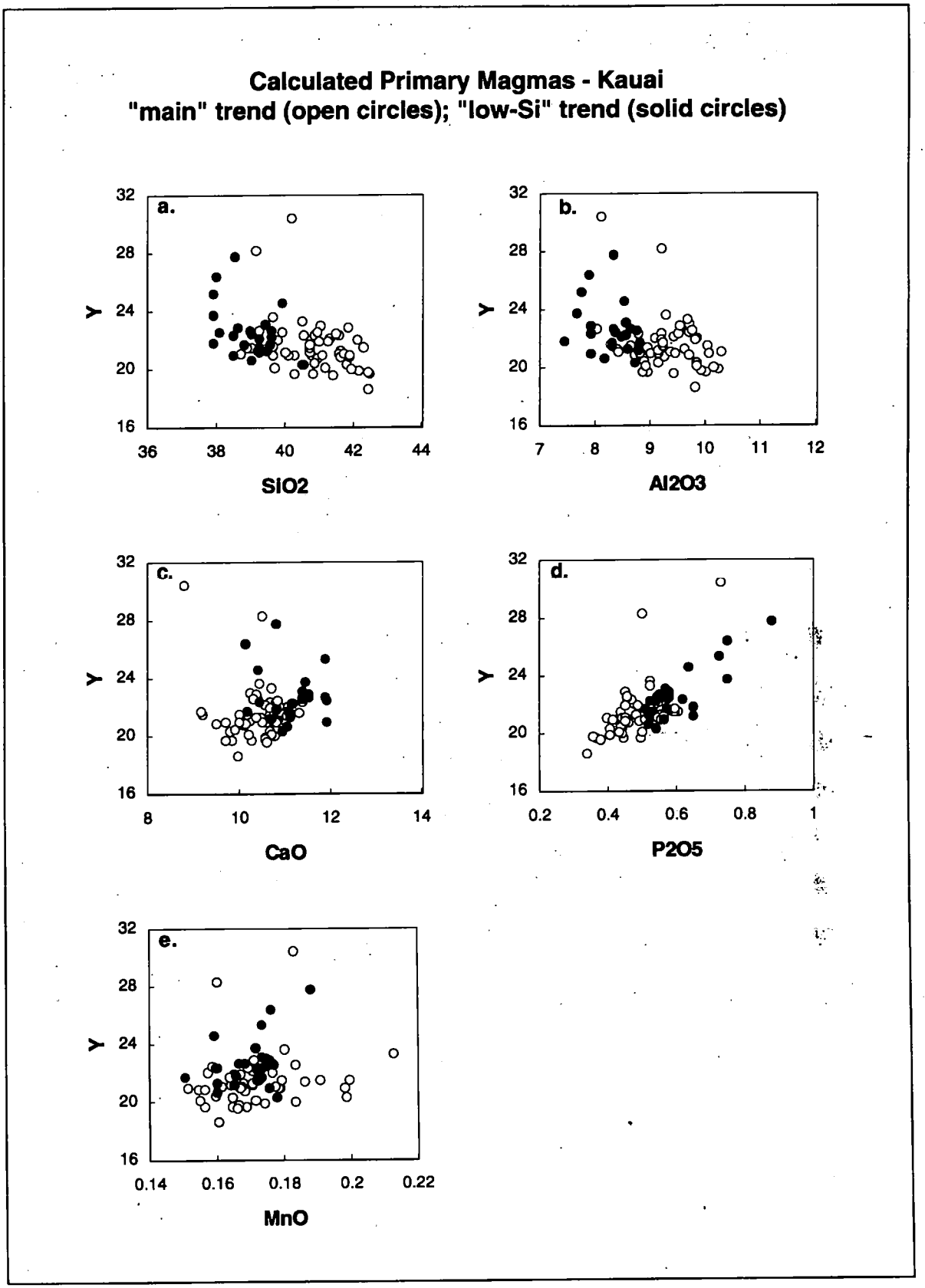

Figure 3-9. Kauai calculated primary magma compositions.
Primary magma compositions calculated as in Figure 3-1 but using K_D = 0.33 for the "low-Si" trend, K_D = 0.30 for the "main" trend.

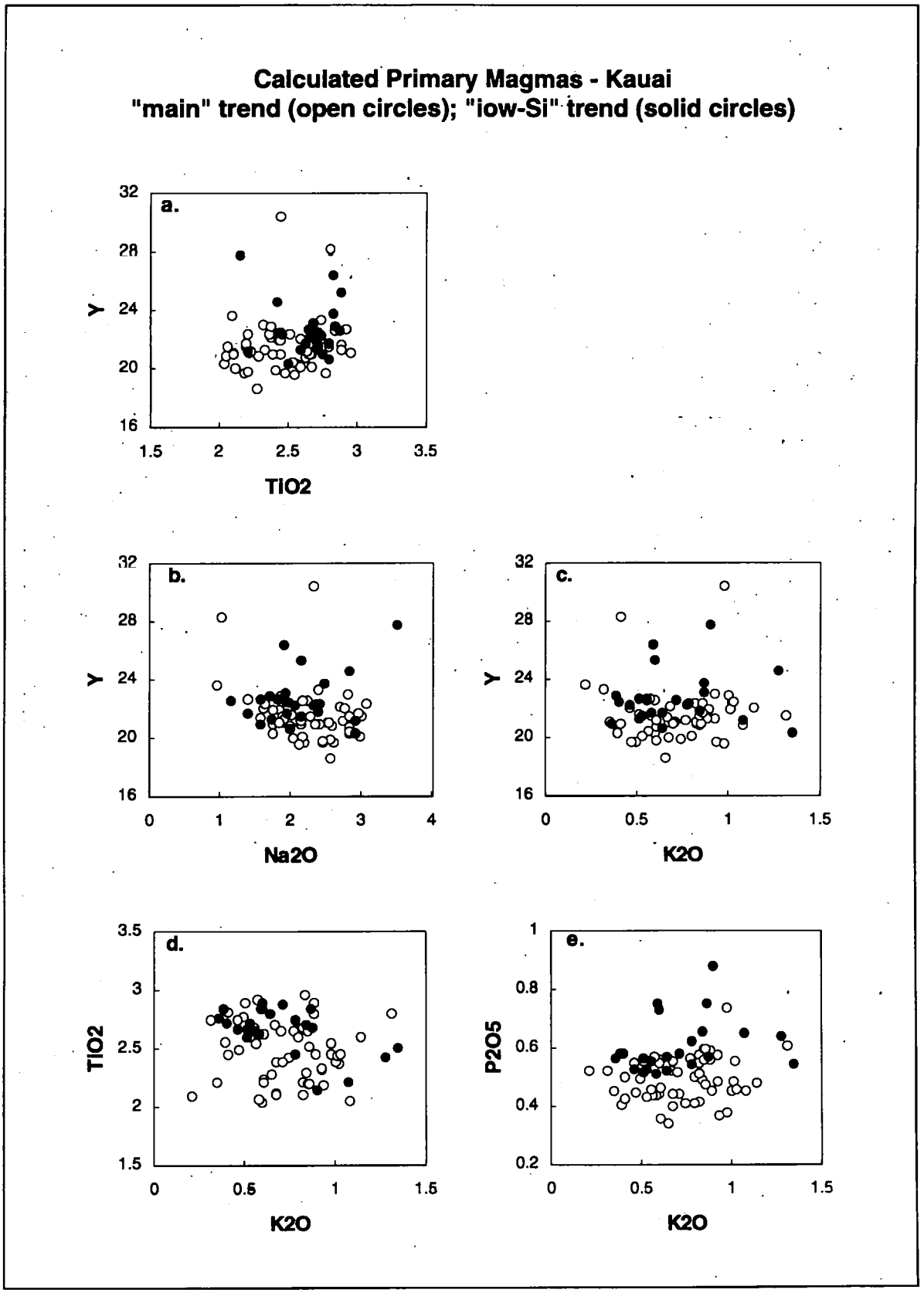

Figure 3-10. Kauai calculated primary magma compositions.
Primary magma compositions calculated as in Figure 3-1 but using K_D = 0.33 for the "low-Si" trend, K_D = 0.30 for the "main" trend.

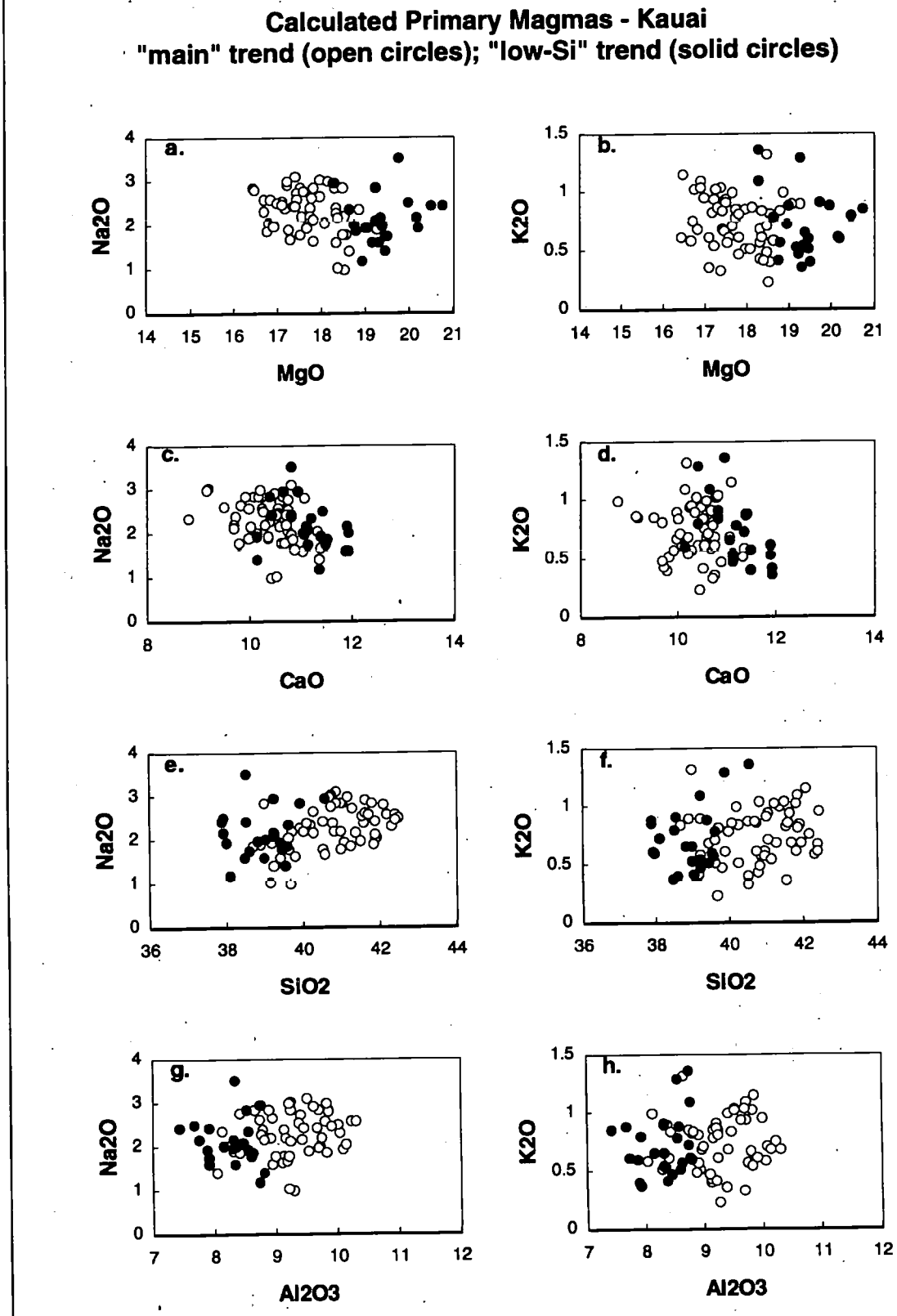

Figure 3-11. Kauai calculated primary magma compositions.
Primary magma compositions calculated as in Figure 3-1 but using K_D = 0.33 for the "low-Si" trend, K_D = 0.30 for the "main" trend.

for sodium but not for potassium or titanium. While TiO_2 correlations may be consistent with incompatible-element behaviour in small melt fractions, the K_2O trends cannot be explained in this way. An alternative explanation for low K_2O at small degrees of melting could, therefore, be the existence of residual potassic phases in the mantle source. It has been suggested in Section 3.5 that amphibole and/or phlogopite may be present in many mantle sources. The low K_2O/Na_2O (ca. 0.36) and generally low TiO_2 concentrations of OIN suggest that the potassic phase is predominantly pargasitic amphibole.

Evidence for the existence of potassic phases in the mantle source of OIN might also be found in the behaviour of trace elements (e.g. Rb, Ba, Nb) which have higher partition coefficients in amphibole and phlogopite compared with other common mantle minerals (Stolz & Davies, 1988; Adam *et al.*, 1993). Fielding's (1992) experimental results (Table 3-3) also indicate that strong prefences for carbonate liquid are shown by certain trace elements, notably Ba, Sr, LREE, and Pb. A more detailed study of trace elements which may be diagnostic in identifying the role of carbonate precursor liquids and residual potassic phases will be undertaken in Chapter 4.

3.7 Comparison between Primary OIB and OIN

A number of major-element correlations have been identified in Section 3.6 which suggest that depth and degree of partial melting, source mineralogy, and carbonate-silicate liquid mixing all contribute to the major element chemistry of OIN. But which, if any, of these correlations are applicable to OIB in general?

The OIB data include compositions ranging from melilitite to tholeiite and therefore represent considerable variation in degree of partial melting. Minor mantle phases, such as amphibole and phlogopite, are likely to be rapidly consumed in near-solidus melt fractions and any correlations observed in OIB are unlikely, therefore, to be controlled by residual potassic phases. In addition, the major-element chemistry of larger

melt fractions will be dominated by silicate liquids rather than carbonate liquids. Major-element variations in OIB will, therefore, reflect depth and degree of partial melting and major phases of the source mineralogy.

Figures 3-3a and 3-12a illustrate negative correlations between SiO_2, Al_2O_3 and MgO in both OIB and OIN but Figure 3-3a also suggests that much of the scatter in OIB could be a consequence of using the same K_D (= 0.30) in the primary magma calculations for OIB regardless of the possibility of carbonate involvement. In Figure 3-12 most elements are plotted against SiO_2. Small variations in K_D affect SiO_2 less than either MgO or Al_2O_3. Inter-element correlations are, therefore, generally clearer and the use of unconstrained ranges of K_D values in calculating primary magma compositions is avoided.

A comparison of OIB and OIN indicates that many of the trends observed in OIN are fundamental features of OIB as a whole. Titanium (Fig. 3-12c) and phosphorus (Fig. 3-12d) behave in the predictable manner of incompatible elements throughout the range of OIB and OIN except that some highly undersaturated OIN are enriched in P_2O_5 and also CaO (Fig. 3-12b) as are a few of the OIB samples shown. Potassium (Fig. 3-12e) does not appear to behave incompatibly in either OIB or OIN but positive correlations between P_2O_5, TiO_2 and K_2O can be demonstrated over part of the range of OIB (i.e. at low concentrations) even though these do not seem to exist in OIN (Fig. 3-10d & e). Despite a strong negative correlation between Al_2O_3 and MgO (Fig. 3-12a) in OIB no correlation (positive or negative) is found between Y and Al_2O_3 (Fig. 3-12f). In fact, yttrium concentrations at any given aluminium concentration are very variable. This absence of correlation could mean that Y is not buffered by garnet in the source of OIB at higher degrees of partial melting than OIN, and that carbonate liquids do not, in general, dominate OIB magmatism. It is much more likely, however, that the OIB data base incompasses so much variation that any individual island correlations are lost. It is worth repeating here that correlations within a large data base of samples which are not co-magmatic have to be treated with caution and, for this reason, this approach is not taken further.

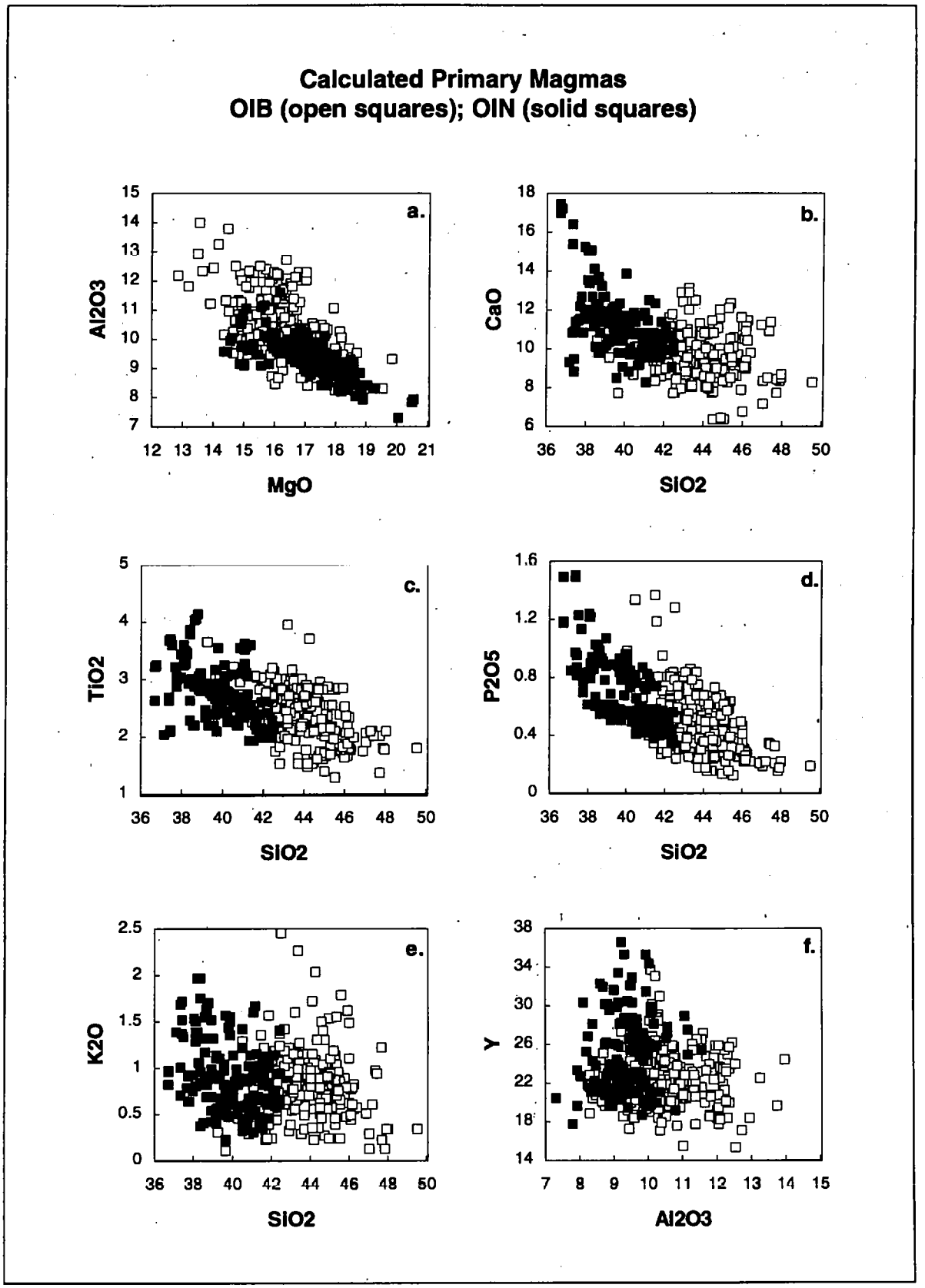

Figure 3-12. Calculated primary magma compositions OIB and OIN. Primary magma compositions calculated as in Figure 3-1 using $K_D = 0.30$ for both OIB and OIN.

The data presented in Section 3.6 suggest that most OIN (but not necessarily all) involve carbonate liquids in their genesis. It has been suggested in Section 3.6 that the calculated estimates of carbonate involvement could be lower limits and that many of the trends observed in OIN could be controlled by mixing of carbonate and silicate liquids. The existence of similar correlations in OIB can be interpreted in two ways. Either all OIB are a consequence of carbonate-silicate mixing in varying proportions or carbonate-silicate liquid partitioning is not responsible for most of the major-element variation observed in OIB and OIN. The treatment of the Kauai "low-Si" trend indicates that fundamental correlations such as those seen in SiO_2 and Al_2O_3 *versus* MgO will remain no matter what correction for carbonate-silicate mixing is made by way of the K_D value. In this case these particular correlations must be mainly attributable to depth and degree of partial melting, and the residual mantle mineralogy.

While Figures 3-3a & 3-12 indicate that most OIN involve carbonate liquids in their genesis it is also evident that a small number of other OIB may also have carbonate precursors. This could be a regional effect but detailed regional investigations of OIB are beyond the scope of this work and the possibility will not, therefore, be pursued. It also appears that amphibole is present in the source of OIN and, probably, in the sources of undersaturated OIB but that amphibole may have been consumed before the degrees of melting appropriate to many OIB have been reached. The role of potassic phases in the source of OIN will be considered again in Chapter 4.

3.8 Major-Element Composition of Primary Continental Nephelinites

The calculated primary compositions of the continental data set (CON) consists of 82 analyses but no volcanic complex or magmatic province is represented by more than eight samples. It is not possible, therefore, to approach the major-element chemistry of continental feldspar-free rocks through a detailed study of any one group of continental samples. Major-element variation diagrams indicate that the CON data set encompasses

more variability in most elements than the OIN data. The absence of a substantial co-magmatic suite within CON which may be taken to be representative of most continental provinces is, thus, a considerable hindrance to establishing the underlying processes which may account for the scatter in these data. However, since feldspar-free rocks are generated in both oceanic and continental environments, similar mantle processes must underpin the observed chemistry of both. The trends established for Kauai can, therefore, be used for comparative purposes and it may be possible to attribute scatter in the data to the effects of continental lithosphere involvement.

When the Kauai trends are superimposed on CON data the correlations deduced for Kauai (and, indeed, for OIB in general) appear also to hold for CON. The correlations are not as strong but overall negative correlations between SiO_2, Al_2O_3 and MgO (Figs. 3-13a & c), and positive correlations between TiO_2 and MgO (Fig. 3-13b) are the same. CON have, however, generally higher CaO, P_2O_5 and MnO (Figs. 3-13d to f), and lower SiO_2 (Fig. 3-13a) than Kauai which suggests a greater proportion of carbonate liquid in many of the magmas. By comparing SiO_2 *versus* MgO for CON (Fig. 3-13a) with the variation in OIN (Fig. 3-6) it appears that K_D values between 0.30 and ca. 0.36 might be appropriate for CON. Using the procedures used in Section 3.6 it can be shown that this implies carbonate additions of up to 20% in continental magmas. TiO_2 (Fig. 3-13b) and P_2O_5 (Fig. 3-13c) correlate positively with MgO. This is consistent with incompatible element enrichment in small silicate melt fractions and carbonate liquid partitioning of phosphorus. Na_2O (Fig. 3-14a) and K_2O (Fig. 3-14b), on the other hand, show poor negative correlations with MgO similar to the patterns seen in the Kauai data. The lack of characteristic incompatible-element behaviour shown by potassium has, in the case of OIN, been taken to indicate the existence of residual potassic phases in the mantle source. Figures 3-14a & b suggest that potassic phases are also present in the continental mantle sources of highly undersaturated volcanic rocks. CON do, however, appear to be generally richer in K_2O (but not in TiO_2) than the Kauai magmas. This has been taken to indicate (Section 3.5) that some continental sources have been metasomatically enriched in potassium. Potassic phases in spinel lherzolites from SE Australia have $(K_2O/Na_2O)_{amph} \cong 0.2$ and $(K_2O/Na_2O)_{mica} \cong 8$

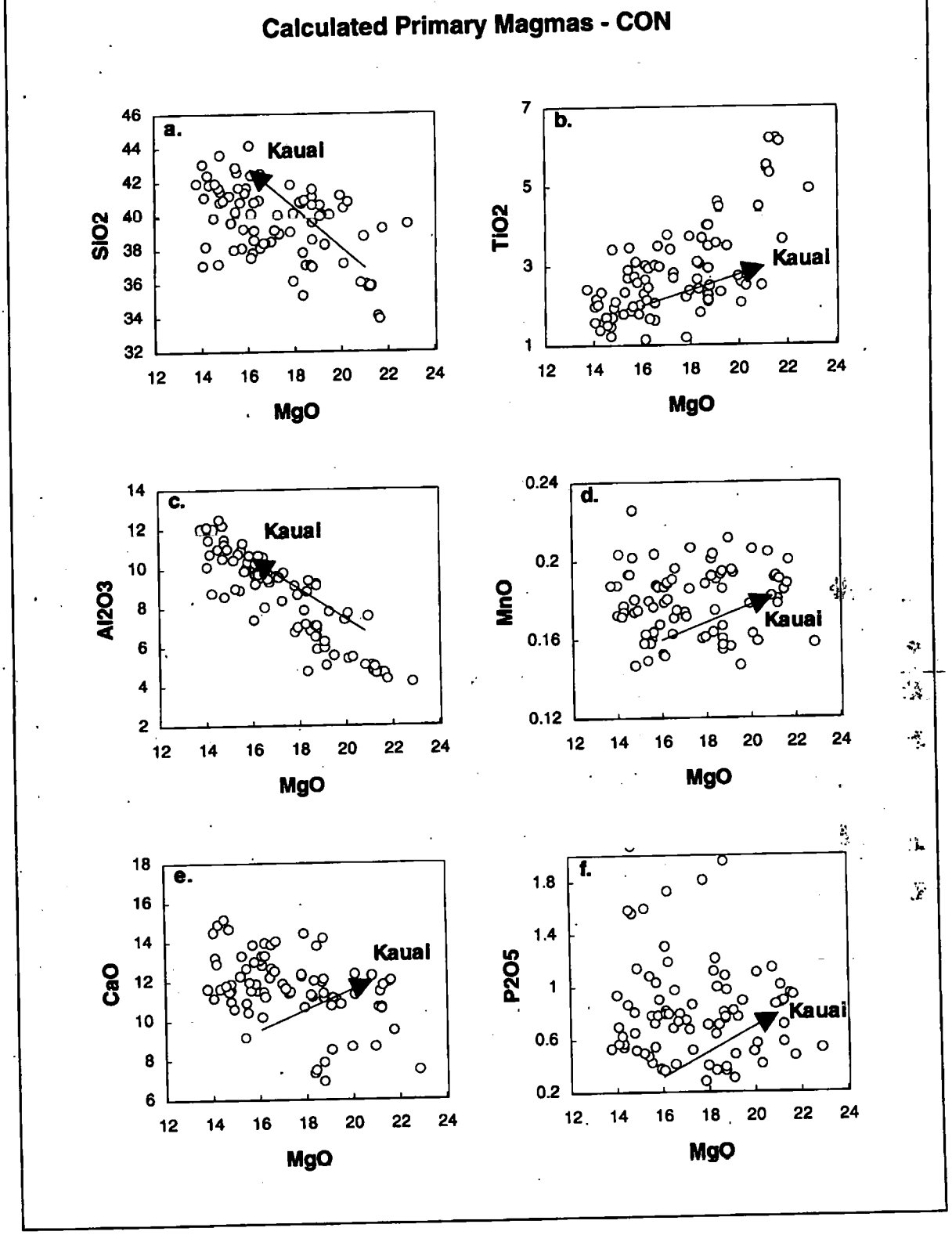

Figure 3-13. Calculated primary magma compositions for all continental nephelinites (CON).
Primary magma compositions calculated as in Figure 3-1 using $K_D = 0.30$ and $Fo_{90.7}$ for CON. Kauai trends are shown by the arrow (cf. Figure 3-5).

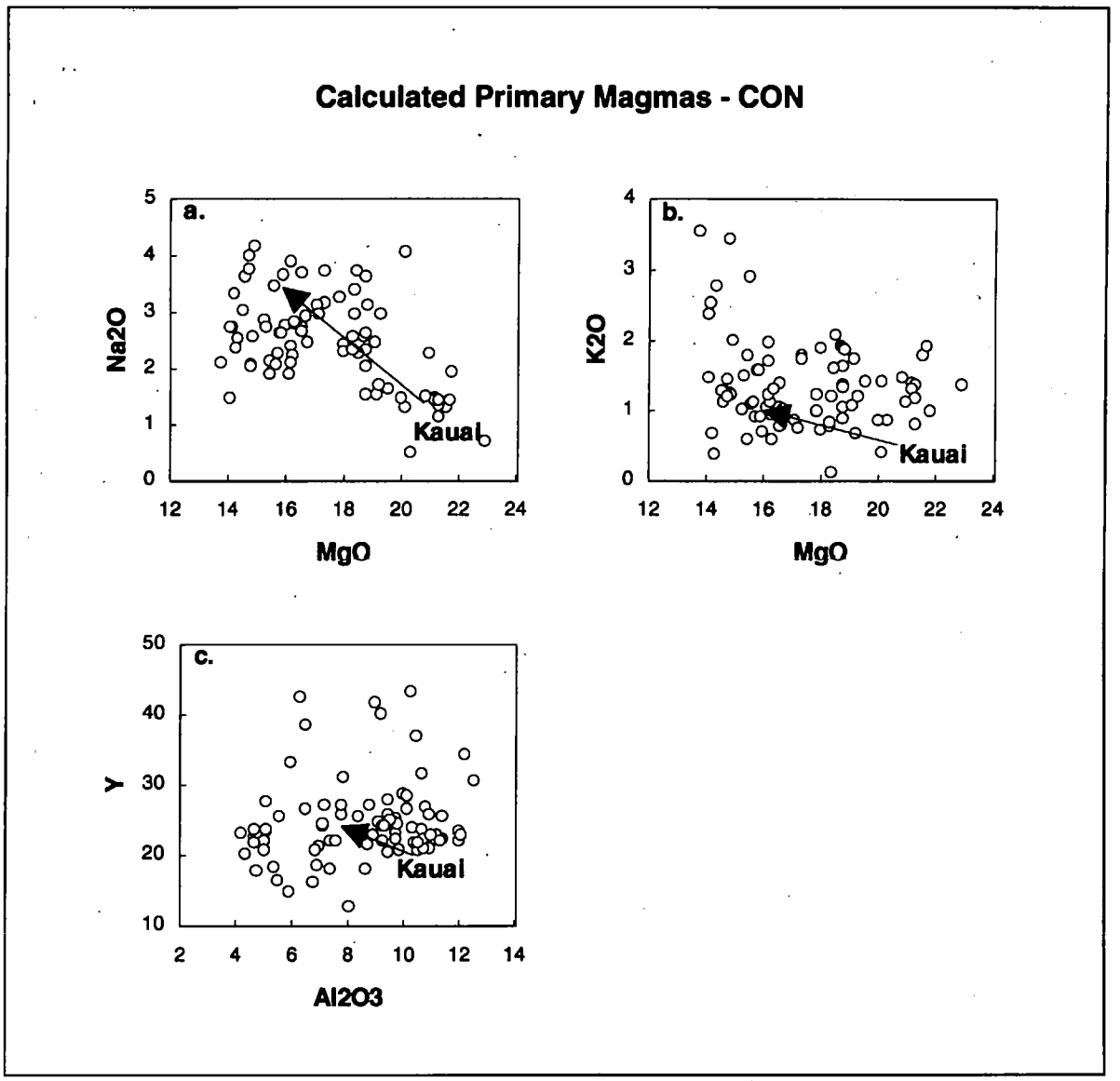

Figure 3-14. Calculated primary magma compositions for all continental nephelinites (CON).
Primary magma compositions calculated as in Figure 3-1 using $K_D = 0.30$ and $Fo_{90.7}$ for CON. Kauai trends are shown by the arrow (cf. Figures 3-9 and 3-11).

(Stolz & Davies, 1988). However, $(K_2O/Na_2O)_{CON} \cong 0.62$ compared with $(K_2O/Na_2O)_{OIN} \cong 0.36$ which suggests that, in general, low-Ti amphibole is the dominant potassic phase in both OIN and CON sources. $(K_2O/Na_2O)_{liquid}$ will always be slightly higher than the same ratio in amphibole because ${}^{amph}D_K \cong {}^{amph}D_{Na}$ and Na is buffered by other mantle phases whereas K is not.

The negative correlation between Y and Al_2O_3 (Fig. 3-9b) in the Kauai data and OIN in general (Fig. 3-12f) does not appear to apply to CON (Fig. 3-14c). The extremely low concentrations of Al_2O_3 in some highly undersaturated continental magmas could be a consequence of high carbonate/silicate liquid in these magmas. In this case a strong negative correlation with Y would be expected together with high concentrations of CaO and P_2O_5 but in fact these features are not observed in low-Al_2O_3 magmas. Alternatively, low Al_2O_3 could be due to a higher proportion of residual aluminous phases in the mantle source. Residual garnet would retain Y in the source at small degrees of partial melting and this could mask the effect of carbonate-silicate liquid partitioning of Y. The correlation between Y and Al_2O_3 observed in the Kauai data is, therefore, lost at low concentrations of Al_2O_3.

Feldspar-free continental magmas may, thus, have been generated from similar mantle sources to their oceanic counterparts by processes involving the mixing of initial carbonate liquids in more voluminous silicate melts. The amount of carbonate liquid involved in continental magmatism may be higher than that involved in the Kauai magmas but it is similar in range (up to ca. 20%) to that required to account for most OIN.

A number of continental compositions lie outside the range of OIN. Some, as has been shown, have low Al_2O_3 (Fig. 3-13c), others have low CaO (Fig. 3-13e), and others still have high P_2O_5 (Fig. 3-13f), TiO_2 (Fig 3-13b) or K_2O (Fig. 3-14b). These differences cannot be accounted for by appealing to carbonate-silicate liquid partitioning and, in these cases, the magmas may be indicating significant variations in the mineralogy and composition of the mantle source. Some of the variation may be due to changes in the

proportions of normal mantle phases. In other cases variation may result from modal and cryptic metasomatism of the mantle source by CO_2- and H_2O-rich fluids during decarbonation reactions as described in Section 3.1. Metasomatism of mantle sources can usually be identified by high concentrations of some trace elements and unusual trace-element ratios. The trace-element evidence for metasomatic enrichment of some continental sources and, in particular, for the existence of potassic phases in the mantle and the involvement of carbonate precursor liquids in the melting process will be addressed in Chapter 5.

3.9 Major-Element Composition of Primary Potassic Continental Rocks

It has already been noted in Section 3.5 that potassic continental rocks have rather different major-element patterns from OIN or CON. The pattern for the Western Rift (Fig. 3-2a) is similar to CON but shows enrichments in K_2O and TiO_2 and depletions in Al_2O_3 and Na_2O. As a result of the foregoing studies of OIN and CON these average compositions suggest carbonate liquid mixing with a silicate component generated in the presence of more garnet than CON from a metasomatically enriched source (high $^{K}C_0$ and $^{Ti}C_0$) containing potassic phases, in this case, principally Ti-rich phlogopite [$(K_2O/Na_2O)_{WR} \cong 3.2$]. The pattern for the New South Wales leucitites (Fig. 3-2b), on the other hand, suggests that carbonate precursor liquids are not involved (low CaO and MnO) and that these magmas are derived by small degrees of silicate melting from a similarly enriched source containing Ti-rich phlogopite [$(K_2O/Na_2O)_{NSW} \cong 3.0$], an aluminous phase (low Al_2O_3) and, possibly, apatite (high P_2O_5). A more detailed study of major-element variation, however, suggests that these interpretations are an over-simplification.

Major-element variation diagrams such as SiO_2 *versus* MgO (Fig. 3-15a) support the involvement of carbonate precursor liquids in some of the Western Rift (WR) magmas. However, it is clear from Fig. 3-15a that the data fall into three clusters defined by katungite and mafurite from the northern end of the rift (Katunga & Bunyaraguru),

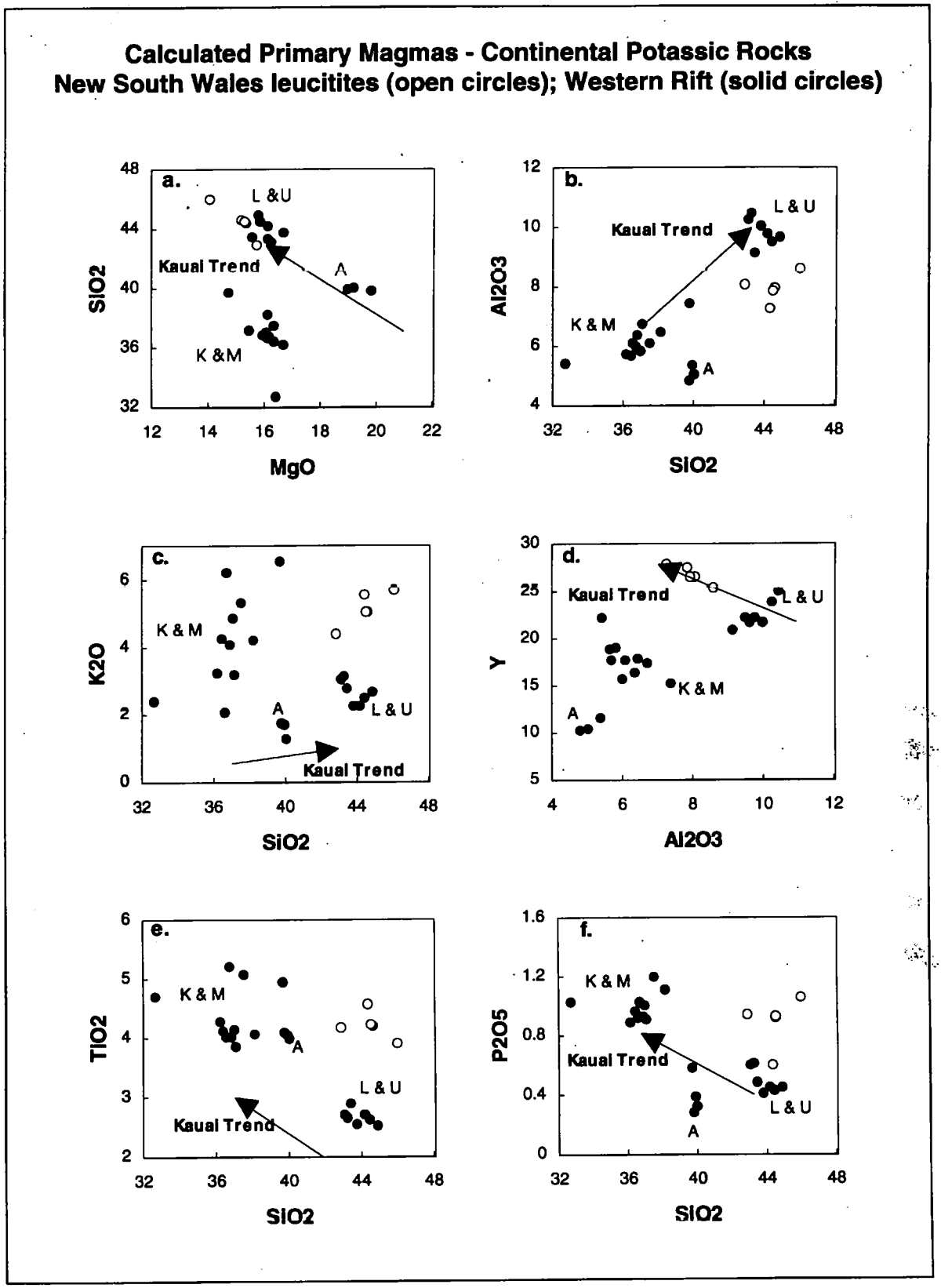

Figure 3-15. Calculated primary magma compositions for potassic continental rocks from the Western Rift, Uganda (kamafugites) and New South Wales, SE Australia (leucitites).
K & M = katungites & mafurites (Katunga & Bunyaraguru, Western Rift)
A = ankaratrites (Katwe, Western Rift)
L & U = leucitites & ugandites (Birunga-Bufumbira, Western Rift)
Primary magma compositions calculated as in Figure 3-1 using $K_D = 0.30$ and $Fo_{90.7}$ for potassic rocks. Kauai trends are shown by the arrow.

ankaratrite also from the northern end of the rift (Katwe), and leucitite and ugandite from further south (Birunga-Bufumbira). By the methods already established for OIN it appears from Figure 3-15a that a carbonate addition of ca. 20% ($K_D \cong 0.36$) is appropriate for the katungite and mafurite samples and that these represent the smallest degrees of partial melting from the deepest sources in this magmatic province. Other major-element variation diagrams, however, show that while the Birunga-Bufumbira samples generally lie close to one end of the Kauai trend, the Katunga, Bunyaraguru and Katwe samples frequently do not. This is particularly noticeable in the case of Al_2O_3 *versus* SiO_2 (Fig. 3-15b) where the Katwe group falls below the Kauai trend. Yttrium and aluminium correlate positively in the Katwe and Birunga data (Fig. 3-15d) but negatively in the katungites and mafurites. Low Al_2O_3 concentrations thus indicate a high proportion of residual garnet in the mantle source of katungite, mafurite and ankaratrite but carbonate liquid partitioning of Y changes the sense of the correlation in the katungites and mafurites. Ugandites and leucitites represent larger degrees of partial melting from shallower sources where the amount of residual garnet in the mantle may be significantly reduced.

The high concentrations of potassium and titanium in all the Western Rift samples compared with typical OIN is shown in Figures 3-15c and 3-15e. The enrichments are taken to indicate high $^{K}C_0$ and $^{Ti}C_0$ in this province. The highest concentrations of K and Ti are found in the smallest degrees of partial melting (katungites and mafurites) and the degree of enrichment is very variable. Lower concentrations of K_2O in the leucitites and ugandites might be a consequence of the higher degrees of partial melting involved in the generation of these magmas and indicate that phlogopite has been stripped from the source. The leucitites and ugandites, however, have $K_2O/Na_2O \cong 1.3$ (for the ankaratrites $K_2O/Na_2O \cong 1.4$). These ratios are closer to typical CON values than those calculated for the katungite and mafurite samples ($K_2O/Na_2O \cong 4.8$) and they suggest that the mantle sources of the leucitites and ugandites contain amphibole as the main potassic phase. This interpretation is consistent with a shallower origin for the leucitite and ugandite magmas. Experimental evidence indicates that phlogopite is stable between about 70 and 150 km along with carbonate phases (dolomite or magnesite) and a H_2O-rich vapour phase. At shallower

depths amphibole is the stable potassic phase and this may coexist with carbonate (dolomite) or CO_2-rich vapour shallower than about 60 km (Olafsson & Eggler, 1983; Brey *et al.*, 1983; Schneider & Eggler, 1986). The generally high concentrations of TiO_2 in Western Rift magmas have been attributed (Section 3.5) to the presence of Ti-rich mica and (kaersutitic) amphibole in the mantle source. These phases appear to be more significant for the katungites, mafurites, and ankaratrites, than the leucitites and ugandites. It should be noted, however, that the mantle may be so extensively metasomatised that the residual source mineralogy may not be dominated by olivine and pyroxene and interpretations of calculated primary magma compositions based on the partitioning of Fe^{2+} and Mg between olivine and liquid will be invalidated. Partition coefficients for a number of trace elements (e.g. Rb, Ba, Sr, and LREE) are markedly different in amphibole and phlogopite and also much higher than for normal mantle phases. The relative roles of these phases in the Western Rift sources will be discussed further in Chapter 5.

Phosphorus concentrations (Fig. 3-15f) are consistent with enrichment in the small degree partial melts by carbonate liquid partitioning and incompatible-element enrichment in silicate fractions. Both the Katunga-Bunyaraguru and Birunga data subsets lie close to the typical oceanic trend provided by the Kauai data. However, the ankaratrite magmas from Katwe seem to be depleted in P_2O_5. A possible explanation for this unusual feature, and the low concentrations of CaO and Al_2O_3, could be that the mantle source for these magmas had been depleted in melt-generating components prior to metasomatic enrichment in potassium and titanium. As there are only three samples of Katwe ankaratrite this topic will not be investigated further.

The New South Wales (NSW) magmas seem to have been derived by similar degrees of melting but from shallower sources than the Western Rift ugandites and leucitites (Fig. 3-15a). In the NSW case there is clear evidence (low-CaO and low-MnO trends, Fig 3-16a & b respectively) that carbonate precursor liquids are not involved in the generation of the magmas. The negative correlation betwen Y and Al_2O_3 (Fig 3-15d) is, therefore, unexpected. If the NSW magmas have been derived entirely from shallow

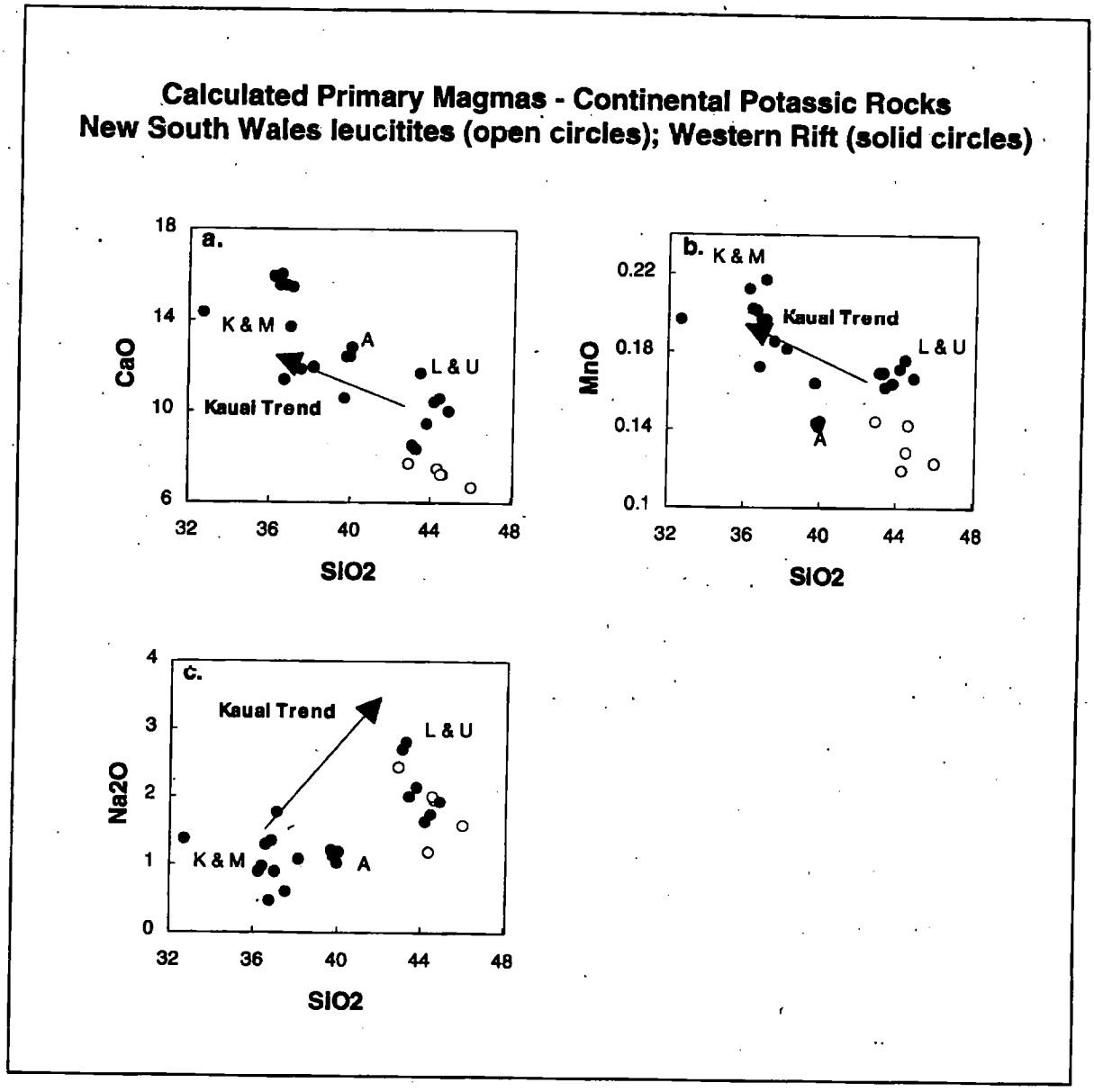

Figure 3-16. Calculated primary magma compositions for potassic continental rocks from the Western Rift, Uganda (kamafugites) and New South Wales, SE Australia (leucitites).
K & M = katungites & mafurites (Katunga & Bunyaraguru, Western Rift)
A = ankaratrites (Katwe, Western Rift)
L & U = leucitites & ugandites (Birunga-Bufumbira, Western Rift)
Primary magma compositions calculated as in Figure 3-1 using $K_D = 0.30$ and $Fo_{90.7}$ for potassic rocks. Kauai trends are shown by the arrow.

lithospheric sources where spinel is the dominant aluminous phase then Y would be expected to show characteristic incompatible-element enrichment in small melt fractions. The low Al_2O_3 of NSW leucitites by comparison with those from the Western Rift suggests that the NSW source is somewhat depleted in melt-generating components.

The NSW magmas are more highly enriched in TiO_2, K_2O, and P_2O_5, than the Western Rift leucitites and ugandites. These may, therefore, have come from sources containing significant proportions of Ti-rich amphibole (kaersutite), phlogopite and, possibly, apatite. These minerals may have been added to a depleted source by metasomatic enrichment of the mantle. Some unusual correlations are also found within this suite. Negative correlations exist in Na_2O *versus* SiO_2 (Fig. 3-16c), MnO *versus* SiO_2 (Fig. 3-16b) and TiO_2 *versus* SiO_2 (Fig. 3-15e) while in K_2O *versus* SiO_2 (Fig. 3-15c) and P_2O_5 *versus* SiO_2 (Fig. 3-15f) the correlations are positive. Na, Mn, and Ti seem to behave as incompatible elements and are, therefore, relatively more enriched in the smaller melt fractions but this is not so for K_2O and P_2O_5. Futhermore, K_2O/Na_2O for these samples varies between ca. 2 and 5 which indicates considerable source heterogeneity with respect to potassium. For modal batch melting at small F, if ^{bulk}D value > 1 then concentration in the liquid increases with increasing partial melting, whereas for non-modal melting, which is more appropriate for metasomatised sources containing accessory phases, if P >1 and $^{bulk}D < 1$ then concentration will also increase with increasing F. The change in concentration of an element with degree of melting thus depends on the balance between the proportions of phases entering the melt and the bulk partition coefficient for that element. In the case of the New South Wales magmas it appears to be more likely that minor K- and P-rich phases are being consumed as melting proceeds.

The NSW leucitite suite consists of only five samples. The source region of the magmas is clearly shallow, extensively metasomatised, and extremely heterogeneous. As was suggested in the discussion of the Western Rift ugandites and leucitites, the distribution of Fe^{2+} and Mg between crystals and melt may not be controlled by olivine when the source can be shown to be extensively metasomatised. The calculated primary

magmas for the NSW suite may have no validity in this case. For these reasons the subtle variations indicated by the NSW trends may be no more than an artifact of the data used in the diagrams.

3.10 Summary

Study of the major-element variation in calculated primary magma compositions of ocean island basalts (OIB), ocean island nephelinites (OIN), continental nephelinites (CON) and the potassic continental variants of these rock types has identified a number of features which can be related to the depth and degree of partial melting required to produce feldspar-free volcanic rocks, to the mineralogy of the source regions from which they are derived, and to the mantle processes which may be involved in the generation of the magmas. These are

(i) Certain correlations (e.g. SiO_2 *versus* MgO, negative; Al_2O_3 *versus* MgO, negative) exist between major elements in all the data sets examined (including OIB as a whole). Feldspar-free volcanic rocks are in general terms, therefore, part of a polybaric partial melting continuum in which magmas generated from a four phase mantle lherzolite mineralogy become more MgO-rich, and SiO_2- and Al_2O_3-poor, with increasing depth.

(ii) Feldpar-free volcanic rocks lie at the more magnesian end of the polybaric partial melting continuum. These, therefore, represent both the smallest degrees of partial melting and the deepest sources where garnet may be the stable aluminous phase.

(iii) The distribution of Fe^{2+} and Mg between olivine and liquid in OIN magmas is variable (K_D = 0.3 up to 0.4). Most OIN are therefore considered to be the result of mixing varying amounts of a carbonate precursor liquid with the more voluminous silicate melts generated as the mantle decompresses through the solidus for carbonated peridotite.

(iv) Carbonate liquid additions of up to 33% (in the case of Cape Verde) are required to explain the range of OIN but additions of ca. 10% (e.g. Kauai) are most common. These additions must be taken as lower limits since all OIN (and many OIB) could have carbonate liquid precursors. OIB will be dominated by silicate melt fractions. The effect of any carbonate component in OIB will probably be negligible in terms of major-element composition.

(v) Most major-element correlations in OIN are consistent with carbonate-silicate liquid mixing and incompatible-element enrichment in small silicate melt fractions.

(vi) Yttrium concentrations in OIN are controlled by REE partitioning in carbonate liquids and residual garnet in the source.

(vii) Low K_2O concentrations in OIN are due to residual potassic phases in the source. Low K_2O/Na_2O (= 0.36) and low TiO_2 concentrations indicate that a low-titanium, sodic amphibole may be the dominant potassic mineral in the OIN source.

(viii) Residual potassic phases determine K_2O concentrations in OIN and the more undersaturated OIB but may be consumed in larger melt fractions.

(ix) CON magmas are derived from slightly more depleted sources than OIN and show more variation in major-element compositions. The major-element correlations seen in OIN nevertheless apply also to CON. Similar sources and processes are, therefore, involved in the generation of both OIN and CON magmas.

(x) Carbonate liquid additions of up to 20% are often required to explain the composition of CON magmas.

(xi) CON sources contain a greater proportion of potassic phases than OIN sources. K_2O/Na_2O for CON magmas (= 0.62) is higher than for OIN (= 0.36) and titanium concentrations are generally low in both. Low-titanium amphibole is thus the dominant potassic phase in both CON and OIN sources.

(xii) Some CON have unusually low concentrations of Ca and Al, and extremely high concentrations of K, Ti, and P, which lie significantly outside the range of

OIN. These have been derived from sources not directly available to OIN magmas and which may be restricted to the continental lithosphere. Metasomatically enriched continental lithosphere is only a significant source component for a small number of CON magmas.

(xiii) Potassic continental magmas are more highly enriched in Ti than OIN and most CON. Continental lithosphere which may have been extensively metasomatised by K- and Ti-rich fluids is, therefore, contributing to the composition of these magmas.

(xiv) Western Rift potassic magmas have been derived from at least three different source compositions which are both geographically separated and chemically distinct. Katungites and mafurites from the northern end of the rift (Katunga and Bunyaraguru) require a carbonate liquid addition of ca. 20%. Ankaratrites from the north (Katwe) and leucitite and ugandite from further south (Birunga) do not involve carbonate precursor liquids.

(xv) Western Rift magmas have generally high K and Ti, and high K_2O/Na_2O (= 3.2). Ti-rich amphibole and mica is therefore present in the mantle source. Katungites have highest K_2O/Na_2O (= 4.8) and low Al_2O_3. These come from deep mantle sources where a high-Ti phlogopite is stable. Leucitites and ugandites have low K_2O/Na_2O (= 1.3) and high Al_2O_3 and, therefore, originate from shallow depths where amphibole is stable. The ankaratrites may be derived from a depleted mantle source which has subsequently been metasomatically enriched in K and Ti.

(xvi) New South Wales leucitites do not involve precursor carbonate liquids in their generation. They are more highly enriched in K, Ti, and P than the Western Rift leucitites and may also have been derived from shallow mantle sources containing kaersutitic amphibole, Ti-rich phlogopite, and apatite. This source may be depleted mantle which has been extensively metasomatised prior to magma generation.

Chapter 4

Trace-Element Characteristics of Oceanic Feldspar-Free Volcanic Rocks

4.1 Introduction

Intraplate alkaline volcanic rocks are strikingly enriched in incompatible elements and none more so than highly silica-undersaturated feldspar-free varieties, such as nephelinite and melilitite, which represent the smallest melt fractions in both continental and oceanic environments. These rock types are, however, less common in oceanic than continental environments and occur in a more limited range of tectonic settings (Chapter 2). Furthermore, the variety of rock types found, and the range of incompatible-element concentrations and isotopic compositions observed, is significantly smaller in oceanic provinces than in their continental equivalents.

Ocean island magmas are commonly believed to be derived from the asthenosphere (and, possibly, the oceanic lithosphere) and also to be uncomplicated by direct involvement of continental lithosphere in magma generation. Oceanic nephelinites (OIN) are found only in areas of old oceanic lithosphere (Chapter 2). While enough time may have elapsed, since its formation, for the local lithosphere to have become enriched by upwardly-percolating metasomatising fluids or asthenosphere-derived small melt fractions (Chapter 1), it is equally possible that the oceanic lithosphere is as depleted in LILE as the MORB source and that OIN (along with OIB in general) are derived mainly from the asthenosphere. In order to obtain information about the mineralogy and composition of asthenospheric sources, unclouded by the possible effects of input from enriched continental lithosphere, the discussion in Chapter 4 will be restricted to the trace-element characteristics of oceanic nephelinites and melilitites. Data for the equivalent continental volcanics will be presented in Chapter 5.

It is now well established that the MORB and OIB sources undergo considerable cross-contamination (e.g. Saunders *et al.*, 1988; Halliday *et al.*, 1995a) and that chemical and isotopic heterogeneities exist within the OIB source, on a large scale (Hart, 1984) and on a local scale (e.g. Hoernle & Schmincke, 1993b; Davies *et al.*, 1989; Gerlach *et al.*, 1987). Isotopic evidence suggests that OIB have been generated from mixtures of sources involving mantle components that have remained isolated from the convecting asthenosphere for more than 1 Ga and a variety of mechanisms and locations for the isolation of these sources have been proposed (see Sun & McDonough (1989) for recent review). Saunders *et al.* (1988), Sun & McDonough (1989), and Weaver (1991) give compositional ranges for certain trace-element ratios which they believe to be characteristic of HIMU, EMI, and EMII isotopic components. If the source material of any of these components is more fusible than the surrounding mantle, small melt fractions, wherever they occur, may preferentially incorporate heterogeneities in the mantle source and, therefore, carry a diagnostic trace-element signature even though larger melt fractions in the same volcanic complex do not.

Various lines of evidence presented in Chapter 3 were taken to indicate that most highly undersaturated oceanic magmas involve carbonate liquid precursors to more voluminous silicate melting. It was also suggested that many of the magmas were generated from sources containing potassic phases which may have been residual in the melting process or rapidly consumed in the early stages of partial melting. On the basis of the mineralogy of continental mantle xenoliths, and the results of experimental studies, phlogopite and amphibole have been suggested as possible candidates (e.g. Kay & Gast, 1973; Clague & Frey, 1982). In Chapter 3 (Section 3.5), low average K_2O/Na_2O, which is characteristic of the oceanic and many of the continental samples, was taken to indicate amphibole in the source rather than phlogopite. Amphibole may be stabilized by hydration of clinopyroxene in a garnet or spinel lherzolite source without changing the concentration of K in the source, whereas the formation of phlogopite, in which the partition coefficient for potassium is possibly an order of magnitude higher than in amphibole, is thought to be

a consequence of source enrichment in potassium (compilation in Halliday *et al.* (1995b) gives $^{K}D_{amph}$ = 0.22 and $^{K}D_{phlog}$ = 1.5). Melting of phlogopite-bearing peridotite generates magmas with high K_2O/Na_2O (Chapter 3, Section 3.9). However certain we may be that potassic phases exist in the continental lithosphere, their possible presence in the source regions of ocean island basalts has been mentioned in passing by other authors (e.g. Sun & McDonough, 1989; Halliday *et al.*, 1992; McKenzie & O'Nions, 1995) but rarely considered in detail, and interpretations of trace-element data in terms of residual minor phases have been controversial (Beswick & Carmichael, 1978; Frey *et al.*, 1980). Greenough (1988) uses published data for both continental and oceanic provinces to address this problem but his data set is dominated by continental rocks and the ocean islands by Hawaiian data.

Recently published partition coefficients (e.g. compilations in McKenzie & O'Nions, 1995; Halliday *et al.*, 1995b) indicate that a number of trace elements (particularly Rb, Ba, and Nb) are more compatible in amphibole and phlogopite than in other common mantle minerals. Fielding's (1992) experimental results suggest that certain trace elements, notably Ba, Sr, LREE, and Pb, partition more strongly into carbonate liquids than silicate liquids (Chapter 3, Table 3-3). The behaviour of these trace elements in OIN and OIB could, therefore, provide additional evidence for the existence of potassic phases in oceanic mantle sources and the involvement of carbonate liquids in the generation of small melt fractions.

The purpose of this chapter is, therefore, to present a detailed study of trace elements which may be diagnostic in identifying the role of carbonate precursor liquids and residual potassic phases in the generation of highly undersaturated oceanic magmas, and to establish, on the basis of trace-element ratio characteristics, whether isotopically distinct mantle components such as HIMU, EMI, or EMII, might be preferentially involved in the genesis of small melt fractions.

4.2 Trace-Element Data Tables

Trace-element abundances for the 488 feldspar-free volcanic rocks selected for this study appear with the major-element data in Appendix C. Average trace-element compositions for ocean island nephelinite (OIN), continental nephelinite (CON), potassic continental rocks from the Western Rift (Uganda) and New South Wales (SE Australia), and olivine-poor continental nephelinite are given in Appendix Tables E-6 to E-9, respectively. Each of these tables gives averages by island, volcanic complex, or province, as appropriate, and an overall average for the subset of data. Table E-10 of Appendix E presents averages for all the islands represented in the OIB data base. Average trace-element compositions for OIN, OIB, and CON are summarised in Table 4-1 below.

Table 4-1. Summary of Average Trace-Element Compositions

	OIN Average of 169 analyses In brackets - av of 13 islands	OIB Average of 904 analyses In brackets - av of 39 islands	CON Average of 215 analyses In brackets - av of 37 groups
Incompatible trace elements (ppm)			
Rb	31 (39)	29 (30)	54 (51)
Ba	816 (783)	479 (479)	1189 (1208)
Th	7.4 (9.3)	5.3 (5.6)	12.7 (12.7)
Nb	70 (80)	52 (53)	112 (110)
K	8,800 (11,208)	9,796 (10,294)	15,193 (15,276)
La	57 (72)	45 (49)	102 (101)
Ce	110 (140)	89 (96)	196 (194)
Pb	3.5 (4.2)	3.1 (3.4)	7.2 (7.0)
Sr	949 (1031)	717 (764))	1485 (1397)
P	3,404 (4,146)	2,662 (2,924)	4,451 (4,539)
Nd	52 (63)	44 (47)	83 (83)
Zr	247 (294)	255 (276)	337 (333)
Ti	18,465 (19,963)	17,625 (18,525)	18,585 (18,165)
Y	28 (30)	29 (30)	32 (31)
Compatible trace elements (ppm)			
V	308 (300)	277 (277)	300 (290)
Sc	21 (22)	24 (23)	21 (21)
Cr	516 (479)	329 (321)	317 (394)
Ni	350 (296)	191 (188)	201 (228)
Cu	79 (70)	65 (62)	110 (101)
Zn	111 (117)	109 (115)	112 (112)

4.3 Incompatible-Element Characteristics of OIN and OIB

Mantle-normalised incompatible-element concentrations for feldspar-free volcanic rocks from continental provinces (excluding olivine-poor and potassic suites) and oceanic islands are shown in Figure 4-1a. The range of average compositions in the oceanic data is completely overlapped by the range of data from continental provinces but many continental feldspar-free volcanic suites are evidently more highly enriched in incompatible elements. These may represent either smaller melt fractions, or more evolved magmas, or they may have been derived from enriched sources which are, possibly, unavailable in the source regions of the oceanic types. It seems unlikely that very small melt fractions would be erupted more commonly in continental regions than in the ocean basins and there is no generally observed tendency towards more extreme silica-undersaturation on the continents which would support such a conclusion. Sample screening (MgO > 4 wt.%) has excluded all highly evolved rocks from both data groups and, furthermore, the primary magma calculations presented in Chapter 3 suggest that continental and oceanic nephelinites have experienced similar amounts of crystal fractionation. Isotopic ratios, however, strongly indicate the involvement of old enriched sources in some continental magmatism and, as suggested in Chapter 1, the continental lithosphere is the obvious candidate for the source of this enriched mantle material.

Notwithstanding the isotopic and trace-element evidence for the involvement of enriched mantle material in the generation of some continental feldspar-free rocks the mantle-normalised incompatible-element patterns of average oceanic and continental compositions are remarkably similar (Fig. 4-1b). This suggests that the incompatible-element profile of magmas in both environments is dominated by a common source composition and it seems reasonable to conclude that the common source for both continental and oceanic highly undersaturated magmas lies in the asthenosphere. The mantle sources of the continental magmas are considered further in Chapter 5.

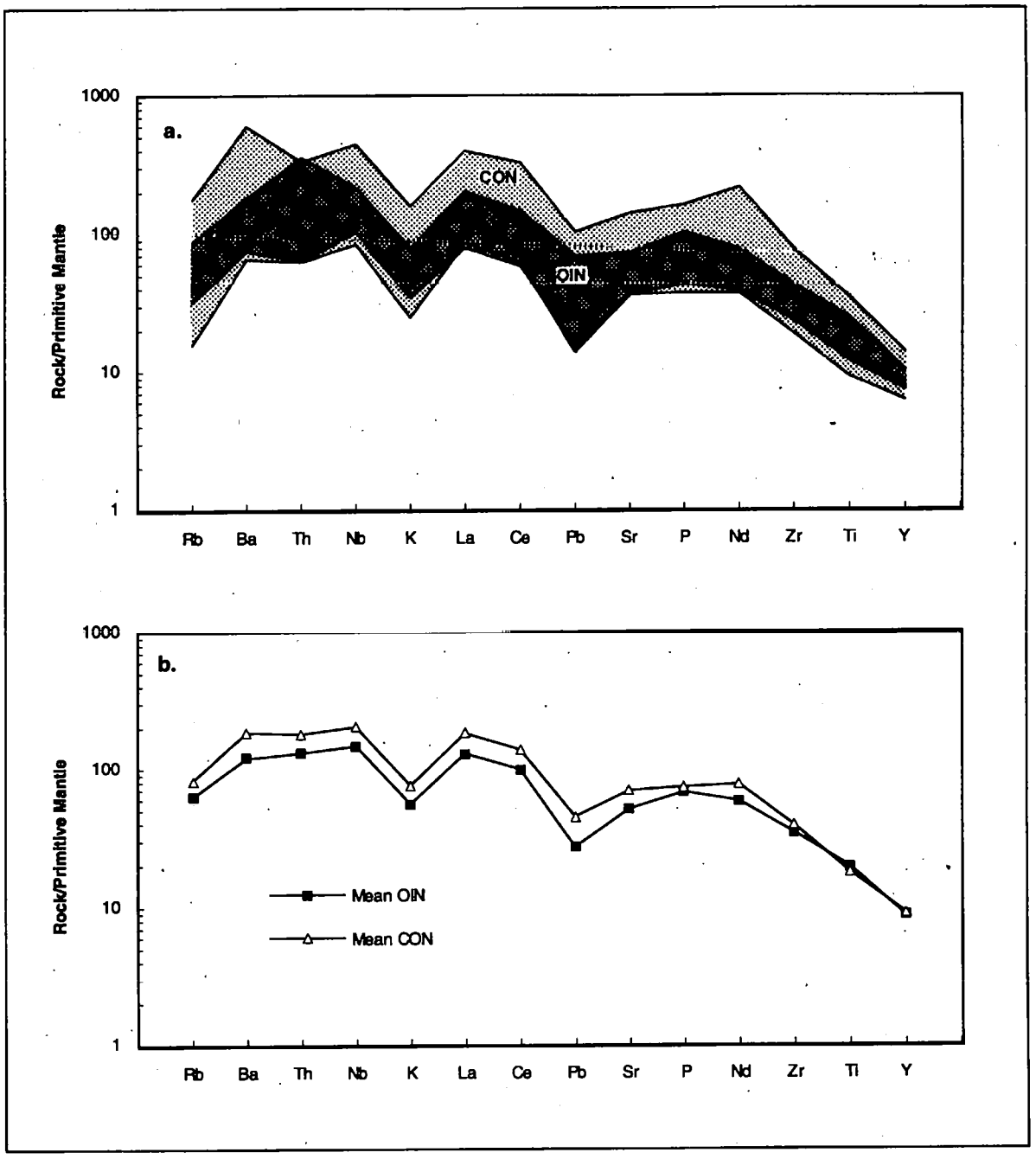

Figure 4-1. Incompatible-element concentrations of feldspar-free volcanic rocks normalised to primitive mantle values (McKenzie & O'Nions, 1995)

a. Range of continental averages (CON) compared with range of ocean island averages (OIN)
b. Mean OIN compared with mean CON (data from Table 4-1)

If an average ocean island nephelinite (OIN) composition has a similar mantle-normalised incompatible trace-element pattern to an average continental nephelinite (CON) composition (Fig. 4-1b), despite the possible involvement of enriched continental lithosphere in the continental magmas, it would be surprising if average OIN and average OIB (Table 4-1) were significantly different from each other. Figure 4-2a shows that the normalised abundances of average OIB and OIN are indeed very similar but OIN, as would be expected, is somewhat more enriched. OIB are generally considered to be generated from a mantle assemblage containing olivine, orthopyroxene, clinopyroxene, and garnet and/or spinel (e.g. Feigenson *et al.,* 1983). When the entire OIB and OIN data sets are plotted on Ce/Y *versus* Zr/Nb diagrams on which melting curves calculated for primitive and depleted lherzolite compositions are superimposed (Figs. 3a & b), it seems that, in terms of these elements, most OIB and OIN are indeed generated from this source mineralogy. Feldspar-free samples appear to represent magmas derived from primitive lherzolite but the data fall on trends lying almost parallel to the y-axis and cross-cutting the partial melting vectors. This suggests that many of the magmas are generated at depths equivalent to the garnet-spinel transition zone.

The order of elements in Figure 4-2a is of decreasing incompatibility from left to right for magmas derived from a garnet-spinel lherzolite source. A striking feature in the patterns of both OIB and OIN, therefore, is the low normalised abundance of Rb, K, and Pb. These anomalies may be a consequence of the source having been previously depleted in Rb, K, and Pb, or of the retention of these elements in residual phases during partial melting, or they may be due to the mobility of LFSE in secondary processes such as alteration, or, indeed, any combination of these processes. The differences between average OIB and OIN become clearer on an OIB-normalised diagram (Fig. 4-2b). OIN are evidently more enriched than OIB in all incompatible elements but, relative to OIB, OIN are not as enriched in Rb, K, and Pb, as other incompatible elements. Even in a previously depleted source, Rb, K, and Pb, would be expected to behave as other incompatible elements and, therefore, the predicted pattern for average OIN, normalised to OIB, would be linear and approximately parallel to the OIB line. The differences between OIB and OIN

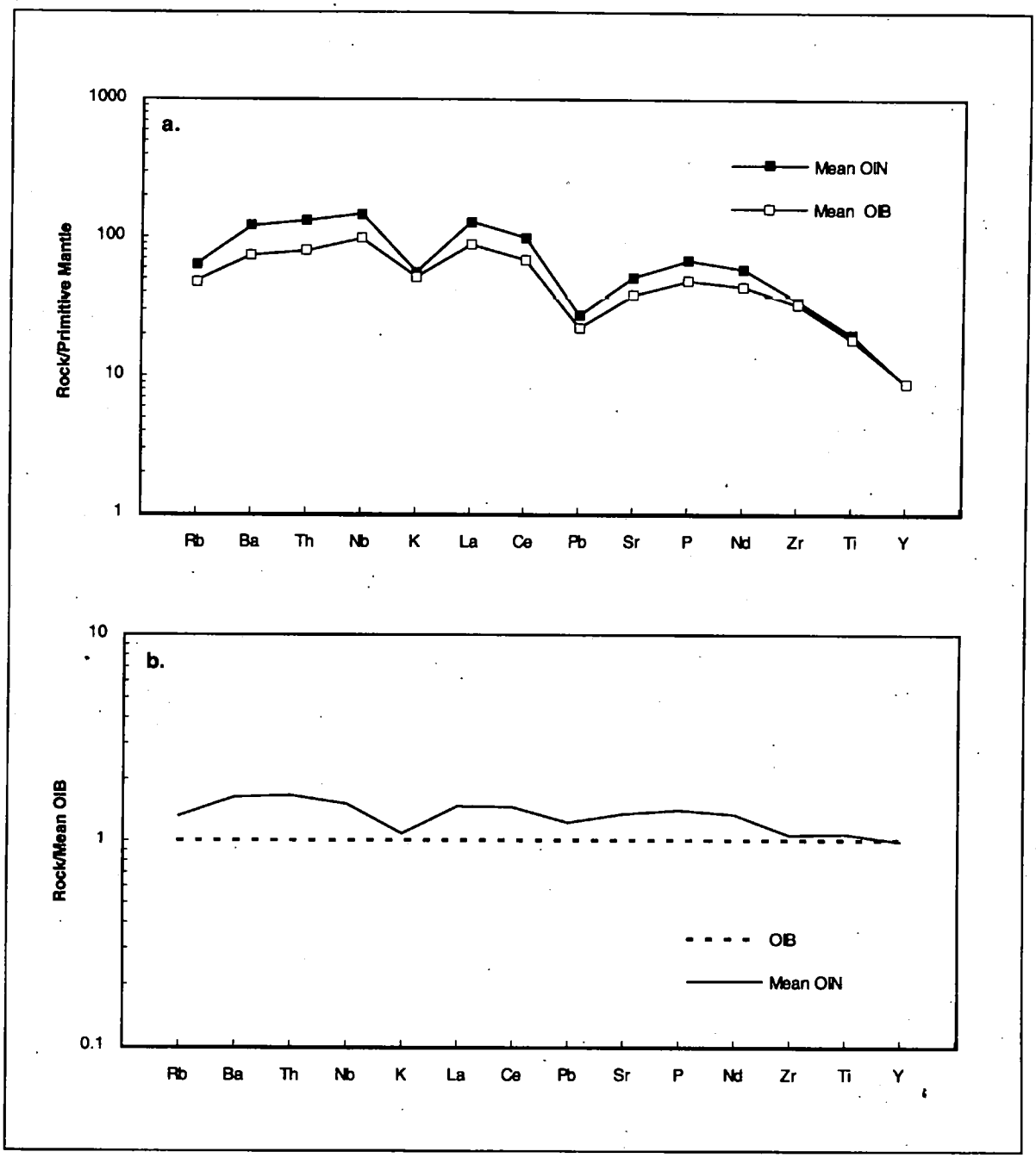

Figure 4-2. Ocean Island incompatible-element concentrations (OIN and OIB) normalised to

a. Primitive mantle values (McKenzie & O'Nions, 1995)
b. Calculated Mean OIB composition (Table 4-1)

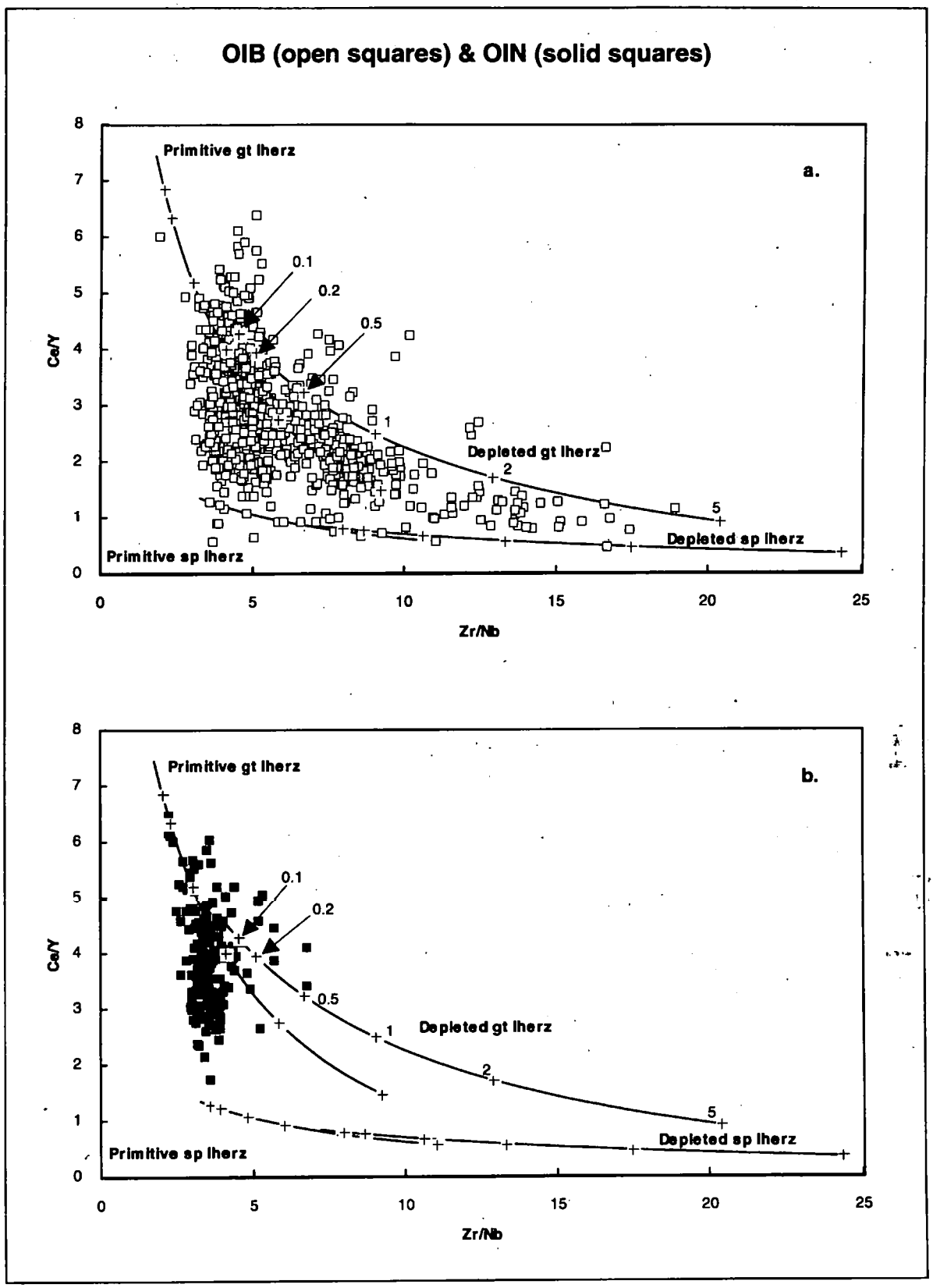

Figure 4-3. OIB and OIN shown against model melting curves of primitive and depleted garnet and spinel lherzolites. Cross symbols on melting curves refer to degrees of partial melting from 0.1% to 5% as shown on the curve for depleted garnet lherzolite. Model curves were calculated using the non-modal batch melting equation of Shaw (1970) $C_l/C_0 = 1/(D+F-PF)$. Source mineralogy, primitive and depleted source concentrations, and partition coefficients, are taken from compilations in McKenzie & O'Nions (1991) and McKenzie & O'Nions (1995).

must, therefore, be attributable to a process which has a greater effect on the composition of OIN than OIB. It was proposed in Chapter 3 that alteration is unlikely to affect OIN more than OIB. If this is so, there remains only the possibility that potassic phases are residual in the mantle source of OIN and, therefore, that these have been consumed before the degrees of melting appropriate to many OIB have been reached. In this case, the anomalously low concentrations of Rb, K, and Pb, shown in mantle-normalised OIB and OIN (Fig. 2a) may be a source characteristic on which the consequences of secondary effects, such as residual potassic phases and/or post-eruption LFSE mobility, have been superimposed. Large-scale Rb-, K-, and Pb-depletion in the upper mantle may be a consequence of major differentiation processes such as crust extraction (e.g. Sun & McDonough, 1989; McKenzie & O'Nions, 1995).

The similarity in incompatible-element composition between feldspar-free volcanic rocks and larger melt fractions from the same islands is shown in the series of mantle-normalised and OIB-normalised diagrams which form Figures 4-4 to 4-8. All the ocean islands on which feldspar-free volcanic rocks occur are represented in these diagrams except Ambitle (Tanga and Feni Islands, off the coast of New Ireland, SW Pacific). The incompatible trace-element pattern of the highly undersaturated rocks from Ambitle is so different from that of other ocean islands (being enriched in Rb, K, Pb, and Sr, and highly depleted in all other incompatible elements, particularly Nb) that a substantially different source is indicated. New Ireland is an island arc but the Tanga and Feni Islands themselves are not part of an arc system (Chapter 2). However, the mantle sources of the magmas may well have been extensively modified by subduction processes associated with the long history of complex arc systems in that part of the Pacific Ocean. The samples from Ambitle have not, therefore, been considered further in this chapter.

The deficiency in Rb, K, and Pb in both OIN and OIB, by comparison with other incompatible elements, is apparent in most of the mantle-normalised examples illustrated in Figures 4-4 to 4-8 and in a number of cases, for example Principe (Fig. 4-4c), Ponape (Fig. 4-5c), and Kauai (Fig. 4-6a), the normalised concentrations of these elements

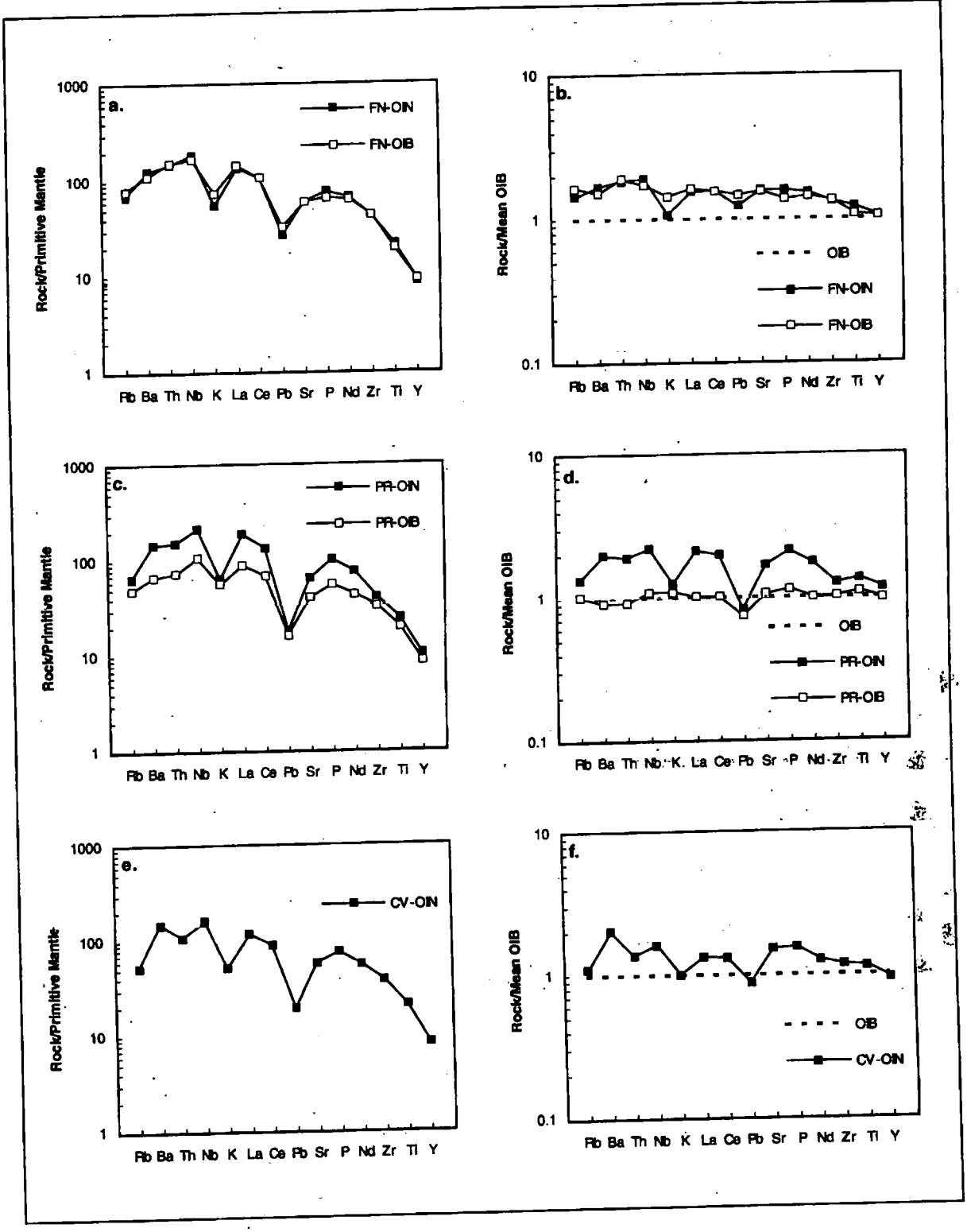

Figure 4-4. Ocean Island incompatible-element concentrations (OIN and OIB) normalised to primitive mantle values (McKenzie & O'Nions, 1995) and a calculated Mean OIB composition (Table 4-1) for

Central Atlantic Islands
a. & b. Fernando de Noronha (FN)
c. & d. Principe (PR)
e. & f. Cape Verde (CV)

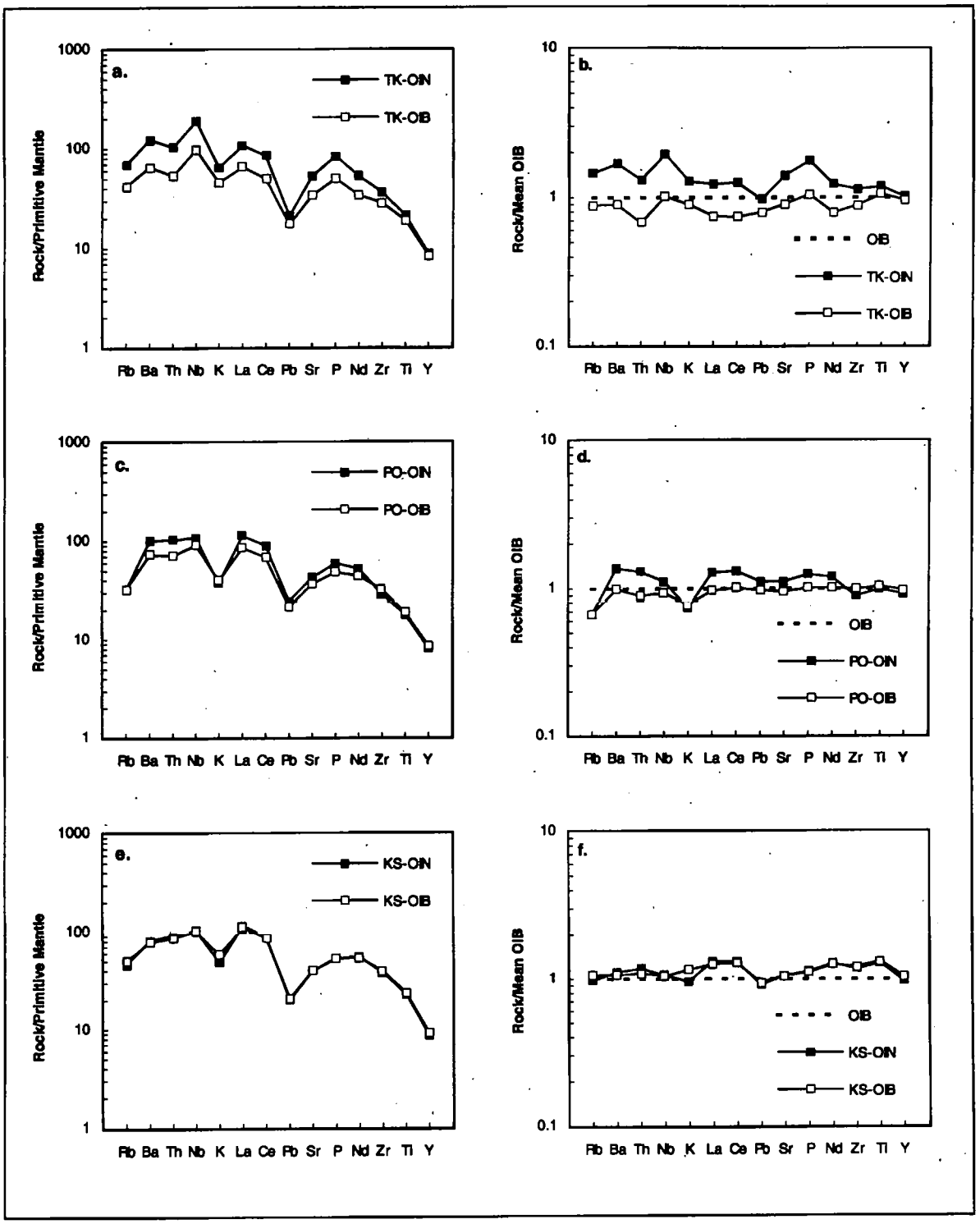

Figure 4-5. Ocean Island incompatible-element concentrations (OIN and OIB) normalised to primitive mantle values (McKenzie & O'Nions, 1995) and a calculated Mean OIB composition (Table 4-1) for

Caroline Islands, W Pacific.
a. & b. Truk (TK)
c. & d. Ponape (PO)
e. & f. Kusaie (KS)
Truk is the oldest and most westerly island. Kusaie is the youngest and most easterly.

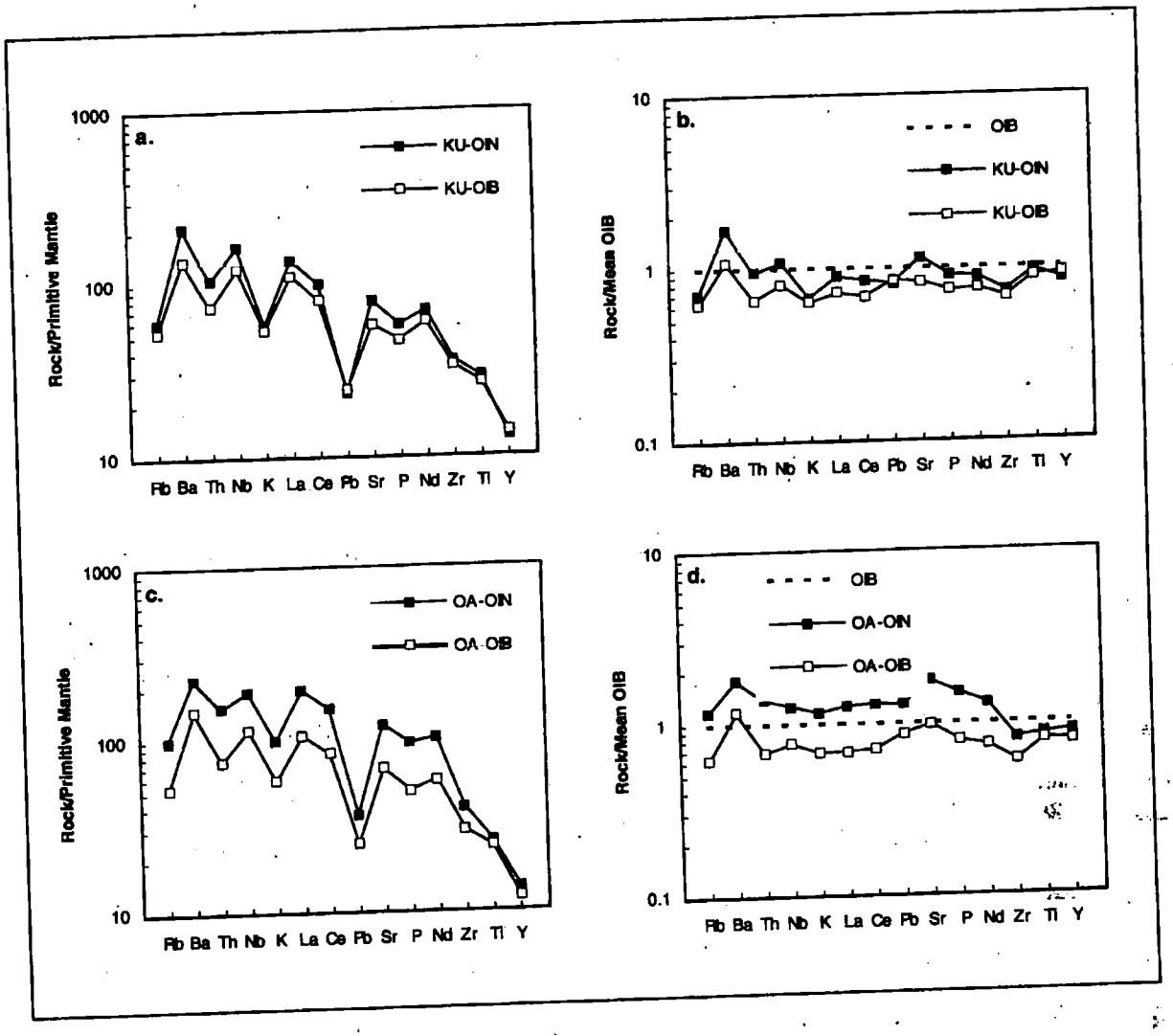

Figure 4-6. Ocean Island incompatible-element concentrations (OIN and OIB) normalised to primitive mantle values (McKenzie & O'Nions, 1995) and a calculated Mean OIB composition (Table 4-1) for

Hawaiian Islands.
a. & b. Kauai (KU)
c. & d. Oahu (OA)

in OIN are barely distinguishable from those of OIB from the same islands. In two instances, Fernando de Noronha (Fig. 4-4a) and Kusaie (Fig. 4-5e), the smaller melt fractions actually have lower concentrations of K than the larger melt fractions. OIB-normalised diagrams for Principe (Fig. 4-4d), Ponape (Fig. 4-5d), Kauai (Fig. 4-6b), Grande Comore (Fig. 4-7b), and Moheli (Fig. 4-7d), illustrate well the anomalous behaviour of Rb, Pb, and particularly K, in OIN compared with OIB from the same islands. However, not all islands follow this pattern. For example, Rb, Pb, and K for Truk (Fig. 4-5b), Oahu (Fig. 4-6d), and Samoa (Fig. 4-8b), appear to behave incompatibly in both small and large melt fractions. Samoa and Aitutaki (Cook Islands) are both within the DUPAL region of the SW Pacific but have noticeably different patterns. Samoa is strongly enriched in Rb and K relative to Ba (Fig. 4-8b) while Aitutaki (Fig. 4-8d) mimics the depletion in these elements characteristic of most other islands but shows a marked enrichment in Th and Pb, and depletion in Nb relative to La, giving a pattern similar to that of the nephelinite samples from the alkaline province around the Sea of Japan (Fig. 4-8f). Nb depletion is a characteristic of island arc magmas. The highly undersaturated samples from Aitutaki and Japan may, therefore, represent magmas that have incorporated subduction-modified mantle material. Since these samples are not typical of OIN or OIB from other islands, intraplate ocean island magmatism may, in general, be free of significant contributions from a subduction-modified source. Alternatively, modified mantle may be so efficiently mixed into the asthenosphere by convection that the potential for the chemical signature to appear in trace-element profiles of most ocean island magmas is lost.

The overall similarity of the normalised patterns shown in Figures 4-4 to 4-8 suggests that the majority of oceanic feldspar-free rocks are derived from very similar sources and may, in many cases, be derived from the same source, or mixture of sources, as larger degrees of melting in the same volcanic complex. However, as already mentioned, the characteristic anomalies shown by K, Rb, and Pb, could be attributed to a number of processes and, given the possible role of potassic phases in the sources of OIN (Chapter 3), it is important to establish whether secondary processes have had any effect on the

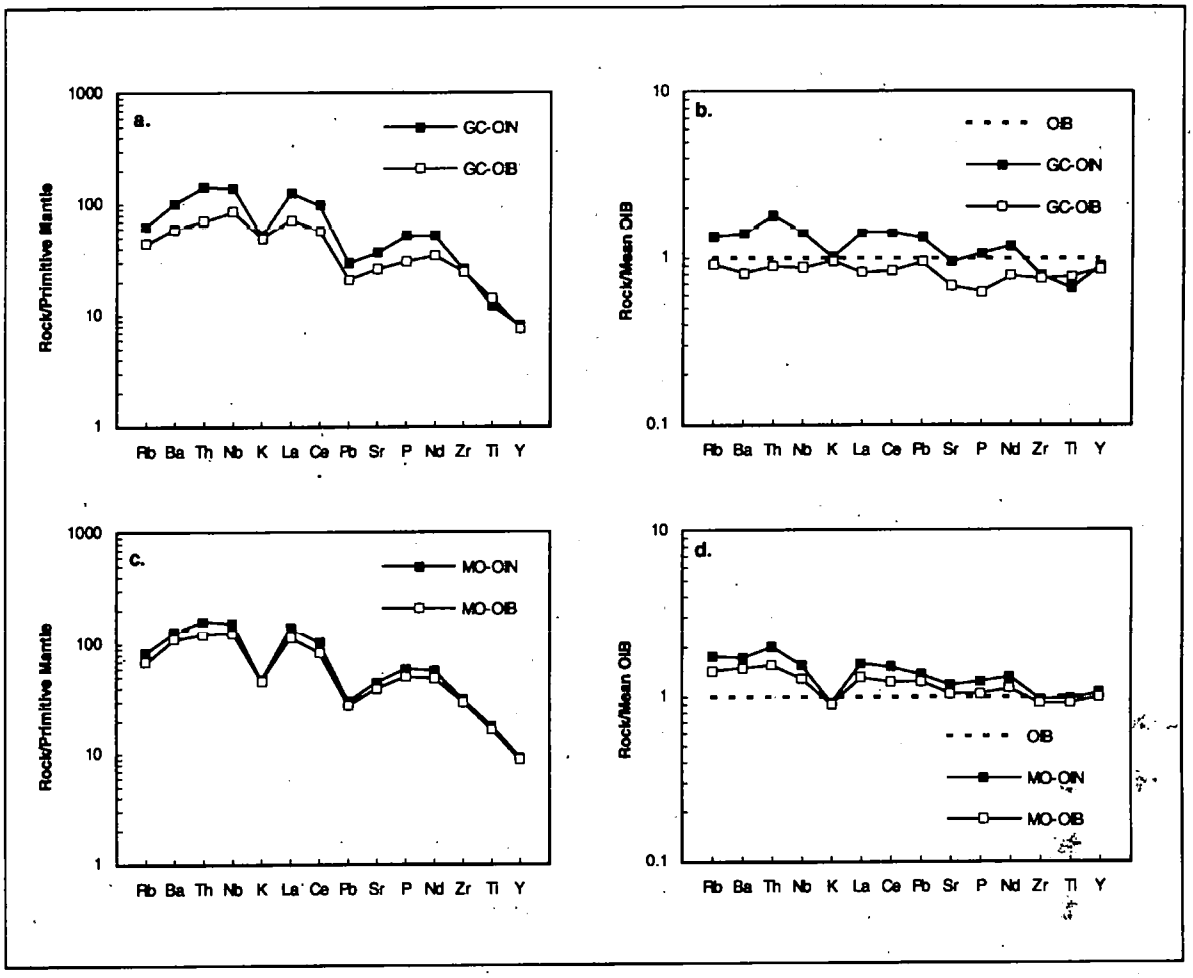

Figure 4-7. Ocean Island incompatible-element concentrations (OIN and OIB) normalised to primitive mantle values (McKenzie & O'Nions, 1995) and a calculated Mean OIB composition (Table 4-1) for

Comores Islands.
a. & b. Grand Comore (GC)
c. & d. Moheli (MO)
Grand Comore is the youngest and most westerly of the Comores Islands.

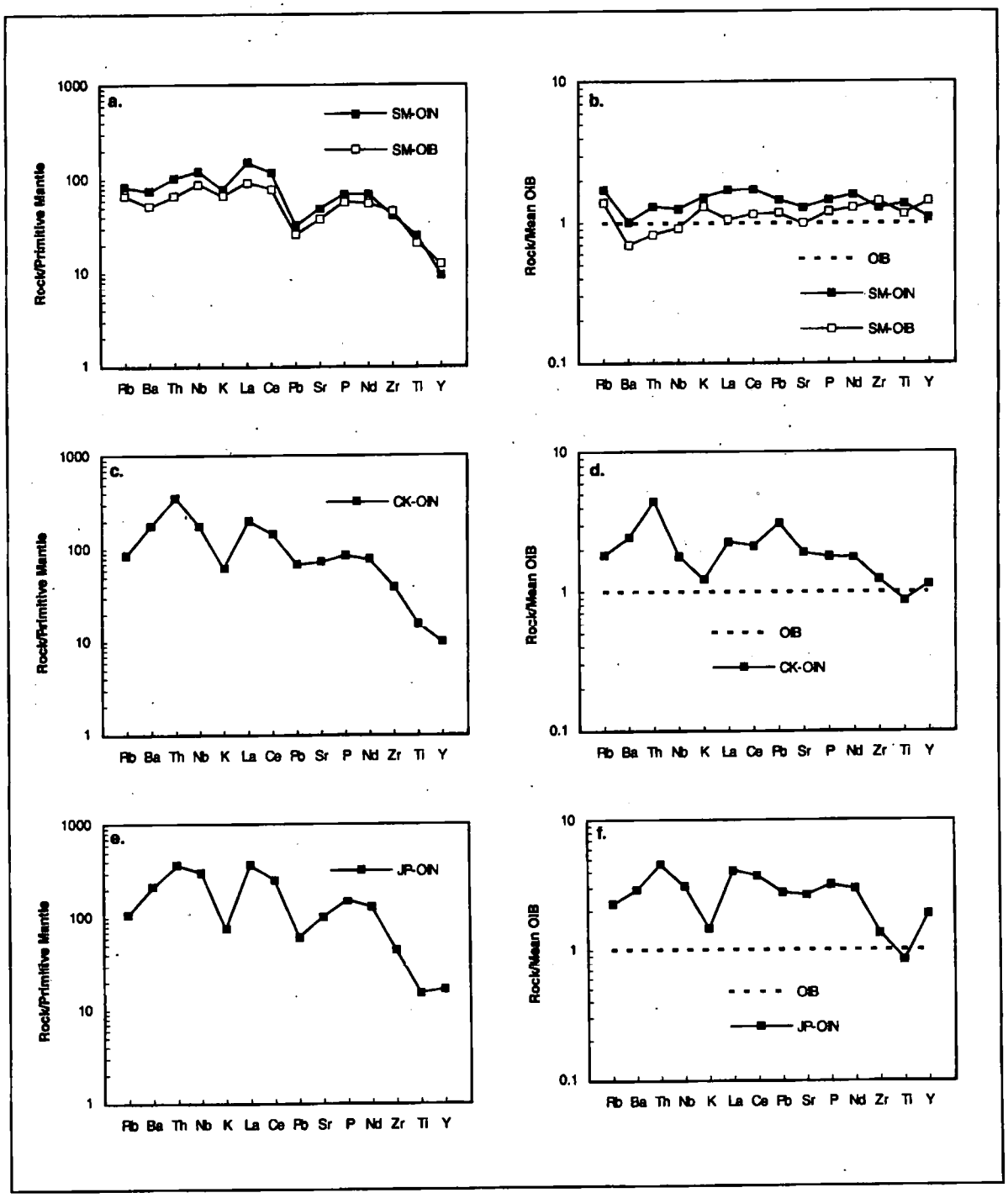

Figure 4-8. Ocean Island incompatible-element concentrations (OIN and OIB) normalised to primitive mantle values (McKenzie & O'Nions, 1995) and a calculated Mean OIB composition (Table 4-1) for

Pacific DUPAL Islands and Sea of Japan.
a. & b. Upolo, Samoa (SM)
c. & d. Aitutaki, Cook Islands (CK)
e. & f. Nagahama, Honshu, Japan (JP)

observed concentrations and the extent to which trace-element mobility may negate models of source composition and evolution based on these elements.

4.4 Incompatible-Element Mobility in OIN and OIB

Clague & Frey (1982) expressed concern that much of the scatter shown in diagrams involving LFSE (K, Rb, Sr, and Ba) reflects susceptibility to secondary, post-eruption processes such as volatile loss during cooling and tropical weathering. Alkali loss during and immediately after eruption is difficult to detect after the event and, therefore, impossible to quantify. Clague & Frey (1982), however, demonstrated that Rb depletion correlated positively with volatile content and alteration of glass in the matrices of tholeiitic rocks and, therefore, that LFSE were unreliable indicators of source mineralogy and composition.

If Rb and K loss are responsible for the anomalies shown in Figures 4-2a & b then it affects both OIN and OIB and, possibly, OIN to a greater extent than OIB. Assuming K to be as incompatible as Nb during melting of anhydrous mantle lherzolite, it is possible to estimate the loss of K required to produce the observed anomaly in Figure 4-2a. This is approximately 45% K-loss from mean OIB and 60% from mean OIN. These figures indicate substantial mobility of K and other LFSE in secondary processes. If it is assumed that OIB and OIN are derived from depleted sources and that mean OIB is essentially unaffected by LFSE mobility, then the preferential loss of K from mean OIN (estimated from Fig. 4-2b) is about 30%. Highly undersaturated rocks, by virtue of their mineralogy, may be more susceptible to alteration and mobility of LFSE than OIB but there is no general inverse correlation between volatile content (as represented by LOI) and Rb/HFSE or K/HFSE which would support this. A more detailed survey of individual islands within the global OIB data base for which sufficient samples are present to establish trends and identify scatter has, therefore, been used to investigate the mobility of

K, Rb, Ba, and Sr, in OIN and OIB. These elements have been plotted against Nb which is a HFSE and immobile in secondary alteration processes.

OIB and OIN for the Hawaiian islands are shown for K *versus* Nb, Rb *versus* Nb, Ba *versus* Nb, and Sr *versus* Nb, in Figure 4-9. These diagrams show that most of the data fall on well-defined trends passing through, or close to, the origin. The tendency for Rb and K to intercept the Nb axis is presumably a result of the loss of these elements from groundmass glass in the tholeiitic rocks as deduced by Clague & Frey (1982). Such loss does not appear to apply to most of the Hawaiian data. However, the cloud of points that lies below the trend on the Rb *versus* Nb and K *versus* Nb diagrams represents, almost exclusively, highly undersaturated rocks from Oahu and Kauai. These are the two oldest Hawaiian islands for which data have been obtained and the samples may have lost alkalies simply by being subjected to weathering for a longer time. Less undersaturated samples from these same islands, however, lie on, or close to, the main trend even though they have LOI in the same range as the highly undersaturated rocks. This suggests that low Rb and K in the nephelinites and melilitites is not a consequence of more intense mobilisation of alkalies resulting from post-eruptive alteration, although preferential loss of volatiles from the cooling magmas during, or soon after, eruption cannot be discounted. The highly undersaturated magmas could, therefore, have been generated from a different source, and in the case of Oahu, this has been demonstrated isotopically by Clague & Frey (1982). Ba and Sr correlate well with Nb and there is no evidence for substantial loss of these elements from any group of samples within the Hawaiian data set.

Similar diagrams for OIB from the Mascarene islands are shown in Figure 4-10. The low-Rb and low-K clouds below the trends, in this case, consist of samples from Rodrigues which is older than Reunion but overlaps in age with Mauritius. The samples from Mauritius included in the OIB data base span the three stages of volcanic activity on the island and almost all lie on the trends. As in Figure 4-9, there is no evidence for Ba or Sr loss from the Mascarene samples so if LFSE mobility has affected the Rodrigues samples it is restricted to loss of Rb and K. The Rodrigues samples are neither highly

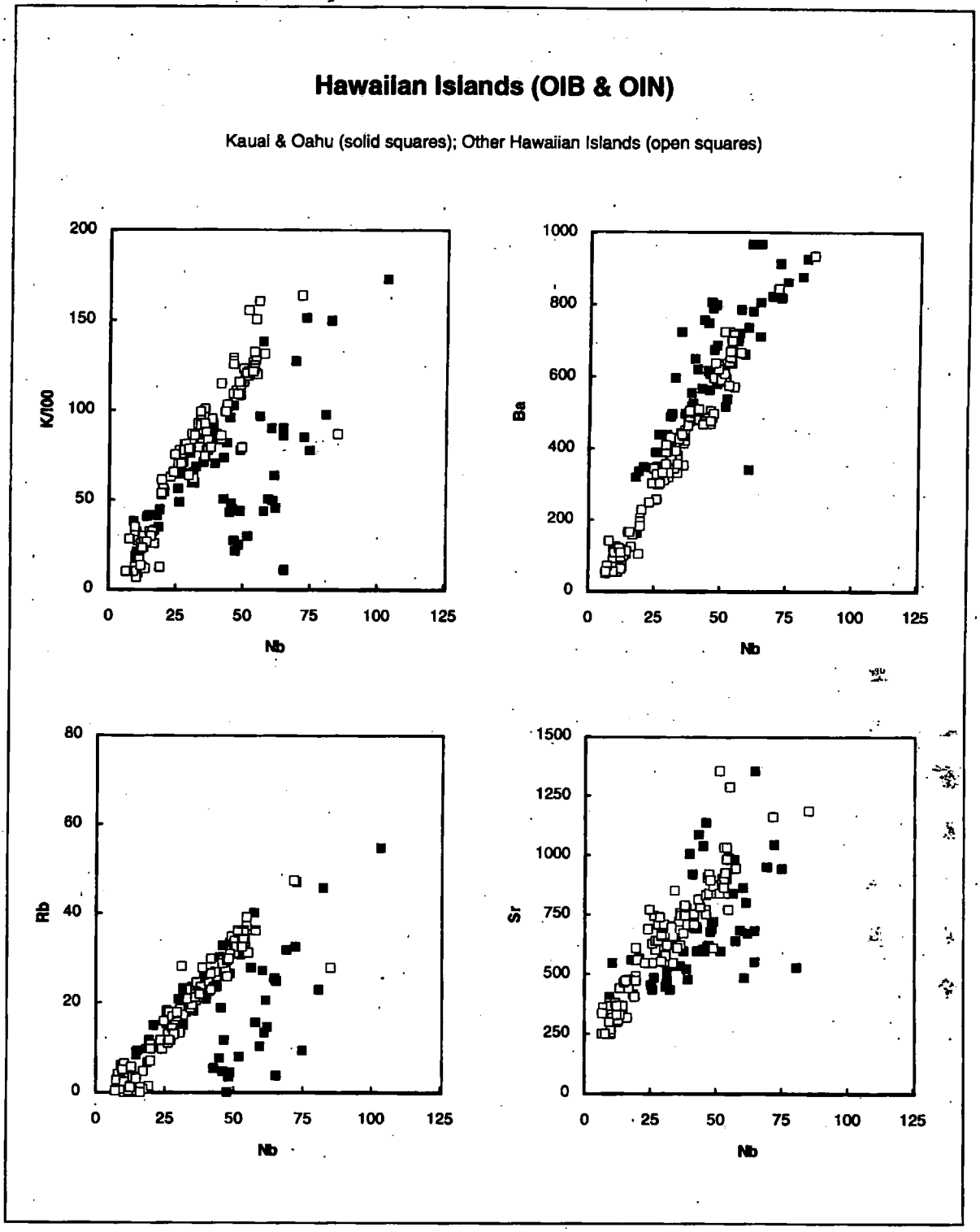

Figure 4-9. LFSE *versus* HFSE for Hawaiian Islands

Kauai and Oahu are shown by solid symbols. All other islands by open symbols. Kauai and Oahu are the only Hawaiian islands on which highly undersaturated post-erosional magmas have been erupted.

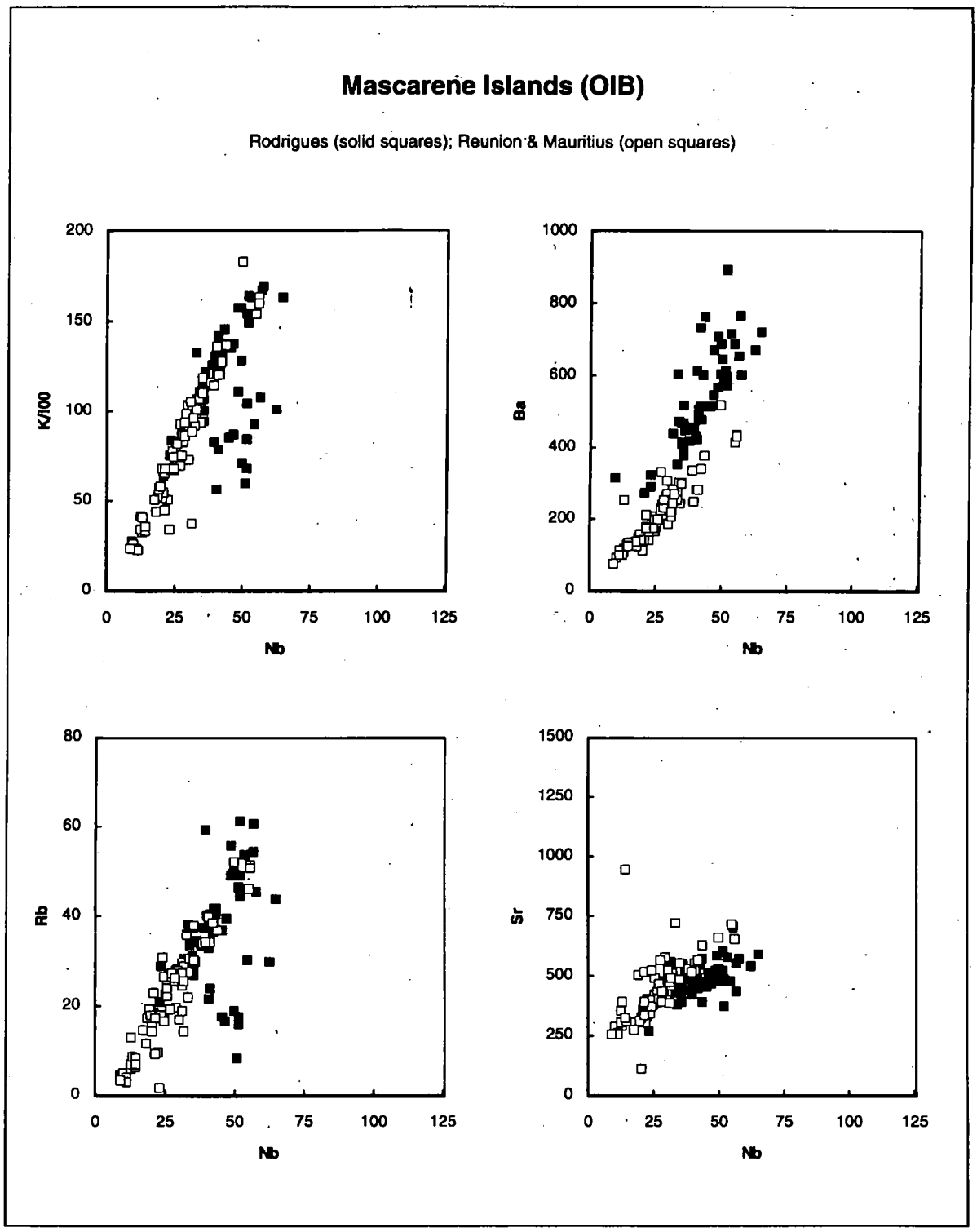

Figure 4-10. LFSE *versus* HFSE for Mascarene Islands

Rodrigues is shown by solid symbols. Mauritius and Reunion by open symbols. None of the samples from these islands which are included in the OIB data base is highly undersaturated.

undersaturated nor is there evidence that they are substantially more altered than samples from Reunion and Mauritius. It is possible, therefore, that some of the Rodrigues magmas were derived from a source with a different mineralogy or composition from the other Mascarene Islands.

A surprising feature of Figures 4-9 and 4-10 is that the gradients of the trends in Rb *versus* Nb and Ba *versus* Nb are different. The data for the Hawaiian and Mascarene Islands are shown superimposed in Figure 4-11a & b. These diagrams suggest that there are definable regional variations in Rb and Ba composition which cannot be related to degree of silica undersaturation. Furthermore, the processes of secondary alteration might be highly variable in effect and produce scatter which would tend to obscure any fundamental structure within the OIB data set. If Ba loss is not significant (Figs. 4-9 and 4-10) then the Ba/Nb differences might be due to regional variations in source mineralogy or source characteristics. If regional differences can be distinguished in Ba/Nb (Fig. 4-11b), it seems reasonable to assume that the differences in Rb/Nb (Fig. 4-11a) might also be a consequence of variation in the source characteristics or mineralogy from which the magmas were derived. In this case it is tempting to suppose that the low Rb and K in the highly undersaturated samples from Kauai and Oahu (Fig. 4-9) could be attributable to source differences rather than preferential loss of Rb and K from the highly undersaturated suites.

Rb *versus* Nb and Ba *versus* Nb for OIB and OIN are shown on Figures 4-12a & b respectively. The trends formed by OIB from the Hawaiian Islands, the Mascarene Islands, and the Gulf of Guinea Islands, are superimposed on these diagrams for reference. Figure 4-12a shows that most OIN and an appreciable number of OIB lie below the Hawaiian Rb/Nb reference line. Many OIN also lie below the Gulf of Guinea line. OIB from DUPAL islands follow the Mascarenes (high Rb/Nb) trend but samples from all other ocean islands lie below the Hawaiian trend with the exception of those from Moheli which range from low to very high Rb in both OIB and OIN. Considerable structure actually exists within the low Rb/Nb data. A detailed investigation of OIB is, however, outside the

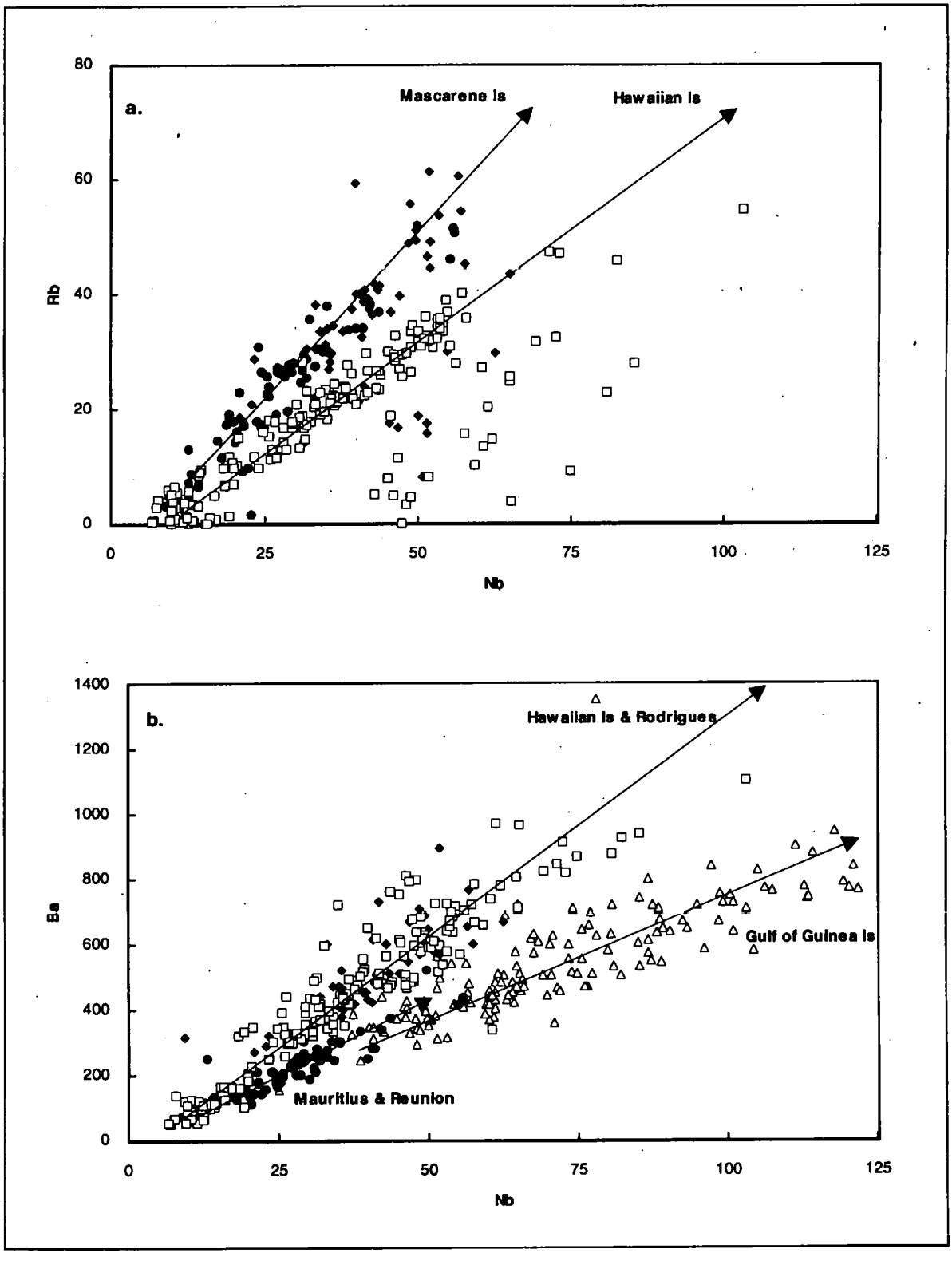

Figure 4-11. Data trends (OIB and OIN combined) from Figures 4-9 and 4-10 superimposed. Ba *versus* Nb for Gulf of Guinea Islands is added to Figure 4-11b. The Gulf of Guinea Islands are not shown on Figure 4-11a because Rb/Nb is much more variable and lies on a broad general trend at lower Rb/Nb than the Hawaiian trend.

Gulf of Guinea Islands	open triangles
Hawaiian Islands	open squares
Rodrigues	solid diamonds
Mauritius & Reunion	solid circles

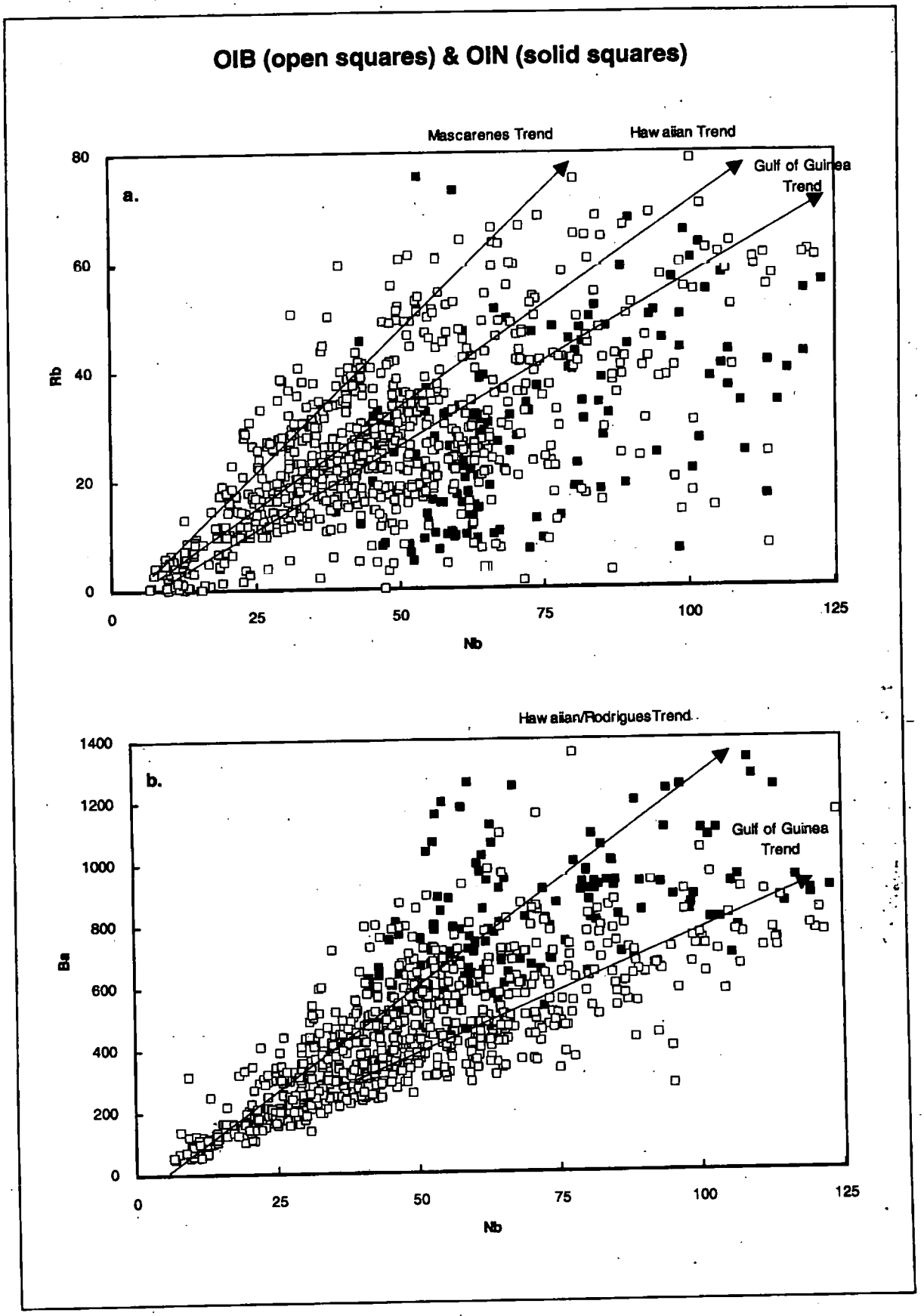

Figure 4-12. LFSE *versus* HFSE for OIB and OIN

OIN are shown by solid symbols. Trends indicate regional variations in the OIB data base which can be clearly identified (cf. Fig. 4-11).

scope of this work but it should be noted that the low Rb/Nb group includes the strongly HIMU islands (St Helena, Rurutu, and Madeira) which define significantly more shallow angled trends than the Hawaiian data. In Figure 4-12b most of the OIB and OIN samples fall between the Hawaiian and Gulf of Guinea trends. There are, however, some notable exceptions. The Kauai and Oahu nephelinite and melilitite samples deviate towards high-Ba compositions as do some highly undersaturated rocks from Cape Verde and Moheli, whereas OIB from DUPAL islands follow the Hawaiian trend closely but deviate to higher Ba compositions at higher Nb.

It appears to be extremely difficult to demonstrate conclusively that LFSE mobility has not affected LILE concentrations in OIN and OIB. It is equally difficult to show unequivocally that it has. Four lines of evidence have been presented which indicate that secondary alteration processes may not be responsible for the low Rb and K observed in most OIN and many OIB:

(i) High losses of K (up to 60%) required to account for normalised-K anomalies and a preferential loss of 30% K from OIN if OIB are assumed to be derived from depleted sources.

(ii) LFSE might be expected to be similarly affected by secondary alteration processes but there is no correlation between low Rb and low Ba in OIN.

(iii) Clear regional variations in Rb/Nb and Ba/Nb in OIB and OIN which are unrelated to degree of undersaturation and might be obscured by the levels of LFSE mobility indicated above.

(iv) No general correlation between LOI and low Rb in OIB or OIN.

While it must be accepted that each of these is largely circumstantial, taken together they do suggest that Rb and K in OIN may be indicative of regional and temporal variations in the source of the magmas rather than post-eruption LFSE mobility.

4.5 Incompatible-Element Sequences in OIN

Comparisons of incompatible element concentrations in MORB, which represent large degrees of melting and have lower abundances of incompatible elements, and OIB, which result from smaller degrees of partial melting and have higher concentrations, allow the incompatible elements to be placed sequentially according to the degree of incompatibility. In general, the order of increasing compatibility in oceanic basalts is thought to be

Rb≅Ba<Th<U≅Nb≅K<La<Ce≅Pb(<Mo)≅Sr<P≅Nd<Zr<Ti<Y

(Sun & McDonough, 1989).

The normalised incompatible-element diagrams presented in Section 4.3 suggest that Rb, K, and Pb, may be less incompatible during the partial melting events which generate OIN than is generally believed and in Section 4.4 it was concluded that this is unlikely to be attributable to the preferential loss of LFSE from the highly undersaturated rocks. In this case, it should be possible to devise an order of trace-element incompatibility appropriate to small melt fractions by comparing incompatible-element concentrations in OIN and OIB in much the same way as for MORB and OIB.

A series of histograms, in which the frequencies of trace-element ratios in the OIN data set can be compared with the frequencies of the same ratios in the OIB global data base, have been used to generate such a sequence for highly undersaturated OIN. The process used involves comparing the mode of the frequency distribution of the two data sets for each element ratio. For example, in Figure 4-13a the mode of Nb/Y distribution for OIN lies at a higher Nb/Y value than the mode for OIB. This indicates that as the degree of partial melting decreases, the concentration of Nb increases more than the concentration of Y, and suggests that Nb is more incompatible than Y. This is in agreement with Sun & McDonough's (1989) sequence and, since Nb is thought to be significantly more incompatible than Y, the distinction betweeen the modes is, as expected, very clear. Similar diagrams for Rb/Ba (Fig. 4-13b) and Rb/Nb (Fig. 4-13c), however, show that the modes of Rb/Ba and Rb/Nb are at lower Rb/Ba and Rb/Nb values in OIN than in OIB.

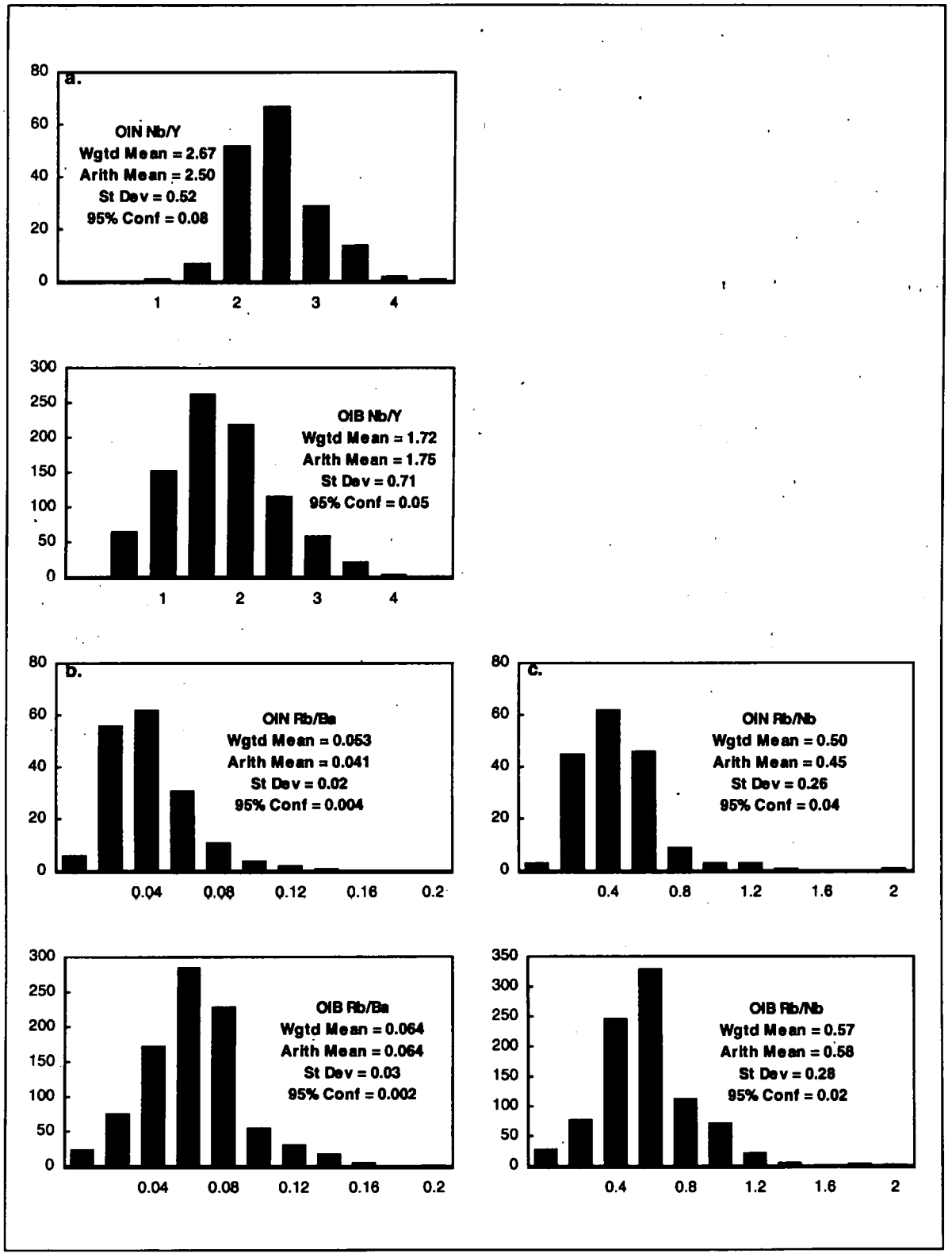

Figure 4-13. Frequency distributions of selected incompatible-element ratios in OIN and OIB.

OIN and OIB for each element ratio are shown as a pair of diagrams placed vertically for ease of comparison of the distribution modes. Horizontal scale is the value of the incompatible-element ratio; vertical scale is the frequency of occurrence.

Arith mean = arithmetic mean of all the data in the data base

Wgtd mean = an average of individual island averages

Since Rb is generally thought to be at least as incompatible as Ba and substantially more incompatible than Nb, higher modes for OIN (as seen in the OIN-OIB relationship for Nb/Y) would be expected. This suggests that Rb is actually less incompatible than both Ba and Nb. K/Nb (Fig. 4-14a) and K/Pb (Fig. 4-14b) show, with similar reasoning, that K and Nb are not, in fact, similarly incompatible and that K is less incompatible than Pb in OIN, while Figures 4-14c & d indicate that Pb itself is somewhat less incompatible than both Ce and Nd. Phosphorus, on the other hand, seems to be more incompatible than Nd (Fig. 4-15a) and also Ce, and is possibly similar to La (Fig. 4-15b). Other incompatible elements appear to retain the relative positions in the sequence given by Sun & McDonough (1989) and the numerous trace-element ratio diagrams which are required to confirm this are not, therefore, reproduced here. Despite the anomalous behaviour of some elements, Y remains the least incompatible element in the sequence.

Using incompatible-element ratio comparisons in this way it might be possible to pinpoint exactly the incompatibility of Rb, K, P, and Pb relative to the other trace elements. There is an obvious difficulty with this approach: the OIB data base is larger and more robust than the OIN data set. Each diagram shows the position of the frequency maximum and the calculated arithmetic mean of the data base. A weighted mean, which compensates for unequal sampling between islands and is the average of averages calculated for each island, is also given. In the case of OIB these figures are almost the same for all trace-element ratios but this is not so in the OIN data set which, as a consequence of the rarity of the rock type, is biased by data from only three islands. This problem is indicated in the 95% confidence intervals which are smaller for OIB than OIN. Higher standard deviations in OIB than OIN, however, reflect a greater range of partial melting represented in the OIB data base and are not a result of unequal sampling. As a consequence of the bias in the OIN data set, bimodality in the frequency patterns of some trace element ratios (e.g. Fig. 4-14d) makes interpretation difficult and tends to invalidate the use of the mode of the frequency distribution and, possibly, the arithmetic mean of the data set as an indicator of the average character of OIN. This problem is particularly acute when ratios are used in which the elements are very close in incompatibility and the modal

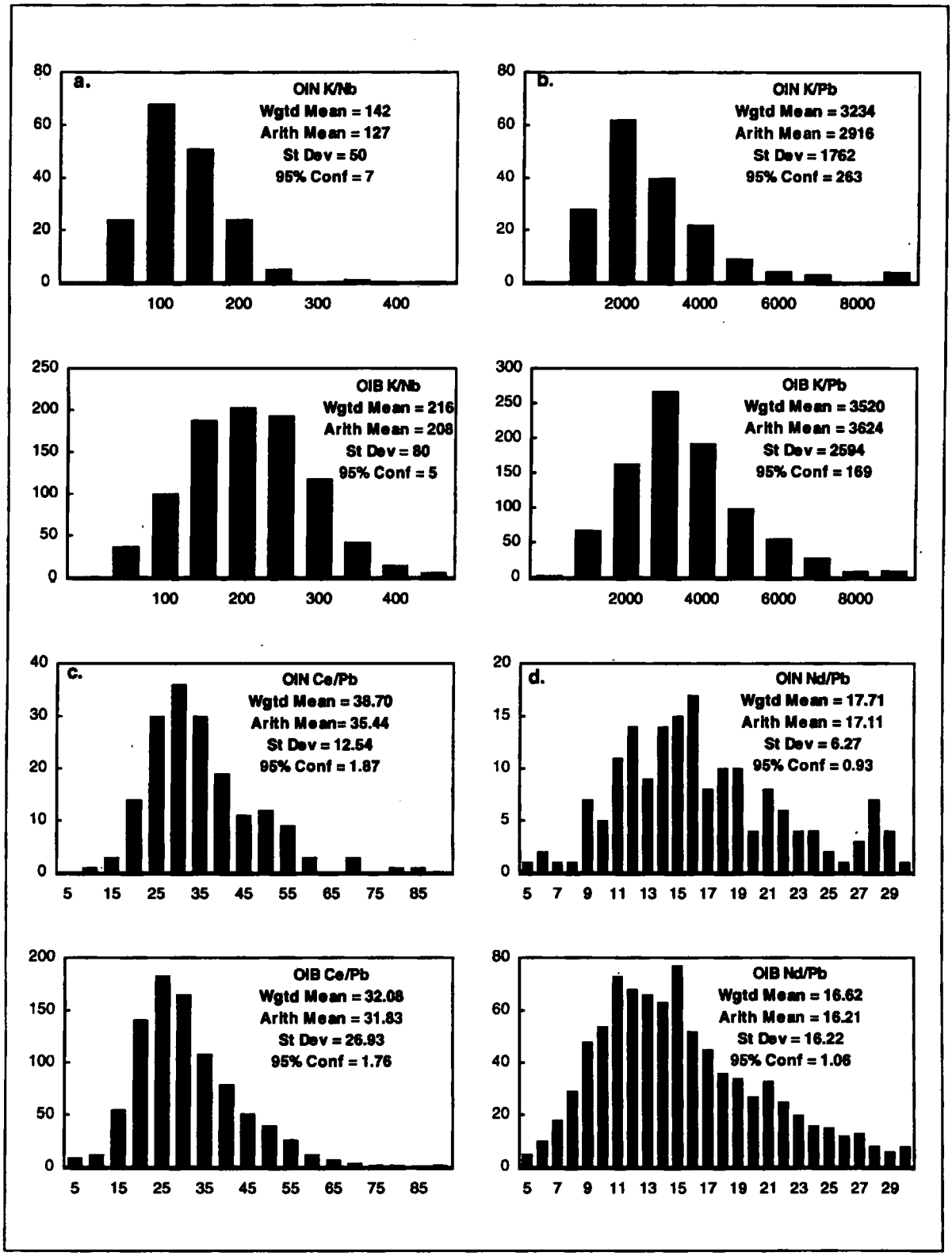

Figure 4-14. Frequency distributions of selected incompatible-element ratios in OIN and OIB. Placement of OIN and OIB pairs and scales as in Figure 4-13.
Arith mean = arithmetic mean of all the data in the data base
Wgtd mean = an average of individual island averages

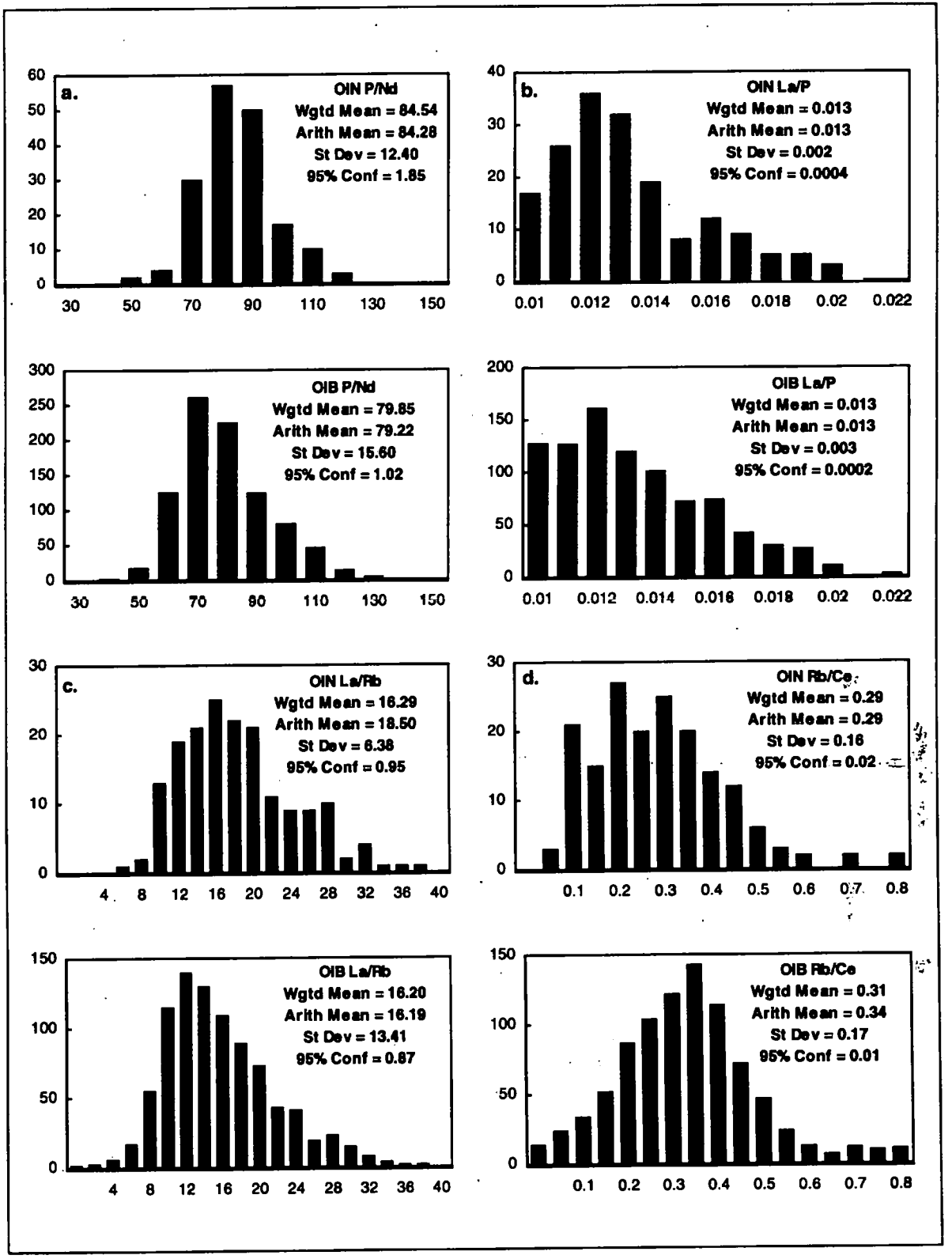

Figure 4-15. Frequency distributions of selected incompatible-element ratios in OIN and OIB. Placement of OIN and OIB pairs and scales as in Figure 4-13.
Arith mean = arithmetic mean of all the data in the data base
Wgtd mean = an average of individual island averages

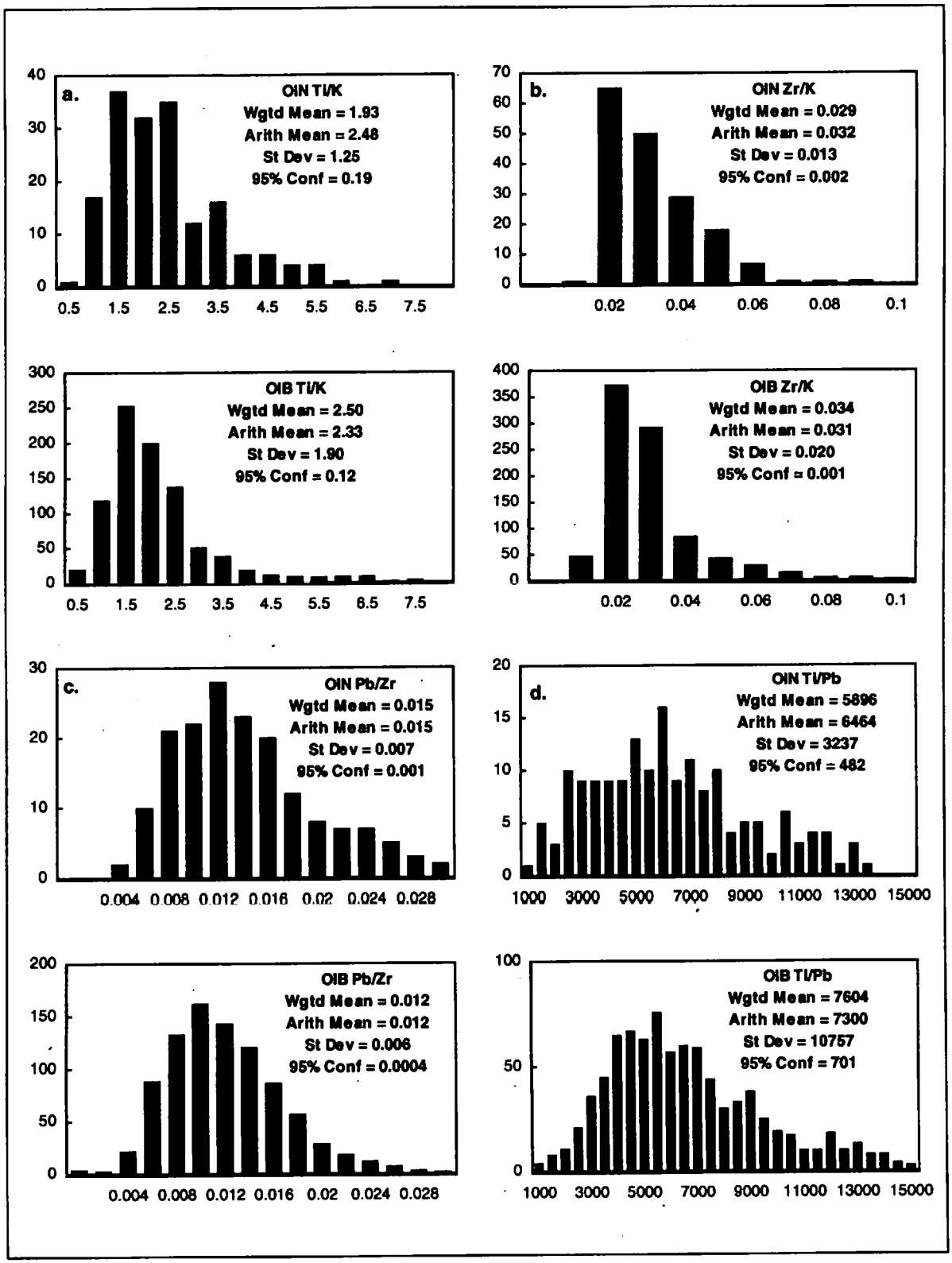

Figure 4-16. Frequency distributions of selected incompatible-element ratios in OIN and OIB. Placement of OIN and OIB pairs and scales as in Figure 4-13.
Arith mean = arithmetic mean of all the data in the data base
Wgtd mean = an average of individual island averages

differences are subtle (e.g Fig. 4-16b). In practice, therefore, the three means have been used together in assessing the relative incompatibility of particular elements. In almost all cases the conclusion is the same regardless of which mean is used. In the few ambiguous cases the weighted OIN mean is used in preference to the others.

La/Rb (Fig. 4-15c) and Rb/Ce (Fig. 4-15d) distributions suggest that the incompatibility of Rb is less than that of La and similar to the incompatiblity of Ce. From Ti/K and Zr/K (Figs. 4-16a & b) it appears that K is similar to Zr and possibly less than Ti, while Pb is more incompatible than Zr and possibly similar to Ti (Figs. 16c & d). In conclusion then the trace-element compatibility order for highly undersaturated magmas appears to be

$$Ba<Th<Nb<La\equiv P<Rb\equiv Ce<Nd<Pb\equiv Ti<Zr\equiv K<Y$$

The distinctions are subtle but the sequence has an overall similarity to that derived from consideration of MORB and OIB (cf. sequence from Sun & McDonough, 1989 shown on page 107) with the important exception that Rb, K and, to a lesser extent Pb, appear to behave more compatibly during the smaller degrees of partial melting considered here and P more incompatibly.

In Section 4.3 it was suggested that the Rb, K, and Pb, anomalies in the normalised incompatible trace-element profiles of OIB and OIN could be due to source depletion by large-scale mantle differentiation processes such as extraction of the continental crust, to retention in residual mantle phases during partial melting, to loss of these elements in secondary alteration processes, or to a combination of these processes. The evidence presented in Section 4.4 indicates that LFSE mobility has not significantly affected OIB in general and that there is no convincing reason to assume that OIN have preferentially lost alkalies. As a result two related possibilities can be considered. Firstly, that Rb, K, and Pb, anomalies indicate increased compatibility of these elements due to the presence of potassic phases in the source of both OIN and OIB. In which case, in order to account for the lower concentratons of these elements in OIN than in OIB from the same island, K and Rb would have to be retained in the source more efficiently at the degrees of

partial melting relevant to OIN. And secondly, that sources of OIB and OIN may have been depleted in incompatible trace elements by continental crust extraction and the small remaining differences between OIB and OIN may be due to the effects of residual potassic phases in the source of OIN which have, in general, been consumed before the degrees of melting appropriate to most OIB have been reached. However, it is also conceivable that OIB and OIN are dominated by a component derived from subducted oceanic crust which has been depleted in K, Rb, and Pb, by slab-dewatering processes during subduction. If this component is more fusible than the surrounding mantle material it will be preferentially incorporated in small melt fractions giving lower abundances of K, Rb, and Pb, in OIN.

The position of P in the sequence shown above suggests an additional factor needs to be considered: that some incompatible trace elements have been preferentially enriched in OIN magmas. Phosphorus partitions strongly into carbonate liquids ($^{L_s/L_c}D_P$ = 0.2; Table 3-3, Chapter 3). The elevation of P in the sequence may indicate, therefore, that OIN, and possibly some OIB, are carbonate-silicate liquid mixtures. In this case, the concentrations of trace elements which partition strongly into carbonate liquids (e.g. Ba, Sr, REE) might be substantially increased in very small melt fractions whereas the concentrations of other elements (e.g. Rb and K) are determined only by the silicate melting. The effect on incompatible-element concentrations of mixing carbonate precursor liquids with more voluminous silicate melting is considered in Section 4.6.

4.6 Carbonate-Silicate Liquid Mixtures

Theoretical curves for silicate melts and carbonate-silicate mixed melts can be calculated for the enrichment (C_L/C_0) of a range of incompatible trace elements at various degrees of partial melting (F) using Shaw's (1970) non-modal batch melting equation

$$C_L/C_0 = 1 / (D + F - PF)$$

as follows.

$$F = c + s$$

where c and s are the melt fractions of carbonate and silicate respectively, and the proportion (m) of carbonate in the carbonate-silicate mixture is given by

$$m = c / (c + s)$$

therefore $m = c/F$.

Bulk D for silicate liquids (^{L_s}D) is calculated for each element from the modal proportions of garnet lherzolite calculated by McKenzie & O'Nions (1991) and partition coefficients compiled by McKenzie & O'Nions (1991 and 1995).

Bulk D for carbonate liquids (^{L_c}D) is given by

$$^{L_c}D = {}^{L_s/L_c}D \cdot {}^{L_s}D$$

and obtained from ^{L_s}D, calculated above, and Fielding's (1992) coefficients for element partitioning between carbonate and silicate liquids ($^{L_s/L_c}D$).

Bulk D for mixed carbonate-silicate liquids ($^{L_{sc}}D$) is given by

$$^{L_{sc}}D = m \cdot {}^{L_c}D + (1-m) \cdot {}^{L_s}D$$

therefore $^{L_{sc}}D = (c/F) \cdot {}^{L_c}D + (1-(c/F)) \cdot {}^{L_s}D$.

P is calculated for basaltic liquids using the partition coefficients compiled by McKenzie & O'Nions (1991 and 1995) and estimates of the proportions of phases entering the melt given by Johnson *et al.* (1990).

Thus for carbonate-silicate mixed melts the enrichment is given by

$$^{L_{sc}}C_L/C_0 = 1 / ({}^{L_{sc}}D + F - PF)$$

and for silicate melts by

$$^{L_s}C_L/C_0 = 1 / ({}^{L_s}D + F - PF).$$

These calculations have been performed assuming c = 0.001 (i.e. carbonate melt derived by ca. 0.1% partial melting) and a range of F from 0.001 to 0.05 (i.e. 0.1% to 5% partial melting and, therefore, 100% to 20% carbonate in the mixed melt).

Theoretical enrichment curves for selected elements derived by the above method are shown in Figure 4-17. These indicate that highly incompatible trace elements (Ba, Th, Nb, and K) are enriched in both silicate melts and carbonate-silicate mixed melts regardless of the trace-element partitioning between carbonate and silicate liquids. For example, Ba (Fig. 4-17a) partitions strongly into carbonate liquid ($^{L_s/L_c}D_{Ba} < 0.1$) but

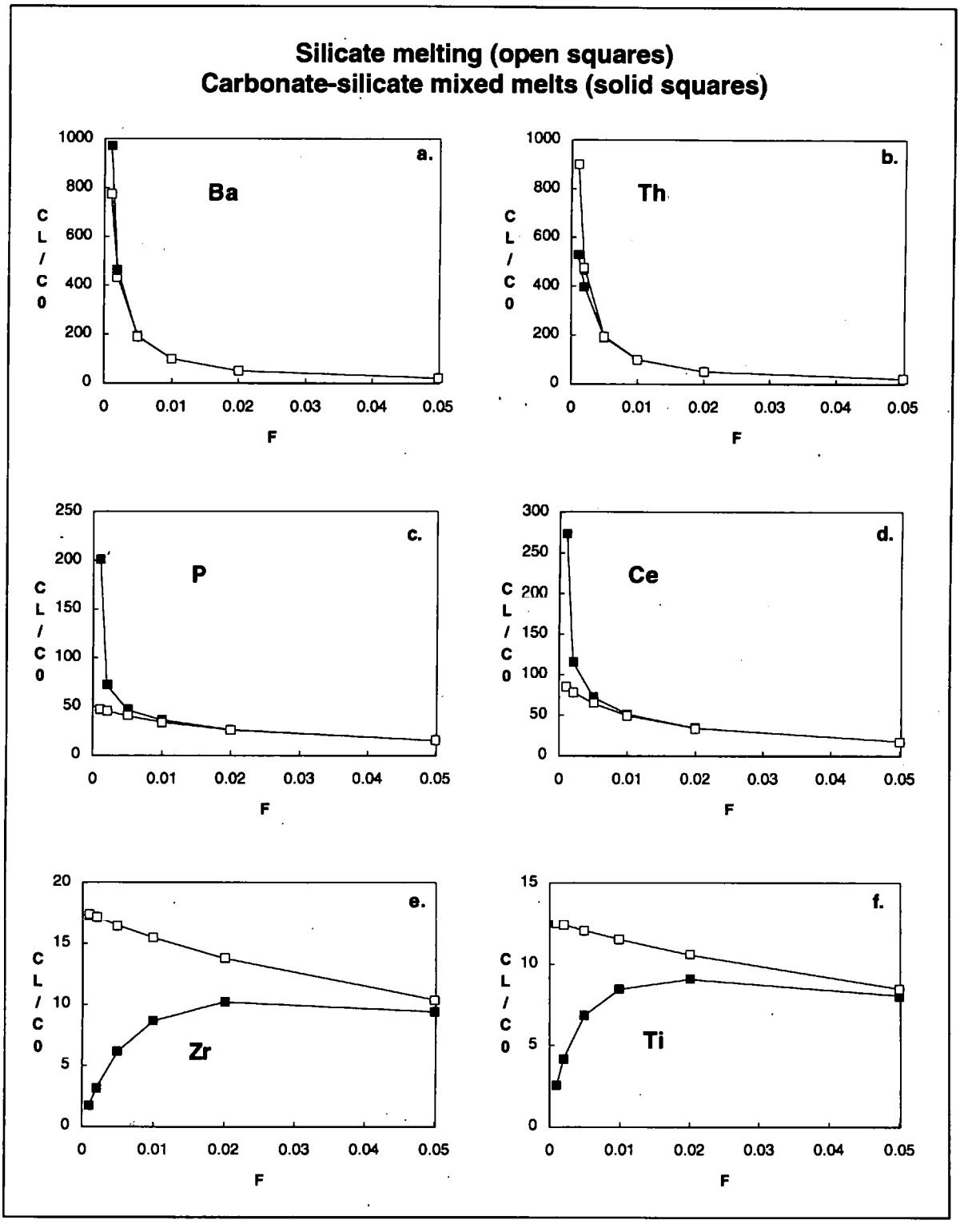

Figure 4-17. Theoretical trace-element enrichment curves for pure silicate melting and silicate melting with a 0.1% carbonate precursor melt addition over a range of F (0.1% to 5% partial melting).

C_l/C_0 calculated using the non-modal batch partial melting equation $C_L/C_0 = 1/(D+F-PF)$ (Shaw, 1970).
Modal proportions of garnet lherzolite from McKenzie & O'Nions (1991); partition coefficients for silicate melting from compilations in McKenzie & O'Nions (1991 & 1995); coefficients for silicate-carbonate liquid partitioning from Fielding (1992); proportions of phases entering basaltic liquids from Johnson *et al.*(1990).

enrichment in Ba in the mixed carbonate-silicate melt is only apparent at very small degrees of partial melting (ca. $F < 0.002$). The same is true for Th (Fig. 4-17b) but in this case silicate melts have higher concentrations at very small F because Th partitions strongly into silicate liquids ($^{Ls/Lc}D_{Th} = 8$). Trace-element enrichments of Nb ($^{Ls/Lc}D_{Nb} = 1.2$), K ($^{Ls/Lc}D_{K} = 1.5$), and Pb ($^{Ls/Lc}D_{Pb} = 0.5$) are similarly difficult to distinguish when $F > 0.002$ whereas the curves for Rb ($^{Ls/Lc}D_{Rb} = 1$) are identical. Most other incompatible elements are less incompatible than the group discussed above and tend to favour carbonate liquids (e.g. $^{Ls/Lc}D_{Sr} = 0.1$; $^{Ls/Lc}D_{P} = 0.2$; $^{Ls/Lc}D_{La} = 0.2$; $^{Ls/Lc}D_{Ce} = 0.25$; $^{Ls/Lc}D_{Nd} = 0.3$; and $^{Ls/Lc}D_{Y} = 0.8$). Even so, the difference between silicate melts and carbonate-silicate mixtures in, for example, P (Fig. 4-17c) and Ce (Fig. 4-17d) becomes apparent at only slightly higher degrees of melting (ca. $F < 0.005$) than in the highly incompatible elements. For elements which are not highly incompatible and which strongly favour silicate liquids, e.g. Zr ($^{Ls/Lc}D_{Zr} = 10$) and Ti ($^{Ls/Lc}D_{Ti} = 5$), silicate and carbonate-silicate mixed melts are clearly distinguishable over the entire range of F shown (Figs. 4-17e & f). The presence of a carbonate precursor in more voluminous silicate melting should theoretically, therefore, result in lower concentrations of Zr and Ti in the mixed melts up to at least 5% partial melting and, possibly, higher concentrations of LREE, Sr, and P, in small melt fractions derived by less than 1% partial melting.

In order to establish the role of carbonate-silicate melts in the generation of OIN and OIB a number of incompatible elements need to be considered simultaneously. The same is true if minor mantle phases, for example amphibole or phlogopite, are suspected in the source regions, and if large-scale processes, such as extraction of the continental crust, have affected the source composition. The most convenient way of developing a theoretical model for the mineralogy and composition of the source of OIN and OIB and the melting processes involved is, therefore, by means of a series of mantle-normalised incompatible-element diagrams. Theoretical incompatible-element concentrations can be calculated for a range of degrees of partial melting. These generate a family of normalised trace-element patterns and by varying a number of model parameters (e.g. modal mineralogy, partition coefficients, carbonate addition, source characteristics) the effect of the changes on the

theoretical patterns can be assessed. At each stage the theoretical patterns are compared with the actual patterns for average OIN and OIB for goodness of fit. A theoretical model for the source of OIN is developed in this way in Section 4.7.

4.7 Melting Models for OIN and OIB Sources

In Section 4.3 it was suggested that, in terms of the trace-element ratios used in Figure 4-3, OIN and OIB could be generated from a garnet or garnet-spinel lherzolite source. Initially, therefore, a garnet lherzolite source mineralogy has been used to model source composition and partial melting processes, starting with pure silicate melting, then progressing to the effects of adding a small amount of carbonate precursor liquid (generated by 0.1% melting) to the silicate melt, and finally considering the effects of depletion of the mantle source by continental crust extraction. Normalised abundances ($^{La}C_L/C_0$ and $^{Lu}C_L/C_0$) were obtained for a range of degrees of partial melting using the equations derived in Section 4.6. Depleted mantle abundances were calculated by mass balance assuming that 40% of the total mass of the mantle has been processed in the extraction of continental crust (with bulk elemental abundances given by Taylor & McClennan, 1985) from primitive mantle (with abundances given by McKenzie & O'Nions, 1995). $^{La}C_L/C_0$ and $^{Lu}C_L/C_0$ for primitive mantle were then scaled accordingly. The process was repeated with the addition of amphibole to the source. The model incompatible-element patterns were, in each case, compared with the normalised average compositions of OIB and OIN (Table 4-1).

The proportions of phases in the mantle sources were taken to be 0.60 ol, 0.20 opx, 0.18 cpx, and 0.02 gt, for the garnet lherzolite model, and 0.60 ol, 0.20 opx, 0.16 cpx, 0.02 gt, and 0.02 amph, for the amphibole-garnet peridotite model. The mineral proportions for anhydrous garnet lherzolite estimated by McKenzie & O'Nions (1991) are similar (0.598 ol, 0.211 opx, 0.076 cpx, 0.115 gt) but these proportions gave poor agreement between the theoretical concentrations of Y and those observed in OIB and

OIN. The concentration of Y in small melt fractions is largely controlled by the amount of garnet in the source. The proportion of garnet assumed for the anhydrous-source model was therefore reduced until an acceptable agreement for Y was obtained. The proportion of clinopyroxene was increased accordingly so that the proportion of fertile components remained constant. Having fixed the amount of garnet, the proportion of amphibole in hydrated lherzolite sources was estimated by achieving a reasonable agreement between theoretical and observed concentrations of K and the proportion of clinopyroxene was reduced by this amount. The mineral proportions chosen in this way are in broad agreement with those assumed by Francis & Ludden (1995) for partial melting of anhydrous garnet lherzolite and Halliday *et al.* (1995b) for amphibole-bearing lherzolite. The proportions of mantle phases entering the melts were assumed to be 0.03 ol, 0.03 opx, 0.44 cpx, and 0.50 gt, for garnet lherzolite (Johnson *et al.*, 1990) and -0.17 cpx, -0.50 gt, and 1.67 amph, for an amphibole-bearing lherzolite source (Francis & Ludden, 1995). Depleted mantle abundances have been calculated by McKenzie & O'Nions (1995) but the source of the bulk continental crustal abundances used by these authors in their calculations is unclear. The depleted mantle abundances calculated here are, therefore, similar to but subtlely different from those given by McKenzie & O'Nions (1995).

Figure 4-18a indicates that the model melting patterns generated for silicate melting in an anhydrous garnet lherzolite source are poor approximations to the normalised abundances of average OIN and average OIB compositions. The model predicts higher abundances of highly incompatible elements, much higher concentrations of K and Pb, and lower abundances of LREE, Zr, and Ti than are observed. The addition of a carbonate precursor liquid (Fig. 4-18b) does little to improve the match, except in the case of LREE, whereas predicted Zr and Ti fail to account for the observed abundances fairly comprehensively. Silicate melting of a depleted garnet lherzolite source (Fig. 4-18c) improves the fit of highly incompatible elements in OIB and OIN to the model patterns and also, to some extent, the fit of K and Pb. With the addition of carbonate melt (Fig. 4-18d), the LREE match is also improved. Carbonate-silicate liquid mixing seems to be necessary, therefore, to account for the LREE enrichment in OIN and OIB. However, in all the cases

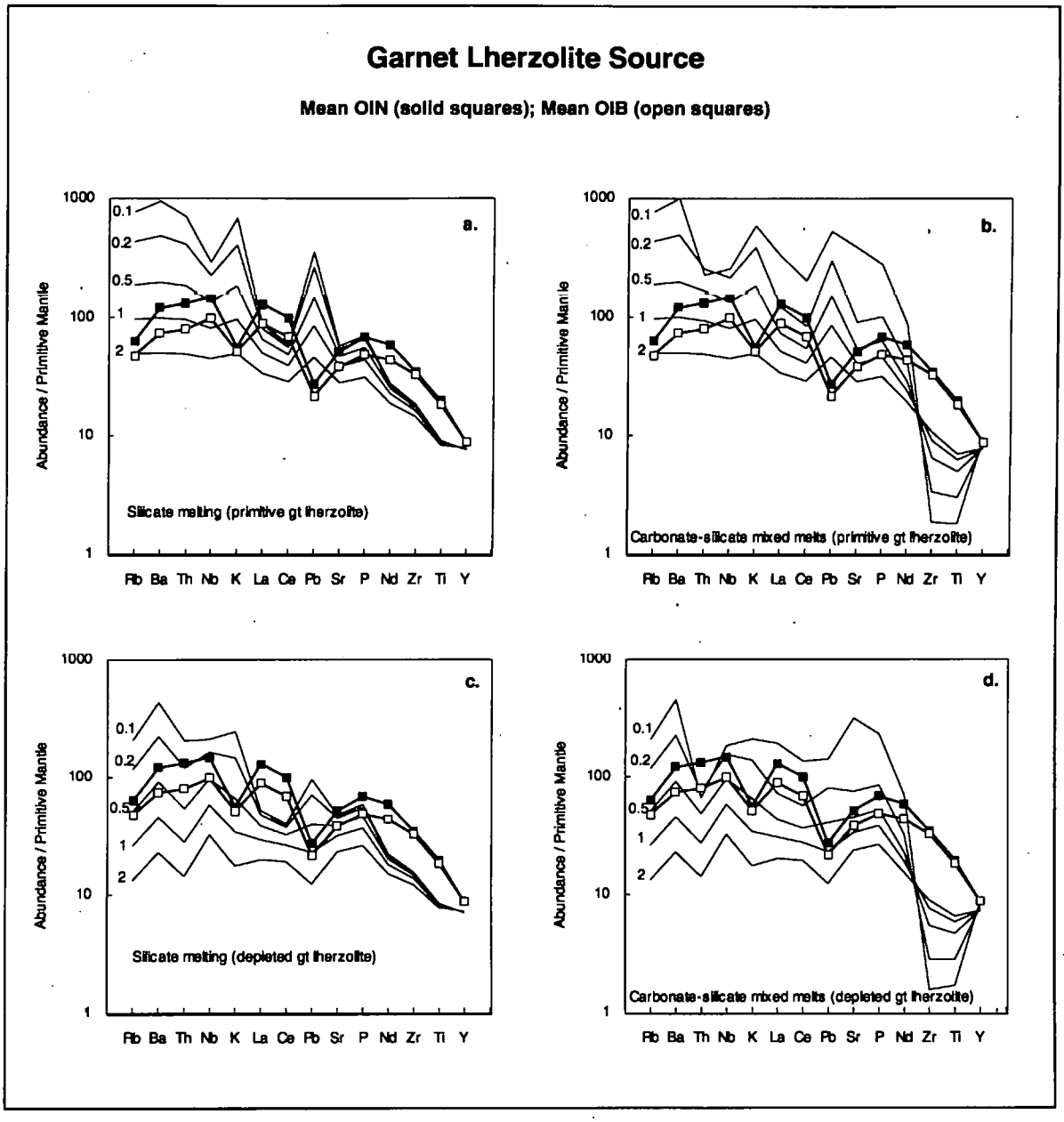

Figure 4-18. Theoretical mantle-normalised incompatible-element patterns calculated for degrees of partial melting ranging from 0.1% to 2% of primitive and depleted garnet lherzolites. Mean OIN and Mean OIB from Table 4-1. Primitive garnet lherzolite is assumed to have been depleted by the extraction of continental crust with bulk elemental abundances given by Taylor & McClennan (1985). Depleted mantle abundances calculated by mass balance assuming 40% of the total mantle mass has been processed.
P abundance in depleted source taken from McKenzie & O'Nions (1995).
Source mineralogy: ol = 0.6, opx = 0.2, cpx = 0.18, gt = 0.02, based on McKenzie & O'Nions (1991) and Halliday *et al.* (1995b). Melting proportions of mantle phases from Johnson *et al.* (1990).
Partition coefficients from compilation in Halliday *et al.* (1995b). Primitive mantle normalising values from McKenzie & O'Nions (1995).
Carbonate precursor liquid assumed to have been generated by 0.1% partial melting of the same source. Carbonate-silicate partition coefficients from Fielding (1992).

examined so far, Zr and Ti abundances are much higher in both OIN and OIB than predicted by these models.

The addition of a small amount of amphibole to a primitive source reduces significantly the predicted concentrations of K at small degrees of partial melting (i.e. $F < 0.012$) but still produces a rather poor fit and does little to reduce the abundances of the highly incompatible elements and Pb in pure silicate melting (Fig. 4-19a), nor is the match improved for these elements by carbonate liquid addition (Fig. 4-19b). The calculated abundances for silicate melting in a depleted amphibole-garnet peridotite source are shown in Figure 4-19c. The fit of most incompatible elements (particularly K) to the average compositions is acceptable but LREE, Pb, Zr, and Ti are still poor. Carbonate liquid addition to the silicate melt (Fig. 4-19d) raises the predicted levels of LREE and also improves the fit of Sr and P without disturbing the fit of the patterns elsewhere. The most appropriate model for the generation of OIN that can be achieved within these simple options is, therefore, approximately 0.2% partial melting of a depleted amphibole-garnet peridotite source with a carbonate liquid precursor melt generated by 0.1% partial melting. OIB may be ca. 0.5% partial melting of the same source. Nevertheless, the model fails in a number of respects: Th and, particularly, Zr and Ti concentrations are higher than predicted in both OIN and OIB, and Pb is significantly lower.

The calculated model patterns are, however, based on a number of assumptions and parameters (e.g. partition coefficients, melting proportions, source mineralogy, crustal abundances etc) and changing any one, or a combination, of these might significantly affect the outcome. For example, the mineral/melt partition coefficients used in the calculations are those compiled by Halliday *et al.* (1995b) from the results of recent experiments and from recently published mineral data. Other compilations exist (e.g. McKenzie & O'Nions, 1991 and 1995) and it is noticeable that estimates of $^{amph}D_K$ vary considerably (0.2 to 1.2). Estimates of $^{amph}D_{Ti}$ are similarly variable. Changing $^{amph}D_K$ and $^{amph}D_{Ti}$ can have a considerable effect on predicted abundances of K and Ti. However, using different compilations of partition coefficients does not significantly affect the patterns for

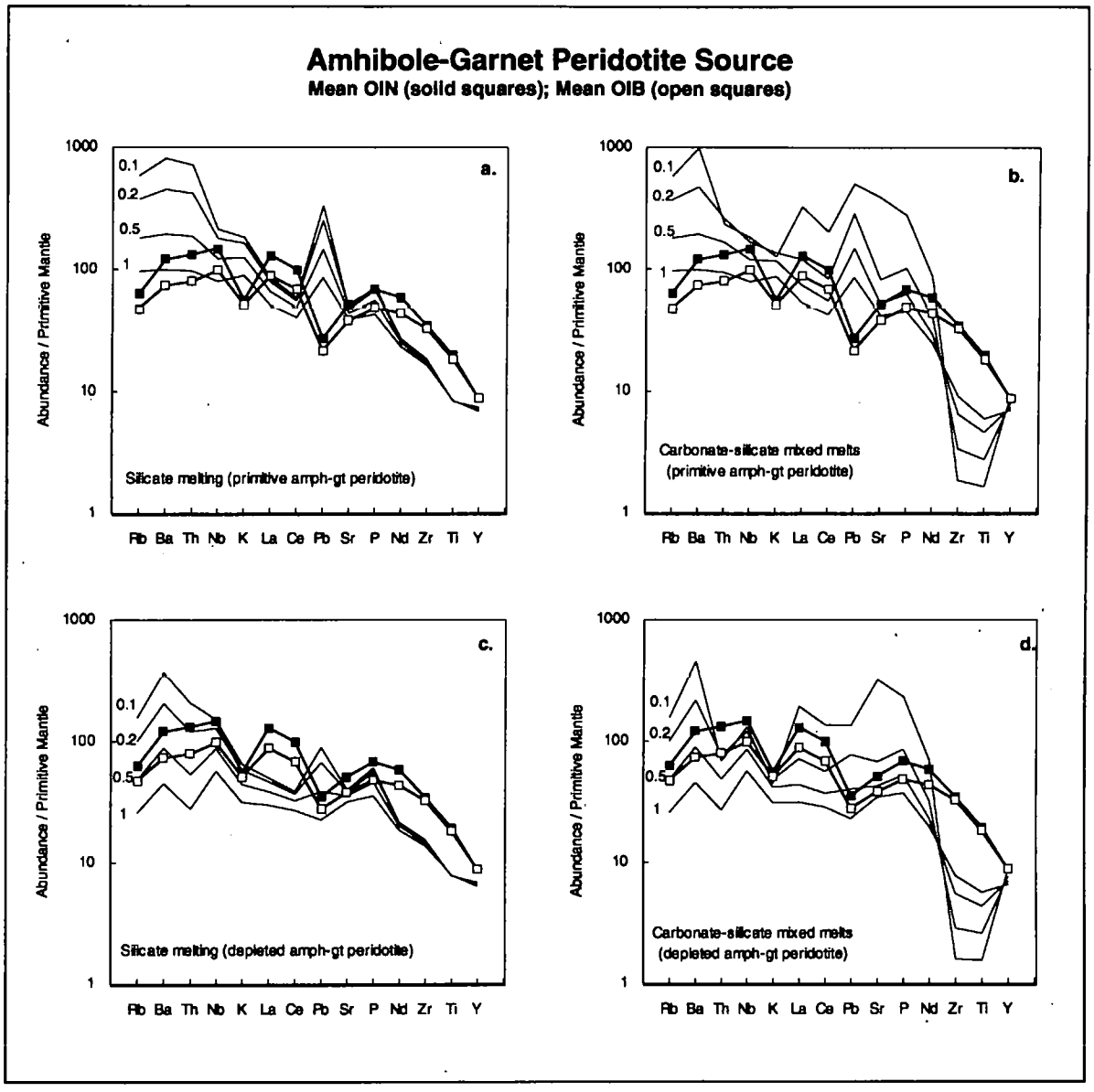

Figure 4-19. Theoretical mantle-normalised incompatible-element patterns calculated for degrees of partial melting ranging from 0.1% to 1% of primitive and depleted amphibole-garnet peridotites. Mean OIN and Mean OIB from Table 4-1.
Primitive amph-gt peridotite is assumed to have been depleted by the extraction of continental crust with bulk elemental abundances given by Taylor & McClennan (1985). Depleted mantle abundances calculated by mass balance assuming 40% of the total mantle mass has been processed.
P abundance in depleted source taken from McKenzie & O'Nions (1995). Source mineralogy: ol = 0.6, opx = 0.2, cpx = 0.16, gt = 0.02, amph =0.02, based on McKenzie & O'Nions (1991) and Halliday *et al.* (1995b). Melting proportions of mantle phases from Francis & Ludden (1995) and Johnson *et al.* (1990). Amph totally consumed at ca. 1.2% partial melting.
Partition coefficients from compilation in Halliday *et al.* (1995b). Primitive mantle normalising values from McKenzie & O'Nions (1995).
Carbonate precursor liquid assumed to have been generated by 0.1% partial melting of the same source. Carbonate-silicate partition coefficients from Fielding (1992).

highly incompatible elements and does nothing to improve the fit of Zr or Th. Changing the source mineralogy within the range of published and, therefore, presumably acceptable mineral proportions has, in general, only subtle effects on the model patterns. The source compositions used in these models were in broad agreement with the compositions proposed by Halliday *et al.* (1995b) and McKenzie & O'Nions (1991) and were chosen to give the best fits at Y and K. The carbonate addition was chosen to give the best fit of LREE.

Clearly no unique solution can be obtained from this type of model because of the number of variables involved. Neither does a match between the observed concentrations and the abundances predicted by the model indicate that the preferred solution has any basis in reality. The success of models of this type depends heavily on the reasonableness of the parameters chosen for the modelling. However, there seems to be little to be gained from fine-tuning the parameters in order to obtain a better agreement with observed averages. Given the use of reasonable parameters, the success of the model developed above indicates only that the constraints imposed may be relevant to the magma generation studied. It is equally obvious from the high levels of Zr, Ti, and Th, in OIN and OIB, that some major process or component has been omitted. This process may be the remobilisation of asthenosphere-derived small melt fractions which have been incorporated into the base of the oceanic lithosphere. Addition of a lithospheric component is difficult to model as further assumptions have to be made about the incompatible-element concentrations of the original melts and the extent to which they might be involved in OIN and OIB genesis. However, since the remobilised melt has probably been generated from a similar source as the magma which it enriches, the general effect of adding a small silicate-melt fraction will be to elevate incompatible-element abundances according to the reciprocal of their respective bulk partition coefficients, producing melts which are significantly enriched in the highly incompatible elements. While most of the incompatible-element budget might be controlled by the mantle sources and processes described earlier in this Section, remobilisation of silicate melts from the lithosphere might

provide a means of enriching OIN and OIB in strongly carbonate-phobic elements. This is an entirely speculative suggestion, however, and is not taken further.

A simple test of the applicability of the model proposed earlier is to compare the normalised OIN and OIB averages for each island on which OIN occur with the patterns predicted by the preferred model. These comparisons are shown in Figures 4-20 to 4-23 which illustrate both silicate melting and carbonate-silicate mixed melting models for a depleted amphibole-garnet peridotite source. In each case, the carbonate-silicate model provides a better approximation to LREE abundances and most other incompatible elements than the pure silicate model. Japan (Fig. 4-23e & f), however, is a fairly poor fit to both. As suggested in Section 4.3, Japan may have a subduction-modified enriched source to which neither of these models applies. In individual cases, i.e. Fernando de Noronha (Fig. 4-20 b), Principe (Fig. 4-20d), Cape Verde (Fig. 4-20f), Truk (Fig. 4-22b), and Aitutaki (Fig. 4-23f) the fit of Nb appears to become a problem. For these islands Nb in OIN is higher than predicted by the carbonate-silicate melting model. It is possible that Nb may have become enriched in these magmas by a similar process to that responsible for the high levels of Zr, Ti, and Th. In no case, however, does either model predict the abundances of Zr and Ti observed. Ignoring Th, Ti, and Zr, the match of the carbonate-silicate melting model to the observed abundances is remarkably good for the Comores Islands (Figs. 4-21 b & d), Ponape and Kusaie (Figs. 4-22d & f), Kauai and Oahu (Figs. 4-23 b & d) and Samoa (Fig. 4-23f), and, apart from Nb, agrees well with the observed abundances from the Atlantic Islands (Fig. 4-20).

4.8 Amphibole-Bearing Sources

A number of incompatible-element diagrams using K on the x axis produce data distributions which can be enclosed in a wedge-shaped envelope (e.g. Fig. 4-24), OIN typically having higher concentrations of the y-axis element than OIB for the same range of K. Data distributions of this type using K and Rb on the x axis have been reported by

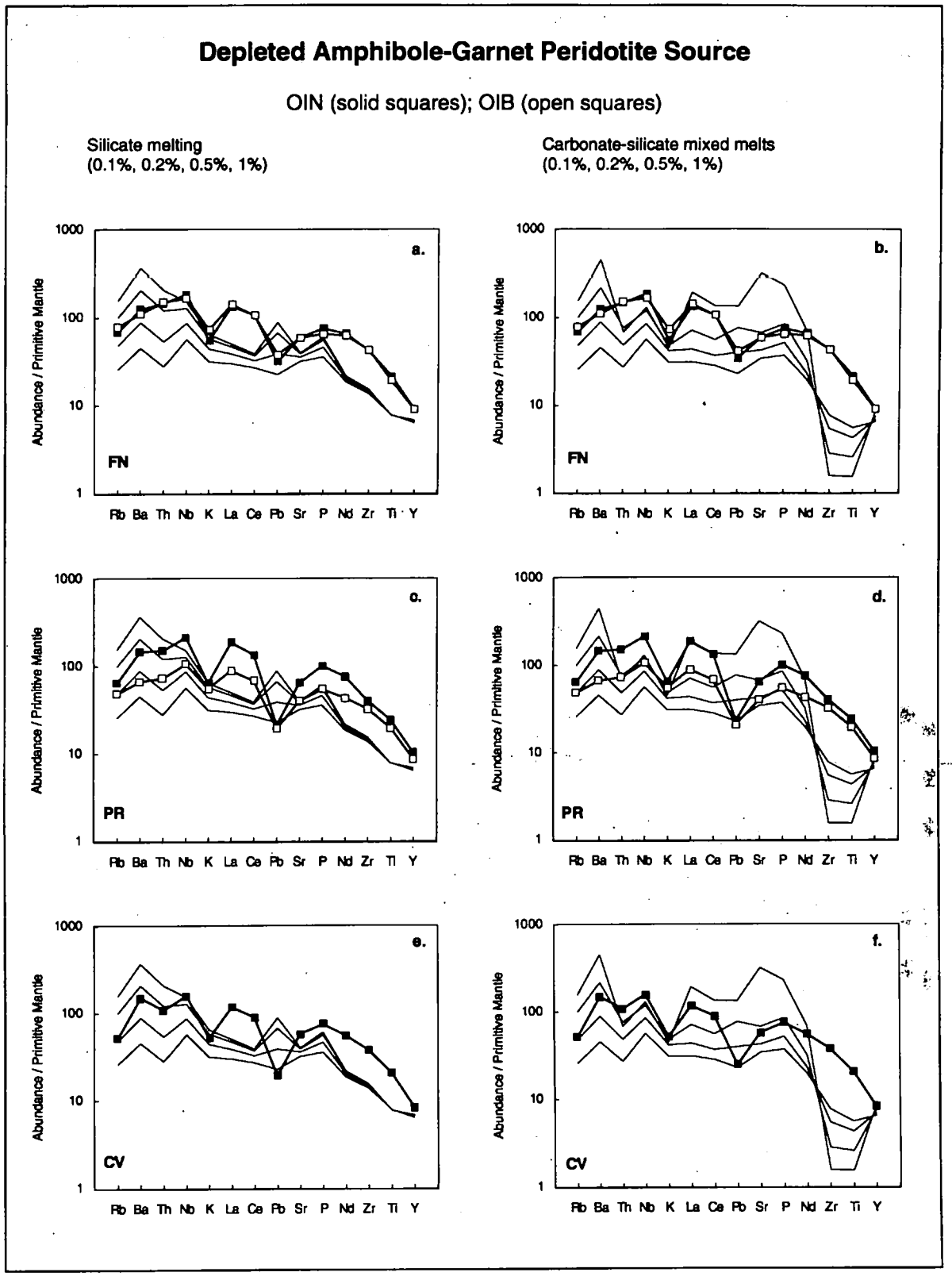

Figure 4-20. Theoretical mantle-normalised incompatible-element patterns for depleted amphibole-garnet peridotite. Model parameters as in Fig. 4-19.
Mean Ocean Island abundances from Appendix E, Table E-6 (OIN) and Table E-10 (OIB).

Atlantic Ocean Islands
FN = Fernando de Noronha
PR = Principe, Gulf of Guinea
CV = Cape Verde

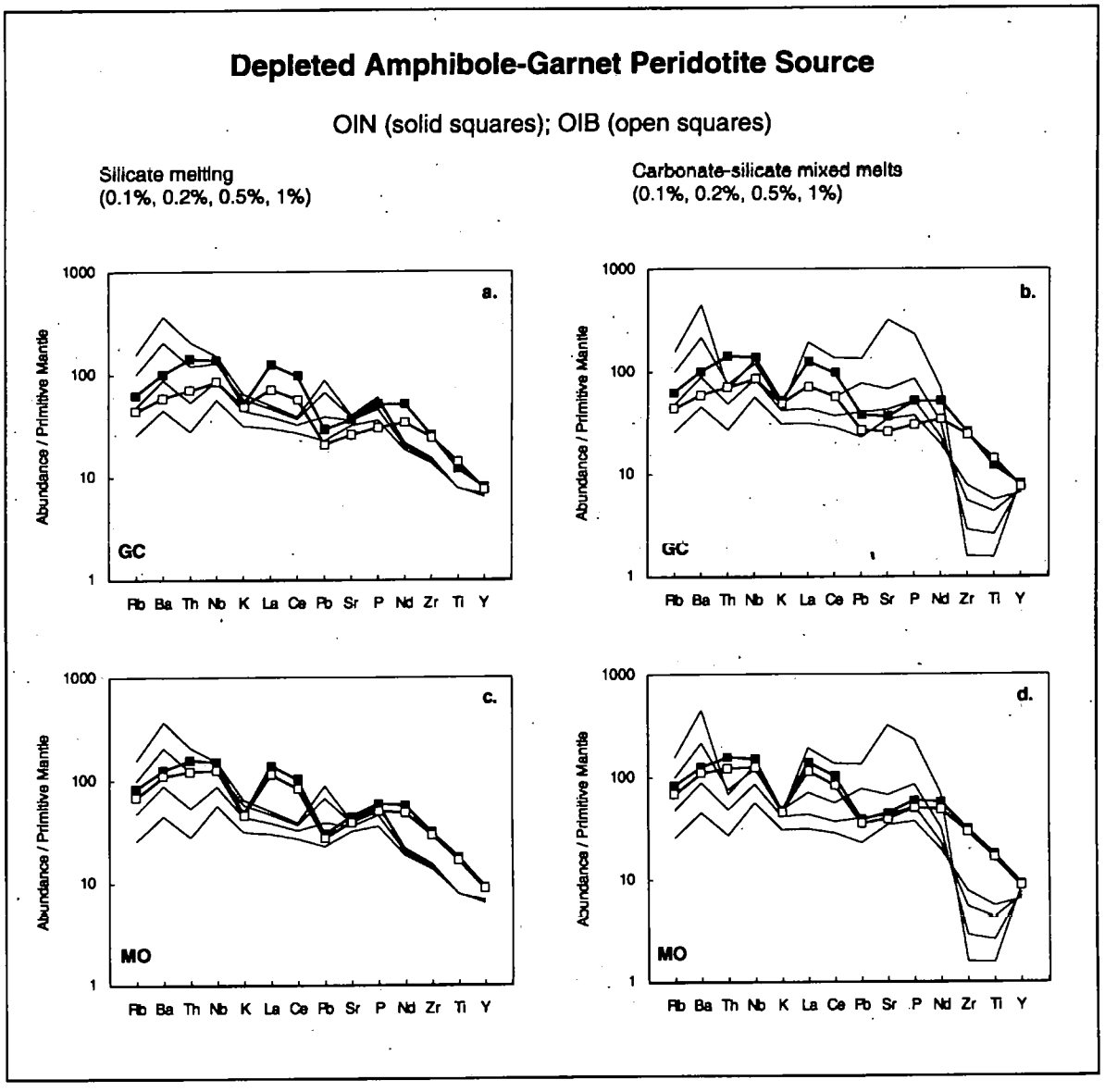

Figure 4-21. Theoretical mantle-normalised incompatible-element patterns for depleted amphibole-garnet peridotite. Model parameters as in Fig. 4-19. Mean Ocean Island abundances from Appendix E, Table E-6 (OIN) and Table E-10 (OIB).

Indian Ocean - Comores Islands
GC = Grand Comore
MO = Moheli

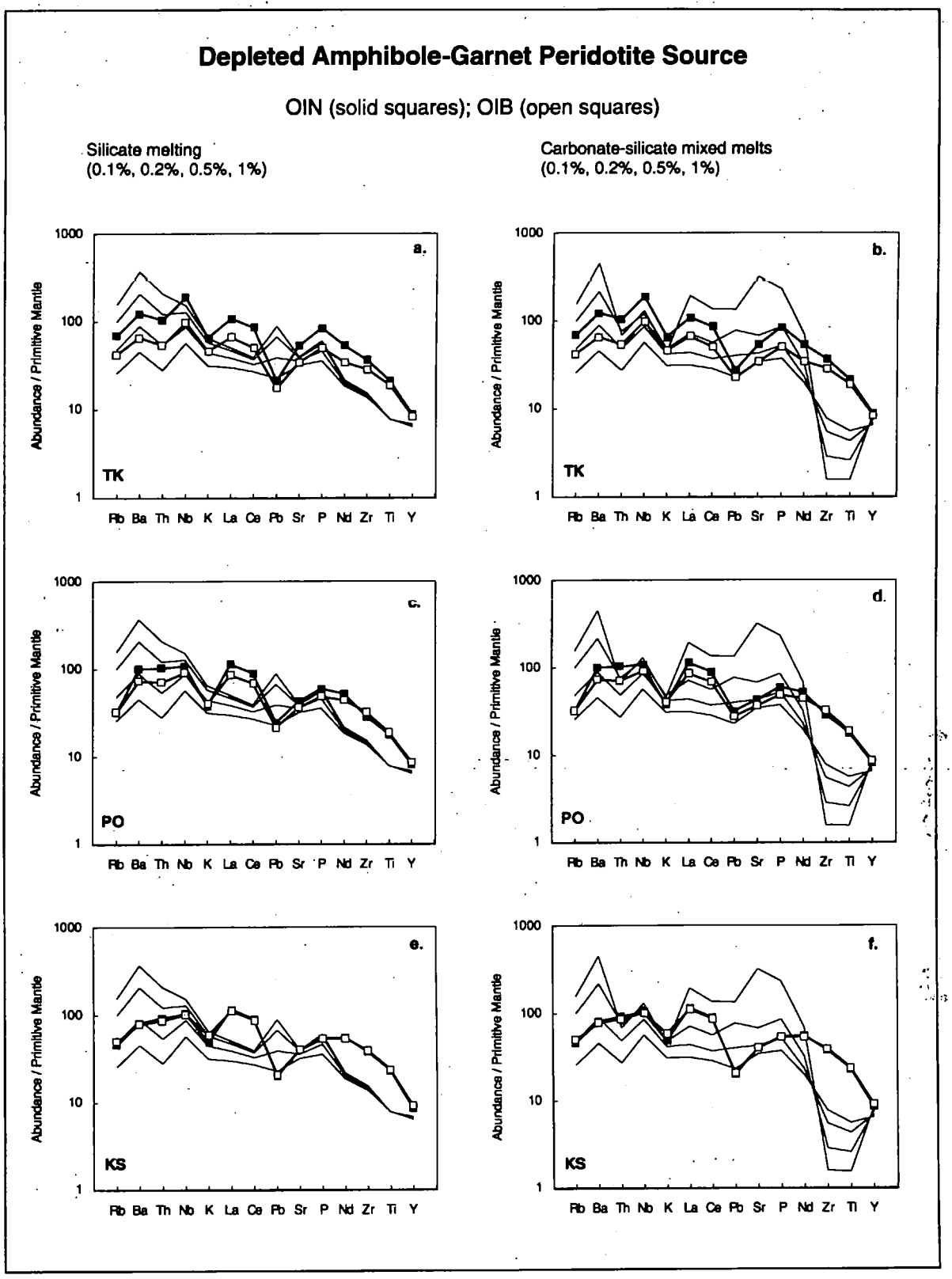

Figure 4-22. Theoretical mantle-normalised incompatible-element patterns for depleted amphibole-garnet peridotite. Model parameters as in Fig. 4-19.
Mean Ocean Island abundances from Appendix E, Table E-6 (OIN) and Table E-10 (OIB).

Pacific Ocean - Caroline Islands
TK = Truk
PO = Ponape
KS = Kusaie

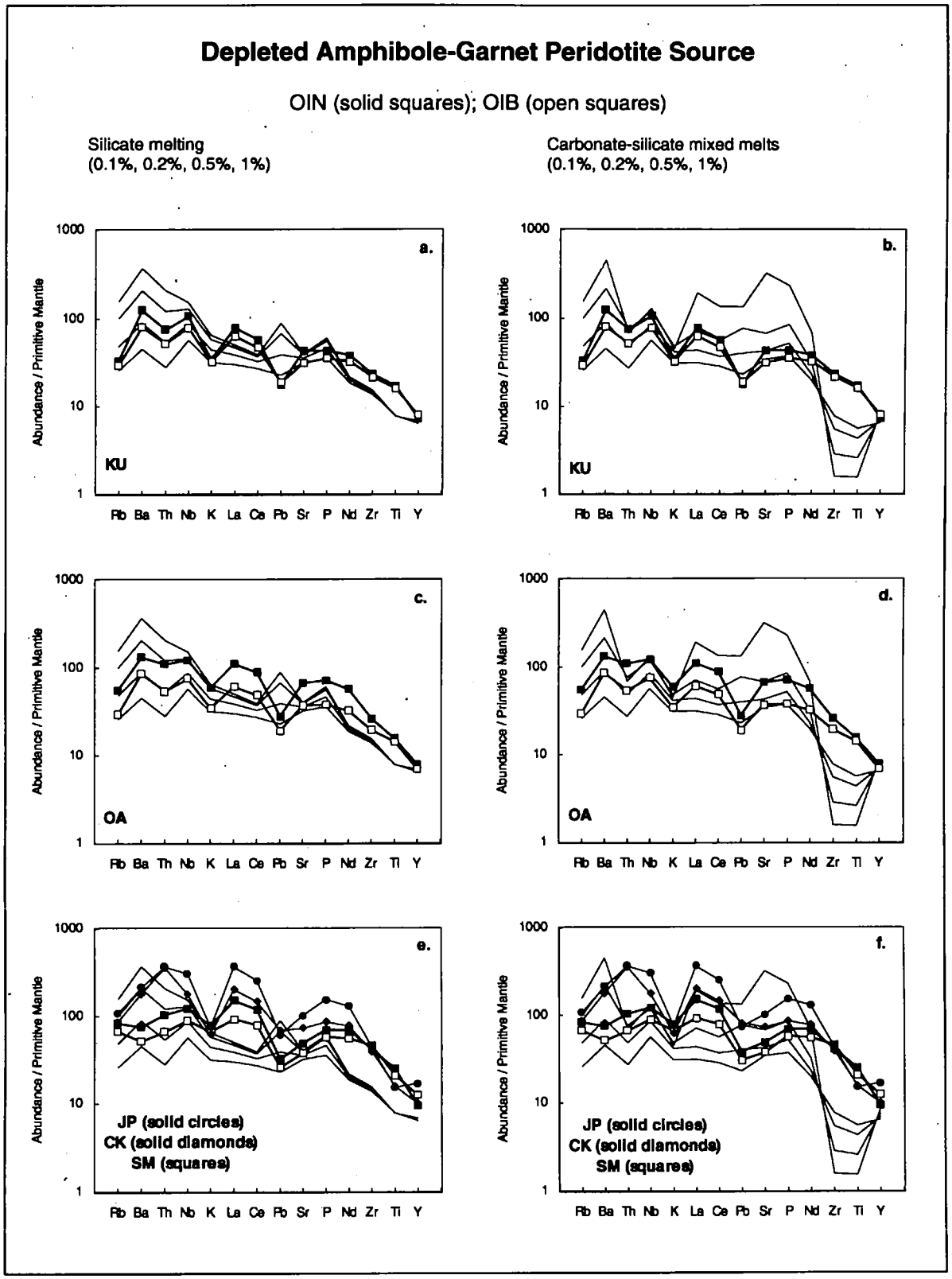

Figure 4-23. Theoretical mantle-normalised incompatible-element patterns for depleted amphibole-garnet peridotite. Model parameters as in Fig. 4-19. Mean Ocean Island abundances from Appendix E, Table E-6 (OIN) and Table E-10 (OIB).

Pacific Ocean Islands
KU = Kauai, Hawaiian Islands
OA = Oahu, Hawaiian Islands
JP = Japan, CK = Aitutaki, Cook Islands, SM = Upolo, Samoa

Francis & Ludden (1995) and Greenough (1988) respectively. These have been modelled by assuming that a potassic phase (amphibole or phlogopite), in which $^{min}D_K > 1$ or $^{min}D_{Rb} > 1$, is progressively consumed during partial melting. In this case, K and Rb increase during the initial stages of melting, the nose of the wedge indicates the point at which the potassic phase disappears and increased melting thereafter produces magmas progressively depleted in K or Rb. Greenough (1988) produced a family of melting curves to fit a range of individual data sets only by changing the source composition of the plotted elements. However, Greenough acknowledges that the modelling parameters used to generate the melting curves do not produce a unique fit to the data distribution. Nevertheless, he shows that by selecting reasonable values for the modelling parameters, theoretical melting curves with a characteristic wedge shape can be generated and, as he suggests, these could reflect the influence of potassic phases during small degrees of melting and its disappearance in the formation of higher melt fractions.

Similar theoretical model curves have been produced for silicate and carbonate-silicate liquid mixtures from primitive and depleted amphibole-garnet peridotite. These are compared with primary OIB and OIN data (Figs. 4-24 to 4-27). Calculated primary compositions (Chapter 3) are used in this case to remove any effect that may be due to olivine fractionation. Primary compositions have not been used in the normalised diagrams presented up to this point because the olivine additions required to restore OIN to primary compositions result in a reduction of only ca. 12% in trace-element concentrations. This reduction is barely detectable on the log scales used in normalised diagrams but makes a significant difference when the same data are plotted on a linear scale. The same source mineralogy has been used in the calculations as before (60% ol, 20% opx, 16% cpx, 2% gt, 2% amph), but partition coefficients have been taken from the compilation given by McKenzie & O'Nions (1995) which suggests that $^{amph}D_K = 1.2$. From mass balance calculations between average olivine nephelinite, garnet, clinopyroxene, and amphibole, Francis & Ludden (1995) suggest that amphibole melts to 0.6 liquid + 0.1 cpx + 0.3 gt. For a source with 2% amphibole this indicates that amphibole disappears at about 1.2% partial melting. At this point the source mineralogy has been recalculated and melting curves for

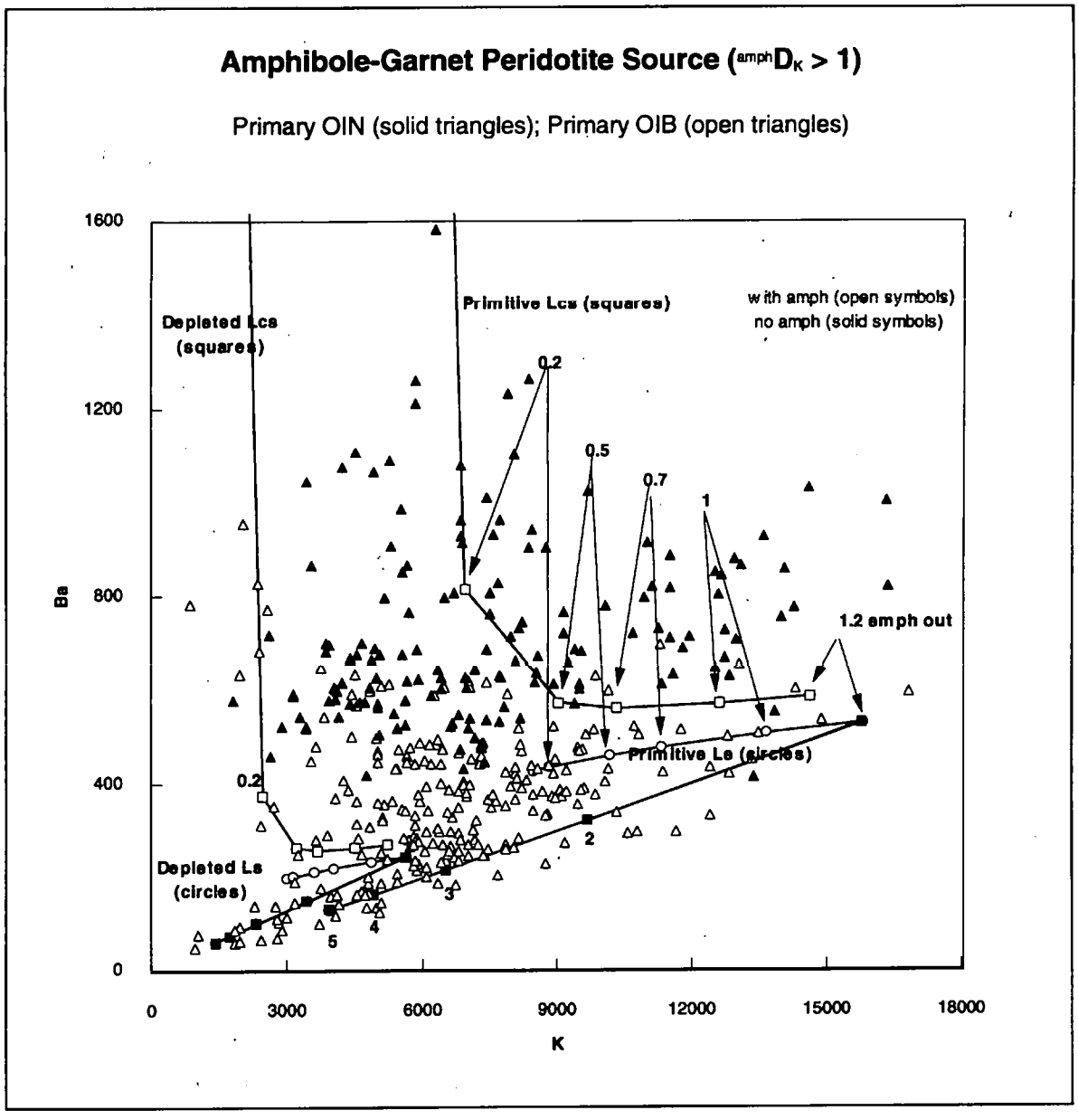

Figure 4-24. Theoretical partial melting curves for degrees of partial melting ranging from 0.1% to 5% of primitive and depleted amphibole-garnet peridotite where $^{amph}D_K > 1$. Amphibole totally consumed at ca. 1.2% partial melting.
Lcs = carbonate-silicate mixed melt
Ls = silicate melt
Source mineralogy and melting proportions as in Fig. 4-19. Depleted mantle abundances calculated as for Fig. 4-19. Partition coefficients and primitive mantle composition from compilation in McKenzie & O'Nions (1995).
Carbonate precursor liquid assumed to have been generated by 0.1% partial melting of same source. Mis-match of Lcs curves at 1.2% melting is an artifact of the calculations which start with a finite amount of carbonate melt, i.e. $F \neq 0$.
Primary OIN and OIB calculated for all samples with MgO > 10% by dilution with olivine additions required to restore magma compositions to equilibrium with mantle olivine (Fo_{90}) using $K_D = 0.30$ for distribution of Fe^{2+} and Mg between olivine and co-existing silicate melt (Chapter 3).

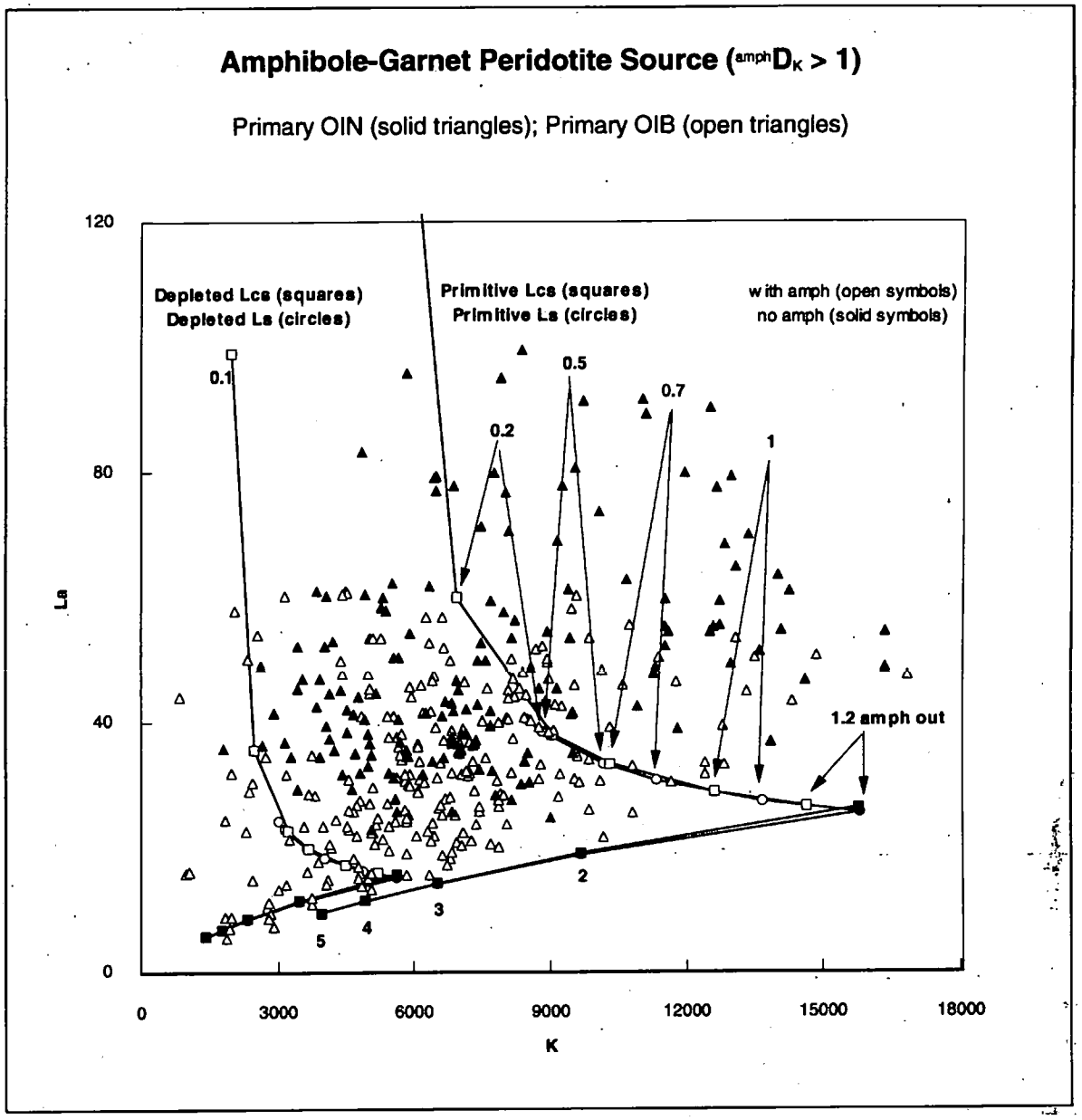

Figure 4-25. Theoretical partial melting curves for degrees of partial melting ranging from 0.1% to 5% of primitive and depleted amphibole-garnet peridotite where $^{amph}D_K > 1$. Amphibole totally consumed at ca. 1.2% partial melting.
Lcs = carbonate-silicate mixed melt
Ls = silicate melt
Parameters and calculations as in Fig. 4-24.

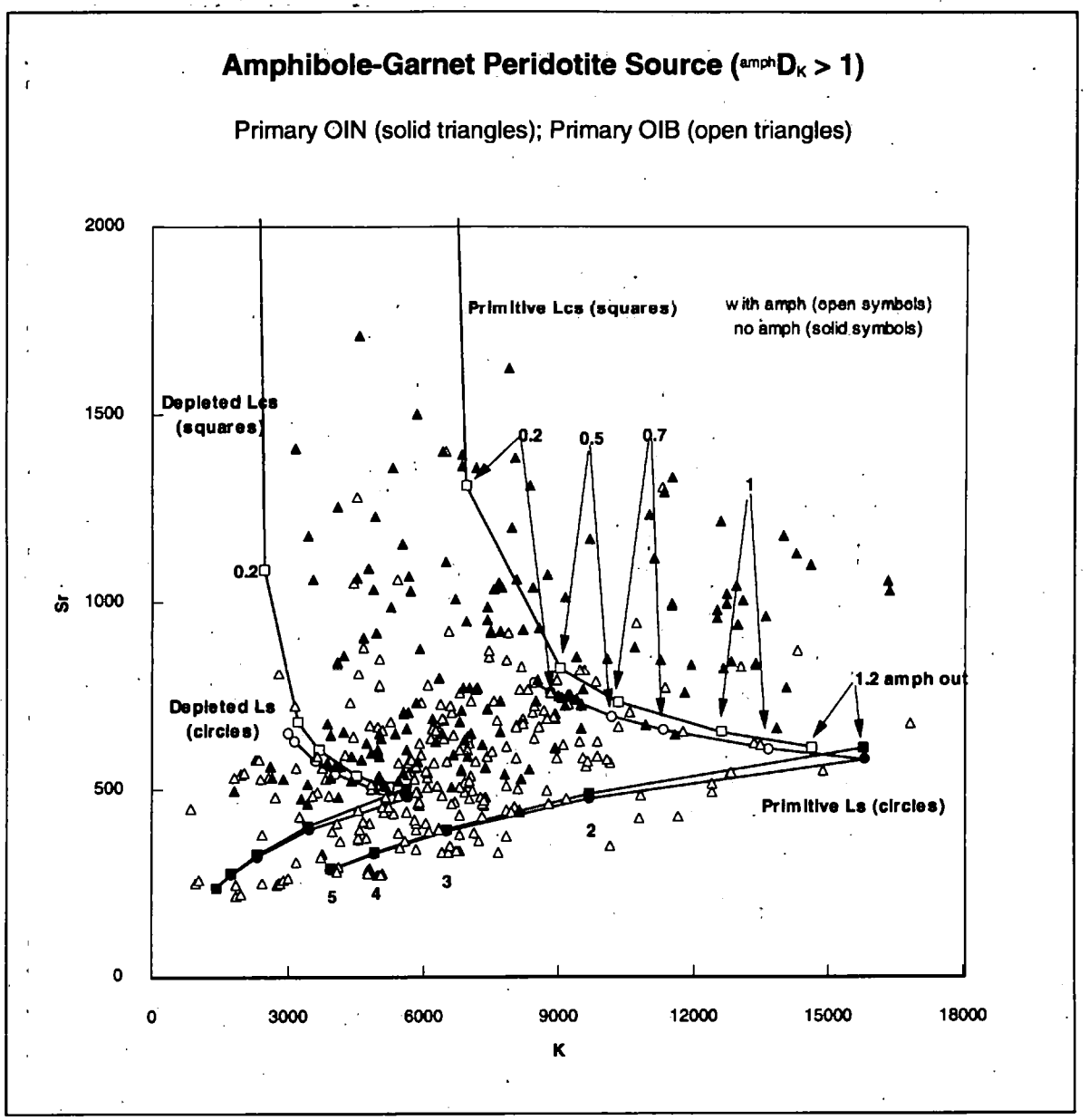

Figure 4-26. Theoretical partial melting curves for degrees of partial melting ranging from 0.1% to 5% of primitive and depleted amphibole-garnet peridotite where $^{amph}D_K > 1$. Amphibole totally consumed at ca. 1.2% partial melting.
Lcs = carbonate-silicate mixed melt
Ls = silicate melt
Parameters and calculations as in Fig. 4-24.

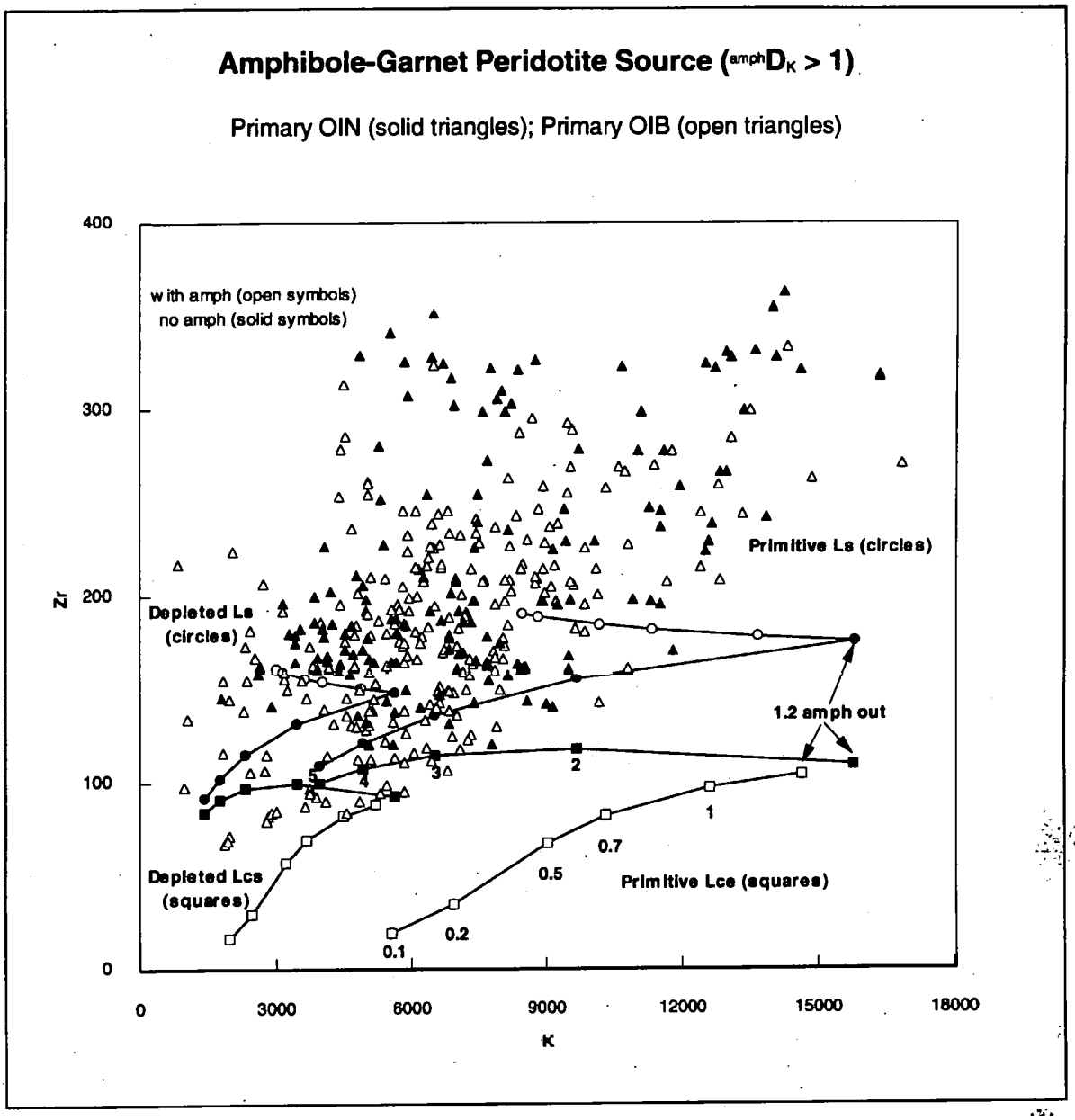

Figure 4-27. Theoretical partial melting curves for degrees of partial melting ranging from 0.1% to 5% of primitive and depleted amphibole-garnet peridotite where $^{amph}D_K > 1$. Amphibole totally consumed at ca. 1.2% partial melting.
Lcs = carbonate-silicate mixed melt
Ls = silicate melt
Parameters and calculations as in Fig. 4-24.

the amphibole-free source generated using the melting proportions suggested by Johnson *et al.* (1990) for basaltic liquids derived from garnet lherzolite sources.

This process was used to generate plots of Ba *versus* K (Fig. 4-24), La *versus* K (Fig. 4-25), Sr *versus* K (Fig. 4-26), and Zr *versus* K (Fig. 4-27). These elements were chosen because carbonate-silicate liquid partition coefficients (Fielding, 1992) indicate that they might be diagnostic in determining the role of carbonate precursor liquids in the generation of OIN and OIB. The data distributions and fit to the theoretical melting curves shown in Figures 4-24, 4-25, and 4-26 are consistent with OIN having been produced by between 0.2% and 0.5% melting from variably depleted amphibole-bearing sources by carbonate-silicate melt mixing. Although not shown on these diagrams, individual island trends for OIN are negatively correlated with K. Most OIB, on the other hand, are positively correlated and appear to be consistent with 2% to 5% melting of an amphibole-free source. Carbonate-silicate and pure silicate curves are, however, indistinguishable at these levels of partial melting, and a role for carbonate in OIB in general cannot, therefore, be ruled out. The position of the theoretical melting curves on these diagrams can be adjusted to improve the fit to the data but, as in the case of the earlier melting models, this process cannot be constrained other than by assessing the reasonableness of the chosen assumptions and parameter values. Consequently, this approach is not pursued here.

Figure 4-27 is a clear indication of the Zr enrichment in OIN and OIB discussed in Section 4.7. The curves for carbonate-silicate liquids and pure silicate liquids are clearly separated on this diagram but there is no tendency for OIN or OIB to follow the carbonate-silicate curves or even to be distributed parallel to them but at higher Zr abundances. In fact, apart from a few high-Zr OIN samples, OIB and OIN are indistinguishable on this diagram and it fails completely to substantiate the evidence presented so far for the existence of potassic phases in the mantle and an essential role for carbonate in the generation of OIN. Since silicate melting models also fail to model Zr abundances it has been assumed that some other process or component (possibly from the oceanic lithosphere) is responsible for the Zr enrichment. Other trace elements, however, seem to

indicate that the effects of residual potassic phases and carbonate.liquid additions might be significant in the generation of OIN magmas.

4.9 Mantle Components

In recent years, considerable effort has been applied to establishing the trace-element characteristics which might accompany the range of isotopic ratios found in OIB and MORB (e.g. Saunders *et al.*, 1988; Sun & McDonough, 1989; Weaver, 1991; Halliday *et al.*, 1995a). Trace-element ratios are more variable than isotopic compositions and without the isotope data which can be used to identify islands lying close to presumed end-member compositions (e.g. HIMU, EM) it would be very difficult to discover characteristic trace-element ratios which might relate to these isotopically distinct components. Thirteen diagnostic trace-element ratio ranges which have been published so far are presented in Table 4-2. In many cases the ratio bands are based on relatively few samples for which isotope data have been obtained. No doubt as more data become available the distinctions may become more blurred or more clearly defined. The ratios used mostly involve HFS elements and those LILE which, from multi-element normalised diagrams, are obviously characteristic of the source components. However, for some ratios, it is not possible to distinguish between HIMU, EMI, and EMII easily (e.g. Th/Nb) and the distinction between EMI and EMII is often ambiguous (e.g. K/Nb, Ba/Th).

In an attempt to discover whether highly undersaturated magmas are derived preferentially from any of these sources arithmetic means of the same thirteen trace-element ratios have been calculated for all the islands represented in the OIN data base, together with means for OIB from the same islands (Table 4-2). The ranges and means appropriate to average OIB and average OIN are also presented in Table 4-2. A comparison between these ranges should indicate which sources are available during melting and whether any of these are more strongly represented in highly undersaturated magmas. There are a number of problems with this approach. Firstly, OIN do not occur on DUPAL

Table 4-2 Average Trace-Element Ratios for OIN and OIB compared with HIMU, EMI, and EMII.

	**	HIMU	EMI	EMII		Mean*	CV	PR	FN	TD	GC	MO	KU	OA	TK	PO	KS	SM	CK	JP
Ce/Pb	(iii)	29-38	14.5-24	25-31	OIB	31		41	30	66	26	27	25	25	23	29	32	26		
					OIN	39	45	68	38	49	31	35	32	33	38	36	43	33	19	40
Nb/Pb	(iii)	18-23	8.5-15.9	12.1-12.2	OIB	17.15		24.24	16.47	30.35	14.88	15.77	16.11	15.82	13.65	15.29	14.97	11.91		
					OIN	23.33	31.79	41.79	25.78	33.00	17.10	19.95	22.87	18.35	32.91	17.00	20.41	13.30	9.01	18.18
Nb/Th	(iii)	10-17	9.1-11.5	9.1	OIB	10.72		11.60	8.49	12.34	9.96	9.21	11.80	14.07	14.88	10.86	10.64	11.62		
					OIN	10.17	12.34	10.93	9.90	17.75	7.53	7.80	11.18	8.60	14.14	8.48	10.62	9.11	3.85	6.44
Ba/Th	(ii)	39-85	80-204	57-105	OIB	95		88	64	77	83	98	136	199	125	99	89	77		
					OIN	100	139	89	81	151	67	83	162	113	111	93	98	67	47	55
Th/La	(ii)	0.099-0.164	0.089-0.147	0.108-0.183	OIB	0.10		0.10	0.13	0.08	0.12	0.13	0.08	0.10	0.08	0.10	0.09	0.09		
					OIN	0.12	0.12	0.10	0.14	0.08	0.15	0.14	0.12	0.13	0.12	0.11	0.10	0.09	0.22	0.13
Ba/La	(ii)	6.2-9.3	11.3-19.1	7.3-13.5	OIB	9.75		8.88	8.18	6.17	9.91	11.82	13.36	18.34	9.32	10.04	8.14	6.96		
					OIN	11.67	15.63	9.18	10.96	12.24	9.84	11.12	19.41	14.24	13.57	10.52	8.45	5.90	10.60	6.95
La/Nb	(ii)	0.64-0.77	0.78-1.32	0.79-1.19	OIB	0.96		0.86	0.96	1.02	0.85	0.92	0.93	0.83	0.91	0.94	1.03	0.95		
					OIN	0.91	0.75	0.88	0.76	0.72	0.93	0.95	0.76	0.96	0.58	1.05	1.13	1.25	1.16	1.22
Ba/Nb	(i)	6.9	17.6	13.3	OIB	9.04		7.61	7.80	6.29	8.39	10.71	10.89	14.26	8.42	9.34	8.37	6.59		
	(ii)	4.7-6.9	9.1-22.1	6.4-13.3	OIN	10.13	11.23	8.12	8.11	8.45	8.96	10.57	14.39	13.77	7.93	11.09	9.45	7.35	12.32	8.50
Ce/Nb	(i)	1.60		2.05	OIB	1.89		1.69	1.77	2.17	1.75	1.71	1.71	1.79	1.68	1.92	2.15	2.15		
					OIN	1.79	1.45	1.63	1.53	1.55	1.83	1.78	1.43	1.96	1.16	2.13	2.21	2.50	2.14	2.18
Rb/Nb	(ii)	0.30-0.43	0.69-1.41	0.58-0.87	OIB	0.58		0.54	0.65	0.23	0.60	0.63	0.46	0.45	0.66	0.42	0.69	0.89		
					OIN	0.51	0.39	0.34	0.42	0.64	0.53	0.70	0.38	0.54	0.42	0.34	0.55	0.77	0.57	0.41
Th/Nb	(i)	0.10		0.13	OIB	0.09		0.09	0.13	0.08	0.10	0.11	0.07	0.08	0.07	0.10	0.09	0.09		
	(ii)	0.071-0.123	0.094-0.130	0.105-0.168	OIN	0.11	0.09	0.09	0.10	0.06	0.13	0.13	0.09	0.12	0.07	0.12	0.11	0.11	0.26	0.16
Zr/Nb	(ii)	2.7-5.5	3.5-11.1	4.4-7.8	OIB	6.58		5.10	4.64	4.83	4.83	4.28	6.74	5.75	8.04	5.86	7.10	9.42		
					OIN	3.81	3.79	2.95	3.62	4.13	2.84	3.36	3.51	3.39	3.03	4.18	5.92	5.31	3.53	2.30
K/Nb	(i)	175	400	280	OIB	226		204	210	96	229	162	192	194	280	171	340	292		
	(ii)	66-187	194-523	203-378	OIN	146	124	110	109	183	138	111	125	184	128	130	194	237	132	92
	(iii)	160-180	270-430	200-250																

Island acronyms as given in Figures 4-3 to 4-7. *OIN mean does not include JP. **Data from: (i) Saunders *et al.* (1988); (ii) Weaver (1991); (iii) Sun & McDonough (1989)

islands (strongly EMI and EMII), except on Samoa (1 sample) and Aitutaki (2 samples), or on the strongly HIMU islands. All other islands lie within a field defined by DMM, HIMU, and EMI end-member compositions on isotope ratio diagrams. As a result, OIB have frequently been considered to be variable mixtures of these end-member components and OIN, as with OIB in general, would be expected to signal trace-element ratios characteristic of the prevalent mantle (PREMA) composition. However, end-member components are largely a convenient way of describing trends on isotope-ratio diagrams. The existence of end-member source components for most OIB cannot be established by any direct means and the composition of a supposed mixture does not give unambiguous information about the parentage of the mixture. Interpretations of isotope-ratio diagrams and trace-element ratio characteristics based on presumed end-member component mixing could, therefore, be misleading. Secondly, some of the trace-element ratios are strongly partial-melting dependent (e.g. Zr/Nb) and must, therefore, be used with caution. Finally, the OIN ranges in many cases vary very little from the OIB ranges.

In matching the island averages for each of the thirteen trace-element ratios to the bands set out in Table 4.2, the conclusions reached were that either a ratio is obviously partial melting dependent (e.g. Zr/Nb), completely ambiguous (e.g. La/Nb, Th/Nb, Ce/Nb, Th/La, Ce/Pb), or indicates an EMI affinity (e.g. Ba/Nb, Ba/Th, Ba/La) and a HIMU affinity (e.g. Rb/Nb, K/Nb, Nb/Pb) in both OIB and OIN. For those ratios where EMI and HIMU are indicated, OIN appears to be more strongly HIMU- or EMI-orientated than OIB from the same island. The ability of highly undersaturated magmas to be more strongly HIMU- and EMI-orientated than larger degrees of melting suggests that OIN sample HIMU- and EMI-type source materials more efficiently than OIB. In this case, these source materials must be more readily fusible than the host mantle in which they reside and the apparent dominance of HIMU or EMI in OIN and complementary OIB depends on the relative availability of each type of source material during partial melting processes.

In Section 4.7 it was shown that OIN and OIB could be derived from a depleted mantle source by the production of an initial small amount of carbonate liquid which becomes incorporated in more voluminous silicate melting. The mantle source was assumed to have been depleted by the extraction of the continental crust from 40% of the mass of the mantle and the lower abundances of Rb and K in OIN to be due to the presence of residual amphibole in the mantle source. The possibility of a heterogeneous mantle source for OIB and OIN in which certain components are more readily incorporated into small melt fractions has implications for the origin of the Rb, K, and Pb, anomalies in OIN and OIB. A currently popular hypothesis is that HIMU magmas are generated from the dehydration residue of subducted oceanic lithosphere (e.g. Saunders *et al.*, 1988; Sun & McDonough, 1989; Weaver, 1991) which has accumulated in the deep mantle, either near the core-mantle boundary or at the 670 km discontinuity. This source is thought to have high HFSE/LILE and HFSE/LREE due to mobility of LILE and LREE in dewatering processes. If Rb, K, and Pb behave incompatibly during melting, small melt fractions from a source already depleted in LILE in this way are not likely to show stronger Rb, K, and Pb deficiencies than OIB from the same source unless small degrees of partial melting preferentially incorporate the depleted source material. If slab material (eclogite) is more readily fusible than the surrounding mantle it may not be necessary to appeal to residual amphibole to account for the low abundances of Rb and K in OIN relative to OIB.

In Section 4.8 it was shown that K concentrations in small melt fractions increase as degree of partial melting increases but then decrease as partial melting increases through the range of partial melting appropriate to most OIB. This pattern is not consistent with the model described above. The incorporation of large amounts of K-depleted source material in small melt fractions which is progressively diluted by "normal" (higher-K) mantle as melting progresses would be expected to produce negative correlations throughout the range of melting shown on incompatible-element diagrams such as Figure 4-24. The model melting curves shown in Figures 4-24 to 4-27 suggest that the distribution of data can be explained if the sources of OIN and some OIB contain small amounts of

amphibole which are residual at small degrees of partial melting but which are consumed before the degrees of melting appropriate to most OIB are reached. Potassic phases can only be stable at relatively shallow depths, <70 km for amphibole and 70-170 km for phlogopite (Wendlandt & Eggler, 1980b; Schneider & Eggler, 1986). It is possible, therefore, that either HIMU-type magmas equilibrate with potassic phases at shallow depths or that HIMU source material resides in the upper mantle at shallower depths than previously believed (*cf.* McKenzie & O'Nions, 1983; Hawkesworth *et al.*, 1986; McKenzie & O'Nions, 1995).

4.10 Summary

Feldspar-free basic volcanic rocks represent the smallest degrees of partial melting in the OIB source region. Study of the trace-element variation in ocean island nephelinites (OIN) and ocean island basalts (OIB) has revealed features which can be related to the mineralogy of the source regions from which OIN and OIB are derived and to the mantle processes which may be involved in the generation of the magmas. The results of these studies are consistent with the evidence presented in Chapter 3 for the involvement of carbonate precursor liquids in OIN and for the presence of potassic phases in the source. Incompatible trace-element modelling has permitted certain constraints to be imposed on the mineralogy and composition of oceanic intraplate mantle sources. These constraints have implications for the evolution of the oceanic mantle and the origin of isotopically distinct mantle components such as HIMU, EMI, and EMII. The main conclusions from Chapter 4 are

(i) Oceanic nepehelinites (OIN) have a much smaller range of incompatible-element concentrations than their continental counterparts (CON). The range of CON overlaps that of OIN but extends to higher concentrations in the more highly incompatible elements. Some CON magmas may have incorporated

material from continental lithosphere which has been enriched by metasomatising fluids or asthenosphere-derived small melt fractions.

(ii) Normalised incompatible-element patterns are similar for average OIN and average CON. The composition of magmas in both environments may, therefore, be dominated by melts derived from the asthenosphere. Incompatible-element patterns for average OIB and average OIN are also similar but OIN, as would be expected for small melt fractions, are more enriched in incompatible elements than OIB.

(iii) Relative to primitive mantle, both OIB and OIN are depleted in Rb, K, and Pb, but OIN are more depleted in these elements than OIB. There is no firm evidence to suggest that OIB, in general, have been affected by secondary LFSE mobility on the scale required to produce the anomalies. It is also considered unlikely that OIN have been preferentially subjected to secondary alteration processes. The source of OIN and OIB is either depleted in Rb, K, and Pb, or these elements are retained in potassic phases in the mantle source.

(iv) Mean values of a number of incompatible-element ratios have been calculated. In each case, mean OIB has been compared with mean OIN to derive a relative compatibility sequence appropriate to OIB. In order of increasing compatibility this is

$$Ba<Th<Nb<La\cong P<Rb\cong Ce<Nd<Pb\cong Ti<Zr\cong K<Y$$

Apart from Rb and K (and, to a lesser extent, Pb and P) this is similar to the sequence proposed by Sun & McDonough (1989).

(v) Highly incompatible trace elements (Ba, Th, Nb, K) are strongly enriched in small melt fractions of both silicate and carbonate-silicate mixtures regardless of trace-element partitioning between carbonate and silicate. The presence of carbonate in a mixed melt can only be detected at very small degrees of partial melting ($F < 0.002$). With more compatible elements which favour carbonate liquids (Sr, P, REE, Y) carbonated melts are, theoretically, distinguishable at $F < 0.005$ but with the elements which strongly favour silicate liquids (Zr, Ti) the

presence of carbonate should be detectable throughout the range of partial melting appropriate to OIB.

(vi) For small melt fractions (up to 1% partial melting), the involvement of carbonate precursors in more voluminous silicate melting should result in liquids with lower concentrations of Zr and Ti and higher concentrations of LREE, Sr, and P.

(vii) Melting models based on HFS trace-element ratios suggest that OIB and OIN can be derived from a lherzolite mineralogy at depths corresponding to the field of garnet stability or the garnet-spinel transition zone. Most OIN can be derived from primitive lherzolite but many OIB require a depleted mantle component in the source region.

(viii) Multi-element melting models indicate that neither OIN nor OIB can be generated by silicate melting of a primitive garnet lherzolite source. A successful fit of average OIN and OIB compositions to theoretical normalized incompatible-element patterns has been obtained by assuming a carbonate-silicate melt derived by 0.2 - 0.5% partial melting of a depleted amphibole garnet peridotite. This is not a unique solution but the constraints imposed on the preferred model, by assuming reasonable values for the model parameters, may also be relevant to the generation of OIN and OIB.

(ix) Both source depletion and residual amphibole were required in the models to account for the Rb, K, and Pb, anomalies characteristic of OIN and OIB. A carbonate precursor liquid, derived by 0.1% melting, was required to account for the high concentrations of REE, Sr, and P.

(x) None of the models predicted the high concentrations of Zr, Ti, and Th, in OIN and OIB. The possibility that asthenosphere-derived small melt fractions are incorporated into the base of the oceanic lithosphere and are involved in subsequent melting events has not been considered in the models. Most of the incompatible-element budget may be controlled by the combined effects of source depletion, carbonate precursor liquids, and residual amphibole, but

remobilisation of silicate melts from the lithosphere is considered a viable means of enriching OIN and OIB in strongly carbonate-phobic elements.

(xi) Theoretical calculations for increasing degrees of partial melting of amphibole garnet peridotite (where $^{amph}D_K > 1$) predict that the K concentration in melts increases with degree of partial melting until all the amphibole is consumed. Thereafter K concentration decreases as degree of melting increases.

(xii) The concentration of K in OIN increases with partial melting whereas K concentration in OIB decreases. On incompatible-element *versus* K diagrams individual data sets can be matched to specific wedge-shaped theoretical melting curves by assuming progressively K-depleted sources. The melting curves are, as before, model dependent (see viii above).

(xiii) The OIB source is regionally heterogeneous in LFSE concentrations. Strongly HIMU islands are characterised by magmas with low Rb/Nb and Ba/Nb. OIN, regardless of provenance, have low Rb/Nb but generally have high Ba/Nb similar to OIB from DUPAL islands.

(xiv) OIN have trace-element ratios which are characteristic of HIMU and EMI and are more strongly HIMU- or EMI-orientated than OIB from the same islands. HIMU and EMI source material may be more fusible than host mantle and more efficiently sampled by OIN.

(xv) Derivation of OIN from subducted slab material which has been depleted in LILE by dewatering processes may account for the stronger HIMU character and lower K-concentration in OIN, compared with associated OIB, if OIN preferentially sample the slab material. This model is not, however, consistent with the positive correlation between K concentration and degree of partial melting observed in OIN.

(xvi) Subducted slab is thought to accumulate at the 670 km discontinuity or to penetrate into the lower mantle. Potassic phases are stable in the mantle at depths of 70-170 km. OIN either equilibrate with potassic phases at shallow depths or HIMU source material may reside in the upper mantle at shallower depths than previously considered.

Chapter 5

Trace-Element Characteristics of Continental Feldspar-Free Volcanic Rocks

5.1 Introduction

Highly silica-undersaturated feldspar-free volcanic rocks are more common in continental provinces than in oceanic environments and occur in a greater range of tectonic settings (Chapter 2). In addition, the variety of rock types found and the range of incompatible-element abundances and isotopic compositions observed is significantly larger.

Ocean island magmas are commonly believed to be derived from the convecting asthenosphere and to be free of any component which has been derived directly from the continental lithosphere. Continental magmas may also be derived from the asthenosphere but must pass through continental lithosphere before reaching the surface. The continental lithosphere is older and thicker than oceanic lithosphere and has the capability to store, for long periods of time, the products of lithospheric mantle interaction with upwardly percolating metasomatising fluids and small melt fractions derived from the asthenosphere which may be incorporated and retained in its base. These processes could be responsible for local lithospheric mantle enrichment in incompatible elements which could be superimposed on earlier enrichment events related to ancient subduction processes active during the formation and assembly of the local continental crust. The continental lithospheric mantle may be variably enriched in a variety of incompatible elements and, therefore, has the capacity to impose higher concentrations of incompatible-elements and considerably more variation in continental magma compositions than is observed in OIN.

Continental lithosphere may be Archaean, Proterozoic or, more rarely, Phanerozoic in age. Apart from kimberlites, highly undersaturated magmas do not occur in cratonic regions underlain by thick Archaean lithosphere but are generally restricted to the younger mobile belts surrounding the cratons. The oceanic lithosphere is Phanerozoic in age. Oceanic nephelinites occur only in areas of old oceanic lithosphere and, as has already been stated, are much rarer than continental nephelinites. The abundance of continental highly undersaturated volcanic rocks in areas of Proterozoic lithosphere, therefore, suggests that lithospheric age and thickness are critical to the generation of this magma type. Phanerozoic lithosphere may be too depleted to contribute significantly to alkaline magmas while Archaean lithosphere may be too thick to allow the passage of asthenosphere-derived magmas to the surface and too refractory for melting of lithospheric material to occur.

Continental intraplate alkaline volcanic provinces are almost invariably associated with extensional tectonic regimes. They are found most commonly within rift systems (e.g. East African Rift) and on the passive margins of ocean basins which developed from continental rift systems (e.g. East Greenland). However, they also occur in rift systems resulting from continental collision (e.g. Rhine Graben), extensional marginal basins associated with collision zones (e.g. Pannonian Basin, Hungary), in provinces co-linear with lines of structural weakness which result from earlier orogenic episodes (e.g. Balcones, Texas), in regions of major transcurrent faulting (e.g. Thailand), and areas of rapid uplift (e.g. SW United States). Many major provinces involve more than one of these tectonic features (e.g. uplift and rifting in East Africa). A small number of occurrences appear to be related to hot spot activity (e.g. the Bushmanland-Namaqualand and Cape Province melilitites).

Rifts have frequently been described as active or passive (Sengor & Burke, 1978) although, in practice, it is difficult to categorize rift systems unambiguously. Many rifts are thought to evolve through passive to active stages and the magmas erupted in each stage may vary in composition depending on the degree of lithosphere involvement.

Passive rifts are caused by differential stresses in the lithosphere (McKenzie, 1978). In this case, lithospheric stretching is followed by mantle upwelling. Passive rifting is characterized by small amounts of crustal extension and lithospheric attenuation. Relative to active rifts, the volume of volcanic products is low and asthenosphere-derived magmas might acquire a lithospheric mantle signature on their way to the surface. Active rifting is a consequence of mantle plume activity. In this case, asthenospheric upwelling causes uplift and rifting. Active rifts are more extended than passive rifts and have larger volumes of volcanic products. Lithospheric thinning on this scale suggests that the volcanism in active rifts might be dominated by magmas derived exclusively from asthenospheric sources.

Various lines of evidence presented in Chapter 3 were taken to indicate that most highly undersaturated magmas in both oceanic and continental environments involve carbonate liquid precursors to more voluminous silicate melting and that many of the magmas were generated from sources containing potassic phases which may have been residual in the melting process or rapidly consumed in the early stages of partial melting. Low average K_2O/Na_2O in oceanic and most continental feldspar-free volcanic rocks was taken to indicate amphibole rather than phlogopite in the source region. In Chapter 4 it was suggested that source depletion and residual amphibole might be responsible for the low concentrations of Rb, K, and Pb, in highly undersaturated oceanic magmas, while the high concentrations of LREE, Sr, and P, in carbonate magmas can arise from liquid immiscibility processes in the continental mantle possibly from a parental CO_2-rich olivine nephelinite melt (Twyman & Gittins, 1987; Le Bas, 1987; Gittins, 1989). The separation of the two magma types may be accompanied by extensive fractionation of olivine and, therefore, olivine-poor nephelinites may simply be highly evolved variants of olivine-rich varieties that have been derived from more highly carbonated magmas.

It was also suggested in Chapter 4 that there may be considerable regional variability in the concentration of some highly incompatible trace elements (Rb and Ba) and that this may be related to source composition or mineralogy. However certain we may be that oceanic and continental sources have amphibole as the main potassic phase,

potassic continental provinces have, by definition, high K_2O/Na_2O and must have been derived from K-enriched sources which may contain phlogopite rather than amphibole. The presence of phlogopite in continental sources may be indicated by the behaviour of Rb in the magmas ($^{Rb}D_{amph}$ = 0.023 whereas $^{Rb}D_{phlog}$ = 1.7, Halliday *et al.*, 1995b) and would suggest that the magmas have been derived from greater depths than most continental magmas, i.e. 70-150 km (Olafsson & Eggler, 1983; Brey *et al.*, 1983; Schneider& Eggler, 1986).

This Chapter makes a detailed study of the trace-element composition of highly undersaturated rocks from sodic and potassic continental provinces and, using the models developed in Chapter 4, attempts to assess the contribution of the continental lithosphere to continental magmas in relation to tectonic environment, to identify the extent of carbonate involvement in continental magmatism, and to establish the relative importance of amphibole and phlogopite in the source region. The trace-element characteristics of olivine-poor nephelinites from carbonatite-nephelinite associations will be investigated in order to define a relationship between olivine-poor and olivine-rich nephelinites and to seek evidence for the operation of liquid immiscibility in highly carbonated magmas.

5.2 Trace-Element Data Tables

Trace-element abundances for the 488 feldspar-free volcanic rocks selected for this study appear with the major-element data in Appendix C. Average trace-element compositions for ocean island nephelinite (OIN), continental nephelinite (CON), potassic continental rocks from the Western Rift, Uganda (WR), and New South Wales, SE Australia (NSW), and olivine-poor continental nephelinite (COP) are given in Appendix Tables E-6 to E-9, respectively. Each of these tables gives averages by island, volcanic complex, or province, as appropriate, and an overall average for the subset of data. Average trace-element compositions for CON, WR, NSW, and COP are summarised in Table 5-1.

Table 5-1 Summary of Average Trace-Element Compositions

	CON Av of 215 analyses (av of 37 groups)	WR Av of 53 analyses	NSW Av of 6 analyses	COP Av of 89 analyses (av of 25 groups)
Incompatible trace elements (ppm)				
Rb	54 (51)	122	159	85 (78)
Ba	1189 (1208)	2007	1801	1857 (1669)
Th	12.7 (12.7)	19.6	11.3	18.8 (17.0)
Nb	112 (110)	173	113	203 (172)
K	15,193 (15,276)	34,702	49,895	24,989 (23,910)
La	102 (101)	148	130	137 (126)
Ce	196 (194)	290	257	242 (224)
Pb	7.2 (7.0)	7.7	11.9	14.5 (13.5)
Sr	1485 (1397)	1957	1537	2163 (2025)
P	4,451 (4,539)	3,491	4,189	4,277 (4,364)
Nd	83 (83)	114	119	92 (84)
Zr	337 (333)	352	681	493 (439)
Ti	18,585 (18,165)	25,958	27,817	13,669 (13,968)
Y	32 (31)	21	30	38 (38)
Compatible trace elements (ppm)				
V	300 (290)	306	213	255 (253)
Sc	21 (21)	22	17	8 (8)
Cr	317 (394)	547	357	42 (56)
Ni	201 (228)	244	326	39 (52)
Cu	110 (101)	112	54	79 (82)
Zn	112 (112)	92	114	143 (145)

5.3 Incompatible-Element Characteristics of CON

Mantle-normalised incompatible-element patterns of average continental (CON) and oceanic (OIN) feldspar-free compositions have been shown to be remarkably similar (Section 4.3, Chapter 4) and it was proposed that the incompatible-element profile in both environments is, therefore, dominated by a common source composition and that the common source for the magmas lies in the asthenosphere. Primitive mantle-normalised abundances (Fig. 5-1a) indicate that CON are generally more enriched in incompatible elements than OIN. CON may, therefore, represent smaller melt fractions, or more evolved

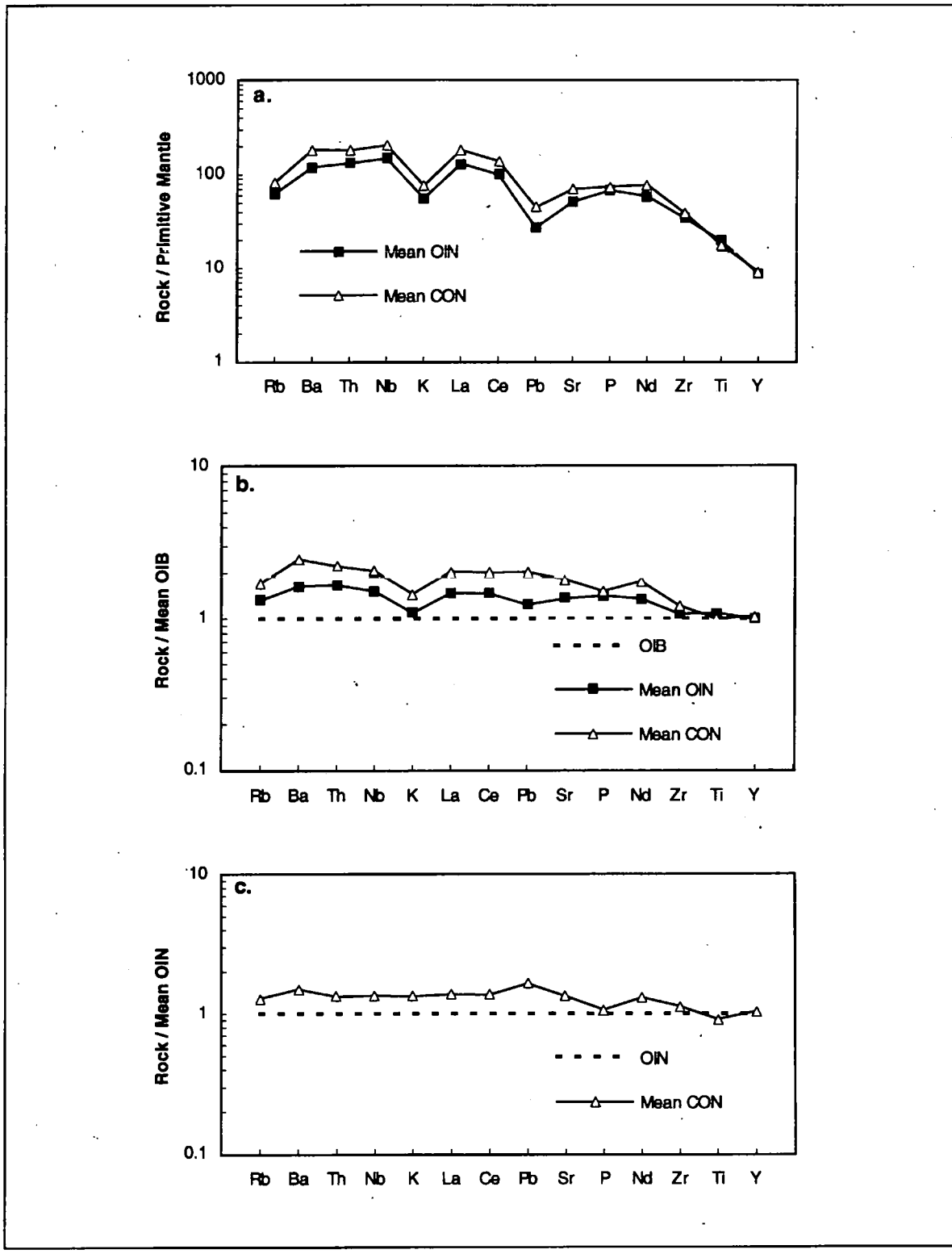

Figure 5-1. Incompatible-element concentrations of feldspar-free volcanic rocks. Average OIN & CON (data from Table 4-1, Chapter 4) normalised to

a. Primitive mantle values (McKenzie & O'Nions, 1995)
b. Calculated Mean OIB composition (Table 4-1)
c. Calculated Mean OIN composition (Table 4-1)

magmas, or they may have been derived from enriched sources which are unavailable in the source regions of the oceanic types. As discussed in Chapter 4, it seems unlikely that extremely small melt fractions would be erupted more commonly in continental regions than in the ocean basins and there is no generally observed tendency towards more extreme silica-undersaturation on the continents which would support such a conclusion. Furthermore, sample screening (MgO > 4 wt.%) has excluded all highly evolved rocks from both data groups. However, only 40% of the CON samples obtained for this study have MgO > 10 wt.% as opposed to 85% of the OIN samples. This suggests that CON may, in general, be more evolved than OIN but the primary magma calculations presented in Chapter 3 indicate that mafic continental and oceanic nephelinites have experienced similar amounts of crystal fractionation. Isotopic ratios, on the other hand, strongly indicate the involvement of old enriched sources in some continental magmatism and, as suggested in Chapter 1, the continental lithosphere is the obvious candidate for the source of this enriched mantle material.

Subtle differences in normalised abundance are enhanced if OIN and CON are normalised to mean OIB (Fig. 5-1b). This diagram suggests that CON may be preferentially enriched in Ba and Pb, and depleted in P and Ti, relative to other incompatible elements. Normalising to a mean OIN composition (Fig. 5-1c) shows these small anomalies more clearly. The Ba and Pb enrichment may be a consequence of crustal contamination, a consistent difference in source mineralogy, or involvement of a lithospheric source which has been differentially enriched in mobile elements by upwardly percolating fluids from the asthenosphere.

Crustal contamination is normally associated with SiO_2-rich magmas with high concentrations of LILE. If crustal contamination is responsible for an almost two-fold Pb-enrichment in CON then an upper crustal input with high Pb is indicated in order to retain the highly silica-undersaturated major-element characteristics. Simple mass balance calculations indicate that 82 parts of magma with average OIN composition (Pb = 4.2 ppm, Table E-6) with 18 parts of upper crustal material (Pb = 20 ppm, Taylor & McClennan,

1985) produces the observed 7 ppm Pb in average CON (Table 5-1). This is equivalent to about 20% crustal contamination of average OIN. Crustal contamination on this scale would raise SiO_2 content of average OIN from 39% to about 43.5 wt.% and it is unlikely that magmas with this amount of silica would be feldspar-free. Furthermore, other trace-element abundances in average CON are higher than would be achieved by contamination with only 20% upper crustal material. The lower crust has significantly lower abundances of highly incompatible trace elements than the upper crust. If contamination with lower crustal material is considered then the required level of contamination is so high that the major-element chemistry would be substantially changed and the magmas could no longer be classified as nephelinites.

Phlogopite and amphibole have different propensities for Pb and Ba ($^{phlog}D_{Pb}$ = 0.0043, $^{amph}D_{Pb}$ = 0.019, $^{phlog}D_{Ba}$ = 1.5, $^{amph}D_{Ba}$ = 0.010, Halliday *et al.*, 1995b). If CON are derived from phlogopite-bearing sources rather than amphibole peridotite, small melt fractions may be more enriched in Pb. However, by the same reasoning, the partitioning of Ba in phlogopite and amphibole suggests that CON sources contain amphibole rather than phlogopite. Amphibole and phlogopite are extremely variable in Ba content and this is reflected in the variability of published partition coefficients. The coefficients compiled by Halliday *et al.* (1995b) may not be appropriate to most CON. Ba and Pb enrichment may therefore be a source characteristic of CON, or due to some other process such as silicate-carbonate liquid partitioning (Section 5.4), rather than a consequence of K-mineral/liquid partitioning. Depletions in Ti and P may be due, respectively, to the fractionation of pyroxene and magnetite, and apatite. Opaque oxides and apatite are common phenocryst phases in continental feldspar-free rocks. Ti-depletion in magmas derived from phlogopite-bearing sources could be due to the stabilisation of ilmenite which is residual in the melting process. The high solubility of Ti in basic magmas, however, indicates that the existence of residual Ti-bearing phases is unlikely (Ryerson & Watson, 1987).

When CON are plotted on a Ce/Y *versus* Nb/Zr diagram (Fig. 5-2) on which melting curves calculated for primitive and depleted lherzolite compositions and the field

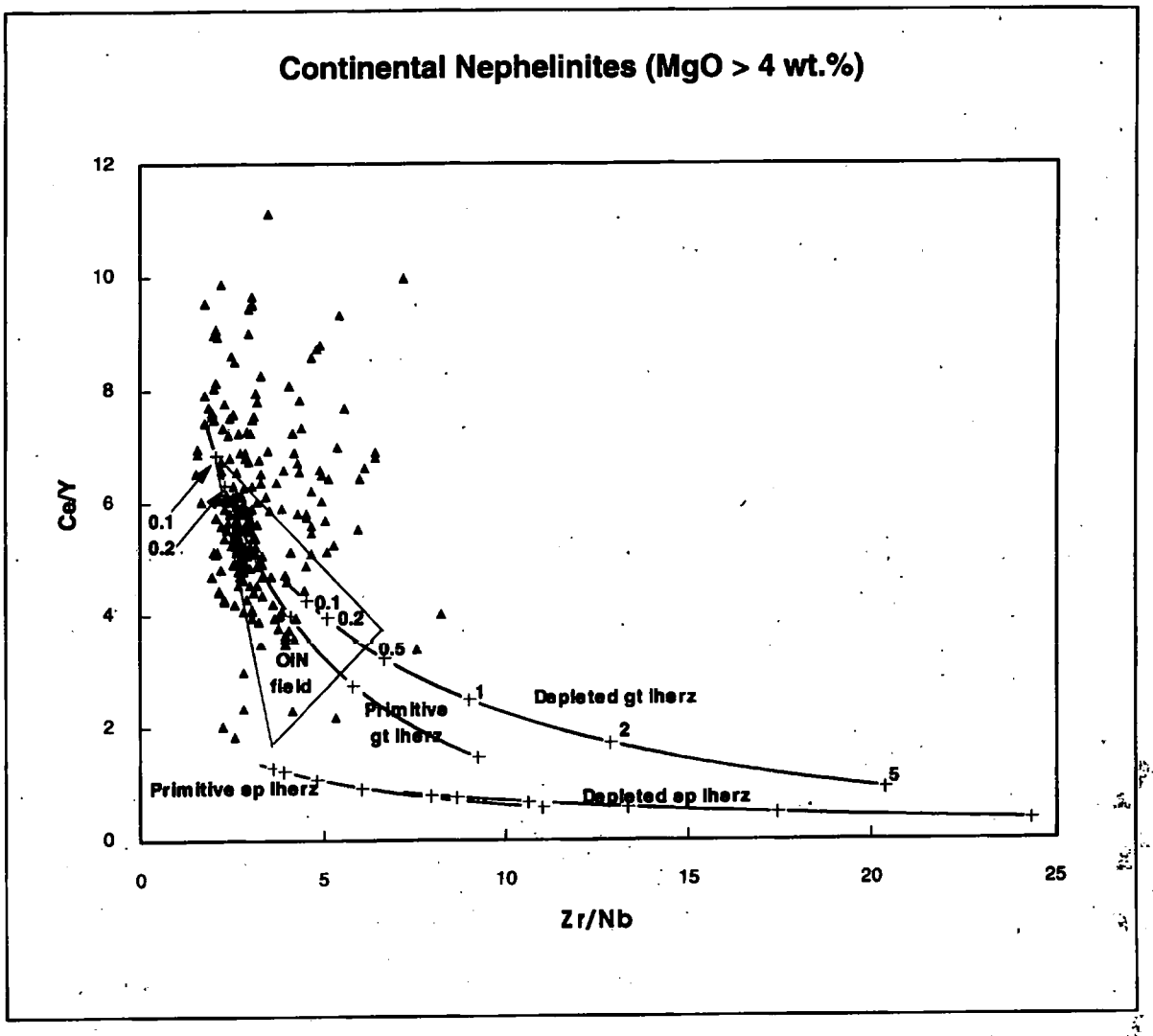

Figure 5-2. Ce/Y *versus* Zr/Nb (CON) shown against model melting curves of primitive and depleted garnet and spinel lherzolites. Cross symbols on melting curves refer to degrees of partial melting from 0.1% to 5% as shown on the curve for depleted garnet lherzolite. Model curves were calculated using the non-modal batch melting equation of Shaw (1970) $C_l/C_o = 1/(D+F-PF)$. Source mineralogy, primitive and depleted source concentrations, and partition coefficients, are taken from compilations in McKenzie & O'Nions (1991) and McKenzie & O'Nions (1995). OIN field from Fig. 4-3, Chapter 4.

of OIN data are superimposed, it appears that, in terms of these elements, many CON can be generated from a lherzolite mineralogy but that a similar number fall outside the boundaries defined by the melting curves. These have high Ce/Y, indicating LREE enrichment of the source (cf. Fig. 5-1c), but generally similar Zr/Nb. Most CON which can be derived from 'normal' lherzolite sources seem to follow the primitive garnet lherzolite melting curve but, as in the case of OIN (cf. Fig. 4-3b), a number fall on trends lying almost parallel to the y-axis and cross-cutting the partial melting curves. Some CON may, therefore, be generated from depths equivalent to the garnet-spinel transition zone.

Incompatible-element abundances of mean compositions from thirty-seven continental provinces are shown in a series of mantle-normalised and OIB-normalised diagrams (Figs. 5-3 to 5-7). These diagrams indicate that feldspar-free rocks from continental provinces are much more variable in composition than those from oceanic islands (cf. Figs. 4-4 to 4-8). Some have an overall similarity to OIN patterns (e.g. N Kenya, Fig. 5-3d & f; S Africa, Fig. 5-4f; Germany, Fig. 5-5d; Thailand, Fig. 5-7d) but others are strikingly dissimilar (e.g. N Kenya, Fig. 5-3b; Greenland, Fig. 5-6b; Colorado Plateau, Fig. 5-7f). Those provinces which have patterns fairly similar to OIN often differ from OIN in the same way. For example, preferential Pb enrichment is common (e.g. Figs. 5-3d & f), while Rb, K, and sometimes Ba, are generally less enriched than other incompatible elements (e.g. Figs. 5-7b & d). 'Exotic' patterns are generated by low Nb and Ti in the case of the SW United States (Fig. 5-7f), and low Th and LREE in Tugtilik and Gardiner, Greenland (Fig. 5-6b) and Nuanetsi (Fig. 5-4d).

In Section 4.4 of Chapter 4 it was demonstrated that OIB are distinctly heterogeneous in Rb and Ba composition and that OIN lie in the low Rb/Nb and high Ba/Nb parts of the OIB spectrum. These differences cannot be related to degree of undersaturation and may, therefore, be a consequence of source characteristics or the mineralogy from which the magmas were derived. In Figures 5-8 (Rb *versus* Nb) and 5-9 (Ba *versus* Nb), CON are shown superimposed on the appropriate OIN fields and diagnostic OIB trends (cf. Fig. 4-12). CON seem also to have low Rb/Nb and high Ba/Nb

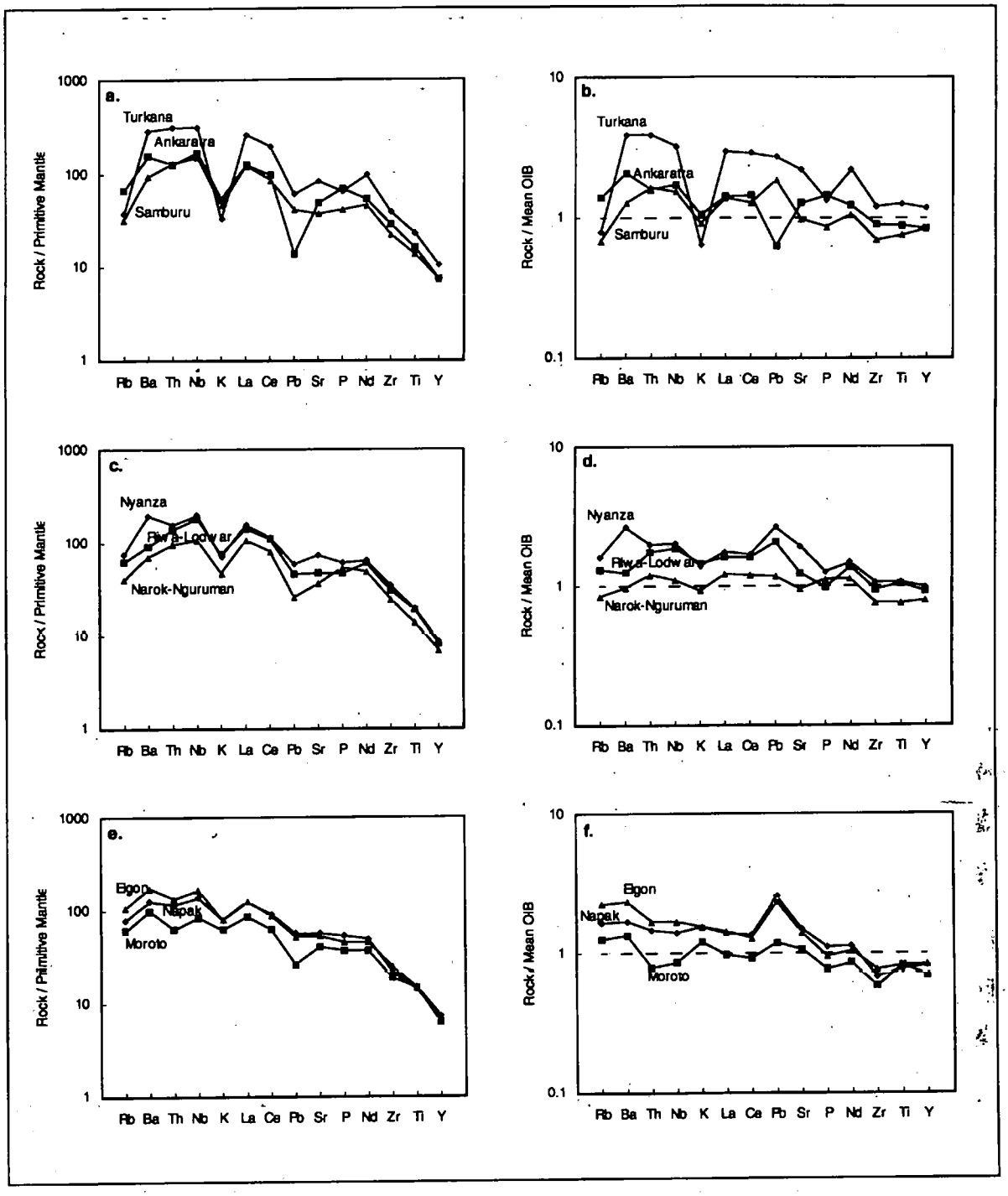

Figure 5-3. Continental incompatible-element concentrations normalised to primitive mantle values (McKenzie & O'Nions, 1995) and a calculated Mean OIB composition (Table 4-1, Chapter 4) for

a. & b. Malagasy: Ankaratra; N Kenya: Turkana, Samburu
c. & d. N Kenya: Lodwar & Riwa, Nyanza Rift, Narok-Nguruman
e. & f. N Kenya: Moroto, Napak, Elgon

Mean abundances of continental provinces from Appendix E, Table E-7.

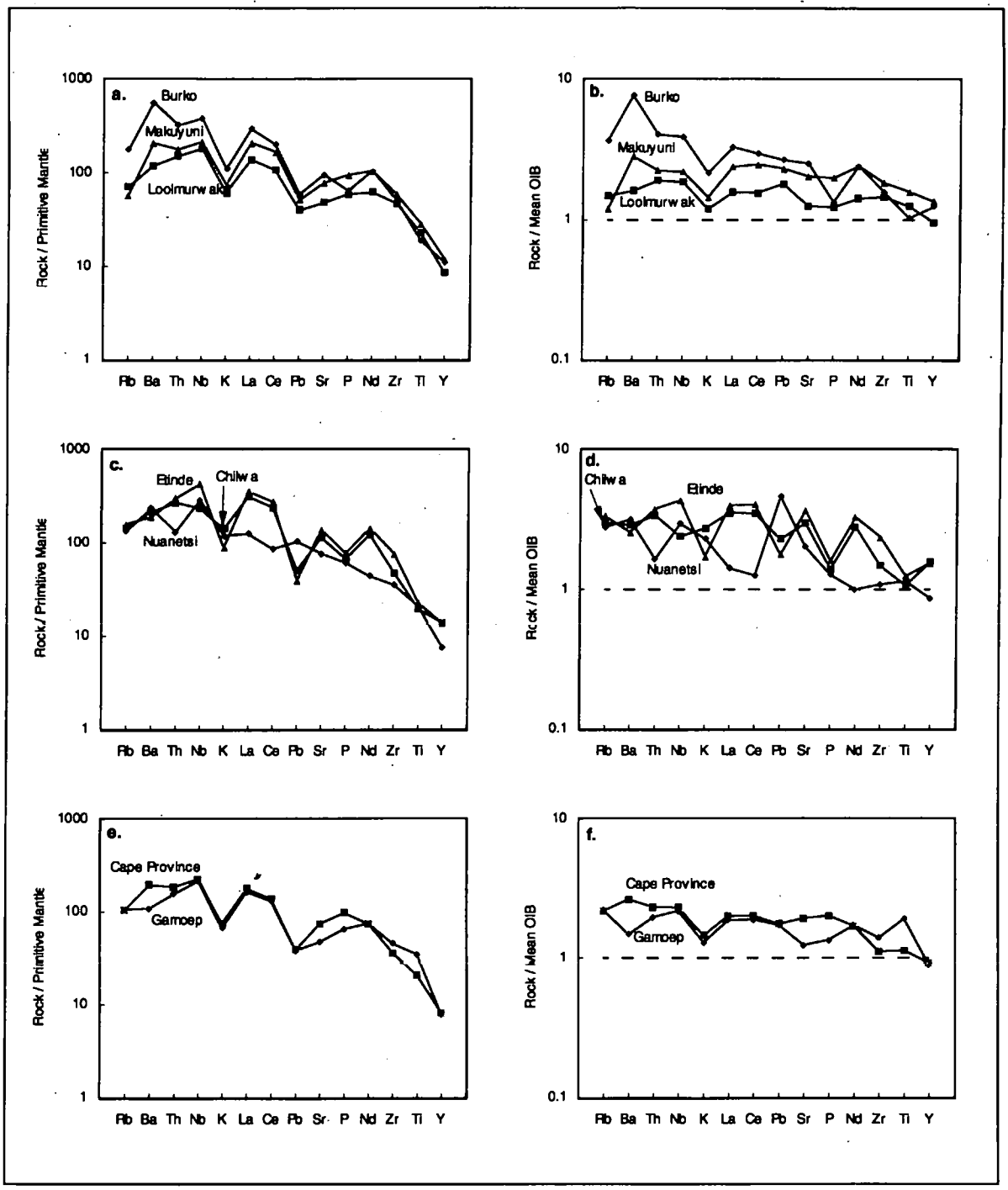

Figure 5-4. Continental incompatible-element concentrations normalised to primitive mantle values (McKenzie & O'Nions, 1995) and a calculated Mean OIB composition (Table 4-1, Chapter 4) for

a. & b. Tanzania: Loolmurwak, Burko, Makuyuni
c. & d. Malawi: Chilwa; Zimbabwe: Nuanetsi; Cameroon: Etinde
e. & f. South Africa: Cape Province, Gamoep

Mean abundances of continental provinces from Appendix E, Table E-7.

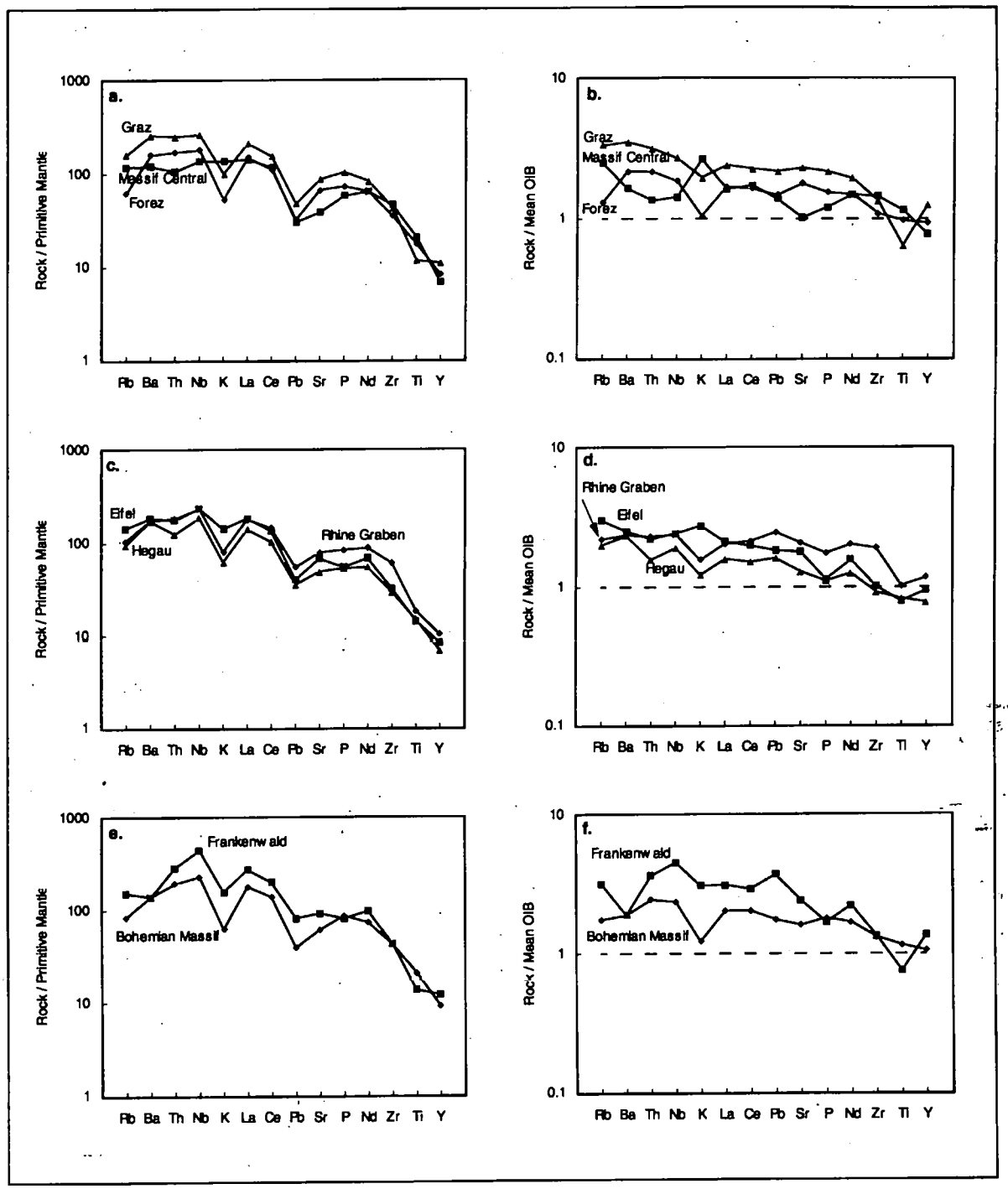

Figure 5-5. Continental incompatible-element concentrations normalised to primitive mantle values (McKenzie & O'Nions, 1995) and a calculated Mean OIB composition (Table 4-1, Chapter 4) for

a. & b. France: Massif Central, Forez; Austria: Graz
c. & d. Germany: Eifel, Rhinegraben, Hegau
e. & f. Germany: Frankenwald; Czech: Bohemian Massif

Mean abundances of continental provinces from Appendix E, Table E-7.

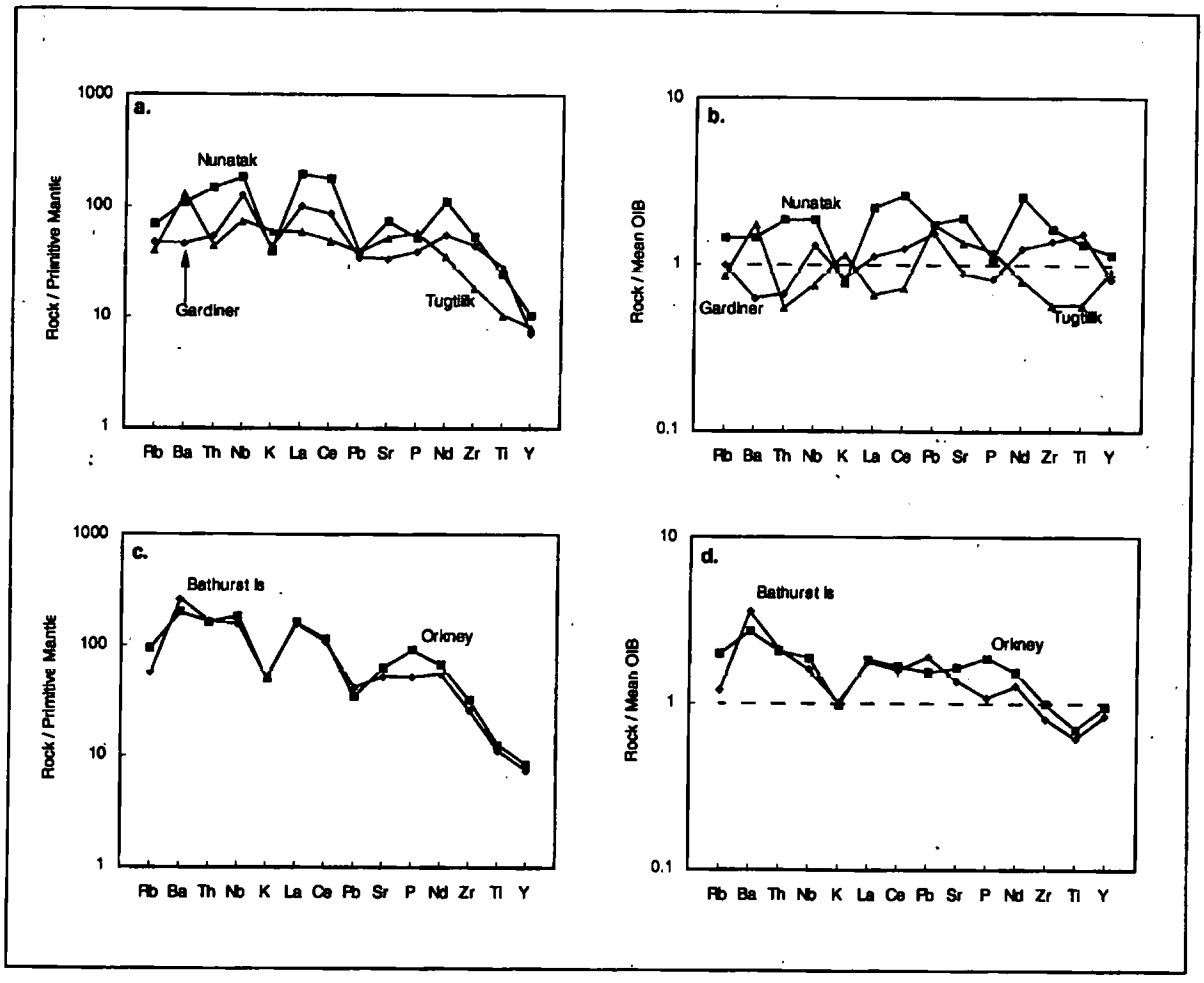

Figure 5-6. Continental incompatible-element concentrations normalised to primitive mantle values (McKenzie & O'Nions, 1995) and a calculated Mean OIB composition (Table 4-1, Chapter 4) for

a. & b. Greenland: Nunatak, Gardiner, Tugtilik
c. & d. NW Territories: Bathurst Island; NE Scotland: Orkney

Mean abundances of continental provinces from Appendix E, Table E-7.

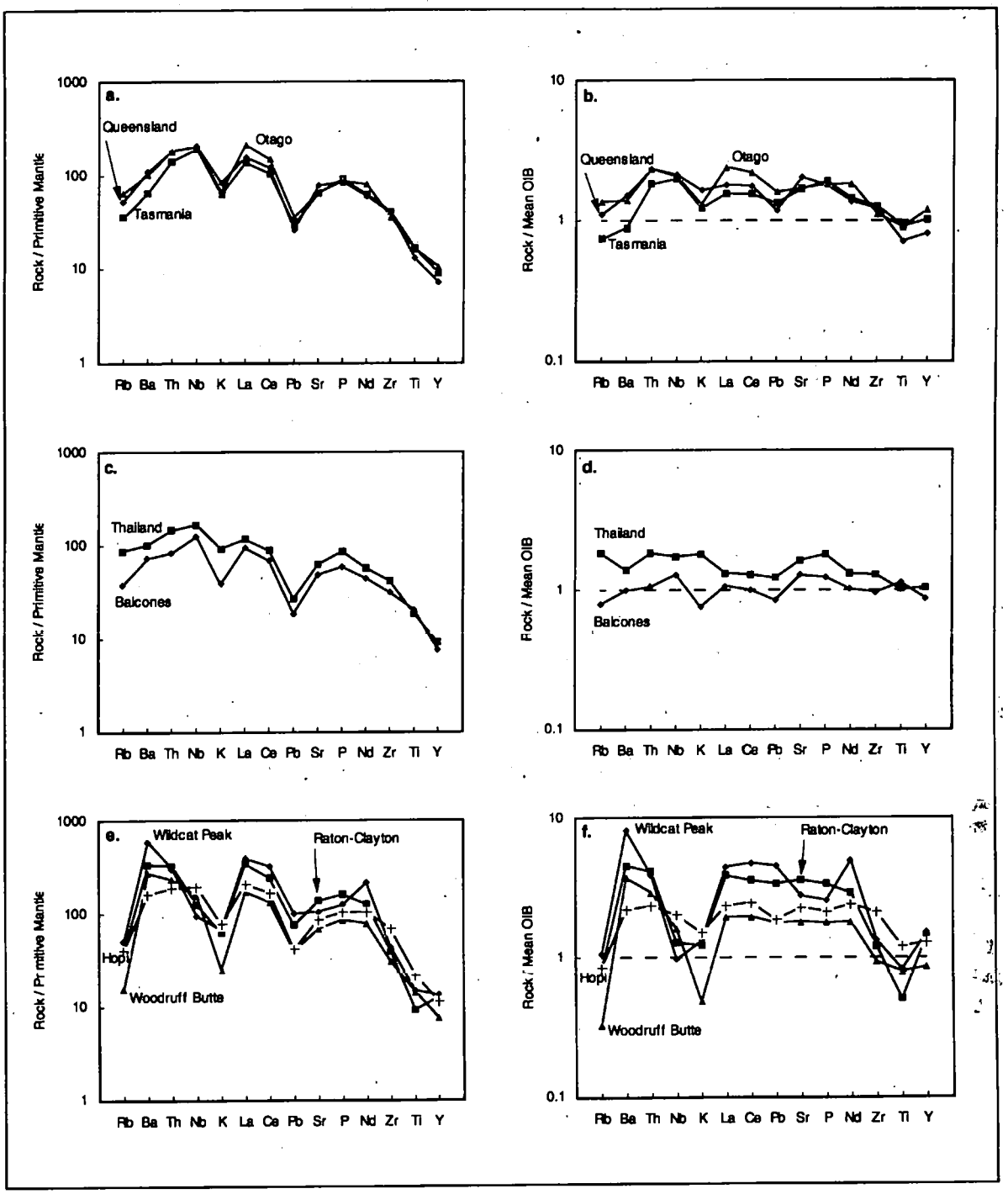

Figure 5-7. Continental incompatible-element concentrations normalised to primitive mantle values (McKenzie & O'Nions, 1995) and a calculated Mean OIB composition (Table 4-1, Chapter 4) for

a. & b. Australasia: Queensland, Tasmania, Otago
c. & d. Thailand: Chantaburi; United States: Balcones
e. & f. United States: Wildcat Peak, Wood Ruff Butte, Hopi Buttes, Raton-Clayton

Mean abundances of continental provinces from Appendix E, Table E-7.

but a large number are either more evolved than OIN or have been derived from significantly more enriched sources than the OIN source (Figs. 5-8a & 5-9a). CON primary magmas were calculated for samples with MgO > 10 wt.% and, in this case, most of the calculated primary compositions fall in the OIN field (Figs. 5-8b and 5-9b). However, some CON primary magmas have much higher Ba than most OIN and others are much lower in Ba. As with OIB and OIN, considerable structure exists within the Rb/Nb and Ba/Nb data for CON which may be related to regional differences in source composition or mineralogy.

The extent of regional heterogeneity in CON provinces is indicated by the incompatible-element profiles normalised to mean OIN (Figs. 5-10 to 5-12). These diagrams show that while most CON provinces are, on average, somewhat more enriched in incompatible elements than OIN, a number, for example Samburu (Fig. 5-10b), Narok-Nguruman (Fig. 5-10c), Moroto (Fig. 5-10e), Tugtilik and Gardiner (Fig. 5-11b), and Balcones (Fig. 5-12b), have generally lower concentrations. Others, for example Turkana (Fig. 5-10a), Burko (Fig. 5-10b), Chilwa and Etinde (Fig. 5-10d), Graz (Fig. 5-11a), Frankenwald (Fig. 5-11e), and SW United States (Fig. 5-12c) are much more highly enriched. This set of diagrams also accentuate Pb enrichment relative to OIN (e.g. Kenya Rift, Figs. 5-10a, c, & e) and the Ba, Rb, and K variability in CON. Preferential Ba enrichment can be seen in Burko (Fig. 5-10b), Bathurst Is (Fig. 5-11d), and the SW United States (Fig. 5-12c), while Gamoep (Fig. 5-10f), Gardiner (Fig. 5-11b), Frankenwald (Fig. 5-11e), and SE Australia (Fig. 5-12a) are depleted in Ba relative to other incompatible elements. High Rb and K appear in the Massif Central (Fig. 5-11a), the Eifel (Fig. 5-11c), and Thailand (Fig. 5-12b), but Turkana (Fig. 5-10a), Tugtilik (Fig. 5-11b), and SW United States (Fig. 5-12c) have low Rb and K, and SE Australia (Fig. 5-12a) has low Rb with normal K.

Clearly there is considerable variation in the composition of CON compared with OIN and this probably reflects involvement of old enriched source material which is

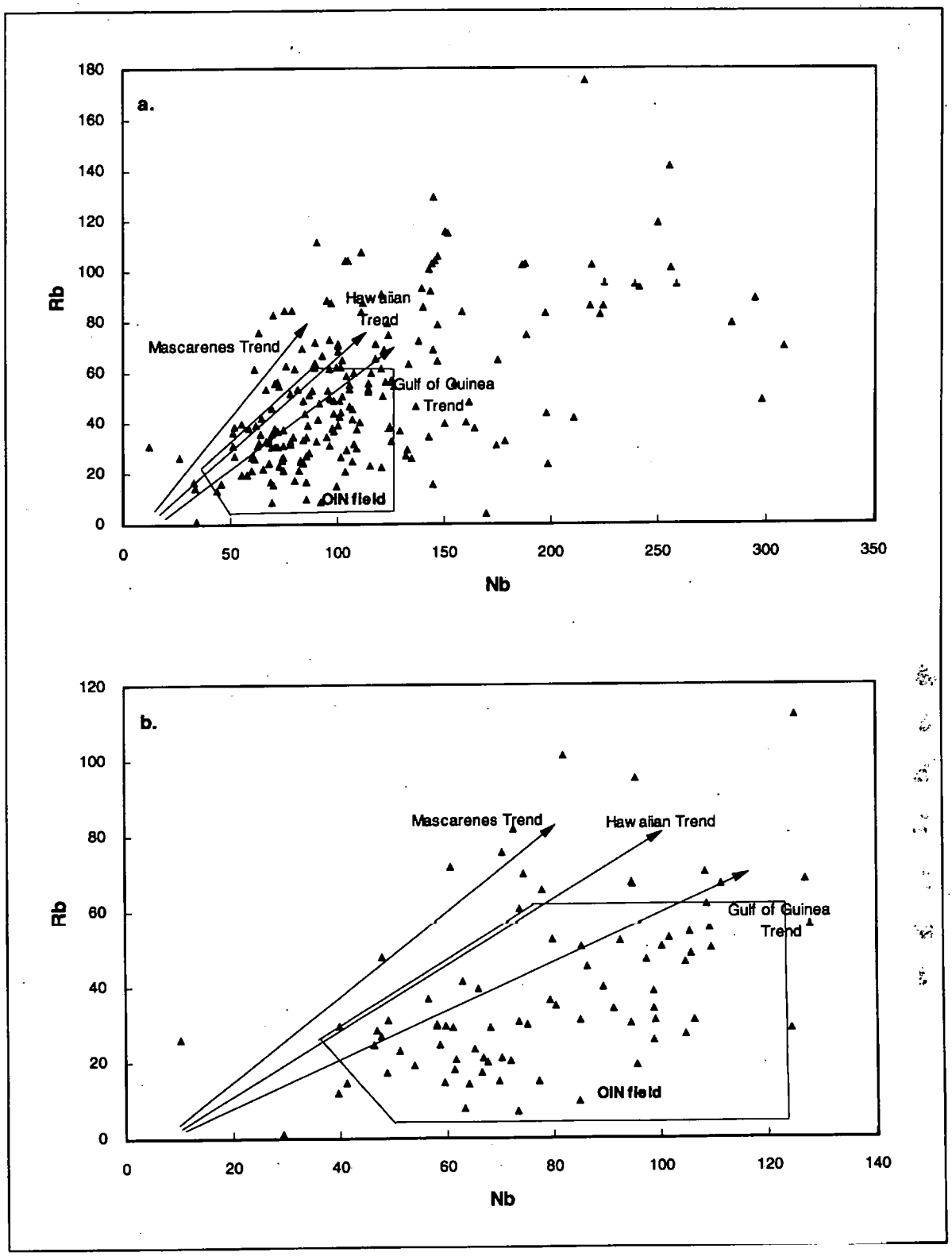

Fig 5-8. Rb *versus* Nb for CON with data trends from Fig. 4-12 (Chapter 4) superimposed.

a. CON, MgO > 4 wt.%.

b. CON calculated primary magma compositions only. Primary magmas calculated for samples with MgO > 10 wt.% as in Section 3.4 (Chapter 3) using $K_D = 0.30$ but an equilibrium forsterite content of $Fo_{90.7}$.

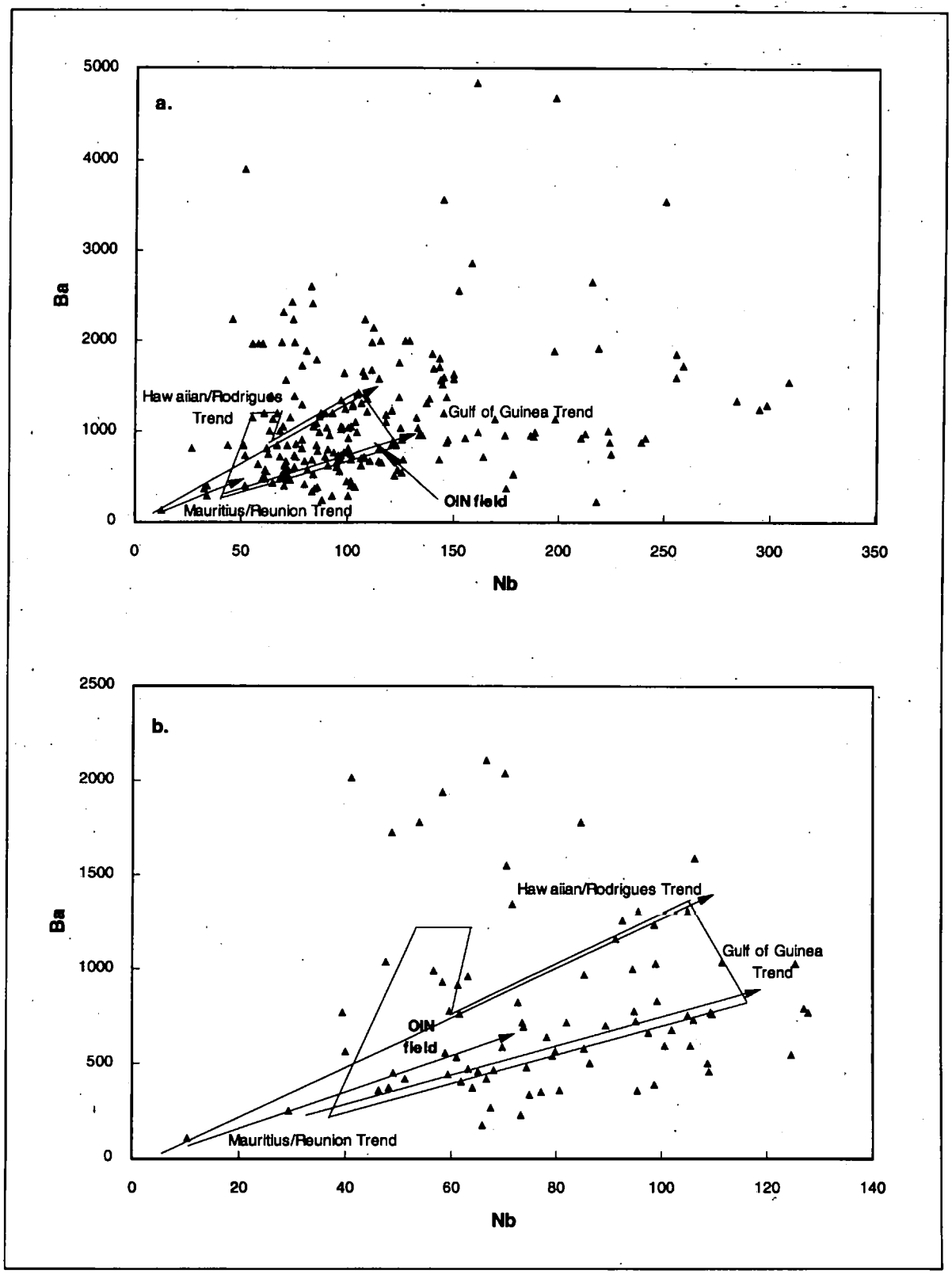

Fig 5-9. Ba *versus* Nb for CON with data trends from Fig. 4-12 (Chapter 4) superimposed.

a. CON, MgO > 4 wt.%

b. CON calculated primary magma compositions only.
Primary magmas calculated for samples with MgO > 10 wt.% as in Section 3.4 (Chapter 3) using $K_D = 0.30$ but an equilibrium forsterite content of $Fo_{90.7}$.

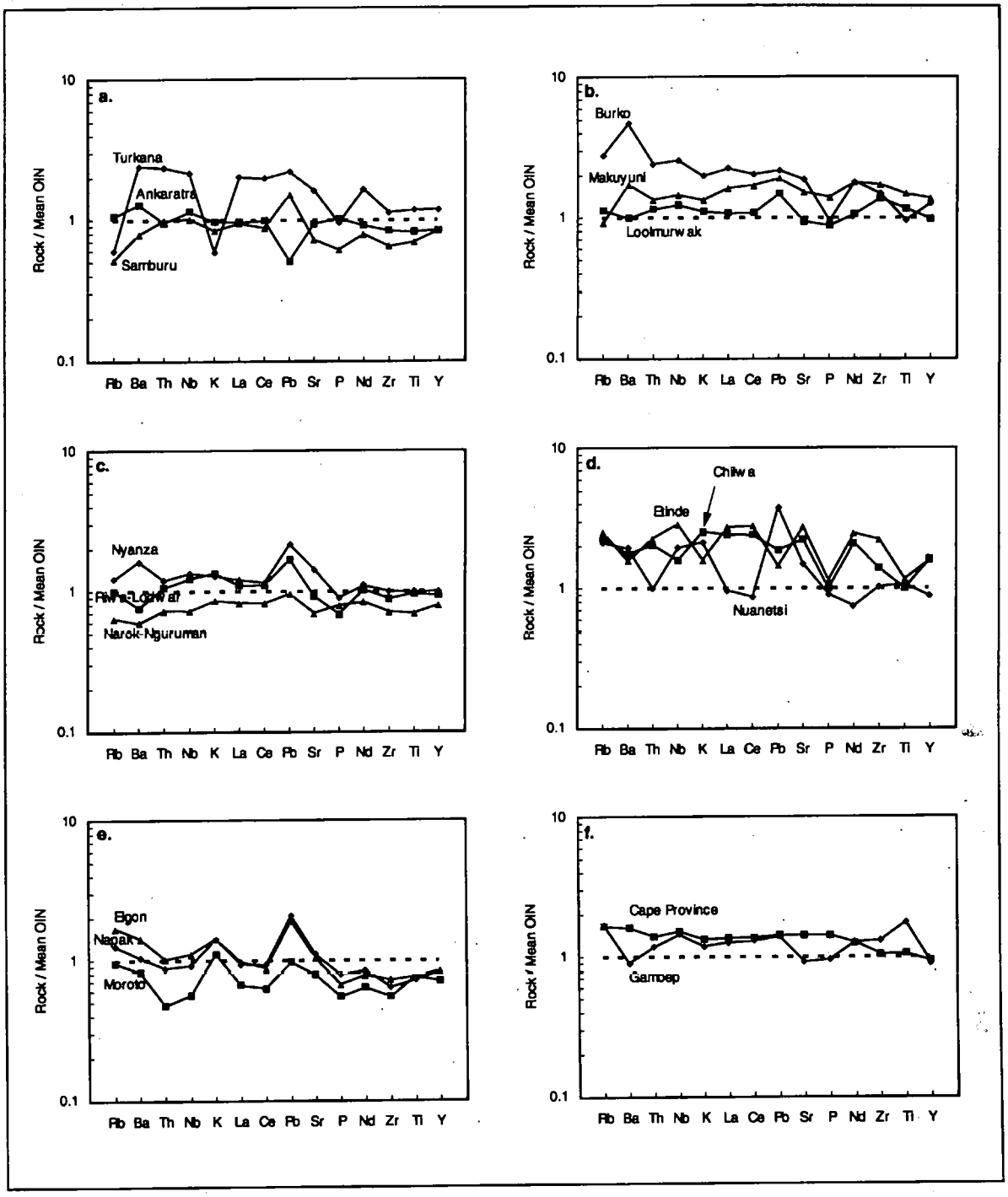

Figure 5-10. Continental incompatible-element concentrations normalised to a calculated Mean OIN composition (Table 4-1, Chapter 4) for

a. Malagasy: Ankaratra; N Kenya: Turkana, Samburu
b. Tanzania: Loolmurwak, Burko, Makuyuni
c. N Kenya: Lodwar & Riwa, Nyanza Rift, Narok-Nguruman
d. Malawi: Chilwa; Zimbabwe: Nuanetsi; Cameroon: Etinde
e. N Kenya: Moroto, Napak, Elgon
f. South Africa: Cape Province, Gamoep

Mean abundances of continental provinces from Appendix E, Table E-7.

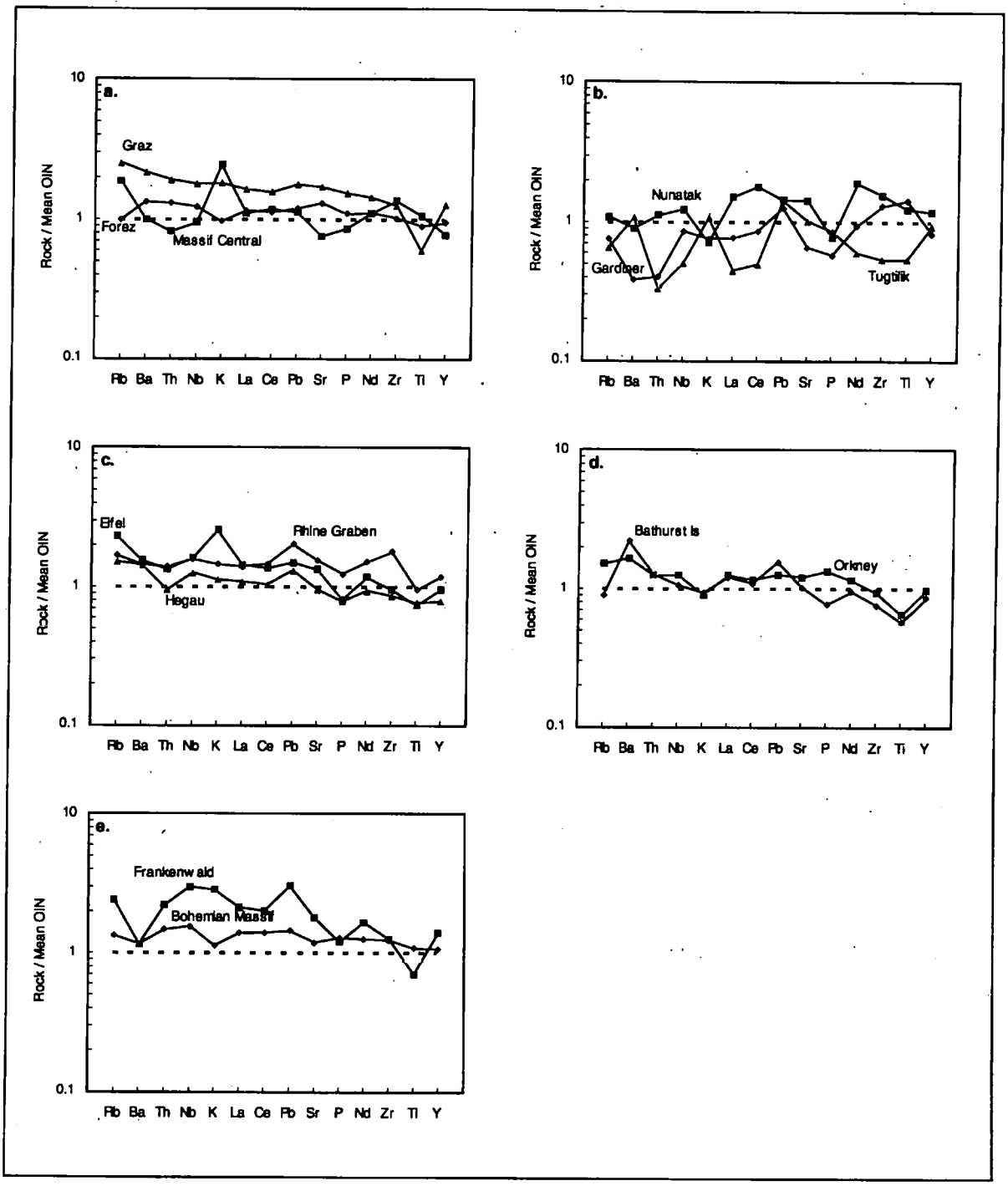

Figure 5-11. Continental incompatible-element concentrations normalised to a calculated Mean OIN composition (Table 4-1, Chapter 4) for

a. France: Massif Central, Forez; Austria: Graz
b. Greenland: Nunatak, Gardiner, Tugtilik
c. Germany: Eifel, Rhinegraben, Hegau
d. NW Territories: Bathurst Island; NE Scotland: Orkney
e. Germany: Frankenwald; Czech: Bohemian Massif

Mean abundances of continental provinces from Appendix E, Table E-7.

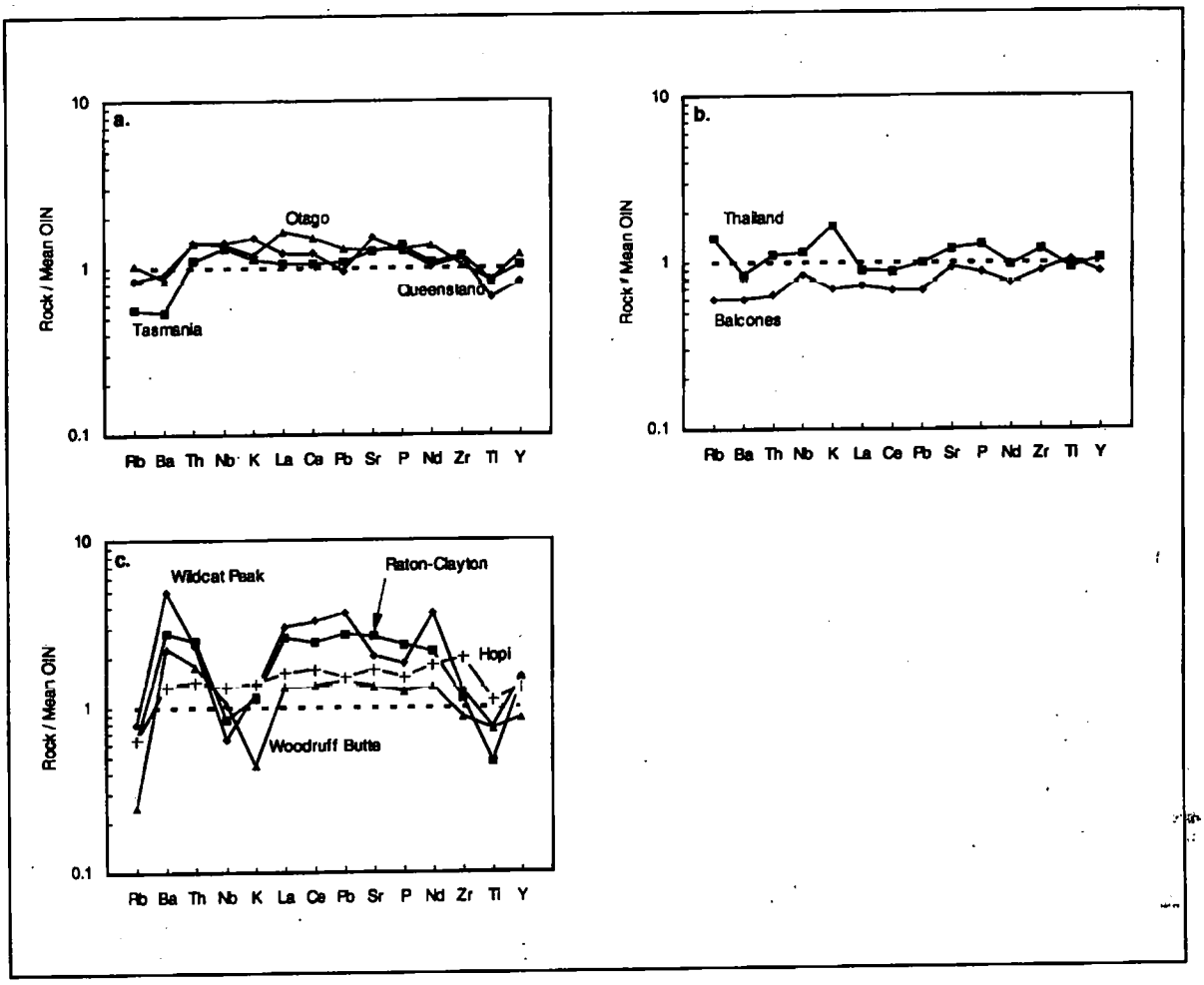

Figure 5-12. Continental incompatible-element concentrations normalised to a calculated Mean OIN composition (Table 4-1, Chapter 4) for

a. Australasia: Queensland, Tasmania, Otago
b. Thailand: Chantaburi; United States: Balcones
c. United States: Wildcat Peak, Wood Ruff Butte, Hopi Buttes, Raton-Clayton

Mean abundances of continental provinces from Appendix E, Table E-7.

derived from continental lithospheric mantle. However, a detailed investigation of CON provinces is outside the scope of this work and will not, therefore, be pursued further.

5.4 Melting Models for CON Sources

In Chapter 4, Section 4.7, various possible source compositions, source mineralogies, and partial melting processes were investigated in order to develop a model which may be applicable to the generation of OIN and OIB. By comparing average OIN and OIB incompatible-element profiles with the abundances predicted by the various melting models, it became clear that simple silicate melting of a garnet lherzolite source is inappropriate for OIN and OIB (Figs. 4-20 to 4-23). The range of models devised indicate that the mantle source must be depleted in Rb, K, and Pb (possibly by crustal extraction), in order to account for the low abundances of these elements observed in both OIN and OIB, and that a carbonate precursor liquid (derived by 0.1% melting) could account for the high concentrations of LREE, Sr, and P. Furthermore, since OIN are often more depleted in K than OIB from the same source, it was suggested in Section 4.7 that the OIN source contains a small amount of amphibole, stabilised as a result of the hydration of clinopyroxene. The amphibole may be residual at small degrees of partial melting but consumed before the degrees of melting appropriate to OIB are reached.

In Section 5.3 it was proposed that, in terms of Ce/Y *versus* Zr/Nb, many CON can be generated from a garnet or garnet-spinel lherzolite source. The results of the OIN source modelling in Chapter 4 suggest that this may be a considerable over-simplification as a model of the CON source. Figure 5-1a shows that average OIN and average CON have similar mantle-normalised incompatible-element patterns but that CON are, on average, somewhat more enriched in incompatible elements than OIN. The model developed for the OIN source (Fig. 4-19d) should also, therefore, be appropriate for CON magmas. CON, however, are considerably more variable in composition than OIN (cf. Figs. 5-3 to 5-7 with Figs. 4-4 to 4-8). For this reason it is more realistic to compare average trace-element

profiles for individual continental provinces with the abundances predicted by the preferred model.

In Figures 5-13 to 5-15 average incompatible-element concentrations of the thirty-seven continental provinces shown in Figures 5-10 to 5-12 are superimposed on the theoretical melt compositions predicted for carbonate-silicate mixed melts derived from a depleted amphibole-garnet peridotite source. A consistent feature of these diagrams is that, as with OIN, higher concentrations of Zr, Ti and, particularly, Th are observed in CON than are predicted by the model (cf. Figs. 4-20 to 4-23). Apart from the fit of these elements, for a small number of provinces (Moroto - Fig 5-13e, Narok-Nguruman - Fig 5-13c, Balcones - Fig 5-15b) the model appears to be as adequate a representation of CON magma compositions as it is of OIN magmas. However, for the majority of provinces, the model consistently fails to account for high levels of Nb and, in some cases (Turkana - Fig. 5-13a, Burko - Fig. 5-13b, Etinde & Chilwa - Fig. 5-13d, Frankenwald - Fig. 5-14e, SW United States - Fig. 5-15c), for high concentrations of LREE.

The mass-balance calculations shown in Chapter 3 (Section 3.6) indicate that, on the basis of major-element chemistry, OIN may be carbonate-silicate mixed magmas where the carbonate addition is about 10%. Cape Verde appears to have a much higher proportion of carbonate (20-33%) but, in general, OIN seem to contain less than 20% carbonate. However, it was stressed in Chapter 3 that these results represent lower limits of carbonate involvement because OIB, in general, may incorporate small amounts of carbonate liquid which are not identifiable in the trace-element profiles at larger degrees of partial melting. Carbonate liquids strongly favour Ba, Sr, P, and LREE, and in Chapter 4 (Section 4.6) it was shown that the influence of carbonate could be responsible for high concentrations of LREE, Sr, and P in OIN. Small silicate melt fractions are also highly enriched in Ba but, for somewhat more compatible elements such as LREE, Sr, and P, the high concentrations of these elements may be controlled by the carbonate fraction. In this case, the relative LREE enrichment of some CON over OIN (e.g. Burko, Chilwa, Etinde) may be due to a greater proportion of carbonate in CON magmas. Silicate magmas in

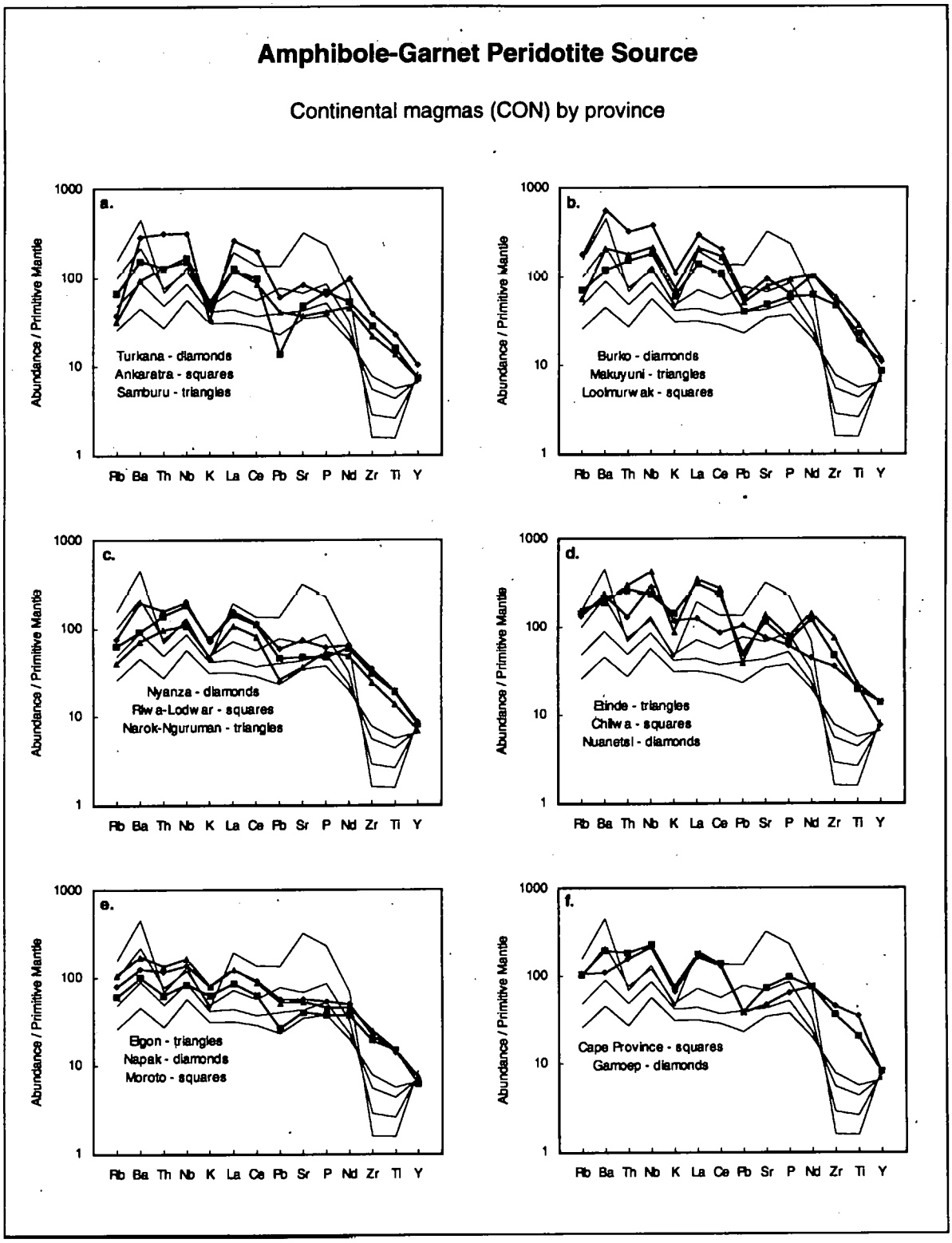

Figure 5-13. Theoretical mantle-normalised incompatible-element patterns for depleted amphibole-garnet peridotite for 0.1, 0.2, 0.5, and 1% partial melting with a carbonate precursor liquid derived by 0.1% melting of the same source. Model parameters as in Fig. 4-19 (Chapter 4). Mean abundances of continental provinces from Appendix E, Table E-7.

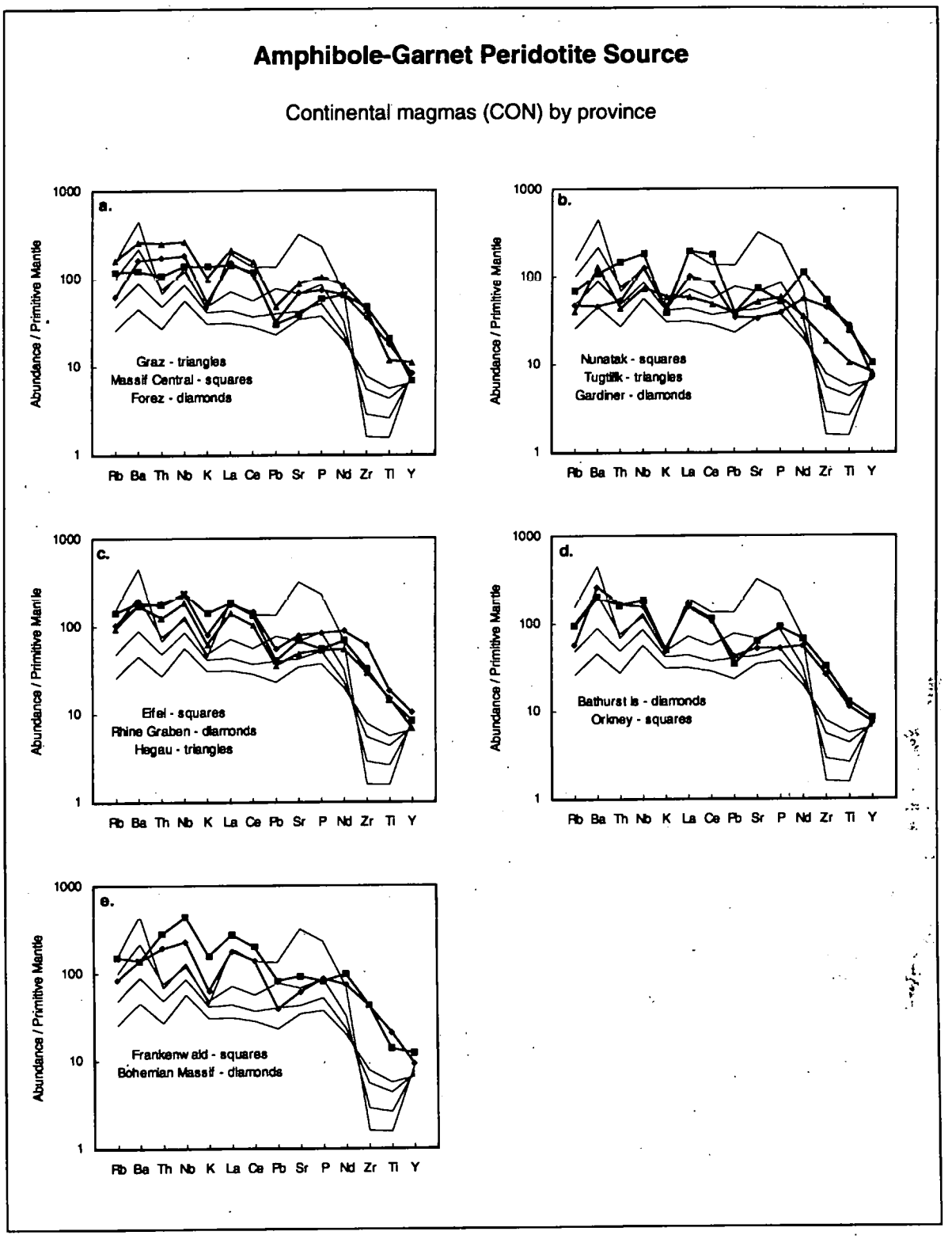

Figure 5-14. Theoretical mantle-normalised incompatible-element patterns for depleted amphibole-garnet peridotite for 0.1, 0.2, 0.5, and 1% partial melting with a carbonate precursor liquid derived by 0.1% melting of the same source. Model parameters as in Fig. 4-19 (Chapter 4). Mean abundances of continental provinces from Appendix E, Table E-7.

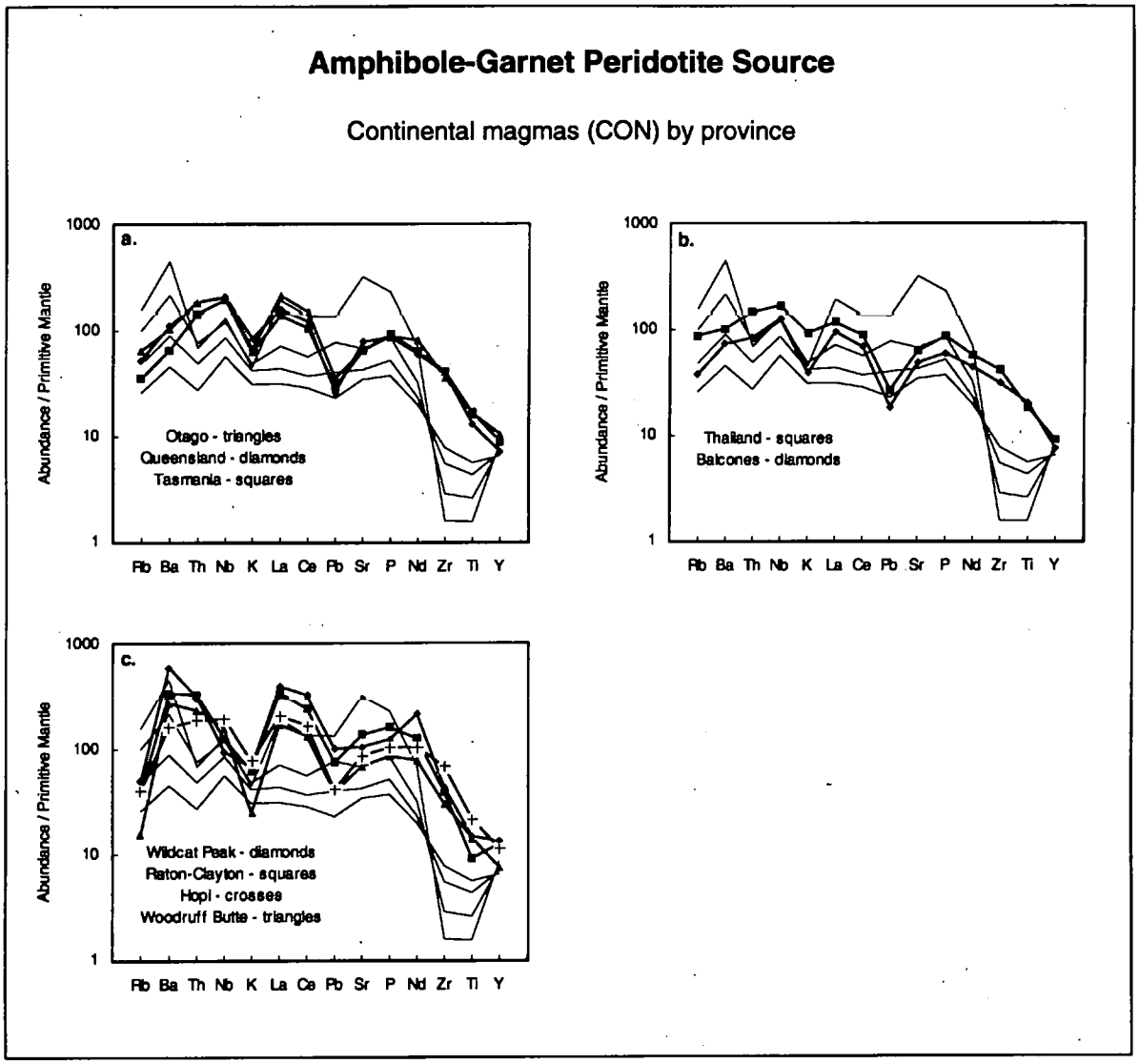

Figure 5-15. Theoretical mantle-normalised incompatible-element patterns for depleted amphibole-garnet peridotite for 0.1, 0.2, 0.5, and 1% partial melting with a carbonate precursor liquid derived by 0.1% melting of the same source. Model parameters as in Fig. 4-19 (Chapter 4). Mean abundances of continental provinces from Appendix E, Table E-7.

Chilwa and N Tanzania are associated with carbonatite complexes but this is not the case for Etinde and by no means all carbonatite provinces (e.g. Nyanza Rift) have associated silicate magmas where strong LREE-enrichment is a prominent feature.

Incompatible elements which are not partitioned strongly into carbonate or which are highly incompatible in silicate melting require the involvement of an additional process or some variation in the source composition. Others (e.g. McKenzie & O'Nions, 1991; Watson, 1993) have found by using REE-inversion techniques that two-stage melting is necessary to account for the budget of REE in some undersaturated ocean island magmas. In Chapter 4 (Section 4.7), therefore, it was proposed that asthenosphere-derived OIN magmas have incorporated remobilized silicate melt fractions which have percolated upwards from the asthenosphere and solidified in the base of the lithosphere. These remobilized melts have probably been generated from similar sources as the magmas which they enrich and this process would, therefore, elevate incompatible element abundances according to the reciprocal of their respective bulk partition coefficients, producing melts which are significantly enriched in the highly incompatible elements. While the incompatible-element budget of most OIN may be controlled by asthenospheric processes and source compositions, remobilization of silicate melts from the lithosphere was considered in Chapter 4 as a likely means of enriching OIN and OIB in strongly carbonate-phobic elements such as Zr, Ti, and Th.

The continental lithosphere is generally older than the oceanic lithosphere. The base of the continental lithosphere may, therefore, have become substantially more enriched than the oceanic lithosphere by the process of melt accumulation. In this case, the particularly high concentrations of Th and Nb of most CON magmas by comparison with the abundances predicted by the preferred model may be due to the incorporation of more lithospheric mantle material. It is also possible that the somewhat higher average concentrations of Ba and Pb in CON are a reflection of the operation of this process. Ba is enriched in both silicate and carbonate melts while Pb is more compatible than Ba but does not favour carbonate liquids as strongly as Sr, P, and LREE ($^{Ls/Lc}D_{Pb} = 0.5$; Fielding, 1992).

A general increase in the amount of carbonate in CON magmas would be signalled by consistently higher LREE, Sr, and P concentrations. Since this is not observed it seems likely that Ba and Pb enrichment could be due to the remobilisation of silicate melts from the lithosphere.

A small number of provinces have extremely unusual incompatible-element profiles (low Nb, or low Th and LREE) by comparison with OIN. Low Th and LREE (Nuanetsi, E Greenland) suggest that the highly undersaturated magmas may have been derived from an extremely depleted source. These magmas were erupted in the initial stages of thermal events which led to continental fragmentation when heat flow from the mantle might have been exceptionally high, the regional geotherm steep and, therefore, the temperature of the base of the lithosphere substantially raised (Upton, 1988; Bristow, 1984).

The highly undersaturated volcanics of the SW United States are characterised by low Nb. This was a feature of Cenozoic alkaline magmatism in the Basin and Range province up to 5 m.y. ago, the Transition Zone surrounding the Colorado Plateau, and on the Plateau itself. Alkaline magmatism in the SW United States followed the cessation of subduction of the Farallon plate beneath the western USA and is related to uplift of the Colorado Plateau and to lithospheric extension and subsidence in the Basin and Range Province. Fitton *et al.* (1988, 1991) have suggested that the continental lithosphere in this region has been substantially modified by slab-derived fluids during the subduction episode. It is believed that slab de-watering processes enrich the overlying mantle in LILE but that HFSE (particularly Nb) are retained in the slab. This process is thought to account for the low-Nb signature of calc-alkaline magmas in general and may be inherited by alkaline magmas when intra-plate volcanic activity follows rapidly after suduction. The fact that a low-Nb signature is found in small melt fractions in this province suggests a significant lithospheric mantle input, in this case providing an unusual signature, but it may also be indicative of the importance of lithospheric components to the composition of CON

in general. In this case, CON may be a feature of passive rifting, as defined in Section 5.1, rather than of active rifting.

Most of the mafic highly undersaturated magmas in the Kenya part of the East African rift system are Miocene in age and were erupted from central-vent volcanoes on the western flanks of the developing rift structure, while the younger highly undersaturated volcanic rocks in the Western Rift have incorporated material from an extremely enriched lithospheric source (cf. Chapter3 and Section 5.6). Mafic nephelinites and melilitites, however, are extremely rare among the recent volcanic products in the Kenya Rift. In the East African rift system, uplift is thought to have preceded rifting, as proposed for active rifts (Section 5.1). Nephelinites from the European rift systems, which are thought to be passive rifts resulting from continental collision, also have chemical features which can be attributed to the involvement of enriched continental lithosphere. The evidence from the East African Rift and the European rifts suggests that rifts may pass through a passive to an active stage (as suggested in Section 5.1) but the nature of the rifting is difficult to ascertain from the chemical composition of the magmas. Other tectonic environments in which CON are found (e.g. major transcurrent faulting, and in association with orogen-related strucural weaknesses) might be characterised by a strong lithospheric signature in the associated magmas because lithospheric attenuation is small in such regions. The undersaturated rocks from Thailand appear to have such a signature but, of all the continental rocks studied in this work, those from the Balcones province are the most similar to OIN and, therefore, may be dominated by asthenosphere-derived magmas.

The variability of Rb and K in CON provinces and the depletion of these elements relative to OIN in some provinces has already been mentioned (Section 5.3). The behaviour of Rb and K in CON magmas may be indicative of the relative importance of phlogopite and amphibole in the source regions because phlogopite is rich in Rb and K ($^{Rb}D_{phlog}$ = 1.7, $^{K}D_{phlog}$ = 1.5 - from compilation in Halliday *et al.*, 1995b) whereas amphibole favours K over Rb ($^{Rb}D_{amph}$ = 0.023, $^{K}D_{amph}$ = 0.22). Published partition coefficients for Rb and K in amphibole can vary by an order of magnitude. For example, McKenzie &

O'Nions (1995) give $^{Rb}D_{amph}$ = 0.2, $^{K}D_{amph}$ = 1.2. This probably reflects the large variation found in amphibole compositions with respect to Na and K. The probability of amphibole and/or phlogopite in the source of CON is discussed in Section 5.5.

5.5 Amphibole- and Phlogopite-Bearing Sources

In Chapter 4, Section 4.8, a number of incompatible-element diagrams with K on the x-axis suggested that the concentration of K in OIN small melt fractions appears to increase as the degree of partial melting increases, whereas in OIB the K abundance decreases. Model melting curves were calculated for primitive and depleted amphibole-garnet peridotite sources with, and without, the involvement of carbonate precursor liquids. The model curves showed that K abundance should increase until all the amphibole has been consumed in melting, at which point, K concentration should decrease as partial melting increases. The sharp inflection in the melting curve could only be produced if it was assumed that $^{K}D_{bulk} > 1$ for modal melting or $P > 1$ for non-modal melting. When superimposed on the calculated primary magma compositions of OIN and OIB (Figs. 4-24 to 4-26) it appeared that the composition of OIN and its relationship to OIB could be modelled simply by varying the degree of depletion of the amphibole-bearing source and the extent of carbonate involvement.

Using the theoretical curves calculated for amphibole-garnet peridotite in Chapter 4, primary CON magmas were assessed in the same way. Ba *versus* K and La *versus* K are shown in Figures 5-16b & d, respectively. Sr *versus* K and Zr *versus* K appear in Figures 5-17b & d. The CON primary data on these diagrams are negatively correlated with K and, in relation to the theoretical melting curves, are distributed similarly to OIN. This is consistent with CON being small degrees of partial melting of amphibole-garnet peridotite. However, as the D values for K in phlogopite and amphibole are similar ($^{K}D_{amph}$ = 1.2; $^{K}D_{phlog}$ = 1.5) a similar data distribution would be expected for phlogopite-bearing sources and, as has already been noted, it is the behaviour of Rb during partial melting that

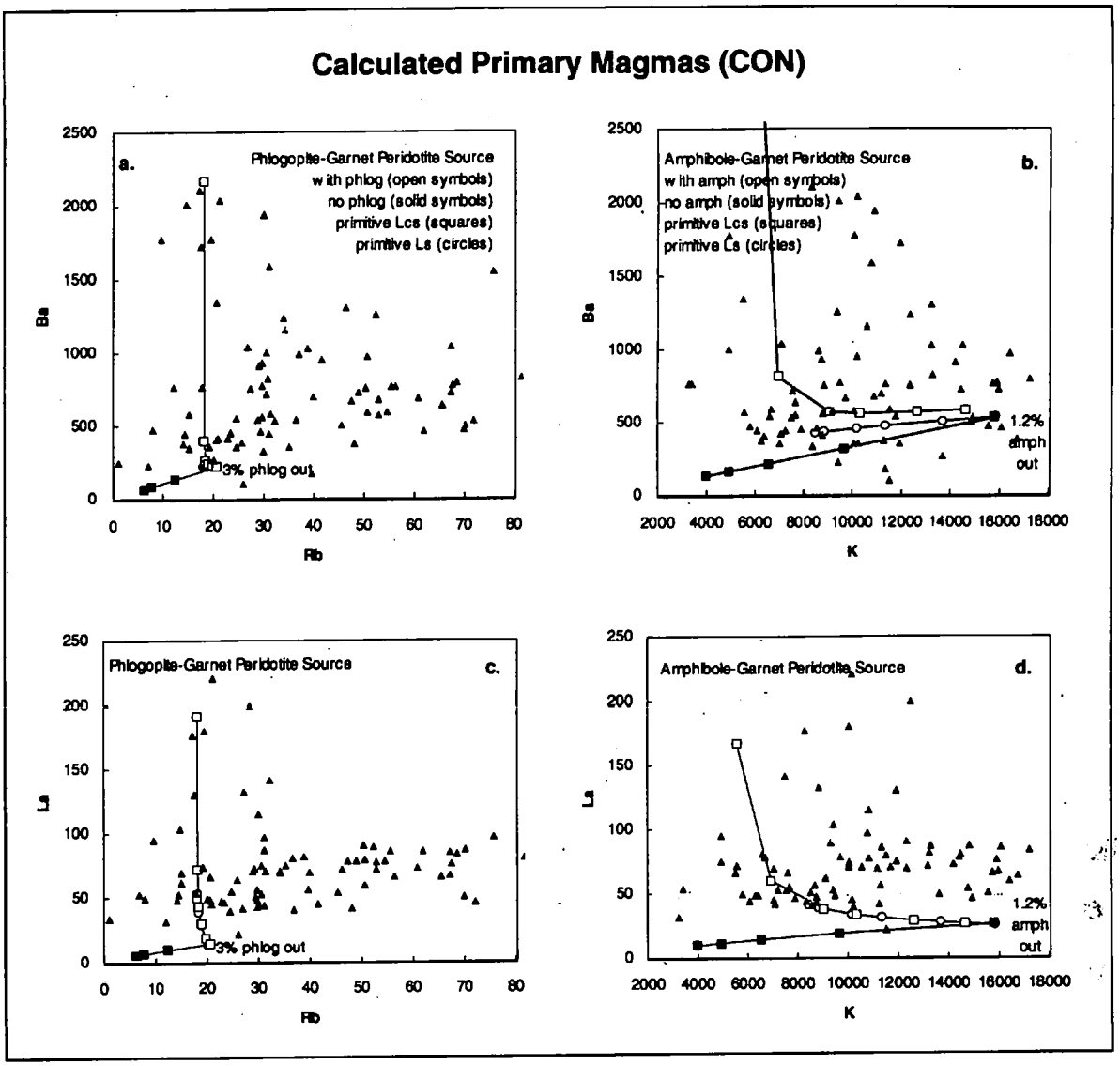

Figure 5-16. Theoretical partial melting curves for primitive phlogopite-garnet peridotite (a. and c.) and amphibole-garnet peridotite (b. and d.) where respectively $^{phlog}D_{Rb} > 1$ and $^{amph}D_K > 1$. Degrees of partial melting (%): 0.1, 0.2, 0.5, 1, 2, 3, 5, 8, 10, for phlogopite-bearing source, and 0.1, 0.2, 0.5, 0.7, 1, 1.2, 2, 3, 4, 5, for amphibole-bearing source. Phlogopite and amphibole totally consumed at 3% and 1.2% partial melting respectively.
Lcs = carbonate-silicate mixed melt
Ls = silicate melt
Amph-gt peridotite model calculated as in Fig. 4-19 (Chapter 4). Partition coefficients and primitive mantle composition from McKenzie & O'Nions (1995).
Phlog-gt peridotite source mineralogy: ol = 0.6, opx = 0.2, cpx = 0.16, gt = 0.02, phlog = 0.02. Melting proportions of mantle phases from Greenough (1988) and Johnson *et al.* (1990). Partition coefficients from compilation in Halliday *et al.* (1995b). Primitive mantle composition from McKenzie & O'Nions (1995).
Carbonate precursor liquid as Fig. 4-24. Primary CON calculated for all samples with MgO > 10 wt.% by dilution with olivine additions required to restore magma compositions to equilibrium with mantle olivine ($Fo_{90.7}$) using $K_D = 0.30$ for distribution of Fe^{2+} and Mg between olivine and co-existing silicate melt (Chapter 3).

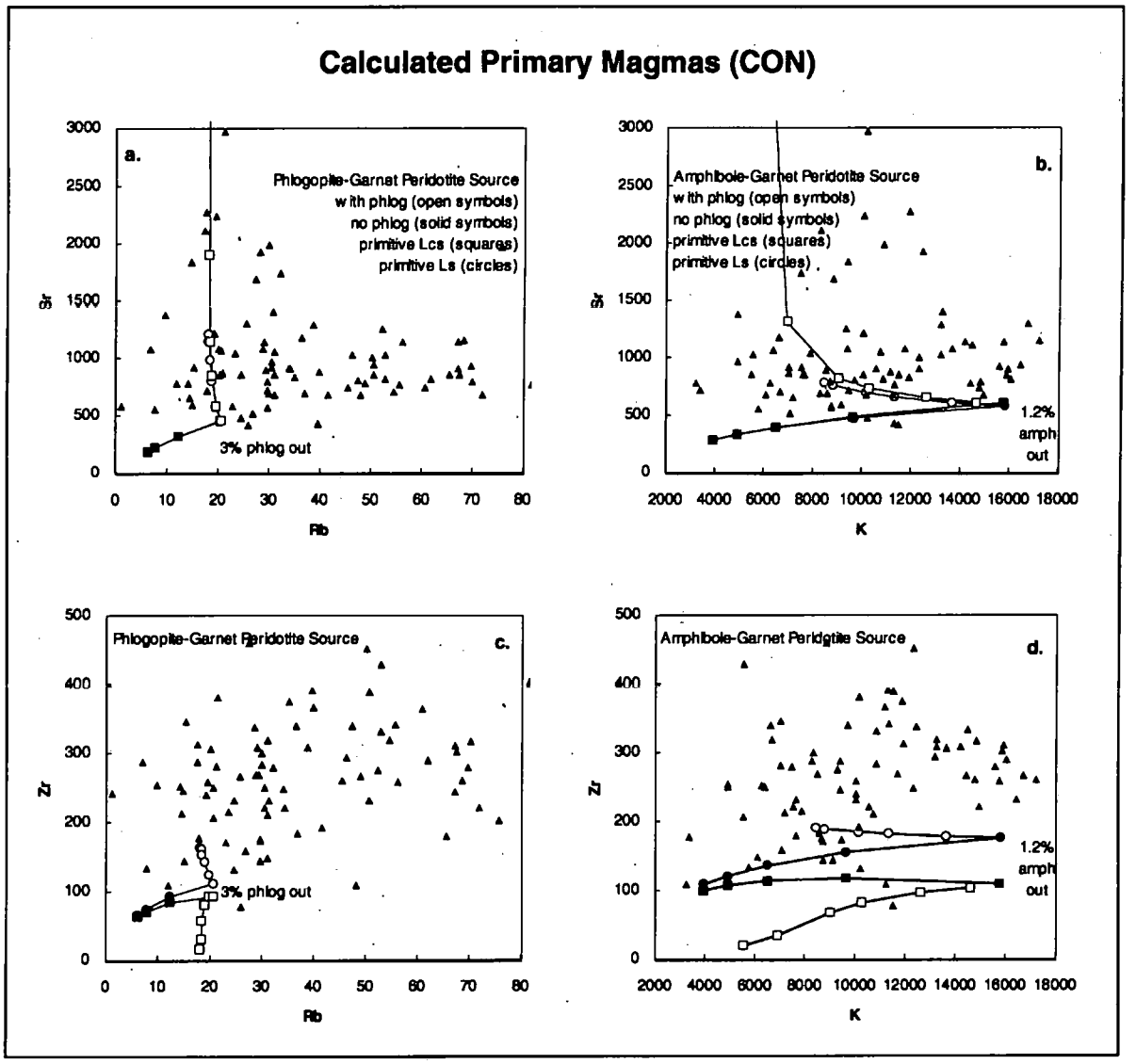

Figure 5-17. Theoretical partial melting curves for primitive phlogopite-garnet peridotite (a. and c.) and amphibole-garnet peridotite (b. and d.) where respectively $^{phlog}D_{Rb} > 1$ and $^{amph}D_K > 1$. Degrees of partial melting as Fig. 5-16. Phlogopite and amphibole totally consumed at 3% and 1.2% partial melting respectively.
Lcs = carbonate-silicate mixed melt
Ls = silicate melt
Parameters and calculations as in Fig. 5-16.

should be diagnostic in distinguishing amphibole- from phlogopite-bearing sources. As in the case of OIN, the data distribution in Zr *versus* K (Fig. 5-17d) does not follow the predicted melting curves.

The same model parameters were used to calculate melting curves for phlogopite-garnet peridotite assuming the same source mineralogy as before but with 2% phlogopite instead of amphibole. In this case, melting proportions of phlogopite-peridotite were assumed to be 0.01 ol, 0.03 opx, 0.12 cpx, 0.17 gt, and 0.67 phlog (Greenough, 1988; after Modreski & Boettcher, 1973) and partition coefficients were taken from the compilation in Halliday *et al.* (1995b). In these models phlogopite is totally consumed at 3% partial melting. Ba *versus* Rb and La *versus* Rb are shown in Figures 5-16a & c, respectively, and Sr *versus* Rb and Zr *versus* Rb in Figures 5-17a & c. It is immediately apparent from these diagrams that CON are considerably more enriched in Rb than is predicted by the theoretical melting curves for primitive mantle. This indicates that if CON are to be derived from phlogopite-bearing sources the source must be substantially enriched in Rb. It is also apparent from Figures 5-16 and 5-17 that none of the model melting curves fits the data and that the data do not have the characteristic negative correlations seen in the diagrams with K on the x-axis. In fact, for most CON, Rb is positively correlated with Ba, La, and Sr and appears to behave as an incompatible element throughout partial melting. There are a small number of data points which lie close to the low Rb-high La and low Rb-high Sr trends defined by the model curves for carbonated magmas derived from primitive phlogopite-garnet peridotite (Figs. 5-16c and 5-17a). These are the only CON magmas which appear to have been derived from phlogopite bearing sources.

The effects on melt compositions of the partitioning of K and Rb in phlogopite and amphibole can also be seen in Figure 5-18 (Rb/Sr *versus* K/Rb) on which the field of OIN has been superimposed. A small number of OIN extend to high values of K/Rb and Rb/Sr. These are from the Hawaiian Islands (Kauai and Oahu) and the Comores Islands (Moheli), respectively. The whole CON data set has been plotted on this diagram because

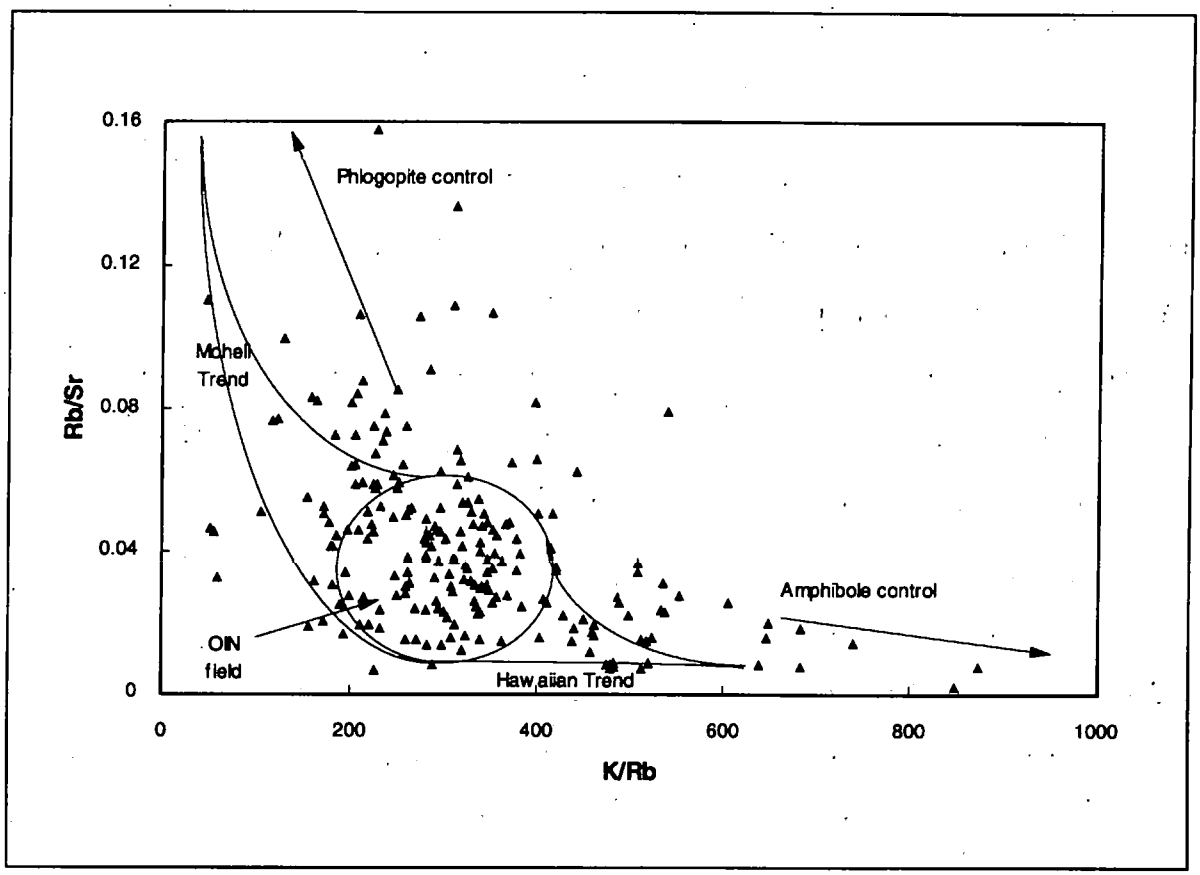

Figure 5-18. Continental magmas (CON), MgO > 4 wt.%, shown with amphibole and phlogopite control lines from Davis (1991). 'OIN field' indicates range of most OIN. The Hawaiian and Moheli trends are defined by a small number of samples. Most samples from these islands and samples from all other islands on which OIN occur fall within the OIN field.

the use of trace-element ratios disposes of the need to calculate primary trace-element compositions for the data. It is, however, assumed that olivine is the only fractionating phase and that the trace-element ratios of the original magmas have not been disturbed by crystal fractionation. In view of the low MgO contents of many CON compared with OIN this may not be a valid assumption. However, Figure 5-18 was repeated using only those samples with MgO > 10% and the same conclusions could be drawn. Figure 5-18 shows that most CON fall within the OIN field but a small number have either higher K/Rb (notably SE Australia, SW United States) or higher Rb/Sr (S Africa, Eifel, Cantal in the Massif Central) than most OIN. Some provinces include both high K/Rb and high Rb/Sr rocks. For example, among the Miocene volcanoes of the the Kenya Rift, Moroto has high K/Rb but Elgon and Napak tend to have high Rb/Sr and volcanics from the Samburu district have high K/Rb. N Tanzania, Chilwa, and the Greenland provinces are also strikingly variable in Rb composition. As partial melting increases, the presence of phlogopite in the mantle source imposes progressively lower K/Rb and higher Rb/Sr characteristics on magma compositions, whereas amphibole generates magmas with progressively higher K/Rb, and a Rb/Sr value which gradually decreases. The phlogopite and amphibole controls on magma composition (from Davis, 1991) are also shown on Figure 5-18.

As in the case of OIN, CON magmas seem to be the products of mantle sources where amphibole is the stable potassic phase. Only a small number appear to have been derived from phlogopite-bearing peridotite and this can be a characteristic of an entire province or individual magmas within a province otherwise dominated by amphibole. Most CON lie around the melting curves for residual amphibole in Figures 5-16d and 5-17b but it is difficult to assess with certainty the role of carbonate in CON magmas from these diagrams because the curves are partially overlapping. All that can be deduced is that many samples are either the result of extremely small degrees of silicate melting (< 0.1%), derived by silicate melting from variably depleted amphibole-bearing sources, or are carbonated melts from this source mineralogy. A number of CON have La and Sr concentrations which lie beyond the limit of the theoretical curves for silicate melting.

These magmas are strong candidates for the involvement of carbonate liquids in magma generation.

5.6 Trace-Element Compositon of Potassic Continental Rocks

On the basis of major-element chemistry it was deduced in Chapter 3 (Section 3.9) that potassic continental magmas have been derived from sources that have been extensively metasomatised and enriched in incompatible elements. Western Rift kamafugitic magmas appear to have been produced from at least three chemically distinct and geographically separated sources. The requirement for carbonate precursor liquids appears to be variable, being high in the northern end of the rift (katungites and mafurites from Katunga and Bunyaraguru) and absent in the south (ugandites and leucitites from Birunga). The New South Wales leucitites do not appear to involve carbonate liquids in their generation.

The overall enrichment in incompatible elements of the New South Wales and Western Rift magmas by comparison with primitive mantle, mean OIB, and mean OIN, is shown in Figures 5-19 a, b, & c, respectively. The incompatible-element patterns bear only a superficial resemblance to OIN and CON patterns and it can be assumed that the magmas have incorporated a melt component derived from a highly metasomatised and enriched lithospheric source. The level of enrichment and the incompatible element profile of the two suites is similar but the New South Wales magmas are strikingly depleted in Th and Nb and enriched in Pb and Zr by comparison with the average Western Rift composition and slightly more enriched in K and Rb. Both suites are depleted in P relative to other incompatible elements and, on the basis of Y abundance, appear to have been derived from HREE-depleted sources or from sources with more residual garnet than OIN. Ce/Y *versus* Zr/Nb for the Western Rift and New South Wales (Fig. 5-20a) shows that in terms of these elements none of the magmas from either province has been generated from a 'normal' primitive or depeleted lherzolite source.

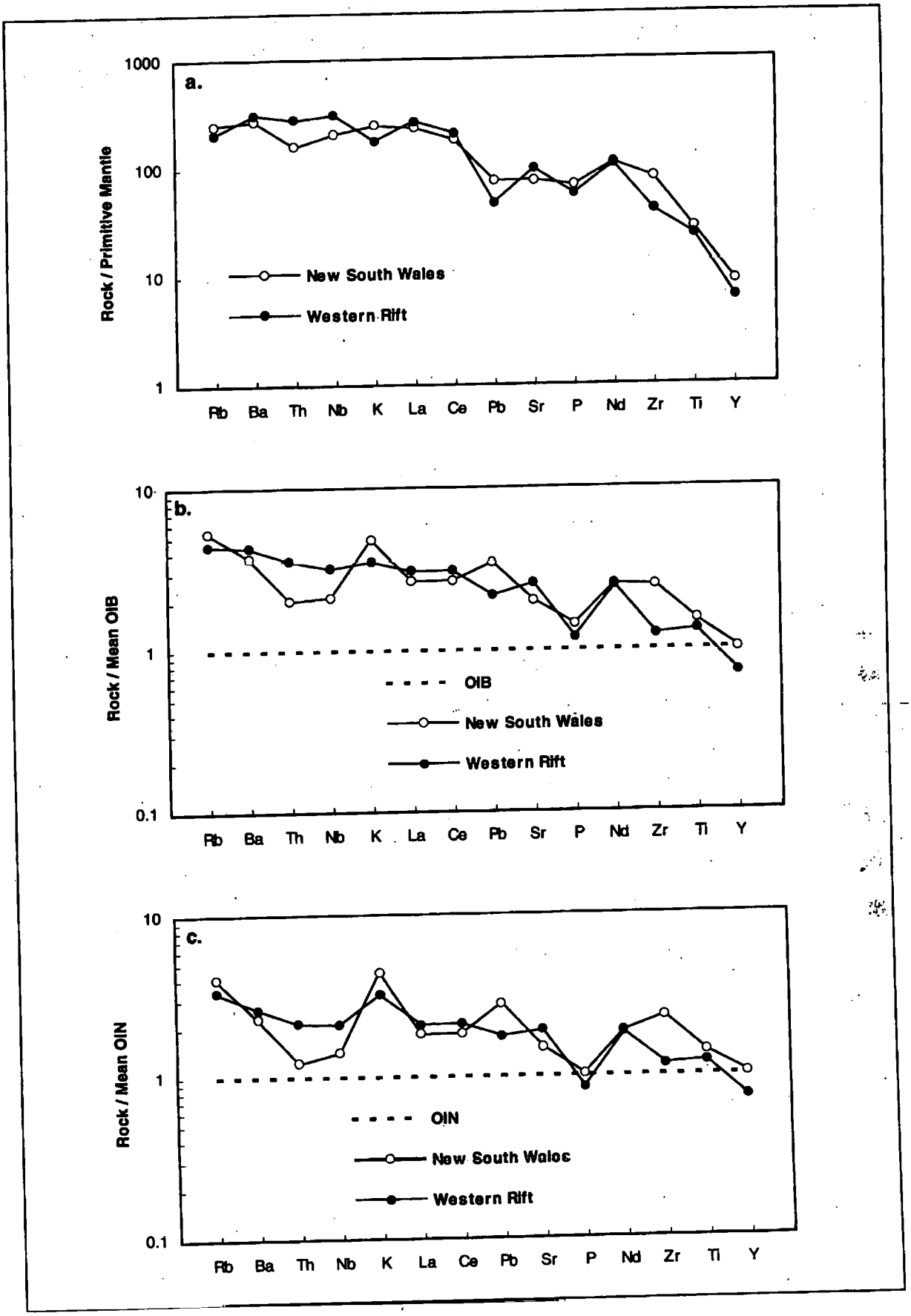

Figure 5-19. Average incompatible-element concentrations of potassic feldspar-free volcanic rocks from New South Wales and the Western Rift (data from Table 5-1). Normalising values as in Fig. 5-1.

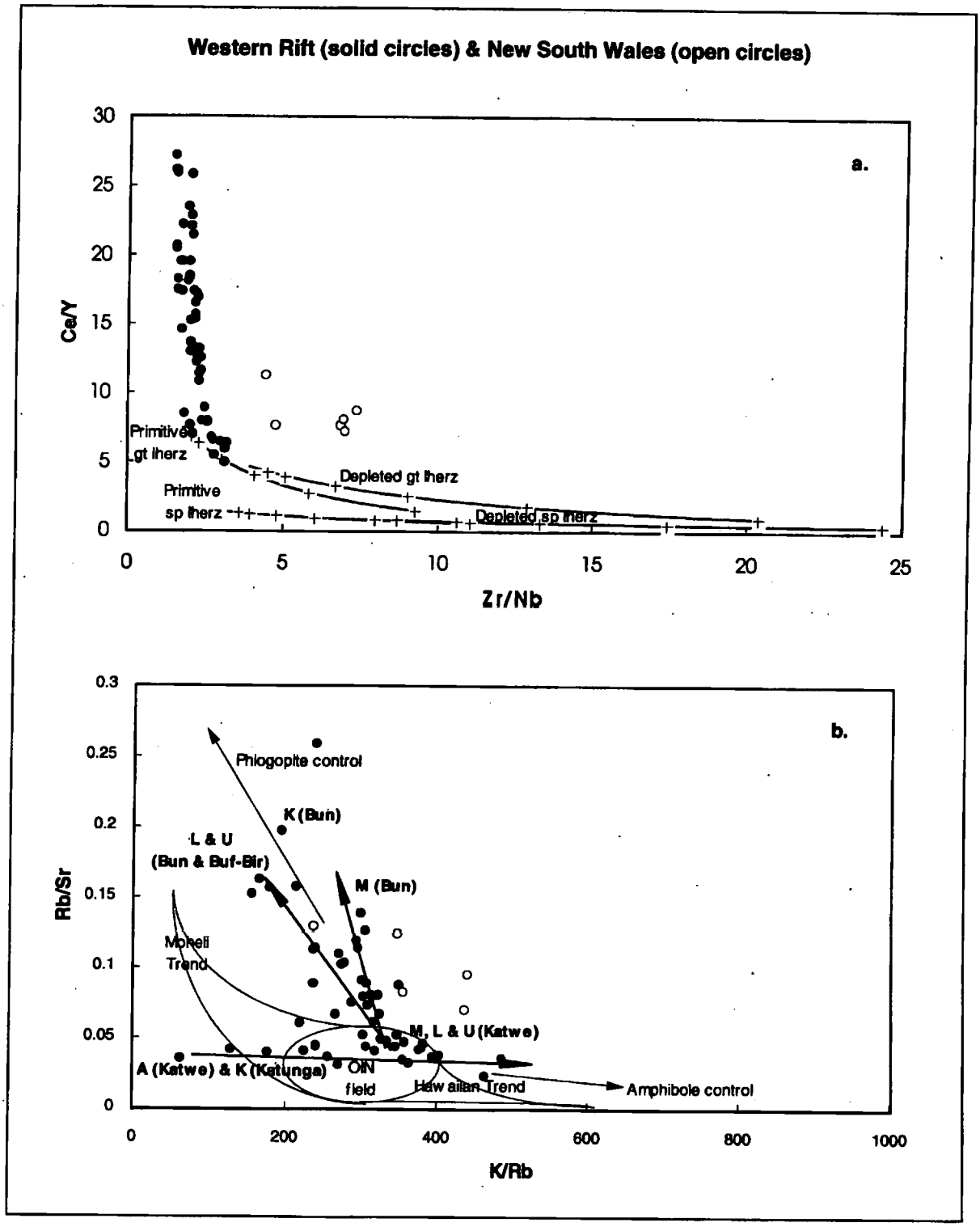

Figure 5-20. Potassic continental rocks from the Western Rift and New South Wales.

a. Ce/Y *versus* Zr/Nb shown against model melting curves of primitive and depleted garnet and spinel lherzolites calculated as in Fig. 5-2. Cross symbols on melting curves refer to degrees of partial melting (0.1%, 0.2%, 0.5%, 1%, 2%, 5%) increasing from the left.

b. Rb/Sr *versus* K/Rb shown with amphibole and phlogopite control lines from Davis (1991). 'OIN field' indicates range of most OIN.
K = katungite, M = mafurite, L = leucitite, U = ugandite, A = ankaratrite
Bun = Bunyaraguru, Buf-Bir = Bufumbira-Birunga

In such highly enriched sources it is possible that phlogopite is a significant component of the source mineralogy. Rb/Sr *versus* K/Rb with the OIN field superimposed is shown in Figure 5-20b. About half of the Western Rift samples, mainly from the northern end (katungites from Katunga, ankaratrites from Katwe, and mafurites, leucitites, and ugandites from Katwe), fall within or very close to the OIN field. However leucitites, mafurites, and a single katungite from Bunyaraguru, follow the phlogopite control path as do the leucitites and ugandites from Bufumbira and Birunga, and the New South Wales leucitites. These observations are at variance with the conclusions of Chapter 3 that katungite is derived from deep mantle sources where phlogopite is stable whereas ugandites and leucitites have a shallower source with amphibole as the main potassic phase. It appears from Figure 5-20b that all the Western Rift magmas are derived from highly enriched phlogopite-bearing sources and the position of the OIN field is irrelevant to inferences about the existence or otherwise of amphibole in the source. In this case ugandites and leucitites are simply larger degrees of melting of a phlogopite-bearing source.

La *versus* Rb and *versus* K for the Western Rift and New South Wales are shown in Figures 5-21b and 5-21c respectively. Theoretical melting curves were not calculated for the highly enriched sources of these magmas because the model parameters (e.g. modal mineralogy, melting proportions, and partition coefficients) are not well constrained. The characteristic wedge-shaped melting curves which apply to amphibole- and phlogopite-bearing sources (cf. Fig. 5-16) are, however, shown qualitatively on Figures 5-21b & c. The distribution of data suggests that phlogopite might be residual during the generation of katungite and mafurite but that it has been consumed before the degrees of melting appropriate to leucitite, ugandite, and ankaratrite are reached. These diagrams do not preclude the existence of both amphibole and phlogopite in the source or the presence of a variety of other minor phases, (e.g. apatite). With such high levels of incompatible-element enrichment and a woeful shortage of reliable trace-element partitioning coefficients for possible minor phases in the mantle, it is difficult to

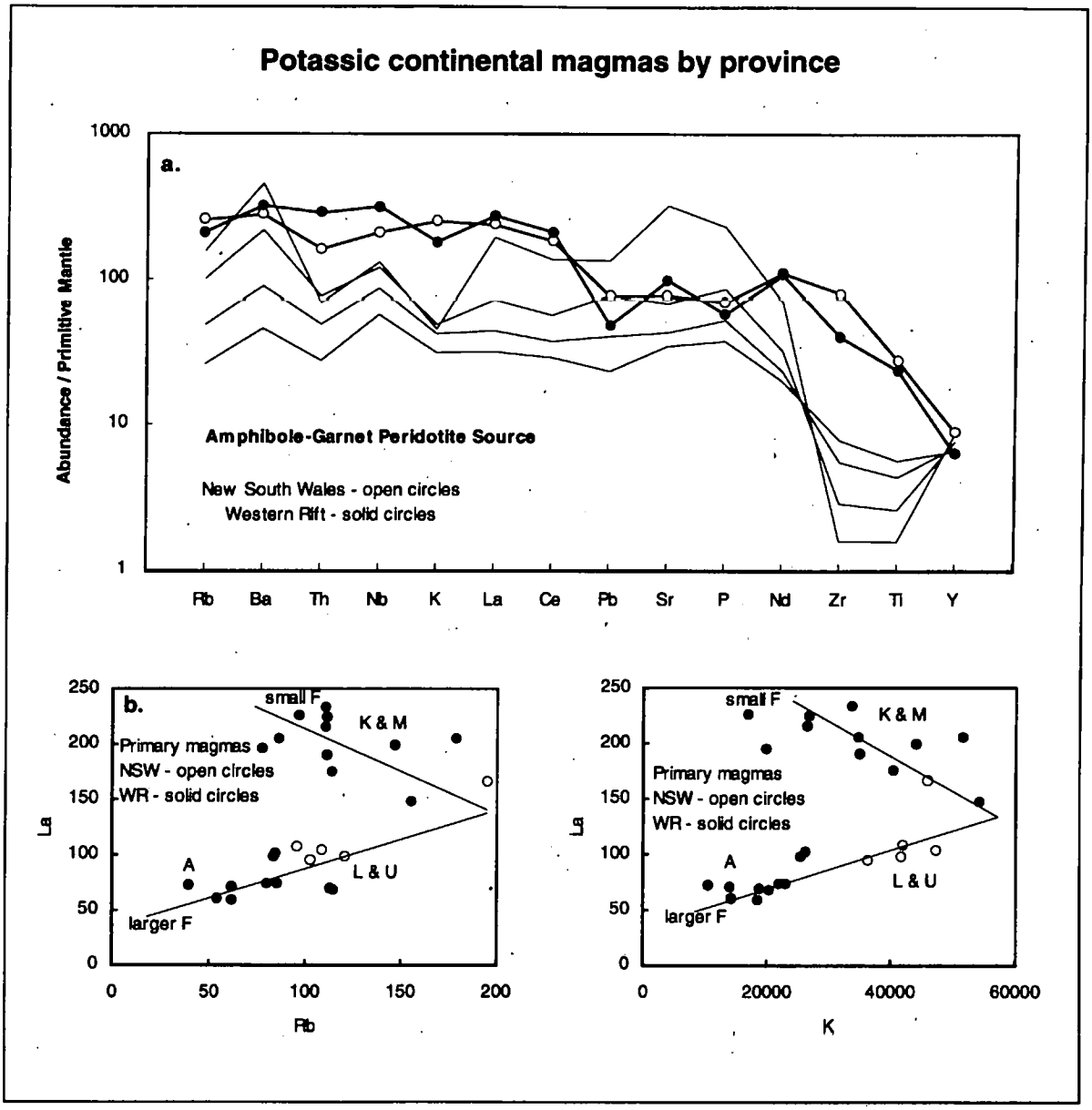

Figure 5-21. a. Theoretical mantle-normalised incompatible-element patterns for depleted amphibole-garnet peridotite for 0.1, 0.2, 0.5, and 1% partial melting with a carbonate precursor liquid derived by 0.1% melting of the same source. Model parameters as in Fig. 4-19 (Chapter 4). Mean abundances of New South Wales and Western Rift provinces from Table 5-1.

b. La *versus* Rb for calculated primary magma compositions of potassic continental rocks. Schematic partial melting curves for an enriched phlogopite-garnet peridotite source after Fig. 5-16. K & M = katungites & mafurites, L & U = leucitites and ugandites, A = ankaratrites.

c. La *versus* K as b. Schematic partial melting curves for an enriched amphibole- or phlogopite-garnet peridotite source after Fig. 5-16.

substantiate speculation about more complex source mineralogies with meaningful models. Modelling of Western Rift and New South Wales magma sources in this study has not, therefore, been extended beyond consideration of amphibole- and phlogopite-peridotite mineralogies. There do, however, appear to be regional differences (between Katwe, Bunyaraguru, and Bufumbira) which could be related to the extent of metasomatic enrichment and the influence of both phlogopite and amphibole in the source.

The theoretical incompatible-element profiles for melting of an amphibole-garnet peridotite source with a carbonate precursor liquid are compared to the Western Rift and New South Wales average compositions in Figure 5-21a. Although the abundances of LREE are higher than can be accounted for by the addition of carbonate liquid assumed in this model, the enrichment in Sr in the Western Rift magmas also indicates the involvement of carbonate in magma generation and supports the conclusion from Chapter 3 that this may be higher (ca. 20%) than assumed in the model. The low abundances of P indicate that a process other than carbonate-silicate liquid partitioning is controlling the P abundance in the magmas. This may be source depletion prior to metasomatic enrichment by K-rich fluids, residual apatite, or apatite fractionation.

As with CON, potassic magmas have, in addition to high Rb and K, higher abundances of Th, Nb, Zr and Ti, than predicted, but Pb does not appear to be anomalous in the Western Rift magmas. The decoupling of the behaviour of Pb from that of elements which favour carbonate liquids or which might be enriched remobilized lithospheric melts, is difficult to explain, as is the relative enrichment in Zr and depletion in Th and Nb observed in the New South Wales suite. Southeast Australia was close to the active margin of the Indo-Austalian plate throughout the Mesozoic and the folded belts parallel to the continental margin may represent a series of collisions resulting from the subduction of the Pacific plate beneath the continental margin. Continental intraplate volcanism associated with extensional tectonics has the ability to sample the continental lithospheric mantle as the magmas rise to the surface. The lithosphere may be extensively modified during subduction processes and the evidence from calc-alkaline volcanics suggests that

subduction-modified lithosphere becomes enriched in LILE but not in HFSE, particulary not in Nb. The low Nb signature in the New South Wales leucitites may therefore indicate that the local lithosphere has experienced the effects of an earlier subduction episode and that this lithospheric component is contributing to the magma composition (cf. SW United States, Section 5.4). The low Th may indicate that the source had been depleted in incompatible elements prior to the metasomatic enrichment event which is responsible for the highly potassic character of the magmas (cf. Nuanetsi and E Greenland, Section 5.3).

5.7 Olivine-Poor Continental Nephelinites

Le Bas (1987, 1989) has classified nephelinitic rocks as belonging to the carbonatite-nephelinite (olivine-poor) association or the basalt-nephelinite (olivine-rich) association. Olivine-poor melanephelinite is almost totally absent from ocean islands but occurs commonly in continental rift provinces usually associated with carbonatite complexes. There is still no concensus about the origin of carbonatite magmas. They may be primary melts from the mantle, derived by carbonate-silicate liquid immiscibility, or the end-products of fractional crystallization of a silicate melt, and parental melts may be derived from depleted or metasomatised lithosphere, the asthenosphere with lithosphere contamination, or from the asthenosphere-lithosphere boundary. Each of these models has been invoked in recent work, but regardless of which model appears appropriate for a particular occurrence, rifting, lithospheric attenuation, and thermal erosion of the lithosphere by upwelling asthenosphere, appear to have been critical in generating the highly carbonated primary or parental magmas.

It is, however, generally agreed that conjugate silicate and carbonate magmas can arise by liquid immiscibility processes in the sub-continental mantle. The parental magma in this process is thought to be CO_2-rich olivine nephelinite in composition and separation of the two liquids may be accompanied by extensive fractionation of olivine. If this is the case, olivine-poor nephelinites may simply be highly evolved olivine-rich nephelinites derived from asthenospheric sources and more highly carbonated magmas.

There may be no need to appeal to fundamentally different processes or sources within the lithosphere, to account for the difference in mineralogy.

The normalised incompatible-element abundances of OIN, CON and olivine-poor continental nephelinites (COP) are shown in Figure 5-22. Mantle-normalised patterns of average compositions from the three data groups (Fig. 5-22a) are very similar and suggest that average CON and COP could be related to OIN, and to each other, by crystal fractionation processes. However, CON and OIN also appear to be similar on this diagram yet there is evidence that many CON magmas have some input from enriched continental lithosphere which is not available to OIN (cf. Section 5.3). Normalising to OIB (Fig. 5-22b) and OIN (Fig. 5-22c) accentuates small differences between the average compositions. OIB normalising (Fig. 5-22b) shows that the differences in composition between OIN and CON are subtle and, as discussed in Section 5.3, involve Pb and possibly Ba. The relative enrichment in Pb, and to a lesser extent in Nb and Sr, of COP over CON is striking. These differences are shown even more clearly by the OIN-normalised diagram (Fig. 5-22c). The striking depletions in P and Ti by comparison with OIN and CON suggest, however, that crystal fractionation processes involving pyroxene, magnetite, and apatite, have affected the incompatible-element composition of COP magmas.

A possible explanation for the overall enrichment of COP over CON and the relative enrichment in Pb, Nb, and Sr, lies in the partitioning of these elements between carbonate and silicate liquids. As discussed in Chapter 3, silicate melting probably occurs in the high-temperature central region of a thermal anomaly. The presence of carbonate lowers the solidus temperature of peridotite and small melt fractions of a carbonated source may, therefore, be derived from the large volume of mantle surrounding the melt zone. In this case, highly carbonated magmas may have scavenged trace elements from a large volume of mantle and become extremely enriched in most incompatible trace elements, particularly those elements which partition strongly into carbonate. Separation, by liquid immiscibility processes is likely, therefore, to generate silicate fractions which are more highly enriched in incompatible elements than is generally observed in CON. Furthermore,

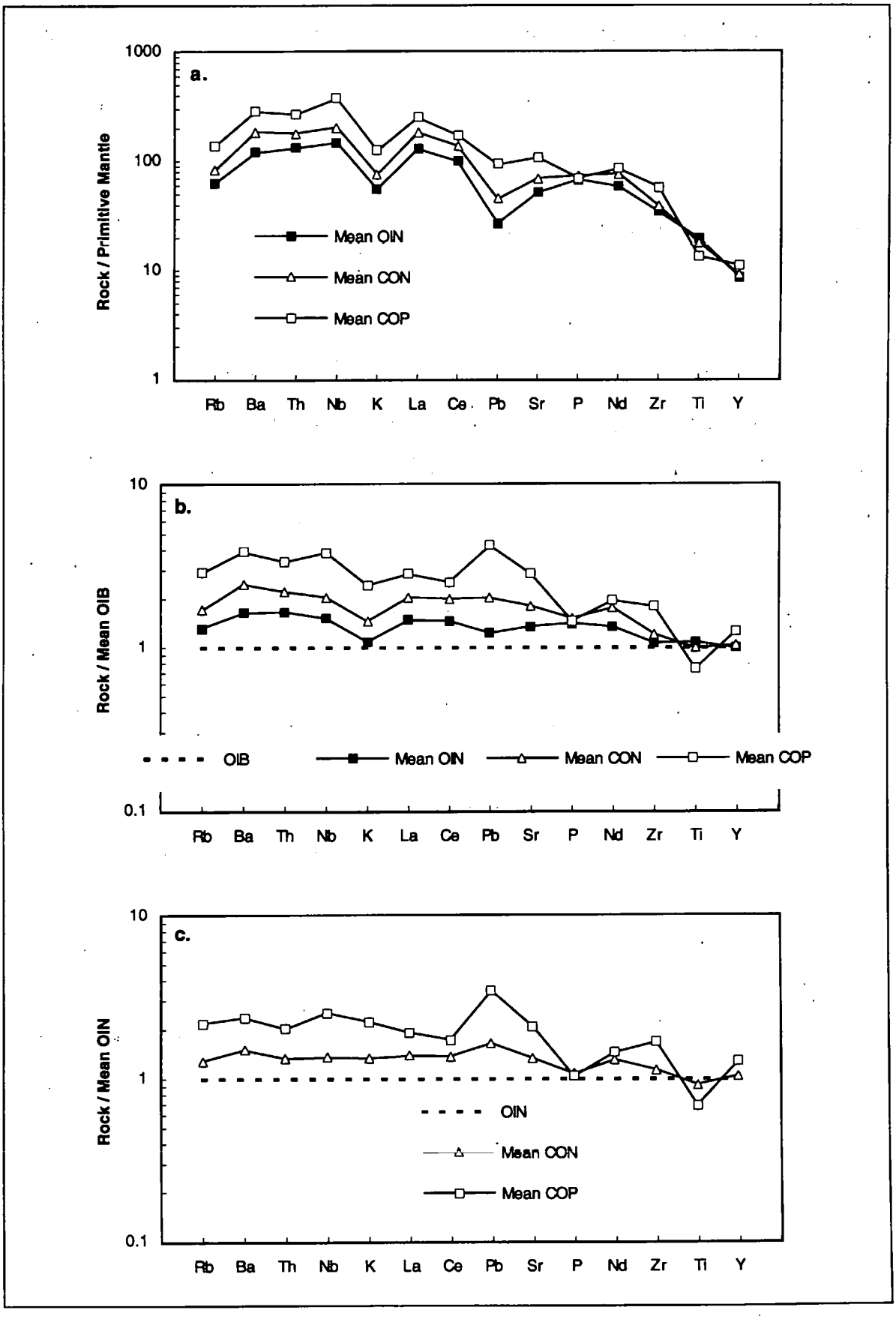

Figure 5-22. Average incompatible element concentrations of continental olivine-poor nephelinites (COP) compared with average OIN and CON (data from Table 5-1 & Table 4-1, Chapter 4). Normalising values as in Fig. 5-1.

during the separation of the silicate fraction, elements which partition very strongly into carbonate (Ba, Sr, LREE) would be expected to enrich the carbonate fraction but those which favour carbonate less strongly (Pb and Nb) could be similarly enriched in both fractions.

However, as an explanation of the observed variation, carbonate-silicate liquid partitioning is not completely satisfactory because Fielding's (1992) partition coefficients for the partitioning of trace-elements between carbonate and silicate liquids suggest that Pb should be rather less enriched in the silicate fraction than strongly carbonate-phobic elements such as Th and Zr ($^{Ls/Lc}D_{Pb} = 0.5$, $^{Ls/Lc}D_{Th} = 8$, $^{Ls/Lc}D_{Zr} = 10$). It is possible, however, that Th and Zr have been almost completely excluded from highly carbonated mixed magmas during their formation. In which case, the relative enrichment of incompatible trace elements in the silicate fraction must depend on a balance between the degree of enrichment in the original mixed magma and subsequent partitioning between conjugate liquids on separation.

Fielding's (1992) experiments on natural nephelinitic compositions indicate that most Ls/Lc partition coefficients are pressure and melt composition sensitive. Elements which partition strongly into carbonate at high pressures (P, Sr, Ba, REE) do so less strongly at lower pressures and when the silicate melt is basic in composition with a low degree of polymerization. HFSE (Zr, Nb, Pb, Th) coefficients appear to be unaffected by pressure. Highly carbonated magmas may be generated at high pressures but separate at lower pressures. The two-stage partitioning process is, therefore, likely to distort the incompatible-element pattern which would be predicted on the basis of Fielding's (1992) data, by somewhat enriching the silicate magma in elements which normally favour carbonate (e.g. Ba, Sr) and, relatively, depleting the magma in those which favour silicate (e.g. Th, Zr). Those incompatible elements with no strong preference for either silicate or carbonate (e.g. Pb, Nb), will be less affected and may become markedly enriched in the silicate fraction during subsequent differentiation if they are not removed from the magma

by fractionating phases. $^{Ls/Lc}D_{Pb}$ is unreliable (Fielding, 1992) due the very low relative yield of Pb^+ in the ion probe analysis.

An alternative process which may account for the differential enrichment in incompatible elements observed in COP by comparison with CON involves crustal contamination. The depth at which separation of carbonate and silicate fractions by liquid immiscibility takes place is still debated but sites within the upper mantle (Twyman & Gittins, 1987) or lower continental crust (Le Bas, 1987) have been proposed. During the formation and subsequent evolution of the magma reservoirs there is considerable scope for AFC processes to take place.

Crustal contamination would be expected to enrich magmas in LILE and particularly in Pb (cf. Section 5.1). As already pointed out, this process would affect the major-element chemistry, particularly the silica content. However, Si is strongly carbonate-phobic and, in highly undersaturated magmas, fractionation of olivine, which may have higher SiO_2 than a highly carbonated magma, would drive the SiO_2 content of the magma down. Any raising of SiO_2 as a result of crustal contamination might, therefore, be compensated by an SiO_2 reduction due to extensive olivine fractionation. This process might be plausible for an upper crustal contaminant which could raise the magma concentration of Pb without an overwhelming rise in silica (upper crustal Pb = 20 ppm, SiO_2 = 66 wt.%; Taylor & McClennan, 1985), but is difficult to envisage for contamination with lower crustal material which has substantially lower abundances of Pb without a concomitant reduction in SiO_2 content (lower crustal Pb = 4 ppm, SiO_2 = 54.4 wt.%; Taylor & McClennan, 1985). However, as in the case of CON, large amounts of crustal contamination would be required to account for the trace-element abundances found in olivine-poor nephelinites and, although enrichment in some trace elements by crustal contamination could be masked by the much greater effect of trace-element enrichment by carbonate-slicate liquid partitioning, any effect due to crustal assimilation is likely to be subsidiary to the silicate-carbonate liquid partitioning effects.

On the basis of the data gathered in this study it is difficult to exclude crustal contamination from the generation of olivine-poor nephelinites. However, Pb enrichment is also a feature of CON in general. It is likely, therefore, that the source of Pb in CON and COP is similar. Since CON have been shown to involve lithospheric mantle sources in their genesis and are considered to be free of crustal components (Section 5.3), COP may also have reacted with enriched lithospheric mantle material. Other workers (e.g. Paslick *et al.*, 1995) have used radiogenic isotope data to assess the relative importance of asthenospheric mantle, lithospheric mantle, and the crust, to the genesis of olivine-poor continental nephelinites. Paslick *et al.* (1995) have discounted crustal contributions to the silicate rocks of N Tanzania on the basis of major-element chemistry and Pb-isotope systematics. They also suggest that the silicate magmas are the result of immiscible separation of silicate and carbonate melt fractions from asthenosphere-derived carbonated melts and, on the basis of the radiogenic isotope data, that the magmas have been contaminated by enriched lithospheric mantle in the process.

5.8 Summary

Feldspar-free basic volcanic rocks represent the smallest degrees of partial melting in oceanic and continental intraplate environments. Study of the trace-element variation in mafic continental nephelinites (CON) and oceanic nephelinites (OIN) has revealed common features which can be related to the mineralogy of the source regions from which highly undersaturated magmas are derived and to the mantle processes which may be involved in their genesis. The results of these studies are consistent with the evidence presented in Chapters 3 and 4 for the involvement of carbonate liquids in the generation of small melt fractions in intraplate environments and for the presence of potassic phases in the source. Continental nephelinites and potassic continental magmas may be contaminated with components derived from enriched continental lithospheric mantle as they rise to the surface. Incompatible trace-element modelling has allowed a number of constraints to be placed on the mineralogy and composition of continental

magma sources. These constraints have implications for the genesis of olivine-poor nephelinites which are common in continental carbonatite provinces. The main conclusions from Chapter 5 are

(i) Normalised incompatible-element patterns are similar for average OIN and average CON. The composition of magmas in both environments may, therefore, be dominated by melts derived from the asthenosphere. The strong depletion, relative to primitive mantle, in Rb, K, and Pb, is present in both OIN and CON and indicates that they are derived from variably depleted mantle sources containing potassic phases.

(ii) CON are, on average, more enriched than OIN and may have incorporated material from the continental lithosphere which has been enriched by metasomatising fluids or asthenosphere-derived small melt fractions. The old continental lithosphere may be substantially more enriched than younger oceanic lithosphere. Individual CON provinces can be generally more enriched or less enriched than OIN, or, selectively enriched or depleted in particular elements.

(iii) CON may, in general, be somewhat more evolved than OIN but it is assumed that olivine is the main fractionating phase and that trace-element ratios are not disturbed. However, CON are depleted in P and Ti, relative to OIN, which indicates some fractionation of pyroxene, magnetite, and apatite.

(iv) On average, CON are significantly more enriched in Pb than OIN and this is not attributable to crustal contamination or to partitioning by residual potassic phases in the mantle source. Pb enrichment could be indicative of lithospheric-mantle components in the magmas.

(v) Continental provinces are much more variable in incompatible-element composition than OIN. Many continental magmas are derived from sources more highly enriched or more variably enriched than primitive garnet- or spinel-lherzolite mineralogies. Some provinces are similar to OIN but have higher Pb abundances. In others, Rb, Ba, and K, are extremely variable.

(vi) The multi-element melting model preferred for OIN (carbonate-silicate mixed melts derived by varying degrees of partial melting of depleted amphibole-garnet peridotite) is only partially successful as a model for CON provinces. As in the case of OIN, the model fails to account for high concentrations of Th, Zr, and Ti, and also for high Nb in CON. In Chapter 4, remobilization of silicate melts which have been frozen in the lithosphere is considered a viable means of enriching small melt fractions in carbonate-phobic elements.

(vii) The preferred melting model also fails to account for high LREE in some provinces. This could be due to a greater proportion of carbonate in some CON magmas compared with OIN.

(viii) Unusual incompatible-element profiles have been attributed to derivation from highly depleted lithospheric sources in regions where high heat flow accompanies continental fragmentation and, when lithospheric extension and intraplate volcanism follows soon after subduction-related volcanism, to the sampling of lithospheric mantle which has been modified by slab-derived fluids during subduction.

(ix) CON are most commonly associated with supposed passive rift systems and the early stages of rifting (possibly passive evolving to active) in active rift systems. They are also associated with major transcurrent faulting and orogen-related structural weaknesses. These tectonic environments are thought to be characterised by low lithospheric attenuation and thermal erosion of the lithosphere and might be expected to be associated with magmas with the strongest lithospheric signature. The evidence from CON provinces is ambiguous and does not fit this simple division of rift systems or with the expected behaviour of other extensional tectonic regimes.

(x) As with OIN, most CON can be accounted for by assuming amphibole-bearing sources but cannot be modelled by theoretical partial melting curves for phlogopite-garnet peridotite. Rb behaves as an incompatible element in the genesis of CON. A small number of CON with high Sr and LREE which represent highly carbonated magmas could be modelled by the theoretical

curves for a phlogopite-bearing source. These characterise the highly undersaturated rocks of an entire province or individual magmas within a province otherwise dominated by amphibole.

(xi) Potassic continental magmas have been derived from sources which have been extensively metasomatised and enriched in incompatible elements. Chemically distinct and geographically separated sources are identified in a single magmatic province (WR) which may be due to variation in the involvement of carbonate in magmatism and to the relative importance of amphibole and phlogopite in the source.

(xii) Potassic continental rocks are by definition highly enriched in K, but are also enriched in other incompatible elements by comparison with OIN and most CON. They have, therefore, been derived from phlogopite- and amphibole-bearing sources even though trace-element ratios are similar to those of OIN.

(xiii) Partial melting trends for phlogopite-garnet and amphibole-garnet peridotites indicate that phlogopite and probably amphibole are residual in the generation of katungite and mafurite (WR) whereas ugandites and leucitites (including NSW leucitites) are derived by larger degrees of melting when the potassic phases have been consumed.

(xiv) New South Wales leucitites and Western Rift kamafugites are similar in incompatible-element pattern but NSW magmas are depleted in Th and Nb and enriched in Pb and Zr by comparison. This may be due to derivation from a depleted source which has been selectively enriched in incompatible elements during an earlier subduction event.

(xv) Low P in both NSW and WR magmas could be due to source depletion, residual apatite, or apatite fractionation but is not investigated here.

(xvi) Low abundances of Ti and P by comparison with CON and OIN suggest that continental olivine-poor nephelinites (COP) could be related to CON and OIN by crystal fractionation processes involving olivine, pyroxene, magnetite, and apatite.

(xvii) Fractionation of olivine from a highly carbonated melt with low silica would result in magmas which retain their highly silica undersaturated character despite low (<4 wt.%) MgO.

(xviii) COP are more enriched in Pb, Nb, and Sr than CON. This may be due to the partitioning of trace elements between mantle and highly carbonated liquids during the formation of the magma and the partitioning between carbonate and silicate liquids during immiscible separation of the silicate fraction at lower pressure.

(xix) AFC processes involving crustal contaminants are discounted on the grounds of major-element chemistry, incompatible-element abundances, and Pb isotope systematics.

(xx) On the basis of available isotope data, most COP appear to have been derived from asthenospheric sources and have incorporated lithospheric mantle material during separation of carbonate and silicate melt fractions in the upper mantle.

Chapter 6
Conclusion

6.1 Strategy

The highly silica undersaturated magmas which form feldspar-free volcanic rocks, although rare, have been erupted at some time on most continents and in all major ocean basins. The samples analyzed in the course of this study numbered 488 in all. Of these 174 were from 15 individual oceanic islands and a further 314 were from 39 different continental provinces or volcanic centres. The continental subset included 59 samples from the potassic suites of the Western Rift and New South Wales and 40 samples of olivine-poor nephelinite from continental carbonatite-nephelinite associations. At the same time 904 samples of ocean island rocks from 39 islands, ranging in composition from tholeiite to melilitite, were assembled and analyzed to provide internally consistent data which were directly comparable.

The large amounts of data obtained have been difficult to present meaningfully. Most volcanic complexes are represented by only a few samples and igneous provinces can display considerable chemical variation both within each province and compared with others. This is particularly true for the continental rocks which are distinctly more variable in composition than those from the oceanic islands. In order to see through the variation to characteristics which may be common to all highly undersaturated magmas, average compositions were calculated for each island, volcanic centre, or igneous province, where feldspar-free volcanic rocks occur. These averages have been compared with average OIB abundances calculated from the ocean island data. The mean OIB composition is considered to be robust due to the large number of data included. For one island, Kauai, a substantial number (81) of nephelinite samples were obtained. The inferences drawn from the Kauai data were used as a basis for comparing islands less well represented.

The main objectives of this study were to establish the relative importance of asthenosphere and lithosphere in the generation of nephelinitic magmas in different tectonic settings, to identify minor phases which may be present in the mantle sources of nephelinitic magmas, to provide evidence for the involvement of CO_2- or H_2O-rich fluids in the magmas, and to consider the findings in relation to a number of currently debated issues in igneous petrology. The use of average compositions helped to identify the major and trace elements which proved to be diagnostic in pursuing these objectives. At each stage of interpretation it was tempting to revert to individual occurrences and to make local inferences. To do this properly would have required more data and field information than were available, so data from specific volcanic centres and provinces were used only to reveal the general applicability of the models devised. More detailed analysis of the data base was considered to be beyond the scope of the project. The continental and oceanic subsets were, however, used extensively in ratio-ratio and inter-element diagrams but without sample or province identification beyond that necessary to identify anomalies or explain features.

Each Chapter ends with a summary of the results and conclusions and their relevance to the stated objectives. These have been extensively cross referred but an overview of the main conclusions is presented in the next Section.

6.2 Overview

Highly silica-undersaturated basic magmatism is associated with intraplate volcanic activity and occurs within extensional tectonic regimes in continental areas or as late-stage, post-erosional volcanism on oceanic islands. It is restricted almost entirely to the continental circum-cratonic Proterozoic lithosphere and to the margins of the ocean basins where the Phanerozoic oceanic lithosphere is older. This is attributed to the significance of the age and previous history of the local lithosphere. Oceanic lithosphere is,

in general, too young and depleted to be involved in the generation of highly enriched small melt fractions while Archaean lithosphere may be too thick to allow the passage of asthenosphere-derived magmas and too refractory to contribute to the magma composition.

The magmas responsible for both oceanic (OIN) and continental (CON) nephelinites are dominated by asthenosphere-derived melts (cf. Fitton & Dunlop, 1985; Thompson, 1985) but continental magmas have more variable incompatible-element profiles than OIN and have incorporated enriched material, unavailable to oceanic magmas, from the continental lithosphere (cf. Menzies, 1987). The extensional provinces in which nephelinitic rocks occur are rift systems, which have been categorized as active or passive (Sengor & Burke, 1978), regions of transcurrent faulting, and zones of orogen-related structural weakness. As a result of lithospheric thinning caused by plume-related uplift, extension, and thermal erosion of the lithosphere, well-developed active rifts are the least likely of these to involve lithospheric sources. Highly undersaturated rocks characterise the early stages of development of the East African Rift system but are absent from recent rift-floor volcanics. While the East African Rift may be unchallenged as an example of an active rift system (Buck, 1986), and may have evolved from a passive to an active stage (Mohr, 1982; Almond, 1986), the data for other provinces are ambiguous in associating lithosphere involvement with extensional style.

Major-element correlations indicate that OIN, CON and OIB as a whole are part of a polybaric partial melting continuum (cf. O'Hara, 1968) in which magmas generated from garnet or garnet-spinel lherzolite become MgO-rich and Al_2O_3- and SiO_2-poor with increasing depth. OIN and CON lie at the more magnesian, silica-deficient end of this spectrum and represent the smallest degrees of partial melting and the deepest sources. The mantle sources are primitive or variably depleted in incompatible elements, possibly by crustal extraction (cf. McKenzie & O'Nions, 1995). Trace-element ratios suggest that the OIB source is regionally heterogeneous in Rb and Ba, and that this cannot be easily attributed to LFSE mobility in secondary alteration processes. OIN have low Rb/Nb and generally high Ba/Nb similar to OIB from HIMU and EMI islands (cf. Saunders *et al.*,

1988; Weaver, 1991; Sun & McDonough, 1989). This is not surprising since OIN from strongly EMII islands are extremely rare. The chemical variation in OIN indicates that they do not acquire their HIMU characteristics by preferentially sampling deep-mantle subducted slab material.

Nephelinitic rocks are enriched in elements which partition strongly into carbonate melts and also incompatible elements which are enriched an small silicate melt fractions. Carbonate involvement in the genesis of both OIN and CON magmas, and the more undersaturated potassic rocks from the Western Rift (WR), is indicated by consistently high concentrations of Ca, Mg, Mn, Sr, P, and REE, and low concentrations of Si and Al. These features are attributed to the mixing of carbonate precursor liquids, derived by 0.1% melting, with more voluminous silicate melts generated as the mantle decompresses through the solidus for carbonate peridotite (Fielding, 1992). Carbonate additions of ca. 10% are indicated for OIN and up to 20% for most CON although ca. 33% has been calculated for the Cape Verde melilite-nephelinites. These results are consistent with the experimental evidence presented by Allen *et al.* (1975), Merrill & Wyllie (1975), Eggler (1978) and Wendlandt & Eggler (1980a). Carbonate liquids may also be involved in some undersaturated OIB magmas but are not thought to be a general feature of OIB. Carbonated magmas should be strongly depleted in Ti, Zr, and Th, but this is not observed. Enrichment of carbono-phobic elements in both OIN and CON is attributed to the involvement of lithospheric mantle which carries the products of lithospheric mantle interaction with upwardly percolating continuously- or episodically-derived small melt fractions from the asthenosphere which may be incorporated and retained in its base (McKenzie & O'Nions,1991; Watson & McKenzie, 1991; Watson, 1993). The continental lithosphere may also have been metasomatically enriched by the passage of H_2O- and CO_2-rich fluids from the asthenosphere (e.g. Bailey, 1983; 1985) and by slab-derived fluids in earlier subduction events (e.g. Fitton *et al.*, 1988; 1991).

OIN and CON are highly enriched in most incompatible elements but depleted in Rb, K and Pb by comparison with primitive mantle, and OIN are generally more

depleted in these elements than OIB from the same islands. This is attributed to derivation from depleted mantle and the presence of potassic phases in the mantle source. K_2O/Na_2O is low and K abundance increases with increasing partial melting in OIN and CON whereas Rb decreases. This indicates derivation from amphibole-garnet lherzolite sources. Amphibole is residual at small degrees of partial melting (0.2 to 0.5% for most OIN and CON) but consumed before the larger degree of partial melting approriate to most OIB are reached (cf. Greenough, 1988; Francis & Ludden, 1995). Amphibole is assumed to have been stabilised in mantle sources by hydration of pyroxene. The requirement for amphibole in the source of OIN implies that HIMU magmas are either derived from shallow depths or equilibrate with shallow mantle before eruption. For a few high K_2O/Na_2O samples the presence of phlogopite in the mantle source is indicated by variation of Rb and K. These are almost exclusively continental provinces where the lithosphere has been metasomatically enriched by the migration of H_2O- and CO_2-rich fluids (Foley *et al.*, 1986). Phlogopite suggests a deeper mantle source (70-170km) for these magmas. The Western Rift (WR) and New South Wales (NSW) samples have high K_2O/Na_2O and have involved components derived from metasomatically K- and Ti-enriched lithosphere in which phlogopite is stable (cf. Hawkesworth *et al.*, 1985; Wilkinson & Le Maitre, 1987). Within province variation may be due to degree of partial melting, the effects of amphibole in the source, and the apparent absence of carbonate precursor melts in the genesis of NSW leucitites and WR leucitites and ugandites (cf. Edgar *et al.*, 1976; Wendlandt & Eggler, 1980a, 1980b).

CON are, in general, more enriched in incompatible elements and more evolved than OIN. Olivine is the main fractionating phase accompanied by pyroxene, magnetite, and apatite. Olivine-poor nephelinites (COP) are also enriched in incompatible elements but have similar normalised profiles to OIN and CON. COP may be derived by liquid immiscibility from highly carbonated asthenospheric melts in the upper mantle or lower crust (e.g. Church & Jones, 1995) and contaminated by lithospheric mantle (e.g. Paslick *et al.*, 1995). Elements which partition strongly into carbonate liquids during formation at high pressures do so less strongly in the low-pressure regime which may apply when liquid

immiscibility takes place (Fielding, 1992). COP are related to olivine-rich CON by two-stages of silicate-carbonate liquid partitioning which may produce subtle changes in predicted abundances of carbono-phile elements due to the pressure-effect on partition coefficients. Liquid immiscibility processes are accompanied by extensive fractionation of olivine, pyroxene, magnetite and apatite which also increases abundances of incompatible elements in COP. High Pb abundances in CON and COP may be a result of lithospheric contamination. Crustal contamination of highly silica-undersaturated CON and COP, on the scale required to account for the high Pb, is considered unlikely on the grounds of major-element chemistry and Pb isotope systematics (cf. Paslick *et al.*, 1995).

6.3 Concluding Remarks

One of the problems which has not been addressed in this work is how minor mantle phases can be retained in source regions which undergo substantial melt extraction prior to the eruption of highly undersaturated suites. This difficulty may be overcome in continental provinces where the feldspar-free volcanic rocks are an early feature of the volcanic activity but it is less easy to explain for provinces where highly undersaturated magmas dominate every stage of tectonic evolution, and for ocean islands where the magmas are erupted after a long shield-building phase involving larger degrees of partial melting. In addressing similar problems, Spiegelman & McKenzie (1987) developed equations which can be used to derive analytical solutions for matrix corner flow to account for melt extraction processes at mid-ocean ridges and in island arcs. This work suggests that small melt fractions from a wide melting zone can be drawn into a much smaller central region which underlies the surface manifestation of volcanism.

The consequences of the integration of liquids obtained by different degrees of partial melting from the same source, but travelling through the melting regime along different flow lines, has been taken up by O'Hara (1995). His models indicate that for incompatible elements where bulk D is approximately equal to the average mass fraction of

melt extracted, relative concentrations will be substantially reduced over that predicted for simple equilibrium or fractional melting. The deficit varies with the shape of the melting region and results in steepened chondrite-normalised REE patterns and selective LREE in liquid and source.

The simple melting models developed in this work for the petrogenesis of highly undersaturated feldspar-free volcanic rocks indicate that the mantle sources of the magmas which give rise to these rock types are depleted in highly incompatible elements prior to melting but that the magmas involve carbonate precursor liquids and, possibly, small melt fractions from the lithosphere which may be derived from metasomatically enriched material or remobilised asthenospheric melts which have been trapped in the base of the lithosphere. As O'Hara remarks "The interpreter has to choose between a simple model of the melting process married to a complex pattern of geological processes and a complex model of the melting process married to a potentially simpler pattern of processes." The models presented in this work involve liquid integration but largely represent the former situation. Clearly there is scope for re-interpretation of the data presented here in the light of O'Hara's work and also avenues for further research into the effects of pressure on carbonate-silicate partitioning of trace elements and the consequences of two-stage partitioning on magma composition.

References

Abbey, S. (1983) Studies in "standard samples" of silicate rocks and minerals. *Geol. Surv. Canada* **83-15**: Paper.

Adam, J., Green, T.H. & Sie, S.H. (1993) Proton microprobe determined partitioning of Rb, Sr, Ba, Y, Zr, Nb and Ta between experimentally produced amphiboles and silicate melts with variable F content. *Chem. Geol.* **109**: 29-49.

Allègre, C.J. (1982) Chemical geodynamics. *Tectonophysics* **81**:109-32.

Allègre, C.J. & Turcotte, D.L. (1985) Geodynamic mixing in the mesosphere boundary layer and the origin of oceanic islands. *Geophys. Res. Lett.* **12**: 207-10.

Allen, J.C., Boettcher, A.L. & Marland, G. (1975) Amphiboles in andesite and basalt: I Stability as a function of P-T-fO_2. *Am. Mineral.* **60**:1069-85.

Almeida, F.F.M. (1958) Geologia e Petrologia do Arquipelago de Fernando de Noronha. *Div. Geol. e Min., Depto. Nac. Prod. Min., Minist. da Agric.*, Monog. 13: Revised edition, 181pp. Rio de Janeiro.

Almeida, F.F.M. (1961) Geologia e Petrologia da Ilha da Trinidade. *Div. Geol. e Min., Depto. Nac. Prod. Min., Minist. da Agric.*, Monog. 18, 197pp. Rio de Janeiro.

Almond, D.C. (1986) Geological evolution of the Afro-Arabian dome. *Tectonophysics* **131**: 301-32.

Aoki, K., Yoshida, T., Yusa, K. & Nakamura, Y. (1985) Petrology and geochemistry of the Nyamuragira volcano, Zaire. *J. Volcanol. Geotherm. Res.* **25**: 1-28.

Bailey, D.K. (1974) Nephelinites and ijolites. In: Sørensen, H. ed., *The Alkaline Rocks*: 53-66. Wiley.

Bailey, D.K. (1982) Mantle metasomatism - continuing chemical change within the Earth. *Nature* **296**: 525-30.

Bailey, D.K. (1983) The chemical and thermal evolution of rifts. *Tectonophysics* **94**: 585-97.

Bailey, D.K. (1985) Fluids, melts, flowage and styles of eruption in alkaline ultramafic magmatism. *Trans. Geol. Soc. S. Afr.* **88**: 449-57.

Baker, B.H. (1987) Outline of the petrology of the Kenya Rift alkaline province. In: Fitton, J.G. & Upton, B.G.J. eds., *Alkaline Igneous Rocks.* Geol. Soc. Sp. Pub. No. 30: 293-312. Blackwell.

Baker, B.H., Williams, L.A.J., Miller, J.A. & Fitch, F.J. (1971) Sequence and geochronology of the Kenya Rift volcanics. *Tectonophysics* **11**: 191-215.

Baker, B.H., Mohr, P.A. & Williams, L.A.J. (1972) Geology of the Eastern Rift System of Africa. *Geol. Soc. Am. Sp. Pub.* **136**, 67pp.

Baker, P.E. (1973) Islands of the South Atlantic. In: Nairn, A.E.M. & Stehli, F.G. eds., *The Ocean Basins and Margins Vol. 1: The South Atlantic:* 493-553. Plenum Press, London.

Baker, P.E. (1992) Oceanic islands and the mantle: historical perspectives. *J. Volcanol. Geotherm. Res.* **50**: 17-32.

Barr, S.M. & James, D.E. (1990) Trace element characteristics of Upper Cenozoic basaltic rocks of Thailand, Kampuchea and Vietnam. *J. of Southeast Asian Earth Sciences,* **Vol. 4, No. 3**: 233-42.

Barr, S.M. & Macdonald, A.S. (1981) Geochemistry and geochronology of late Cenozoic basalts of southeast Asia. *Geol. Soc. Am. Bull.* **92**: 1069-1142.

Basaltic Volcanism Study Project (1981) *Basaltic Volcanism on the Terrestrial Planets.* Pergamom Press Inc., New York. 1286pp.

Baxter, A.N. (1986) Petrochemistry of the late Palaeozoic alkali lamprophyre dykes from N Scotland. *Trans. Roy. Soc. Edin., Earth Sciences* **77**: 267-77.

Bell, K. ed. (1989) *Carbonatites: Genesis and Evolution.* Unwin-Hyman. 618pp.

Bell, K. & Powell, J.L. (1969) Strontium isotopic studies of alkalic rocks: the potassium-rich lavas of the Birunga and Toro-Ankole regions, East and Central equatorial Africa. *J. Pet.* **10**: 536-72.

Bergman, S.C. (1987) Lamproites and other potassium-rich igneous rocks: a review of their occurrence, mineralogy and geochemistry. In: Fitton, J.G. & Upton, B.G.J. eds., *Alkaline Igneous Rocks.* Geol. Soc. Sp. Pub. No. 30: 103-90. Blackwell.

Beswick, A.E. & Carmichael, I.S.E. (1978) Constraints on mantle source compositions imposed by phosphorus and rare earth elements. *Contrib. Min. Pet.* **67**: 317-30.

Boctor, N.Z. & Yoder, H.S. (1986) Petrology of some melilite-bearing rocks from Cape Province, Republic of South Africa: relationship to kimberlites. *Am. J. Sci.* **286**: 513-539.

Boettcher, A.L., Mysen, B.O. & Modreski, P.J. (1975) Melting the mantle: phase relationships in natural and synthetic peridotite-H_2O and peridotite-H_2O-CO_2 C-H-O-S with application to kimberlite. In: Ahrens, L.H., Press, F., Runcorn, S.K. & Urey, H.C. eds., *Physics and Chemistry of the Earth Vol. 9*: 855-67. Pergamom Press.

Boettcher, A.L. & O'Neil, J.R. (1980) Stable isotope, chemical and petrographic studies of high-pressure amphiboles and micas: evidence for metasomatism in the mantle source regions of alkali basalts and kimberlites. *Am. J. Sci.* **280A**: 594-621.

Boyd, F.R. (1987) High- and low-temperature garnet peridotite xenoliths and their possible relation to the lithosphere-asthenosphere boundary beneath southern Africa. In: Nixon, P.H. ed., *Mantle Xenoliths*: 403-12. Wiley.

Bracey, D.R. & Andrews, J.E. (1974) Western Caroline Ridge: relic island arc? *Mar. Geophys. Res.* **2**: 111-125.

Brey, G., Brice, W.R., Ellis, D.J., Green, D.H., Harris, K.L. & Ryabchikov, I.D. (1983) Pyroxene-carbonate reactions in the upper mantle. *Earth Planet. Sci. Lett.* **62**: 63-74.

Bristow, J.W. (1984) Nephelinites of the North Lebombo and South-East Zimbabwe. *Spec. Pub. Geol. Soc. S. Africa* **13**: 87-104.

Brooks, C.K. (1976) The Fe_2O_3/FeO ratio of basalt analyses: an appeal for a standardised procedure. *Bull. Geol. Soc. Denmark* **25**: 117-20.

Brooks, C.K. & Nielsen, T.F.D. (1982) The Phanerozoic development of the Kangerdlugssuaq area, East Greenland. *Medd. om Gronland, Geoscience* **9**.

Brooks, C.K., Pedersen, A.K. & Rex, D.C. (1979) The petrology and age of alkaline mafic lavas from the nunatak zone of central East Greenland. *Geological Survey of Greenland Bull. No.* **133**.

Buck, W.R. (1986) Small-scale convection induced by passive rifting: the cause for uplift of rift shoulders. *Earth Planet. Sci. Lett.* **77**: 362-72.

Bultitude, R.J. & Green, D.H. (1967) Experimental study at high pressures on the origin of olivine nephelinite and olivine melilite nephelinite magmas. *Earth Planet Sci. Lett.* **3**: 325-37.

Bultitude, R.J. & Green, D.H. (1971) Experimental study of crystal-liquid relationships at high pressure in olivine nephelinite and basanite compositions. *J. Pet.* **12**: 121-47.

Church, A.A. & Jones, A.P. (1995) Silicate-carbonate immiscibility at Oldoinyo Lengai. *J. Pet.* **36**: 869-90.

Clague, D.A. & Frey, F.A. (1982) Petrology and trace-element geochemistry of the Honolulu volcanics, Oahu: implications for the oceanic mantle below Hawaii. *J. Pet.* **23**: 447-504.

Cohen, R.S. & O'Nions, R.K. (1982) Identification of recycled continental material in the mantle from Sr, Nd and Pb isotope investigations. *Earth Planet. Sci. Lett.* **61**: 73-84.

Coombs, D.S., Cas, R.A., Kawachi, Y., Landis, C.A., McDonough, W.F. & Reay, A. (1986) Cenozoic volcanism in north, east and central Otago. In: Smith, I.E.M. ed., *Late Cenozoic Volcanism in New Zealand.* Roy. Soc. NZ Bull. **23**.

Coombs, D.S. & Wilkinson, J.F.G. (1969) Lineages and fractionation trends in undersaturated volcanic rocks from the east Otago volcanic province (New Zealand) and related rocks. *J. Pet.* **10**: 440-501.

Courtney, R.C. & White, R.S. (1986) Anomalous heat flow and geoid across the Cape Verde rise: evidence for dynamic support from a thermal plume in the mantle. *Geophys. J. Roy. Astr. Soc.* **87**: 815-68.

Cox, K.G., Johnson, R.L., Stillman, C.J., Vail, J.R. & Wood, D.N. (1965) The geology of the Nuanetsi igneous province. *Phil. Trans. Roy. Soc.* **A257**: 71-218.

Crossley, R. (1979) The Cenozoic stratigraphy and structure of the western part of the rift valley in southern Kenya. *J. Geol. Soc. Lond.* **136**: 393-405.

Crossley, R. & Knight, R.M. (1981) Volcanism in the western part of the rift valley in southern Kenya. *Bull. Volcanol.* **44**: 117-28.

Cundari, A. (1973) Petrology of the leucite-bearing lavas in New South Wales. *J. Geol. Soc. Australia* **20, 4**: 465-94.

Cundari, A. (1989) Central and southern New South Wales: East Australian leucitite suite. In: Johnson, R.W. ed., *Intraplate Volcanism in Eastern Australia and New Zealand:* 131-2. Cambridge University Press.

Dalrymple, G.B., Journal, R.D. & Clague, D.A. (1975) K-Ar ages of some volcanic rocks from the Cook and Austral Islands. *Geol. Soc. Am. Bull.* **86**: 1463-7.

Davies, G.R., Norry, M.J., Gerlach, D.C. & Cliff, R.A. (1989) A combined chemical and Pb-Sr-Nd isotope study of the Azores and Cape Verdes hotspots: the geodynamic implications. In: Saunders, A.D. & Norry, M.J. eds., *Magmatism in Ocean Basins.* Geol. Soc. Sp. Pub. No. 42: 231-55. Blackwell.

Davis, J.M. (1991) The geochemical evolution of basic and intermediate mid- to late-Tertiary volcanism from the Mogollon-Datil volcanic field, southwestern New Mexico, U.S.A. Unpub. PhD Thesis. The Open University.

Dawson, J.B. (1984) Contrasting types of upper mantle metasomatism. In: Kornprobst, J. ed., *Kimberlites II*: 289-94. Proc. Third Int. Kimberlite Conf. Elsevier.

Dawson, J.B. (1989) Sodium carbonatite extrusions from Oldoinyo Lengai, Tanzania: implications for carbonatite complex genesis. In: Bell, K. ed., *Carbonatites: Genesis and Evolution:* 255-77. Unwin-Hyman.

Dawson, J.B. (1992) Neogene tectonics and volcanicity in the North Tanzania sector of the Gregory Rift Valley: contrasts with the Kenya sector. *Tectonophysics* **204**: 81-92.

Dawson, J.B. & Powell, D.G. (1969) The Natron-Engaruka explosion crater area, northern Tanzania. *Bull. Volcanol.* **33**: 791-817.

Dawson, J.B., Smith, J.V. & Jones, A.P. (1985) A comparative study of bulk rock and mineral chemistry of olivine melilitites and associated rocks from East and South Africa. *Neues Jahrbruch Miner. Abh.* **152, 2**: 143-175.

de Jongh, W.K. (1973) XRF-analysis using theoretical influence coefficients. *X-Ray Spectrometry* **2**: 151.

De la Roche, H., Leterrier, P., Grandclaude, P. & Marchal, M. (1980) A classification of volcanic and plutonic rocks using the R1-R2 diagram and major element analyses: its relationships with current nomenclature. *Chem. Geol.* **29**: 183-210.

Dillon, W.P. & Sougy, J.M.A. (1974) Geology of West Africa and Canary and Cape Verde Islands. In: Nairn, A.E.M. & Stehli, F.G. eds., *The Ocean basins and Margins Vol. 2: The North Atlantic*: 315-91. Plenum Press, London.

Downes, H. (1987) Tertiary and Quaternary volcanism in the Massif Central, France. In: Fitton, J.G. & Upton, B.G.J. eds., *Alkaline Igneous Rocks.* Geol. Soc. Sp. Pub. No. 30: 517-30. Blackwell.

Duncan, R.A., Hargraves, R.B. & Brey, G.P. (1978) Age, palaeomagnetism and chemistry of melilite basalts in the southern Cape, South Africa. *Geol. Mag.* **115**: 317-396.

Duncan, R.A. & McDougall, I. (1989) Plate tectonic setting. In: Johnson, R.W. ed., *Intraplate Volcanism in Eastern Australia and New Zealand:* 13-18. Cambridge University Press.

Dunlop, H.M. & Fitton, J.G. (1979) A K-Ar and Sr-isotope study of the volcanic rocks of the island of Principe, West Africa - evidence for mantle heterogeneity beneath the Gulf of Guinea. *Contrib. Min. Pet.* **71**: 125-31.

Edgar, A.D. (1974) Experimental studies. In: Sørensen, H. ed., *The Alkaline Rocks*: 355-89. Wiley.

Edgar, A.D. (1987) The genesis of alkaline magmas with emphasis on their source regions: inferences from experimental studies. In: Fitton, J.G. & Upton, B.G.J. eds., *Alkaline Igneous Rocks.* Geol. Soc. Sp. Pub. No. 30: 29-52. Blackwell.

Edgar, A.D. & Arima, M. (1983) Conditions of phlogopite crystallization in ultrapotassic volcanic rocks. *Min. Mag.* **47**: 11-19.

Edgar, A.D., Green, D.H. & Hibberson, W.O. (1976) Experimental petrology of a highly potassic magma. *J. Pet.* **17**: 339-56.

Eggler, D.H. (1978) The effect of CO_2 upon partial melting of peridotite in the system Na_2O-CaO-Al_2O_3-MgO-SiO_2-CO_2 to 35kb, with an analysis of melting in a peridotite-H_2O-CO_2 system. *Am. J. Sci.* **278**: 305-43.

Eggler, D.H. (1989) Kimberlites: how do they form? In: Ross, J. ed., *Kimberlites and Related Rocks Vol. I.* Geol. Soc. Am. Sp. Pub. No. 14: 489-504. Blackwell.

Embey-Isztin, A., Downes, H., James, D.E., Upton, B.G.J., Dobosi, G., Ingram, G.A., Harmon, R.S. & Scharbert, H.G. (1993) The petrogenesis of Pliocene alkaline volcanic rocks from the Pannonian Basin, Eastern Central Europe. *J. Pet.* **34**: 317-344.

Emerick, C.M. & Duncan, R.A. (1982) Age progressive volcanism in the Comores archipelago, western Indian Ocean and implications for Somali plate tectonics. *Earth Planet. Sci. Lett.* **60**: 415-28 and (1983) Errata, *Ibid.* **62**: 439.

Ewart, A., Chappell, B.W. & Menzies, M.A. (1988) An overview of the geochemical and isotopic characteristics of the Eastern Australian Cainozoic volcanic provinces. *J. Pet. Special Lithosphere Issue*: 225-74.

Falloon, T.J. & Green, D.H. (1989) The solidus of carbonated fertile peridotite. *Earth Planet. Sci. Lett.* **94**: 364-70.

Falloon, T.J. & Green, D.H. (1990) The solidus of carbonated fertile peridotite under fluid saturated conditions. *Geology* **18**: 195-99.

Feigenson, M.D., Hofmann, A.W. & Spera, F.J. (1983) Case studies on the origin of basalt II. The transition from tholeiitic to alkalic volcanism on Kohala volcano, Hawaii, *Contrib. Min. Pet.* **84**: 390-405.

Fielding, K.D. (1992). *Element partitioning between coexisting carbonate and silicate liquids*. Unpub. PhD Thesis, University of Edinburgh.

Fitton, J.G. (1987) The Cameroon line, West Africa: a comparison between oceanic and continental volcanism. In: Fitton, J.G. & Upton, B.G.J. eds., *Alkaline Igneous Rocks*. Geol. Soc. Sp. Pub. No. 30: 273-92. Blackwell.

Fitton, J.G. & Dunlop, H.M. (1985) The Cameroon Line, West Africa, and its bearing on the origins of oceanic and continental alkali basalt. *Earth Planet. Sci. Lett.* **72**: 23-38.

Fitton, J.G. & Hughes, D.J. (1977) Petrochemistry of the volcanic rocks of the island of Principe, Gulf of Guinea. *Contrib. Min. Pet.* **64**: 257-72.

Fitton, J.G. & Hughes, D.J. (1981) Strontian melilite in a nephelinite lava from Etinde, Cameroon. *Min. Mag.* **44**: 261-64.

Fitton, J.G. & James, D. (1986) Basic volcanism associated with intraplate linear features. *Phil. Trans. Roy. Soc. Lond.* **A317**: 253-66.

Fitton, J.G., James, D., Kempton, P.D., Ormerod, D.S. & Leeman, W.P. (1988) The role of lithospheric mantle in the generation of late cenozoic basic magmas in the western United States. *J. Pet. Special Lithosphere Issue*: 331-50.

Fitton, J.G., James, D., & Leeman, W.P. (1991) Basic magmatism associated with late Cenozoic extension in the western United States: compositional variations in space and time. *J. Geophys. Res.* **Vol. 96, No. B8**: 13693-711.

Fitton, J.G. & Upton, B.G.J. eds. (1987) *Alkaline Igneous Rocks*. Geol. Soc. Lond. Sp. Pub. No. 30. Blackwell. 568pp.

Flower, M.J.F. (1972) Petrology of volcanic rocks from Anjouan, Comores archipelago. *Bull. Volcanol.* **36**: 238-50.

Flower, M.J.F. (1973) Evolution of basaltic and differentiated lavas from Anjouan, Comores archipelago. *Contrib. Min. Pet.* **38**: 237-60.

Fodor, R.V., Bauer, G.R. & Keil, K. (1982) Ultramafic inclusions and megacrysts in olivine nephelinite, Aitutaki Island, Cook Islands. *New Zealand J. Geol. Geophys.* **25**: 67-76.

Foley, S.F., Taylor, W.R. & Green, D.H. (1986) The role of fluorine and oxygen fugacity in the genesis of the ultrapotassic rocks. *Contrib. Min. Pet.* **94**: 183-92.

Francis, D. & Ludden, J. (1995) The signature of amphibole in mafic alkaline lavas, a study in the northern Canadian cordillera. *J. Pet.* (submitted).

Frey, F.A., Green, D.H. & Roy, S.D. (1978) Integrated models of basalt petrogenesis: a study of quartz tholeiites to olivine melilitites from South Eastern Australia utilizing geochemical and experimental petrological data. *J. Pet.* **19**: 463-513.

Frey, F.A., Roden, M.F. & Zindler, A. (1980) Constraints on mantle source composition imposed by phosphorus and rare earth elements. Critical comments on paper by A.E. Beswick & I.S.E. Carmichael. *Contrib. Min. Pet.* **67**: 317-330. *Contrib. Min. Pet.* **75**: 165-173.

Gass, I.G., Mallick, D.I.G. & Cox, K.G. (1973) Volcanic Islands of the Red Sea. *J. Geol. Soc. Lond.* **129**: 275.

Gerlach, D.C., Cliff, R.A., Davies, G.R., Norry, M. & Hodgson, N. (1988) Magma sources of the Cape Verdes archipelago: isotopic and trace-element constraints. *Geochem. Cosmochem. Acta* **52**: 2979-92.

Gerlach, D.C., Stormer, J.C. Jr. & Mueller, P.A. (1987) Isotopic geochemistry of Fernando de Noronha. *Earth Planet. Sci. Lett.* **85**: 129-44.

Gittins, J. (1989) The origin and evolution of carbonatite magma. In: Bell, K. ed., *Carbonatites: Genesis and Evolution*: 580-600. Unwin-Hyman.

Gleadow, A.J.W. & Brooks, C.K. (1979) Fission track dating, thermal histories and tectonics of igneous intrusions in East Greenland. *Contrib. Min. Pet.* **71**: 45-60.

Govindaraju, K. (1994) 1994 compilation of working values and sample description for 383 geostandards. *Geostandards Newsletter* **18**: Special Issue.

Green, D.H. & Ringwood, A.E. (1964) Fractionation of basalt magmas at high pressures. *Nature* **201**: 1276-9.

Green, D.H. & Ringwood, A.E. (1966) The genesis of basaltic magmas. *Dept. Geophys. Geochem. Australian Nat. Univ. Pub.* **444**: 118-205.

Green, D.H. & Ringwood, A.E. (1967) The genesis of basaltic magmas. *Contrib. Min. Pet.* **15**: 103-90.

Greenough, J.D. (1988) Minor phases in the Earth's mantle: evidence from trace- and minor-element patterns in primitive alkaline magmas. *Chem. Geol.* **69**: 177-92.

Gupta, A.K. & Yagi, K. (1980) *Petrology and Genesis of Leucite-Bearing Rocks*. Springer-Verlag. 252pp.

Halliday, A.N., Davies, G.R., Lee, D-C., Tommasini, S., Paslick, C.R., Fitton, J.G. & James, D.E. (1992) Lead isotopic evidence for young trace-element enrichment in the oceanic upper mantle. *Nature* **359**: 623-7. Correction (1993). *Nature* **362**: 184.

Halliday, A.N., Lee, D-C., Tommasini, S., Davies, G.R., Paslick, C.R., Fitton, J.G. & James, D.E. (1995a) Incompatible trace elements in OIB and MORB and melt enrichment in the sub-oceanic mantle. *Earth Planet. Sci. Lett.* (submitted).

Halliday, A.N., Lee, D-C., Tommasini, S., Davies, G.R., Paslick, C.R., Fitton, J.G. & James, D.E. (1995b) Highly incompatible trace elements in Earth's mantle. *Earth Planet. Sci. Lett.* (submitted).

Harris, P.G. (1957) Zone refining and the origin of potassic basalts. *Geochem. Cosmochem. Acta* **12**:195-208.

Hart, S.R. (1984) The DUPAL anomaly: a large scale isotope anomaly in the southern hemisphere mantle. *Nature* **309**: 753-57.

Hart, S.R., Gerlach, D.C. & White, W.M. (1986) A possible new Sr-Nd-Pb mantle array and consequences for mantle mixing. *Geochem. Cosmochem. Acta* **50**: 1551-57.

Hawkesworth, C.J., Fraser, K.J. & Rogers, N.W. (1985) Kimberlites and lamproites: extreme products of mantle enrichment processes. *Trans. Geol. Soc. S. Afr.* **88**: 439-47.

Hawkesworth, C.J., Mantovani, M.S.M., Taylor, P.N. & Palacz, Z. (1986) Evidence from the Parana of south Brazil for a continental contribution to DUPAL basalts. *Nature* **322**: 356-59.

Hayes, D.E. & Rabinowitz, P.D. (1975) Mesozoic magnetic lineations and the magnetic quiet zone off northwest Africa. *Earth Planet. Sci. Lett.* **28**: 105-15.

Hernandez, J. (1971) *Le Volcanisme Tertiare des Monts du Forez et de la Plaine de Montbrison.* Unpub. PhD Thesis, Université Paris.

Higazy, R.A. (1954) Trace elements of volcanic ultrabasic potassic rocks of southwestern Uganda and adjoining parts of the Belgian Congo. *Bull. Geol. Soc. Am.* **65**: 39-70.

Hoernle, K. & Schmincke, H-U. (1993a) The petrology of the tholeiites through melilite nephelinites on Gran Canaria, Canary Islands: crystal fractionation, accumulation, and depths of melting. *J. Pet.* **34**: 573-97.

Hoernle, K. & Schmincke, H-U. (1993b) The role of partial melting in the 15Ma geochemical evolution of Gran Canaria: a blob model for the Canary hotspot. *J. Pet.* **34**: 599-626.

Hofmann, A.W. & White, W.M. (1982) Mantle plumes from ancient oceanic crust. *Earth Planet. Sci. Lett.* **57**: 421-36.

Irvine, T.N. & Baragar, W.R.A. (1971) A guide to the chemical classification of the common volcanic rocks. *Canad. J. Earth Sci.* **8**: 523-48.

Jacques, A.L. & Green, D.H. (1980) Anhydrous melting of peridotite at 0-15kb pressure and the genesis of tholeiitic basalts. *Contrib. Min. Pet.* **73**: 287-310.

Johnson, K.T., Dick, H.J.B. & Shimuzu, N. (1990) Melting in the oceanic upper mantle: an ion microprobe study of diopsides in abyssal peridotites. *J. Geophys. Res.* **95**: 2661-2678.

Johnson, R.W., Wallace, D.A. & Ellis, D.J. (1976) Feldspathoid-bearing volcanic rocks and associated types from volcanic islands off the coast of New Ireland, Papua New Guinea. In: Johnson, R.W. ed., *Volcanism in Australasia:* 297-316. Elsevier, Amsterdam.

Johnson, R.W. ed. (1976) *Volcanism in Australasia.* Elsevier, Amsterdam. 405pp.

Johnson, R.W. ed. (1989) *Intraplate Volcanism in Eastern Australia and New Zealand.* Cambridge University Press. 408pp.

Kay, R.W. & Gast, P.W. (1973) The rare earth content and origin of alkali-rich basalts. *J. Geology* **81,6**: 653-82.

Keating, B.H., Mattey, D.P., Helsley, C.E., Naughton, J.J., Epp, D., Lazarewicz, A. & Schwank, D. (1984) Evidence for a hot spot origin of the Caroline Islands. *J. Geophys. Res.* **89, B12**: 9937-48.

King, B.C. (1970) Vulcanicity and rift tectonics in East Africa. In: Clifford, T.N. & Gass, I.G. eds., *African Magmatism and Tectonics*: 263-84. Oliver & Boyd, Edinburgh.

King, B.C. & Chapman, G.R. (1972) Volcanism of the Kenya Rift Valley. *Phil. Trans. Roy. Soc. Lond.* **A271**: 185-208.

King, B.C., Le Bas, M.J. & Sutherland, D.S. (1972) The history of the alkaline volcanoes and intrusive complexes of eastern Uganda and western Kenya. *J. Geol. Soc.* **128**: 173-205.

Kjarsgaard, B.A. & Hamilton, D.L. (1989) The genesis of carbonatites by immiscibility. In: Bell, K. ed., *Carbonatites: Genesis and Evolution*: 388-404. Unwin-Hyman.

Knutson, J. (1989) East Australian volcanic geology. In: Johnson, R.W. ed., *Intraplate Volcanism in Eastern Australia and New Zealand:* 89-157. Cambridge University Press.

Kornprobst, J. ed. (1984) *Kimberlites I: Kimberlites and Related Rocks* (466pp); *Kimberlites II: The mantle and crust-mantle relationships* (393pp). Proc. Third Internat. Kimberlite Conf. Elsevier.

Koster van Groos, A.F. (1975) The effect of high CO_2 pressure on alkalic rocks and its bearing on the formation of alkaline ultrabasic rocks and associated carbonatites. *Am. J. Sci.* **275**: 163-85.

Kuno, H. (1959) Origin of Cenozoic petrographic provinces of Japan and surrounding areas. *Bull. Volcanol.* **20**: 37-76.

Kushiro, I. (1972) Effects of water on the composition of magmas formed at high pressures. *J. Pet.* **13**: 311-34.

Kushiro, I. & Kuno, H. (1963) Origin of primary basalt magmas and classification of basaltic rocks. *J. Pet.* **4**: 75-89.

Lanphere, M.A. & Dalrymple, G.B. (1980) Age and strontium isotopic composition of the Honolulu volcanic series, Oahu, Hawaii. *Am. J. Sci.* **280A**: 736-51.

Laughlin, A.W., Aldrich, M.J., Shafiqullah, M. & Husler, J. (1986) Tectonic implications of the age, composition and orientation of lamprophyre dikes, Navajo volcanic field, Arizona. *Earth Planet. Sci. Lett.* **76**: 361-74.

Le Bas, M.J. (1977) *Carbonatite-Nephelinite Volcanism.* Wiley, London. 347pp.

Le Bas, M.J. (1978a) Nephelinite volcanism at plate interiors. *Bull. Volcanol.* **41-4**.

Le Bas, M.J. (1978b) Are olivine-poor nephelinites a primary melt product from the mantle? *Bull. Volcanol.* **41-4**.

Le Bas, M.J. (1987) Nephelinites and Carbonatites. In: Fitton, J.G. & Upton, B.G.J. eds., *Alkaline Igneous Rocks.* Geol. Soc. Sp. Pub. No. 30: 53-84. Blackwell.

Le Bas, M.J. (1989a) Diversification of carbonatite. In: Bell, K. ed., *Carbonatites: Genesis and Evolution*: 428-47. Unwin-Hyman.

Le Bas, M.J. (1989b) Nephelinitic and basanitic rocks. *J.Pet.* **30**: 1299-312.

Le Bas, M.J., Le Maitre, R.W., Streckeisen, A. & Zanettin, B. (1986) A chemical classification of volcanic rocks based on the total alkali-silica diagram. *J. Pet.* **27**: 745-50.

Le Bas, M.J., Rex, D.C. & Stillman, C.J. (1986) The early magmatic chronology of Fuerteventura, Canary Islands. *Geol. Mag.* **123(3)**: 287-98.

Le Maitre, R.W. (1976) The chemical variability of some common igneous rocks. *J. Pet.* **17**: 589-637.

Le Maitre, R.W. (1984) A proposal by the IUGS Subcommission on the Systematics of Igneous Rocks for a chemical classification of volcanic rocks based on the total alkali-silica (TAS) diagram. *Australian J. Earth Sci.* **31**: 243-55.

Maaløe, S., James, D., Smedley, P., Peterson, S. & Garmann, L.B. (1992) The Koloa volcanic suite of Kauai, Hawaii. *J. Pet.* **33**: 761-84.

McKenzie, D.P. (1978) Some remarks on the development of sedimentary basins. *Earth Planet. Sci. Lett.* **40**: 25-32.

McKenzie, D.P. (1984) The generation and compaction of partially molten rock. *J.Pet.* **25**: 713-65.

McKenzie, D. (1985) The extraction of magma from the crust and mantle. *Earth Planet. Sci. Lett.* **74**: 81-91.

McKenzie, D. & O'Nions, R.K. (1983) Mantle reservoirs and ocean island basalts. *Nature* **301**: 229-31.

McKenzie, D. & O'Nions, R.K. (1991) Partial melt distributions from inversion of rare earth element concentrations. *J. Pet.* **32**: 1021-91.

McKenzie, D. & O'Nions, R.K. (1995) The source regions of ocean island basalts. *J. Pet.* **36**: 133-59.

Marcelot, G., Rancon, J.Ph. & Demange, J. (1985) The potassic series of Karisimbi volcano (Virunga range, Rwanda): volcanological and petrological aspects. *J. Volcanol. Geotherm. Res.* **26**: 99-129.

Mattey, D.P. (1982) The minor and trace element geochemistry of volcanic rocks from Truk, Ponape and Kusaie, Eastern Caroline Islands: the evolution of a young hot spot trace across old Pacific Ocean crust. *Contrib. Min. Pet.* **80**: 1-13.

Meen, J.K. (1987) Mantle metasomatism and carbonatites: an experimental study of a complex relationship. *Geol. Soc. Am. Sp. Pub.* **215**: 91-100.

Meen, J.K., Ayers, J.C. & Fregau, E.J. (1989) A model for mantle metasomatism by carbonated alkaline melts: trace-element and isotopic compositions of mantle source regions of carbonatite and other continental igneous rocks. In: Bell, K. ed., *Carbonatites: Genesis and Evolution*: 464-99. Unwin-Hyman.

Menzies, M. (1987) Alkaline rocks and their inclusions: a window on the Earth's interior. In: Fitton, J.G. & Upton, B.G.J. eds., *Alkaline Igneous Rocks*. Geol. Soc. Sp. Pub. **30**: 15-27. Blackwell.

Menzies, M. & Rama Murthy, V. (1980a) Mantle metasomatism as a precursor to the genesis of alkaline magmas - isotope evidence. *Am. J. Sci.* **280A**: 622-38.

Menzies, M. & Rama Murthy, V. (1980b) Enriched mantle: Nd and Sr isotopes in diopsides from Kimberlite nodules. *Nature* **283**: 634-36.

Merrill, R.B. & Wyllie, P.J. (1975) Kaersutite and kaersutite eclogite from Kakanui, New Zealand - water excess and water deficient melting relations to 30 kilobars. *Geol. Soc. Am. Bull.* **86**: 555-70.

Mertes, H. & Schmincke, H-U. (1985) Mafic potassic lavas of the Quaternary west Eifel field (western Germany). I Major and trace elements. *Contrib. Min. Pet.* **89**: 330-45.

Minarik, W.G. & Watson, E.B. (1991) Bulk iron diffusion in dunite through interstitial carbonate melts. *EOS* **72**: 17.

Minato, M., Gorai, M. & Hunahashi, M., eds.(1965) *The Geologic Development of the Japanese Islands.* Tsukiji Shokan Co. Ltd. 442pp.

Mitchell, R. (1986) *Kimberlites.* Plenum Press. 442pp.

Mitchell, R.H. & Bergman, S.C. (1991) *Petrology of Lamproites.* Plenum Press, New York. 447pp.

Mitchell, R.H. & Platt, R.G. (1983) Primitive nephelinitic volcanism associated with rifting and uplift in the Canadian Arctic. *Nature* **303**: 609-12.

Mitchell, R.H. & Platt, R.G. (1984) The Freeman's Cove volcanic suite: field relations, petrochemistry, and tectonic setting of nephelinite-basanite volcanism associated with rifting in the Canadian Arctic archipelago. *Canad. J. Earth Sci.* **21**: 428-36.

Mitchell-Thomé, R.C. (1970) *Geology of the South Atlantic Islands.* Gebruder Borntraeger, Berlin. 367pp.

Modreski, P.J. & Boettcher, A.L. (1973) Phase relationships of phlogopite in the system K_2O-MgO-CaO-Al_2O_3-SiO_2-H_2O to 35 kilobars:a better model for micas in the interior of the Earth. *Am. J. Sci.* **273**: 385-414.

Mohr, P. (1982) Musings on continental rifts. In: Palmason, G. ed., *Continental and Oceanic Rifts*: 293-309. Am. Geophys. Union. Washington.

Moore, A.E. & Erlank, A.J. (1979) Unusual olivine zoning - evidence for complex physico-chemical changes during the evolution of olivine melilitite and kimberlite magmas. *Contrib. Min. Pet.* **700**: 391-406.

Mysen, B.O. & Boettcher, A.L. (1975) Melting of hydrous mantle: II Geochemistry of crystals and liquids formed by anatexis of mantle peridotite at high pressures and high temperatures as a function of controlled activities of water, hydrogen and carbon dioxide. *J. Pet.* **16**: 549-93.

Mysen, B.O. & Kushiro, I. (1977) Compositional variations of coexisting phases with degrees of melting of peridotite in the upper mantle. *Am. Mineral.* **62**: 843-65.

Nakamura, E., Campbell, I.H. & Sun, S-S. (1985) The influence of subduction processes on the geochemistry of Japanese alkaline basalts. *Nature* **316**: 55-8.

Nakamura, Y. & Tatsumoto, M. (1988) Pb, Nd, and Sr isotopic evidence for a multi-component source for rocks of the Cook-Austral Islands and heterogeneities of mantle plumes. *Geochem. Cosmochem. Acta* **52**: 2909-24.

Natland, J.H. (1980) The progression of volcanism in the Samoan linear volcanic chain. *Am. J. Sci.* **280A**: 709-35.

Nkoumbou, C., Deruelle, B. & Velde, D. (1995) Petrology of Mt Etinde nephelinite series. *J. Pet.* **36**: 373-95.

Norrish, K. & Hutton, J.T. (1969) An accurate X-ray spectrographic method for the analysis of a wide range of geological samples. *Geochem. Cosmochim. Acta* **33**: 431-53.

Nougier, J., Cantagrel, J.M. & Karche, J.P. (1986) The Comores archipelago in the western Indian Ocean: volcanology, geochronology and geodynamic setting. *J. African Earth Sci.* **Vol. 5, No. 2**: 135-45.

Odling, N.W. & Randle, H.A. (1992) The partitioning of trace elements between fluid and melt. *Terra Abstracts* **4**: 32.

O'Hara, M.J. (1965) Primary magmas and the origin of basalts. *Scot. J. Geol.* **1**: 19-40.

O'Hara, M.J. (1968) The bearing of phase equilibria studies in synthetic and natural systems and the origin and evolution of basic and ultrabasic rocks. *Earth Planet. Sci. Lett.* **4**: 69-133.

O'Hara, M.J. (1995) Trace element geochemical effects of integrated melt extraction and 'shaped' melting regimes. *J. Pet.* **36**: 1111-32.

Olafsson, M. & Eggler, D.H. (1983) Phase relations of amphibole-carbonate and phlogopite carbonate peridotite: petrologic constraints on the asthenosphere. *Earth Planet. Sci Lett.* **64**: 305-15.

O'Nions, R.K. (1987) Relationships between chemical and convective layering in the Earth. *J. Geol. Soc. Lond.* **144**: 259-74.

Palacz, Z.A. & Saunders, A.D. (1986) Coupled trace element and isotope enrichment in the Cook-Austral-Samoa Islands, southwest Pacific. *Earth Planet. Sci. Lett.* **79**: 270-80.

Paslick, C., Halliday, A., James, D. & Dawson, J.B. (1995) Enrichment of the continental lithosphere by OIB melts: isotopic evidence from the volcanic province of northern Tanzania. *Earth Planet. Sci. Lett.* **130**: 109-26.

Phelps, D.W., Gust, D.A. & Wooden, J.L. (1983) Petrogenesis of the mafic feldspathoidal lavas of the Raton-Clayton volcanic field, New Mexico. *Contrib. Min. Pet.* **84**: 182-90.

Rabinowitz, P.D., Coffin, M.F. & Falvey, D. (1983) The separation of Madagascar and Africa. *Science* **220**: 67-9.

Reynolds, R.C. (1963) Matrix corrections in trace element analysis by X-ray fluorescence: estimation of the mass absorption coefficient by Compton scattering. *Am. Mineral.* **48**: 1133-43.

Richter, P. & McKenzie, D. (1984) Dynamic models for melt segregation from a deformable matrix. *J. Geol.* **92**: 729-40.

Ringwood, A.E. (1982) Phase transformations and differentiation in subducted lithosphere: implications for mantle dynamics, basalt petrogenesis and crustal evolution. *J. Geol.* **90**: 611-43.

Ringwood, A.E. (1989) Constitution and evolution of the mantle. In: Ross, J. ed., *Kimberlites and Related Rocks Vol I.* Geol. Soc. Am. Sp. Pub. No. 14: 457-85. Blackwell.

Roden, M.F., Frey, F.A. & Clague, D.A. (1984) Geochemistry of tholeiitic and alkalic lavas from the Koolau Range, Oahu, Hawaii: implications for Hawaiian volcanism. *Earth Planet. Sci. Lett.* **69**: 141-58.

Roden, M.F., Smith, D. & McDowell, F.W. (1979) Age and extent of potassic volcanism on the Colorado Plateau. *Earth Planet. Sci. Lett.* **43**: 279-84.

Roeder, P.L. & Emslie, R.F. (1970) Olivine-liquid equilibrium. *Contrib. Min. Pet.* **29**: 275-89.

Rosendahl, B.R. (1987) Architecture of continental rifts with special reference to East Africa. *Ann. Rev. Earth Planet. Sci.* **15**: 445-503.

Ross, J. ed. (1989) *Kimberlites and Related Rocks Vol. I: Their composition, occurrence, origin and emplacement; Kimberlites and Related Rocks Vol. II: Their mantle/crust setting, diamonds and diamond exploration.* Proc. 4th Int. Kimberlite Conf. Geol Soc. Am. Sp. Pub. No. 14. Blackwell. 1271pp.

Ryerson, F.J. & Watson, E.B. (1987) Rutile saturation in magmas: implications for Ti-Nb-Ta depletion in island arc magmas. *Earth Planet. Sci. Lett.* **86**: 225-39.

Sahama, Th. G. (1974) Potassium-rich alkaline rocks. In: Sørensen, H. ed., *The Alkaline Rocks*: 96-108. Wiley.

Saunders, A.D., Norry, M.J. & Tarney, J. (1988) Origin of MORB and chemically depleted mantle reservoirs: trace element constraints. *J. Pet. Special Lithosphere Issue*: 415-45.

Schmincke, H-U. (1973) Magmatic evolution and tectonic regime in the Canary, Madeira and Azores Island groups. *Geol. Soc. Am. Bull.* **84**: 633-48.

Schmincke, H-U. (1982) Volcanic and chemical evolution of the Canary Islands. In: von Rad, U., Hinz, K., Sarnthein, M., & Seibold, E. eds., *Geology of the Northwest African Margin*: 273-306. Springer-Verlag, New York.

Schneider, M.E. & Eggler, D.H. (1986) Fluids in equilibrium with peridotite minerals: implications for mantle metasomatism. *Geochem. Cosmochem. Acta* **50**: 711-24.

Sengor, A.H.C. & Burke, K. (1978) Relative timing of rifting and volcanism in earth and its tectonic implications. *Geophys. Res. Lett.* **5**: 419-21.

Shaw, D.M. (1970) Trace element fractionation during anatexis. *Geochem. Cosmochem. Acta* **34**: 237-43.

Shoemaker, E.M., Roach, C.H. & Byers, F.M. (1962) Diatremes and uranium deposits in the Hopi Buttes, Arizona. In: *Petrologic studies: a volume in honour of A.F. Buddington:* 327-55. Geol. Soc. Am.

Sørensen, H., ed. (1974) *The Alkaline Rocks*. Wiley. 622pp.

Spencer, A.B. (1969) Alkalic Igneous Rocks of the Balcones province, Texas. *J. Pet.* **10,2**: 272-306.

Spiegelman, M. & Mckenzie, D. (1987) Simple 2-D models for melt extraction at mid-ocean ridges and island arcs. *Earth Planet. Sci. Lett.* **83**: 137-52.

Stolz, A.J. & Davies, G.R. (1988) Chemical and isotopic evidence from spinel lherzolite xenoliths for episodic metasomatism of the upper mantle beneath southeast Australia. *J. Pet. Special Lithosphere Issue*: 303-30.

Streckeisen, A. (1980) Classification and nomenclature of volcanic rocks, lamprophyres, carbonatites and melilitic rocks: IUGS Subcommission on the Systematics of Igneous Rocks. *Geol. Rundsch.* **69,1**: 194-207.

Strong, D.F. (1972a) The petrology of the lavas of Grande Comore. *J.Pet.* **13,2**: 181-217.

Strong, D.F. (1972b) Petrology of the Island of Moheli, western Indian Ocean. *Geol. Soc. Am. Bull.* **83**: 389-406.

Strong, D.F. (1974) Volcanic couples and deep mantle plumes. *Nature* **247**, 191-3.

Strong, D.F. & Flower, M.F.J. (1969) The significance of sandstone inclusions in lavas of the Comores archipelago. *Earth Planet. Sci. Lett.* **7**: 47-50.

Sun, S-S. & McDonough, W.F. (1989) Chemical and isotopic systematics of oceanic basalts: implications for mantle composition and processes. In: Saunders, A.D. & Norry, M.J. eds., *Magmatism in the Ocean Basins*. Geol. Soc. Sp. Pub. No. 42: 313-45. Blackwell.

Sutherland, F.L. (1989) Tasmania and Bass Strait. In: Johnson, R.W. ed., *Intraplate Volcanism in Eastern Australia and New Zealand*: 143-9. Cambridge University Press.

Sutherland, F.L., Hollis, J.D. & Robertson, A.D. (1989) Central Queensland: Springsure. In: Johnson, R.W. ed., *Intraplate Volcanism in Eastern Australia and New Zealand*: 103. Cambridge University Press.

Taylor, S.R. & McClennan, S.M. (1985) *The continental crust: its composition and evolution.* Blackwell, London. 312pp.

Theisen, R. & Vollach, D. (1967) *Tables of X-ray mass absorption coefficients.* Verlag Stahleisen MBH, Dusseldorf.

Thibault, Y., Edgar, A.D. & Lloyd, F.E. (1992) Experimental investigation of melts from carbonated phlogopite lherzolite: implications for metasomatism in the continental lithospheric mantle. *Am. Mineral.* **77**: 784-94.

Thompson, R.N. (1985) Asthenospheric source of Ugandan ultrapotassic magma. *J. Geol.* **93**: 603-8.

Tilley, C.E. & Yoder, H.S. (1964) Pyroxene fractionation in mafic magma at high pressure and its bearing on basalt genesis. *Carn. Inst. Wash. Yrbk.* **63**: 114-21.

Treiman, A.H. & Schedl, A. (1983) Properties of carbonatite magma and processes in carbonatite magma chambers. *J. Geol.* **91**: 437-47.

Turner, G., Burgess, R. & Bannon, M. (1990) Volatile-rich mantle fluids inferred from inclusions in diamond and mantle xenoliths. *Nature* **344**: 653-5.

Twyman, J.D. & Gittins, J. (1987) Alkalic carbonatite magmas: parental or derivative? In: Fitton, J.G. & Upton, B.G.J. eds., *Alkaline Igneous Rocks*. Geol. Soc. Sp. Pub. No. 30: 85-94. Blackwell.

Upton, B.G.J. (1982) Oceanic Islands. In: Nairn, A.E.M. & Stehli, F.G. eds., *The Ocean Basins and Margins Vol. 6: Indian Ocean*: 585-648. Plenum.

Upton, B.G.J. (1988) History of tertiary igneous activity in the N Atlantic borderlands. In: Morton, A.C. & Parsons, L.M. eds., *Early Tertiary Volcanism and the Opening of the NE Atlantic*. Geol Soc. Sp. Pub. 39: 429-53. Blackwell.

Upton, B.G.J., Mitchell, R.H., Long, A. & Aspen, P. (1992) Primitive olivine melanephelinite dykes from the Orkney Islands, Scotland. *Geol. Mag.* **129(3)**: 319-24.

Varne, R. (1965) *The Geology of Moroto Mountain, Karamoja, North-Eastern Uganda.* Unpub. PhD Thesis, University of Leeds.

Vollmer, R. & Norry, M.J. (1983) Possible origin of K-rich volcanic rocks from Virunga, East Africa, by metasomatism of continental crustal material: Pb, Nd, and Sr isotopic evidence. *Earth Planet. Sci. Lett.* **64**: 374-86.

Wallace, D.A., Johnson, R.W., Chappel, B.W., Arculus, R.J., Perfit, M.R. & Crick, I.H. (1983) Cainozoic volcanism of the Tabar, Lihir, Tanga and Feni Islands, Papua New Guinea: geology, whole-rock analyses, and rock-forming mineral compositions. *Bur. Min. Res., Geol. & Geophys. Rep.* **243**.

Wallace, M.E. & Green, D.H. (1988) An experimental determination of primary carbonatite magma composition. *Nature* **335**: 343-5.

Walsh, J. & Dodson, R.G. (1969) Geology of Northern Turkana. *Kenya Geol. Surv. Rep. No.* **82**, 42pp.

Wass. S.Y. & Rogers, N.W. (1980) Mantle metasomatism: precursor to continental alkaline volcanism. *Geochem. Cosmochem. Acta* **44**: 1811-23.

Watson, S. (1993) Rare earth element inversions and percolation models for Hawaii. *J. Pet.* **34**: 763-84.

Watson, S. & McKenzie, D. (1991) Melt generation by plumes: a study of Hawaiian volcanism. *J. Pet.* **32**: 501-37.

Weaver, B.L. (1991) The origin of ocean island basalt end-member compositions: trace element and isotopic constraints. *Earth Planet. Sci. Lett.* **104**: 381-97.

Wedepohl, K.H. (1985) Origin of the Tertiary basaltic volcanism in the northern Hessian depression. *Contrib. Min. Pet.* **89**: 122-43.

Wendlandt, R.F. & Eggler, D.H. (1980a) The origins of potassic magmas. 1, Melting relations in the system $KAlSiO_4$-Mg_2SiO_4-SiO_2 and $KAlSiO_4$-MgO-SiO_2-H_2O-CO_2 to 30 kilobars. *Am. J. Sci.* **280**: 385-420.

Wendlant, R.F. & Eggler, D.H. (1980b) The origins of potassic magmas. 2, Stability of phlogopite in natural spinel lherzolite and in the system $KAlSiO_4$-MgO-SiO_2-H_2O-CO_2 at high pressures and temperatures. *Am. J. Sci.* **280**: 421-58.

White, W.M. (1985) Sources of oceanic basalts: radiogenic isotope evidence. *Geology* **13**: 115-18.

Whitford-Stark, J.L. (1983) Cenozoic volcanic and petrochemical provinces of mainland Asia. *J. Volcanol. Geotherm. Res.* **19**: 193-222.

Wilkinson, J.F.G. & Le Maitre, R.W. (1987) Upper mantle amphiboles and micas and TiO_2, K_2O and P_2O_5 abundances and $100Mg/(Mg+Fe^{2+})$ ratios of common basalts and andesites: implications for modal mantle metasomatism and undepleted mantle compositions. *J. Pet.* **28**: 37-73.

Williams, H. (1936) Pliocene volcanoes of the Navajo-Hopi country. *Bull. Geol. Soc. Am.* **47**: 111-71.

Wilshire, H.G. (1987) A model of mantle metasomatism. *Geol. Soc. Am. Sp. Pub.* **215**: 47-60.

Wilson, M. & Downes, H. (1991) Tertiary-Quaternary extension-related alkaline magmatism in Western and Central Europe. *J. Pet.* **32**: 811-50.

Wimmenauer, W. (1974) The alkaline province of Central Europe and France. In: Sørensen, H. ed., *The Alkaline Rocks*: 238-70. Wiley.

Wood, B.G.M. (1985) The mechanics of progressive deformation in crustal plates - a working model for Southeast Asia. *Geol. Soc. Malaysia Bull.* **18**: 55-99.

Wood, B.H. & Hay, R.F. (1970) Geology of the Cook Islands. *New Zealand Geol. Surv. Bull.* **82**.

Wood, C.P. (1968) *A geochemical study of E African alkaline lavas and its relevance to the petrogenesis of nephelinites*. Unpub. PhD Thesis, University of Leeds.

Wood, C.P. (1978) Petrology of Aitutaki, Cook Islands. *New Zealand J. Geol. Geophys.* **21**: 761-5.

Woolley, A.R. (1987) *Alkaline Rocks and Carbonatites of the World. Part 1: North and South America*. British Museum (Natural History) London. 216pp.

Woolley, A.R. (1989) The spatial and temporal distribution of carbonatites. In: Bell, K. ed., *Carbonatites: Genesis and Evolution*: 15-37. Unwin-Hyman.

Woolley, A.R. & Garson, M.S. (1970) Petrochemical and tectonic relationship of the Malawi carbonatite-alkaline province and the Lupata-Lebombo volcanics. In: Clifford, T.N. & Gass, I.G. eds., *African Magmatism and Tectonics*: 237-62. Oliver & Boyd, Edinburgh.

Woolley, A.R. & Jones, G.C. (1987) The petrochemistry of the northern part of the Chilwa alkaline province, Malawi. In: Fitton, J.G. & Upton, B.G.J. eds., *Alkaline Igneous Rocks*. Geol. Soc. Sp. Pub. No. 30: 335-56. Blackwell.

Worner, G., Zindler, A., Staudigel, H. & Schmincke, H-U. (1986) Sr, Nd, and Pb isotope geochemistry of Tertiary and Quaternary alkaline volcanics from West Germany. *Earth Planet. Sci. Lett.* **79**: 107-19.

Wright, T.L. (1984) Origin of Hawaiian tholeiite: a metasomatic model. *J. Geophys. Res.* **89**: 3233-52.

Wright, E. & White, W.M. (1987) The origin of Samoa: new evidence from Sr, Nd, and Pb isotopes. *Earth Planet. Sci. Lett.* **81**: 151-62.

Wyllie, P.J. (1987) Discussion of recent papers on carbonated peridotite, bearing on mantle metasomatism and magmatism. *Earth Planet. Sci. Lett.* **82**: 391-7.

Wyllie, P.J. (1989) Origin of carbonatites: evidence from phase equilibria studies. In: Bell, K. ed., *Carbonatites: Genesis and Evolution*: 500-45. Unwin-Hyman.

Wyllie, P.J. & Huang, W.L. (1975) Influence of mantle CO_2 in the generation of carbonatites and kimberlites. *Nature* **257**: 297-99.

Wyllie, P.J. & Rutter, M. (1986) Experimental data on the solidus for peridotite-CO_2 with applications to alkaline magmatism and mantle metasomatism. *EOS* **67**: 390.

Yoder, H.S.Jr. & Tilley, C.E. (1962) Origin of basalt magmas: an experimental study of natural and synthetic systems. *J. Pet.* **3**: 343-532.

Ziegler, P.A. (1982) *Geological Atlas of Western and Central Europe*. Elsevier, Amsterdam. 130pp.

Zindler, A. & Hart, S. (1986) Chemical Geodynamics. *Ann. Rev. Earth Planet. Sci.* **14**: 493-571.

Zindler, A. & Jagoutz, E. (1988) Mantle cryptology. *Geochem. Cosmochem. Acta* **52**: 319-33.

Zindler, A., Jagoutz, E. & Goldstein, S. (1982) Nd, Sr and Pb isotopic systematics in a three-component mantle: a new perspective. *Nature* **298**: 519-23.

Appendix A

Distribution of Feldspar-Free Volcanic Rocks

A.1 Introduction

The following information refers to the samples analysed in the course of this study or to the location of samples for which recently-published data are used for comparative purposes. The details presented include location, tectonic environment, age, and the associated volcanic products. The sources of the samples are given in Appendix F.

A.2 Atlantic Ocean Islands

Feldspar-free volcanic rocks occur on Trinidade, Fernando de Noronha, Principe, the Cape Verde Islands and the Canary Islands.

A.2.1 Trinidade

Close to latitude 20°S, a chain of submarine mountains and guyots extends more than 1140 km eastwards from the coast of Brazil into the South Atlantic following the line of a major fracture zone in the oceanic crust. At the eastern end, some 2130 km west of the mid-Atlantic ridge, the eroded summits of two Pliocene to Recent volcanoes are exposed and form Trinidade Island and Martin Vaz rocks (48 km east of Trinidade). These represent the youngest volcanism along the chain. The Trinidade volcano rises about 5500 m from the sea floor and the island itself reaches 600 m above sea level (Mitchell-Thomé, 1970; Baker, 1973).

Five volcanic formations have been recognised on Trinidade (Almeida, 1961) which range in age from 3.6 Ma to <0.2 Ma. The two oldest formations are characterised by nephelinitic and phonolitic pyroclastics, flows, and high-level intrusions, while ankaratrite (biotite olivine melanephelinite) and tannbuschite (olivine melanephelinite) pyroclastic deposits and lava flows dominate the three youngest formations. Nephelinite (often containing leucite) and phonolite are the most abundant rock types found, and these are more silica-undersaturated, more alkaline, and more sodic than other ocean island volcanism in the Atlantic (Almeida, 1961). The only known rocks to have been collected from Martin Vaz are ankaratrite, similar to those found on Trinidade, and a haüyne-rich nephelinite (Mitchell-Thomé, 1970).

A.2.2 Fernando de Noronha

The Fernando de Noronha archipelago is a cluster of small islands of Cenozoic age, aligned NE-SW, 3° 50′ south of the equator, 345 km from the coast of Brazil and 830 km from the mid-Atlantic ridge. The volcanic structure rises 4300 m from the sea floor and the island reaches 320 m above sea level (Baker, 1973).

Three volcanic episodes have been identified (Almeida, 1958) which span the period 11.8 Ma to 1.7 Ma. The Remedios Formation is the basal relic of an old volcanic structure and consists of alkaline pyroclastic rocks cut by strongly alkaline intrusions (dykes, plugs and domes). The younger Quixaba Formation (3.2 to 1.7 Ma), consists of basal pyroclastics and flows of ankaratrite, melilite ankaratrite, olivine melanephelinite and, more rarely, alkali basalt, erupted onto the eroded remnants of the Remedios Formation. It is exposed over some two-thirds of Fernando de Noronha island. The São José Formation is a single flow of olivine nephelinite/basanite containing peridotite xenoliths. It is exposed off the north-west coast of Fernando de Noronha island and appears to be similar in age to the rocks of the Remedios Formation (Mitchell-Thomé, 1970). Samples from the Quixaba Formation are used in this study (Gerlach *et al.*, 1988).

A range of sea mounts extends westwards from Fernando de Noronha across the continental shelf towards the Brazilian coast. Volcanic rocks of similar types are found along this structure. As in the case of Trinidade, the islands represent the youngest volcanism along a volcanic chain which follows the line of a major fracture zone in the oceanic crust. The Fernando de Noronha rocks are less strongly alkaline than the rocks found on Trinidade and more similar in petrology and chemical composition to those from the Gulf of Guinea islands.

A.2.3 Principe and Etinde(Cameroon line)

The Gulf of Guinea islands, Bioko (formerly Fernando Poo), Principe, São Tomé and Pagalu (formerly Annobon), form the oceanic sector of the Cameroon line of volcanoes which extends 1600 km south-westwards from the Cameroon Highlands into the South Atlantic. Bioko and Pagalu are composed almost entirely of alkaline basaltic lavas which include picritic basalt, ankaramite and, occasionally, basanite. These are overlain on Pagalu by a small group of trachytic rocks. On Principe and São Tomé more undersaturated rocks (limburgite and basanite) are found. There is no apparent age progression along the Cameroon line or along the oceanic sector of the chain.

Principe lies 1° 40' north of the equator, 2700 km east of the mid-Atlantic ridge, and rises some 4000 m from the sea floor. The island reaches 948 m above sea level (Baker, 1973). The volcanism ranges from Miocene to Recent in age. An older series of transitional basalt lavas (24 to 19 Ma) is overlain by a younger series of basanitic flows (5.6 to 3.5 Ma) which include an isolated olivine melanephelinite lava flow which is used in this study (Fitton & Hughes, 1977; Dunlop & Fitton, 1979). The younger series is overlain by phonolitic lavas in the northern part of the island.

Etinde is a Quaternary (<1 Ma) nephelinite volcano, 1713 m high, which rises from the south-west flanks of Mt Cameroon on the coast of the Republic of Cameroon. The lavas vary from olivine melanephelinite to leucite nephelinite (Fitton & Hughes, 1981; Fitton, 1987; Nkoumbou *et al.*, 1995) and are the only feldspar-free volcanic rocks known in the continental sector of the Cameroon line.

A.2.4 Cape Verde Islands

The Cape Verde Islands lie between latitudes 15° and 17°N, about 500 km from the west coast of Africa and 1500 km east of the mid-Atlantic ridge (Baker, 1973). The ten main islands of the group are underlain by thickened oceanic crust, Jurassic to Cretaceous in age (Hayes & Rabinowitz, 1975). Following the intrusion of nepheline syenite and carbonatite ring complexes, the structure was uplifted by tectonic disturbances lasting from the middle Cretaceous until upper Miocene times and now forms a topographic anomaly 1000 km in diameter and rising up to 2 km above the adjacent ocean floor.

The islands appear to have been volcanically active since the early Tertiary (Dillon & Sougy, 1974). The alkaline volcanic rocks now exposed were erupted onto the eroded intrusive complex and range in age from Miocene (>20 Ma) to Recent, becoming younger to the south-west. Fogo and Brava are the only historically active centres in the island group. The island of Fogo was last active in 1951. It rises 6000 m from the sea floor and the summit is 2830 m above sea level (Baker, 1973).

Volcanic products on the islands are either basaltic or phonolitic in composition. The basaltic rocks grade, with increasing silica-undersaturation, from alkali basalt through basanite into nephelinite, olivine melanephelinite and strongly undersaturated melilitite. Nephelinitic flows and dykes have been reported on most of the islands of the Cape Verdes archipelago. The samples used in this study are from the highly undersaturated Malhadra Pedra Formation on Maio (Gerlach *et al.*, 1987; Davies *et al.*, 1989) which are Miocene (6.8 to 6.9 Ma) in age.

A.2.5 Canary Islands

The Canary Islands are a 600 km-long chain of seven volcanic islands which lie off the southern coast of Morocco between latitudes 28° and 29°N. The islands to the east are older (80 to 30 Ma) than those in the west (4 to 2 Ma) but all have remained active until Recent times. Hoernle & Schmincke (1993a; 1993b) have suggested that the volcanism is a consequence of a plume impinging on the base of a relatively thick part of the slow-moving oceanic plate.

The visible part of the Canary Islands consists of Miocene and Pliocene basaltic lavas overlying a basal sequence of plutonic rocks, representing oceanic upper mantle and lower crustal rocks, with associated submarine lavas (Schmincke, 1973). Carbonatite intrusions, similar to those found on the Cape Verde Islands, probably exist in the Canary Islands but carbonatite is only exposed on Fuerteventura (Le Bas *et al.*, 1986). Tectonic uplift began here, as in the Cape Verdes, in the middle Cretaceous (Dillon & Sougy, 1974). Volcanism was re-established in the middle Miocene and large composite shield volcanoes, composed of alkali olivine basalt and its differentiated products, were built on the eroded basal complex.

A second burst of volcanic activity began in the Pleistocene after a period of quiescence and eruptions have occurred intermittently during the past three centuries. Volcanic products on the eastern islands (Lanzarote and Fuerteventura) have been less

alkaline than those on Gran Canaria, Tenerife and La Gomera, in the central part of the chain (Schmincke, 1982). Nephelinite and melilite nephelinite dominate the Llanos de Pez Formation (3.2 to 1.8 Ma) and the early Quaternary eruptions (1.8 to 1 Ma) on Gran Canaria. Recent volcanic rocks are less undersaturated.

A.3 Indian Ocean Islands

Nephelinite and olivine melanephelinite lavas occur in the Comores archipelago on the islands of Gran Comoro, Moheli and Mayotte (Nougier *et al.*, 1986) which lie between latitudes 10° and 13°S and form a NW-SE trending chain, 275 km long, across the northern end of the Mozambique Channel. The apparent decrease in age of the volcanism from SE to NW has been interpreted as due to the movement of the lithosphere in a direction ESE over a mantle plume which currently lies beneath Gran Comoro (Flower, 1972; Emerick & Duncan, 1982; 1983) and, alternatively, as the result of a very slowly spreading axis, along the line of the Comoro ridge, which is transected by transform fractures (Upton, 1982). This model is similar to that proposed by Gass *et al.* (1973), for the islands at the southern end of the Red Sea. The Comores Islands will be considered here along with related undersaturated volcanism occurring on Madagascar itself.

A.3.1 Gran Comoro (Njazidja)

Gran Comoro is the westernmost and youngest (Pliocene to Recent) of the Comores Islands and consists of two coalescing shield volcanoes: La Grille (rising 1087 m above sea level) to the north and Kartala (reaching 2361 m) to the south. Both volcanoes are clearly associated with major fissure zones (Upton, 1982).

Kartala has erupted only basaltic lavas and has been more productive than La Grille, erupting at least fourteen times since 1857. Unlike Kartala, La Grille has no clearly defined summit crater and is covered in small cinder cones aligned along fissures. The lavas are undersaturated basanite and olivine melanephelinite (Strong, 1972a; Flower, 1973) and are probably associated with a post-erosional rejuvenation phase. The volcanic products from the two volcanoes have very different incompatible trace-element patterns and must therefore represent different degrees of partial melting of chemically distinct mantle sources (Strong, 1972a). Despite the proximity of the centres, the plumbing systems of the two volcanoes appear to have remained separate (Strong, 1974).

A.3.2 Moheli

Moheli lies 40 km to the south-east of Gran Comoro and rises to 790 m above sea level (Upton, 1982). The island is an eroded shield volcano of Pliocene to Pleistocene age (Emerick & Duncan, 1983) which is thought to be composed of two series of undersaturated lavas: an older series exposed in the east and a younger series forming the more mountainous area in the west. A still younger phase of activity produced small flows in the west and north and cinder cones, aligned with fissures, along the length of the island

(Strong, 1972b). The lavas range from alkali olivine basalt through basanite to olivine melanephelinite, and the more evolved derivatives of these rock types.

A.3.3 Malagasy (formerly Madgascar)

Late Miocene to Recent lavas (Emerick & Duncan, 1983) belonging to the same petrographic province as the Comores Islands are found at Mont Ambre and Isle Nose-Be at the northern end of Madgascar and also in the central Ankaratra Mountains (Nougier *et al.*, 1986). These lavas represent a minor phase of volcanism which produced alkali basalt, limburgite, basanite and nephelinite in small-scale fissure eruptions. The Ankaratra Mountains are the type locality of ankaratrite, an olivine melanephelinite containing biotite and sometimes melilite. Samples from the Ankaratra volcano are included in this study.

A.4 Pacific Ocean Islands

Feldspar-free volcanic rocks represent a post-erosional rejuvenation episode on Kauai and Oahu in the Hawaiian chain (central Pacific), on Truk, Ponape and Kusaie in the Caroline Islands (western Pacific), on Aitutaki in the Cook Islands archipelago and Upolo in the Samoan group (both in the south Pacific).

A.4.1 Aitutaki (Cook Islands)

Aitutaki is situated in the southern group of the Cook Islands archipelago at 18° 50'S and 159° 50'W. The island originated in the Eocene/Oligocene as one of fourteen submarine volcanoes (Fodor *et al.*, 1982). The first stage of volcanic activity occurred at about 8 Ma with a second stage between 1.9 and 0.7 Ma (Nakamura & Tatsumoto, 1988). The island is composed mainly of olivine melanephelinite flows and pyroclastic material (Wood & Hay, 1970; Wood, 1978) which are about 0.7 m.y. old (Dalrymple *et al.*, 1975). The sub-aerial undersaturated volcanism represents a post-erosional phase of activity similar to that found on other islands in the Pacific Ocean.

A.4.2 Upolo (Samoan Islands)

The eastern islands (Upolo and Tutuila) of the Samoan group are more deeply eroded and incised than the western islands and consist of lavas which date from the late Pliocene. The apparently younger age of the islands in the west may be due to the long period of quiescence which has followed the shield building stage and voluminous post-erosional activity which gives the western islands a youthful appearance. Shield-building volcanism gets younger to the east (Natland, 1980).

The Recent volcanism on Upolo consists of alkali olivine basalt, basanite, and olivine melanephelinite which represent a substantial portion of the total volcanic products (Wright & White, 1987). Natland (1980) considers the near-simultaneous eruption of post-erosional lavas along 1500 km of the Samoan Island chain in Pleistocene to historic times to be a result of lateral bending of the Pacific plate at the point where the axis of the

Tonga-Kermadec trench swings from an orientation almost due north-south to a line trending 70° west of north. Upolo currently lies at the point where lateral bending becomes significant while the islands further west are moving along the line of the flexure as subduction of the Pacific plate beneath the Australian plate continues.

A.4.3 Truk, Ponape and Kusaie (Caroline Islands)

The Caroline Islands and the associated Caroline ridge extend eastwards from the Mariana trench into the western Pacific. The eastern Caroline Islands lie between 7° - 9 °N and 151° - 163°E on ocean floor of Jurassic age. Most of the islands in the chain are atolls but Truk (12 to 8 Ma), Ponape (8 to 4 Ma) and Kusaie (2 to 1 Ma) are volcanic islands consisting of eroded alkali basalt shield volcanoes which are younger than the atolls in the same group (Mattey, 1982). All three islands have olivine melanephelinite flows from the post-erosional episode of volcanism which post-dated the shield-building phase by up to 6 m.y.

A.4.4 Kauaii and Oahu (Hawaiian Islands)

The feldspar-free volcanic rocks on these islands represent the final stage of evolution of the volcanic structures and were erupted after a considerable period of quiescence and erosion of the associated shield volcanoes.

Oahu lies 210 km north-west of the currently active island of Hawaii. The island consists of two tholeiitic shield volcanoes, Waianae and Koolau, which were active in the Tertiary (Roden *et al.*, 1984). The subaerial eruptions of the Koolau shield have been dated, by Lanphere & Dalrymple (1980), at 2.7 to 1.8 Ma. Quaternary (0.6 to 0.3 Ma) highly undersaturated volcanism forms the Honolulu volcanic series, the remnants of which are found over the eastern half of the island. The melanephelinite and melilite nephelinite flows and pyroclastic deposits are associated with thirty-seven small vents on the flanks and in the caldera of the eroded Koolau shield (Clague & Frey, 1982).

Kauai lies some 200 km north west of Oahu and is the northernmost of the major islands in the Hawaiian chain. The island consists of a typical Hawaiian shield volcano of Tertiary age (ca. 5.6 to 3.9 Ma). The post-erosional volcanic episode reached a peak of activity at about 1.2 Ma after a period of quiescence lasting 0.27 m.y. The rocks of this phase form the Koloa volcanic series (Maaløe *et al.*, 1992). While similar to the Honolulu series the rocks are, in general, less undersaturated than their equivalents on Oahu. Olivine melanephelinite and, more rarely, melilite nephelinite flows are associated with about forty cinder and tuff cones distributed, as in Oahu, over the eastern half of the island. The cones, however, are smaller than the vents on Oahu.

A.4.5 Ambitle (Feni Islands)

The Tabar, Lihir, Tanga and Feni groups of islands in the south-west Pacific form a 260 km-long chain roughly parallel to the coast of the Tertiary island arc system of New Ireland and about 50 km to the north-east (Wallace *et al.*, 1983). The islands are not

associated directly with any island arc system or mantle plume trace, and the tectonic setting of the islands is still uncertain. Volcanism may be a consequence of major faulting due to isostatic readjustments between normal oceanic crust to the north-east and thickened oceanic crust in the Bismarck Sea and New Ireland region to the south-west. Evidence of sea-level changes in the reefs around the islands support this hypothesis (Johnson *et al.*, 1976).

The volcanic rocks are Pliocene to Pleistocene in age but there is no evidence of an age progression along the chain. A wide range of rock types is present (strongly alkaline nephelinite and basanite, transitional basalt, tephrite, phonolite and quartz trachyte), and potassic compositions ($K_2O/Na_2O > 0.5$) are more common than sodic varieties on all the island groups. Strongly undersaturated rocks occur in the Tanga and Feni groups but the only feldspar-free rocks known are from Ambitle in the Feni group (Johnson *et al.*, 1976).

A.4.6 Nagahama (Japan)

Alkaline rocks of Quaternary age occur in a small province situated on the north-eastern coast of the Sea of Japan and extending from south-western Honshu and northern Kyushu into North Korea and Manchuria (Nakamura *et al.*, 1985). The province also includes the islands of Oki and Iki in the Sea of Japan off the northern coast of Honshu (Kuno, 1959). The volume of alkaline rocks is small but it includes isolated occurrences of olivine melanephelinite and melilite nephelinite at Nagahama, south-west Honshu (Minato *et al.*, 1965). Alkaline volcanism in the circum-Japan Sea belt may be related to the formation of the Japan Sea behind the active trench-arc system which began at the end of the Palaeogene (Minato *et al.*, 1965).

A.5 Australasia

A number of examples of nephelinite volcanism associated with basalts and allied extrusive rocks of Mesozoic to Holocene age occur along the east coast of Australia from the Torres Strait to Tasmania, a total distance of some 4400 km. Volcanic rocks of a similar age and composition are also found in New Zealand on both islands. New Zealand straddles the tectonically active boundary between the Pacific plate and the Indo-Australian plate. Widespread Cenozoic volcanism is found on the South Island, and is almost entirely on the Pacific plate. Nephelinite is rare but occurs in the Otago province.

A.5.1 Eastern Australia

Nephelinite and melilite nephelinite are reported as flows and plugs in many localities in Queensland, New South Wales, Victoria and, particularly, in Tasmania. These are generally Cenozoic (<35 Ma) in age. Two samples included in this study are from Mt Sterculia in the Springsure district of central Queensland. Mt Sterculia is a massive nephelinite peak 26 m.y. old (Sutherland *et al.*, 1989). Eight samples are from north and central Tasmania and are 35 to 25 m.y. old (Sutherland, 1989).

The eastern Australian leucitite suite (16 to 6 Ma) forms a 90 km-wide strip extending 640 km south from Byrock in New South Wales to Cosgrove in Victoria, with most of the total outcrop being around Bygalorie, Tullibigeal and Lake Cargelligo (Cundari, 1973). The potassic suite lies about 200 km inland from the Cenozoic alkaline rocks of the eastern Australian highlands and appears to be younger at the southern end (Cundari, 1989). Samples from olivine leucitite flows at Byrock and Lake Cargelligo have been analysed in the course of this study.

A.5.2 New Zealand

The late Tertiary rocks of the east and central Otago province on the south island of New Zealand are termed the Dunedin Volcanic Group (Coombs *et al.,* 1986). The Dunedin volcano is a major subaerial basanitic shield volcano constructed from 13 to 10 m.y. ago (Coombs & Wilkinson, 1969). Rocks of the Dunedin group include melanephelinite, basanite, alkali basalt, and evolved derivatives of these types, and they can be found up to 95 km from the Dunedin volcano. Two samples of olivine nephelinite from the Middlemarch area, 50 km north west of Dunedin, have been analysed. These rocks were erupted from peripheral vents which appear to have been short-lived monogenetic centres. The nephelinite is similar in composition to the Pliocene lava found at the summit of Siberia Hill in the Kakanui Mountains to the north.

A.6 South-East Asia

Upper Cenozoic alkaline volcanic rocks form an extensive igneous province in Thailand, Kampuchea, Laos, Vietnam and Malaysia (Barr & MacDonald, 1981) where they have been erupted in an area of uplift and complex transcurrent faulting and extensional tectonics (Wood, 1985; Whitford-Stark, 1983).

A.6.1 Thailand

Olivine melanephelinite occurs in minor amounts in several localities in the Chantaburi-Trat area of south-eastern Thailand, at approximately 12°-13°N and 102°-103° E. The five samples included here are from Chantaburi close to the border with Kampuchea (Barr & James, 1990).

A.7 North America

Nephelinitic rocks are found in the Cretaceous Balcones igneous province in Texas, and in the Raton-Clayton volcanic field in New Mexico which is part of the extensive late Cenozoic igneous province in the south-western United States (Fitton *et al.,* 1988; 1991). Isolated occurrences of feldpar-free volcanic rocks are also found on the Colorado Plateau in Arizona.

A.7.1 Balcones Igneous Province, Texas

The Balcones province forms a narrow elongate area some 300 km long from east of Austin to west of Uvalde in Texas, approximately 28°-31°N and 99°-100°W. The province is roughly co-linear with the buried Ouachita structural belt and slightly north of the SW-NE trending Balcones fault zone. Igneous activity in the form of shallow intrusions and minor submarine volcanism took place at 86 to 63 Ma in the upper Cretaceous, some 150 million years after the deformation in the Ouachita belt and approximately 60 million years before the movement on the Balcones faults. About half of the exposed rocks are melilite olivine nephelinite and a third olivine melanephelinite, with minor amounts of phonolite, basanite, and basalt (Spencer, 1969). The six nephelinitic samples analyzed are from Uvalde county, Texas.

A.7.2 Raton-Clayton Volcanic Field, New Mexico

The Raton-Clayton volcanic field covers about 2000 km^2 in north-eastern New Mexico (approximately 36°-37°N and 103°-104°W) and extends over the state line into Colorado (Stormer, 1972). The age of the igneous rocks ranges from Pliocene to Recent (<2500 yrs). Phonolitic sills of Miocene age are exposed in the south-west of the region and these are overlain unconformably by younger basaltic flows. Feldspathoidal rocks (basanite, olivine melanephelinite and melilite olivine nephelinite) occur as flows, plugs, and dykes, and are younger than the basaltic lavas (Phelps *et al.*, 1983). Eleven samples collected in this region have been included in this study.

A.7.3 Colorado Plateau (Arizona part)

The Navajo field (approximately 35° - 37°N, 100° - 111°W) consists mainly of dykes and volcanic necks which are thought to be related to the uplift of the Colorado Plateau (Laughlin *et al.*, 1986) and to have been emplaced between 34 and 19 Ma, with a peak of activity around 25 Ma (Roden *et al.*, 1979).

The Hopi Buttes (about 35° N and 110° W) are often considered to be part of the same igneous province but the rocks are sodic in composition and were mostly erupted in the Pliocene (ca. 5 Ma). Four samples from the Hopi Buttes have been analyzed. Shoemaker *et al.* (1962) estimate that about three hundred diatremes were emplaced in a small area 50 km by 55 km. Volcanism was explosive and pyroclastic deposits and lava flows appear to have been erupted into shallow fresh water. Volcanic necks, dykes and the remnants of lava flows now capping mesas, yield feldspar-free monchiquitic rocks which are petrographically similar to each other and contain abundant analcime (Williams, 1936).

Isolated occurrences of monchiquite grading into olivine leucitite are known but these are unrelated to either of the above provinces. Two samples from monchiquite dykes bearing melilite and nepheline are included in this study. These are from Wildcat Peak (ca. 20 Ma) and Woodruff Butte (ca. 8 Ma).

A.8 The North Atlantic Borderlands

The early Tertiary to Recent volcanism of eastern Greenland (Upton, 1988) and Bathurst Island, in the North West Territories of Canada (Mitchell & Platt, 1983; 1984), is considered to be associated with the opening of the North Atlantic.

A.8.1 Greenland

Highly undersaturated alkaline rocks have been reported from dykes and sheets in the Gardiner ultramafic complex, at the western end of the Kangerdlugssuaq fjord in central east Greenland (about 68°N and 34°W), and in the Tugtilik coastal dyke swarm 220 km to the south (around 66°N, 35°W). Nephelinite flows cap nunataks to the north in Arnold Eschers Land and Hobbs Land (73°-74°N, 28°-29°W). These rocks range in age from 58 to 44 Ma (Brooks *et al.*, 1979) and were contemporaneous with the volcanic activity in the Gardiner complex (50.3 Ma; Brooks & Nielsen, 1982) but are a little older than the Tugtilik dyke swarm (44 to 19 Ma; Gleadow & Brooks, 1979).

A.8.2 Bathurst Island, North-West Territories, Canada

The Freeman's Cove area on Bathurst Island consists of five agglomerate-filled vents, about seventy-five dykes and small plugs, and a number of sills, within an area of some 800 km^2 at the south-east end of the island (Mitchell & Platt, 1984). The volcanism appears to be controlled by major north-east- and north-trending faults, and occurred at about 47 Ma. Olivine melanephelinite is the most abundant rock type and fifteen samples have been analyzed.

A.9 Europe

Feldspar-free volcanic rocks of the late Tertiary to Quaternary magmatic province in western and central Europe occur in the Massif Central (France), the Rhenish Massif (Germany), the Rhine graben (southern Germany), the Bohemian Massif (Czechoslovakia and Germany), and the Pannonian Basin (Austria and Hungary). The main phases of volcanic activity occurred in the Miocene and Pliocene. Pleistocene volcanic rocks are restricted to a few widely scattered locations.

A suite of monchiquitic (olivine melanephelinite) dykes in the Orkney Islands are Permian in age and are contemporaneous with the basaltic magmatism in south and central Scotland (Upton *et al.*, 1992). Although not part of the European magmatic province the Orkney rocks are included in this geographical section.

A.9.1 France

Most of the volcanism in the Massif Central is only mildly alkaline and highly undersaturated nephelinite is rare (Downes, 1987). Two samples of leucite melanephelinite from the Cantal volcano (11 to 2.5 Ma) are included in this study.

Isolated occurrences of melilite nephelinite and olivine melanephelinite of lower Miocene age are found as dykes and lavas at Marcoux and La Guillanche, near Montbrison in Les Monts du Forez to the east of the Massif Central (Hernandez, 1971). The Forez horst is bordered to the east and west by the Loire and d'Allier rifts respectively. Two samples from this district have been analysed.

A further isolated volcanic complex at Essey-la-Côte, 50 km north-west of Vosges, consists of three olivine melanephelinite plugs. An international standard, BE-N, is from this locality. The volcanism at Essey-la-Côte probably relates to alkaline volcanism associated with the Rhine rift system to the east.

A.9.2 Germany

Nephelinitic volcanism (66 Ma) associated with the Rhine graben is found on the eastern flanks of the rift at Katzenbuckel east of Heidelberg, at Spessart south of Frankfurt, and in the Miocene to lower Pliocene volcanic plugs of the Hegau district to the south-east of Freiburg and east of the Black Forest. Nephelinite is also associated with melilitite in the diatremes of the Urach volcanic area south of Stuttgart (Wimmenauer, 1974). In the Rhine graben itself, nephelinite, and limburgite of nephelinitic composition, occur as part of the Kaiserstuhl volcanic complex near Freiburg. A single melilitite outcrop is found nearby at Mahlberg on the eastern edge of the graben. The carbonatitic Kaiserstuhl complex is Miocene in age (7 to 14 Ma) and is the type locality of limburgite. Samples from all these localities have been analysed.

At the northern end of the Rhine graben more extensive volcanic activity occurred in the Eifel district and in the north Hessian depression. Volcanism in the Eifel district began in the Eocene and was associated with uplift of the Rhenish Massif. Volcanic activity later extended eastwards and westwards at the time of renewed uplift in the Pleistocene and continued until about 10000 years ago (Mertes & Schmincke, 1985). Leucite nephelinite and melilite nephelinite occur in both the East and West Eifel provinces (Mertes & Schmincke, 1985; Worner *et al.*, 1986). Magmatism is generally potassic although sodic varieties are also present. Olivine melanephelinite, leucitite and leucite nephelinite from the East Eifel have been analysed in the course of this study.

Volcanic activity in the North Hessian Depression began at around 20 Ma, reached a climax at 13 to 14 Ma, and finally ended at 7 Ma with the eruption of basanite and olivine melanephelinite (Wedepohl, 1985). Volcanic rocks occur as scattered necks and plugs in the graben north of the Vogelsberg volcano, and to the east in the Rhon area. Olivine melanephelinite from north of Kassel and the Rhon are included here.

A.9.3 Bohemian Massif, Czechoslovakia

The Bohemian massif occupies most of western Czechoslovakia but Tertiary volcanism is restricted to the northern area. Olivine melanephelinite, olivine leucitite and melilite nephelinite occur at many localities between Marktredwitz, in the Oberpfalz, and lower Silesia in Poland.

The two main volcanic areas are Doupovské Hory (Oligocene-Miocene) and Ceské Stredohorí (Böhmisches Mittelgebirge) which is a complex of flows, plugs and dykes of Oligocene to Pliocene age. Many smaller volcanoes are distributed some 40 km to the north and south of the main centres between Plzen and Dresden. Quaternary volcanic activity occurs near Cheb, in north-west Czechoslovakia on the border with Germany, and almost due east near Bruntal in northern Moravia, close to the border with Poland (Wimmenauer, 1974). Samples included in this study are from north-western Czechoslovakia and lower Saxony (Erzegebirge) close to the border between the former East Germany and Czechoslovakia.

A.9.4 The Pannonian Basin, Austria and Hungary

The Pannonian Basin extends from eastern Austria across the Hungarian Plains to western Romania. Alkaline volcanism occurred in the northern part of the basin during the Pliocene and closely followed subduction-related calc-alkaline volcanism, of Eocene to Pliocene age (Embey-Isztin *et al.*, 1993). The Pannonian Basin is bounded by the Alpine, Carpathian, and Dinaride orogenic belts, and has usually been interpreted as an inter-arc basin in which extension and subsidence have been active since the Palaeogene.

Feldspar-free volcanic rocks occur only at Stradner Kogel, in the Graz Basin, which lies on the west side of the Pannonian Basin in south-eastern Austria. The Stradner Kogel nephelinite flow is 1.9 million years old and extends over several tens of square kilometres (Embey-Isztin *et al.*, 1993).

A.9.5 Orkney Islands, North-East Scotland

Two suites of late Permian dykes are found in the Orkney Islands (Upton *et al.*, 1992). The north to north-east trending suite are olivine melanephelinite in composition and appear to be unique in the British Isles (Baxter, 1986). Three samples from mainland Orkney are included in this study.

A.10 Eastern Africa

Feldspar-free volcanic rocks (olivine melanephelinite, nephelinite and melilite nephelinite) occur on the margins of the East African rift in a province stretching from Turkana to northern Tanzania. The volcanic rocks of the western rift are highly potassic. Feldspar-free melilitite, melilite nephelinite, olivine melanephelinite, leucite nephelinite, and ankaratrite occur in the northern part of this branch of the rift but the volcanic rocks become less undersaturated further to the south. The oldest (Early Cretaceous) volcanic rocks associated with the East African rift system occur in Malawi and Mozambique where nephelinite dykes and plugs are associated with intrusive carbonatite complexes.

A.10.1 The Eastern Rift, Kenya and Tanzania

Volcanism appears to have begun in the eastern rift at about 30 Ma and was followed soon after (22 to 15 Ma) by explosive activity from the central-vent volcanoes on the Kenya-Uganda border (Baker *et al.*, 1971; King & Chapman, 1972). These Miocene-Pliocene volcanoes are aligned parallel to and on the western side of a half-graben which developed in northern Kenya at about 12 Ma (Baker, 1987). The volcanoes overlie a group of earlier (Oligocene-early Miocene) carbonatitic intrusive complexes (King *et al.*, 1972). Elgon, Napak and Kadam are dominated by olivine-poor melanephelinite associated with intrusive carbonatite, but further to the north, at Moroto, Toror and Yelele, both olivine-poor melanephelinite and olivine-rich melanephelinite are found without carbonatitic intrusive rocks. Kisingiri, Tinderet and Londiani lie in the E-W trending Kavirondo trough to the south and were also active in the Miocene-Pliocene. Kisingiri overlies an earlier carbonatitic intrusive complex and younger carbonatite complexes (Ruri Hills, 10 Ma; Homa Mt., 1 Ma) lie to the east. The Kisingiri lavas belong to the olivine-poor association while the Tinderet-Londiani complex has both associations (Le Bas, 1977). Samples from Elgon, Napak, Moroto, and Kisingiri have been analyzed in the course of this work.

Minor amounts of olivine melanephelinite, associated with extensive flood basalts and phonolites, occur as flows and dykes of Miocene age (ca. 30 Ma) in northern Turkana (Walsh & Dodson, 1969) and in the Samburu district of northern Kenya but these generally appear near the base of the volcanic sequence. Three samples from these localities have been included. Volcanism to the east of the northern end of the rift system post-dates full graben development which occurred at about 4 Ma. It is less strongly alkaline, and is often associated with widespread fissure eruptions and monogenetic cones. Olivine melanephelinite of Pliocene-Pleistocene age has been reported in the Aberdares and in the Nyambeni ranges (Baker, 1987).

A number of nephelinite occurrences are found on the shoulders of the Narok-Nguruman escarpment on the western side of the southern end of the Kenya rift system (Crossley, 1979). At Narok four olivine melanephelinite plugs of Pleistocene age are associated with extensive ash deposits. Further to the south, the Kishalduga lavas include olivine-poor melanephelinite and phonolite flows of Miocene age (Crossley & Knight, 1981). Samples from Narok and the Kishalduga sequence have been included in this study. West of Lake Magadi nephelinitic (micro-ijolite or ngurumanite) dykes intrude ankaratrite lavas of Pliocene age while Olorgesaile, a trachytic volcano capped with phonolitic nephelinite of the same age, is situated on the floor of the rift valley near the lake (Baker, 1987).

In northern Tanzania the rift system is less distinct and more splayed out. A major phase of Tertiary rifting gave rise to a broad depression and was followed by the eruption of considerable volumes of basaltic and trachytic magmas from large shield volcanoes. This volcanism was separated, by a second phase of faulting, from upper Pleistocene to Recent explosive activity which produced more limited quantities of nephelinite, phonolite and carbonatite (Dawson, 1989).

Olivine-poor melanephelinite associated with phonolite and intrusive carbonatite is characteristic of the Quaternary shield volcanoes in the western part of the province while the volcanoes further to the east are generally of mixed association having both olivine-poor and olivine-rich varieties. The nephelinitic Tanzanian volcanoes can be divided into two groups: an older group (ca. 8-2 Ma) which includes Shombole and Oldoinyo Sambu (north of Lake Natron), Mosonik (south of Lake Natron), Lemagrut, Elanairobi, Olmoti, Loolmalasin, Ngorongoro, Sadiman and Oldeani (crater highlands), Gelai, Kitumbeini, Tarosero and Essimingor (central zone), and the Shira and Mawenzi centres of Killimanjaro; and a younger group (<1.2 Ma) including Meru, Monduli and Burko (central zone), Oldoinyo Lengai and Kerimasi (south of Lake Natron), Kwaraha and Hanang (south of Lake Manyara), and the Kibo vent of Killimanjaro (Dawson, 1992), although Kibo and Tarosero were first active before the second phase of faulting. Nephelinite samples from Sadiman, Lemagrut, Burko and Hanang have been included in this study with a single olivine melilite melanephelinite from Oldoinyo Loolmurwak, one of many recent explosion craters and tuff cones in the Natron-Engaruka area (Dawson & Powell, 1969)

A.10.2 The Western Rift, Uganda and Zaire

The volcanic rocks of the western rift are strongly potassic. Three main volcanic areas have been identified, two of which are characterised by highly undersaturated rocks of Pliocene-Recent age. Samples from both areas have been analyzed.

The northernmost area, Toro-Ankole in western Uganda, consists of small tuff cones and craters scattered over an area some 50 km across north of Lake Edward. Lava flows are rare but a number of katungite flows (olivine melilitite devoid of pyroxene) emanate from the Katunga volcano in the south-east of the area. Two other volcanic fields in the area, Katwe-Kikorongo and Bunyaruguru north-west of Katunga, are noted for pyroclastic deposits containing ejected blocks of katungite, mafurite (olivine kalsilitite), ugandite (olivine melaleucitite), leucitite, and leucite ankaratrite and, more rarely, flows of the same composition. Carbonatite is not exposed but occurs as volcanic bombs in the pyroclastics at Katwe and in the Fort Portal area further to the north (Higazy, 1954; Bell & Powell, 1969).

The Virunga volcanic field lies about 100 km further south, to the north of Lake Kivu, and includes the Bufumbira area. It is composed of eight large central-vent volcanoes but is dominated by the currently active Nyiragongo and Nyamuragira volcanoes situated at the junction of the Kamatembe graben, the Albert rift, and the Bufumbira depression (Marcelot *et al.*, 1985). Volcanic activity is Pliocene to Recent in age and appears to get younger to the west. Nyamuragira is a leucite-basanite volcano (Aoki *et al.*, 1985) but Nyiragongo is composed of melilitite, leucitite and melilite nephelinite lavas (Vollmer & Norry, 1983). Volcanism in Virunga is generally less undersaturated and less explosive than in the Toro-Ankole area and volcanic products comprise mainly leucitite and ugandite flows. South of Lake Kivu the volcanism is of the basaltic association (King, 1970).

A.10.3 Chilwa Province, Malawi Rift

The Chilwa province in southern Malawi and northern Mozambique lies at the southern end of the East African rift system at the junction with the E-W trending Zambezi rift (Woolley & Garson, 1970). The province as a whole has a diameter of 300-400 km and is situated on a large domal area of uplift. Numerous carbonatite intrusive centres of lower Cretaceous age (135 to 105 Ma) are associated with olivine-poor melanephelinite dykes, cone sheets and plugs at Tundulu, Nathace Hill and Chilwa Island in the northern part of the province. Seven samples from the intrusions in this area have been analyzed. The Chilwa magmatism post-dated the final phases of the Karoo volcanic cycle by about 30 Ma but it is closely associated with uplift and rifting that may have been initiated during Karoo times (Woolley, 1987).

A.11 Southern Africa

Highly undersaturated volcanic rocks occur in two widely separated areas of southern Africa and in distinctly different associations at Nuanetsi, in south-eastern Zimbabwe, and in the Cape Province and Bushmanland-Namaqualand regions of South Africa.

A.11.1 Nuanetsi Province, Zimbabwe

The Nuanetsi Igneous Province is situated in the south-eastern corner of Zimbabwe (formerly Southern Rhodesia) at the intersection of the Limpopo lineament and a zone of intense Karoo and post-Karoo volcanicity (the volcanic monocline of the Lebombo) which can be traced from Natal in South Africa to the Zambezi River (Cox *et al.*, 1965).

Olivine-poor melanephelinite lavas (Mashikiri Formation) and dykes occur in the northern Lebombo and north-eastern Soutpansberg regions of South Africa, and the Sabi region of Zimbabwe, at the base of the Karoo volcanic succession. Four samples have been analyzed in the course of this study. Although volumetrically insignificant compared with the overlying picritic and tholeiitic sequences, geochronological data suggest that undersaturated volcanism was associated with the emplacement of carbonatite complexes in south-eastern Zimbabwe and north-eastern South Africa at the onset of the major eastern Karoo volcanic episode which was associated with the fragmentation of eastern and western Gondwanaland in the Jurassic at 206 to 166 Ma (Bristow, 1984).

A.11.2 Sutherland Commonage and Riversdale district, Cape Province

Olivine melilitite associated with kimberlite diatremes is found on Sutherland Commonage within the Orange River Belt adjacent to the Kapvaal craton (Boctor & Yoder, 1986). The melilitite has been dated at 75 Ma and is a little older than melilitite from the Spiegel River in the Riversdale district (63 Ma). The Riversdale locality lies

within the Cape Fold Belt to the south of Sutherland and the samples included in this study are from small (200 m diameter) isolated plugs. The five samples from Sutherland Commonage come from individual outcrops which may be part of a sill, a ring dyke, or single plugs (Dawson *et al.*, 1985).

A.11.3 Gamoep, Namaqualand-Bushmanland Province

The Bushmanland Plateau is situated south of the Orange River and approximately 100 km inland (Moore & Erlank, 1979). A large number of diatremes and plugs occur in a dense cluster around the village of Gamoep and represent the youngest (38.5 Ma) phase of volcanism in South Africa (Duncan *et al.*, 1978). The volcanic plugs form prominent round hills in the same area as older kimberlite pipes and include olivine melanephelinite and olivine melilitite. Ten samples from the vicinity of Gamoep have been analyzed.

A.12 Conclusion

In all, 174 samples of melanephelinite and melilitite from ocean islands have been analyzed in the course of this study together with 314 samples of olivine-rich and olivine-poor melanephelinite, melilitite, and the potassic equivalents of these types, from continental volcanic provinces.

In addition 904 samples covering the entire range of magmatic compositions found on oceanic islands and a number of continental suites which include highly undersaturated volcanic products have been analyzed for comparative purposes.

Appendix B

Analytical Techniques

B.1 Introduction

The feldspar-free volcanic rocks selected for this study numbered 488 in all. These were prepared for chemical analysis by X-ray fluorescence at Edinburgh University along with 904 samples of ocean island volcanic rocks.

B.2 Sawing, Crushing, and Grinding

Approximately 50g of material was cut from each rock sample using a diamond saw. The material selected was free from alteration, veining, amygdales, and inclusions. The cut pieces were crushed and the chips ground in a tungsten carbide barrel for 3 minutes.

In a number of cases the rock sample was too small to obtain 50g of chips. These were all fine-grained rocks which contained only very small phenocrysts and a smaller weight of chips (but not less than 15g) could be used. In these cases the grinding time was reduced according to the weight of material.

B.3 X-Ray Fluorescence Analysis (XRF)

Samples were analysed for 10 major and 17 trace elements at Edinburgh University using Philips PW1450 and PW1480 wavelength-dispersive, automatic, sequential X-ray fluorescence spectrometers fitted with Rh anode side-window X-ray tubes. The original analytical work was carried out using the PW1450 but some trace elements (Pb, Th, Ba, REE) were subsequently repeated using the PW1480 with calibrations more appropriate to nephelinite compositions and trace-element concentrations.

To correct for instrument drift on the PW1450, all sample measurements were ratioed to a monitor measurement which was obtained with each group of three samples analyzed. An average sample measurement was calculated from four repeat measurements for each element. With the PW1480, monitors were used to update the current calibration before each batch of samples was analyzed and samples were, routinely, measured once only.

B.3.1 Glass Disc Preparation for Major-Element Analysis

Major-element analysis was carried out on fused glass discs prepared by a method based on that of Norrish & Hutton (1969) and described by Fitton & Dunlop (1985). Rock powders were dried in an oven overnight at 110°C. Approximately 1g of

each powder was ignited for 20 minutes in a Pt-5%Au crucible at 1100°C and a value for LOI (= H_2O loss + CO_2 loss - O_2 gain) was calculated from the weight change. The ignited powder was then fused for 20 minutes at 1100°C using a lithium borate flux (Johnson Matthey Spectroflux® 105) with a 5:1 (flux:sample) dilution. The molten material was poured from the crucible onto a graphite plate and pressed into a disc by lowering an aluminium plunger onto the globule. The casting operation was carried out on a hotplate at 220°C and the glass disc allowed to anneal at this temperature for 10 minutes before cooling.

Spectroflux® 105 contains 47% lithium tetraborate ($Li_2B_4O_7$), 37% lithium oxide (Li_2O) and 16% Lanthanum Oxide (La_2O_3) as a heavy absorber.

B.3.2 Pellet Preparation for Trace-Element Analysis

Approximately 6g of rock powder was mixed with 4 drops of binding agent (2% PVA in distilled water). The mixture was placed in a steel mold, surrounded and backed by boric acid powder, and compressed at 8 tons to form a 40mm diameter pellet using a hydraulic press.

B.3.3 Calibration

The spectrometer was calibrated for major- and trace-element analysis using USGS and CRPG standard samples. Most of the calibrations relevant to this study used the concentrations ("usable" values) for international standards given by Abbey (1983). A more up-to-date compilation of working values appears in Govindaraju (1994). Gradient, intercept, and root mean square deviation of the standards about the regression line for each element were checked for consistency between each batch of samples analyzed.

B.3.4 Interference and Matrix Corrections

Analytical lines were, in general, chosen to provide high intensity with minimal interference from other elements. Line overlap factors for trace-elements (from PW1450) were calculated using synthetic glass standards. These were prepared from pure oxide mixtures of basalt and granite composition, spiked with stoichiometric trace-element compounds. Line overlap corrections were made for Rb on Y, Sr on Zr, Y on Nb, V on Cr, Ce on Nd, Ca on Sc, V on Ti and the back interference of Ti on V, Ti on La, and Ba on Ti.

The use of flux containing a heavy absorber (La_2O_3) for major-element analysis produces glass discs with a relatively constant matrix composition. Linearity of major-element calibration lines was generally excellent but root mean square deviation could be improved, particularly for SiO_2, by making matrix corrections. Iterative mass absorption corrections were applied using the coefficients tabulated by Theisen & Vollach (1967) and usually only one iteration was necessary.

Trace-element line intensities (from PW1450) were corrected using the major-element analysis obtained from the glass disc and the coefficients given by Theisen & Vollach (1967). Again a high degree of linearity was obtained in calibration lines,

particularly for elements where international standards have well-established concentrations. Trace-element data obtained more recently from the PW1480 were corrected for matrix effects using the RhKα Compton scatter peak (Reynolds, 1963) for Pb and Th and theoretical alpha factors (de Jongh, 1973) for Ba, La, and Ce.

B.3.5 Data Checks

Average major- and trace-element counts were calculated from four measurements for each element. Major-element data were screened by the total of the measured oxides plus LOI. The analysis of samples with totals lying outside the range 99.4 to 100.4 wt.% were repeated using new glass discs to confirm the total or to obtain an analysis in the expected range.

Monitors were used on both the PW1450 and PW1480 to correct for long-term instrument drift. However, with each batch of samples analyzed for major and trace elements an international standard (BE-N) was measured as an unknown sample against the current calibration data to ensure consistency between batches. The data are given in Table B-1.

Table B-1 Long-term reproducibility, repeat analyses of BE-N

PW1450: (wt.%)	5/85	1/86	5/86 (New Flux)	12/86	3/87	6/88 (New Flux)	12/88
SiO_2	38.29	38.31	38.42	38.51	38.43	38.36	38.29
Al_2O_3	10.21	10.18	10.06	10.12	10.08	10.17	10.19
Fe_2O_3	12.75	12.69	12.89	12.94	12.90	12.83	12.79
MgO	13.12	13.06	13.31	13.24	13.23	13.29	13.32
CaO	13.82	13.79	13.98	14.01	13.99	13.88	13.91
Na_2O	3.32	3.41	3.15	3.18	3.24	3.21	3.27
K_2O	1.395	1.378	1.428	1.431	1.437	1.406	1.398
TiO_2	2.612	2.591	2.620	2.597	2.622	2.626	2.630
MnO	0.201	0.202	0.199	0.198	0.201	0.200	0.202
P_2O_5	1.064	1.059	1.009	1.016	1.017	1.049	1.057

PW1450: (ppm)	11/85	7/86	1/87	8/87	1/89	PW1480:	12/92
Nb	115	112	111	113	113		
Zr	271	267	269	268	270		
Y	28	29	29	29	30		
Sr	1393	1395	1405	1404	1408		
Rb	49	49	49	49	49		
Th	12.3	12.1	13.0	13.1	12.2		10.4
Pb	3.1	2.9	3.2	5.6	4.1		4.0
Zn	124	125	126	124	126		
Cu	79	79	81	78	80		
Ni	273	275	274	275	271		
Cr	367	372	373	376	378		
Ce	157	149	158	147	161		154
Nd	70	69	67	72	72		66
La	89	81	91	87	85		84
V	247	250	249	244	241		
Ba	1067	1066	1049	1060	1064		
Sc	23	21	24	24	21		

For major elements the same glass disc was used throughout the life of a batch of flux (usually 12-18 months). Making a new set of standards for each new flux batch introduces a sample reproducibility component into the analysis comparisons for BE-N (see Table B-2 below). This has the effect of periodically resetting the longer-term reproducibility measure for major elements. However, for trace elements the same pressed-powder pellet was used throughout this study.

B.3.6 Precision and Accuracy

Analytical precision is essentially a measure of reproducibility. There are two components to reproducibility: the ability of the spectrometer to reproduce results when repeatedly analyzing the same sample, and the ability of the analyst to manufacture samples which give the same results when analyzed. In general, for major elements, instrument reproducibility is better than sample reproducibility but for trace elements it is similar to or worse than sample reproducibility.

Reproducibility was assessed by preparing five glass discs and five pressed pellets from a typical feldspar-free rock sample (a melilite nephelinite from the Honolulu Volcanic Series, Oahu - 43652). The discs and pellets were made from the same rock powder batch. Each of the five pairs of discs and pellets were measured five times for major and trace elements respectively. To assess machine reproducibility the mean and standard deviation was calculated from the five repeat analyses of one disc or pellet. To assess manufacturing reproducibility the mean and standard deviation was calculated from the mean of five repeat analyses for each disc or pellet. These results are presented in Table B-2.

Accuracy is a measure of the absolute quality of the analysis and is more difficult to estimate. To some extent accuracy depends on the quality of the calibration which can be quantified as the root mean square deviation (rmsd), expressed in wt.% or ppm, of the calibration data about the regression line. Typical rmsd from calibration data are given in Table B-2. For major elements precision and accuracy are comparable, whereas for trace elements precision is much better than accuracy. This probably reflects the accuracy of the values recommended for the standards used in the trace-element calibrations. Inter-laboratory agreement on standard values is much better for major elements than for trace elements.

B.4 Data Comparisons

Representative samples were selected for trace-element analysis by neutron activation (INAA) at the Open University and isotope dilution (ID) at Leeds University. The results were compared with the XRF results obtained in Edinburgh and it was found, for a small number of samples, that the concentrations of La, Ce, and Nd given by XRF were substantially lower (up to 50%) than those obtained by INAA and ID on the same powders, although the INAA and ID results agreed very well with each other. The samples

Table B-2 Typical Reproducibility (Standard Deviation) and Accuracy (rmsd) data

	Instrument Reproducibility (sample 43652)		Sample Reproducibility (sample 43652)		Accuracy (rmsd)
(wt.%)	Mean (n=5)	St Dev	Mean (n=5)	St Dev	
SiO_2	39.42	0.03	39.39	0.06	0.22
Al_2O_3	11.33	0.02	11.33	0.05	0.12
Fe_2O_3	14.30	0.02	14.27	0.05	0.05
MgO	13.26	0.03	13.24	0.06	0.08
CaO	12.76	0.01	12.75	0.06	0.05
Na_2O	3.68	0.03	3.64	0.10	0.06
K_2O	1.151	0.007	1.149	0.005	0.02
TiO_2	2.454	0.009	2.450	0.013	0.01
MnO	0.215	0.002	0.216	0.003	0.01
P_2O_5	0.932	0.003	0.941	0.023	0.01
Total	99.51	0.08	99.42	0.14	
LOI	0.42		0.42	0.02	
(ppm)					
Nb	52.4	0.6	52.6	0.4	2.4
Zr	166.7	0.9	166.9	1.0	14.8
Y	29.3	0.3	29.1	0.3	3.4
Sr	1070.1	2.1	1070.2	2.9	9.6
Rb	30.4	0.4	30.4	0.4	3.5
Th	6.8	0.4	6.8	0.4	2.8
Pb	4.4	0.5	4.0	0.4	4.0
Zn	123.4	0.7	123.3	0.8	5.0
Cu	84.6	1.1	84.7	0.9	5.3
Ni	310.3	2.6	310.6	2.6	4.3
Cr	488.4	2.1	487.7	1.1	11.0
Ce	115.2	5.2	114.3	3.5	13.5
Nd	62.4	3.4	61.7	3.5	3.6
La	59.5	2.4	58.0	3.3	5.6
V	300.3	2.5	300.4	2.8	11.5
Ba	745.8	9.3	746.4	6.7	39.0
Sc	29.7	0.9	29.2	1.5	2.4

affected were highly undersaturated melilitites and melilite nephelinites from the Western Rift, Uganda. These samples all contain perovskite which has high concentrations of REE.

When a single phase concentrates particular trace elements the matrix corrections based on the bulk rock composition may not be appropriate. The problem becomes acute at long wavelengths where X-ray penetration depths are not much greater than the average particle size. The very large differences in Ca and Ti content between perovskite and the bulk rock result in large differences in the absorption of La, Ce, and Nd L-radiation. Increasing the grinding time of the Western Rift samples improved the agreement but it was not possible to reproduce INAA and ID results even with 30 minutes grinding.

By melting 10g of rock powder in a new Pt-5%Au crucible at 1300°C and then cooling the crucible and contents fairly rapidly, it was possible to recover all the melted material as a glass block. This was then ground in a small tungsten carbide barrel, pressed, and analysed for La, Ce, and Nd as before. The results were recalculated to a 'wet' basis

using the LOI from the relevant major-element analysis and were found to agree closely with those obtained by INAA and ID. All the perovskite-bearing Western Rift rocks were, therefore, prepared for trace-element analysis using this method and these results have been used in this study. Chemical heterogeneity did not appear to affect trace-element concentrations in any other mineralogical composition analyzed in this study.

Appendix C

Major- and Trace-Element Data

Ocean Island Nephelinites (174 samples)
Continental Nephelinites (215 samples)
Potassic Continental Kamafugites and Leucitites (59 samples)
Olivine-poor Continental Nephelinites (89 samples)

Ocean Island Nephelinites (OIN)

	Ambitle	Japan				Samoa	Aitutaki	
Sample	AMB1	78-60	78-61	78-62	78-64	UPO7	AT4-46I	AT4-45
(wt.%)								
SiO_2	45.80	36.32	36.65	36.31	36.33	41.21	38.12	38.24
Al_2O_3	10.30	11.52	11.67	11.39	11.69	11.38	11.47	11.59
Fe_2O_3	11.05	15.00	15.33	15.28	15.44	14.53	14.48	14.68
MgO	9.16	9.31	9.75	9.29	8.79	11.93	11.04	11.19
CaO	14.52	14.13	12.78	14.32	13.54	9.73	12.26	11.94
Na_2O	3.02	3.69	3.74	3.72	4.50	3.65	4.74	4.79
K_2O	2.17	1.43	1.99	1.49	2.40	1.90	1.61	1.42
TiO_2	0.72	2.58	2.64	2.60	2.60	4.23	2.67	2.69
MnO	0.19	0.32	0.33	0.33	0.33	0.17	0.21	0.21
P_2O_5	0.56	2.11	2.12	2.13	2.26	0.98	1.20	1.20
Total	97.49	96.39	97.01	96.85	97.87	99.71	97.80	97.95
(p.p.m.)								
Cr	162	166	167	168	139	425	201	200
Ni	53	110	111	110	94	355	162	162
Cu	150	39	36	45	38	54	53	47
Zn	82	146	150	151	154	157	142	144
V	310	205	208	200	209	294	179	180
Sc	40	22	22	22	21	16	13	13
Rb	29	63	72	61	70	51	51	57
Ba	160	1598	1705	759	1487	489	1108	1247
Th	1	25	26	26	25	7	24	26
Nb	2	156	164	167	169	67	94	97
La	15	195	197	204	206	83	111	111
Ce	35	344	350	372	366	166	205	204
Pb	82	10	10	12	6	5	11	10
Sr	1277	2102	1328	1988	2736	984	1496	1419
Nd	26	134	141	140	146	75	81	86
Zr	74	368	373	385	382	353	337	338
Y	15	57	57	59	59	33	34	35

Ocean Island Nephelinites (OIN) - continued

	Kusaie					Ponape				Truk				
Sample	KS13	KS14	KS5	KS8	KS18	PO65	PO66	PO67	PO72	TUU30	TUU31	TUU32	TT51	TT52
(wt.%)														
SiO_2	38.79	37.13	37.45	40.24	40.17	38.64	40.93	40.55	40.87	37.94	37.85	37.83	37.99	38.07
Al_2O_3	10.26	10.68	9.80	10.20	10.47	10.36	11.02	10.79	11.09	10.93	11.01	11.06	11.13	11.17
Fe_2O_3	14.05	16.78	16.66	13.27	13.85	13.31	13.69	13.47	13.11	13.01	13.02	12.97	12.39	12.32
MgO	13.61	8.61	9.44	15.13	14.71	15.41	13.10	13.14	14.11	12.93	12.81	12.56	13.04	12.96
CaO	12.84	11.17	10.88	11.99	11.83	12.42	11.53	11.84	12.24	12.96	12.79	12.79	14.27	14.17
Na_2O	3.65	1.69	1.44	3.21	2.42	3.04	3.21	2.38	2.56	3.39	3.39	3.46	3.47	3.53
K_2O	1.03	1.90	1.52	0.60	0.88	0.92	1.25	0.98	0.51	1.63	1.67	1.68	1.47	1.47
TiO_2	3.43	5.65	4.55	2.87	3.25	2.93	3.43	3.37	2.50	3.79	3.78	3.77	3.43	3.45
MnO	0.22	0.19	0.22	0.21	0.19	0.20	0.20	0.19	0.20	0.21	0.20	0.20	0.19	0.19
P_2O_5	1.18	0.44	0.45	0.87	0.84	0.93	0.81	0.71	0.90	1.32	1.32	1.36	0.94	1.00
Total	99.04	94.22	92.40	98.58	98.61	98.17	99.17	97.42	98.09	98.11	97.84	97.68	98.29	98.32
(p.p.m.)														
Cr	579	486	593	820	676	597	455	437	574	431	420	402	466	469
Ni	345	214	258	459	414	415	351	346	340	232	224	227	235	232
Cu	76	82	81	66	79	66	73	67	66	68	75	70	83	87
Zn	117	120	122	107	104	105	106	101	106	99	100	102	90	90
V	334	513	431	304	323	297	292	282	256	298	305	303	343	337
Sc	27	32	30	24	25	24	20	21	27	30	28	29	29	30
Rb	22	39	30	28	26	15	24	31	10	41	43	42	45	44
Ba	688	383	446	681	456	773	632	586	630	701	790	732	934	862
Th	10	3	4	11	5	10	6	5	8	7	8	7	7	8
Nb	68	43	46	65	56	64	59	55	59	106	107	114	90	99
La	88	49	47	85	49	73	59	55	63	59	65	61	55	58
Ce	178	80	101	160	108	149	108	113	134	128	124	134	109	103
Pb	5	2	2	4	2	6	3	2	4	4	4	2	3	3
Sr	1141	498	637	1060	670	933	818	782	879	1057	1080	1118	1050	1048
Nd	89	39	45	74	54	62	51	51	62	64	61	62	48	52
Zr	355	291	311	337	320	244	253	247	238	351	350	352	251	260
Y	39	24	25	32	28	29	28	27	29	32	32	33	28	29

Ocean Island Nephelinites (OIN) - continued

	Kauai																	
Sample	SM2	SM11	SM13	SM15	SM20	SM21	SM22	SM23	SM25	SM26	SM36	SM38	SM39	SM41	SM48	SM51	SM53	SM54
(wt.%)																		
SiO_2	40.24	40.53	40.87	41.82	41.15	41.40	41.79	40.89	39.00	40.46	42.32	41.84	42.32	39.52	41.02	40.88	40.93	42.64
Al_2O_3	10.86	11.26	11.15	10.71	11.40	10.76	10.96	10.87	10.50	8.94	11.10	10.03	10.06	10.87	10.38	10.42	10.32	11.01
Fe_2O_3	15.02	15.60	15.38	14.15	14.61	14.57	14.39	14.55	13.72	13.97	13.94	13.69	13.88	15.61	14.97	15.61	15.44	14.63
MgO	11.59	11.83	11.84	10.49	12.19	13.04	12.94	13.03	12.43	18.61	14.02	15.89	16.66	13.46	14.09	13.35	13.55	13.70
CaO	11.93	12.05	11.86	13.00	12.04	12.10	11.94	12.35	12.78	11.04	11.46	10.85	10.70	12.24	11.33	11.37	11.49	11.19
Na_2O	3.18	2.17	2.89	2.90	3.29	3.09	3.30	3.51	3.51	1.64	2.78	2.89	2.30	1.12	3.18	2.57	3.29	2.89
K_2O	0.61	0.49	0.51	1.00	1.09	0.78	1.06	1.17	1.29	0.42	0.81	0.61	0.58	0.26	0.68	0.56	0.66	0.74
TiO_2	3.37	3.15	2.98	2.70	2.73	2.72	2.65	2.70	2.64	2.50	2.62	2.08	2.07	2.45	2.95	2.92	2.95	2.55
MnO	0.19	0.20	0.20	0.20	0.21	0.20	0.19	0.20	0.20	0.19	0.19	0.20	0.19	0.21	0.19	0.19	0.19	0.18
P_2O_5	0.60	0.50	0.52	0.70	0.68	0.63	0.55	0.63	0.78	0.51	0.44	0.45	0.44	0.61	0.52	0.53	0.51	0.38
Total	97.59	97.79	98.20	97.67	99.39	99.28	99.78	99.88	96.86	98.29	99.68	98.52	99.20	96.34	99.30	98.39	99.32	99.90
(p.p.m.)																		
Cr	654	543	445	667	493	460	553	556	500	692	535	967	707	587	443	510	490	515
Ni	1012	662	307	727	318	321	330	336	284	634	363	1531	600	424	386	394	367	354
Cu	72	89	73	95	95	77	86	84	107	71	91	100	98	94	104	93	96	97
Zn	117	123	120	121	122	109	115	123	123	100	93	106	99	119	103	109	105	99
V	378	364	348	272	302	295	312	308	288	285	302	292	278	326	302	316	315	298
Sc	21	20	17	21	15	14	15	12	17	21	17	20	16	17	13	18	17	15
Rb	10	7	9	28	27	23	28	28	32	16	46	20	19	5	36	18	22	22
Ba	661	668	637	668	738	707	606	702	680	884	638	572	608	674	756	677	667	583
Th	5	5	4	7	7	4	5	5	7	5	3	5	4	5	5	5	4	4
Nb	59	57	54	70	60	54	50	56	58	56	43	45	45	52	51	53	51	41
La	45	43	36	45	49	46	37	40	47	37	34	33	32	42	39	41	41	36
Ce	85	69	68	90	93	82	75	87	91	78	67	66	64	84	67	72	69	60
Pb	3	3	2	3	5	2	2	3	9	1	3	3	2	2	4	6	2	4
Sr	683	585	629	827	861	805	745	840	817	593	747	600	599	580	715	754	721	588
Nd	43	38	41	50	49	46	36	40	48	38	33	33	33	46	33	35	37	30
Zr	204	222	213	209	191	188	176	185	182	166	152	134	136	170	187	196	196	161
Y	24	25	26	27	27	25	24	26	25	21	22	21	22	28	23	23	24	21

Ocean Island Nephelinites (OIN) - continued

Kauai - continued

Sample	SM55	SM56	SM67	SM77	SM80	SM88	SM109	SM113	SM116	SM119	SM124	SM125	SM126	SM127	SM128	SM129	SM140	SM141
(wt.%)																		
SiO_2	41.14	42.01	40.14	41.72	40.76	41.89	41.87	39.27	39.83	37.85	39.71	38.77	39.59	39.50	42.69	42.61	42.35	41.48
Al_2O_3	11.34	10.56	9.75	10.86	9.48	10.73	11.80	10.24	9.98	9.59	10.24	9.98	10.35	10.45	11.16	10.97	11.32	10.61
Fe_2O_3	14.81	14.04	15.97	14.25	14.74	14.77	14.01	15.46	15.46	14.43	14.97	15.61	15.66	15.62	14.20	14.31	13.65	14.83
MgO	13.84	15.54	13.04	12.22	13.69	10.96	12.28	14.07	14.19	16.08	14.00	13.93	13.79	13.74	13.39	13.79	11.74	13.79
CaO	11.30	11.20	10.56	12.44	12.11	11.69	11.72	12.63	11.86	12.47	12.25	11.75	12.43	12.33	11.47	11.68	12.75	11.93
Na_2O	2.15	2.13	2.81	2.93	3.09	3.18	2.93	1.81	2.55	1.29	1.84	3.27	2.52	2.05	2.74	2.71	3.19	2.40
K_2O	0.80	0.71	1.18	0.41	0.68	1.04	0.77	0.77	0.69	0.78	0.53	1.52	0.93	0.82	1.05	0.67	1.31	1.11
TiO_2	2.68	2.21	2.93	2.56	2.52	2.81	2.42	3.09	3.23	3.15	3.09	3.22	3.09	3.08	2.43	2.44	2.99	2.87
MnO	0.20	0.19	0.22	0.19	0.19	0.19	0.19	0.21	0.20	0.19	0.20	0.21	0.20	0.21	0.19	0.18	0.18	0.19
P_2O_5	0.50	0.46	0.88	0.52	0.63	0.60	0.46	0.60	0.62	0.64	0.62	0.70	0.58	0.60	0.41	0.39	0.55	0.43
Total	98.76	99.04	97.46	98.10	97.88	97.85	98.43	98.13	98.60	96.45	97.43	98.94	99.15	98.38	99.72	99.77	100.04	99.64
(p.p.m.)																		
Cr	602	704	554	608	768	649	413	432	443	569	538	416	430	440	535	533	476	539
Ni	445	554	521	448	724	427	311	326	407	483	396	325	334	327	373	366	282	359
Cu	102	98	83	76	82	89	95	98	83	93	78	90	97	100	91	83	102	79
Zn	110	105	139	104	121	133	95	116	108	129	99	110	112	120	103	99	101	110
V	321	291	288	327	281	293	275	350	308	325	324	333	358	345	287	313	320	342
Sc	17	16	15	17	12	15	12	14	15	18	19	18	15	16	18	21	19	22
Rb	25	25	23	7	10	34	12	20	10	29	16	39	26	22	26	14	33	32
Ba	771	547	877	605	643	745	662	971	714	1640	785	918	614	1461	626	560	703	606
Th	4	4	8	5	5	5	4	5	5	5	4	7	5	4	4	4	5	3
Nb	47	49	81	52	60	60	43	61	56	64	58	65	59	61	41	39	54	46
La	39	27	64	48	41	44	32	36	43	43	48	49	40	41	32	25	40	31
Ce	70	63	116	67	82	85	57	80	79	71	88	92	69	69	51	47	85	54
Pb	3	2	4	2	3	3	3	4	3	3	3	2	2	4	3	3	4	2
Sr	647	629	527	609	733	722	756	802	691	649	641	773	687	848	603	582	759	596
Nd	33	29	66	36	41	41	32	41	42	47	41	51	35	37	27	27	41	33
Zr	169	143	282	163	200	197	138	215	226	218	209	229	216	215	134	133	193	177
Y	24	21	37	24	24	26	24	24	26	25	25	25	23	24	22	22	25	22

Ocean Island Nephelinites (OIN) - continued

	Kauai - continued																	
Sample	SM145	SM146	SM147	SM150	SM151	SM153	SM154	SM155	SM156	SM157	SM158	SM159	SM160	SM161	SM162	SM163	SM164	SM168
(wt.%)																		
SiO_2	37.33	37.55	40.54	42.15	39.24	38.53	38.13	39.07	39.22	39.00	38.80	39.49	42.02	39.00	39.43	38.27	41.36	39.33
Al_2O_3	9.02	9.21	10.26	11.50	10.43	9.69	9.20	9.01	10.03	9.91	9.65	9.59	10.93	10.09	10.12	9.31	11.19	10.50
Fe_2O_3	16.02	15.53	14.49	13.99	14.80	14.81	14.72	15.73	14.44	14.73	14.26	15.23	14.44	14.63	14.25	14.90	13.94	13.87
MgO	14.92	15.45	13.68	11.23	13.36	14.59	14.59	15.00	14.00	13.86	14.23	13.38	12.74	13.72	13.71	14.42	12.38	9.03
CaO	13.14	11.87	12.72	12.01	13.51	12.92	13.87	12.75	13.35	13.24	13.76	13.10	11.91	13.27	13.50	13.55	12.30	16.53
Na_2O	2.91	2.23	1.84	2.36	2.12	2.28	1.85	1.57	2.27	2.56	2.29	2.34	2.14	2.45	2.15	2.02	2.10	2.37
K_2O	1.02	0.70	0.96	1.28	0.62	0.75	0.42	0.65	1.02	0.63	0.46	0.59	1.16	0.55	0.65	0.46	1.16	0.50
TiO_2	3.28	3.32	2.80	2.43	3.15	3.26	3.20	3.27	3.14	3.23	3.13	3.34	2.73	3.17	3.10	3.34	2.78	3.97
MnO	0.20	0.21	0.19	0.19	0.19	0.20	0.20	0.20	0.20	0.21	0.20	0.20	0.20	0.21	0.20	0.21	0.19	0.20
P_2O_5	0.79	0.88	0.53	0.54	0.63	0.67	0.66	0.64	0.67	0.63	0.67	0.64	0.52	0.63	0.65	0.68	0.55	0.74
Total	98.63	96.93	98.02	97.67	98.04	97.70	96.85	97.87	98.33	97.98	97.45	97.90	98.77	97.71	97.75	97.15	97.95	97.03
(p.p.m.)																		
Cr	491	450	563	421	454	497	479	502	501	451	529	486	579	430	494	457	557	465
Ni	339	350	310	242	320	367	379	372	386	321	331	362	318	326	328	336	306	144
Cu	101	108	90	72	81	94	93	85	45	71	43	90	82	93	54	90	82	84
Zn	122	128	118	101	104	107	109	130	101	103	101	107	117	105	101	106	111	99
V	351	309	320	272	357	359	358	349	347	359	366	377	323	353	353	380	320	431
Sc	21	17	21	15	19	20	20	14	18	16	19	20	19	18	18	21	19	33
Rb	33	19	19	26	9	19	10	15	21	13	12	11	25	10	10	9	23	7
Ba	914	1196	718	2939	1261	948	644	468	1062	783	943	1245	1036	651	1181	576	1070	536
Th	8	9	5	4	4	6	5	5	6	6	7	5	4	6	6	7	4	7
Nb	72	89	53	44	59	66	66	63	64	63	63	67	52	62	58	64	53	72
La	60	64	43	29	44	55	40	50	44	46	51	41	35	44	45	50	38	53
Ce	108	122	81	66	84	83	89	83	88	89	96	82	71	88	88	90	64	104
Pb	4	6	3	2	2	2	2	2	3	2	2	4	3	2	2	3	3	2
Sr	1046	1081	1515	884	1214	1173	1544	1221	1018	1013	1153	988	635	1408	1357	1305	1181	956
Nd	51	56	39	38	39	39	43	43	43	39	45	41	37	46	46	45	39	56
Zr	289	308	207	168	205	207	216	237	197	206	198	214	188	200	189	199	183	245
Y	26	31	25	25	26	25	24	25	27	26	26	25	26	26	27	27	25	31

Ocean Island Nephelinites (OIN) - continued

Kauai - continued

Sample	SM169	SM171	SM172	SM175	SM176	SM177	SM196	SM198	SM205	SM315	SM328	SM337A	SM344	SM349	SM350	SM361	SM362	SM363
(wt.%)																		
SiO_2	41.64	38.74	39.49	41.07	38.72	37.46	40.52	41.02	38.60	42.04	40.21	38.98	38.47	40.04	39.93	38.98	39.36	38.04
Al_2O_3	11.13	9.63	9.71	10.55	9.77	9.11	10.88	11.03	9.96	10.42	10.27	9.88	9.46	10.25	10.43	10.54	10.50	9.79
Fe_2O_3	14.09	14.79	14.18	14.67	14.60	15.49	14.53	14.70	16.39	14.59	15.50	16.16	15.89	14.88	14.88	15.52	14.85	15.76
MgO	12.31	14.19	14.65	13.08	14.20	15.20	13.54	13.56	13.61	14.29	13.48	13.87	15.16	14.04	13.51	14.08	13.99	14.04
CaO	12.43	13.05	12.70	12.23	13.93	14.00	12.04	11.64	11.98	11.58	11.67	12.22	12.17	12.12	12.21	12.05	12.11	12.90
Na_2O	2.26	2.37	2.65	2.01	1.85	2.53	2.70	2.47	2.26	2.65	2.51	2.24	2.06	2.63	2.46	1.18	1.68	2.98
K_2O	1.18	0.76	0.89	1.03	0.60	0.71	0.36	0.63	1.06	0.91	0.96	1.05	0.93	0.95	0.88	0.47	0.70	0.97
TiO_2	2.81	3.30	3.11	2.81	3.12	3.40	3.08	3.02	3.35	2.32	3.11	3.40	3.31	2.98	3.01	3.21	3.13	3.04
MnO	0.18	0.19	0.20	0.19	0.20	0.20	0.24	0.21	0.24	0.22	0.18	0.20	0.20	0.19	0.19	0.18	0.18	0.20
P_2O_5	0.52	0.62	0.62	0.52	0.66	0.86	0.59	0.52	0.71	0.46	0.60	0.66	0.62	0.63	0.64	0.57	0.61	0.77
Total	98.55	97.62	98.18	98.15	97.65	98.95	98.48	98.79	98.14	99.46	98.47	98.66	98.26	98.71	98.13	96.78	97.10	98.47
(p.p.m.)																		
Cr	590	448	498	590	576	493	490	496	493	693	495	488	488	536	501	486	421	497
Ni	293	360	329	315	384	363	324	345	392	444	415	376	353	392	370	755	371	342
Cu	83	41	78	87	74	85	78	83	99	91	102	93	90	82	83	84	78	80
Zn	112	103	100	117	105	129	107	95	114	114	121	113	114	109	112	117	104	128
V	326	356	347	327	348	343	335	295	350	307	318	360	351	310	307	299	297	332
Sc	25	20	22	20	23	23	17	17	13	22	11	13	15	18	15	21	17	16
Rb	25	18	16	19	14	13	8	8	27	26	32	29	26	22	17	12	19	24
Ba	731	850	995	1157	746	1003	518	650	573	520	1122	527	1025	604	715	1196	890	723
Th	5	6	6	4	6	8	4	3	6	4	6	6	6	6	6	5	5	7
Nb	53	62	61	54	62	78	52	47	67	46	63	65	62	59	60	55	54	59
La	35	41	46	37	46	66	41	33	44	28	43	44	47	40	38	60	50	52
Ce	71	83	85	79	74	111	82	67	90	66	71	81	90	78	73	92	87	108
Pb	3	2	3	2	3	2	3	3	2	2	2	3	3	2	2	3	3	3
Sr	907	1145	1495	1089	1884	1502	595	655	738	611	824	655	865	727	737	528	572	1095
Nd	36	43	41	44	47	61	38	29	45	31	40	39	37	41	37	47	42	46
Zr	186	200	192	189	189	279	183	179	223	145	206	233	226	215	218	188	184	240
Y	26	24	25	25	27	30	26	25	26	23	24	25	24	24	24	32	26	28

Ocean Island Nephelinites (OIN) - continued

	Kauai - continued									Oahu						
Sample	SM364	SM366	SM385	SM430	SM431	SM451	2521-32	2521-34	HWK1	KA5	8127-85	8127-86	2521-16	2521-40	43651	43652
(wt.%)																
SiO_2	39.79	41.24	38.13	40.78	40.76	42.52	42.18	40.56	37.36	42.55	36.43	36.35	40.20	39.13	36.13	39.43
Al_2O_3	10.26	11.05	10.04	11.04	11.10	12.83	11.12	9.34	9.27	12.90	10.44	10.03	10.88	11.51	10.34	11.42
Fe_2O_3	14.63	14.39	15.08	15.07	15.21	14.94	14.88	13.88	15.29	13.95	17.58	16.93	14.37	14.20	17.65	14.22
MgO	13.45	13.41	13.94	12.16	12.07	8.22	11.68	16.19	14.14	8.74	11.45	10.00	13.82	13.13	12.36	13.35
CaO	12.51	11.46	13.04	10.98	11.03	12.32	11.68	11.70	13.82	11.57	12.66	12.17	12.32	12.93	12.11	12.85
Na_2O	3.40	3.35	4.23	3.60	3.57	3.24	2.52	3.12	3.00	4.21	4.93	5.44	3.99	4.04	5.14	3.48
K_2O	1.54	0.60	1.09	1.01	1.04	1.27	0.96	1.45	1.05	0.94	1.83	2.08	0.99	1.24	1.81	1.15
TiO_2	2.91	2.91	2.59	2.62	2.65	3.56	3.13	2.67	3.42	2.67	2.82	2.86	2.49	2.47	2.64	2.47
MnO	0.19	0.17	0.23	0.21	0.20	0.20	0.18	0.19	0.21	0.21	0.23	0.25	0.21	0.23	0.24	0.21
P_2O_5	0.77	0.49	1.06	0.72	0.72	0.51	0.49	0.58	0.91	0.84	1.09	1.19	0.81	1.00	1.11	0.98
Total	99.44	99.05	99.41	98.19	98.33	99.61	98.83	99.68	98.45	98.56	99.47	97.29	100.05	99.88	99.52	99.57
(p.p.m.)																
Cr	544	470	414	551	574	198	575	728	485	360	305	244	516	472	375	500
Ni	411	352	305	327	327	113	407	560	348	237	244	205	340	312	271	312
Cu	100	100	86	70	59	110	85	53	90	101	73	65	85	76	71	78
Zn	101	93	142	132	135	110	125	106	134	120	204	206	114	114	210	117
V	290	314	292	297	297	401	343	337	352	266	290	245	297	306	282	326
Sc	15	14	15	17	19	24	21	21	18	21	11	10	21	28	13	30
Rb	32	8	26	23	23	31	35	37	28	9	47	55	23	33	46	30
Ba	823	642	807	621	599	516	630	699	938	867	821	1104	760	808	926	751
Th	7	5	8	5	5	3	4	5	8	7	7	10	7	7	10	7
Nb	69	47	65	41	42	46	49	55	85	75	73	103	44	46	82	45
La	54	36	65	46	51	33	50	40	67	58	65	76	47	51	78	54
Ce	100	69	131	86	95	72	76	77	128	107	133	160	106	104	142	113
Pb	4	3	5	3	4	3	2	2	3	5	7	2	4	4	5	3
Sr	952	658	1356	920	920	780	611	768	1189	947	1731	1670	1090	1135	1738	1036
Nd	49	30	69	42	47	42	52	36	63	48	69	76	50	57	72	55
Zr	280	183	198	202	204	241	177	173	309	252	265	315	158	157	255	160
Y	30	23	34	26	26	27	44	22	29	28	24	28	25	29	26	29

Ocean Island Nephelinites (OIN) - continued

	Grande Comore							Moheli									
Sample	GC33	GC51	GC124	72/6	72/7	72/9	72/178	MO2	MO9	MO11	MO12	MO14	MO16	MO17	MO32	MO34	MO104
(wt.%)																	
SiO_2	41.50	42.74	39.63	42.07	42.28	41.55	41.27	39.86	41.26	40.22	40.41	40.49	41.02	38.84	41.38	44.69	42.71
Al_2O_3	9.86	13.57	10.86	9.68	10.11	11.14	11.14	10.19	9.51	9.56	10.56	11.49	10.78	11.53	12.53	16.73	12.75
Fe_2O_3	12.78	13.29	15.17	11.94	12.22	12.51	12.54	13.55	13.94	14.36	13.72	14.55	13.54	15.02	14.88	10.39	13.77
MgO	17.58	10.70	10.86	19.62	18.46	15.59	14.90	13.89	17.50	18.11	13.09	11.33	13.36	11.47	9.63	4.20	8.31
CaO	11.30	10.67	12.25	10.58	10.81	12.34	12.60	12.58	9.55	9.96	13.16	11.66	12.94	12.80	10.61	8.42	10.87
Na_2O	2.82	4.34	4.25	1.89	2.57	3.04	2.76	3.89	2.51	1.54	2.86	3.18	2.54	2.84	3.15	6.84	3.55
K_2O	1.28	1.64	1.80	0.87	0.90	1.11	1.15	1.62	0.65	0.44	0.66	1.46	0.56	1.34	1.20	2.79	1.76
TiO_2	1.93	2.32	3.12	1.43	1.63	1.93	1.95	2.74	2.75	2.84	2.90	2.75	2.59	3.01	2.81	2.43	2.24
MnO	0.20	0.22	0.25	0.18	0.19	0.21	0.21	0.23	0.20	0.19	0.20	0.23	0.20	0.23	0.22	0.21	0.26
P_2O_5	0.59	0.65	1.13	0.53	0.63	0.74	0.76	1.00	0.75	0.83	0.90	0.92	0.78	0.74	0.80	0.82	0.87
Total	99.84	100.14	99.32	98.78	99.80	100.14	99.28	99.54	98.60	98.04	98.47	98.05	98.29	97.82	97.21	97.51	97.09
(p.p.m.)																	
Cr	1093	369	377	1141	994	823	767	662	511	558	554	367	709	352	217	19	376
Ni	600	223	218	746	703	468	435	417	716	762	310	276	355	196	182	25	168
Cu	80	62	66	81	82	85	84	84	56	46	72	76	84	86	54	36	63
Zn	88	107	138	82	90	91	90	110	113	116	99	126	96	108	141	132	113
V	242	239	249	203	216	252	253	258	241	241	269	247	289	314	244	178	201
Sc	27	23	18	28	26	28	30	20	15	18	22	19	25	28	20	9	17
Rb	31	61	46	45	24	34	37	45	16	32	73	52	22	58	68	75	34
Ba	556	742	890	521	610	656	686	914	552	463	761	938	670	932	844	1284	1330
Th	8	12	12	7	9	11	11	15	7	7	9	14	8	11	12	26	19
Nb	64	101	96	58	61	72	74	82	57	59	60	84	62	106	90	177	109
La	54	64	100	45	64	78	81	97	58	57	67	89	58	84	75	147	99
Ce	102	136	183	102	122	155	151	182	114	115	137	165	119	149	141	252	183
Pb	3	6	5	4	4	5	5	6	4	3	4	6	3	6	6	17	
Sr	613	757	1037	506	666	752	771	1026	648	640	1016	1018	714	879	908	1938	1200
Nd	42	54	84	42	48	63	59	76	48	52	57	71	53	64	60	87	71
Zr	181	325	324	144	156	195	199	240	227	333	227	276	220	274	347	400	333
Y	22	30	40	21	23	27	29	34	25	26	30	37	28	32	33	39	41

Ocean Island Nephelinites (OIN) - continued

Moheli - continued

Sample	MO116	MO117	MO120	MO121	MO123	MO126	MO133	MO134	MO135	MO136	MO137	MO138	MO158	MO159	MO161	MO191
(wt.%)																
SiO_2	39.77	38.71	39.48	39.49	39.39	39.49	41.49	41.16	39.61	40.92	41.11	41.11	41.19	41.52	42.09	41.87
Al_2O_3	11.28	10.28	11.78	11.67	11.51	10.87	10.89	11.13	10.55	11.08	10.53	10.83	12.33	9.88	11.77	11.26
Fe_2O_3	15.45	14.08	15.32	15.37	15.63	15.08	13.96	14.47	14.29	14.16	14.05	14.17	14.78	13.68	14.12	13.05
MgO	10.16	13.60	9.05	9.29	10.10	10.50	12.06	11.69	11.75	11.67	12.19	11.68	9.89	17.82	11.85	15.46
CaO	11.78	13.13	12.15	11.98	11.08	12.33	11.38	11.59	13.20	11.61	11.95	11.36	11.61	10.05	11.76	11.49
Na_2O	4.21	3.35	4.63	4.37	4.86	4.35	3.27	2.35	2.84	2.69	2.87	3.38	3.58	1.86	2.94	2.56
K_2O	2.00	1.68	1.67	1.59	1.00	1.97	0.54	0.37	0.57	0.78	0.57	0.62	0.97	1.17	0.54	1.08
TiO_2	3.14	3.10	2.78	2.75	3.12	3.10	4.14	4.31	3.45	4.16	3.78	4.12	3.08	2.10	2.49	2.01
MnO	0.25	0.22	0.30	0.30	0.24	0.26	0.18	0.19	0.20	0.19	0.18	0.18	0.22	0.21	0.22	0.20
P_2O_5	1.14	0.86	1.16	1.15	1.09	1.17	0.61	0.64	0.96	0.65	0.65	0.60	0.82	0.55	0.65	0.57
Total	99.18	99.02	98.32	97.95	98.01	99.11	98.51	97.90	97.42	97.90	97.88	98.04	98.45	98.84	98.44	99.54
(p.p.m.)																
Cr	327	508	252	260	196	362	513	535	529	510	573	539	354	626	445	784
Ni	191	311	173	184	156	206	285	290	277	276	302	287	185	613	272	454
Cu	61	86	64	66	55	66	70	69	71	72	67	71	74	69	74	84
Zn	140	106	130	135	133	136	96	99	103	99	98	98	112	105	114	95
V	253	294	238	237	243	246	320	342	294	330	300	332	281	231	274	245
Sc	22	23	18	20	20	17	24	20	27	19	24	24	23	26	23	29
Rb	63	50	37	34	7	66	51	106	25	61	14	76	105	47	90	50
Ba	816	931	953	866	841	891	800	847	711	793	690	786	784	618	794	618
Th	12	11	18	21	12	13	6	5	9	6	7	7	10	7	8	7
Nb	102	93	107	115	98	99	53	54	69	56	55	53	85	61	74	69
La	89	86	119	126	81	100	54	58	61	59	51	53	63	51	71	55
Ce	175	163	218	228	166	184	93	98	123	98	96	92	128	91	125	111
Pb	3	6	6	6	4	8	3	2	3	2	3	2	4	2	4	4
Sr	1086	907	1238	1263	1039	1183	611	667	660	638	554	612	881	613	787	612
Nd	77	70	94	96	69	80	48	45	58	46	46	44	57	44	55	47
Zr	345	264	325	340	332	336	186	188	215	193	190	188	285	213	233	199
Y	39	32	45	47	39	41	24	26	27	25	25	24	32	24	30	25

Ocean Island Nephelinites (OIN) - continued

	Fernando de Noronha								Trinidade		Principe	Cape Verde			
Sample	FDN18	FDN20	FDN31	FDN33	FDN74	FDN76	FDN98	FDN106	TD3	TD6	P18	LM45	80/180A	80/180B	80/178
(wt.%)															
SiO_2	36.72	36.85	38.66	40.00	39.52	39.95	37.24	37.78	41.21	41.03	37.01	37.39	36.71	37.24	37.32
Al_2O_3	10.37	10.33	10.95	10.94	10.38	9.79	10.22	10.36	11.28	11.57	10.88	7.36	9.56	10.18	10.17
Fe_2O_3	14.97	15.22	13.54	13.11	13.31	13.17	14.55	14.46	12.39	14.14	14.28	13.81	12.02	12.10	12.14
MgO	12.30	12.77	11.81	12.86	13.65	13.52	13.16	13.23	13.44	8.29	12.24	20.70	14.45	13.71	14.21
CaO	12.86	12.82	13.03	12.67	12.86	12.09	13.03	13.04	11.96	12.36	13.19	12.97	17.42	16.79	15.53
Na_2O	3.00	2.92	3.49	3.60	3.26	2.57	3.33	2.67	2.05	1.94	2.97	2.34	3.18	2.89	3.67
K_2O	2.00	2.03	1.13	1.23	1.04	0.83	0.89	1.46	1.74	1.49	1.55	1.14	0.95	0.72	1.02
TiO_2	4.35	4.38	3.49	3.31	3.40	3.11	3.65	3.87	3.19	4.30	4.15	2.99	2.62	2.71	2.71
MnO	0.20	0.20	0.20	0.19	0.19	0.19	0.22	0.21	0.17	0.17	0.21	0.18	0.20	0.20	0.19
P_2O_5	1.16	1.12	1.01	0.91	0.95	1.03	1.29	1.02	0.48	0.89	1.42	1.06	1.50	1.54	1.51
Total	97.93	98.64	97.32	98.82	98.57	96.24	97.57	98.10	97.91	96.18	97.91	99.93	98.60	98.07	98.46
(p.p.m.)															
Cr	337	339	380	382	540	459	332	405	733	319	339	708	340	327	314
Ni	146	145	116	203	292	364	158	110	329	146	196	686	279	263	266
Cu	89	92	42	51	60	53	53	49	67	85	59	61	75	90	87
Zn	124	116	104	101	108	114	117	107	94	123	114	103	101	100	98
V	330	330	286	288	313	280	284	309	315	492	311	286	225	262	254
Sc	22	23	21	22	22	17	21	22	25	27	24	21	23	22	21
Rb	55	56	50	48	32	19	43	39	39	59	40	31	25	17	25
Ba	893	913	850	744	709	645	903	813	580	693	950	612	1232	1243	1278
Th	11	12	9	7	10	11	13	10	3	6	11	10	12	14	13
Nb	120	123	98	76	86	80	120	104	64	88	117	65	95	113	110
La	75	72	64	67	76	85	88	71	38	74	104	69	95	98	101
Ce	151	143	133	128	151	185	158	148	83	160	191	125	184	195	189
Pb	6	4	3	3	3	6	5	3	2	3	3	3	5	5	5
Sr	1395	1329	1057	930	1137	1498	1259	992	690	828	1290	1152	1623	1539	1324
Nd	72	69	68	60	70	86	74	71	43	71	82	56	83	93	87
Zr	421	427	346	268	320	351	399	365	253	381	345	226	305	333	324
Y	31	31	30	28	31	36	36	32	20	34	35	26	33	36	35

Ocean Island Nephelinites (OIN) - continued

	Cape Verde - continued															
Sample	80/100	ZM28	ZM31	ZM37	ZM43	ZM45	ZM49	ZM51	ZM54	ZM91	ZM94	ZM96	ZM97	ZM131	ZM133	ZM223
(wt.%)																
SiO_2	40.06	38.22	38.23	38.10	38.54	37.93	37.94	36.70	39.65	38.49	38.25	38.65	38.58	38.28	38.41	36.74
Al_2O_3	9.71	9.74	9.87	9.21	10.20	9.87	9.71	9.15	10.58	10.28	10.32	10.03	10.23	10.37	9.97	9.11
Fe_2O_3	11.96	12.58	12.58	12.94	12.64	12.44	11.91	12.08	13.33	12.71	12.38	12.84	12.60	12.73	12.58	12.15
MgO	13.82	14.88	14.50	15.21	13.30	14.73	15.18	14.84	12.65	13.12	12.93	13.41	13.38	13.51	16.20	15.03
CaO	14.11	15.15	15.31	15.20	14.47	15.36	16.26	16.99	13.68	14.47	14.93	14.03	14.25	14.25	12.97	17.19
Na_2O	2.85	3.00	2.27	2.15	3.24	2.50	2.73	2.28	3.11	3.19	2.98	2.70	3.01	2.97	2.03	2.52
K_2O	0.68	1.99	1.07	0.82	1.67	0.92	1.08	0.83	0.79	1.66	1.87	1.80	1.73	2.08	1.16	0.97
TiO_2	3.31	3.45	3.52	3.64	4.25	3.45	2.73	3.23	3.93	4.30	4.09	4.38	4.26	4.00	3.59	3.25
MnO	0.17	0.19	0.19	0.19	0.19	0.18	0.18	0.18	0.18	0.19	0.18	0.19	0.18	0.19	0.18	0.18
P_2O_5	0.93	0.90	0.87	0.80	0.97	0.84	1.07	1.18	0.87	0.96	0.99	0.96	0.98	1.08	0.79	1.19
Total	97.60	100.10	98.41	98.25	99.45	98.21	98.79	97.46	98.75	99.37	98.92	99.00	99.18	99.46	97.88	98.31
(p.p.m.)																
Cr	883	643	589	618	648	547	704	665	589	614	611	663	614	608	587	660
Ni	317	333	308	312	252	311	330	308	285	247	251	274	252	266	296	317
Cu	78	90	77	81	77	84	72	105	60	60	76	76	77	79	78	95
Zn	93	92	91	90	91	92	92	89	92	88	84	89	88	94	94	92
V	311	309	309	315	345	312	287	311	333	358	358	348	350	340	326	309
Sc	22	28	26	29	28	25	27	25	26	28	25	29	28	24	26	26
Rb	18	48	39	31	43	34	34	27	13	40	48	46	40	50	19	22
Ba	1001	826	920	813	915	936	1005	1081	689	936	1090	910	976	1057	820	1105
Th	8	6	6	5	6	5	9	9	6	4	6	6	5	5	6	10
Nb	85	86	85	82	81	82	85	102	74	79	81	79	80	83	81	101
La	63	55	46	44	69	50	76	78	60	53	49	58	54	51	49	77
Ce	139	107	93	87	104	97	135	144	123	112	97	104	118	114	95	153
Pb	3	1	3	3	3	2	3	4	2	2	3	2	2	3	3	4
Sr	1175	1038	1091	1019	1060	1041	1257	1364	964	1111	1162	816	1011	1111	898	1385
Nd	69	53	45	42	57	43	63	63	63	55	49	50	56	54	52	65
Zr	347	321	332	327	346	301	291	317	340	352	340	348	349	335	306	310
Y	28	27	26	26	28	25	28	30	29	28	29	28	29	29	25	30

Continental Nephelinites (CON)

	Malagasy		Turkana, N Kenya			Riwa & Lodwar Hill, N Kenya				Samburu, N Kenya		
Sample	ANK8	ANK9	T71	T78	T80	RIWA1	RIWA2	RIWA3	LOD1	8-428	11-108	KS7309
(wt.%)												
SiO_2	40.20	40.15	38.51	38.86	34.83	38.22	41.80	41.93	39.92	42.84	41.71	38.01
Al_2O_3	11.01	9.87	11.53	11.70	10.01	10.39	12.63	7.52	11.73	12.54	11.52	8.68
Fe_2O_3	11.86	12.40	15.82	15.40	13.76	15.66	15.18	13.81	14.71	11.74	12.22	15.08
MgO	14.73	15.58	7.48	7.32	6.76	8.89	5.86	14.24	6.98	10.64	12.72	15.83
CaO	12.93	13.01	13.90	13.92	17.81	14.31	11.16	13.69	12.78	12.01	12.64	12.36
Na_2O	1.95	2.45	3.37	3.11	2.82	4.07	5.46	3.65	5.30	3.99	3.06	3.33
K_2O	0.61	2.02	1.09	0.87	0.42	1.62	2.05	1.37	2.22	1.27	0.77	1.36
TiO_2	2.75	2.71	4.11	4.06	3.59	3.36	2.92	2.47	4.04	2.13	2.23	2.60
MnO	0.18	0.18	0.26	0.28	0.24	0.22	0.27	0.18	0.23	0.18	0.18	0.22
P_2O_5	1.10	0.84	0.91	0.98	0.83	0.74	0.75	0.31	0.81	0.49	0.41	0.85
Total	97.32	99.20	96.98	96.50	91.07	97.49	98.09	99.17	98.72	97.81	97.45	98.32
(p.p.m.)												
Cr	546	728	64	54	56	225	11	1084	67	461	615	607
Ni	348	396	50	41	40	74	27	253	55	180	214	457
Cu	67	83	238	199	152	154	195	221	129	104	122	74
Zn	88	89	100	92	94	104	141	83	114	83	78	141
V	256	300	378	363	321	382	303	290	377	297	317	256
Sc	25	28	26	21	17	28	12	33	20	30	39	22
Rb	31	51	31	24	16	38	56	27	34	17	9	35
Ba	1023	988	966	1143	3564	605	685	404	691	672	523	652
Th	9	9	23	23	20	7	13	4	15	10	8	10
Nb	97	87	174	198	145	75	126	52	143	80	69	95
La	77	61	144	153	138	66	96	44	108	70	54	78
Ce	149	127	273	294	263	127	185	94	213	125	101	142
Pb	3	1	8	8	12	3	16	4	6	5	4	10
Sr	983	958	1178	1497	2371	847	1294	538	1107	685	604	954
Nd	61	55	108	112	94	55	78	39	88	49	39	62
Zr	256	235	324	386	290	207	325	148	360	166	147	259
Y	27	24	35	39	33	25	34	18	35	24	23	29

Continental Nephelinites (CON) - continued

	Moroto, E Uganda				Napak, E Uganda								
Sample	V151A	V259	V322	V534	SUN14	SUN16	SUN21	SUN86	SUN87	SUN89	SUN90	SUN189	SUN193
(wt.%)													
SiO_2	43.13	41.27	42.78	39.98	42.41	43.24	42.56	42.57	42.38	41.40	41.69	40.42	39.79
Al_2O_3	14.42	8.95	9.60	10.92	10.84	11.29	13.63	13.15	13.01	12.47	13.17	14.40	13.80
Fe_2O_3	13.67	14.35	12.51	13.66	14.03	13.69	14.48	14.70	14.65	14.79	14.58	12.04	12.85
MgO	5.95	10.05	10.36	10.05	7.48	6.77	5.22	6.04	5.74	5.15	5.84	5.23	4.78
CaO	9.94	14.54	15.13	13.49	14.47	13.20	10.76	11.56	11.21	12.20	12.01	13.22	13.45
Na_2O	4.95	3.06	4.45	3.08	3.38	3.60	4.58	2.04	4.63	3.03	3.65	6.24	5.36
K_2O	2.02	1.37	1.66	0.93	1.32	1.66	2.50	2.39	1.51	1.89	1.19	2.20	2.59
TiO_2	2.31	2.91	1.92	3.02	2.31	2.19	2.48	2.51	2.48	2.53	2.48	2.38	2.29
MnO	0.21	0.20	0.20	0.20	0.21	0.21	0.23	0.21	0.22	0.22	0.21	0.19	0.22
P_2O_5	0.61	0.47	0.49	0.51	0.71	0.78	0.79	0.72	0.67	0.71	0.71	0.75	0.90
Total	97.21	97.17	99.09	95.85	97.15	96.61	97.23	95.88	96.50	95.38	95.53	97.05	96.04
(p.p.m.)													
Cr	21	305	620	287	86	71	11	18	17	21	20	7	5
Ni	27	112	157	127	43	38	12	16	18	19	18	7	9
Cu	84	151	173	153	160	149	158	157	149	151	147	162	194
Zn	115	90	76	95	115	111	133	130	132	121	120	110	131
V	255	394	243	355	344	299	266	296	274	291	254	290	302
Sc	18	33	30	29	26	20	16	16	16	17	16	17	13
Rb	40	39	31	39	33	33	55	56	37	54	56	49	68
Ba	1151	731	126	569	719	853	1152	842	597	1203	668	532	763
Th	6	6	1	5	6	8	7	8	8	7	8	10	11
Nb	55	52	12	62	68	67	73	72	72	67	71	84	93
La	50	56	27	56	61	66	72	69	63	63	64	68	80
Ce	104	102	52	94	117	131	127	125	125	129	120	148	142
Pb	5	5	2	5	7	9	11	8	10	8	9	8	9
Sr	1140	741	500	855	1050	914	1267	1215	1606	1167	1164	752	1029
Nd	48	46	25	41	49	50	56	52	50	50	52	60	61
Zr	176	187	93	188	173	170	206	200	199	184	190	180	189
Y	23	24	15	23	22	24	26	25	26	25	25	24	28

Continental Nephelinites (CON) - continued

	Elgon, E Uganda					Homa Mtn, Nyanza, Kenya				N Ruri Hills, Nyanza, Kenya
Sample	ELG5	ELG6	ELG1	ELG2	ELG4	1279	HC116A	H182	HF563	N595
(wt.%)										
SiO_2	41.59	43.72	39.31	41.27	42.02	35.49	36.45	42.73	39.54	41.66
Al_2O_3	9.11	7.60	7.52	9.13	13.95	8.01	7.89	11.48	9.21	7.93
Fe_2O_3	13.93	15.57	14.41	14.09	12.77	13.93	14.39	11.21	14.43	14.66
MgO	8.18	7.93	10.58	8.77	5.59	13.45	13.77	5.42	6.29	9.31
CaO	17.44	14.59	18.16	14.93	9.38	16.53	15.89	12.69	14.92	15.66
Na_2O	2.83	1.38	1.99	2.75	5.36	2.66	2.63	5.51	3.03	2.02
K_2O	1.47	1.73	1.74	2.05	2.63	2.18	2.40	0.79	0.97	1.14
TiO_2	2.21	2.94	2.70	2.45	2.42	4.29	4.28	2.76	3.98	3.22
MnO	0.22	0.24	0.21	0.23	0.37	0.22	0.22	0.21	0.23	0.16
P_2O_5	0.46	0.41	0.50	0.63	1.19	0.81	0.81	0.77	1.04	0.76
Total	97.44	96.11	97.08	96.28	95.68	97.56	98.73	93.57	93.63	96.53
(p.p.m.)										
Cr	167	60	309	266	2	624	585	81	60	334
Ni	70	49	108	111	8	181	175	36	29	105
Cu	204	222	259	209	272	155	152	125	150	217
Zn	93	133	102	107	172	104	118	110	110	94
V	290	345	286	299	334	355	351	292	380	316
Sc	38	30	36	31	3	24	23	17	22	36
Rb	38	64	62	85	84	65	79	38	40	33
Ba	645	727	477	912	2863	886	917	1769	4847	6242
Th	6	11	8	10	12	11	12	17	25	8
Nb	58	89	62	79	158	147	147	124	160	78
La	46	64	54	73	113	76	97	106	158	70
Ce	85	123	81	135	193	140	196	207	300	122
Pb	10	9	4	9	9	4	5	13	14	5
Sr	842	940	867	1033	1619	1311	1335	1855	1469	794
Nd	37	46	34	53	76	51	84	81	121	66
Zr	165	235	140	186	336	298	302	304	285	214
Y	21	20	19	24	44	24	24	27	31	24

Continental Nephelinites (CON) - continued

Rangwa - Kisingiri, Nyanza, Kenya

Sample	RR85	RR585	RR589	RR610-1	RR656	RR657	RR659	RR663	RR672	RR674	RR695-1	RR695-2	RR703
(wt.%)													
SiO_2	41.04	44.73	43.78	40.45	37.78	42.52	41.11	41.91	43.07	42.63	41.25	43.20	42.74
Al_2O_3	14.11	14.32	13.98	7.36	9.99	14.32	12.43	12.52	11.52	13.61	10.14	7.07	12.02
Fe_2O_3	12.69	12.93	12.89	15.58	13.73	12.75	14.68	15.40	13.67	13.30	14.89	13.01	14.66
MgO	4.68	4.29	5.10	9.96	6.33	5.27	7.02	6.56	7.32	4.69	5.78	9.94	5.80
CaO	11.99	8.94	10.71	16.89	17.32	10.87	13.00	10.79	13.50	11.48	13.66	17.59	11.96
Na_2O	4.87	6.51	3.89	1.78	3.42	5.66	3.19	4.36	3.43	5.84	4.16	2.58	3.61
K_2O	2.48	2.48	2.63	0.56	2.57	2.37	1.49	2.01	1.57	1.87	2.26	1.29	2.08
TiO_2	3.04	2.62	2.64	3.55	3.62	2.77	3.30	3.13	2.79	2.83	3.90	3.24	3.18
MnO	0.23	0.22	0.21	0.22	0.28	0.25	0.24	0.23	0.23	0.25	0.21	0.18	0.24
P_2O_5	0.99	0.82	0.87	0.78	1.09	1.10	0.78	0.74	0.82	0.84	0.81	0.49	0.93
Total	96.11	97.85	96.70	97.11	96.10	97.88	97.23	97.64	97.92	97.33	98.05	98.59	97.22
(p.p.m.)													
Cr	7	11	31	285	62	11	17	16	159	30	67	242	61
Ni	6	22	23	86	32	18	42	42	66	23	45	88	34
Cu	213	111	107	220	291	167	141	112	131	100	245	175	113
Zn	125	119	127	108	121	116	109	116	97	140	104	74	112
V	302	235	311	371	426	257	301	313	312	266	354	310	296
Sc	11	8	10	39	12	8	15	15	19	10	24	44	14
Rb	56	62	62	25	63	56	41	44	62	51	60	31	50
Ba	923	1052	1056	1050	957	1590	1672	856	1196	892	721	498	1340
Th	20	12	10	9	12	12	11	9	9	15	9	6	9
Nb	155	102	97	84	134	114	107	85	89	121	108	72	97
La	132	91	80	74	82	99	98	73	84	108	75	47	79
Ce	257	166	162	140	149	196	186	153	173	204	132	97	151
Pb	11	12	20	9	7	12	9	8	8	12	7	15	10
Sr	2024	1307	1554	981	1159	1575	3011	1257	1355	1657	870	638	1306
Nd	105	71	69	57	60	82	79	64	78	88	58	37	70
Zr	378	315	292	244	344	349	297	266	273	352	323	218	281
Y	38	31	29	25	35	36	31	30	29	36	26	19	30

Continental Nephelinites (CON) - continued

	Kaksingiri - Gembe, Nyanza, Kenya								Usaki - Wasaki, Nyanza, Kenya						
Sample	K2	K17	K38	K53	K61	K66	K91	K93	U921	U926	U955	U1137	U1144	U1145	U1270
(wt.%)															
SiO_2	39.80	40.90	38.46	33.84	39.99	41.24	43.60	38.16	43.25	42.72	40.32	37.69	40.37	39.04	40.92
Al_2O_3	10.37	11.93	10.46	9.00	10.43	9.32	10.65	9.87	13.29	13.16	9.45	10.05	8.13	11.93	7.35
Fe_2O_3	14.28	14.79	14.78	14.38	15.23	15.31	14.42	15.10	14.12	13.79	16.39	14.41	15.79	13.41	15.89
MgO	7.66	6.30	7.31	6.86	7.10	8.21	7.96	6.85	5.62	5.17	7.38	6.95	9.38	6.83	10.95
CaO	16.61	14.27	14.78	22.30	15.45	15.76	12.62	18.53	10.75	11.50	15.41	18.55	16.20	14.17	15.54
Na_2O	2.43	1.22	1.63	3.83	2.65	1.12	3.78	2.26	3.54	3.35	3.04	1.18	2.87	2.50	0.68
K_2O	1.37	1.75	2.46	2.08	1.55	1.24	1.32	0.52	2.33	2.38	0.92	1.47	1.61	1.80	1.15
TiO_2	3.09	3.42	3.49	3.22	3.76	3.31	2.79	3.50	2.83	2.78	3.70	3.56	3.46	3.14	3.32
MnO	0.25	0.21	0.27	0.27	0.22	0.22	0.20	0.25	0.23	0.23	0.24	0.26	0.22	0.24	0.21
P_2O_5	0.77	0.78	1.29	1.18	0.93	0.82	0.62	0.78	0.76	0.74	0.90	0.94	0.77	1.10	0.55
Total	96.64	95.56	94.91	96.97	97.30	96.54	97.94	95.82	96.73	95.81	97.76	95.06	98.80	94.14	96.55
(p.p.m.)															
Cr	147	6	44	26	48	208	157	51	53	136	99	85	488	80	422
Ni	50	12	43	34	53	64	79	37	31	393	54	285	687	88	112
Cu	154	305	276	233	222	212	177	267	82	82	226	259	192	220	191
Zn	124	117	140	127	115	114	104	123	124	125	119	126	106	136	105
V	347	329	394	319	416	343	290	408	265	265	395	382	340	309	343
Sc	21	19	12	18	18	26	27	18	12	13	24	15	40	8	38
Rb	62	28	73	49	46	34	32	15	67	48	27	47	39	57	36
Ba	292	1209	1359	990	703	413	824	449	1196	956	788	1309	1177	541	1395
Th	10	9	10	11	13	9	9	12	8	9	11	13	8	12	6
Nb	100	87	138	162	107	80	78	100	93	92	86	137	86	126	64
La	79	65	95	115	86	75	72	83	83	80	73	100	64	95	57
Ce	73	132	184	187	175	148	132	157	150	150	143	186	121	177	97
Pb	7	8	9	9	9	8	5	8	11	8	12	7	6	7	5
Sr	1502	1827	1699	1804	1962	1489	924	1814	1413	1889	1983	1539	836	1818	689
Nd	65	57	76	70	69	64	58	64	70	68	62	70	52	75	45
Zr	282	276	388	372	295	256	257	286	262	262	287	322	233	345	214
Y	31	27	40	44	29	26	27	30	31	30	28	34	26	35	22

Continental Nephelinites (CON) - continued

	Narok - Nguruman, S Kenya					Loolmurwak, N Tanzania	Burko, N Tanzania		Makuyuni Jnctn, N Tanzania				
Sample	SK244-2	SK209-1	SK419-1	SK410-1	1467	BD105	BD435	BD436	MANY1	MANY3	MANY4	MANY5	MANY6
(wt.%)													
SiO_2	41.26	44.69	39.93	39.38	39.97	38.37	40.24	42.68	41.27	41.49	40.8	42.38	40.87
Al_2O_3	8.51	8.61	8.43	7.99	9.30	7.17	11.46	14.51	11.06	11.67	10.6	7.26	12.00
Fe_2O_3	15.72	12.13	12.82	12.46	13.36	14.62	13.45	12.03	15.23	14.60	14.85	14.71	14.38
MgO	15.39	10.61	18.76	18.60	13.76	15.67	6.42	4.25	5.43	5.81	5.92	9.27	5.80
CaO	10.07	15.24	12.72	13.11	12.63	12.53	14.15	10.55	11.87	11.17	12.63	16.13	11.79
Na_2O	1.72	2.24	2.42	2.41	4.16	2.26	4.04	2.74	2.86	4.00	3.43	1.59	4.29
K_2O	1.01	1.23	0.78	0.77	1.98	1.48	1.87	3.47	2.38	2.72	1.77	0.71	1.42
TiO_2	3.18	2.66	1.35	1.30	3.15	3.87	3.53	2.86	5.17	4.78	5.34	4.48	4.74
MnO	0.21	0.18	0.19	0.19	0.21	0.21	0.25	0.24	0.25	0.25	0.24	0.19	0.26
P_2O_5	0.58	0.42	1.10	1.08	0.57	0.83	1.04	0.76	1.56	1.28	1.58	0.87	1.37
Total	97.64	98.00	98.50	97.28	99.08	97.01	96.44	94.09	97.10	97.77	97.18	97.59	96.92
(p.p.m.)													
Cr	718	478	808	809	1029	685	41	8	5	19	17	489	13
Ni	563	138	840	882	255	370	43	20	20	34	30	116	25
Cu	11	139	112	116	150	122	136	85	114	134	125	207	152
Zn	138	87	92	93	100	123	120	121	140	146	137	109	145
V	291	289	227	222	272	275	317	236	358	336	371	374	318
Sc	27	40	21	17	30	33	13	10	16	17	19	35	14
Rb	17	27	14	17	51	44	44	176	37	55	23	38	26
Ba	515	487	394	369	565	772	4683	2656	1999	1998	1242	561	969
Th	9	6	5	4	9	11	21	24	13	14	13	8	15
Nb	69	60	34	33	96	98	198	215	129	127	120	71	135
La	61	56	59	60	60	77	144	177	125	127	121	81	127
Ce	120	99	117	121	117	150	267	300	258	260	251	164	256
Pb	2	5	3	3	8	6	8	11	8	10	8	5	9
Sr	755	679	680	677	831	964	1701	2139	1565	1334	1434	2002	1483
Nd	55	44	53	57	56	67	109	119	127	121	120	83	115
Zr	247	200	158	153	291	404	445	423	583	545	542	332	521
Y	26	21	23	22	29	29	36	39	44	45	44	30	43

Continental Nephelinites (CON) - continued

	Chilwa Province, Malawi						Nuanetsi Province, Zimbabwe			
Sample	MAL9	MAL6	MAL7	MAL8	MAL1	MAL2	NTS8	NTS14	NTS206	NTS218
(wt.%)										
SiO_2	45.30	33.94	37.62	35.56	39.61	36.65	41.56	43.76	41.29	43.75
Al_2O_3	15.88	9.99	11.44	11.06	7.86	11.27	11.65	15.77	12.35	11.59
Fe_2O_3	10.48	14.57	16.29	10.94	9.19	10.54	15.81	11.76	14.41	14.38
MgO	4.37	9.58	9.54	8.82	6.18	10.04	5.64	4.28	5.90	7.16
CaO	8.18	12.65	11.42	13.95	9.95	16.17	8.77	5.53	7.77	9.93
Na_2O	6.40	0.84	1.28	1.89	3.12	1.64	6.25	7.79	7.18	4.59
K_2O	4.39	3.60	2.66	2.95	4.22	2.67	2.33	3.94	2.98	2.28
TiO_2	2.82	4.32	4.96	2.46	3.01	2.22	4.31	3.07	3.82	2.97
MnO	0.23	0.30	0.26	0.22	0.16	0.21	0.21	0.19	0.22	0.20
P_2O_5	0.79	1.40	0.94	1.35	0.14	1.04	0.92	1.04	0.92	0.55
Total	98.84	91.20	96.42	89.20	83.42	92.45	97.43	97.12	96.83	97.38
(p.p.m.)										
Cr	54	394	266	512	143	421	18	69	59	71
Ni	53	507	64	204	51	187	44	39	49	78
Cu	34	52	50	65	58	74	305	160	275	258
Zn	109	138	110	104	97	88	131	125	140	120
V	157	260	315	231	389	244	489	236	433	495
Sc	12	26	20	18	42	27	9	2	9	25
Rb	91	115	72	106	65	85	69	103	84	76
Ba	1241	2566	1037	1371	374	1729	1519	1923	1884	753
Th	6	39	13	19	28	9	10	12	11	3
Nb	121	152	90	147	175	79	145	219	198	63
La	103	396	183	183	63	108	81	82	91	21
Ce	229	746	339	354	137	201	132	147	166	38
Pb	6	12	4	13	4	8	17	19	17	10
Sr	1789	2289	2126	4470	818	2197	1531	1899	1844	889
Nd	101	274	138	124	75	87	52	60	60	18
Zr	638	529	362	291	391	226	289	424	328	163
Y	43	67	42	39	67	30	26	31	27	20

Continental Nephelinites (CON) - continued

	Cape Province, S Africa							Gamoep, Bushmanland - Namaqualand									
Sample	BD1231	BD1234	BD1235	BD1238	SU1	RIV1	RIV2	BD1207	BD1211	BD1220	BD1224	N1	N2	N3	N4	N5	N6
(wt.%)																	
SiO_2	34.90	29.75	33.48	29.88	33.71	36.87	36.76	39.94	35.65	40.58	33.20	35.26	35.61	33.09	35.82	35.63	35.36
Al_2O_3	7.62	6.57	7.75	6.62	7.52	7.47	7.50	6.97	5.39	6.90	5.32	5.51	4.96	5.25	5.29	4.89	5.50
Fe_2O_3	12.34	14.41	11.76	12.18	11.70	14.50	14.54	15.24	16.45	14.94	17.08	16.76	16.44	17.14	16.17	16.51	16.72
MgO	17.71	18.43	17.75	17.92	18.42	17.04	16.95	12.00	19.53	14.44	17.89	18.33	20.00	18.41	19.53	20.21	18.57
CaO	14.36	19.48	15.47	20.01	15.27	12.60	12.79	13.69	11.29	9.89	13.51	11.79	11.89	13.46	12.81	12.23	11.57
Na_2O	1.05	2.06	1.00	1.61	0.94	2.73	2.79	2.06	1.55	1.81	1.49	1.48	1.52	1.61	1.58	1.48	1.26
K_2O	2.01	0.91	2.36	1.01	2.25	2.03	2.03	1.81	1.47	2.02	2.03	1.51	1.36	2.17	1.55	1.22	0.88
TiO_2	3.43	2.96	3.36	2.98	3.29	4.23	4.26	4.40	5.75	5.31	7.01	6.84	5.78	6.87	4.68	5.51	6.80
MnO	0.19	0.29	0.20	0.24	0.20	0.20	0.21	0.19	0.20	0.18	0.21	0.20	0.20	0.21	0.21	0.20	0.20
P_2O_5	0.83	1.98	1.02	3.05	0.96	0.85	0.81	1.12	1.06	0.34	1.07	0.78	0.92	1.04	1.19	0.92	0.63
Total	94.43	96.82	94.14	95.49	94.25	98.50	98.64	97.41	98.35	96.42	98.80	98.45	98.66	99.26	98.83	98.81	97.47
(p.p.m.)																	
Cr	822	768	836	791	883	695	696	507	659	301	524	654	677	517	721	652	607
Ni	501	442	455	445	496	421	423	477	705	420	602	667	746	635	723	771	674
Cu	93	59	98	144	97	83	81	103	117	96	131	99	122	124	102	122	131
Zn	92	112	86	92	86	110	111	109	118	134	117	118	115	114	120	113	112
V	290	358	370	240	305	295	296	284	327	264	353	363	285	337	289	285	365
Sc	29	24	33	17	28	21	21	22	19	18	15	18	22	22	21	19	19
Rb	65	33	87	40	84	71	72	44	53	130	80	61	55	69	53	49	60
Ba	1288	537	2141	1587	1683	765	821	455	630	1197	572	852	709	517	795	692	652
Th	9	26	9	19	10	9	8	10	9	22	11	10	9	9	12	8	9
Nb	102	178	112	150	111	100	101	102	106	145	123	121	106	122	115	101	116
La	78	143	82	129	96	71	80	95	84	93	99	95	80	96	95	81	86
Ce	171	273	157	256	164	168	157	201	164	175	187	193	163	192	209	157	170
Pb	3	6	5	16	7	5	2	5	10	16	3	3	3	3	5	6	5
Sr	1003	1756	1910	2024	1760	961	907	1046	908	1298	902	844	857	922	1054	834	771
Nd	65	107	68	111	69	72	70	99	84	67	83	79	72	86	100	67	72
Zr	289	282	365	267	301	327	321	474	412	385	358	377	345	325	473	352	351
Y	25	39	25	32	24	26	26	32	25	38	26	24	24	26	29	23	23

Continental Nephelinites (CON) - continued

	Etinde, Cameroon														
Sample	C20	C21	C22	C23	C24	C31	C32	C33	C34	C35	C127	C129	C133	C134	C150
(wt.%)															
SiO_2	40.54	40.95	40.43	40.12	40.04	39.04	40.17	40.53	39.94	39.97	37.98	40.39	40.22	39.80	39.60
Al_2O_3	15.31	14.73	14.56	15.24	14.56	15.14	15.37	16.32	14.04	14.86	14.56	15.24	16.47	12.92	12.75
Fe_2O_3	11.44	12.38	12.34	12.28	12.34	11.53	11.24	12.28	12.02	12.30	11.78	11.71	12.30	13.71	13.91
MgO	4.55	4.13	5.26	5.11	5.28	4.69	4.30	4.52	5.27	5.18	5.72	5.09	4.25	8.03	8.03
CaO	13.12	12.96	13.65	13.70	14.01	13.67	13.09	11.92	14.75	13.98	12.17	13.31	11.37	15.64	14.98
Na_2O	4.93	4.80	4.32	4.30	3.47	3.72	3.66	4.09	2.89	3.85	3.21	5.17	4.92	2.46	2.69
K_2O	2.82	2.01	2.93	1.61	2.61	2.70	2.58	3.13	0.68	2.05	2.78	0.58	3.70	0.45	1.66
TiO_2	3.69	3.50	4.04	4.08	4.06	3.70	3.61	3.52	3.66	4.12	3.45	3.90	3.48	4.50	4.49
MnO	0.31	0.42	0.30	0.28	0.30	0.34	0.34	0.30	0.32	0.29	0.36	0.29	0.31	0.20	0.20
P_2O_5	1.07	0.92	1.14	1.21	1.18	1.31	1.08	1.21	0.98	1.32	1.10	1.13	1.20	0.68	0.67
Total	97.77	96.80	98.95	97.93	97.84	95.82	95.45	97.83	94.57	97.92	93.11	96.71	98.21	98.38	98.98
(p.p.m.)															
Cr	11	7	5	4	4	24	12	7	26	0	5	5	10	110	118
Ni	16	13	13	12	14	17	14	15	21	12	10	13	14	44	48
Cu	67	90	67	88	70	47	68	101	67	90	75	95	105	116	117
Zn	140	202	130	123	129	147	152	142	155	124	165	128	139	95	97
V	385	389	432	441	434	381	385	343	455	473	419	411	340	442	448
Sc	11	6	12	12	13	10	8	8	15	13	4	9	7	39	40
Rb	79	49	87	287	83	89	70	142	96	42	119	86	95	73	88
Ba	1349	1289	876	978	1004	1250	1560	1601	761	935	3546	229	1733	686	743
Th	27	16	25	23	25	29	27	22	20	23	20	23	22	7	8
Nb	284	299	224	212	223	295	308	256	225	211	250	218	259	97	97
La	231	174	226	199	225	246	230	196	181	210	196	216	201	100	95
Ce	465	295	444	427	461	481	445	395	362	422	363	459	396	195	199
Pb	6	9	7	5	7	6	6	2	11	5	11	8	4	3	3
Sr	3287	3157	2210	2590	2407	3235	3290	1949	2922	2638	6947	1886	2950	1572	1051
Nd	174	121	191	178	192	182	166	156	139	182	141	181	151	96	94
Zr	735	991	682	630	680	723	775	539	698	621	735	666	527	421	409
Y	55	60	47	47	48	56	59	44	48	45	54	48	44	30	29

Continental Nephelinites (CON) - continued

	Orkney, NE Scotland			Massif Central, France		Monts du Forez, France		Rhine Graben, Germany			
Sample	ORK9	ORK11	ORK12	42974	42466	MC4	MC1	KG5	KT8	G3	KATZ1
(wt.%)											
SiO_2	39.78	39.34	37.43	42.93	43.75	38.06	38.04	40.79	39.18	37.55	38.87
Al_2O_3	10.48	9.71	11.40	9.17	8.89	10.12	9.77	10.00	10.45	12.39	12.82
Fe_2O_3	11.40	10.93	12.37	11.91	11.31	12.10	11.53	12.02	12.17	11.58	14.68
MgO	15.06	15.13	12.13	14.52	13.43	15.35	16.42	15.09	15.43	10.23	4.60
CaO	12.36	13.03	12.86	11.26	11.40	14.04	14.53	11.75	13.15	10.62	7.83
Na_2O	1.78	1.13	2.54	2.19	2.15	2.69	1.81	2.32	2.69	2.46	6.63
K_2O	1.22	1.16	1.27	3.00	3.58	1.61	0.99	0.93	1.61	2.08	3.16
TiO_2	2.23	1.88	2.39	3.54	3.56	3.12	2.88	2.77	2.61	3.37	3.92
MnO	0.19	0.19	0.21	0.16	0.15	0.21	0.20	0.17	0.19	0.17	0.36
P_2O_5	1.30	1.05	1.46	0.80	0.83	1.04	1.04	0.73	0.79	0.54	2.66
Total	95.78	93.55	94.06	99.48	99.04	98.35	97.21	96.56	98.27	90.99	95.52
(p.p.m.)											
Cr	974	881	508	1077	1131	700	807	511	809	160	5
Ni	422	534	267	331	284	345	382	421	380	119	15
Cu	59	53	58	87	75	62	62	83	61	50	94
Zn	81	74	98	86	83	87	83	91	99	90	258
V	240	230	254	293	283	331	334	232	360	332	201
Sc	26	27	21	30	31	31	31	24	33	27	1
Rb	66	52	59	63	85	39	38	31	47	83	101
Ba	1185	1301	1415	715	859	1047	1044	731	1320	618	1861
Th	12	10	13	8	7	11	13	6	10	7	29
Nb	118	78	104	76	76	100	97	75	106	70	256
La	90	78	100	75	84	83	82	54	73	53	219
Ce	161	137	187	153	179	157	158	103	152	96	466
Pb	5	5	6	5	5	4	6	3	4	4	23
Sr	1183	1166	1409	763	794	1309	1413	933	1049	783	3599
Nd	72	64	81	68	73	75	66	45	65	46	227
Zr	303	206	309	376	420	313	291	225	297	256	1312
Y	29	27	32	24	23	29	28	21	24	24	72

Continental Nephelinites (CON) - continued

	Vogelsberg	Eifel, Germany							Hegau, Germany		Frankenwald, Germany	
Sample	KG1	E1	E2	E4	LV2803	LV3415	LV3429	LV3511	LV3512	RG1	RG2	G33	G20
(wt.%)													
SiO_2	37.03	44.22	44.23	38.94	41.11	42.06	41.53	41.93	42.56	38.84	39.00	39.59	39.30
Al_2O_3	8.83	16.66	16.65	13.58	12.10	13.19	13.60	13.25	13.92	9.22	10.43	15.30	15.04
Fe_2O_3	12.01	10.03	10.09	11.25	10.78	10.35	10.64	10.81	10.31	11.43	11.27	11.30	11.31
MgO	18.32	4.25	4.29	9.00	12.06	10.36	9.37	10.77	9.29	18.82	14.86	4.41	4.49
CaO	13.33	10.08	10.03	14.16	13.96	12.75	12.71	12.79	12.62	13.31	15.04	12.91	13.07
Na_2O	2.28	5.49	5.45	3.75	2.91	2.32	2.64	2.80	3.41	2.18	1.82	5.67	5.26
K_2O	1.03	4.57	4.53	3.59	2.69	3.91	4.02	3.06	3.43	1.71	1.33	3.94	3.72
TiO_2	2.24	1.98	1.99	3.00	2.29	2.64	2.74	2.59	2.56	2.36	2.76	2.31	2.34
MnO	0.20	0.26	0.28	0.21	0.22	0.21	0.21	0.20	0.19	0.19	0.20	0.36	0.30
P_2O_5	1.47	0.80	0.80	0.69	0.73	0.58	0.64	0.60	0.61	0.69	0.80	1.16	1.12
Total	96.76	98.33	98.34	98.16	98.84	98.37	98.11	98.77	98.90	98.75	97.50	96.94	95.94
(p.p.m.)													
Cr	738	39	39	120	409	246	233	262	238	1261	763	10	13
Ni	564	25	26	63	175	154	125	130	99	488	271	22	23
Cu	32	34	32	53	64	75	54	62	62	77	75	79	69
Zn	108	98	98	73	70	74	78	78	73	76	83	134	121
V	206	347	344	430	336	387	407	367	353	339	365	404	391
Sc	19	8	7	23	27	22	22	27	31	32	33	9	9
Rb	27	103	103	75	71	104	108	112	104	68	51	95	94
Ba	1145	969	951	1374	1100	1429	1988	794	1104	937	1305	881	931
Th	16	17	17	10	11	10	10	9	11	8	9	21	20
Nb	132	187	188	124	118	105	111	91	104	100	102	239	241
La	112	152	153	75	91	93	88	80	77	77	78	155	149
Ce	211	280	274	152	178	154	157	148	152	136	154	276	285
Pb	1	12	12	2	6	7	8	5	5	4	7	15	11
Sr	2210	2145	2154	1128	1206	764	988	707	984	810	1166	1868	1834
Nd	78	99	97	65	70	65	68	60	62	56	63	103	108
Zr	312	325	326	273	259	242	254	252	262	232	275	361	378
Y	29	38	37	27	27	26	27	25	25	22	25	42	41

Continental Nephelinites (CON) - continued

	Bohemian Massif, Czechoslovakia						Graz Basin, Austria						
Sample	BM9	BM10	BM12	77-101	77-134	77-136	A4	A5	A6	A7	STK210	STK211	STK212
(wt.%)													
SiO_2	36.66	36.69	40.74	39.06	41.34	38.65	39.81	40.81	40.42	39.74	40.40	40.29	40.52
Al_2O_3	12.56	11.41	13.76	10.68	11.36	11.27	13.71	13.96	13.79	13.53	13.84	13.85	13.87
Fe_2O_3	13.81	15.41	12.38	11.80	12.19	13.34	11.29	11.02	11.00	11.45	11.40	11.40	11.29
MgO	5.04	7.20	4.34	17.15	13.69	12.44	6.63	6.26	6.67	6.33	6.34	6.41	6.28
CaO	15.99	16.29	11.97	10.27	12.66	13.22	14.08	12.53	12.96	13.15	13.01	13.03	12.87
Na_2O	3.90	2.47	4.59	2.65	3.91	3.66	5.14	6.81	5.92	6.61	6.36	6.42	6.55
K_2O	0.78	1.10	3.05	1.20	0.98	2.01	1.76	2.58	1.93	2.44	2.81	2.81	2.80
TiO_2	4.83	5.14	3.97	2.54	1.88	3.11	2.00	1.95	1.95	2.00	2.02	2.00	2.01
MnO	0.30	0.25	0.28	0.19	0.20	0.24	0.27	0.26	0.26	0.28	0.27	0.27	0.27
P_2O_5	1.36	1.35	1.26	1.40	0.96	1.00	1.47	1.44	1.41	1.47	1.49	1.51	1.51
Total	95.21	97.30	96.32	96.95	99.17	98.92	96.16	97.62	96.31	97.00	97.93	97.98	97.96
(p.p.m.)													
Cr	23	5	3	567	572	424	69	71	74	69	72	67	65
Ni	11	14	8	364	355	198	57	60	59	57	57	58	57
Cu	127	186	49	75	64	207	25	29	32	29	30	29	32
Zn	117	106	131	88	96	107	105	100	105	104	99	95	99
V	484	491	386	284	215	320	189	179	186	181	186	180	183
Sc	16	23	8	27	29	31	10	11	11	7	11	9	11
Rb	29	54	75	30	70	57	86	101	93	92	104	103	116
Ba	1047	669	989	1222	683	847	1696	1718	1861	1813	1608	1570	1640
Th	13	10	19	17	11	13	17	18	18	17	19	17	18
Nb	133	115	189	109	83	123	140	143	140	143	145	144	150
La	102	90	135	107	71	91	119	124	119	117	119	111	112
Ce	208	184	269	195	136	184	223	224	231	219	221	204	208
Pb	8	2	11	5	4	7	8	8	7	8	7	7	8
Sr	1522	1012	1870	1143	909	902	1687	1694	1834	1795	1760	1772	1801
Nd	96	80	105	73	54	72	92	89	92	92	91	91	92
Zr	459	404	574	241	192	310	367	371	368	376	371	373	371
Y	34	31	43	29	25	29	38	37	37	39	39	39	40

Continental Nephelinites (CON) - continued

	Gardiner, Greenland			Nunatak Zone, Greenland			Tugtilik, Greenland		
Sample	55201E	20385A	29918	200147	240426	240427	20730	20738A	20748
(wt.%)									
SiO_2	39.17	39.02	34.49	40.72	40.01	39.80	44.23	42.58	38.57
Al_2O_3	5.57	4.87	5.49	8.15	5.19	7.51	14.93	9.62	14.82
Fe_2O_3	18.73	17.24	14.28	14.21	14.77	14.90	11.15	10.77	11.54
MgO	14.44	18.31	13.56	13.93	18.60	13.29	5.29	10.68	4.30
CaO	9.97	10.67	8.45	12.83	11.38	12.88	10.01	16.46	10.85
Na_2O	0.97	2.21	3.46	2.66	1.73	2.95	7.34	2.62	7.83
K_2O	1.82	1.13	0.13	0.91	0.68	1.28	1.75	0.43	2.15
TiO_2	6.58	4.12	3.55	3.53	4.58	4.28	1.56	1.52	2.30
MnO	0.21	0.23	0.19	0.23	0.20	0.25	0.20	0.19	0.26
P_2O_5	0.70	0.52	0.42	0.73	0.49	0.98	0.72	0.62	1.10
Total	98.16	98.32	84.03	97.90	97.62	98.10	97.18	95.50	93.71
(p.p.m.)									
Cr	974	818	1133	1528	1631	1212	59	571	12
Ni	774	771	490	350	663	268	43	140	10
Cu	218	244	116	179	200	173	119	130	25
Zn	164	140	103	112	100	118	94	64	106
V	411	317	343	330	303	364	276	314	360
Sc	26	23	24	32	36	31	8	33	1
Rb	53	34	1	42	54	33	26	13	37
Ba	236	375	294	622	579	907	820	854	850
Th	5	4	2	8	7	17	2	4	4
Nb	88	85	34	91	81	125	27	44	51
La	76	50	39	92	73	159	24	35	38
Ce	172	106	83	208	168	374	54	71	82
Pb	9	5	2	5	4	9	8	6	4
Sr	581	776	680	1346	1054	2015	948	862	1337
Nd	89	48	42	101	75	184	30	35	50
Zr	523	339	281	389	437	551	141	122	212
Y	31	23	21	31	24	51	25	24	36

Continental Nephelinites (CON) - continued

Bathhurst Island, NW Territories, Canada

Sample	BI60	BI69	BI136	BI207	BI211	BI213	BI245	BI247	BI253	BI258	BI260	BI266	BI268	BI270	BI272
(wt.%)															
SiO_2	42.03	43.27	40.80	43.54	41.19	41.51	38.63	41.68	38.12	43.08	42.91	41.25	39.87	42.96	40.92
Al_2O_3	13.42	13.34	12.34	13.29	11.88	12.37	12.10	11.82	11.18	13.52	13.06	11.95	11.10	12.69	11.46
Fe_2O_3	10.74	10.58	11.29	10.64	11.46	11.23	11.55	12.00	10.88	10.14	8.88	11.38	11.14	10.41	12.69
MgO	8.53	10.41	12.03	8.45	10.47	11.27	9.91	14.12	12.74	7.38	7.09	9.51	14.00	8.30	13.67
CaO	13.34	12.29	12.48	13.45	14.04	13.10	16.79	12.51	13.42	14.56	16.44	13.13	15.34	13.32	13.23
Na_2O	3.14	3.03	2.22	4.26	3.27	2.84	1.45	2.17	3.48	3.77	2.14	3.07	3.09	3.00	2.97
K_2O	1.85	1.64	1.38	1.15	1.18	1.36	0.78	1.19	0.69	1.43	1.34	1.15	1.32	1.29	1.14
TiO_2	2.02	1.72	1.85	1.69	2.04	2.12	2.00	2.06	2.08	1.67	1.72	1.95	1.74	1.71	2.24
MnO	0.21	0.19	0.20	0.17	0.18	0.19	0.19	0.18	0.18	0.18	0.16	0.18	0.20	0.16	0.18
P_2O_5	0.60	0.62	0.69	0.85	0.56	0.57	1.40	0.57	0.65	0.88	0.71	0.61	0.87	0.62	0.74
Total	95.89	97.09	95.28	97.49	96.27	96.56	94.79	98.31	93.42	96.62	94.46	94.19	98.66	94.46	99.24
(p.p.m.)															
Cr	304	307	346	240	500	481	247	540	319	265	264	274	433	229	324
Ni	200	211	261	157	284	244	169	360	251	165	169	231	280	197	325
Cu	62	57	56	48	63	63	77	69	43	58	50	58	74	65	73
Zn	87	87	75	90	82	88	85	87	72	80	88	84	81	90	85
V	220	186	210	183	238	243	234	236	241	178	173	205	264	191	237
Sc	28	26	22	26	33	34	27	31	34	24	29	26	33	26	28
Rb	62	38	37	49	42	46	25	31	21	23	33	28	32	31	32
Ba	1894	1368	1251	1643	1138	1059	2237	813	1398	2000	5576	1195	1611	1573	1017
Th	9	14	13	16	7	7	25	6	8	18	16	8	13	11	6
Nb	80	109	99	98	65	70	107	62	75	115	90	61	108	71	63
La	62	76	77	120	46	49	177	51	69	134	120	70	98	92	61
Ce	124	137	140	201	96	101	297	99	129	215	175	122	197	148	109
Pb	5	8	6	9	5	5	12	4	3	9	9	6	8	8	4
Sr	1065	1002	977	1429	797	746	1629	754	891	1533	1103	897	1067	1052	858
Nd	54	56	54	74	42	44	104	41	53	80	70	49	76	56	50
Zr	247	276	239	232	210	213	235	182	215	263	236	191	215	207	191
Y	28	25	24	28	25	25	30	23	23	28	27	23	26	25	24

Continental Nephelinites (CON) - continued

	Queensland, E Australia		Tasmania					Otago, N Zealand	Chantaburi-Trat, Thailand				
Sample	Q1	Q2	TAS2	TAS3	TAS6	TAS7	TAS8	OT1	TM1	TM2	NB1-2	NB2	PNR1
(wt.%)													
SiO_2	40.90	40.91	40.76	37.51	41.78	38.20	36.13	40.47	40.64	39.86	40.97	41.30	42.04
Al_2O_3	11.29	11.80	8.73	9.56	11.33	9.53	10.19	12.88	11.64	11.77	12.42	12.69	12.59
Fe_2O_3	11.45	14.12	14.17	14.22	14.52	16.69	15.71	14.52	14.46	14.80	15.04	14.71	11.73
MgO	13.92	10.84	14.80	15.68	11.93	13.80	11.26	8.52	10.76	9.60	8.10	8.16	8.24
CaO	10.88	9.37	12.60	13.09	8.47	10.88	14.87	11.38	9.98	9.97	10.38	10.11	12.10
Na_2O	4.28	4.70	2.85	3.69	4.49	2.87	5.38	4.64	4.00	5.11	4.36	4.30	2.42
K_2O	2.08	2.01	0.94	1.31	2.03	1.43	1.86	1.62	2.39	2.60	1.95	2.00	2.26
TiO_2	2.14	2.28	2.96	2.64	2.64	3.16	2.70	2.79	3.19	3.20	3.28	3.26	2.68
MnO	0.18	0.22	0.21	0.22	0.21	0.23	0.27	0.25	0.20	0.21	0.20	0.20	0.18
P_2O_5	1.17	1.25	1.24	1.31	1.33	1.10	1.45	1.23	1.24	1.35	1.33	1.25	0.88
Total	98.29	97.49	99.26	99.23	98.72	97.89	99.82	98.28	98.50	98.45	98.02	97.97	95.10
(p.p.m.)													
Cr	467	336	632	500	453	428	185	180	177	132	59	63	192
Ni	364	272	403	412	386	348	162	129	201	150	90	94	141
Cu	53	47	61	64	40	48	87	51	47	47	47	47	57
Zn	105	149	129	122	163	162	152	133	134	157	159	150	113
V	176	139	236	236	146	198	224	203	239	206	201	200	177
Sc	16	8	20	21	10	14	18	11	15	10	10	12	15
Rb	27	39	17	21	25	9	38	40	89	43	50	53	37
Ba	401	1042	392	390	330	288	722	670	610	760	703	735	516
Th	10	16	9	11	7	8	16	13	11	11	10	11	8
Nb	102	124	86	104	83	92	164	110	95	101	96	96	71
La	66	109	77	81	61	67	93	118	64	69	70	72	46
Ce	138	202	155	145	133	132	172	211	119	133	135	131	100
Pb	1	7	5	4	4	4	7	6	3	6	4	4	4
Sr	1344	1762	1019	1324	1335	1360	1424	1311	1184	1238	1406	1409	995
Nd	52	77	75	60	66	63	76	87	63	65	69	66	47
Zr	276	399	384	262	378	363	356	306	356	380	372	364	295
Y	24	26	35	30	27	28	36	36	32	33	33	33	28

Continental Nephelinites (CON) - continued

	Raton-Clayton, New Mexico											Wildcat Peak, Arizona
Sample	855284	8551861	NM98A	NM98AL	NM98B	NM99	NM100	NM101	NM103	NM104	NM105	AZ101
(wt.%)												
SiO_2	36.84	40.26	37.17	38.60	37.57	36.93	40.76	41.78	42.08	36.77	40.79	39.52
Al_2O_3	12.63	12.76	12.62	11.32	12.72	12.11	13.37	13.90	13.88	11.60	12.80	9.83
Fe_2O_3	12.66	12.62	12.40	13.59	12.49	12.17	10.98	11.04	11.02	11.16	12.25	11.66
MgO	8.84	9.53	9.53	10.60	9.55	10.19	9.72	10.03	10.81	11.08	9.97	12.14
CaO	15.61	13.01	15.66	15.32	15.66	15.74	13.20	13.04	13.08	16.26	13.49	14.55
Na_2O	4.97	4.23	4.86	4.07	5.05	4.62	3.93	4.57	4.04	4.18	3.38	3.01
K_2O	1.52	1.69	1.47	1.24	1.51	1.45	2.09	1.64	1.26	1.35	1.57	1.64
TiO_2	1.33	2.00	1.32	1.48	1.34	1.33	1.71	1.65	1.68	1.37	2.00	2.54
MnO	0.29	0.21	0.28	0.31	0.29	0.29	0.22	0.23	0.21	0.25	0.22	0.18
P_2O_5	2.50	2.01	2.62	2.24	2.64	3.07	1.93	1.78	1.75	2.30	2.08	1.74
Total	97.19	98.30	97.94	98.77	98.82	97.91	97.90	99.65	99.81	96.31	98.54	96.81
(p.p.m.)												
Cr	99	219	98	113	93	126	203	216	250	315	199	513
Ni	150	157	154	173	146	182	157	174	197	232	154	233
Cu	57	48	57	52	58	38	48	39	41	63	46	119
Zn	121	119	119	124	119	125	98	97	94	103	116	120
V	203	235	199	224	199	196	213	219	216	204	233	241
Sc	16	17	21	26	24	23	26	26	26	25	25	21
Rb	27	31	25	22	26	25	20	20	16	22	36	31
Ba	1991	1977	2429	2612	2248	2414	1976	1966	2238	1969	2327	3905
Th	30	15	30	26	30	30	17	19	17	26	15	22
Nb	75	69	74	83	74	83	58	55	46	60	70	51
La	239	132	237	219	252	262	136	148	115	200	137	218
Ce	424	238	435	392	448	481	249	270	219	358	251	457
Pb	13	13	14	13	9	9	12	12	10	11	13	16
Sr	3128	2564	2926	2620	3327	3519	2617	2599	2043	2472	2380	2113
Nd	160	101	168	157	171	185	109	112	96	136	106	233
Zr	247	257	346	357	365	453	373	356	274	287	341	368
Y	51	37	51	50	51	52	37	39	34	41	38	46

Continental Nephelinites (CON) - continued

	Woodruff Butte, Arizona	Hopi Buttes, Arizona				Balcones, Texas					
Sample	AZ162	AZ19	AZ20	AZ21	AZ69	TX3	473	529	767	82005	82020
(wt.%)											
SiO_2	38.55	40.44	42.56	41.54	41.17	38.21	39.02	37.92	38.93	38.28	38.29
Al_2O_3	9.50	11.91	10.27	11.50	11.08	10.52	10.13	10.31	10.38	9.70	9.88
Fe_2O_3	12.51	12.75	12.35	14.09	13.81	13.13	12.55	12.72	13.24	12.91	12.84
MgO	16.07	5.77	12.51	9.57	9.80	14.02	14.87	14.75	14.17	15.44	15.16
CaO	14.06	11.76	11.28	11.01	10.75	12.96	13.90	14.59	12.74	14.58	13.12
Na_2O	2.82	4.47	2.35	2.91	3.34	3.45	2.96	2.83	3.27	2.57	3.07
K_2O	0.60	1.75	1.90	2.23	1.63	0.93	0.99	0.81	0.83	0.96	1.08
TiO_2	2.46	3.54	3.33	4.21	3.75	4.11	3.05	3.19	3.75	3.10	3.64
MnO	0.19	0.23	0.17	0.18	0.20	0.19	0.20	0.20	0.19	0.18	0.21
P_2O_5	1.20	2.31	0.88	1.14	1.45	0.81	0.82	1.02	0.73	0.83	0.77
Total	97.96	94.93	97.62	98.37	96.97	97.14	98.49	98.35	98.23	98.55	98.04
(p.p.m.)											
Cr	561	44	451	229	218	451	599	478	484	529	576
Ni	457	33	362	185	181	293	337	314	332	303	386
Cu	70	24	81	72	62	58	66	55	62	55	54
Zn	104	208	105	134	140	107	93	93	104	100	111
V	245	176	260	275	252	326	289	280	302	276	301
Sc	21	11	22	20	18	20	23	20	22	20	24
Rb	10	4	32	35	29	23	25	22	16	26	31
Ba	1792	1137	1016	1089	987	461	477	427	409	580	486
Th	16	22	9	8	14	6	7	5	6	5	8
Nb	85	170	68	85	104	73	68	65	70	61	71
La	95	191	82	79	108	50	48	52	53	58	53
Ce	189	412	154	162	222	107	82	96	97	92	102
Pb	6	9	5	5	7	3	4	2	3	2	4
Sr	1385	2703	1272	1486	1514	944	1093	1123	847	892	940
Nd	85	190	69	86	109	45	43	50	49	49	52
Zr	257	1040	344	435	518	308	225	265	277	240	282
Y	26	62	27	32	37	27	23	26	27	25	29

Potassic Continental Rocks (COK)

New South Wales, E Australia

Sample	NSW5	NSW6	NSW1	NSW2	NSW3	NSW4
(wt.%)						
SiO_2	46.54	43.11	44.92	45.00	44.97	45.01
Al_2O_3	9.42	8.96	8.33	8.77	8.81	10.73
Fe_2O_3	10.60	12.01	11.53	11.56	11.60	10.36
MgO	10.73	12.09	10.37	11.65	11.25	8.52
CaO	7.33	8.56	8.62	8.04	8.10	8.41
Na_2O	1.74	2.71	1.36	2.17	2.25	1.16
K_2O	6.24	4.86	6.38	5.59	5.65	7.31
TiO_2	4.27	4.62	5.25	4.64	4.72	4.33
MnO	0.13	0.16	0.14	0.16	0.14	0.14
P_2O_5	1.16	1.04	0.69	1.01	1.05	0.83
Total	98.17	98.12	97.59	98.57	98.54	96.80
(p.p.m.)						
Cr	355	408	281	468	449	182
Ni	303	302	308	396	391	254
Cu	38	61	61	46	49	69
Zn	121	119	111	113	114	107
V	175	242	214	207	210	228
Sc	13	21	17	18	17	19
Rb	119	114	224	106	135	255
Ba	1644	1560	1785	1069	1104	3643
Th	9	9	18	9	9	14
Nb	95	104	148	102	104	126
La	114	106	192	119	110	140
Ce	241	225	360	236	222	255
Pb	10	11	16	10	9	15
Sr	1686	1375	1724	1111	1093	2231
Nd	108	108	152	118	121	108
Zr	701	708	653	705	724	598
Y	28	30	32	29	31	33

Potassic Continental Rocks (COK) - continued

	Western Rift, Uganda																	
Sample	15010A	C4407	C4409	C4414	C3946	C3948	C3994	C4078	C6073	C6143	C4788	C4793	C4801	C5963	C5967	C6066	C3991	C4774
(wt.%)																		
SiO_2	36.77	36.63	35.80	36.07	36.29	36.97	40.69	41.08	40.31	40.69	39.11	37.15	36.29	38.80	37.75	40.15	39.72	41.02
Al_2O_3	6.24	6.74	6.22	6.11	6.53	7.01	5.92	7.67	7.41	7.70	8.16	6.76	6.71	7.96	7.56	7.49	7.49	5.65
Fe_2O_3	12.36	12.24	12.82	12.59	12.37	11.89	11.18	10.27	10.30	10.37	12.24	12.55	12.35	12.06	12.22	10.62	11.31	11.32
MgO	13.80	14.00	13.74	13.77	13.82	14.16	22.69	17.24	17.62	17.28	9.78	12.72	12.26	9.45	10.62	16.67	14.35	22.69
CaO	14.61	16.42	17.38	16.77	17.15	16.10	7.24	10.58	10.36	10.43	14.22	13.23	12.76	13.42	14.00	10.34	10.74	8.28
Na_2O	0.95	1.42	0.98	1.03	1.39	1.83	0.64	0.72	0.64	0.74	1.37	0.65	0.53	1.70	1.26	0.96	1.24	0.86
K_2O	5.20	4.31	3.52	4.58	2.20	3.31	4.77	6.55	6.94	6.66	5.61	5.93	6.95	6.00	4.92	7.03	6.61	3.26
TiO_2	4.43	4.24	4.67	4.45	4.30	4.01	4.67	3.45	3.41	3.43	4.66	5.65	5.83	4.47	4.74	3.33	5.00	3.87
MnO	0.23	0.21	0.23	0.22	0.22	0.20	0.15	0.16	0.17	0.16	0.22	0.21	0.19	0.21	0.21	0.17	0.17	0.14
P_2O_5	1.07	0.99	0.96	1.03	0.99	0.95	0.16	0.51	0.71	0.50	1.04	1.33	1.16	1.25	1.30	0.46	0.59	0.34
Total	95.67	97.18	96.30	96.62	95.24	96.43	98.09	98.22	97.88	97.94	96.40	96.18	95.02	95.32	94.58	97.22	97.21	97.41
(p.p.m.)																		
Cr	551	646	611	579	566	630	1065	907	936	942	164	542	868	169	180	837	700	1057
Ni	258	256	236	246	235	247	923	478	514	492	83	167	196	75	81	486	371	934
Cu	114	128	138	136	126	116	48	53	77	64	160	148	146	150	159	92	109	78
Zn	94	96	105	102	98	92	68	73	71	77	90	88	87	100	102	75	87	80
V	244	187	172	251	194	220	154	225	222	235	194	174	151	277	273	196	189	149
Sc	35	31	30	29	24	31	15	24	25	26	18	20	19	15	20	20	18	17
Rb	122	117	122	120	104	115	205	186	193	187	124	163	201	130	101	192	158	175
Ba	2410	2333	2385	2318	2584	2408	1830	3216	3126	2416	2771	3129	3261	2762	2720	3467	2131	1464
Th	32	30	33	33	28	25	14	21	22	21	30	26	24	30	28	22	19	9
Nb	242	224	250	247	223	206	125	152	156	150	262	246	239	257	257	151	178	101
La	188	248	246	205	243	225	121	141	153	110	230	222	230	237	240	146	149	82
Ce	371	474	501	422	494	471	227	289	312	224	476	461	453	484	480	298	298	176
Pb	5	8	9	8	9	7	4	7	8	8	12	8	9	9	10	7	6	3
Sr	3559	2663	2698	2962	2607	2618	1041	1560	1383	1647	2951	3095	2675	2859	2687	1512	1798	1151
Nd	138	177	192	152	186	177	81	113	120	84	181	177	172	180	186	114	114	66
Zr	381	334	375	379	335	304	213	256	235	253	538	469	478	513	511	260	347	167
Y	20	17	19	20	19	18	10	15	15	15	22	20	18	22	21	17	15	9

Potassic Continental Rocks (COK) - continued

Western Rift, Uganda - continued

Sample	C6095	C6098	C6099	C5545	C5621	C5994	C5549	C5566	C5595	C5619	C5620	C5624	C5775	C5783	C5805	C5809	C5812	C5816
(wt.%)																		
SiO_2	40.75	41.58	41.84	39.74	39.99	41.12	39.58	37.54	39.75	42.03	39.08	36.85	32.29	40.75	42.81	37.39	37.30	39.01
Al_2O_3	7.22	7.83	6.26	10.73	8.51	5.45	6.30	9.60	6.81	8.75	10.18	8.99	5.69	11.03	8.40	9.56	7.69	8.72
Fe_2O_3	11.15	11.15	11.93	13.88	14.15	10.87	15.43	14.27	14.67	13.38	13.84	14.08	12.62	13.71	13.18	14.80	13.86	14.35
MgO	16.77	16.25	20.89	4.91	7.86	23.73	11.03	5.68	11.11	9.79	6.35	6.17	14.78	5.00	9.00	5.99	9.56	7.68
CaO	9.20	9.00	7.36	13.08	14.86	8.50	16.29	13.52	15.81	13.22	13.14	14.58	15.02	12.43	13.43	14.55	16.19	14.38
Na_2O	0.82	2.39	0.77	3.51	1.81	1.34	1.49	3.91	1.29	1.59	2.59	2.47	1.43	3.12	3.35	2.57	2.07	2.12
K_2O	5.15	2.88	5.01	4.46	3.69	1.26	2.28	4.27	2.15	3.99	5.29	5.34	2.51	4.88	1.41	3.86	4.31	4.26
TiO_2	5.21	4.90	4.10	5.13	5.68	3.80	5.36	5.36	5.13	4.75	6.02	5.38	4.94	5.31	4.63	5.53	5.61	5.72
MnO	0.14	0.14	0.15	0.26	0.21	0.14	0.19	0.26	0.18	0.19	0.24	0.25	0.21	0.25	0.20	0.26	0.21	0.22
P_2O_5	0.22	0.19	0.31	1.20	0.85	0.37	0.38	1.30	0.49	0.55	1.06	1.30	1.08	1.16	0.58	1.38	0.90	0.82
Total	96.64	96.32	98.61	96.88	97.60	96.56	98.32	95.71	97.39	98.25	97.79	95.40	90.56	97.64	96.98	95.87	97.69	97.27
(p.p.m.)																		
Cr	912	837	1240	25	131	1228	421	7	523	384	43	10	579	52	420	15	344	278
Ni	494	461	833	24	53	904	106	22	126	110	37	29	163	33	106	26	99	50
Cu	92	91	94	121	166	71	84	227	105	131	200	199	137	97	140	238	159	159
Zn	80	80	74	129	93	81	66	123	76	79	100	113	87	115	79	121	87	94
V	184	183	177	514	530	163	350	532	380	398	530	510	379	481	371	536	428	479
Sc	16	17	17	13	25	19	39	9	37	28	12	13	31	10	21	14	26	24
Rb	181	109	174	102	94	170	71	90	79	106	140	91	81	118	91	69	94	109
Ba	3320	2200	1191	1818	1819	1338	973	1974	2077	1303	2060	2166	2549	1642	2416	3590	1379	1796
Th	12	13	9	26	26	10	11	12	11	17	29	11	28	30	19	14	24	22
Nb	136	133	97	271	199	94	104	252	114	140	244	243	207	250	152	259	217	192
La	117	111	77	213	148	82	80	167	90	115	214	164	205	176	117	176	166	172
Ce	224	217	153	404	281	177	156	279	158	231	442	292	403	337	224	319	331	346
Pb	6	5	4	14	9	3	3	14	5	6	11	13	10	13	8	14	6	10
Sr	2031	1798	673	3127	1908	4772	1071	2491	1926	1329	2277	2537	2204	2676	2195	2945	2199	1644
Nd	93	86	56	145	105	71	69	104	65	98	175	107	162	128	84	113	128	136
Zr	300	285	150	571	408	179	240	579	258	277	474	538	428	544	307	605	432	416
Y	13	13	9	26	21	10	13	25	15	17	24	23	23	27	17	25	22	20

Potassic Continental Rocks (COK) - continued

Western Rift, Uganda - continued

Sample	C1001	C5791	C2815	C1943	C2782	C2787	C2792	C2813	C2820	C2838	C3023	C9872	C2870	WR1	WR2	WR3	WR7
(wt.%)																	
SiO_2	39.85	43.68	45.30	43.76	44.15	45.37	43.52	44.27	43.77	43.62	38.42	39.05	43.61	42.91	39.33	44.52	44.77
Al_2O_3	6.49	9.10	10.27	10.29	14.08	10.80	12.17	11.54	12.37	12.47	14.95	14.76	13.93	6.68	14.85	10.80	10.35
Fe_2O_3	14.86	12.53	11.58	11.84	11.81	12.02	12.23	12.76	12.16	13.16	14.50	14.05	12.86	12.16	13.55	12.36	12.14
MgO	10.89	9.88	9.78	11.40	6.31	11.84	10.22	11.80	10.21	8.16	4.16	4.47	7.35	18.51	4.19	12.61	12.88
CaO	16.57	12.41	12.47	13.18	10.36	11.19	10.14	10.91	9.92	11.30	12.10	12.53	10.18	9.37	11.91	11.58	11.53
Na_2O	1.54	2.30	1.93	2.25	4.07	2.14	3.22	2.45	3.34	2.64	4.83	4.70	3.02	1.33	5.84	1.81	1.89
K_2O	1.64	4.09	3.45	3.13	4.25	2.96	3.63	2.58	3.74	3.38	4.77	4.72	3.92	3.21	5.36	2.50	2.69
TiO_2	5.14	4.27	3.89	3.26	3.19	2.83	3.21	2.93	3.12	3.69	3.20	3.21	3.70	3.94	2.81	2.98	2.85
MnO	0.19	0.19	0.16	0.18	0.21	0.19	0.20	0.19	0.20	0.21	0.29	0.28	0.21	0.17	0.31	0.19	0.19
P_2O_5	0.41	0.56	0.50	0.54	0.87	0.51	0.71	0.47	0.72	0.62	1.77	1.69	0.73	0.49	1.47	0.51	0.47
Total	97.59	99.00	99.29	99.83	99.28	99.84	99.24	99.91	99.55	99.24	98.99	99.46	99.50	98.77	99.62	99.86	99.77
(p.p.m.)																	
Cr	481	519	779	857	140	901	657	937	671	335	7	5	207	1205	2	932	982
Ni	120	133	160	206	59	233	223	278	230	69	27	27	71	641	34	243	255
Cu	91	125	99	75	44	60	50	67	47	39	180	142	41	87	177	40	41
Zn	81	79	76	78	97	82	102	94	101	97	126	128	103	81	127	87	84
V	422	357	363	325	277	297	281	296	283	364	303	317	335	243	287	330	322
Sc	43	26	35	26	13	24	18	27	18	26	0	0	19	25	9	37	38
Rb	51	105	134	96	114	90	100	71	100	119	111	113	106	96	133	125	125
Ba	953	1321	1286	1213	1475	1069	1295	901	1256	1065	1932	1651	1269	3229	2248	919	951
Th	11	19	16	10	25	13	22	10	21	13	18	18	16	10	23	12	12
Nb	106	138	112	93	164	84	139	77	142	111	188	180	125	111	243	86	81
La	93	135	92	84	131	83	117	68	121	91	161	142	108	75	182	77	75
Ce	177	261	170	159	257	156	228	125	236	160	306	277	205	139	347	147	153
Pb	4	7	8	5	12	7	10	7	12	9	4	5	9	4	5	6	6
Sr	1627	1303	848	877	1553	878	1260	781	1245	1060	2362	2174	1193	927	2790	768	800
Nd	70	110	73	67	104	70	98	58	96	78	123	125	87	64	135	64	63
Zr	242	294	267	250	420	252	355	241	363	310	370	377	344	272	438	267	260
Y	13	17	22	24	33	24	28	25	30	29	40	40	31	16	41	25	24

Olivine-poor Continental Nephelinites (COP)

	Riwa, N Kenya	Lodwar, N Kenya	Moroto,E Uganda		Napak, E Uganda				Elgon, E Uganda	
Sample	RIWA2	LOD1	V151A	V171	SUN4	SUN21	SUN189	SUN193	ELG3	ELG4
(wt.%)										
SiO_2	41.80	39.92	43.13	42.39	45.26	42.56	40.42	39.79	40.02	42.02
Al_2O_3	12.63	11.73	14.42	14.70	16.17	13.63	14.40	13.80	15.54	13.95
Fe_2O_3	15.18	14.71	13.67	13.71	11.58	14.48	12.04	12.85	11.76	12.77
MgO	5.86	6.98	5.95	3.19	2.80	5.22	5.23	4.78	3.93	5.59
CaO	11.16	12.78	9.94	9.60	9.39	10.76	13.22	13.45	11.69	9.38
Na_2O	5.46	5.30	4.95	7.22	4.89	4.58	6.24	5.36	6.98	5.36
K_2O	2.05	2.22	2.02	3.05	3.23	2.50	2.20	2.59	2.71	2.63
TiO_2	2.92	4.04	2.31	2.53	1.94	2.48	2.38	2.29	2.44	2.42
MnO	0.27	0.23	0.21	0.27	0.25	0.23	0.19	0.22	0.24	0.37
P_2O_5	0.75	0.81	0.61	0.76	0.71	0.79	0.75	0.90	0.84	1.19
Total	98.09	98.72	97.21	97.41	96.22	97.23	97.05	96.04	96.16	95.68
(p.p.m.)										
Cr	11	67	21	6	9	11	7	5	6	2
Ni	27	55	27	16	7	12	7	9	11	8
Cu	195	129	84	192	39	158	162	194	219	272
Zn	141	114	115	148	144	133	110	131	125	172
V	303	377	255	241	161	266	290	302	316	334
Sc	12	20	18	5	3	16	17	13	4	3
Rb	56	34	40	69	86	55	49	68	104	84
Ba	685	691	1151	928	1512	1152	532	763	926	2863
Th	13	15	6	11	15	7	10	11	11	12
Nb	126	143	55	107	107	73	84	93	98	158
La	96	108	50	84	98	72	68	80	72	113
Ce	185	213	104	157	174	127	148	142	131	193
Pb	16	6	5	6	12	11	8	9	10	9
Sr	1294	1107	1140	1202	1627	1267	752	1029	1099	1619
Nd	78	88	48	65	69	56	60	61	49	76
Zr	325	360	176	296	273	206	180	189	195	336
Y	34	35	23	37	31	26	24	28	27	44

Olivine-poor Continental Nephelinites (COP) - continued

	Homa Mtn, Nyanza, Kenya						Rangwa-Kisingiri, Nyanza, Kenya				
Sample	HC420	HC474	H182	HF218	HF231	HF608	RR85	RR198	RR585	RR657	RR674
(wt.%)											
SiO_2	48.05	47.46	42.73	49.70	49.49	49.41	41.04	48.92	44.73	42.52	42.63
Al_2O_3	18.12	17.28	11.48	18.70	18.51	18.85	14.11	16.37	14.32	14.32	13.61
Fe_2O_3	5.91	6.84	11.21	5.78	5.92	5.42	12.69	9.46	12.93	12.75	13.30
MgO	1.92	3.13	5.42	1.44	1.65	0.97	4.68	0.74	4.29	5.27	4.69
CaO	6.04	6.91	12.69	4.65	5.61	5.27	11.99	4.92	8.94	10.87	11.48
Na_2O	8.29	8.27	5.51	9.70	8.62	8.36	4.87	9.99	6.51	5.66	5.84
K_2O	4.22	4.13	0.79	4.56	4.48	4.86	2.48	5.00	2.48	2.37	1.87
TiO_2	0.97	1.24	2.76	0.86	0.90	0.68	3.04	1.25	2.62	2.77	2.83
MnO	0.23	0.18	0.21	0.18	0.19	0.21	0.23	0.21	0.22	0.25	0.25
P_2O_5	0.25	0.33	0.77	0.23	0.22	0.21	0.99	0.13	0.82	1.10	0.84
Total	93.99	95.75	93.57	95.78	95.58	94.23	96.11	97.00	97.85	97.88	97.33
(p.p.m.)											
Cr	56	97	81	43	48	19	7	8	11	11	30
Ni	15	25	36	12	14	7	6	7	22	18	23
Cu	20	32	125	14	16	7	213	32	111	167	100
Zn	160	152	110	148	150	164	125	150	119	116	140
V	125	146	292	112	123	88	302	204	235	257	266
Sc	1	3	17	2	2	1	11	0	8	8	10
Rb	81	89	38	93	95	132	56	110	62	56	51
Ba	9943	7809	1769	5361	1072	1042	923	2631	1052	1590	892
Th	53	50	17	51	51	54	20	14	12	12	15
Nb	704	663	124	739	739	779	155	111	102	114	121
La	129	165	106	96	127	208	132	93	91	99	108
Ce	193	265	207	169	218	323	257	149	166	196	204
Pb	18	17	13	16	18	21	11	34	12	12	12
Sr	790	975	1855	826	1399	1102	2024	1923	1307	1575	1657
Nd	86	87	81	60	65	87	105	46	71	82	88
Zr	821	759	304	912	869	887	378	375	315	349	352
Y	22	23	27	20	21	24	38	25	31	36	36

Olivine-poor Continental Nephelinites (COP) - continued

	N Ruri Hills, Nyanza, Kenya	Londiani, Nyanza, Kenya	Narok-Nguruman, S Kenya	
Sample	N90	14-1034	SK293-1	SK451-1
(wt.%)				
SiO_2	49.40	43.70	42.59	42.64
Al_2O_3	18.70	13.51	20.95	21.08
Fe_2O_3	6.23	11.94	8.48	8.40
MgO	0.79	1.28	3.28	2.46
CaO	5.86	10.48	6.18	6.16
Na_2O	9.25	6.02	7.65	8.22
K_2O	4.32	3.23	3.74	4.15
TiO_2	1.04	1.37	2.47	2.41
MnO	0.20	0.48	0.21	0.23
P_2O_5	0.39	0.41	0.66	0.76
Total	96.16	92.42	96.20	96.51
(p.p.m.)				
Cr	8	7	0	0
Ni	5	5	5	6
Cu	40	24	142	140
Zn	142	212	148	138
V	111	465	181	183
Sc	0	0	2	0
Rb	92	82	69	78
Ba	1905	2923	1322	1609
Th	31	14	13	14
Nb	195	323	175	168
La	149	180	84	71
Ce	252	241	155	138
Pb	24	26	4	5
Sr	2000	4567	1527	1439
Nd	71	54	57	49
Zr	431	381	505	468
Y	31	26	40	40

Olivine-poor Continental Nephelinites (COP) - continued

	Burko, N Tanzania			Makuyuni Jctn, N Tanzania	Hanang, N Tanzania							
Sample	BD439	BD445	BD450	MANY2	HCT779	HCT782	HCT785	HCT787	HCT791	HCT798	HCT799	HCT803
(wt.%)												
SiO_2	44.43	44.13	45.31	47.66	43.94	45.20	46.95	48.15	49.74	46.51	49.70	43.77
Al_2O_3	16.07	16.32	17.16	16.66	11.67	11.78	13.62	14.96	13.84	12.60	14.08	13.88
Fe_2O_3	8.36	8.89	7.19	7.10	10.58	10.03	10.12	9.02	8.52	9.56	8.47	9.52
MgO	2.76	2.15	0.95	0.58	2.03	1.91	1.39	1.23	2.08	1.43	2.09	1.62
CaO	8.60	9.13	10.18	5.58	15.18	14.63	10.08	7.33	7.15	12.07	7.40	10.28
Na_2O	5.22	6.69	9.71	8.72	6.29	4.56	8.11	10.03	7.00	6.67	7.17	8.56
K_2O	5.01	4.66	4.40	3.92	3.11	3.06	2.90	4.18	4.79	3.57	4.84	3.45
TiO_2	1.22	1.74	0.94	0.71	1.49	1.43	1.30	1.14	1.18	1.23	1.19	1.35
MnO	0.32	0.29	0.31	0.23	0.32	0.30	0.31	0.28	0.27	0.30	0.24	0.29
P_2O_5	0.44	0.43	0.67	0.17	0.98	0.94	0.44	0.29	0.37	0.54	0.37	0.51
Total	92.42	94.42	96.82	91.32	95.58	93.83	95.22	96.59	94.94	94.47	95.53	93.22
(p.p.m.)												
Cr	3	4	4	1	5	5	7	2	7	9	4	8
Ni	6	6	5	4	7	5	7	4	6	7	7	9
Cu	26	37	22	22	116	94	58	40	55	70	48	37
Zn	230	197	209	183	182	193	229	212	183	200	177	190
V	170	179	85	64	302	263	232	193	162	251	163	205
Sc	0	3	0	0	1	5	0	1	2	2	1	4
Rb	108	75	88	94	77	89	78	132	162	125	157	65
Ba	2725	2032	1857	1962	1739	1867	1884	1858	2672	2032	2343	2815
Th	27	35	55	44	7	8	10	12	14	9	14	11
Nb	240	272	300	170	168	163	184	169	145	178	146	185
La	195	243	345	203	79	88	104	101	341	120	98	138
Ce	295	387	616	326	120	124	138	137	137	157	136	197
Pb	39	25	34	35	26	31	36	38	33	36	33	31
Sr	5553	4602	3650	1397	2596	2608	2999	2730	3659	3219	3666	2823
Nd	86	121	199	88	43	42	47	52	80	53	47	67
Zr	924	839	855	393	596	594	650	631	576	509	582	564
Y	41	48	67	45	36	36	35	30	94	32	32	38

Olivine-poor Continental Nephelinites (COP) - continued

	Chilwa Province, Malawi			Dorowa-Shawa, Zimbabwe		Nuanetsi Province, Zimbabwe				
Sample	MAL3	MAL5	MAL9	DS1	DS2	NTS8	NTS14	NTS200	NTS206	NTS221
(wt.%)										
SiO_2	40.24	41.03	45.30	43.87	46.02	41.56	43.76	44.84	41.29	44.15
Al_2O_3	13.90	15.09	15.88	15.33	16.06	11.65	15.77	15.77	12.35	16.29
Fe_2O_3	13.81	8.85	10.48	10.76	7.28	15.81	11.76	10.14	14.41	9.95
MgO	3.85	1.97	4.37	4.15	3.70	5.64	4.28	3.36	5.90	3.38
CaO	9.77	8.53	8.18	5.44	7.60	8.77	5.53	3.69	7.77	3.65
Na_2O	5.52	7.52	6.40	10.40	10.84	6.25	7.79	10.09	7.18	9.78
K_2O	1.98	3.51	4.39	2.73	1.62	2.33	3.94	1.73	2.98	1.75
TiO_2	3.58	2.22	2.82	3.12	0.60	4.31	3.07	2.91	3.82	2.86
MnO	0.27	0.47	0.23	0.22	0.16	0.21	0.19	0.21	0.22	0.21
P_2O_5	1.98	0.64	0.79	0.85	1.40	0.92	1.04	1.34	0.92	1.37
Total	94.90	89.82	98.84	96.87	95.27	97.43	97.12	94.05	96.83	93.38
(p.p.m.)										
Cr	4	2	54	18	19	18	69	2	59	3
Ni	6	4	53	22	21	44	39	9	49	12
Cu	11	4	34	179	30	305	160	136	275	137
Zn	137	176	109	156	102	131	125	147	140	145
V	190	180	157	255	87	489	236	257	433	245
Sc	6	0	12	1	5	9	2	-2	9	0
Rb	89	104	91	77	30	69	103	34	84	41
Ba	1567	4729	1241	2371	1004	1519	1923	3487	1884	4713
Th	18	0	6	17	1	10	12	20	11	19
Nb	149	299	121	256	53	145	219	293	198	273
La	143	185	103	104	12	81	82	109	91	109
Ce	289	329	229	187	28	132	147	185	166	188
Pb	8	12	6	23	23	17	19	25	17	23
Sr	1607	3761	1789	1734	861	1531	1899	2469	1844	2704
Nd	137	114	101	67	17	52	60	66	60	68
Zr	612	1346	638	389	177	289	424	423	328	388
Y	48	67	43	39	17	26	31	33	27	34

Olivine-poor Continental Nephelinites (COP) - continued

	Etinde, Cameroon											
Sample	C20	C21	C22	C33	C126	C128	C129	C130	C131	C132	C133	C152
(wt.%)												
SiO_2	40.54	40.95	40.43	40.53	38.60	41.76	40.39	38.76	42.66	39.91	40.22	39.99
Al_2O_3	15.31	14.73	14.56	16.32	15.00	16.58	15.24	15.05	17.39	17.61	16.47	17.54
Fe_2O_3	11.44	12.38	12.34	12.28	11.62	10.65	11.71	11.77	9.95	9.60	12.30	9.69
MgO	4.55	4.13	5.26	4.52	3.78	3.79	5.00	3.30	2.71	3.70	4.25	3.74
CaO	13.12	12.96	13.65	11.92	12.20	11.31	13.31	13.02	8.79	10.94	11.37	10.87
Na_2O	4.93	4.80	4.32	4.09	5.46	6.07	5.17	5.76	6.41	7.17	4.92	6.95
K_2O	2.82	2.01	2.93	3.13	2.75	1.20	0.58	3.59	4.48	3.50	3.70	3.87
TiO_2	3.69	3.50	4.04	3.52	3.26	3.51	3.90	3.31	2.55	2.92	3.48	2.95
MnO	0.31	0.42	0.30	0.30	0.43	0.30	0.29	0.44	0.38	0.30	0.31	0.29
P_2O_5	1.07	0.92	1.14	1.21	0.92	0.94	1.13	0.95	0.68	0.90	1.20	0.89
Total	97.77	96.80	98.95	97.83	94.02	96.10	96.71	95.95	95.99	96.55	98.21	96.77
(p.p.m.)												
Cr	11	7	5	7	5	4	5	6	4	3	10	3
Ni	16	13	13	15	7	9	13	8	9	11	14	11
Cu	67	90	67	101	36	47	95	35	44	87	105	86
Zn	140	202	130	142	206	134	128	210	193	141	139	136
V	385	389	432	343	350	385	411	362	378	332	340	323
Sc	11	6	12	8	2	6	9	0	3	5	7	5
Rb	79	49	87	142	92	89	86	93	345	98	95	110
Ba	1349	1289	876	1601	1800	1099	229	1594	1203	846	1733	961
Th	27	16	25	22	16	30	23	15	15	23	22	24
Nb	284	299	224	256	317	272	218	333	316	280	259	276
La	231	174	226	196	202	244	216	222	156	217	201	210
Ce	465	295	444	395	360	472	459	399	280	407	396	395
Pb	6	9	7	2	15	8	8	14	20	12	4	12
Sr	3287	3157	2210	1949	6178	3606	1886	3610	2836	2145	2950	2399
Nd	174	121	191	156	131	182	181	143	97	150	151	150
Zr	735	991	682	539	1007	736	666	1010	904	631	527	633
Y	55	60	47	44	65	52	48	66	54	46	44	46

Olivine-poor Continental Nephelinites (COP) - continued

	Eifel, Germany				Frankenwald, Germany				Rhine Graben, Germany	
Sample	G30	E1	E2	E4	G31	G32	G33	G20	KATZ1	RG6
(wt.%)										
SiO_2	46.53	44.22	44.23	38.94	48.97	47.90	39.59	39.30	38.87	38.12
Al_2O_3	16.30	16.66	16.65	13.58	17.00	16.77	15.30	15.04	12.82	16.57
Fe_2O_3	9.14	10.03	10.09	11.25	7.71	8.52	11.30	11.31	14.68	8.87
MgO	5.04	4.25	4.29	9.00	4.58	4.52	4.41	4.49	4.60	2.36
CaO	9.46	10.08	10.03	14.16	7.90	8.75	12.91	13.07	7.83	13.22
Na_2O	4.50	5.49	5.45	3.75	5.22	4.88	5.67	5.26	6.63	4.23
K_2O	4.11	4.57	4.53	3.59	4.65	4.36	3.94	3.72	3.16	2.23
TiO_2	2.19	1.98	1.99	3.00	1.89	2.02	2.31	2.34	3.92	1.41
MnO	0.20	0.26	0.28	0.21	0.19	0.19	0.36	0.30	0.36	0.34
P_2O_5	0.60	0.80	0.80	0.69	0.42	0.54	1.16	1.12	2.66	0.67
Total	98.07	98.33	98.34	98.16	98.52	98.47	96.94	95.94	95.52	88.03
(p.p.m.)										
Cr	31	39	39	120	44	26	10	13	5	8
Nl	36	25	26	63	39	32	22	23	15	8
Cu	33	34	32	53	32	30	79	69	94	94
Zn	90	98	98	73	84	87	134	121	258	186
V	264	347	344	430	238	225	404	391	201	427
Sc	18	8	7	23	18	16	9	9	1	3
Rb	110	103	103	75	149	115	95	94	101	358
Ba	1662	969	951	1374	1096	1787	881	931	1861	6674
Th	12	17	17	10	16	12	21	20	29	18
Nb	117	187	188	124	97	121	239	241	256	322
La	92	152	153	75	83	91	155	149	219	208
Ce	182	280	274	152	149	184	276	285	466	357
Pb	10	12	12	2	11	9	15	11	23	8
Sr	1435	2145	2154	1128	872	1508	1868	1834	3599	3906
Nd	61	99	97	65	43	62	103	108	227	107
Zr	360	325	326	273	432	369	361	378	1312	297
Y	29	38	37	27	25	30	42	41	72	44

Olivine-poor Continental Nephelinites (COP) - continued

	Bohemian Massif, Czechoslovakia	Graz Basin, Austria						Tugtilik, Greenland	
Sample	BM12	A4	A5	A6	A7	STK210	STK211	STK212	20730	20748
(wt.%)										
SiO_2	40.74	39.81	40.81	40.42	39.74	40.40	40.29	40.52	44.23	38.57
Al_2O_3	13.76	13.71	13.96	13.79	13.53	13.84	13.85	13.87	14.93	14.82
Fe_2O_3	12.38	11.29	11.02	11.00	11.45	11.40	11.40	11.29	11.15	11.54
MgO	4.34	6.63	6.26	6.67	6.33	6.34	6.41	6.28	5.29	4.30
CaO	11.97	14.08	12.53	12.96	13.15	13.01	13.03	12.87	10.01	10.85
Na_2O	4.59	5.14	6.81	5.92	6.61	6.36	6.42	6.55	7.34	7.83
K_2O	3.05	1.76	2.58	1.93	2.44	2.81	2.81	2.80	1.75	2.15
TiO_2	3.97	2.00	1.95	1.95	2.00	2.02	2.00	2.01	1.56	2.30
MnO	0.28	0.27	0.26	0.26	0.28	0.27	0.27	0.27	0.20	0.26
P_2O_5	1.26	1.47	1.44	1.41	1.47	1.49	1.51	1.51	0.72	1.10
Total	96.32	96.16	97.62	96.31	97.00	97.93	97.98	97.96	97.18	93.71
(p.p.m.)										
Cr	3	69	71	74	69	72	67	65	59	12
Ni	8	57	60	59	57	57	58	57	43	10
Cu	49	25	29	32	29	30	29	32	119	25
Zn	131	105	100	105	104	99	95	99	94	106
V	386	189	179	186	181	186	180	183	276	360
Sc	8	10	11	11	7	11	9	11	8	1
Rb	75	86	101	93	92	104	103	116	26	37
Ba	989	1696	1718	1861	1813	1608	1570	1640	820	850
Th	19	17	18	18	17	19	17	18	2	4
Nb	189	140	143	140	143	145	144	150	27	51
La	135	119	124	119	117	119	111	112	24	38
Ce	269	223	224	231	219	221	204	208	54	82
Pb	11	8	8	7	8	7	7	8	8	4
Sr	1870	1687	1694	1834	1795	1760	1772	1801	948	1337
Nd	105	92	89	92	92	91	91	92	30	50
Zr	574	367	371	368	376	371	373	371	141	212
Y	43	38	37	37	39	39	39	40	25	36

Olivine-poor Continental Nephelinites (COP) - continued

	Tasmania	Queensland, E Australia		Otago, N Zealand	Chantaburi-Trat, Thailand	Raton-Clayton, New Mexico				
Sample	TAS8	Q1	Q2	OT1	TM2	855284	NM98A	NM98B	NM99	NM101
(wt.%)										
SiO_2	36.13	40.90	40.91	40.47	39.86	36.84	37.17	37.57	36.93	41.78
Al_2O_3	10.19	11.29	11.80	12.88	11.77	12.63	12.62	12.72	12.11	13.90
Fe_2O_3	15.71	11.45	14.12	14.52	14.80	12.66	12.40	12.49	12.17	11.04
MgO	11.26	13.92	10.84	8.52	9.60	8.84	9.53	9.55	10.19	10.03
CaO	14.87	10.88	9.37	11.38	9.97	15.61	15.66	15.66	15.74	13.04
Na_2O	5.38	4.28	4.70	4.64	5.11	4.97	4.86	5.05	4.62	4.57
K_2O	1.86	2.08	2.01	1.62	2.60	1.52	1.47	1.51	1.45	1.64
TiO_2	2.70	2.14	2.28	2.79	3.20	1.33	1.32	1.34	1.33	1.65
MnO	0.27	0.18	0.22	0.25	0.21	0.29	0.28	0.29	0.29	0.23
P_2O_5	1.45	1.17	1.25	1.23	1.35	2.50	2.62	2.64	3.07	1.78
Total	99.82	98.29	97.49	98.28	98.45	97.19	97.94	98.82	97.91	99.65
(p.p.m.)										
Cr	185	467	336	180	132	99	98	93	126	216
Ni	162	364	272	129	150	150	154	146	182	174
Cu	87	53	47	51	47	57	57	58	38	39
Zn	152	105	149	133	157	121	119	119	125	97
V	224	176	139	203	206	203	199	199	196	219
Sc	18	16	8	11	10	16	21	24	23	26
Rb	38	27	39	40	43	27	25	26	25	20
Ba	722	401	1042	670	760	1991	2429	2248	2414	1966
Th	16	10	16	13	11	30	30	30	30	19
Nb	164	102	124	110	101	75	74	74	83	55
La	93	66	109	118	69	239	237	252	262	148
Ce	172	138	202	211	133	424	435	448	481	270
Pb	7	1	7	6	6	13	14	9	9	12
Sr	1424	1344	1762	1311	1238	3128	2926	3327	3519	2599
Nd	76	52	77	87	65	160	168	171	185	112
Zr	356	276	399	306	380	247	346	365	453	356
Y	36	24	26	36	33	51	51	51	52	39

Appendix D

Calculated Primary Magma Compositions

Ocean Island Nephelinites (148 samples)
Continental Nephelinites (82 samples)
Potassic Continental Kamafugites and Leucitites (26 samples)

Primary magma compositions were calculated for samples with MgO > 10 wt.% using the method described by Fitton & James (1986).

The method assumes that samples with MgO > 10 wt.% have lost only olivine by fractional crystallization and that a correction for fractional crystallization can be made by replacing olivine until the magma composition is in equilibrium with a chosen mantle olivine composition. Olivine is added in small incremental amounts. The olivine added must be in equilibrium with the current magma composition and the appropriate olivine composition is, therefore, calculated before each addition. After each increment the magma composition is recalculated and tested for equilibrium with the chosen mantle olivine composition. If equilibrium with mantle olivine is not reached a new equilibrium olivine composition is calculated and the process is repeated.

For this study the composition of mantle olivine was assumed to be Fo_{90} (Boyd, 1987) and equilibrium olivine was added to the magma composition in increments of 0.1 wt.%. The distribution (K_D) of Fe^{2+} and Mg between olivine and melt was taken as 0.30 (Roeder & Emslie, 1970). In the analytical data presented in Appendix C all Fe is expressed as Fe_2O_3. The amounts of Fe_2O_3 and FeO in the sample were therefore calculated on the basis of an assumed Fe_2O_3/FeO. Brooks (1976) recommends Fe_2O_3/FeO = 0.15 for tholeiitic basalts and this figure is commonly used for normalising calculations. However, in the present study Fe_2O_3/FeO = 0.25 was considered appropriate as it reflects the more oxidised nature of highly alkaline rocks.

The procedure for the calculations is iterative and can be carried out using a spreadsheet macro program. The algorithm is as follows.

$\{Fe_2O_3\} = 159.691$ **Comment:** curly brackets

$\{FeO\} = 71.846$ denote molecular weights

$\{MgO\} = 40.311$

$\{SiO_2\} = 60.084$

$\{Fe_2O_3\} / 2 * \{FeO\} = 159.691 / (2 * 71.846) = 1.11134$ ..... **(i)**

$\{MgO\} / \{FeO\} = 40.311 / 71.846 = 0.56108$ ..... **(ii)**

Comment: $[Fe_2O_3^T]$ from the initial analysis represents original Fe_2O_3 (= $[Fe_2O_3^A]$) plus original FeO recalculated as Fe_2O_3 (= $[Fe_2O_3^B]$). Square brackets are used to indicate concentrations. Therefore

$[Fe_2O_3^T] = [Fe_2O_3^A] + [Fe_2O_3^B]$

$[Fe_2O_3^B] = 1.11134 * [FeO]$ **Comment:** using **(i)**. Therefore

$[Fe_2O_3^T] = [Fe_2O_3^A] + (1.11134 * [FeO])$ ..... **(iii)** And

$[Fe_2O_3^A] = [Fe_2O_3^T] - 1.11134 * [FeO]$ ..... **(iv)** But

$[Fe_2O_3^A] = [FeO] * R$

Comment: $R = [Fe_2O_3^A] / [FeO]$ where R is chosen. Therefore

$[Fe_2O_3^T] = ([FeO] * R) + (1.11134 * [FeO])$ **Comment:** using **(iii)**

$[Fe_2O_3^T] = [FeO] * (R + 1.11134)$

$[FeO] = [Fe_2O_3^T] / (R + 1.11134)$ ..... **(v)**

$A = 0$

Comment: The variable, A, sums the olivine increments in wt.% and is initially set to zero. The composition (E_{Fo}) of olivine in equilibrium with the initial or current magma composition is calculated as follows.

$E_{Fo} = 100 / (1+ (0.56108 * 0.3 * [FeO] / [MgO]))$....**(vi)**

Comment: E_{Fo} is calculated as %Fo; 0.56108 = {MgO} / {FeO} (see **(ii)**); [FeO] and [MgO] are calculated from the initial analysis on the first iteration (using **(v)**) but thereafter are current concentrations (see below); 0.3 = $^{ol/Ls}D_{Fe}/^{ol/Ls}D_{Mg}$ (Roeder & Emslie, 1970).

$E_{Fo} < M_{Fo}$.....**(vii)**

false / true

Comment: The equilibrium olivine composition (E_{Fo}) is compared with the chosen mantle olivine composition (M_{Fo}, given as %Fo). If $E_{Fo} \geq M_{Fo}$ than the magma composition is in equilibrium with the current magma composition and the incremental olivine addition process ceases i.e. go to equation **(viii)** and recalculate analysis. If $E_{Fo} < M_{Fo}$ then the procedure for incremental olivine addition is followed until the condition $E_{Fo} \geq M_{Fo}$ is satisfied, as follows.

$A = A + 0.1$

Comment: Add 0.1 wt.% olivine.

$\{MgO\}_{Ol} = 2 * 40.311 * E_{Fo} / 100$
$\{FeO\}_{Ol} = 2 * 71.846 * (100 - E_{Fo}) / 100$
$\{SiO_2\}_{Ol} = 60.084$
$\{Total\}_{Ol} = \{MgO_{Ol}\} + \{FeO_{Ol}\} + \{SiO_{2Ol}\}$

Comment: Calculate molecular wgt of olivine at current equilibrium olivine composition using the formula $(Mg,Fe)_2.SiO_4$.

$MgO_{Ol} = 100 * \{MgO\}_{Ol} / \{Total\}_{Ol}$
$FeO_{Ol} = 100 * \{FeO\}_{Ol} / \{Total\}_{Ol}$
$SiO_{2Ol} = 100 * \{SiO_2\}_{Ol} / \{Total\}_{Ol}$

Comment: Calculate the percentage of each oxide in the current equilibrium olivine.

$[SiO_2] = [SiO_2] + (0.001 * SiO_{2Ol})$
$[FeO] = [FeO] + (0.001 * FeO_{Ol})$
$[MgO] = [MgO] + (0.001 * MgO_{Ol})$

Comment: Recalculate SiO_2, FeO, and MgO for addition of 0.1 wt.% olivine of the composition calculated above to give current concentrations. Return to equation **(vi)**.

[EL] = [EL] * 100 / (100 + A).....**(viii)**

Comment: Equation **(viii)** recalculates all other oxides including $[Fe_2O_3^A]$ calculated in **(iv)** to correct for dilution effect of olivine addition. A = total olivine added in wt. %.

$[Fe_2O_3^T] = [Fe_2O_3^A] + 1.11134 * [FeO]$

Comment: Calculate $[Fe_2O_3^T]$ by converting final [FeO] to $[Fe_2O_3^B]$. and adding to $[Fe_2O_3^A]$ calculated in **(viii)**.

Calculated Primary Compositions - Ocean Island Nephelinites

	Kusale			Ponape				Truk				
Sample	KS13	KS8	KS18	PO65	PO66	PO67	PO72	TUU30	TUU31	TUU32	TT51	TT52
(wt.%)												
SiO_2	38.96	40.25	40.20	38.67	40.91	40.56	40.87	38.15	38.08	38.08	38.14	38.21
Al_2O_3	9.32	9.96	9.89	10.19	9.98	9.86	10.57	10.09	10.13	10.11	10.54	10.58
Fe_2O_3	1.52	1.54	1.56	1.56	1.47	1.46	1.49	1.43	1.42	1.41	1.40	1.39
FeO	11.10	10.50	10.94	10.54	10.84	10.68	10.39	10.33	10.35	10.32	9.85	9.79
MgO	16.82	15.93	16.58	15.98	16.44	16.19	15.74	15.67	15.68	15.66	14.94	14.87
CaO	11.66	11.70	11.18	12.22	10.44	10.82	11.67	11.97	11.77	11.69	13.51	13.42
Na_2O	3.32	3.13	2.29	2.99	2.91	2.18	2.44	3.13	3.12	3.16	3.29	3.34
K_2O	0.93	0.59	0.83	0.90	1.13	0.89	0.49	1.51	1.54	1.53	1.39	1.39
TiO_2	3.11	2.80	3.07	2.88	3.11	3.08	2.38	3.50	3.48	3.45	3.24	3.27
MnO	0.20	0.21	0.18	0.20	0.18	0.17	0.19	0.19	0.19	0.18	0.18	0.18
P_2O_5	1.07	0.85	0.80	0.91	0.73	0.65	0.86	1.22	1.21	1.24	0.89	0.95
Total	98.00	97.47	97.53	97.04	98.15	96.55	97.08	97.19	96.96	96.83	97.35	97.38

	Kaual																
Sample	SM2	SM11	SM13	SM15	SM20	SM21	SM22	SM23	SM25	SM36	SM38	SM39	SM41	SM48	SM51	SM53	SM54	SM55
(wt.%)																		
SiO_2	40.29	40.53	40.81	41.58	41.06	41.30	41.65	40.86	39.19	42.19	41.83	42.32	39.68	40.98	40.84	40.88	42.43	41.09
Al_2O_3	8.95	9.15	9.14	8.79	9.71	9.42	9.63	9.52	9.31	10.24	9.86	10.05	9.29	9.25	8.88	8.91	9.82	10.09
Fe_2O_3	1.47	1.51	1.50	1.38	1.48	1.52	1.50	1.52	1.45	1.53	1.60	1.65	1.59	1.59	1.58	1.58	1.55	1.57
FeO	11.86	12.25	12.10	11.32	11.55	11.49	11.36	11.47	10.89	11.01	10.84	11.00	12.20	11.75	12.20	12.09	11.52	11.64
MgO	17.98	18.58	18.33	17.17	17.51	17.43	17.24	17.39	16.50	16.71	16.45	16.69	18.51	17.83	18.48	18.31	17.45	17.66
CaO	9.83	9.79	9.72	10.67	10.26	10.60	10.49	10.82	11.33	10.57	10.67	10.69	10.46	10.09	9.70	9.92	9.98	10.05
Na_2O	2.62	1.76	2.37	2.38	2.80	2.70	2.90	3.07	3.12	2.57	2.84	2.30	0.96	2.84	2.19	2.84	2.57	1.91
K_2O	0.50	0.40	0.41	0.82	0.93	0.68	0.93	1.02	1.15	0.75	0.60	0.58	0.22	0.61	0.47	0.57	0.66	0.71
TiO_2	2.77	2.56	2.45	2.21	2.32	2.38	2.33	2.37	2.34	2.42	2.04	2.06	2.09	2.63	2.49	2.54	2.27	2.39
MnO	0.16	0.16	0.16	0.16	0.17	0.17	0.17	0.17	0.18	0.17	0.20	0.19	0.18	0.17	0.16	0.16	0.16	0.18
P_2O_5	0.50	0.41	0.43	0.58	0.58	0.56	0.49	0.55	0.69	0.41	0.44	0.44	0.52	0.46	0.45	0.44	0.34	0.44
Total	96.92	97.09	97.41	97.06	98.38	98.24	98.69	98.77	96.14	98.57	97.36	97.97	95.69	98.20	97.45	98.24	98.76	97.73

Calculated Primary Compositions - Ocean Island Nephelinites (continued)

Kaual - continued

Sample	SM56	SM67	SM77	SM80	SM88	SM109	SM113	SM116	SM119	SM124	SM125	SM126	SM127	SM128	SM129	SM140	SM141	SM145
(wt.%)																		
SiO_2	41.96	40.21	41.57	40.75	41.63	41.71	39.44	39.93	37.95	39.81	39.02	39.73	39.66	42.48	42.43	42.12	41.39	37.73
Al_2O_3	10.15	8.12	9.38	8.42	8.73	10.30	8.96	8.77	9.24	9.10	8.66	8.92	9.01	10.01	9.93	9.85	9.42	7.95
Fe_2O_3	1.60	1.58	1.46	1.56	1.43	1.46	1.61	1.62	1.65	1.58	1.61	1.61	1.60	1.52	1.54	1.41	1.57	1.68
FeO	11.09	12.46	11.29	11.60	11.73	11.11	12.09	12.09	11.39	11.76	12.19	12.24	12.20	11.21	11.29	10.87	11.66	12.48
MgO	16.83	18.87	17.10	17.58	17.78	16.83	18.34	18.34	17.28	17.83	18.49	18.55	18.50	16.99	17.10	16.47	17.67	18.91
CaO	10.77	8.80	10.75	10.76	9.52	10.23	11.06	10.42	12.01	10.89	10.19	10.72	10.63	10.29	10.57	11.10	10.60	11.58
Na_2O	2.05	2.34	2.53	2.74	2.59	2.56	1.58	2.24	1.24	1.63	2.84	2.17	1.76	2.46	2.46	2.77	2.13	2.56
K_2O	0.68	0.98	0.35	0.61	0.84	0.68	0.67	0.60	0.76	0.47	1.32	0.80	0.70	0.94	0.61	1.14	0.98	0.90
TiO_2	2.12	2.44	2.22	2.23	2.29	2.11	2.70	2.84	3.03	2.74	2.79	2.67	2.65	2.18	2.21	2.60	2.55	2.89
MnO	0.18	0.18	0.17	0.17	0.15	0.16	0.19	0.17	0.19	0.18	0.18	0.17	0.18	0.17	0.17	0.16	0.17	0.18
P_2O_5	0.44	0.73	0.45	0.56	0.49	0.40	0.52	0.55	0.61	0.55	0.60	0.50	0.52	0.37	0.36	0.48	0.38	0.70
Total	97.88	96.71	97.27	96.96	97.19	97.55	97.17	97.57	95.36	96.54	97.89	98.07	97.42	98.62	98.65	98.98	98.52	97.55

Kaual - continued

Sample	SM146	SM147	SM150	SM151	SM153	SM154	SM155	SM156	SM157	SM158	SM159	SM160	SM161	SM162	SM163	SM164	SM169	SM171
(wt.%)																		
SiO_2	37.83	40.56	41.90	39.41	38.72	38.36	39.24	39.36	39.18	38.95	39.65	41.84	39.18	39.55	38.51	41.27	41.51	38.93
Al_2O_3	8.39	9.20	9.72	9.15	8.83	8.41	8.04	9.10	8.84	8.86	8.30	9.53	9.00	9.15	8.40	9.83	9.71	8.67
Fe_2O_3	1.68	1.54	1.41	1.54	1.60	1.60	1.67	1.56	1.56	1.56	1.57	1.50	1.55	1.53	1.60	1.46	1.46	1.58
FeO	12.15	11.42	11.15	11.64	11.64	11.58	12.28	11.37	11.59	11.24	11.94	11.40	11.52	11.24	11.70	11.05	11.16	11.62
MgO	18.42	17.30	16.92	17.66	17.63	17.54	18.63	17.23	17.57	17.05	18.09	17.27	17.47	17.05	17.75	16.76	16.92	17.63
CaO	10.81	11.40	10.15	11.85	11.77	12.67	11.37	12.10	11.82	12.64	11.33	10.39	11.84	12.20	12.23	10.80	10.84	11.74
Na_2O	2.03	1.65	2.00	1.86	2.08	1.69	1.40	2.05	2.28	2.10	2.02	1.87	2.19	1.94	1.82	1.85	1.97	2.13
K_2O	0.63	0.86	1.09	0.54	0.68	0.38	0.58	0.93	0.56	0.43	0.51	1.01	0.49	0.59	0.41	1.02	1.03	0.69
TiO_2	3.02	2.51	2.06	2.76	2.97	2.92	2.92	2.84	2.88	2.88	2.89	2.38	2.82	2.80	3.02	2.44	2.45	2.97
MnO	0.19	0.17	0.16	0.17	0.18	0.19	0.18	0.18	0.18	0.18	0.17	0.17	0.18	0.18	0.19	0.17	0.16	0.17
P_2O_5	0.80	0.47	0.45	0.55	0.61	0.60	0.57	0.61	0.56	0.61	0.56	0.45	0.56	0.58	0.62	0.49	0.46	0.55
Total	95.96	97.08	96.99	97.14	96.71	95.93	96.86	97.33	97.04	96.50	97.02	97.82	96.80	96.83	96.24	97.12	97.65	96.68

Calculated Primary Compositions - Ocean Island Nephelinites (continued)

	Kauai - continued																	
Sample	SM172	SM175	SM176	SM177	SM196	SM198	SM205	SM315	SM328	SM337A	SM344	SM349	SM350	SM361	SM362	SM363	SM364	SM366
(wt.%)																		
SiO_2	39.58	41.02	38.91	37.77	40.54	40.98	38.92	41.92	40.27	39.22	38.71	40.11	40.02	39.19	39.50	38.39	39.89	41.17
Al_2O_3	9.05	9.22	8.86	8.24	9.68	9.77	8.32	9.47	8.82	8.39	8.43	9.15	9.16	9.21	9.37	8.46	9.08	9.84
Fe_2O_3	1.57	1.53	1.57	1.67	1.54	1.55	1.63	1.58	1.58	1.63	1.68	1.58	1.55	1.61	1.58	1.62	1.54	1.53
FeO	11.19	11.56	11.49	12.12	11.45	11.56	12.72	11.48	12.12	12.57	12.40	11.69	11.69	12.14	11.67	12.30	11.52	11.35
MgO	16.98	17.52	17.41	18.38	17.37	17.55	19.28	17.42	18.38	19.06	18.79	17.73	17.74	18.40	17.69	18.66	17.48	17.22
CaO	11.83	10.69	12.63	12.67	10.72	10.31	10.01	10.53	10.02	10.37	10.85	10.83	10.73	10.53	10.81	11.16	11.07	10.21
Na_2O	2.47	1.76	1.68	2.29	2.40	2.19	1.89	2.41	2.15	1.90	1.84	2.35	2.16	1.03	1.50	2.58	3.01	2.99
K_2O	0.82	0.90	0.55	0.64	0.32	0.56	0.88	0.83	0.83	0.89	0.83	0.85	0.77	0.41	0.62	0.84	1.36	0.53
TiO_2	2.89	2.45	2.83	3.07	2.75	2.68	2.79	2.11	2.67	2.89	2.95	2.66	2.64	2.81	2.79	2.63	2.58	2.59
MnO	0.18	0.17	0.18	0.18	0.21	0.18	0.20	0.20	0.15	0.17	0.18	0.17	0.16	0.16	0.16	0.17	0.17	0.16
P_2O_5	0.58	0.45	0.60	0.77	0.52	0.46	0.59	0.42	0.51	0.56	0.55	0.56	0.56	0.50	0.54	0.66	0.68	0.43
Total	97.14	97.25	96.70	97.81	97.50	97.78	97.24	98.34	97.51	97.65	97.20	97.67	97.20	95.99	96.24	97.47	98.36	98.02

	Kauai - continued						Oahu						Samoa	Aitutaki	
Sample	SM385	SM430	SM431	2521-32	2521-34	HWK1	8127-85	8127-86	2521-16	2521-40	43651	43652	UPO7	AT4-46I	AT4-45
(wt.%)															
SiO_2	38.42	40.75	40.72	41.90	40.56	37.75	37.43	37.43	40.24	39.30	37.13	39.56	41.11	38.54	38.64
Al_2O_3	8.88	9.24	9.22	9.24	9.20	8.18	7.80	7.30	9.83	10.25	7.94	10.23	9.65	9.46	9.54
Fe_2O_3	1.59	1.50	1.50	1.47	1.63	1.60	1.56	1.46	1.54	1.50	1.61	1.52	1.46	1.42	1.44
FeO	11.83	11.86	11.97	11.76	10.99	11.97	13.54	13.24	11.33	11.21	13.54	11.23	11.50	11.52	11.65
MgO	17.93	17.98	18.15	17.82	16.68	18.17	20.51	20.07	17.18	17.00	20.53	17.01	17.44	17.47	17.67
CaO	11.53	9.19	9.16	9.70	11.53	12.20	9.46	8.85	11.12	11.51	9.29	11.51	8.24	10.12	9.83
Na_2O	3.74	3.02	2.96	2.09	3.08	2.64	3.68	3.96	3.60	3.60	3.94	3.12	3.09	3.91	3.94
K_2O	0.96	0.85	0.86	0.80	1.42	0.93	1.36	1.52	0.89	1.10	1.39	1.03	1.61	1.33	1.17
TiO_2	2.29	2.20	2.20	2.60	2.63	3.02	2.11	2.08	2.25	2.20	2.03	2.21	3.58	2.20	2.21
MnO	0.20	0.17	0.16	0.15	0.19	0.18	0.17	0.18	0.19	0.20	0.19	0.19	0.14	0.17	0.17
P_2O_5	0.94	0.60	0.60	0.41	0.57	0.80	0.82	0.86	0.73	0.89	0.85	0.88	0.83	0.99	0.99
Total	98.30	97.37	97.50	97.94	98.48	97.44	98.44	96.94	98.90	98.77	98.43	98.49	98.67	97.13	97.25

Calculated Primary Compositions - Ocean Island Nephelinites (continued)

	Moheli																	
Sample	MO2	MO9	MO12	MO14	MO16	MO17	MO116	MO117	MO123	MO126	MO133	MO134	MO135	MO136	MO137	MO138	MO161	MO191
(wt.%)																		
SiO_2	39.92	41.26	40.43	40.50	40.99	39.14	39.91	38.90	39.62	39.69	41.38	41.06	39.75	40.87	41.04	41.03	41.88	41.86
Al_2O_3	9.50	9.51	9.55	9.54	9.89	9.46	8.72	9.32	8.82	8.62	9.46	9.38	8.97	9.43	9.16	9.22	10.10	11.18
Fe_2O_3	1.50	1.66	1.48	1.44	1.48	1.46	1.42	1.52	1.42	1.42	1.44	1.45	1.44	1.43	1.45	1.44	1.44	1.54
FeO	10.72	11.05	10.87	11.55	10.73	11.86	12.26	11.12	12.39	11.98	11.08	11.47	11.34	11.25	11.14	11.25	11.21	10.34
MgO	16.27	17.50	16.49	17.52	16.27	18.00	18.60	16.87	18.78	18.15	16.80	17.38	17.18	17.06	16.89	17.07	16.99	15.70
CaO	11.72	9.55	11.90	9.68	11.87	10.50	9.10	11.91	8.49	9.78	9.89	9.77	11.22	9.89	10.39	9.67	10.09	11.41
Na_2O	3.62	2.51	2.59	2.64	2.33	2.33	3.25	3.04	3.72	3.45	2.84	1.98	2.41	2.29	2.49	2.87	2.53	2.54
K_2O	1.51	0.65	0.59	1.21	0.51	1.10	1.55	1.52	0.76	1.56	0.47	0.31	0.49	0.67	0.50	0.53	0.46	1.07
TiO_2	2.55	2.75	2.63	2.28	2.38	2.47	2.43	2.81	2.39	2.46	3.60	3.64	2.94	3.55	3.29	3.51	2.14	1.99
MnO	0.21	0.20	0.18	0.19	0.18	0.19	0.20	0.19	0.19	0.20	0.15	0.16	0.17	0.16	0.16	0.16	0.19	0.20
P_2O_5	0.93	0.75	0.81	0.76	0.72	0.61	0.88	0.78	0.84	0.93	0.53	0.54	0.81	0.56	0.56	0.51	0.56	0.57
Total	98.46	97.37	97.52	97.32	97.34	97.12	98.32	97.98	97.42	98.24	97.64	97.15	96.73	97.15	97.08	97.27	97.59	98.40

	Grande Comore				Fernando de Noronha								Trinidade	Principe
Sample	GC51	GC124	72/9	72/17B	FDN18	FDN20	FDN31	FDN33	FDN74	FDN76	FDN98	FDN106	TD3	P18
(wt.%)														
SiO_2	42.42	39.79	41.55	41.26	37.32	37.42	38.90	40.06	39.60	40.00	37.65	38.11	41.19	37.50
Al_2O_3	11.58	8.69	11.14	11.09	8.75	8.77	9.59	10.05	9.69	9.15	8.99	9.17	10.80	9.39
Fe_2O_3	1.35	1.44	1.49	1.48	1.50	1.54	1.41	1.43	1.48	1.46	1.52	1.52	1.41	1.47
FeO	10.67	12.02	9.92	9.94	11.79	11.95	10.78	10.41	10.55	10.44	11.47	11.40	9.84	11.31
MgO	16.17	18.21	15.59	15.07	17.88	18.11	16.34	15.79	15.98	15.82	17.38	17.28	14.94	17.15
CaO	9.11	9.80	12.34	12.54	10.85	10.88	11.41	11.63	12.00	11.30	11.47	11.54	11.45	11.39
Na_2O	3.70	3.40	3.04	2.75	2.53	2.48	3.06	3.31	3.05	2.41	2.93	2.36	1.96	2.57
K_2O	1.40	1.44	1.11	1.15	1.69	1.72	0.99	1.13	0.97	0.77	0.78	1.29	1.67	1.34
TiO_2	1.98	2.49	1.93	1.94	3.67	3.72	3.06	3.03	3.18	2.90	3.21	3.42	3.05	3.59
MnO	0.19	0.20	0.21	0.21	0.17	0.17	0.18	0.17	0.18	0.18	0.19	0.18	0.16	0.18
P_2O_5	0.56	0.90	0.74	0.76	0.98	0.95	0.88	0.84	0.89	0.96	1.13	0.90	0.46	1.23
Total	99.12	98.39	99.03	98.18	97.14	97.70	96.60	97.85	97.56	95.40	96.73	97.18	96.95	97.11

Calculated Primary Compositions - Ocean Island Nephelinites (continued)

	Cape Verde																
Sample	80/180A	80/180B	80/178	80/100	ZM28	ZM31	ZM37	ZM43	ZM45	ZM51	ZM54	ZM91	ZM94	ZM96	ZM97	ZM131	ZM223
(wt.%)																	
SiO_2	36.71	37.33	37.35	40.07	38.24	38.28	38.12	38.66	37.95	36.70	39.75	38.63	38.39	38.77	38.69	38.41	36.74
Al_2O_3	9.56	9.93	10.06	9.56	9.68	9.70	9.12	9.65	9.80	9.15	9.57	9.65	9.74	9.46	9.72	9.84	9.11
Fe_2O_3	1.43	1.40	1.43	1.40	1.49	1.47	1.52	1.42	1.47	1.44	1.43	1.42	1.39	1.44	1.42	1.44	1.45
FeO	9.53	9.60	9.63	9.49	9.97	9.97	10.26	10.03	9.86	9.58	10.58	10.10	9.84	10.19	10.01	10.10	9.63
MgO	14.45	14.57	14.59	14.37	15.12	15.11	15.55	15.21	14.97	14.84	16.06	15.30	14.94	15.45	15.16	15.32	15.03
CaO	17.42	16.38	15.36	13.89	15.05	15.04	15.05	13.69	15.25	16.99	12.38	13.59	14.10	13.22	13.53	13.52	17.19
Na_2O	3.18	2.82	3.63	2.81	2.98	2.23	2.13	3.06	2.48	2.28	2.81	2.99	2.82	2.55	2.85	2.81	2.52
K_2O	0.95	0.70	1.01	0.67	1.97	1.05	0.81	1.58	0.91	0.83	0.71	1.56	1.76	1.70	1.64	1.97	0.97
TiO_2	2.62	2.64	2.68	3.26	3.43	3.46	3.60	4.02	3.43	3.23	3.56	4.04	3.86	4.13	4.05	3.80	3.25
MnO	0.20	0.19	0.19	0.17	0.19	0.18	0.19	0.18	0.18	0.18	0.16	0.18	0.17	0.17	0.17	0.18	0.18
P_2O_5	1.50	1.50	1.50	0.91	0.89	0.85	0.79	0.92	0.84	1.18	0.78	0.90	0.93	0.90	0.93	1.03	1.19
Total	97.54	97.08	97.41	96.59	99.00	97.35	97.14	98.42	97.14	96.40	97.80	98.36	97.95	97.99	98.17	98.42	97.24

Calculated Primary Compositions - Continental Nephelinites

	Malagasy		Riwa, N Kenya	Samburu, N Kenya			Moroto, E Uganda			Elgon, E Uganda
Sample	ANK8	ANK9	RIWA3	8-428	11-108	KS7309	V259	V322	V534	ELG1
(wt.%)										
SiO_2	40.20	40.15	41.85	42.62	41.65	38.19	41.10	42.49	40.07	39.53
Al_2O_3	11.01	9.87	7.01	11.29	10.88	8.12	7.19	8.34	9.00	6.13
Fe_2O_3	1.41	1.47	1.53	1.26	1.37	1.68	1.37	1.29	1.34	1.40
FeO	9.40	9.83	10.91	9.47	9.72	11.85	11.51	10.10	11.01	11.50
MgO	14.73	15.58	16.56	14.38	14.74	17.96	17.44	15.31	16.68	17.44
CaO	12.93	13.01	12.77	10.82	11.93	11.57	11.67	13.15	11.11	14.80
Na_2O	1.95	2.45	3.41	3.59	2.89	3.12	2.46	3.86	2.54	1.62
K_2O	0.61	2.02	1.28	1.14	0.72	1.27	1.10	1.44	0.77	1.41
TiO_2	2.75	2.71	2.31	1.92	2.10	2.43	2.33	1.67	2.49	2.20
MnO	0.18	0.18	0.17	0.17	0.17	0.20	0.16	0.18	0.17	0.17
P_2O_5	1.10	0.84	0.29	0.44	0.39	0.80	0.38	0.42	0.42	0.40
Total	96.27	98.11	98.09	97.10	96.57	97.19	96.71	98.25	95.59	96.59

	Homa Mtn, Nyanza, Kenya		Rangwa-Kisingiri, Nyanza, Kenya	Usaki-Wasaki, Nyanza, Kenya
Sample	1279	HC116A	RR610-1	U1270
(wt.%)				
SiO_2	35.97	36.87	40.43	40.81
Al_2O_3	7.27	7.10	5.62	5.74
Fe_2O_3	1.50	1.54	1.42	1.48
FeO	11.01	11.34	12.37	12.49
MgO	16.71	17.22	18.75	18.93
CaO	15.00	14.32	12.90	12.14
Na_2O	2.42	2.37	1.36	0.53
K_2O	1.98	2.16	0.43	0.89
TiO_2	3.89	3.85	2.71	2.59
MnO	0.20	0.20	0.17	0.17
P_2O_5	0.74	0.73	0.59	0.43
Total	96.67	97.71	96.74	96.21

Calculated Primary Compositions - Continental Nephelinites (continued)

	Narok-Nguruman, S Kenya			Loolmurwak, N Tanzania	Chilwa Province, Malawi
Sample	SK244-2	SK209-1	1467	BD105	MAL2
(wt.%)					
SiO_2	41.21	44.23	40.02	38.50	36.96
Al_2O_3	7.68	7.64	8.69	6.78	10.41
Fe_2O_3	1.69	1.28	1.49	1.64	1.16
FeO	12.28	9.78	10.58	11.52	8.54
MgO	18.63	14.85	16.05	17.47	12.95
CaO	9.09	13.52	11.80	11.85	14.95
Na_2O	1.55	1.99	3.89	2.14	1.52
K_2O	0.91	1.09	1.85	1.40	2.47
TiO_2	2.87	2.36	2.94	3.66	2.05
MnO	0.19	0.16	0.19	0.19	0.19
P_2O_5	0.53	0.37	0.54	0.79	0.96
Total	96.62	97.28	98.04	95.95	92.16

	Cape Province, S Africa			Gamoep, Bushmanland - Namaqualand									
Sample	BD1234	RIV1	RIV2	BD1207	BD1211	BD1220	BD1224	N1	N2	N3	N4	N5	N6
(wt.%)													
SiO_2	29.75	36.91	36.82	40.04	35.69	40.59	33.75	35.54	35.61	33.56	35.82	35.63	35.59
Al_2O_3	6.57	7.39	7.39	5.77	5.35	6.23	4.93	5.22	4.96	4.93	5.29	4.89	5.26
Fe_2O_3	1.71	1.71	1.70	1.50	1.94	1.60	1.88	1.89	1.95	1.91	1.92	1.96	1.90
FeO	11.42	11.47	11.50	11.99	13.02	11.73	13.31	13.13	13.03	13.38	12.82	13.09	13.12
MgO	18.43	17.39	17.43	18.18	19.74	17.80	20.16	19.90	20.00	20.31	19.53	20.21	19.88
CaO	19.48	12.46	12.60	11.34	11.22	8.92	12.52	11.18	11.89	12.63	12.81	12.23	11.07
Na_2O	2.06	2.70	2.75	1.70	1.54	1.63	1.38	1.41	1.52	1.51	1.58	1.48	1.20
K_2O	0.91	2.00	2.00	1.50	1.46	1.82	1.88	1.43	1.36	2.03	1.55	1.22	0.84
TiO_2	2.96	4.18	4.20	3.64	5.71	4.79	6.50	6.49	5.78	6.45	4.68	5.51	6.51
MnO	0.29	0.20	0.20	0.15	0.20	0.16	0.19	0.19	0.20	0.20	0.21	0.20	0.19
P_2O_5	1.98	0.84	0.80	0.93	1.05	0.31	0.99	0.74	0.92	0.98	1.19	0.92	0.60
Total	95.55	97.25	97.40	96.74	96.91	95.58	97.49	97.13	97.21	97.88	97.40	97.35	96.17

Calculated Primary Compositions - Continental Nephelinites (continued)

	Orkney, NE Scotland	Monts du Forez, France	Massif Central, France		Rhine Graben, Germany		
Sample	ORK12	MC4	42974	42466	KG5	KT8	G3
(wt.%)							
SiO_2	37.69	38.06	42.93	43.73	40.79	39.18	37.87
Al_2O_3	10.51	10.12	9.17	8.84	10.00	10.45	11.09
Fe_2O_3	1.36	1.44	1.42	1.34	1.43	1.45	1.23
FeO	9.87	9.59	9.44	8.97	9.53	9.65	9.38
MgO	14.99	15.35	14.52	13.61	15.09	15.43	14.22
CaO	11.85	14.04	11.26	11.34	11.75	13.15	9.51
Na_2O	2.34	2.69	2.19	2.13	2.32	2.69	2.20
K_2O	1.17	1.61	3.00	3.56	0.93	1.61	1.86
TiO_2	2.20	3.12	3.54	3.54	2.77	2.61	3.01
MnO	0.19	0.21	0.16	0.15	0.17	0.19	0.15
P_2O_5	1.35	1.04	0.80	0.83	0.73	0.79	0.48
Total	93.52	97.28	98.43	98.05	95.50	97.20	91.02

	Eifel, Germany			Bohemian Massif, Czechoslovakia	
Sample	LV2803	LV3415	LV3511	77-134	77-136
(wt.%)					
SiO_2	41.10	41.98	41.85	41.33	38.85
Al_2O_3	11.78	12.39	12.40	11.05	10.13
Fe_2O_3	1.25	1.16	1.20	1.41	1.43
FeO	8.59	8.35	8.70	9.67	10.60
MgO	13.04	12.66	13.18	14.66	16.07
CaO	13.59	11.99	11.97	12.31	11.89
Na_2O	2.83	2.18	2.62	3.80	3.29
K_2O	2.62	3.67	2.86	0.95	1.81
TiO_2	2.23	2.48	2.42	1.83	2.79
MnO	0.21	0.19	0.18	0.19	0.21
P_2O_5	0.71	0.54	0.56	0.93	0.90
Total	97.94	97.61	97.96	98.14	97.97

Calculated Primary Compositions - Continental Nephelinites (continued)

	Gardiner, Greenland			Nunatak Zone, Greenland			Tugtlilik, Greenland
Sample	55201E	20385A	29918	200147	240426	240427	20738A
(wt.%)							
SiO_2	39.45	39.14	35.11	40.71	40.01	39.90	42.46
Al_2O_3	4.40	4.54	4.94	7.43	5.19	6.55	8.99
Fe_2O_3	1.76	1.91	1.53	1.54	1.76	1.55	1.20
FeO	14.18	13.44	11.27	11.21	11.71	11.71	8.67
MgO	21.48	20.39	17.08	17.00	18.60	17.75	13.17
CaO	7.87	9.94	7.60	11.70	11.38	11.23	15.38
Na_2O	0.77	2.06	3.11	2.43	1.73	2.57	2.45
K_2O	1.44	1.05	0.12	0.83	0.68	1.11	0.40
TiO_2	5.19	3.84	3.19	3.22	4.58	3.74	1.42
MnO	0.17	0.21	0.17	0.21	0.20	0.22	0.18
P_2O_5	0.56	0.49	0.38	0.66	0.49	0.86	0.58
Total	97.25	97.02	84.50	96.94	96.32	97.20	94.91

	Bathhurst Island, NW Territories, Canada								Queensland, E Australia		Tasmania				
Sample	BI69	BI136	BI211	BI213	BI247	BI253	BI268	BI272	Q1	Q2	TAS2	TAS3	TAS6	TAS7	TAS8
(wt.%)															
SiO_2	43.10	40.80	41.14	41.46	41.67	38.15	39.87	40.91	40.90	40.84	40.76	37.64	41.59	38.60	37.02
Al_2O_3	12.46	11.80	10.76	11.58	11.71	11.07	11.10	10.95	11.29	9.80	8.18	9.17	9.60	7.92	8.10
Fe_2O_3	1.17	1.28	1.23	1.25	1.41	1.28	1.32	1.44	1.36	1.39	1.58	1.62	1.46	1.65	1.48
FeO	8.54	9.01	9.26	9.01	9.52	8.64	8.83	10.07	9.08	11.27	11.18	11.23	11.49	12.92	12.35
MgO	12.95	13.65	14.04	13.66	14.43	13.10	14.00	15.25	13.92	17.11	16.94	17.03	17.44	19.58	18.73
CaO	11.48	11.93	12.72	12.27	12.40	13.29	15.34	12.64	10.88	7.78	11.81	12.56	7.18	9.05	11.81
Na_2O	2.83	2.12	2.96	2.66	2.15	3.45	3.09	2.84	4.28	3.90	2.67	3.54	3.81	2.38	4.27
K_2O	1.53	1.32	1.07	1.27	1.18	0.69	1.32	1.09	2.08	1.67	0.88	1.26	1.72	1.19	1.48
TiO_2	1.61	1.77	1.85	1.98	2.04	2.06	1.74	2.14	2.14	1.89	2.77	2.53	2.24	2.63	2.14
MnO	0.18	0.19	0.16	0.18	0.18	0.18	0.20	0.17	0.18	0.18	0.20	0.21	0.17	0.19	0.22
P_2O_5	0.58	0.66	0.51	0.53	0.56	0.64	0.87	0.70	1.17	1.04	1.16	1.26	1.13	0.91	1.15
Total	96.41	94.53	95.71	95.85	97.27	92.54	97.68	98.20	97.28	96.88	98.13	98.06	97.83	97.02	98.75

Calculated Primary Compositions - Continental Nephelinites (continued)

	Chantaburi-Trat, Thailand	Raton-Clayton, New Mexico						Wildcat Peak, Arizona
Sample	TM1	NM98AL	NM99	NM101	NM103	NM104	NM105	AZ101
(wt.%)								
SiO_2	40.61	38.91	37.39	41.68	41.98	37.04	40.76	39.58
Al_2O_3	9.53	9.52	10.59	12.61	12.91	10.82	11.08	9.30
Fe_2O_3	1.41	1.36	1.27	1.19	1.22	1.24	1.26	1.31
FeO	11.53	10.91	9.86	8.96	8.87	8.96	9.94	9.31
MgO	17.48	16.52	14.93	13.58	13.45	13.61	15.08	14.12
CaO	8.16	12.88	13.77	11.83	12.17	15.17	11.68	13.76
Na_2O	3.27	3.42	4.04	4.15	3.76	3.90	2.93	2.85
K_2O	1.96	1.04	1.27	1.48	1.17	1.25	1.36	1.55
TiO_2	2.61	1.24	1.16	1.50	1.56	1.27	1.73	2.40
MnO	0.16	0.26	0.26	0.21	0.20	0.23	0.19	0.17
P_2O_5	1.01	1.88	2.69	1.61	1.63	2.15	1.80	1.64
Total	97.73	97.95	97.23	98.80	98.92	95.64	97.80	96.00

	Woodruff Butte, Arizona	Hopi Buttes, Arizona	Balcones, Texas					
Sample	AZ162	AZ20	TX3	473	529	767	82005	82020
(wt.%)								
SiO_2	38.55	42.44	38.34	39.03	37.97	39.02	38.29	38.31
Al_2O_3	9.50	9.59	9.99	10.07	10.15	9.87	9.68	9.80
Fe_2O_3	1.49	1.37	1.48	1.48	1.49	1.50	1.53	1.51
FeO	9.92	9.84	10.40	9.95	10.08	10.49	10.24	10.18
MgO	16.07	14.91	15.78	15.07	15.29	15.89	15.51	15.43
CaO	14.06	10.53	12.31	13.82	14.36	12.11	14.55	13.01
Na_2O	2.82	2.20	3.28	2.94	2.78	3.10	2.56	3.04
K_2O	0.60	1.78	0.88	0.99	0.80	0.79	0.96	1.07
TiO_2	2.46	3.11	3.90	3.03	3.14	3.56	3.10	3.61
MnO	0.19	0.16	0.18	0.20	0.20	0.18	0.18	0.20
P_2O_5	1.20	0.82	0.77	0.82	1.01	0.70	0.83	0.76
Total	96.86	96.76	97.31	97.39	97.27	97.21	97.42	96.93

Calculated Primary Compositions - Potassic Continental Rocks

	New South Wales, E Australia					Western Rift, Uganda										
Sample	NSW5	NSW6	NSW1	NSW2	NSW3	15010A	C4407	C4409	C4414	C3946	C3948	C4793	C4801	C5967	C3991	C5549	C5595
(wt.%)																	
SiO_2	46.20	42.95	44.50	44.72	44.64	36.89	36.72	36.04	36.26	36.43	36.98	37.39	36.61	38.08	39.72	39.76	39.88
Al_2O_3	8.87	8.36	7.50	8.20	8.14	6.05	6.60	5.92	5.87	6.34	6.98	6.31	6.22	6.69	7.49	5.02	5.59
Fe_2O_3	1.19	1.33	1.24	1.29	1.27	1.43	1.43	1.45	1.44	1.43	1.41	1.39	1.36	1.29	1.34	1.46	1.43
FeO	8.53	9.59	9.32	9.25	9.31	9.81	9.71	10.16	9.99	9.82	9.43	9.98	9.85	9.86	8.97	12.18	11.64
MgO	12.95	14.55	14.14	14.04	14.12	14.86	14.72	15.41	15.16	14.88	14.30	15.14	14.93	14.94	14.35	18.47	17.65
CaO	6.90	7.98	7.76	7.52	7.48	14.17	16.08	16.55	16.11	16.63	16.03	12.34	11.82	12.39	10.74	12.97	12.99
Na_2O	1.64	2.53	1.23	2.03	2.08	0.92	1.39	0.93	0.99	1.34	1.83	0.61	0.49	1.12	1.24	1.19	1.06
K_2O	5.88	4.54	5.75	5.23	5.22	5.05	4.22	3.35	4.40	2.13	3.30	5.53	6.44	4.35	6.61	1.81	1.77
TiO_2	4.02	4.31	4.73	4.34	4.36	4.30	4.15	4.44	4.27	4.17	3.99	5.27	5.40	4.20	5.00	4.27	4.21
MnO	0.13	0.15	0.12	0.15	0.13	0.23	0.20	0.22	0.21	0.21	0.20	0.19	0.18	0.19	0.17	0.15	0.15
P_2O_5	1.09	0.97	0.62	0.95	0.97	1.04	0.96	0.92	0.99	0.96	0.94	1.24	1.07	1.15	0.59	0.30	0.41
Total	97.39	97.26	96.91	97.71	97.71	94.74	96.18	95.40	95.69	94.33	95.40	95.40	94.37	94.25	96.21	97.58	96.79

	Western Rift, Uganda - continued								
Sample	C5775	C1001	C1943	C2787	C2792	C2813	C2820	WR3	WR7
(wt.%)									
SiO_2	32.38	39.97	43.52	45.02	43.15	43.91	43.37	44.28	44.57
Al_2O_3	5.63	5.26	9.46	10.00	10.62	10.39	10.84	10.11	9.84
Fe_2O_3	1.48	1.43	1.29	1.32	1.27	1.37	1.27	1.38	1.37
FeO	10.00	11.79	9.49	9.61	9.90	10.19	9.85	9.84	9.66
MgO	15.16	17.89	14.38	14.57	15.02	15.46	14.92	14.91	14.66
CaO	14.86	13.42	12.13	10.36	8.86	9.82	8.69	10.84	10.96
Na_2O	1.41	1.25	2.07	1.99	2.81	2.21	2.92	1.69	1.80
K_2O	2.48	1.33	2.88	2.74	3.17	2.32	3.28	2.34	2.56
TiO_2	4.88	4.17	3.00	2.62	2.80	2.63	2.73	2.79	2.71
MnO	0.20	0.15	0.17	0.17	0.18	0.17	0.18	0.18	0.18
P_2O_5	1.07	0.33	0.50	0.47	0.62	0.42	0.63	0.47	0.45
Total	89.56	96.98	98.89	98.87	98.39	98.90	98.66	98.84	98.76

Appendix E

Average Major-Element Compositions

E-1 Ocean Island Nephelinites
E-2 Continental Nephelinites
E-3 Potassic Continental Kamafugites and Leucitites
E-4 Olivine-Poor Continental Nephelinites
E-5 Ocean Island Basalts

Average Trace-Element Compositions

E-6 Ocean Island Nepehlinites
E-7 Continental Nephelinites (2 pages)
E-8 Potassic Continental Kamafugites and Leucitites
E-9 Olivine-Poor Continental Nephelinites (2 pages)
E-10 Ocean Island Basalts (2 pages)

Table E-1 Averages of Ocean Island Nephelinites

Major elements (wt.%)

	SiO_2	Al_2O_3	Fe_2O_3	MgO	CaO	Na_2O	K_2O	TiO_2	MnO	P_2O_5
Cape Verde CV (20)*	38.07	9.78	12.53	14.49	15.07	2.78	1.25	3.52	0.19	1.05
Principe PR (1)	37.01	10.88	14.28	12.24	13.19	2.97	1.55	4.15	0.21	1.42
Fernando de Noronha FN (8)	38.34	10.42	14.04	12.91	12.80	3.10	1.33	3.69	0.20	1.06
Trinidade TD (2)	41.12	11.43	13.27	10.87	12.16	1.99	1.61	3.75	0.17	0.68
Grande Comore GC (7)	41.57	10.91	12.92	15.39	11.51	3.09	1.25	2.04	0.21	0.72
Moheli MO (26)	40.74	11.28	14.21	11.91	11.58	3.35	1.14	3.03	0.22	0.83
Oahu OA (7)	38.60	11.08	15.55	11.83	12.37	4.46	1.43	2.63	0.23	1.00
Kauai KU (81)	40.22	10.37	14.82	13.54	12.29	2.56	0.84	2.94	0.20	0.61
Kusaie KS (5)	38.75	10.28	14.92	12.30	11.74	2.48	1.19	3.95	0.21	0.76
Ponape PO (4)	40.25	10.82	13.40	13.94	12.01	2.80	0.92	3.06	0.19	0.84
Truk TK (5)	37.94	11.06	12.74	12.86	13.40	3.45	1.58	3.64	0.20	1.19
Samoa SM (1)	41.21	11.38	14.53	11.93	9.73	3.65	1.90	4.23	0.17	0.98
Aitutaki CK (2)	38.18	11.53	14.58	11.12	12.10	4.77	1.52	2.68	0.21	1.20
Average of 13 Islands	39.39	10.86	13.98	12.72	12.30	3.19	1.35	3.33	0.20	0.95
St Dev	1.51	0.52	0.94	1.32	1.23	0.77	0.30	0.66	0.02	0.24
Average of 169 analyses	39.81	10.56	14.25	13.25	12.50	2.89	1.06	3.08	0.20	0.78
St Dev	1.70	0.96	1.19	2.17	1.40	0.84	0.46	0.61	0.02	0.25
Range - Highest	44.69	16.73	17.65	20.70	17.42	6.84	2.79	5.65	0.30	1.54
Lowest	36.13	7.36	10.39	4.20	8.42	1.12	0.26	1.43	0.17	0.38
Japan JP (4)	36.40	11.57	15.26	9.29	13.69	3.91	1.83	2.61	0.33	2.15
Ambitle AM (1)	45.80	10.30	11.05	9.16	14.53	3.02	2.17	0.72	0.19	0.56

* Number of samples

Table E-2 Averages of Continental Nephelinites

Major elements (wt.%)

	SiO_2	Al_2O_3	Fe_2O_3	MgO	CaO	Na_2O	K_2O	TiO_2	MnO	P_2O_5
Ankaratra, Malagasy (2)*	40.17	10.44	12.13	15.16	12.97	2.20	1.31	2.73	0.18	0.97
Turkana, N Kenya (3)	37.40	11.08	14.99	7.19	15.21	3.10	0.80	3.92	0.26	0.91
Riwa & Lodwar, N Kenya (4)	40.47	10.57	14.84	8.99	12.99	4.62	1.82	3.20	0.22	0.65
Samburu, N Kenya (3)	40.85	10.91	13.01	13.06	12.34	3.46	1.13	2.32	0.19	0.58
Moroto, E Uganda (4)	41.79	10.97	13.55	9.10	13.28	3.88	1.50	2.54	0.20	0.52
Napak, E Uganda (9)	41.83	12.86	13.98	5.92	12.45	4.06	1.92	2.40	0.21	0.75
Elgon, E Uganda (5)	41.58	9.46	14.15	8.21	14.90	2.86	1.92	2.54	0.25	0.64
Nyanza Rift, Kenya (33)	40.68	10.71	14.27	7.35	14.45	3.19	1.73	3.29	0.23	0.85
Narok-Nguruman, S Kenya (5)	41.05	8.57	13.30	15.42	12.75	2.59	1.15	2.33	0.19	0.75
Loolmurwak, N Tanzania (1)	38.37	7.17	14.62	15.67	12.53	2.26	1.48	3.87	0.21	0.83
Burko, N Tanzania (2)	41.46	12.98	12.74	5.34	12.35	3.39	2.67	3.19	0.24	0.90
Makuyuni Jnctn, N Tanzania (5)	41.37	10.52	14.75	6.45	12.72	3.23	1.80	4.90	0.24	1.33
Chilwa, Malawi (6)	38.11	11.25	12.00	8.09	12.06	2.53	3.41	3.30	0.23	0.95
Nuanetsi, Zimbabwe (4)	42.59	12.84	14.09	5.75	8.00	6.45	2.88	3.54	0.20	0.86
Cape Province, S Africa (7)	33.62	7.29	13.06	17.74	15.71	1.74	1.80	3.50	0.22	1.36
Gamoep, Bushmanland (10)	36.01	5.60	16.35	17.89	12.21	1.58	1.60	5.90	0.20	0.91
Etinde, Cameroon (15)	39.98	14.81	12.24	5.29	13.49	3.90	2.15	3.85	0.30	1.08
Orkney, NE Scotland (3)	38.85	10.53	11.57	14.10	12.75	1.82	1.22	2.17	0.19	1.27
Massif Central, France (2)	43.34	9.03	11.61	13.98	11.33	2.17	3.29	3.55	0.16	0.82
Forez, France (2)	38.05	9.95	11.82	15.89	14.29	2.25	1.30	3.00	0.20	1.04
Rhine Graben, Germany (4)	39.10	11.41	12.61	11.34	10.84	3.52	1.94	3.17	0.22	1.18
Eifel & Vogelsberg, Germ'y (9)	41.51	13.53	10.70	9.75	12.49	3.45	3.43	2.45	0.22	0.77
Hegau, Germany (2)	38.92	9.82	11.35	16.84	14.18	2.00	1.52	2.56	0.19	0.75
Frankenwald, Germany (2)	39.44	15.17	11.31	4.45	12.99	5.46	3.83	2.32	0.33	1.14
Bohemian Massif, Czech (6)	38.86	11.84	13.15	9.98	13.40	3.53	1.52	3.58	0.24	1.22
Graz, Austria (7)	40.29	13.79	11.26	6.42	13.09	6.26	2.45	1.99	0.27	1.47
Greenland (9)	39.84	8.46	14.18	12.49	11.50	3.53	1.14	3.56	0.22	0.70
Bathhurst Island, Canada (15)	41.45	12.37	11.00	10.53	13.83	2.93	1.26	1.91	0.18	0.73
Queensland, E Australia (2)	40.91	11.55	12.79	12.38	10.12	4.49	2.04	2.21	0.20	1.21
Tasmania (5)	38.87	9.87	15.06	13.49	11.98	3.85	1.51	2.82	0.23	1.29
Otago, New Zealand (1)	40.47	12.88	14.52	8.52	11.38	4.64	1.62	2.79	0.25	1.23
Chantaburi, Thailand (5)	40.96	12.22	14.15	8.97	10.51	4.04	2.24	3.12	0.20	1.21
Raton-Clayton, New Mex'o (11)	39.05	12.70	12.03	9.99	14.55	4.35	1.53	1.56	0.25	2.26
Wildcat Peak, Arizona (1)	39.52	9.83	11.66	12.14	14.55	3.01	1.64	2.54	0.18	1.74
Woodruff Butte, Arizona (1)	38.55	9.50	12.51	16.07	14.06	2.82	0.60	2.46	0.19	1.20
Hopi Buttes, Arizona (4)	41.43	11.19	13.25	9.41	11.20	3.27	1.88	3.71	0.19	1.45
Balcones, Texas (6)	38.44	10.15	12.90	14.74	13.65	3.02	0.93	3.47	0.19	0.83
Average of 37 groups	39.87	10.91	13.07	10.92	12.79	3.39	1.84	3.03	0.22	1.04
St Dev	1.87	2.06	1.37	3.93	1.55	1.15	0.76	0.84	0.03	0.35
Average of 215 analyses	39.93	11.13	13.18	10.01	13.13	3.41	1.83	3.10	0.23	1.02
St Dev	2.63	2.70	1.82	4.39	2.31	1.48	0.86	1.10	0.04	0.47
Range - Highest	45.30	16.66	18.73	20.21	22.30	7.83	4.57	7.01	0.42	3.07
Lowest	29.75	4.87	8.88	4.13	5.53	0.68	0.13	1.30	0.15	0.14

* Number of samples

Table E-3 Averages of Potassic Continental Rocks

Major elements (wt.%)

	SiO_2	Al_2O_3	Fe_2O_3	MgO	CaO	Na_2O	K_2O	TiO_2	MnO	P_2O_5
New South Wales, Australia (6)*	44.93	9.17	11.28	10.77	8.17	1.90	6.01	4.64	0.15	0.96
St Dev	1.09	0.84	0.65	1.26	0.48	0.58	0.84	0.35	0.01	0.17
Range - Highest	46.54	10.75	12.01	12.09	8.62	2.71	7.31	5.25	0.16	1.16
Lowest	43.11	8.33	10.36	8.52	7.33	1.16	4.86	4.27	0.13	0.69
Western Rift, Uganda (53)	40.20	8.85	12.62	11.77	12.57	2.02	4.18	4.33	0.20	0.80
St Dev	2.94	2.62	1.27	4.90	2.62	1.19	1.47	0.94	0.04	0.39
Range - Highest	45.37	14.95	15.43	23.73	17.38	5.84	7.03	6.02	0.31	1.77
Lowest	32.29	5.45	10.27	4.16	7.24	0.53	1.26	2.81	0.14	0.16

* Number of samples

Table E-4 Averages of Olivine-poor Continental Nephelinites

Major elements (wt. %)

	SiO_2	Al_2O_3	Fe_2O_3	MgO	CaO	Na_2O	K_2O	TiO_2	MnO	P_2O_5
Riwa & Lodwar, N Kenya (2)*	40.86	12.18	14.95	6.42	11.97	5.38	2.14	3.48	0.25	0.78
Moroto, E Uganda (2)	42.76	14.56	13.69	4.57	9.77	6.08	2.54	2.42	0.24	0.69
Napak, E Uganda (4)	42.01	14.50	12.74	4.51	11.71	5.27	2.63	2.27	0.22	0.79
Elgon, E Uganda (2)	41.02	14.75	12.26	4.76	10.54	6.17	2.67	2.43	0.30	1.02
Nyanza, Kenya (12)	46.34	16.20	9.04	2.92	7.93	7.57	3.46	1.75	0.21	0.52
Londiani, Kenya (1)	43.70	13.51	11.94	1.28	10.48	6.02	3.23	1.37	0.48	0.41
Narok-Nguruman, S Kenya (2)	42.61	21.02	8.44	2.87	6.17	7.93	3.94	2.44	0.22	0.71
Burko, N Tanzania (3)	44.62	16.52	8.14	1.95	9.30	7.20	4.69	1.30	0.30	0.51
Makuyuni Jctn, N Tanzania (1)	47.66	16.66	7.10	0.58	5.58	8.72	3.92	0.71	0.23	0.17
Hanang, N Tanzania (8)	46.75	13.30	9.48	1.72	10.51	7.30	3.74	1.29	0.29	0.55
Chilwa, Malawi (3)	42.19	14.96	11.04	3.40	8.83	6.48	3.29	2.87	0.32	1.14
Dorowa-Shawa, Zimbabwe (2)	44.94	15.70	9.02	3.93	6.52	10.62	2.17	1.86	0.19	1.12
Nuanetsi, Zimbabwe (5)	43.12	14.37	12.41	4.51	5.88	8.22	2.54	3.39	0.20	1.11
Etinde, Cameroon (12)	40.39	15.98	11.31	4.06	11.95	5.50	2.88	3.39	0.34	0.99
Eifel, Germany (4)	43.48	15.80	10.13	5.64	10.93	4.80	4.20	2.29	0.24	0.72
Frankenwald, Germany (4)	43.94	16.03	9.71	4.50	10.66	5.26	4.17	2.14	0.26	0.81
Rhine Graben, Germany (2)	38.50	14.69	11.77	3.48	10.53	5.43	2.70	2.66	0.35	1.67
Bohemian Massif, Czech (1)	40.74	13.76	12.38	4.34	11.97	4.59	3.05	3.97	0.28	1.26
Graz, Austria (7)	40.29	13.79	11.26	6.42	13.09	6.26	2.45	1.99	0.27	1.47
Greenland (2)	41.40	14.87	11.34	4.79	10.43	7.58	1.95	1.93	0.23	0.91
Tasmania (1)	36.13	10.19	15.71	11.26	14.87	5.38	1.86	2.70	0.27	1.45
Queensland, E Australia (2)	40.91	11.55	12.79	12.38	10.12	4.49	2.04	2.21	0.20	1.21
Otago, New Zealand (1)	40.47	12.88	14.52	8.52	11.38	4.64	1.62	2.79	0.25	1.23
Chantaburi, Thailand (1)	39.86	11.77	14.80	9.60	9.97	5.11	2.60	3.20	0.21	1.35
Raton-Clayton, New Mex'o (5)	38.06	12.80	12.15	9.63	15.14	4.81	1.52	1.40	0.28	2.52
Average of 89 analyses	42.64	14.85	10.95	4.60	10.38	6.39	3.01	2.28	0.27	0.98
St Dev	3.46	2.13	2.38	2.66	3.02	1.70	1.10	0.93	0.07	0.57
Range - Highest	49.74	21.08	15.81	13.92	15.74	10.84	5.01	4.31	0.48	3.07
Lowest	36.13	10.19	5.42	0.58	3.65	3.75	0.58	0.60	0.16	0.13
Average of 25 groups	42.11	14.49	11.52	5.12	10.25	6.27	2.88	2.33	0.27	1.00
St Dev	2.74	2.15	2.26	3.05	2.47	1.53	0.87	0.80	0.06	0.48

* Number of samples

Table E-5 Averages of Ocean Island Basaltic Rocks

Major elements (wt.%)

	SiO_2	Al_2O_3	Fe_2O_3	MgO	CaO	Na_2O	K_2O	TiO_2	MnO	P_2O_5
Hawaii (15)*	48.63	14.16	13.33	6.95	10.10	2.66	0.73	3.00	0.19	0.38
Kahoolawe (7)	49.44	13.51	13.31	9.36	9.69	2.33	0.21	2.42	0.18	0.21
Lanai (4)	50.88	14.31	11.99	7.06	9.98	2.41	0.32	2.18	0.16	0.27
Maui (76)	45.36	14.81	14.20	6.12	10.21	3.36	1.08	3.46	0.21	0.51
Oahu (28)	43.36	11.82	14.15	11.63	11.23	2.95	0.84	2.43	0.19	0.53
Kaui (45)	43.67	11.92	14.27	10.94	11.08	2.59	0.79	2.74	0.19	0.49
Azores (24)	46.61	13.89	11.55	9.95	10.87	2.85	1.12	2.71	0.17	0.46
Madeira (30)	44.09	13.51	13.11	11.01	10.77	2.76	0.85	2.68	0.19	0.60
Canaries (13)	44.14	14.16	12.73	8.53	10.34	3.60	1.44	3.37	0.19	0.83
Cape Verde (20)	38.07	9.78	12.53	14.49	15.07	2.78	1.25	3.52	0.19	1.05
Pagalu (16)	43.73	12.40	13.83	10.30	10.31	2.74	1.17	3.25	0.19	0.97
Sao Tome (77)	44.50	13.56	12.88	8.20	10.52	3.17	1.39	3.35	0.18	0.88
Principe (28)	44.81	13.20	12.99	8.23	10.41	2.88	1.36	3.37	0.16	0.77
Bioko (23)	45.09	13.29	13.55	8.53	10.57	2.91	1.39	3.44	0.19	0.70
Fernando de Noronha (20)	41.36	12.32	12.57	10.04	11.60	3.18	1.78	3.28	0.19	0.92
Trinidade (5)	39.66	12.21	14.18	7.63	11.84	2.91	1.77	3.95	0.23	1.97
Ascension (9)	48.07	15.61	12.98	4.88	8.62	3.79	1.38	3.01	0.21	0.91
St Helena (8)	45.21	14.23	13.47	7.97	10.20	2.85	1.01	3.01	0.20	0.56
Rapa, Australs (11)	44.84	13.22	13.03	9.89	9.61	2.66	1.30	3.32	0.17	0.59
Rurutu, Australs (8)	45.45	14.09	13.77	7.58	9.21	3.53	1.02	3.00	0.20	0.65
Kusaie, Carolines (7)	40.63	11.30	13.76	10.53	11.47	2.52	1.42	4.08	0.19	0.74
Ponape, Carolines (34)	42.88	12.36	13.44	10.36	10.71	2.70	0.97	3.20	0.19	0.68
Truk, Carolines (14)	42.85	13.69	13.07	8.94	10.73	3.25	1.11	3.25	0.18	0.70
Juan Fernandez (7)	47.18	15.34	12.37	6.15	9.65	2.96	0.87	3.52	0.15	0.48
Marion, Prince Edward (4)	46.41	15.05	13.23	7.52	9.67	2.93	1.06	3.10	0.18	0.47
Grande Comore (89)	46.11	13.51	12.88	8.77	11.22	2.98	1.19	2.41	0.19	0.43
Mohell (70)	42.88	12.14	14.00	10.47	11.08	2.97	1.12	2.82	0.20	0.70
Tristan (10)	43.44	15.43	13.62	6.02	10.52	3.08	2.36	3.78	0.18	0.86
Gough (5)	48.12	15.62	10.94	5.78	8.40	3.17	2.43	3.41	0.14	0.72
Kerguelen (13)	44.96	13.15	12.78	10.90	8.67	3.13	1.30	2.47	0.18	0.66
Heard (4)	45.46	11.10	13.07	11.77	9.10	2.47	2.13	3.87	0.17	0.64
Mauritius (52)	46.31	14.62	13.00	7.98	9.80	2.81	1.04	2.73	0.18	0.40
Reunion (23)	46.92	13.84	12.83	8.96	10.81	2.53	0.79	2.63	0.18	0.32
Rodrigues (54)	48.26	16.67	9.85	7.39	9.28	3.40	1.38	1.82	0.14	0.43
Christmas Is, Indian Ocean (8)	45.43	11.70	12.24	10.59	9.58	2.57	1.36	3.07	0.16	0.72
Samoa (4)	46.54	14.50	13.69	6.53	7.99	3.58	1.61	3.60	0.16	0.81
Aitutaki, Cook Is (2)	38.18	11.53	14.58	11.12	12.10	4.77	1.52	2.68	0.21	1.20
Tahiti (25)	45.18	11.77	12.65	11.76	9.93	2.37	1.54	2.89	0.17	0.48
Ua Pou, Marquesas (12)	44.00	13.94	13.32	7.81	10.56	2.92	1.02	3.71	0.19	0.64
Average of 904 analyses	44.87	13.48	13.06	9.01	10.56	2.97	1.18	2.94	0.18	0.61
St Dev	2.99	2.13	1.43	3.40	1.54	0.79	0.54	0.69	0.03	0.30
Range - Highest	52.98	20.20	17.65	20.70	18.38	6.84	3.93	5.65	0.57	3.45
Lowest	36.13	7.36	7.78	4.00	5.69	0.22	0.08	0.66	0.10	0.13
Average of 39 islands	44.84	13.42	13.07	8.94	10.35	2.97	1.24	3.09	0.18	0.67
St Dev	2.79	1.48	0.92	2.07	1.22	0.46	0.46	0.51	0.02	0.30

* Number of samples

Table E-6 Averages of Ocean Island Nephelinites

Trace elements (ppm)

	Rb	Ba	Th	Nb	La	Ce	Pb	Sr	Nd	Zr	Y	V	Sc	Cr	Ni	Cu	Zn
Cape Verde CV (20)*	32	972	7.6	86	65	126	3.0	1157	60	323	29	312	25	597	307	79	93
Principe PR (1)	40	950	10.7	117	104	191	2.8	1290	82	345	35	311	24	339	196	59	114
Fernando de Noronha FN (8)	43	809	10.3	101	75	150	4.2	1200	71	362	32	302	21	397	191	61	111
Trinidade TD (2)	49	636	4.5	76	56	122	2.5	759	57	317	27	403	26	526	237	76	109
Grande Comore GC (7)	40	666	10.0	75	69	136	4.5	729	56	218	27	236	26	795	485	77	98
Moheli MO (26)	52	824	11.1	82	77	144	4.7	898	62	266	32	267	21	448	303	68	114
Oahu OA (7)	35	863	7.7	67	61	124	4.4	1335	61	223	27	288	19	396	274	78	155
Kauai KU (81)	21	809	5.3	57	43	81	2.8	869	42	200	26	326	18	526	403	86	112
Kusaie KS (5)	29	531	6.5	56	64	60	3.1	801	60	323	29	381	27	631	338	77	114
Ponape PO (4)	20	655	7.2	59	62	126	3.8	853	56	245	28	282	23	516	363	68	105
Truk TK (5)	43	804	7.3	103	60	120	3.3	1070	57	313	31	317	29	437	230	77	96
Samoa SM (1)	51	489	7.3	67	83	166	5.0	984	75	353	33	294	16	425	355	54	157
Aitutaki CK (2)	54	1177	24.9	96	111	205	10.7	1458	84	338	35	180	13	201	162	50	143
Average of 13 Islands	39	783	9.3	80	72	140	4.2	1031	63	294	30	300	22	479	296	70	117
St Dev	11	189	5.1	19	19	32	2.1	239	12	56	3	57	5	147	93	11	21
Average of 169 analyses	31	816	7.4	70	57	110	3.5	949	52	247	28	308	21	516	350	79	111
St Dev	18	271	3.9	22	21	40	1.9	306	16	71	5	48	5	157	169	15	19
Range - Highest	106	2939	26.0	177	147	252	16.7	1938	96	427	47	513	33	1141	1531	110	210
Lowest	5	383	2.6	39	25	47	1.3	498	27	133	20						
Japan JP (4)	67	1387	25.5	164	201	358	9.6	2038	140	377	58	206	22	160	106	39	150
Ambitle AM (1)	29	160	0.8	2.2	15	35	81.6	1277	26	74	15	310	40	162	53	150	82

* Number of samples

Table E-7 Averages of Continental Nephelinites

Incompatible trace elements (ppm)

	Rb	Ba	Th	Nb	La	Ce	Pb	Sr	Nd	Zr	Y
Ankaratra, Malagasy (2)*	41	1006	8.9	92	69	138	2.2	970	58	246	26
Turkana, N Kenya (3)	23	1891	21.9	172	145	277	9.3	1682	105	333	36
Riwa & Lodwar, N Kenya (4)	39	596	9.8	99	78	155	7.1	947	65	260	28
Samburu, N Kenya (3)	20	615	9.2	82	68	123	6.4	748	50	191	25
Moroto, E Uganda (4)	37	644	4.4	45	47	88	4.1	809	40	161	21
Napak, E Uganda (9)	49	814	8.1	74	67	129	8.8	1129	53	188	25
Elgon, E Uganda (5)	66	1125	9.4	89	70	124	8.1	1060	49	212	25
Nyanza Rift, Kenya (33)	48	1275	11.1	108	86	162	9.1	1474	69	293	30
Narok-Nguruman, S Kenya (5)	25	466	6.8	58	59	115	4.0	724	53	210	24
Loolmurwak, N Tanzania (1)	44	772	10.6	98	77	150	6.2	964	67	404	29
Burko, N Tanzania (2)	110	3669	22.6	207	161	284	9.2	1920	114	434	38
Makuyuni Jnctn, N Tanzania (5)	36	1354	12.5	116	116	238	8.0	1563	113	505	41
Chilwa, Malawi (6)	89	1386	18.9	127	173	334	7.9	2282	133	406	48
Nuanetsi, Zimbabwe (4)	83	1520	9.2	156	69	120	16.0	1541	47	301	26
Cape Province, S Africa (7)	64	1260	12.9	122	97	192	6.0	1474	80	307	28
Gamoep, Bushmanland (10)	65	707	10.9	116	90	181	5.9	944	81	385	27
Etinde, Cameroon (15)	99	1236	21.1	230	195	387	6.1	2806	156	655	47
Orkney, NE Scotland (3)	59	1300	11.5	100	89	162	5.3	1253	72	273	29
Massif Central, France (2)	74	787	7.6	76	79	166	4.8	779	70	398	23
Forez, France (2)	39	1046	12.1	99	83	157	5.1	1361	71	302	28
Rhine Graben, Germany (4)	66	1132	12.9	127	100	204	8.5	1591	95	522	36
Eifel & Vogelsberg, Germ'y (9)	90	1206	12.4	129	102	189	6.3	1365	74	279	29
Hegau, Germany (2)	60	1121	8.8	101	78	145	5.6	988	60	254	24
Frankenwald, Germany (2)	95	906	20.4	240	152	281	12.8	1851	106	370	42
Bohemian Massif, Czech (6)	52	909	13.6	125	99	196	6.1	1226	80	363	32
Graz, Austria (7)	99	1701	17.8	144	117	219	7.5	1763	91	371	38
Greenland (9)	32	615	5.7	69	65	147	5.8	1067	73	333	29
Bathhurst Island, Canada (15)	35	1718	11.7	85	87	153	6.5	1053	60	223	26
Queensland, E Australia (2)	33	722	13.1	113	87	170	4.1	1553	65	338	25
Tasmania (5)	22	425	10.2	106	76	147	4.6	1292	68	349	31
Otago, New Zealand (1)	40	670	13.1	110	118	211	5.5	1311	87	306	36
Chantaburi, Thailand (5)	54	665	10.3	92	64	124	4.2	1246	62	354	32
Raton-Clayton, New Mex'o (11)	24	2195	23.1	68	189	342	11.6	2745	136	332	44
Wildcat Peak, Arizona (1)	31	3904	21.7	51	218	457	15.6	2113	233	368	46
Woodruff Butte, Arizona (1)	10	1792	16.4	85	95	189	6.1	1385	85	257	26
Hopi Buttes, Arizona (4)	25	1057	13.2	107	115	238	6.4	1744	114	584	39
Balcones, Texas (6)	24	473	5.9	68	52	96	2.9	973	48	266	26
Average of 37 groups	51	1208	12.7	110	101	194	7.0	1397	83	333	31
St Dev	26	759	5.0	44	42	83	3.1	507	37	108	7
Average of 215 analyses	54	1189	12.7	112	102	196	7.2	1485	83	337	32
St Dev	33	850	6.6	54	54	104	3.8	783	41	157	10
Range - Highest	287	6242	38.8	308	396	746	23.4	6947	274	1312	72
Lowest	1	126	1.2	12	21	38	0.5	500	18	93	12

* Number of samples

Table E-7 Averages of Continental Nephelinite (continued)

Compatible trace elements (ppm)

	V	Sc	Cr	Ni	Cu	Zn
Ankaratra, Malagasy (2)*	278	27	637	372	75	88
Turkana, N Kenya (3)	354	21	58	44	196	95
Riwa & Lodwar, N Kenya (4)	338	23	347	102	175	111
Samburu, N Kenya (3)	290	30	561	284	100	101
Moroto, E Uganda (4)	312	27	308	106	140	94
Napak, E Uganda (9)	291	17	28	20	158	123
Elgon, E Uganda (5)	311	28	161	69	233	121
Nyanza Rift, Kenya (33)	330	20	143	93	183	115
Narok-Nguruman, S Kenya (5)	260	27	768	536	105	102
Loolmurwak, N Tanzania (1)	275	33	685	370	122	128
Burko, N Tanzania (2)	277	12	25	31	110	120
Makuyuni Jnctn, N Tanzania (5)	351	20	109	45	146	135
Chilwa, Malawi (6)	266	24	298	177	55	108
Nuanetsi, Zimbabwe (4)	413	11	54	53	249	129
Cape Province, S Africa (7)	308	25	784	455	94	98
Gamoep, Bushmanland (10)	315	20	582	642	115	117
Etinde, Cameroon (15)	412	14	23	18	83	138
Orkney, NE Scotland (3)	242	25	788	408	57	84
Massif Central, France (2)	288	31	1104	307	81	84
Forez, France (2)	333	31	753	364	62	85
Rhine Graben, Germany (4)	281	21	371	234	72	135
Eifel & Vogelsberg, Germ'y (9)	353	21	258	151	52	84
Hegau, Germany (2)	352	32	1012	380	76	79
Frankenwald, Germany (2)	398	9	12	22	74	127
Bohemian Massif, Czech (6)	363	22	266	158	118	107
Graz, Austria (7)	184	10	69	58	29	101
Greenland (9)	335	24	882	390	156	111
Bathhurst Island, Canada (15)	216	28	338	234	61	84
Queensland, E Australia (2)	157	12	402	318	50	127
Tasmania (5)	208	17	4440	342	60	145
Otago, New Zealand (1)	203	11	180	129	51	133
Chantaburi, Thailand (5)	205	12	124	135	49	142
Raton-Clayton, New Mex'o (11)	213	23	176	171	50	112
Wildcat Peak, Arizona (1)	241	21	513	233	119	120
Woodruff Butte, Arizona (1)	245	21	561	457	70	104
Hopi Buttes, Arizona (4)	241	18	235	190	60	147
Balcones, Texas (6)	296	22	520	327	58	102
Average of 37 groups	290	21	394	228	101	112
St Dev	64	7	303	163	54	19
Average of 215 analyses	300	21	317	201	110	112
St Dev	77	9	325	202	67	26
Range - Highest	495	44	1631	882	305	258
Lowest	139	1	0	6	11	64

* Number of samples

Table E-8 Averages of Polassic Continental Rocks

Trace elements (ppm)

	Rb	Ba	Th	Nb	La	Ce	Pb	Sr	Nd	Zr	Y	V	Sc	Cr	Ni	Cu	Zn
New South Wales, Australia (6)*	159	1801	11.3	113	130	257	11.9	1537	119	681	30	213	17	357	326	54	114
St Dev	64	948	4.1	20	32	52	2.9	435	17	48	2	22	3	109	56	11	5
Range - Highest	255	3643	18.4	148	192	360	15.7	2231	152	724	33	242	21	468	396	69	121
Lowest	106	1069	8.5	95	106	222	9.3	1093	108	598	28	175	13	182	254	38	107
Western Rift, Uganda (53)	122	2007	19.6	173	148	290	7.7	1957	114	352	21	306	22	547	244	112	92
St Dev	38	766	7.4	62	56	115	3.0	870	41	115	7	116	9	372	243	50	16
Range - Highest	205	3590	33.2	271	248	501	14.2	4772	192	605	41	536	43	1240	934	238	129
Lowest	51	901	9.2	77	68	125	2.8	673	56	150	9	149	0	2	22	39	66

* Number of samples

Table E-9 Averages of Olivine-poor Continental Nephelinites

Incompatible trace elements (ppm)

	Rb	Ba	Th	Nb	La	Ce	Pb	Sr	Nd	Zr	Y
Riwa & Lodwar, N Kenya (2)*	45	688	13.9	135	102	199	10.8	1201	83	343	34
Moroto, E Uganda (2)	55	1040	8.6	81	67	130	5.6	1171	57	236	30
Napak, E Uganda (4)	64	990	10.6	89	80	148	10.0	1169	61	212	27
Elgon, E Uganda (2)	94	1895	11.6	128	92	162	9.2	1359	63	266	35
Nyanza, Kenya (12)	80	2999	31.7	379	125	216	17.3	1453	77	563	28
Londiani, Kenya (1)	82	2923	13.6	323	180	241	26.0	4567	54	381	26
Narok-Nguruman, S Kenya (2)	74	1465	13.4	172	78	147	4.6	1483	53	486	40
Burko, N Tanzania (3)	90	2205	39.0	271	261	433	32.5	4601	135	873	52
Makuyuni Jctn, N Tanzania (1)	94	1962	43.5	170	203	326	34.6	1397	88	393	45
Hanang, N Tanzania (8)	111	2151	10.6	167	134	143	33.1	3037	54	588	42
Chilwa, Malawi (3)	95	2512	7.5	190	144	282	8.8	2385	118	865	53
Dorowa-Shawa, Zimbabwe (2)	53	1687	9.1	154	58	107	22.6	1298	42	283	28
Nuanetsi, Zimbabwe (5)	66	2705	14.6	225	94	163	20.2	2090	61	370	30
Etinde, Cameroon (12)	114	1215	21.5	278	208	397	9.7	3018	152	755	52
Eifel, Germany (4)	94	1056	16.0	185	132	247	9.3	1815	92	326	36
Frankenwald, Germany (4)	117	1356	15.1	144	105	198	11.2	1421	67	380	31
Rhine Graben, Germany (2)	230	4267	23.5	289	214	412	15.7	3752	167	805	58
Bohemian Massif, Czech (1)	75	989	18.5	189	135	269	10.9	1870	105	574	43
Graz, Austria (7)	99	1701	17.8	144	117	219	7.5	1763	91	371	38
Greenland (2)	31	835	2.8	39	31	68	6.0	1143	40	177	30
Tasmania (1)	38	722	16.1	164	93	172	6.7	1424	76	356	36
Queensland, E Australia (2)	33	722	13.1	113	87	170	4.1	1553	65	338	25
Otago, New Zealand (1)	40	670	13.1	110	118	211	5.5	1311	87	306	36
Chantaburi, Thailand (1)	43	760	11.4	101	69	133	5.5	1238	65	380	33
Raton-Clayton, New Mex'o (5)	25	2210	27.9	72	227	411	11.3	3100	159	353	49
Average of 89 analyses	85	1867	18.8	203	137	242	14.5	2163	92	493	38
St Dev	52	1496	11.8	149	65	115	9.6	1078	44	251	13
Range - Highest	358	9943	55.4	779	345	616	39.2	6178	227	1346	94
Lowest	20	229	0	27	12	28	1.3	752	17	141	17
Average of 25 groups	78	1669	17.0	172	126	224	13.5	2025	84	439	38
St Dev	42	916	9.6	83	59	102	9.4	1051	36	200	9

* Number of samples

Table E-9 Averages of Olivine-poor Continental Nephelinites (continued)

Compatible trace elements (ppm)

	V	Sc	Cr	Ni	Cu	Zn
Riwa & Lodwar, N Kenya (2)*	340	16	39	41	162	128
Moroto, E Uganda (2)	248	11	14	21	138	131
Napak, E Uganda (4)	255	12	8	9	138	129
Elgon, E Uganda (2)	325	4	4	9	245	149
Nyanza, Kenya (12)	188	5	35	16	73	140
Londiani, Kenya (1)	465	0	7	5	24	212
Narok-Nguruman, S Kenya (2)	182	1	0	5	141	143
Burko, N Tanzania (3)	145	0	3	6	28	212
Makuyuni Jctn, N Tanzania (1)	64	0	1	4	22	183
Hanang, N Tanzania (8)	221	2	6	6	65	196
Chilwa, Malawi (3)	176	6	20	21	16	140
Dorowa-Shawa, Zimbabwe (2)	171	3	19	21	104	129
Nuanetsi, Zimbabwe (5)	332	3	30	31	202	137
Etinde, Cameroon (12)	369	6	6	12	72	158
Eifel, Germany (4)	378	12	53	34	47	98
Frankenwald, Germany (4)	283	15	28	32	43	98
Rhine Graben, Germany (2)	314	2	7	12	94	222
Bohemian Massif, Czech (1)	386	8	3	8	49	131
Graz, Austria (7)	184	10	69	58	29	101
Greenland (2)	318	5	36	27	72	100
Tasmania (1)	224	18	185	162	87	152
Queensland, E Australia (2)	157	12	402	318	50	127
Otago, New Zealand (1)	203	11	180	129	51	133
Chantaburi, Thailand (1)	206	10	132	150	47	157
Raton-Clayton, New Mex'o (5)	203	22	126	161	50	116
Average of 89 analysos	255	8	42	39	79	143
St Dev	98	7	71	61	65	38
Range - Highest	489	26	467	364	305	258
Lowest	64	0	0	4	4	73
Average of 25 groups	253	8	56	52	82	145
St Dev	94	6	90	75	59	35

* Number of samples

Table E-10 Averages of Ocean Island Basaltic Rocks

Incompatible trace elements (ppm)

	Rb	Ba	Th	Nb	La	Ce	Pb	Sr	Nd	Zr	Y
Hawaii (15)*	11	232	1.4	23	27	49	1.6	566	33	232	34
Kahoolawe (7)	2	86	0.6	12	16	25	1.1	340	17	159	24
Lanai (4)	3	80	0.2	8	13	27	1.1	361	21	142	27
Maual (76)	22	435	2.7	37	33	67	2.1	717	39	243	31
Oahu (28)	18	560	3.8	40	33	68	3.0	745	35	164	24
Kaual (45)	18	521	3.7	43	35	65	3.0	633	36	185	28
Azores (24)	25	354	3.7	43	32	67	3.0	567	36	206	25
Madeira (30)	18	298	4.9	49	41	81	2.0	640	41	240	27
Canaries (13)	30	475	6.7	76	64	127	3.4	949	62	340	31
Cape Verde (20)	32	972	7.6	86	65	126	3.0	1157	60	323	29
Pagalu (16)	34	594	6.2	64	57	112	3.6	886	56	337	34
Sao Tome (77)	38	577	7.3	77	64	123	3.2	983	59	340	31
Principe (28)	30	436	5.1	58	49	96	2.5	802	47	279	30
Bioko (23)	35	519	7.0	73	62	120	3.7	863	57	310	32
Fernando de Noronha (20)	49	725	10.6	91	79	149	5.0	1182	67	369	31
Trinidade (5)	42	853	9.5	125	120	255	4.4	1754	120	586	47
Ascension (9)	25	366	4.5	53	40	81	3.0	559	45	287	39
St Helena (8)	18	367	5.1	50	42	87	2.3	592	42	252	33
Rapa, Australs (11)	33	370	4.6	53	45	86	3.0	748	43	271	26
Rurutu, Australs (8)	20	283	5.2	57	52	104	3.1	755	48	292	33
Kusaie, Carolines (7)	31	508	6.1	55	61	122	3.2	801	59	336	31
Ponape, Carolines (34)	20	472	5.0	49	47	96	3.3	730	48	274	30
Truk, Carolines (14)	26	427	3.8	53	36	71	2.7	690	37	244	29
Juan Fernandez (7)	15	225	2.8	36	31	61	2.4	497	34	242	31
Marion, Prince Edward (4)	18	262	2.7	35	30	64	2.1	541	33	249	30
Grande Comore (89)	27	390	5.0	46	40	81	3.2	519	37	208	26
Moholi (70)	43	715	8.6	68	63	117	4.3	795	53	251	30
Tristan (10)	54	764	8.3	64	67	130	4.7	1182	64	287	29
Gough (5)	41	797	6.3	49	56	108	5.8	907	51	340	28
Kerguelen (13)	30	487	5.8	44	51	103	5.2	849	47	290	29
Heard (4)	45	600	5.1	50	53	94	5.1	722	48	305	27
Mauritius (52)	25	245	3.6	29	27	55	2.6	470	30	216	28
Reunion (23)	19	172	2.4	23	22	47	1.7	387	24	187	27
Rodrigues (54)	35	539	4.7	43	30	55	2.4	481	23	175	31
Christmas Is, Indian Ocean (8)	23	472	4.2	53	43	86	2.4	722	43	261	27
Samoa (4)	41	334	4.6	49	51	111	4.0	755	60	392	43
Aitutaki, Cook Is (2)	54	1177	24.9	96	111	205	10.7	1458	84	338	35
Tahiti (25)	41	402	5.2	41	41	82	3.9	626	45	307	27
Ua Pou, Marquesas (12)	65	610	8.0	61	64	126	4.4	862	59	320	31
Average of 904 analyses	29	479	5.3	52	45	89	3.1	717	44	255	29
St Dev	19	241	3.4	25	23	43	1.7	307	19	94	7
Range - Highest	147	1946	26.0	177	185	400	16.7	3079	172	966	121
Lowest	0	49	0	7	6	10	0	112	6	46	16
Average of 39 islands	30	479	5.6	53	49	96	3.4	764	47	276	30
St Dev	14	232	3.9	23	22	44	1.6	288	18	80	5

* Number of samples

Table E-10 Averages of Ocean Island Basaltic Rocks (continued)

Compatible trace elements (ppm)

	V	Sc	Cr	Ni	Cu	Zn
Hawaii (15)*	297	28	231	102	87	108
Kahoolawe (7)	305	30	412	266	100	113
Lanai (4)	285	29	270	129	93	100
Maui (76)	335	22	114	69	57	114
Oahu (28)	296	24	495	332	84	120
Kauai (45)	304	20	469	316	88	113
Azores (24)	271	28	549	189	48	89
Madeira (30)	306	28	523	241	71	99
Canaries (13)	285	20	256	164	65	111
Cape Verde (20)	312	25	597	307	79	93
Pagalu (16)	286	26	399	293	48	131
Sao Tome (77)	255	21	247	146	51	118
Principe (28)	256	23	223	138	42	113
Bioko (23)	281	23	303	171	60	117
Fernando de Noronha (20)	271	17	297	181	56	110
Trinidade (5)	311	16	220	103	46	153
Ascension (9)	265	24	44	36	35	140
St Helena (8)	263	23	319	165	65	116
Rapa, Australs (11)	226	18	383	235	55	122
Rurutu, Australs (8)	217	18	304	171	73	127
Kusaie, Carolines (7)	384	27	471	268	83	118
Ponape, Carolines (34)	291	23	375	225	66	117
Truk, Carolines (14)	322	27	259	158	71	103
Juan Fernandez (7)	329	27	199	109	62	114
Marion, Prince Edward (4)	274	26	205	110	57	118
Grande Comore (89)	268	29	334	191	89	103
Moheli (70)	261	23	413	250	74	114
Tristan (10)	346	20	66	35	45	112
Gough (5)	227	19	109	90	25	112
Kerguelen (13)	204	20	464	317	55	106
Heard (4)	273	23	476	334	58	121
Mauritius (52)	285	25	244	156	69	106
Reunion (23)	317	32	430	212	77	98
Rodrigues (54)	179	24	220	135	50	63
Christmas Is, Indian Ocean (8)	206	19	436	271	46	117
Samoa (4)	246	14	109	93	25	175
Aitutaki, Cook Is (2)	180	13	201	162	50	143
Tahiti (25)	262	22	607	334	55	114
Ua Pou, Marquesas (12)	306	22	254	112	43	112
Average of 904 analyses	277	24	329	191	65	109
St Dev	62	7	263	146	27	20
Range - Highest	548	50	1534	1012	180	210
Lowest	93	3	0	?	7	50
Average of 39 islands	277	23	321	188	62	115
St Dev	44	5	146	86	18	18

* Number of samples

Appendix F

Sample Sources

F.1 Ocean Island Nephelinites

F.1.1 Atlantic Ocean

Maio, Cape Verde Islands	Dr M J Le Bas, Dept Geology, Leicester University.
Principe, Gulf of Guinea	Dr J G Fitton, Dept Geology & Geophysics, Edinburgh University.
Fernando de Noronha	Dr J C Stormer, Dept Geology, Rice University, Houston, Texas, USA.
Trinidade	TD3 (=75364); TD6 (=87171(915)): Rock Collection, British Museum (Natural History), London. (Dr A R Woolley)

F.1.2 Indian Ocean

Gran Comoro & Moheli, Comores Islands	Prof B G J Upton, Dept Geology & Geophysics, Edinburgh University.

F.1.3 Pacific Ocean

Kauai, Hawaiian Islands	SM-- samples: Prof S Maaløe, Dept Geology, University of Bergen, Bergen, Norway. 2521-32 & -34 (=112521-32 & -34): National Museum of Natural History, Smithsonian Institution, Washington DC, USA. HWK1: Author, Dept Geology & Geophysics, Edinburgh University.
Oahu, Hawaiian Islands	KA5: Dr D P Mattey, Dept Earth Sciences, The Open University, Milton Keynes. 8127-85 & -86 (=88127-85 & -86); 2521-16 & -40 (=112521-16 & -40): National Museum of Natural History, Smithsonian Institution, Washington DC, USA. 43651 & 43652: Department collection, Dept Geology & Geophysics, Edinburgh University.
Kusaie, Ponape & Truk, Caroline Islands	Dr D P Mattey, Dept Earth Sciences, The Open University, Milton Keynes.

Aitutaki, Cook Islands	Dr R V Fodor, Dept Marine, Earth & Atmospheric Sciences, North Carolina State University, Raleigh, North Carolina, USA.
Upolo, Samoa	Dr J Natland, Scripps Institute Oceanography, University of California, San Diego, USA.
Nagahama, Japan	Dr M J Le Bas, Dept Earth Sciences, Leicester University.
Ambitle, Feni Islands	AMB1 (=73680007): Dr R W Johnson, Bureau of Mineral Resources, Geology & Geophysics, Canberra, Australia.

F.2 Continental Nephelinites

F.2.1 Africa

Madagascar (Malagasy)	Department collection, Dept Geology & Geophysics, Edinburgh University.
Turkana Province, N Kenya	Dr H Emeleus, Dept Geological Sciences, Durham University.
Riwa-Lodwar, N Kenya	RIWA1 (=1926,83(11)); RIWA2 & 3 (=1967,P28(1) & (2)); LOD1 (=1936,1333(128)): Rock Collection, British Museum (Natural History), London. (Dr A R Woolley)
Samburu District, N Kenya	Dr M J Le Bas, Dept Earth Sciences, Leicester University.
Moroto, E Uganda	The Curator, Dept Earth Sciences, University of Leeds. (Dr R Varne's collection)
Napak, E Uganda	Dr M J Le Bas, Dept Earth Sciences, Leicester University. (Dr D Sutherland's collection)
Elgon, E Uganda	ELG1, 3 & 5 (=1931,199(6), (2) & (5)); ELG2 (=1970,P44(2)); ELG4 & 6 (=1924,821(37) & (31)): Rock Collection, British Museum (Natural History), London. (Dr A R Woolley)
Nyanza (Kavirondo Trough), Kenya	1279: Author, Dept Geology & Geophysics, Edinburgh University. All other samples: Dr M J Le Bas, Dept Earth Sciences, Leicester University.

Narok-Nguruman Escarpment, S Kenya	SK-- samples: Dr L A J Williams, Dept Environmental Sciences, University of Lancaster. (Dr R Crossley's collection) 1467: Author, Dept Geology & Geophysics, Edinburgh University.
Oldoinyo Loolmurwak, Burko & Hanang, N Tanzania	Prof J B Dawson, Dept Geology & Geophysics, Edinburgh University.
Makuyuni Jnctn, N Tanzania	MANY1 to 6 (=1942,47(13), (20), (18), (15), (17) & (16)): Rock Collection, British Museum (Natural History), London. (Dr A R Woolley)
Chilwa Province, Malawi	MAL1 (=1962,77(4)); MAL2 & 5 (=1935,1211(31) & (137)); MAL6, 7 & 8 (=1957,1056(153), (162) & (151)); MAL9 (=1964,389(33)); MAL3 (=1980,P35): Rock Collection, British Museum (Natural History), London. (Dr A R Woolley)
Nuanetsi Province, Zimbabwe	Dr K G Cox, Dept Geology & Mineralogy, University of Oxford. (Dr M Norry's collection)
Dorowa-Shawa, Zimbabwe	DS1 (=1948,201(8)); DS2 (=1965,P19(6)): Rock Collection, British Museum (Natural History), London. (Dr A R Woolley)
Cape Province, S Africa	BD-- samples: Prof J B Dawson, Dept Geology & Geophysics, Edinburgh University. RIV1 (=1937,200(1)); RIV2 (=1923,660); SU1 (=1924,547): Rock Collection, British Museum (Natural History), London. (Dr A R Woolley)
Gamoep, Bushmanland-Namaqualand Province	BD-- samples: Prof J B Dawson, Dept Geology & Geophysics, Edinburgh University. N1 to 4 (=1937,200(7), (6), (5) & (4)); N5 & 6 (=1924,545 & 546): Rock Collection, British Museum (Natural History), London. (Dr A R Woolley)
Etinde, Cameroon	Dr J G Fitton, Dept Geology & Geophysics, Edinburgh University.

F.2.2 Europe

Orkney, NE Scotland	Prof B G J Upton, Dept Geology & Geophysics, Edinburgh University.
Massif Central & Monts du Forez, France	42974 & 42466: Dr H Downes, Dept Geology, Birkbeck College, University of London. MC4 & MC1: Author, Dept Geology & Geophysics, Edinburgh University.
Rhine Graben, Vogelsburg, Eifel, Hegau & Frankenwald, Germany	RG1, 2 & 6: Prof B G J Upton, Dept Geology & Geophysics, Edinburgh University. G3, G30 to 33, & G20: Department collection, Dept Geology & Geophysics, Edinburgh University. KG1 & 5; KATZ1; KT8; & E-- samples: Author, Dept Geology & Geophysics, Edinburgh University. LV-- samples: Dr H-U Schmincke, Institut für Mineralogie, Ruhr-Universität Bochum, Bochum, Germany.
Bohemian Massif, Czech Republic	77-- samples: Dr M J Le Bas, Dept Earth Sciences, Leicester University. BM9, 10 & 12 (=1934,963(9), (10) & (12)): Rock Collection, British Museum (Natural History), London. (Dr A R Woolley)
Graz Basin, Austria	STK-- samples: Dr A Embey-Isztin, Dept Mineralogy & Petrology, Hungarian Natural History Museum, Budapest, Hungary. A-- samples: Prof B G J Upton, Dept Geology & Geophysics, Edinburgh University.

F.2.3 N Atlantic Borderlands

Gardiner Complex, Nunatak Zone & Tugtilik, E Greenland	Dr T F D Neilsen, Grønlands Geologiske Undersøgelse, Copenhagen, Denmark.
Bathurst Island, NW Territories, Canada	Dr R G Platt, Dept Geology, Lakehead University, Thunder Bay, Ontario, Canada.

F.2.4 Australasia

Springsure District, Queensland, E Australia	Q1 (=DR11597); Q2 (=Mt Sterculia): Dr F L Sutherland, The Australian Museum, Sydney, Australia.

Tasmania	TAS6 (=46397(2912)); TAS7 (=46396(2911)); TAS8 (=Beehive Basalt): Prof D Green, Dept Geology, University of Tasmania, Hobart, Tasmania. TAS2 (=Round Lagoon Plug); TAS3 (=Laughing Jack Marsh (2927)): Dr F L Sutherland, The Australian Museum, Sydney, Australia.
Otago, New Zealand	OT1 (=OU5649): Prof D S Coombs, University of Otago, Dunedin, New Zealand.
Chantaburi-Trat, SE Thailand	Dr S M Barr, Dept Geology, Acadia University, Wolfville, Nova Scotia, Canada.

F.2.5 North America

Raton-Clayton, New Mexico	NM-- samples: Author, Dept Geology & Geophysics, Edinburgh University. 8552848 & 8551861: Dr J C Stormer, Dept Geology, Rice University, Houston, Texas, USA.
Wildcat Peak, Woodruff Butte & Hopi Buttes, Colarado Plateau, Arizona	Dr J G Fitton, Dept Geology & Geophysics, Edinburgh University.
Balcones Province, Texas	TX3: Dr J G Fitton, Dept Geology & Geophysics, Edinburgh University. All other samples: Dr D S Barker, Dept Geological Sciences, The University of Texas at Austin, Austin, Texas, USA.

F.3 Potassic Continental Rocks

Byrock & Lake Cargelligo, New South Wales, E Australia	NSW1 to 4 (=1962,260(19), (21), (20) & (18)): Rock Collection, British Museum (Natural History), London. (Dr A R Woolley) NSW5 & 6: Department collection, Dept Geology & Geophysics, Edinburgh University.
Western Rift, Uganda	C-- samples: The Curator, Dept Earth Sciences, Cambridge University. (Combe-Holmes collection) 15010A: Department collection, Dept Geology & Geophysics, Edinburgh University. WR1 to 3, W7: Author, Dept Geology & Geophysics, Edinburgh University.